
European Commission
JRC CONFERENCE AND WORKSHOP REPORT
10th International Symposium on Transportation Data & Modelling (ISTDM23)
Ispra, 19-22 June 2023
Booklet of abstracts
Duboz, L., Ciuffo, B. (eds.)
2023
Joint Research Centre

Contact information
Name: Biagio Ciuffo
Address: European Commission, Joint Research Centre, Via E. Fermi 2749, I-21027, Ispra (VA), Italy
Email: JRC-SMART-MOBILITY@ec.europa.eu
Tel.: +39 0332 789732

EU Science Hub
https://joint-research-centre.ec.europa.eu

JRC134973

PDF ISBN 978-92-68-07590-6 doi:10.2760/522095 KJ-04-23-881-EN-N

Luxembourg: Publications Office of the European Union, 2023

How to cite this report: *10th International Symposium on Transportation Data & Modelling (ISTDM23) Ispra, 19-22 June 2023 – Booklet of abstracts*, Duboz, L., Ciuffo, B. (eds.) Publications Office of the European Union, Luxembourg, 2023, doi:2760/522095, JRC134973.

Contents

Abstract

The present document collects the main outcomes and most of the works presented during the 10th International Symposium on Transportation Data and Modelling (ISTDM2023), held in Ispra (IT) on 19-21 June 2023. The Symposium was attended by almost 200 participants from 35 different countries from all around the world. The program included three introductory presentations from the ISTDM steering and organizing committees, four key-note speeches, a science-meets-policy-and-industry panel discussion, nine presentations about relevant European initiatives and fourteen parallel sessions to present the works submitted to the Symposium. The challenges posed by transport and mobility to our society call for a better capability to model the transport system and anticipate the impact that new policies, technologies and business models may have on its efficiency and the externalities that it produces. At the same time an unprecedent amount of data is being made available and gives the opportunity to understand transport dynamics as never has been possible hitherto. These two converging factors call for the development of new generations of transport models and data-driven tools. ISTDM2023 has offered an important opportunity to share new ideas and perspectives in this direction.

Foreword

Transport is one of the main pillars of our society. The ubiquitous availability of transport opportunities and the possibility to quickly reach almost anywhere in the world has fuelled and sustained globalisation and the unprecedented economic growth of the last century. But modern transport has had wider social effects beyond providing seamless and effective mobility. The rise of the car has given birth to 'the automotive city' and has transformed public space as well as becoming symbolic of social aspiration and status. The development of the mass production and consumption economic model has gone hand-in-hand with the revolution in vehicle production processes. As a result, any substantial changes in the transport system can have a big knock-on effect on our economic and social systems, especially if we consider that sectors linked to road transport account for about 15% of European Gross Value Added and 10% of European employment.

Yet the sector is following an unsustainable pathway. Productivity losses due to delay and congestion account for approximately 1-2% of EU GDP, not to mention the 26.000 deaths and the 1 million injured on Europe's roads. Yet, road transport and domestic heating are the two main sources of poor air quality in European cities and Road transport is the second largest source of greenhouse gases in Europe. It's also the only main source whose emissions are increasing. Achieving our sustainable development goals requires addressing the challenges posed by the transport system as a whole and by road transport in particular.

Figure 1. Main challenges posed by road transport

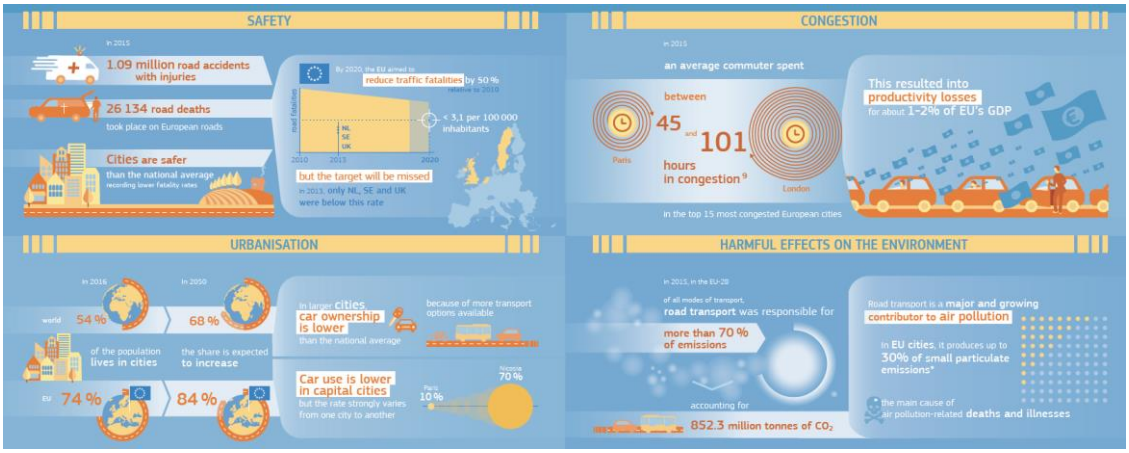

This is no easy task: policy makers face the challenge of having to act on a sector to reduce its externalities while at the same time preserving the economic model it sustains. In other terms, transport policies have a bearing on many, often conflicting, interests, as can be seen from the heated debates that accompany almost all decisions concerning transportation. It is therefore no surprise that high-level strategic actions aimed at regulating road transport usually advocate the deployment of innovative technological solutions that can contribute to cope with both objectives.

The problem is that the intrinsic complexity of the transport system makes it extremely difficult to anticipate the implications of deploying new technologies and solution that may appear highly beneficial may in reality worsen the situation and turn the system in an even more unsustainable path.

The limited reliably of the models and tools available to anticipate the effect of policies, technologies and social trends is very much linked to the historical difficulty to gather data of sufficient quality and granularity about transport and mobility dynamics. But the situation is gradually changing. The unprecedent amount of information that are being increasingly made available combined with the urgency to act on the transport system and make it safer, more efficient and more sustainable call the scientific community to develop new instruments able to deliver with the needed accuracy.

We have a long way to go to achieve this though and having fora where to discuss, exchange ideas, propose new approaches becomes extremely important. This is why when we had the opportunity to host the 10th edition of the International Symposium on Transportation Data and Modelling, we considered it a perfect opportunity to contribute to this process and we applied for it. Fortunately the steering committee liked the proposal and we succeeded to bring ISTDM to Ispra. The rest is history.

Biagio Ciuffo, European Commission Joint Research Centre

Acknowledgements

The organisation of the 10th International Symposium on Transportation Data and Modelling is the result of the collaboration of many people inside and outside the European Commission Joint Research Centre (JRC). From the JRC it involved the whole Decarbonised, Smart and Safe Mobility Portfolio[1], and indeed the Symposium itself represent one of its main deliverables. Among the members of the portfolio, Akos Kriston, Elena Paffumi, Georgios Fontaras, Juan Nicolas Ibanez and Panayotis Christidis, who have played a major role, together with the report's editors and the ISTDM Organising Committee[2], to define the Symposium content, review the contributions received, define the program and chair the scientific sessions.

Another group of colleagues deserving a special mention is the ISTDM Local Organising Committee who supported with the program development and with all the logistic involved in organising the event. Special thanks to Florentin Ungureanu and Barbara Realini for the continuos support provided during the months preceding the event.

The editors also express their gratitude towards the members of the ISTDM Steering and Organizing Committees for their constant support in preparing and advertising the event since the very beginning. In particular the editors are grateful to Jaume Barceló and Masao Kuwahara to have warmly welcomed the proposal to organise ISTDM in Ispra.

Last but not least, the editors would like to express their gratitude to all ISTDM contributors, from the key-note speakers, to the panel members, to all the presenters during plenary and parallel sessions, for the efforts put in contributing to make the Symposium a success.

[1] https://joint-research-centre.ec.europa.eu/jrc-science-and-knowledge-activities/mobility_en
[2] The list of members in the different ISTDM committees is reported in annex 1 (p. 370).

Editors

Louison Duboz, European Commission Joint Research Centre, Ispra (IT)

Biagio Ciuffo, European Commission Joint Research Centre, Ispra (IT)

Introduction

The 10th International Symposium on Transportation Data and Modelling (ISTDM) was organized at the Ispra premises of the European Commission Joint Research Centre (Italy) on June 19-21 2023.

The symposium aimed at discussing processes and challenges to properly model and manage future transport systems in a context of great transformations.

The convergency of technological, social and political trends (e.g. connectivity, automation, electrification, quantum computing, blockchains, new vehicle concepts, new social attitudes towards the provision and consumption of transport opportunities, new policy actions to fight or adapt to the climate change) provides the opportunity to rethink the transportation system to make it safer, cleaner, more efficient and more equitable in the coming decades.

Whether this opportunity will materialise or not will however strongly depend on the capability of policy, industry, academia and citizens to work together towards a common goal. Will our society be apt to the challenge? The role of the scientific community in this process will be crucial. Decision-making to tackle climate-change and fighting against the Covid-19 pandemics have both counted on the evidence provide and the tools made available by the scientific community. The same must happen in the transport sector otherwise the risk to lose the one in a century opportunity to disrupt it will likely be lost.

In order to drive the transformation of the transport sector models and data are needed on the one hand to anticipate possible impacts of new mobility solution, and on the other hand to define the requirements of the future transport system to achieve the sustainable development goals set by our society. In particular, approaches to manage the ever increasing transport complexity in urban contexts with the interaction between traditional services any new mobility options are very much needed.

Conference format

During the four days of the Symposium, 200 among scientists, policy makers, representative of private companies from 35 different countries, met to discuss the latest advancement in the field of transport data and modelling as well as future perspectives on the subject.

The main topics discussed during the Symposium were related to :

- Data collection and processing;
- Innovative research methodologies;
- Challenges in urban mobility modelling;
- Challenges in extra-urban transport modelling.

To get an overall understanding of the state of the research on the different topics parallel sessions were organised including 110 presentations, selected on the basis of extended abstracts submitted at the beginning of 2023. Among the selected abstracts, those expressing explicit consent are part of the present booklet.

In addition to the parallel sessions, plenaries with four key-note speeches, one panel discussion and nine presentations concerning relevant EU initiative completed the program[3]. In the next sections some information on the content of the plenary sessions are provided before presenting the abstracts submitted to the Symposium for presentation during the parallel scientific sessions.

[3] More details on the ISTDM program can be found online at: https://joint-research-centre.ec.europa.eu/events/istdm2023-2023-06-19_en

Setting the scene

ISTDM 2023. Continuing the series on transportation data and modelling

by M. Kuwahara (Tohuku University, JP) and J. Barceló (Universitat Politècnica de Catalunya, ES)

The presentation started by recalling the origins and evolution of the meeting, back in 2002 when Prof. Kuwahara and the late Prof. R. Kitamura organized in Yokohama the first meeting of what was initially called the "International Symposium on Transport Simulation." In 2008, it was considered that the availability of traffic data for model building and for model calibration and validation was a topic that deserved special attention. Therefore, Prof. Kuwahara and Prof. Barceló organized in 2008 in Barcelona an International Workshop on Traffic Data Collection and its Standardization.

Both meetings were held independently, but it became evident soon that, due to the strong dependencies between the main topics of both conferences and the high overlapping of the audiences, it would be better to cooperate, and therefore, in 2021, both meetings merged into a unique meeting addressing data and models. That originated the current "International Symposium on Transportation Data and Modelling."

Figure 2. Research areas, topics, and applications object of the symposium

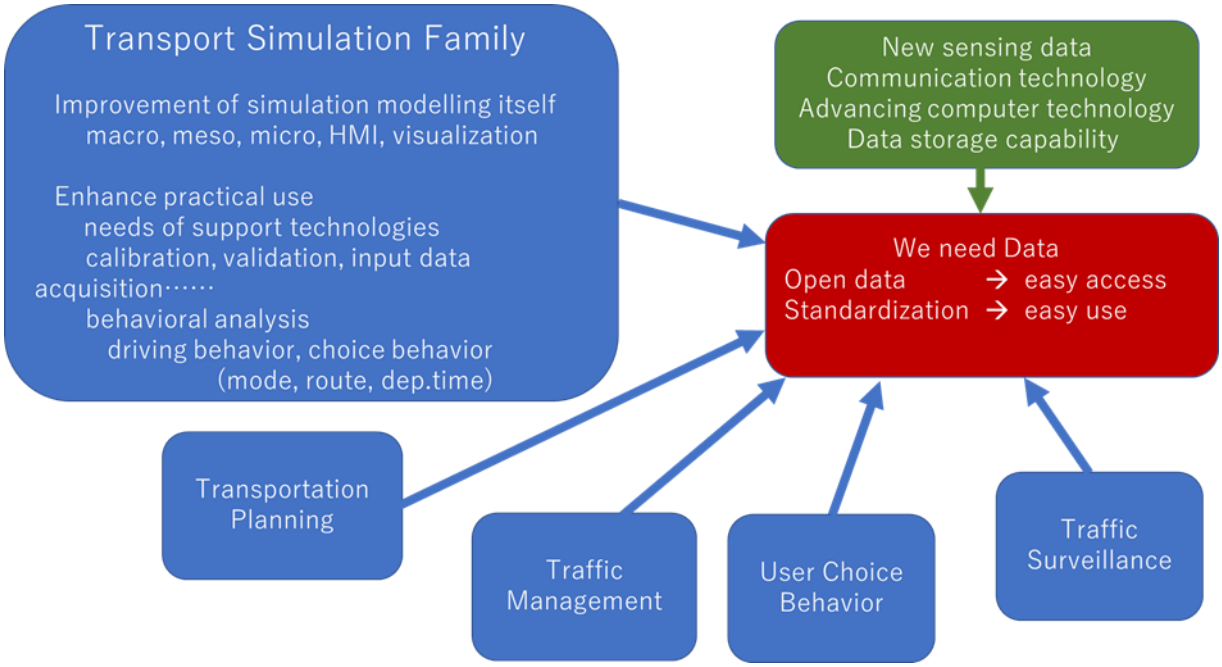

After this historical reminder, the presentation offered a synthetic view of the main areas of research and application that the issues of the symposia have covered (Figure 1).

Using the term "Transportation" instead of "Traffic" to name the symposium was needed to convey the idea that the objectives were extensive and not restricted to particular areas.

After this overview of the origins and trajectory of the symposium, the speakers exposed some thoughts about potential issues for future events in light of the societal and technological changes affecting the transportation world, highlighting which have already made a presence in our series of symposia and which appear still underrepresented If not missing.

Examples of emerging topics in our meetings are Mobility as a Service, micromobility, electric vehicles, connected vehicles, autonomous vehicles, etc. It becomes evident since Jeju meeting the increasing number of papers presented which deal with these topics. However, in the case of connected and autonomous vehicles, the approaches took a look more at the reformulation of traffic flow theory to deal with the new reality than in attempts to reflect in the model other aspects, i.e., those concerning their social implications, or their contribution to sustainability considering the life cycle of the technology.

These thoughts were complemented by a few considerations regarding the other substantial component of our symposium: the data. A simulation output substantially depends on the input data and user behaviors such as route, departure time (=dynamic OD), and mode choices. For instance, when an incident happens, or a new policy is introduced, how do people change their routes, trip times, and modes? To overcome this problem, we need data continuously and may try to use the data-driven approach more.

And getting to this point, the speakers commented on the risks of data-driven approaches. Conventionally, we have modeled user choice behaviors based on the observed data and the developed models plugged into a simulator. However, since more data become available and learning technologies have been well developed, a rising trend considers that a simulator may simulate our behaviors directly from the observed data without mathematical modeling.

However, we warned that the data-driven approach holds the risk of being purely predictive and not descriptive. We may lose the reasoning on traffic condition changes and have difficulty understanding the cause-and-effect relationship. On the contrary a model, in general, formally organizes what we know, or we think we know, about a system to predict how it might behave in the present, future or past, as well as how it might respond to external influence.

To conclude the introductory speech of the Symposium, presenters suggested some of the future trends that can determine the urban Mobility of the future. If it is fundamentally determined by technology (Autonomous and Connected Vehicles, Electric Vehicles, Information and Communication Technologies, ICT), then to inquire about the future of Mobility, **we need models that consider how those technologies configure it and which effects they will have**. That approach Implicitly assumes that technology will be used to do the same things differently. However, suppose other non-technological factors, such as urban forms, will have a relevant influence on shaping Mobility. In that case, asking ourselves about its future requires asking ourselves How cities and the dependencies between Mobility, urban forms, and transport systems will evolve. It assumes using technology to do different things, for example: telecommuting, the 15-minute city, etc. Then: **We need other types of models. Which ones?**

To answer this question it is necessary to i) put more focus on people rather than on vehicles, and ii) overcome the limitation of current traffic simulators, which are mostly used to reproduce traffic conditions but do not simulate pedestrians and public transport simultaneously, in agreement with the original objectives of this series of symposia.

Panel discussion. Driving the transformation in transport: what models, data, technologies and governance?

Moderator: D. McGarry (European Commission JRC, EU).

The objective of this panel discussion is provide a source of inspiration for attendees to prepare their future research plans. The invited panelists were therefore tasked to provide some future perspectives on the expected evolution of transport and mobility as well as on the challenges ahead. To this aim the panel was composed by the following list of transport experts coming from different organizations, countries and roles:

1. L. Castiglioni, Federal Department of the Environment, Transport, Energy and Communications (CH)
2. H. Cornet, UITP (BE)
3. R. Liu, University of Leeds (UK)
4. G. Menzel, Federal Ministry for Climate Action, Environment, Energy, Mobility, Innovation and Technology (AT)
5. R. Shliselberg, Ayalon Highways (IL)
6. E. Silani, e-Novia (IT)
7. T. Victor, Waymo (US)

To stimulate their reflections, panelists were provided with the following questions:

- "Please provide a vision on how you expect or would like transport to evolve in the next decades"
- "According to the vision you have just provided, what is the impact that you would expect on:"
  - "Emissions and energy consumption" (to speakers 1, 2, and 3)
  - "Number of accidents" (to speakers 5 and 7)
  - "Congestion and traffic efficiency" (to speakers 4 and 6)
- "As we know a change in the transport sector has impacts going beyond the business of going around and touching the choices we make in our lives (here for example you can mention what happened in

the NL with eBikes and the possibility to use the bike for longer, etc.). This makes transport so complex and makes it also difficult to foresee the effect of policies applied to it. So my question to the panel is how can we ensure that the visions that you have described achieve the effects that you expect."

- "Some people argue that new technologies may actually contribute to make the personal car even more appealing. What is your opinion on this and how can we avoid this potential negative effect?"

A very animated discussion lasted 75' and touched an impressive number of topics. A shared vision of how transport and mobility will/should evolve in the decades ahead did not emerge given the different perspectives and the complexity of the topic. However it was a common view that to **shape policies able to properly cope with the complexity of the transport sector it will be crucial** to i) take advantage from the ever-increasing amount, quality and granularity of **available data**, ii) to develop **holistic models** able to explicitly capture the links between the transport and the other societal systems and iii) to break the silos between the transport community and **other disciplines**. These were all important messages for the ISTDM community.

A second important point raised by the majority of the panelists is that it will be extremely hard to achieve transport carbon neutrality in the next decades by acting on the supply (namely on vehicles and both physical and digital infrastructure) only without touching the demand ("*the most sustainable mobility is the one that is avoided*"). The **narrative that technological development can sustain an ever-increasing transport demand should be questioned as soon as possible** if we want to avoid that transport will remain one of the non-carbon neutral sectors. Modal shift to active modes and a better integration between transport and land-use planning aimed at rationalizing the need for going around by car should be pursued with priority. Models able to properly capture the effect of mobility policies on overall energy consumption and greenhouse gas emissions will be very important.

Linked to the previous points, a **further "diversification" of transport options was proposed** as a tendency for the future to take into account. In the last decade we have already observed the introduction of new types of mobility solutions, such as e-bikes, scooters, shared mobility, etc. The call to better use the available resources will lead to both **new types of vehicles** (smaller/modular) and to **systems able to maximize the occupancy of existing ones** (both via enhanced traffic management taking advantage of a future widespread connectivity to nudging more sustainable/virtuous behaviors). New models will need to be developed to understand their impact both on traffic flow and on the demand for their adoption.

Among the new topics in ISTDM2023, **safety emerged clearly**. This was reflected also during the panel discussion. The safety of new technologies introduced in the transport field is a fundamental prerequisite for their large-scale deployment. From automated vehicles to droids, from drones to hyperloop systems there is no question that safety assurance will play a major enabling role, but also thinking that these systems can be deployed only when they zero the risk is unfeasible as some of the risks will be visible only when full deployment will be available (the unknown unknowns). To help the process, the availability of **data on the safety performance** of the new systems from when they start the first pilots to when the achieve sufficient maturity,

and of **models able to link traffic scenarios with robust accident probabilities** can certainly play an important role.

The last point that also emerged about the mobility of the future concerns **equity**. The transport system cannot evolve without taking into account the needs of different parts of the society, different locations (urban versus rural) as well as the different requirements that different mobility reasons have (from commuting, to leisure, to shopping, up to tourism different mobility paradigms emerge). **The promotion of a people-centric mobility cannot remain a political slogan, but it's a concept to operationalize**. Living labs and other forms of participatory innovation have to be taken into serious account in order to design a system that is really more sustainable and more equitable. On this subject, the work of the community has been still limited and certainly more could be done to cover this dimension as well.

Key-note speeches

On the two central days of the Symposium, four authoritative key-note speakers enriched the program with their inspirational talks about new trends in data collection and modelling. The points of discussion they generated kept busy the audience during all the social events included in the program. A summary of their content is presented hereafter following the order in which they were presented.

The I-24 MOTION Open-Road Test Bed

by D. Work and D. Gloudemans (Vanderbilt University, US)

This presentation introduced the I-24 MOTION open road testbed led by the Tennessee Department of Transportation on Interstate 24 near Nashville, TN. The purpose of the testbed is to provide an open road experimental facility for testing traffic management and automated vehicle technologies in real freeway traffic. The testbed consists of pole-mounted 4K resolution video cameras providing uninterrupted coverage of the roadway. Video data is processed into vehicle trajectories for all vehicles passing through the testbed. The current length of the testbed is approximately 4 miles long and contains 294 cameras. Testbed specifications, hardware, and design decisions were discussed, as well as the future of the testbed construction.

Urban transportation systems: What are the contributions of the trip-based MFD simulation framework

by L. Leclercq (Gustave Eiffel University, FR, and Technical University of Delft, NL)

This presentation focused on modelling urban traffic dynamics with Network Macroscopic Fundamental Diagrams (MFD). Recent developments in MFD simulation propose two general formulations that can both be applied to multi-reservoir systems. The first is the classical accumulation-based formulation when traffic dynamics in each reservoir is governed by a conservation equation. The second is the more recently developed trip-based formulation when vehicle trips have individual lengths but share a single time-dependent mean speed in each region. The integration of multiclass extensions (mainly to represent public transport) is also presented with a particular focus on the resulting traffic dynamics at the reservoir boundaries. The question of MFD model calibration is then addressed considering two central questions: (i) the regional trip-length estimation and (ii) the scaling of observations to determine the vehicle accumulations and travel productions. Several applications are discussed in the end: validation of the multi-reservoir setting for the city of Lyon, optimization of ride-sharing services, demand-management through tradable credit schemes, optimal routing at the city scale, etc.

Learning and Control for Emerging Mobility Systems

by Andreas A. Malikopoulos (University of Delware, US)

Emerging mobility systems, such as connected and automated vehicles (CAVs) or shared mobility options, are typical cyber-physical systems (CPS) representing systems of subsystems with an informationally decentralized structure. To derive optimal control strategies for such systems, we typically assume an ideal model. However, such model-based control approaches cannot effectively facilitate optimal solutions with performance guarantees due to the discrepancy between the model and the actual system. On the other hand, in most CPS there is a large volume of dynamic data that is added to the system gradually in real time and not altogether in advance. Thus, traditional supervised learning approaches cannot always facilitate robust solutions using data derived a priori. By contrast, applying reinforcement learning approaches directly to the actual CPS might impose significant implications on safety and robust operation of the system. A new framework founded at the intersection of control theory and learning can circumvent these challenges. In this framework, we aim to identify a sufficient information state for the CPS that takes values in a time-invariant space and use this information state to derive separated control strategies. By establishing separated control strategies, we can derive offline the optimal control strategy of the system with respect to the information state, which might not be precisely known due to model uncertainties or the complexity of the system, and then use learning methods to learn the information state online while data are added gradually to the system in real time. This approach could effectively facilitate optimal solutions with performance guarantees in a wide range of emerging mobility systems.

Traffic flow as a complex system

by J. Laval (Georgia Institute of Technology, US)

The talk made the case for a complex system approach to understanding congestion on large urban networks. This paradigm change is prompted by recent findings suggesting a strong analogy between the theory of phase transitions in simple fluids and vehicular traffic flow, provided that the thermal energy of the system is interpreted as the flow of cars through the network. It is shown that the resulting network traffic model belongs to the Kardar-Parisi-Zhang universality class in statistical mechanics. The scaling relationships arising in this universality class are found to be consistent with West's scaling theory for cities. It is shown that congestion costs (delays + fuel consumption) scale superlinearly with city population, possibly and worryingly more so than predicted by West's theory. Implications for sustainability and resiliency are discussed.

Relevant European initiatives

The ISTDM2023 program was completed by the presentation of nine European initiatives on transport and mobility that relevant to the work of scientific community. Policy initiatives, research programs and projects, as well as open source tools were introduced during the different plenaries included in the Symposium program.

Relevant Initiatives 1. Preparing for a common European mobility data space

by D. Gkatzoflias (European Commission Directorate General for Mobility and Transport, EU)

As stated in the Sustainable and Smart Mobility Strategy, the Commission will propose actions to build a common European mobility data space, facilitating access, pooling and sharing of data from existing and future transport and mobility data sources. The aim of the common EMDS is to identify crucial data and increase their availability to support services considered essential across the EU's territory, covering themes from sustainability to multimodality.

A "data space" is not one database or one piece of hardware infrastructure. The common European mobility data space will be a framework for interlinking and federating many different transport data eco-systems that are rather heterogeneous and often difficult to discover or access. It will build on and complement the new European cross-sectoral data legislation, namely the Data Governance Act, the Data Act and the Implementing Act on High Value Datasets. The initiative will notably take due account of data sharing mechanisms proposed in these acts, in existing transport-related passenger and freight ecosystems and legislation (e.g. the ITS Directive establishing the National Access Points), expert groups such as the Digital Transport and Logistics Forum (DTLF) and other national or private initiatives.

To support this initiative, funds are allocated for preparatory and deployment actions under the Digital Europe Programme (DIGITAL) and the Connecting Europe Facility (CEF). A Communication by the Commission is planned for this year where the objectives and proposed way forward will be announced.

Relevant Initiatives 2. The Transport Data Commons Initiative (TDCI)

by V. Knöll (Deutsche Gesellschaft für Internationale Zusammenarbeit DE), P. N. Kishimoto (International Institute for Applied Systems Analysis, AT), J. Dixon (University of Oxford, UK), and J. Tattini (European Commission Joint Research Centre, EU)

The Transport Data Commons Initiative[4] (TDCI) aims to make high quality transport data accessible to the public. It was initiated in 2020 in a co-creation workshop of organisations that believe that better publicly available transport data is urgently needed to enhance climate action in transport. It now gathers a network of professionals from more than 30 organisations worldwide interested in sound and open data and funders who want to sustainably build a better data environment for their projects and global initiatives. The TDCI is developing the Transport Data Commons (TDC), a database with the following features: 1) providing a space for storing, 2) editing and accessing open transport data, encouraging data standards, data cleaning and interoperability of existing databases and 3) enabling active collaboration of data providers and users. The prototype of the TDC is up and running to demonstrate the vision of the initiative and it is ready to move into full operations and absorb more funding in its second year of life. TDC partners extend a warm invitation to join this collective endeavour to like-minded entities and individuals who share our vision and can contribute to data collection & management and mobilisation of funding.

[4] https://www.transport-data.org/

Relevant Initiatives 3. The Transportation Research and Innovation Monitoring System (TRIMIS)

by M. Stepniak and A. Marotta (European Commission Joint Research Centre, EU)

TRIMIS[5] is an integrated transport policy-support tool that provides open-access information on transport research and innovation. TRIMIS was founded in 2017 by the European Commission and it is operated by the Joint Research Centre. The role of TRIMIS project is to collect, curate, analyse and disseminate data on transport research and innovation in Europe and beyond and to analyse technology trends and R&I capacities in transport sector.

During the session the TRIMIS database of transport research and innovation projects was presented. The database contains more than 8.500 projects and it is constantly updated and extended. It covers not only projects funded within the latest Framework Programmes (i.e. Horizon Europe, Horizon 2020 and FP7) but it also gathers data on other relevant European projects (e.g. Interreg, Connecting Europe Facility etc.) as well as projects funded by Member States.

The second part of the presentation focused on TRIMIS Science for Policy support. TRIMIS reports offer in-depth analysis of outcomes of research and innovation activities in a given transport thematic area. They provide necessary background information, including the policy landscape and key challenges. These reports focus on projects results, including delivered solutions, prototypes, tests and deployments, policy recommendations etc., and they conclude highlighting potential research needs. The final part of the presentation introduced TRIMIS dissemination activities, including social media activity and TRIMIS Newsletter.

Relevant Initiatives 4. The JRC Living Lab for Future Mobility Solutions

by B. Ciuffo (European Commission Joint Research Centre, (EU)

The presentation introduced the JRC Living Lab for Future Mobility Solutions launched in 2019. Living labs are experimentation spaces for co-creation, prototyping, testing and upscaling of innovative solutions in real-world settings. Usually in the form of public-private partnerships, Living Labs implement an open innovation model, involving quadruple-helix stakeholders such as research organisations, businesses, governmental actors, and citizens. A key feature setting them apart from other experimentation spaces is the involvement of end users and citizens as co-creators in the experimentation process, instead of passive testers and utilisers. By involving users early-on in the research and development process, this approach allows to address users' preferences and observe the effect of emerging technologies on individuals and society, ultimately improving uptake and acceptance.

In line with the 2030 strategy principle to open up JRC's research infrastructures to external use, the JRC decided in 2019 to host LL initiatives in the Ispra (Italy) and Petten (the Netherlands) sites for the development and testing of smart city solutions[6]. Delivering on EU policy priorities, the ongoing living lab projects focus on digital energy (DES-Lab) and future mobility solutions (FMS-Lab). Thanks to its state-of-the-art infrastructure, its scientific expertise, and its policy support role, the JRC is uniquely positioned to provide a milieu for experimentation in real-life conditions, contributing to citizen-centric innovation and evidence-based policy making.

Since its start the JRC Living Lab has assessed 13 project proposals, eventually leading, as of June 2023, to 6 projects running and 1 more in the pipeline. They concern the co-design and development of an automated electric vehicle platform to implement different types of transport services for passengers and goods, the co-design and testing of automated systems for last-mile parcel deliveries, the testing of a smart-charging infrastructure for electric vehicles, two projects related to the co-design and development of mobility as a service platforms, and one project related to the use of connectivity for the protection of vulnerable road users.Furthermore, the JRC Living Lab is being used in two European Projects, namely the SHOW Horizon 2020 project, and the Green-Log Horizon Europe project.

[5] https://trimis.ec.europa.eu/

[6] Information on the JRC Living Labs can found at https://joint-research-centre.ec.europa.eu/living-labs-jrc_en

Relevant Initiatives 5. The EU approach to CCAM under Horizon Europe

by A. De Candido (European Commission Directorate General for Research and Innovation, EU)

Under Horizon Europe the European Commission has reaffirmed the strategic role of public-private Partnerships in enabling, when possible, through research the achievement of the priority policy objectives. Partnerships enable to jointly develop among all relevant stakeholders a common vision and roadmap on how to move towards the intended goal. Such structured collaboration also allows for the different projects funded under the umbrella of the partnerships to be better integrated into a wider picture favoring sharing of research outcomes and smoother transition between a project and possible follow-up activities. During this session, the European Commission illustrated how, more specifically, the Connected, Cooperative and Automated Mobility Partnership, is allowing to accelerate the transition towards automated mobility that will enable a greener, smarter, less congested and safer road transportation ecosystem. In this respect the timely alignment between research and the necessary framework regulations that will allow for an efficient deployment of automated mobility systems is paramount to reach the objective. International collaboration was also stressed as a must in this domain since the market for the industrial players developing the future automated vehicles is necessarily a global one.

Relevant Initiatives 6. Overview of the on-going European research projects on traffic & network management, transport data and modelling

by T. Tavares (European Climate, Infrastructure and Environment Executive Agency, EU)

Sustainable and competitive mobility and transport services are vital to accommodate the needs of citizens and businesses in and around urban and peri-urban areas. Challenges remain on how to efficiently manage the multimodal traffic and the network taking into account the user needs, existing transport infrastructure and new transport solutions, such as shared services, connected and automated vehicles, and urban air mobility. During this session, CINEA presented how 11 EU-funded projects are tackling these challenges with focus on developing the next generation of network and traffic management for door-to-door transport of passengers and goods. In particular, the session presented the innovative data-driven solutions that are being developed by the these projects to create a multimodal traffic and network management approaches that are dynamic, effective and resilient. More information about these and other EU-funded transport projects can be found on the European Climate, Infrastructure and Environment Executive Agency (CINEA)'s website[7].

Relevant Initiatives 7. The SHOW Horizon 2020 project

by A. Bekiaris, Centre for Research and Technology Hellas (EL)

SHOW seeks to deploy shared, connected, and electrified AV fleets in real-life urban settings across Europe. These coordinated chains include Public Transport (PT), Demand Responsive Transport (DRT), Mobility as a Service (MaaS), and Logistics as a Service (LaaS). SHOW's impact extends to regulations and innovative business models for a sustainable future. Real-life urban demonstrations occur in 20 European cities with each pilot site hosting operational AV services for at least 12 months. SHOW deploys over 70 SAE L4/L5 AVs for passenger and cargo transport, navigating dedicated lanes and mixed traffic, connected to a comprehensive infrastructure network. Already, SHOW has transformed numerous cities where AVs are seamlessly integrated into public transport systems and widely used by the local population, showcasing its practical and impactful approach. Beyond its core mission, SHOW is fostering international collaborations with countries like Japan, the US, and Australia, uniting experts to shape the future of mobility. SHOW's work is driving a transformation toward automation, electrification, cooperativeness, and inclusiveness in urban mobility, setting the stage for a sustainable and innovative transportation future. More information about SHOW can be found on the project website[8].

[7] https://cinea.ec.europa.eu/index_en
[8] https://show-project.eu/

Relevant Initiatives 8. The European type-approval framework for Automated Driving Systems

by M. C. Galassi (European Commission Directorate General for Internal Market, Industry, Entrepreneurship and SMEs, EU)

The presentation outlined the progressive regulatory approach adopted by the European Commission for driving automation. It gave a glimpse into how the new Vehicle General Safety Regulation EU 2019/2144, adopted in July 2022, will be progressively introduced between July 2024 and July 2029. In particular, the new EU-type approval framework for levels 3 and 4 of connected and automated vehicles was discussed with :

- UN Regulation 157, covering the type approval of automated lane-keeping systems (ALKS) for motorway applications;
- Regulation EU 2022/1426 on the type-approval of motor vehicles equipped with Automated Driving System (ADS), covering level 4 driverless vehicles.

In both cases the focus was on requirements and validation methods included in the two legislative acts as well as on all the necessary information and documentation that the manufacturers will need to submit to the type approval authorities, and on the planned in-service reporting. This legal framework allows the introduction of automated vehicles in the EU market and on EU roads and represents the first legal framework of its kind worldwide.

Furthermore, a short overview of the Commission's work to support the development of legislation for assisted driving (level 2) at the UNECE level (Amendment of UN Regulation 79 and drafting of the new Driver Control Assistance Systems – DCAS Regulation), planned to be adopted during 2024, was provided.

Finally, the need to develop for a better legal framework for pre-deployment tests and CCAM Large-Scale Demonstrations in the EU was introduced, which in Europe represent a considerable issue in testing CCAM solutions.

Relevant Initiatives 9. Designed to be safe or designed to be compliant? Lessons learned from the European market surveillance for the safety of vehicles

by F. Minarini (European Commission Joint Research Centre, EU)

Ensuring the safety of vehicles on our roads is of paramount importance for the well-being of society. The Joint Research Centre (JRC) has emerged as a key player in the domain of vehicle safety, spearheading rigorous market surveillance and innovative research initiatives. This abstract provides an overview of JRC's substantial contributions to the field, highlighting its dedication to enhancing vehicle safety standards.

JRC's market surveillance efforts are grounded in a proactive approach to monitoring the compliance of vehicles with established safety regulations. Through tests, JRC conducts thorough assessments of vehicles, identifying

potential safety risks and non-compliance issues. This scrutiny helps safeguard consumers from hazardous vehicles and incentivises manufacturers to maintain high safety standards.

In parallel, JRC places a strong emphasis on research and development, aiming to push the boundaries of vehicle safety. The organization engages in research projects on emerging technologies in particular Advanced Driver Assistance Systems (ADAS) to address the assurance of vehicle safety. The aim is to improve the knowledge on the performance and the limits of these safety systems and to provide input to policy makers to improve existing legislation and to develop new ones to both increase the competitiveness of the Industry and enhance consumer protection. Furthermore, JRC actively collaborates with regulatory bodies and industry leaders to drive the evolution of safety standards and testing methodologies. Through knowledge sharing, standard development, and the establishment of best practices, JRC contributes to the harmonization of safety requirements worldwide.

In the work on market surveillance JRC performed 74 regulatory tests on 17 vehicles and 7 components. The tests resulted in 13 compliances and 11 non compliances. In 2022 alone, the non-compliance rate raised to almost 60% with 7 out of 12 tested vehicles and components. The open question is now to understand the causes of such a high rate of non-conformities as the market surveillance tests are just a repetition of the type approval (homologation) tests.

On the Research side, five use cases are presented. The work revealed how vehicles have very different behaviors in real driving for both the test environment and the conditions of use. Technology allowing compliance in real and various environments exists but some cars look like changing strategy. The concept of safety culture of the manufacturers is also central.

In conclusion, JRC's multifaceted approach to vehicle safety, encompassing comprehensive market surveillance and pioneering research, underscores its commitment to advancing the safety of vehicles on our roads. By promoting compliance, fostering innovation, and collaborating with stakeholders, JRC plays a pivotal role in ensuring that vehicles meet the highest safety standards, thereby enhancing road safety and protecting lives.

Conference Papers

Category 1. Advanced data collection and processing

Data Collection and Processing of Multimodal Trajectories Collected by Aerial Drones

A. Kutscha[a], M. Margreiter[a], K. Bogenberger[a]

[a] *Chair of Traffic Engineering and Control, Technical University of Munich, Germany*

Introduction

Traffic data nowadays becomes more and more important to understand the behaviour and the strategic, tactical, and operative manoeuvres of traffic participants and to increase with this knowledge traffic safety and traffic efficiency. The need for data is therefore interesting in the field of general traffic behaviour but also of individual traffic manoeuvres like turning, overtaking etc. It gets especially important when looking at the traffic behaviour of vulnerable road users (VRU) like cyclists and pedestrians, as proper data sets about those traffic participants are quite rare and therefore also knowledge about their behaviour in the traffic system is quite limited. For motorized traffic most large-scale datasets also stem from observations on freeways, where the sensor density and the need for traffic detection is also higher and therefore data generation is easier. For urban traffic systems with a much higher variety of different traffic participants and also a more complex road network structure it is rather difficult to use (existing) infrastructure-based sensors like on freeways (Motamedidehkordi 2017) to have a full data coverage of all traffic participants and their interactions. This present work goes one step further and elaborates the use of large-scale drone video footage in combination with innovative recognition algorithms to provide a temporal and spatial full overview of the complete set of all traffic participants. This enables further research to study in particular the interactions between different traffic participants especially motorized road users and VRUs with a focus on traffic safety and to better understand the multimodal traffic patterns. Such data contributes significantly to improve traffic safety and optimize the road network operations (Krajewski 2018, Bock 2019). Another benefit is the availability of such a data set to train further video recognition algorithms and neural networks (Barmpounakis 2020).

The data set was gathered within the Munich TEMPUS project (Kutsch 2022), a project to prepare the Munich urban and suburban road network for connected and automated driving.

Experimental Design

The drone surveys were conducted along Rheinstrasse in Munich, Germany, between Bonner Platz and Leopoldstrasse. Six locations were covered by two drones each, as shown in Figure 1. The drones had a flying altitude of 110 meter when taking the videos, resulting in a recording area of 143 meter on 75 meter for each drone location. With the need for an overlap in between the individual locations for reconstructing the whole trajectories throughout the whole stretch, a total length of 700 meter was recorded. The street is highly frequented and can be classified as a main street. The perimeter includes two signalized intersections, one right-of-way-controlled intersection, two non-signalized T-junctions and two signalized pedestrian crossings. Bicycle traffic in this area is mostly guided on a protective lane. For the general traffic and pedestrians in particular, there are several points of interest within the recording area and the immediate surroundings. In addition to a school and a kindergarten, several doctors and pharmacies, as well as numerous shopping facilities, both for groceries and drugstores, and recreational activities are also available. Several restaurants, a sports club and three hotels are located in the area. There are also several access points to public transport, namely a tram and several bus stops on Leopoldstrasse, as well as a Subway access point on Bonner Platz.

Figure 3. The six observation locations in the North of Munich

Source: Authors' elaborations based on Google Earth.

Until today, drones have a maximum flight time of around 30 minutes due the limited battery capacity. Various systems, such as balloons and tethered drones with power supply, have been assessed but do not provide the necessary image stability or are not suitable due to the high costs and the approval process, which is difficult to implement in the city centre. Therefore, in order to create a continuous data set, two drones were used for each location, and a 'shake-hands' was performed in the air so that the drone to be replaced only descended when the following drone was in the air and had fixed the image section. Accordingly, a total of twelve drones were in use. They recorded a total of analysed videos amounting to almost 42 hours from their respective single locations. The recordings were performed on Thursday, October 6 and Wednesday, October 12, 2022. The days in the middle of the week were determined according to surrounding detector data in order to capture the most frequented days in the week. On both days, flights were performed in the afternoon in order to be able to depict the leisure traffic as well as the commuter traffic and therefore the peak-hour. On the first day, the last drone was in the air at 15:35, so that a complete image of the entire stretch could be generated. The recordings were carried out until 18:45. On the second day, the first shots were started even earlier to counteract the earlier sunset. Thus, from 15:00 on all drones were in the air, the end of recording was then accordingly at 18:25.

Due to their altitude and mostly unobstructed viewing angle towards the observed road and sidewalk segments, the drones were able to record all traffic participants in the area. The eleven different classified modes include passenger cars, busses, trucks, trams, motorcycles, (e-)bicycles, pedestrians and (e-)kick-scooters. In addition to that, truck trailers as well as bus trailers (in the city of Munich several high-capacity bus routes operate buses with bus trailers) were also recognized and categorized. In addition to those traffic participants the dataset also contains trajectories of an electrified bicycle Rickshaw from the TEMPUS project (Fehn 2023, Margreiter 2023), (E-)Cargo-Bikes and persons with a wheelchair.

Raw Dataset Description

The raw data consists of one data file per evaluated frame in each individual video, i.e., for each location and drone flight. The evaluation frequency was set to 12.5 frames per second, giving then updated information every 0.08 seconds. Within these files, all detected objects within the respective frame are stored with their attributes listed in Table 1. The object category is stored as a numeric value for each category mentioned in the preceding chapter. Category ID 1 as shown in the example would match to the classification as a car. The track ID is a unique number for an object within each video, making it possible to follow objects throughout the frames. The translation describes the location of the respective object, where the values describe the offset with respect to a reference point, which is given in the UTM 32 N (NIMA 1989) coordinate system and is uniform for the entire data set. The value refers to the centre of the bounding box and the bottom of the object, i.e., on the ground. Besides that, the object dimensions are given as length, width and height. The current velocity and acceleration are given as a vector in the respective coordinate system, as well as the rotation describes the current orientation in that system.

Table 1. Extracted data from drone video footage

Parameter	Descrip[tion	Example value	Unit
category	numeric classification ID	1	[-]
track_id	numeric unique ID	38	[-]
translation	[x, y, z]	[123.0319, 14.0211, 508.6254]	[m]
dimension	[length, width, height]	[4.2998, 1.9754, 1.4882]	[m]
rotation	[x, y, z]	[-0.0011, 0.0016, 0.1227]	[-]
velocity	[x, y, z]	[10.252, 1.2638, -0.0169]	[m/s]
accelaration	[x, y, z]	[0.0577, 0.0071, -0.0001]	[m/s^2]

In addition to the raw dataset, frame matching is performed for each uninterrupted video time series per location. This means that for the videos recorded by two drones in sequence, it is known which frame of the ending video corresponds exactly to the frame of the starting video. Thus, the track IDs for the uninterrupted timelines are available and unique. Due to technical problems, which occasionally led to short interruptions with individual drones, two recording days and six locations, a total of 20 timelines were created. A matching between the locations, as well as further filter applications were not yet carried out and will be described in the next section.

Processing Steps

The raw dataset is cleaned and pre-processed before publication. First, the static objects are tagged. Those static objects which are geospatially outside the street space are sorted out, as they are due to misclassifications. In some places where errors are known to occur, for example at the subway stairways, manual post-processing is done. Static objects that appear temporary but do not move are also filtered out.

The resulting dataset is then merged across the various locations. As described above, the raw data set contains a unique ID for each video per location. To track individual trajectories across multiple locations, the respective track ID must be matched between the locations. Due to the maximum localization error of 15 cm, isolated classification errors, as well as deviations in the speeds, the linking of the trajectories is not quite trivial, especially for pedestrians and cyclists. The linking logic is implemented according to the following description, in order to guarantee a scalable approach.

To ensure the correct time for each location and since the default-times vary slightly between the drones, the dataset is matched on a frame level between the different timelines, choosing one location as a reference timeline, in this case location 2. For each first timestamp, all IDs in the overlapping area need to be determined. Based on their coordinates and thus the Euclidean Distance, their speed vector similarity and the object type, a cross comparison between each object in the respective two overlapping frames is performed and a score for being the same object is calculated. Objects with the respective highest scores are then marked with a global unique ID. Starting from this step, it is now necessary to check for each new frame whether new objects appear in the overlapping section. If this is not the case, the process continues with the next frame. If exactly one object moves into the scope, the IDs can be matched directly. If there are several new IDs in the area under consideration, the scores are determined in each case as before and an allocation is made accordingly. This procedure needs to be repeated for each location change, as well as for each observation gap, which have occurred on a single drone level.

Results and Conclusions

The highly detailed dataset allows applications in traffic flow theory to be developed, validated, and calibrated. For example, the immense ground truth data set can be used to develop car following models, turning behaviour models, link-level traffic flow models, or queue length estimators. In addition, the multimodal trajectories, which include non-motorized road users with a high level of detail, also depict interactions between VRUs and motorized vehicles, both on the open, non-disturbed link, as well as at signalized and non-signalized intersections. Consequently, especially in the presence of different levels of vehicles' connectivity and automation, important conclusions can be derived regarding the impact on traffic flow in urban environments.

Also, regarding traffic safety aspects, having each traffic participant together with the information on the underlying road network, different situations have been captured. Having several different types of intersections, as well as different types of bicycle paths and other infrastructure elements, the dataset is ideally suited for safety analysis.

To enable a wide and global access for scientists and practitioners the drone data set will be published open source. The open data set will include – in addition to the video raw material – all extracted trajectories for all traffic participants continuously in time and space through the whole area covered by all twelve drones at the six locations. It is planned to publish under the Creative Commons CC BY-NC 4.0 license to guarantee easy access and usability for further research.

In beginning of summer 2023 a similar dataset will be gathered in the city of Ingolstadt, Germany, via the KIVI project (Ilic 2022a. Ilic 2022b) funded by the German Federal Ministry of Digital and Transport. Likewise, this data set will be made available open source.

Acknowledgements

This research was funded and supported via the TEMPUS project through the German Federal Ministry for Digital and Transport under the research grant 01MM200008K. The drone data was gathered with the help of Fairfleet and DeepScenario.

References

Barmpounakis, E. and Geroliminis, N., 'On the new era of urban traffic monitoring with massive drone data: The pNEUMA large-scale field experiment.' Transportation Research Part C: Emerging Technologies, 111, 50-71, 2020, doi:https://doi.org/10.1016/j.trc.2019.11.023.

Bock, J., Krajewski, R., Moers, T., Runde, S., Vater, L. and Eckstein, L., 'The inD Dataset: A Drone Dataset of Naturalistic Road User Trajectories at German Intersections', 2019, from https://arxiv.org/abs/1911.07602.

Fehn, F., Engelhardt, R., Margreiter, M. and Bogenberger, K., 'Ride-Parcel-Pooling: Integrating On-Demand Passenger Transportation and City Logistics', PIARC World Road Congress, Prague, Czech Republic, 2023.

Ilic, M., Sautter, N., Margreiter, M., Loder, A. and Bogenberger, K., 'Changing Strategic Alignments in European Urban Traffic Control - Requirements for Future Developments', 10th Symposium of the European Association for Research in Transportation (hEART), Leuven, Belgium, 2022.

Ilic, M., Sautter, N., Margreiter, M., Loder, A. and Bogenberger, K., 'Revisiting Urban Traffic Control in Austria, Germany and Switzerland - Requirements for Future Developments', Transportation Research Board - 101st Annual Meeting Washington, D.C., USA, 2022.

Krajewski, R., Bock, J., Kloeker, L. and Eckstein, L., 'The highD Dataset: A Drone Dataset of Naturalistic Vehicle Trajectories on German Highways for Validation of Highly Automated Driving Systems', 21st International Conference on Intelligent Transportation Systems (ITSC), 2018, doi:10.1109/ITSC.2018.8569552.

Kutsch, A., Margreiter, M., Stüger, P., Fehn, F., Metzger, B., Hamm, L., Engelhardt, R., Ilic, M. and Bogenberger, K., 'TEMPUS - Test Field Munich - Pilot Test for Urban Automated Road Traffic', IEEE 25th International Conference on Intelligent Transportation Systems (ITSC), 2022 doi:10.1109/ITSC55140.2022.9922303.

Margreiter, M., Ilic, M., Joshi, A. and Bogenberger, K., 'A Self-Driving Cycle-Rickshaw for Autonomous Urban Passenger and Freight Transport', PIARC World Road Congress, Prague, Czech Republic, 2023.

NIMA - US National Imagery and Mapping Agency, 'The Universal Grids: Universal Transverse Mercator (UTM) and Universal Polar Stereographic (UPS)' , Edition 1, TM 8358.2 Washington, D.C., 1989.

Motamedidehkordi, N., Margreiter, M., Hoffmann, S. and Busch, F. 'Implications of Automated Vehicles on Freeway Safety and Operations', ITS World Congress Montreal, Canada, 2017.

Use of Origin-Destination data in synthetic travel demand synthesis

B. Mateta[b], E. Côme[a], A. Furno[b], S. Hörla[c], L. Oukhellou[a]

[a] *Université Gustave Eiffel, COSYS, GRETTIA*

[b] *Université Gustave Eiffel, COSYS, LICIT-ECO7*

[b] *IRT SystemX*

Introduction

One way of acquiring an insight into the transportation system of a city is to simulate an adequately generated synthetic population of agents. The generation in itself is a challenging problem, as the population should match the known marginal distributions of the real population while staying as close as possible to the joint distribution of variables observed from an input population sample. Each agent must then be assigned an agenda, stating a chain of activities (e.g. home, work, shopping, other), with their corresponding times and transport modes, along with a chain of locations for each of the activities. The agendas should be plausible at the individual level and ultimately match flows observed from other data sources. When little data is available, each step of the process may be handled by modelling a distribution and sampling from it: socio-economic modalities (Sun and Erath 2015, Sun et al. 2018), activity chains (Joubert et al. 2020, Anda et al. 2020), and activity locations (Ma and Klein 2018, Horl and Axhausen 2021).

We base our research on a state-of-the-art pipeline (Horl and Balac 2021) to create a synthetic population with socio-economic variables and activity chains from three data sources. The socio-economic variables are taken from the census performed by the French statistics institute INSEE, containing micro-data representative of the whole population. The activity chains are taken from the Enquête Ménage Déplacements of the year 2015 (EMD, Cerema 2015) performed by the French agency for urban planning CEREMA, which details the complete agendas of 25 203 persons in the region of Lyon and is available on request.

For the location of activities, we propose a novel data-driven approach, leveraging Origin-Destination (OD)-matrices derived from mobile data from the telecommunications provider Orange, dating from 2019. Mobile data are cheaper and faster to produce than surveys, which make them a good source to update data from older surveys. Works such as (Zilske and Nagel 2015, Yin et al. 2017) propose approaches relying on full trajectories for the generation of population. In contrast with whole trajectory datasets, OD-matrices are lighter and more manageable, and can be fully anonymized (Matet et al. 2021). This makes them more readily available and safer regarding the privacy of transportation users.

Methodology

The first steps of the synthetic travel demand generation are inspired from (Horl and Balac 2021), which focused on Île-de-France and Paris, now with the target area being Lyon and its surroundings:

Table 1. Attributes used in the statistical matching to assign activity chains from EMD to agents from census

Variable	Number of modalities	% of agents with more than 20 matches
Age	4	100%
Gender	2	100%
Occupation	9	95%
Has car (Y/N)	2	94%
Home_status (Owner / Tenant / Social housing)	3	90%
Canton	8	75%

Source: Authors' elaborations and EMD 2015.

Socio-economic variables: The French census contains microdata extensive enough so that no generation is required. In order to have an integer number of agents, we discretize the existing scaling coefficients via TRS (Truncate, Replicate, Sample) (Lovelace and Ballas 2013), i.e., we round the per-person coefficients up with probability equal to its decimal part, and we round it down otherwise.

Activity chains: We assign activity chains from the EMD to persons from the census via a process inspired from statistical matching (Orazio et al. 2006). As in (Horl and Balac 2021), this process is close to a regular join between relational databases, except that each census row is required to match at least 20 EMD rows in order to guarantee sufficient diversity of the associated chains. For census rows for which this is not the case, we successively remove the last variable from the join key. Then, one of the matched EMD rows is randomly drawn, and its activity chain is assigned to the person. This process aims at guaranteeing diversity in the assignment of chains to population agents, as well as joining as many variables as possible. The variables used in the join key are described in Table 1.

While the previous steps correspond to existing approaches for travel demand synthesis (Horl and Balac 2021), we propose the following steps that make direct use of a large-scale Origin-Destination matrix with hourly information that is featured in this research:

- Rescaling: The resulting population is composed of agents equipped with an agenda specifying when they finish their activities and need to go to a new one. Due to data discrepancies, the number of trips performed in each hour of the day by our matched agent population does not match the number of trips observed from mobile data. This is illustrated in (Fig. 1, left), where each point represents the marginal value of a socio-economic modality (in green) or the total number of trips taken for a given hour (in red). The x-coordinate of the point is the truth value from the available data, while the y-coordinate is the total measured in our synthetic population. We perform rescaling via Iterative Proportional Updating (IPU) (Ye 2009), using persons for the upper-level matching and trips on the lower level. The resulting population is consistent both with the socio-economic composition of the real population and the number of trips they take at each timestep of the day.
- Spatialisation: To be complete, the synthetic population requires locations for each activity in their agenda. We interpret the OD-matrices as probability tables of destinations D given the origin O and time T: P(D | O,T). For each agent, we draw a destination from these probability tables each time their activity chain sends them to another activity. We consider each agent to have at most one home, one workplace and one study place. Thus, when the activity specifies that the agent must go home, the home is directly assigned as a destination. The same is true if the agent is going to work or study for the second time in the generation process. For the first time they go to work or study, we draw from the destination probabilities and store the result as the de facto workplace or study place. As a refinement, we take into account the transport modes M of the trips in the activity chains to obtain a probability destination P(D | O,T,M). The transport mode is not specified in the mobile OD data, but can be integrated into the sampling process using Bayes rule: $P(D \mid O,T,M) \propto P(M \mid O,D,T) \times P(D \mid O,T)$. As an estimation of P(M | O,D,T), we consider that the mode M depends only on the distance L between origin O and destination D. Using all trips from the EMD, we obtain an empirical probability distribution P(M | L(O,D)) discretized to individual bins of 1km.

Results

The resulting synthetic population is expected to behave like the real population, so we evaluate it on all the available indicators about the composition or mobility of the real population. Note that as the input data sources disagree over those indicators from the start, simply matching indicators from various input sources is already a satisfying result.

- Socio-economic composition of the population: (Fig. 1) illustrates how our population matches the official census better than the transport survey EMD. As the EMD represents only a small number of people, it is normal that the totals have a high variance.

Figure 4. Left : Marginals of the synthetic population versus what is expected from the data sources. Right : Matching of the socio-economic marginals of our rescaled synthetic population (in magenta) compared to the transport survey EMD (in light green).

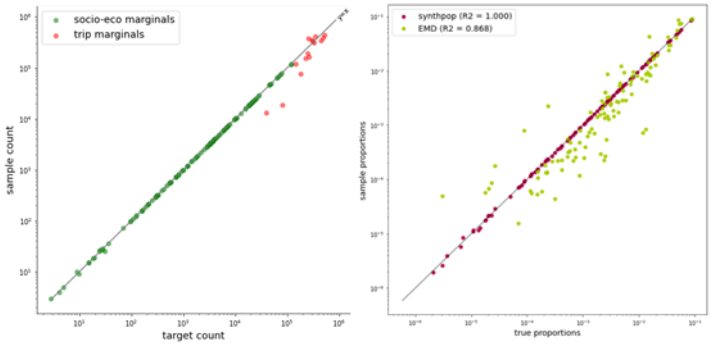

Source: Own elaborations.

— Number of trips by hour: (Fig. 2) illustrates the distribution of trips during a typical day in the OD-matrix from 2019 taken as a ground truth (in orange), our synthetic data (in magenta), and the survey EMD from 2015 (in green). We see that in this case our population is also able to fit the ground truth source better than the official survey.

Figure 2. Distribution of trips taken during the day.

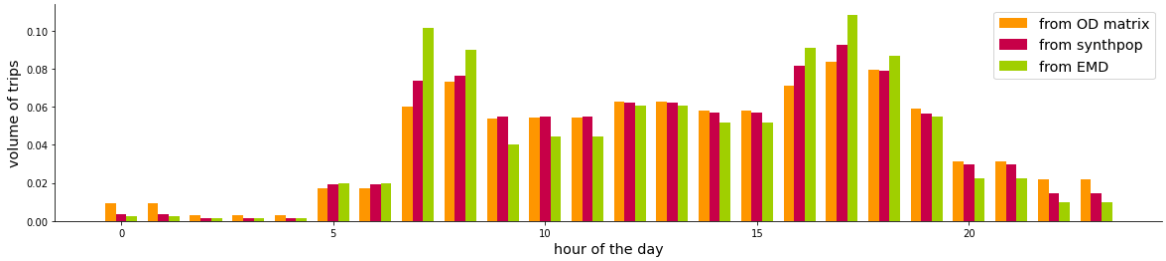

Source: Authors' elaborations.

— P(D|OT): (Fig. 3) illustrates how our distribution of destinations fits the P(D | O,T) derived from the OD matrix. We see that our synthetic demand is highly correlated to the actual observations.

Figure 3. $P(D \mid O,T)$, from our synthetic data w.r.t. ground truth value from the OD-matrix. The black line represents y=x.

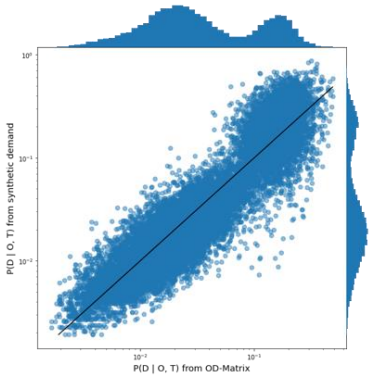

Source: Authors' elaborations.

Conclusion and future works

In this paper, we illustrate how OD matrices from mobile data can be used to improve the generation process for synthetic travel demand data. We show that they can mitigate uncertainties or outdated information in

travel surveys regarding flows by time of day and in between zones, while still making use of the included activity chain structures. As OD-matrices can be anonymized, our approach is also relevant to leverage the richness of mobile data without the computational cost nor the privacy hazard that come with full trajectory data. The results may be further enhanced by the integration of socio-economic dependencies in the location drawing, as it is known for example that the socio-professional categories have an impact on the commute distance.

Acknowledgments

This research is supported by the French ANR research projects MOBITIC (grant number ANR-19-CE22-0010) and PROMENADE (grant number ANR-18-CE22-0008).

References

Anda, C., Ordonez Medina, S. A., Axhausen, K., Synthesising digital twin travellers: Individuals travel demand from aggregated mobile phone data, 2020.

Fournier, N., Christofa, E., Akkinepally, A., Lima Azevedo, C., Integrated population synthesis and workplace assignment using an efficient optimization-based person-household matching method, Transportation 48, 2021.

Hörl, S., Axhausen, K., Relaxation-discretization algorithm for spatially constrained secondary location assignment, Transportationmetrica A: Transport Science, 2021

Hörl, S., Balac, M., Synthetic population and travel demand for Paris and Île-de-France based on open and publicly available data, Transportation Research Part C: Emerging Technologies 130, 2021

Joubert, J., de Waal, A., Activiy-based travel demand generation using Bayesian networks, Transportation Research Part C: Emerging Technologies 120, 2020

Ma, T.-y., Klein, S., Bayesian networks for constrained location choice modeling using structural restrictions and model averaging, European Journal of Transport and Infrastructures Research 18, 2017

Matet, B., Côme, E., Furno, A., Bonnetain, L., Oukhellou, L., El Faouzi, N.-E., A lightweight approach for origin-destination matrix anonymization, 2021, pp. 487-492.

D'Orazio, M., Zio, M., Scanu, M., Statistical Matching: Theory and Practice, 2006

Sun, L., Erath, A., A Bayesian network approach for population synthesis, Transportation Research Part C: Emerging technologies 61, 2015, pp. 49-62.

Sun, L., Erath, A., Cai, M., 'A hierarchical mixture modelling framework for population synthesis', Transportation Research Part B: Methodological 114, 2018, pp. 199-212.

Ye, X., Konduri, K., Pendyala, R., Sana, B., Waddel, P., Methodology to match distributions of both household and person attributes in generation of synthetic populations, Transportation Research Board, 2009

Yin, M., Sheehan, M., Feygin, S., Paiement, J.-F., Pozdnoukhov, A., A generative model of urban activities from cellular data, IEEE Transactions on Intelligent Transportation Systems PP, 2017.

Zilske, M., Nagel, K., A simulation-based approach for constructing all-day travel chains from mobile phone data, Procedia Computer Science 52, 2015, pp. 468-475.

Cerema, lil-1023: Enquête Ménage Déplacement, Lyon / Aire métropolitaine lyonnaise, 2015.

Robust OD matrix estimation method under low sampling rate, by utilizing multiscale information of questionnaire data

Y. Mochizuki[a] , A. J. Pel[b], C. van Hinsbergen[c], J. Urata[a]

[a] *Department of Civil Engineering, University of Tokyo, Tokyo, Japan*

[b] *Faculty of Civil Engineering and Geosciences, Delft University of Technology, the Netherland*

[c] *Fileradar B.V., the Netherland*

Introduction

Estimating Origin-Destination (OD) matrix is a fundamental yet important problem in the transportation research field, since most transportation models or simulators require an OD matrix as an input. That is why the estimation of OD matrix has been developed with many approaches exploiting various types of data source. For the OD matrix estimation, methods using traffic counts such as Van Zuylen \& Willumsen (1980) [1] or Maher (1983) [2] have been well-known and widely used since they were proposed. However, traffic counts are not collected in many cases and impose a huge investment cost. Therefore, a method of the OD matrix estimation from travel questionnaire data, which is collected much quicker, easier and cheaper is required in many cities for transportation measures. Tough travel questionnaire data has problems in the OD matrix estimation mainly originated from low sampling rate, such as sparsity of collected OD pairs and bias in the collected number of travels. The purpose of this study is to ease the effect of these problems and produce a robust OD matrix estimates from questionnaire data even with low sampling rates. Our proposed method takes both aggregate variables and the number of trips between each OD pair as fitting target and estimate OD matrix robustly.

We incorporate both IPF and Gravity Model in our proposed method, making the output OD matrix fit to both on aggregate level and on each OD pair level. In general cases, data on aggregate level is more reliable than that on each OD pair level, while the latter one has detailed information necessary to estimate a fine-grained OD matrix. By utilizing data of both resolution levels, the method can estimate the robust OD matrix with any sampling rate of questionnaire. Nejad et al. (2021) [3] developed a method for population synthesis which considers data of different reliability using copulas functions and random sampling. We build a method of the same concept for the OD matrix estimation, applying IPF and Gravity Model. These two methods work as an OD estimation, but both have problems related to sampling rate when they are run alone. IPF suffers from a zero-cell problem (Müller \& Axhausen, 2010) [4], meaning having no sample in OD pairs which actually have unsampled trips, which ruins the accuracy of OD matrix on the individual OD pair level especially when zoning is fine-grained. On the other hand, the constrained versions of Gravity Model (Ortúzar \& Willumsen, 1990) [5] is only fit to aggregated trips, not individual OD pairs, ignoring the detailed information about the number of observed trips in each OD pair even when questionnaire data is informative.

Methodology

In this section, a new method for the OD matrix estimation is proposed. Firstly, we introduce data used for the estimation, and then the algorithm is explained.

Our method uses two kinds of trip data in the estimation. One is a sampled trip data collected through questionnaire. We denote the scaled number of trips from zone i to j as T'_{ij}, which is obtained by simply dividing the sampled trip count by the sampling rate. T'_{ij} is not a good estimate of the real OD matrix, as the questionnaire includes bias coming from sampling. The other is the number of trips on aggregated level. In this paper, we adopted three types of aggregated values in the experiment, so algorithm is shown using those values. However, aggregated values used in this method can be any subset of OD pairs, which makes the method flexible. Three types of aggregated values used in this paper are the total number of trips originate in zone i as T'_i the number of trips absorbed in zone j as T'_j and the aggregated number of trips which originate in zone i and absorbed in zone j such that $i \in I, j \in J$ as T'_{IJ}. One possible way to obtain the aggregated information is referring to an outer source such as national census data. In case data other than questionnaire is not available, aggregating the collected trips in questionnaire and dividing the aggregated value by sampling rate can provide estimates of aggregated trips. The aggregated values are basically more reliable and robust to bias than T'_{ij}, as each choice has more samples through aggregation.

Algorithm Gravity Model with Iterative Proportional Fit to Marginal Target

Input: Trips in each OD pair T'_{ij}, Trips on marginal levels T'_i, T'_J, T'_{IJ},

Features of each zone, each pair of zones P_i, P_j, C_{ij}

Step 1: Setting and First Estimation

1.1 set all Balancing Factors $a = 1$

1.2 estimate Gravity Model Parameters β

$\widehat{\boldsymbol{\beta}} = argmin\ Loss\big(G\big(\boldsymbol{\beta}, O_i, D_j, C_{ij}, a = 1\big), T'_{ij}\big)$

1.3 calculate OD matrix from Model Equation

$\widehat{T_{ij}} = G\big(\beta, P_i, P_j, C_{ij}, a = 1\big)$

Step 2: Iterative fitting Process to data with different reliability

while (till the criterion is met) **do**

2.1 update Balancing Factors

$$a_i = a_i * \{T'_i / \sum_j \widehat{T_{ij}}\}^{\frac{1}{\beta_2}}, a_j = a_j * \{T'_j / \sum_i \widehat{T_{ij}}\}^{\frac{1}{\beta_3}}, a_{IJ} = a_{IJ} * \{T'_{IJ} / \sum_{i\in I, j\in J} \widehat{T_{ij}}\}^{\frac{1}{\beta_4}}$$

2.2 update Gravity Model Parameters β

$\widehat{\boldsymbol{\beta}} = \boldsymbol{argmin\ Loss}\big(\boldsymbol{G}\big(\boldsymbol{\beta}, \boldsymbol{P_i}, \boldsymbol{P_j}, \boldsymbol{C_{ij}}, \boldsymbol{a}\big), \boldsymbol{T'_{ij}}\big)$

2.3 update OD matrix from Model Equation

$\widehat{T_{ij}} = G\big(\beta, P_i, P_j, C_{ij}, a\big)$

end while

Output: OD matrix $\widehat{T_{ij}}$ calculated by Gravity Model Equation with Parameters $\widehat{\boldsymbol{\beta}}$ and Balancing Factor a

$$\widehat{T_{ij}} = G\big(\beta, P_i, P_j, C_{ij}, a\big)$$
$$= \exp(\beta_1) \cdot (a_i P_i)^{\beta_2} \cdot \big(a_j P_j\big)^{\beta_3} \cdot \big(a_{IJ} C_{ij}\big)^{\beta_4}, for\ i, j \in I, J \quad (1)$$

In our method, the estimated number of trips $\widehat{T_{ij}}$ from zone i to j is calculated by the function $G(\cdot)$ in shape of gravity model, which is shown in equation (1). P_i is the population in zone i and C_{ij} is a cost feature between zone i and j, both features are commonly used in gravity model (Ortuzar & Willumsen, 1990 [5]). β is the vector of parameters in gravity model and a is a set of balancing factors. We need to calibrate $\boldsymbol{\beta}$ and a to obtain a good, estimated value $\widehat{T_{ij}}$. The whole calibration process is shown in algorithm1. We iteratively update parameters $\boldsymbol{\beta}$ and a. While we use the aggregated number of trips data T'_i, T'_j, and T'_{IJ} in calibration of balancing factors a, we calibrate gravity model parameters $\boldsymbol{\beta}$ using the sampled trip information T'_{ij}. For the loss function $Loss(\cdot, \cdot)$, we used RMSE.

The output OD matrix has two preferred features for the OD matrix estimation from questionnaire data. The first one is fitting in multiple zonal resolutions. The output OD matrix is almost perfectly fit to the aggregated trip number data T'_i, T'_j, and T'_{IJ}, but not to the sampled trip data T'_{ij}. This is because we use the same number of parameters for fitting the aggregated trip number, while we just introduced 4 parameters for fitting the sampled trip number. By this difference in fitting, the method can produce the OD matrix which follows more reliable aggregate source as well as utilizing the information of sampled data in a gravity model. The second one is filling the sparsity of the sampled data. Unlike any IPF method, referenced values used in calibrating Balancing Factor are values produced with Gravity Model, so we have few zero-cells in the estimated OD matrix even when sampling rate is small, and the sampled OD matrix is sparse.

Numerical Experiment

In order to validate our method, we evaluated its estimation performance on the real inter-zonal OD matrix in Switzerland 2010 (National Passenger Traffic Model2010). The OD data split the whole area of Switzerland into 2944 small zones and includes daily passenger traffic among them. Total daily trips are more than 2 million including intra-zonal trips, so the OD matrix is sparse considering there are $(2944^2 - 2944)$ pairs of OD zones. We set the OD matrix as our ground truth data and created sampled data which we used for the estimation from it. We randomly sampled trips from the ground truth OD with several sampling rates and set them as a questionnaire data T'_{ij}. In addition, we made the aggregated data T'_i, T'_j, T'_{IJ} by aggregating either the ground truth data or the questionnaire data. Using these two datasets and features about zones (population and distance between each zone), we estimated OD matrix and calculated RMSE using all OD pairs as performance evaluation.

We estimated OD matrix with three methods. The first method is our proposed algorithm. We generated marginal data by aggregating the sampled trips in forms of T'_i, T'_j, T'_{IJ}, assuming the proposed algorithm just utilizes data from the questionnaire. The second one is a constrained Gravity Model known as Furness Model with cost bin function (Ortúzar & Willumsen, 1990 [5]]), in which we used the marginal data from the questionnaire the same as in the proposed method. The third one is IPF method commonly used to deal with bias. In IPF, we set the aggregated values of the ground truth data as target values, meaning that we assume precise information other than the questionnaire data. All the three methods include fitting procedure to the marginal data, but the usage of other data is different. While the proposed method fits the estimated values by gravity model to the marginal data, IPF fits the original sampled trip data to the marginal data. Furness method just considers aggregated level and uses questionnaire data to calculate the aggregated values and cost function for each distance range bin.

Figure1 show the estimated result from each method, under three sampling rates $0.1, 0.05, 0.01$. We plotted the number of trips in the ground truth data on x-axis and the estimated number of trips by each method on y-axis over all $(2944^2 - 2944)$ OD pairs. Sampled trips represents the number of trips between each OD pair sampled from the ground truth and multiplied by $1/sampling\ rate$. With higher sampling rate, you can get more precise sampled trip data and less OD pairs in which no trip is observed.

Graphs show that our proposed method produced the OD matrix with high evaluation score under all sampling rates. When sampling rate goes down, the number of OD pairs which have no trips observed sharply increases since we set a fine-grained zoning. As a result, IPF suffered from a zero-cell problem. On the other hand, the estimates of the proposed method and Furness method were stable even under low sampling rate. The fitting procedure to the marginal trip data T'_i, T'_j, T'_{IJ} worked and eased the sparsity in sampled questionnaire data. When we obtain comparatively large samples of questionnaire, Furness method does not improve well in estimation while our proposed method performed quite well along with IPF method. We can say that utilizing detailed OD data T'_{ij} is essential to accomplish high accuracy of the estimate with large samples.

Figure 5. Results of the OD Estimation

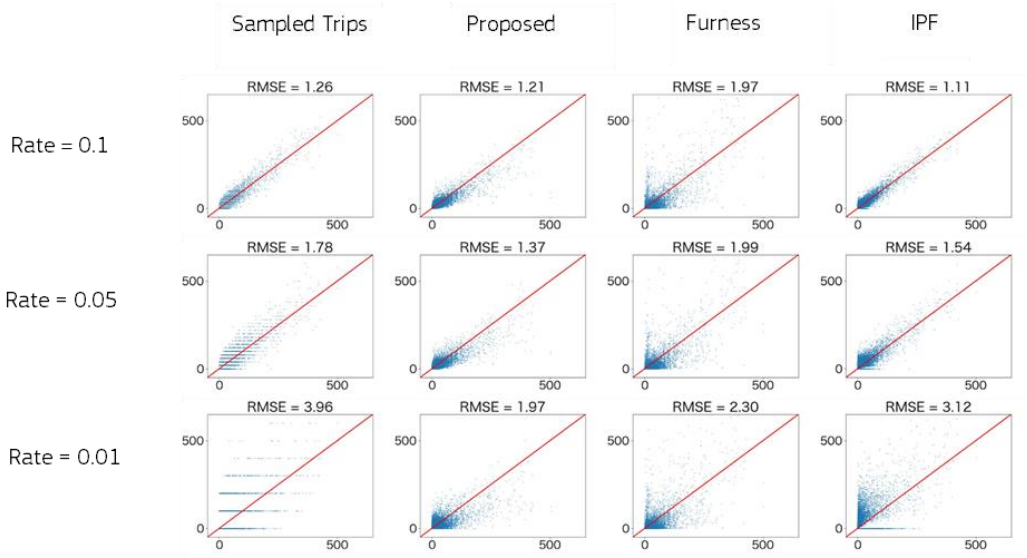

Summary

In this study, we proposed a new method for the OD estimation from questionnaire data in case the sampled data is sparse. In numerical experiments, our method produced a robust estimation of OD matrix under any sampling rate, because of the algorithm which includes the fitting on several data aggregation levels. The best method for the estimation from questionnaire has been chosen based on data sparsity, which is up to sampling rate and spatial resolution of zoning. However, the proposed method can output the sufficient estimation under any data sparsity, compared to other methods. Thus, model choice is now much easier and the OD estimation from questionnaire data involves less trial and error, as our model can perform well in different settings of sampling rate.

References

Van Zuylen, H. J. and Willumsen, L. G. (1980). The most likely trip matrix estimated from traffic counts. *Transportation Research Part B: Methodological*, 14(3):281–293.

Maher, M. (1983). Inferences on trip matrices from observations on link volumes: A bayesian statistical approach. *Transportation Research Part B: Methodological*, 17(6):435–447.

Nejad, M. M., Erdogan, S., and Cirillo, C. (2021). A statistical approach to small area synthetic population generation as a basis for carless evacuation planning. *Journal of Transport Geography*, 90:102902.

Muller, K. and Axhausen, K. W. (2010). Population synthesis for microsimulation: State of the art.¨ *Arbeitsberichte Verkehrs-und Raumplanung*, 638.

de Dios Ortúzar, J. and Willumsen, L. G. (2011).´ *Modelling transport*. John wiley & sons

Full-scale experimentation of a mixed traditional and GPS-individual travel survey in Paris Region

D.,NGUYEN-LUONG[a]

[a]*Institut Paris Region, 15 rue Falguière, 75740 Paris Cedex 15, France.*

The traditional Global Travel Survey ("Enquête Globale Transport" or EGT in french) in Paris Region is a very important tool of observation and measure of the persons' mobility. The methodology benefits of a background of more than forty years. But there is a scientific consensus to consider that the EGT is not exempt from flaws: the deficiencies concerning short trips (especially walk trips), infrequent trips and stops during trips chain which are not always declared, the deficiencies about routes, the inaccuracies about distances, the inaccuracies about durations, the complexity of the paper diary survey which makes it difficult to be managed, the increasing refusal to welcome at home pollsters and the problem of the cost.

So a consortium of 14 partners (*), led by Institut Paris Region, has conducted a full-scale GPS-person travel survey in Paris Region for the first time in Europe. The survey took place from october 2022 to march 2023. 3500 participants were followed during seven days with a specific GPS-data recorder (not a smartphone), representative of a population of 9 million people aged 15 and over. This GPS recorder is a light and passive battery-powered device. A passive monitoring is the best suited method to minimize the burden on survey participant : the traveler had nothing to do except turned it on before his first trip of the day, carried it all day, turned it off in the end of the day, and reloaded the battery three times in the week.

A simple diary was requested to be filled every evening by each participant, under the form of checkboxes. It took only 3 minutes per day to fill the diary. Then the GPS tracks were analyzed automatically by algorithms which detect the trips and their features (departure and arrival time, origin and destination points, home and work or school purposes, modes). Because the algorithms were far to be perfect so far, it was necessary to complement this first automatized approach with a classical survey where each participant was called back by phone to check or complete the information. Especially, our algorithms do not recognize the trip purposes except home and work/school so this post-survey allowed to complete the information of purposes. Each call lasts in average only 15 minutes.

The method of recruitment to build a representative sample by the quota method was also innovative (many channels including social networks) and a financial incentive was proposed. The survey resulted in a database of 80 000 trips that we are still working on.

This database brings, on one hand, new information about routes (big data) but very short trips which are often omitted in the traditional survey, are not better detected by the algorithms. On the other hand, accuracy on fundamental attributes is provided such as distances and durations. The new added value is the collection of trips data on seven days and not only on one day in the traditional methodology. The total cost is about 2,5 times less.

This full-scale experimentation shows that it is interesting to introduce GPS tracking in a new methodology of person-travel survey but it is still necessary to complement it with a human traditional light survey.

Acknowledgment

We gratefully acknowledge the partners of the consortium: Région IDF, CD 77, CD 78, CD 91, CD 95, Ville de Paris, RATP, SNCF Transilien, RATP CAP IDF, KEOLIS IDF, TRANSDEV IDF, IFPEN and Vinci Autoroutes.

Application of Graph Neural Network to Traffic Information Big Data and Evaluation by Sites

R. Ogata[a], T. Miyazaki[a], Y. Kikuchi[a], Y. Murano[a], H. Sugawara[a]

[a] *Yachiyo Engineering Co., Ltd.*

Introduction

Since former President Barack Obama's efforts to promote open government in the United States, public organisations have been opening their data to the public in recent years. Traffic data is also becoming more open, and studies are being conducted to avoid traffic congestion.

In considering how to utilize traffic volume data, Miyazaki et al. (2023) focused on the publicly available traffic data of England and studied to predict traffic congestion using a decision tree model LightGBM. Long Short Term Memory (LSTM) is also often used for time series forecasting and was applied in traffic congestion forecasting (Fu et al., (2016); Zhao et al., (2017)). In addition, many methods based on Graph Neural Networks (GNN), which acquire spatial features through graph structures, have been developed in recent years and have demonstrated the highest accuracy on various benchmark datasets (Yu et al., (2018); Wu et al., (2019); Jiang et al., (2022); etc.). However, when considering decision tree models or RNN models such as LSTM, the number of target sites in many studies is limited to one or a few. In addition, the evaluation of the benchmark dataset only includes an overall evaluation of all sites, not individual sites. Ogata et al. (2023) conducted a site-by-site evaluation, but this was a comparison of only LightGBM and GNNs, and there was no study using RNN methods commonly used in time-series forecasting.

The purpose of this paper is to compare short-time speed predictions by sites using traffic data in England. We use methods including not only LightGBM and GNN but also LSTM and clarify the differences in the evaluations by model for each site.

Methodology

Data

The WebTRIS Traffic Flow API of National Highways (Highways England, 2023), which provides an overview of the traffic situation in England since 2015, allows users to download historical traffic volume data for various roads in England. In this study, time series traffic data at each observation site were downloaded from the WebTRIS Traffic Flow API, as in Miyazaki et al. (2022).

As in Ogata et al. (2023), a total of 170 sites were selected within a 30 km radius of Birmingham Town Hall. The data period was from January 1, 2016, to December 31, 2019, and used 2016 and 2017 as training data, 2018 as validation data, and 2019 as test data. Data were provided in 15-min intervals, and average speed (Avg mph) and total volume (Total Volume) were used. The average speed and total number of vehicles for 3 h (12 times) from the current situation to 2 h and 45 min ago were used as inputs, along with dummy variables (0 to 6) for the time of day (15-min time units, normalised to 0 to 1) and the day of the week. Because LightGBM and LSTM were used in training and inference for each of the 170 target sites individually, input data was also used for each site. Moreover, GNN uses the data of all sites as input data as training and inference were conducted for all sites at once. The output of each model is the average speed from 15 min to 180 min ahead for all 12 time periods.

Model

In this paper, the models were compared using machine learning methods. As in Ogata et al. (2023), the models used were LightGBM and Graph Wavenet, which is one of the GNNs that have been studied extensively in recent years. In addition to them, LSTM, which is commonly used for time series forecasting, was also used in the study.

The problem is that decision tree models such as LightGBM and RNN models, including LSTM, cannot account for spatial site-to-site dependencies. Moreover, GNNs are expected to improve accuracy by capturing the relationship between sites in a graph structure. Graph Convolutional Networks (GCN) are commonly used for GNNs in the field of traffic flow, but the Graph WaveNet used in this paper introduced the "self-adaptive adjacency matrix" method, which was able to acquire spatially independent relationships between sites and achieves high accuracy. For more information, please refer to the paper by Wu et al. (2019).

The Python library “optuna” (Akiba, 2019) was used for hyperparameter search in LightGBM, and the optimal parameters were adjusted for each site. As LSTM is computationally expensive, multiple attempts were conducted to set parameters. The number of epochs was set to 200 (it was stopped if there were no updates with an accuracy of 40 epochs) and the layers were set as the LSTM layer (32 neurons) + Dropout (0.3) layer + Dense layer. The hyperparameters of Graph WaveNet were set to default, and the number of epochs was set to 300.

Results

The Mean Average Percentage Error (MAPE) and the coefficient of determination (R2) were used for a uniform evaluation of all sites. Figure 1 (left) shows the average values of the calculated evaluation indices for all sites. The lower the value of MAPE, the better the accuracy, and the higher the value of the coefficient of determination, the better the accuracy. The results show that LSTM is more precise at making predictions 30 and 45 min in advance, whereas GNN is better at making predictions at other times. Because LSTM makes predictions based on past time series information, the accuracy of predictions made 30 and 45 min ahead of time was improved by capturing past features, however, predictions made beyond that point were judged to have benefited from features related to the time of day or other locations. As reported by Ogata et al. (2023), Graph WaveNet automatically acquires the spatio-temporal dependencies of the sites, which contributed to its high accuracy.

Next, Figure 1 (right) shows the results of calculating the percentage of sites where the GNN is superior to the LightGBM and LSTM at each prediction time. Root Mean Square Error (RMSE) was used here to evaluate each site. The GNN was superior to most prediction times throughout, and there were many sites where the GNN had a consistent advantage in comparison to LightGBM (Ogata et al., (2023)). Moreover, GNN was inferior to LSTM in predicting 30 and 45 min ahead of time. As a result, LSTM was superior in the evaluation of all sites for both 30 and 45 min predictions, as described earlier (Figure 1 (left)). Both LightGBM and LSTM were found to be more accurate than GNN in some cases and at some sites. 〖RMSE〗_i^(model1-model2) is defined in the following equation, with LightGBM and LSTM compared to GNN. Note that i is the predicted time index; e.g., i =3 represents 45 (=15x3) min ahead.

$$RMSE_i^{model1-model2} = RMSE_i^{model1} - RMSE_i^{model2}$$

The results of the three models comparison for the entire prediction time, i = 1 to 12 averages for 〖RMSE〗_i^model, confirmed that the GNN was superior at 70% of all sites. Since LSTM showed high accuracy at 30 and 45 min ahead, Figure 2 shows the 30-min-ahead prediction results 〖RMSE〗_2^(GNN-LSTM) of LSTM and GNN, which shows overall high accuracy, sorted by 〖RMSE〗_2^(GNN-LSTM) values (ascending order from left to right). The results show LSTM was superior at most sites. Partial autocorrelations were calculated using the Python library “statsmodels” (Perktold, 2023) for the sites with the largest differences, Id = 3753 (LSTM advantage) and Id = 9234 (GNN advantage), and the results are shown in Figure 3 (left and middle). The figure shows that the correlation at Id=3753 has a high value of 0.8 at lag = 1. Moreover, at Id = 9234, the lag decreases gently as the lag increases. The LSTM advantage in the 30 and 45 min ahead predictions was attributed to the high partial autocorrelation at lag = 1. A comparison of partial autocorrelation averages for LSTM-advantage and GNN-advantage sites confirmed a similar trend (Figure 3 (right)). These results indicate that the high partial autocorrelation of the LSTM at lag = 1 is the reason for its high accuracy in predicting 30 and 45 min ahead of time.

Figure 1. (left) Accuracy comparison of LightGBM (blue line), LSTM (green line) and GNN (red line) (MAPE (solid line, left axis), R2 (dotted line, right axis) (Right) Percentage of sites where GNN is superior (vs LightGBM: blue line, vs LSTM: green line)

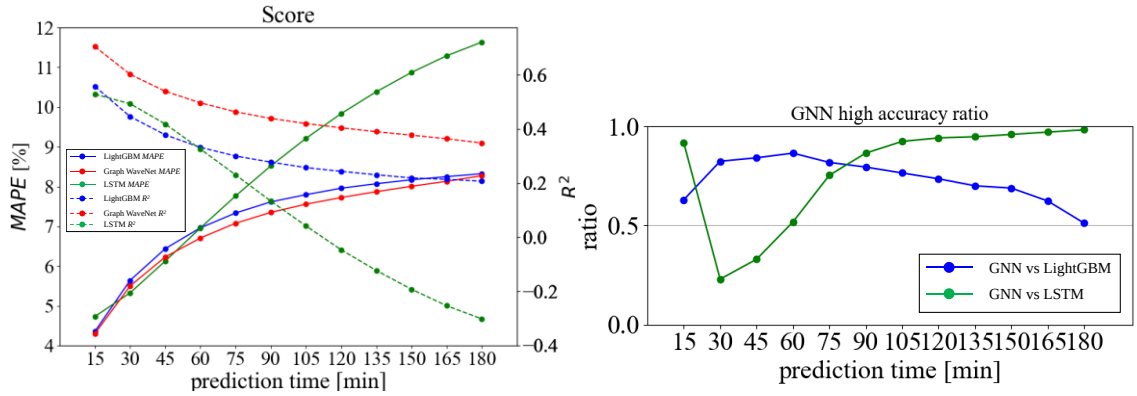

Source: Authors' elaborations.

Figure 2. Comparison of LSTM and GNN (30 min ahead forecast, 〖RMSE〗_2^GNN-〖RMSE〗_2^LSTM)

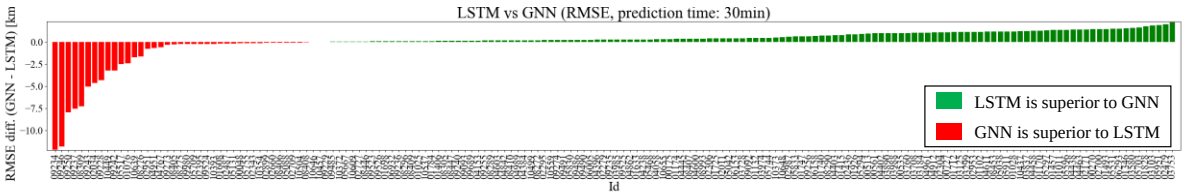

Source: Authors' elaborations.

Figure 3. Partial Autocorrelation (left: Id=3753, middle: Id=9234, right; LSTM/GNN advantage sites mean)

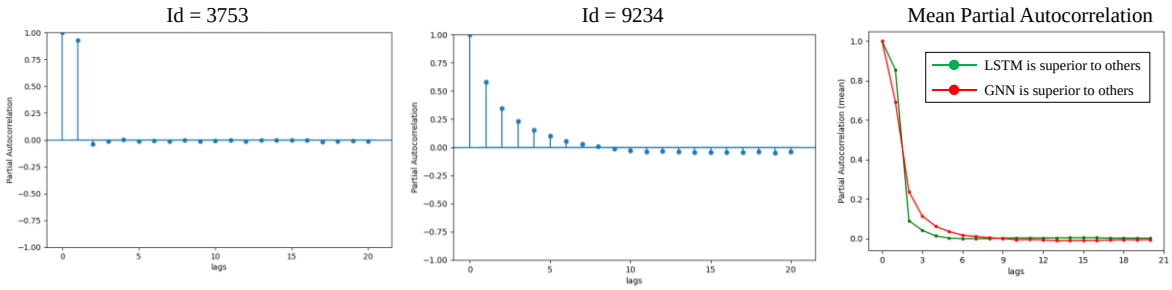

Source: Authors' elaborations.

Conclusion

In this paper, we compare the results of average speed predictions from 15 to 180 min ahead of time by applying LightGBM, LSTM, and Graph WaveNet as GNN, to open data in England. In the evaluation of all 170 sites, the GNN was superior in the average of all predicted times, but the LSTM may be superior depending on the value of partial autocorrelation, such as 30 min ahead or 45 min ahead in this study. However, when predicting at all sites with large data sets, LSTM should be treated with caution because of the large computational cost during training.

As a later issue, this study has been discussed by MAPE, R2, and RMSE, but has not been able to clarify the differences in characteristics between sites from a traffic engineering point of view. We understand that clarifying this is also an important issue to consider. In addition, because GNN handles all sites at once, the adjacent matrix calculation requires significant amount of memory when using large datasets. In this study, GNNs showed high accuracy in 2-3 h ahead-of-time predictions, and we believe that reducing the computational

cost of GNNs will lead to more effective and efficient traffic management. Moreover, GNNs that take into account the relationship between data at different times of the day have been developed in recent years, and there is a possibility that they can provide accuracy in predicting 30 or 45 min in advance. Therefore, the study of improving the computational efficiency of the GNN and introducing relationships between data in time series is a subject for future work.

References

Akiba, T., Sano, S., Yanase, T., Ohta, T., Koyama, M., 'Optuna: A Next-generation Hyperparameter Optimization Framework', 2019, arXiv:1907.10902.

Fu, R., Zhang, Z., Li, L., 'Using LSTM and GRU Neural Network Methods for Traffic Flow Prediction', Proc. 31st Youth Academic Annu.Conf. Chin. Assoc. Autom. (YAC), 2016, pp. 324-328.

Highways England, 'WebTRIS Traffic Flow API', https://webtris.highwaysengland.co.uk/api/swagger/ui/index. (Accessed 3rd February 2023)

Jiang, R., Wang, Z., Yong, J., Jeph, P., Chen, Q., Kobayashi, Y., Song, X., Fukushima, S., Suzumura, T., 'Spatio-Temporal Meta-Graph Learning for Traffic Forecasting', 2022, arXiv:2211.14701v3.

Miyazaki, T., Oosawa, A., Kikucih, Y., Sugawara, H., 'Open traffic data of England and short-term traffic congestion prediction with AutoML', Intelligence, Informatics and Infrastructure, Vol. 3, No. J2, 2022, pp. 268-276.

Miyazaki, T. , Ogata, R. , Y., Murano, Kikuchi, Y., Sugawara, H., 'AI short-term speed prediction on an arterial road of england', Intelligence, Informatics and Infrastructure, 2023. (in press)

Ogata, R., Miyazaki, T. , Kikuchi, Y., Murano, Y., Sugawara, H., 'Comparison of Gradient Boosting Decision Tree and Graph Neural Networks for Short-Time Speed Prediction', Intelligence, Informatics and Infrastructure, 2023. (in press)

Perktold, J., Seabold, S., Taylor, J., statsmodels-developers, 'statsmodels', https://www.statsmodels.org/stable/index.html. (Accessed 3rd February 2023)

Yu, B., Yin, H., Zhu, Z., 'Spatio-Temporal Graph Convolutional Networks: A Deep Learning Framework for Traffic Forecasting', 2018, arXiv:1709.04875v4.

Wu, Z., Pan, S., Long, G., Jiang, J., Zhang, C., 'Graph WaveNet for Deep Spatial-Temporal Graph Modeling', 2019, arXiv:1906.00121v1.

Zhao, Z, Chen, W., Wu, X., Chen, P. C. Y. and Liu, J. 'LSTM network: A deep learning approach for short-term traffic forecast', IET Intelligent Transport Systems, Vol. 11, No. 2, 2017, pp. 68-75.

Data Valuation in Collaborative Urban Traffic Forecasting

D. Pavlyuk[a], , J. Perevozcikova[a]

[a] *Transport and Telecommunication Institute, Latvia*

Introduction

Urban traffic forecasting is an indispensable intelligent transportation system (ITS) component. Providing great practical value for everyday mobility and transportation scheduling, accurate traffic forecasts become a point of intensive research for decades. The modern methodology of traffic forecasting focused on the city level by utilising the power of spatiotemporal relationships of traffic flows (Ermagun and Levinson, 2018). A wide range of spatiotemporal models is successfully adopted for traffic forecasting, e.g., graph convolutional neural networks, GNN (Wang et al., 2019), vector autoregressive models, VAR (Pavlyuk, 2017), k-nearest neighbours algorithm, KNN (Cai et al., 2016). Nevertheless, the vast majority of modern traffic forecasting methods rely on large-scale centralized data both for training and operational usage of models. In real settings, traffic data is generally collected and managed by different parties: state and municipal organisations, public transport operators, road maintenance companies, navigation software providers, and others. Sharing the traffic data and creating the centralised database for model training is associated with additional costs for the parties, such as direct costs of channels for data transferring and indirect costs like the risk of data privacy violation and the potential threat of data leakage. These issues lead to developing schemes for collaborative traffic learning that allow keeping data locally for parties and training the network-wide traffic forecasting model.

Federated learning, FL, (Yang et al., 2019) is one of the emerging frameworks for effective collaborative training and usage of the model by multiple data providers. In federated learning, each data provider uses its private data for training the global model or a part of the global model and shares the entire resulting model or model training results like gradients. As a result, a good balance between achieving the overall model accuracy and preserving data privacy is obtained. Recently, federated learning has become a popular approach in the traffic forecasting domain. Liu et al. (2020) proposed a deep learning model, based on the gated recurrent unit and the FL architecture for preserving the privacy of traffic data. Zhang et al. (2021) presented an FL-based approach for collaborative training of the network topology information and related attention mechanisms. Meese et al. (2022) utilised blockchain technology for secure FL-based real-time traffic prediction. The intensive development of the FL framework and its growing number of applications in the traffic forecasting domain reveals a huge potential for distributed collaborative traffic forecasting.

Motivation is the key success factor of any collaboration, including FL-based collaborative traffic forecasting. Participation in collaborative traffic forecasting incurs costs, so a rewarding mechanism is crucial for potential participant parties. For ensuring fairness in collaborative learning, the reward should correspond to the contribution of each party. There are different forms of this reward in FL: improved accuracy of traffic forecasting for the party-managed part of the network (local model), access to the network-wide model with improved accuracy (global model), access to the distributed computational power, and even monetary compensation or reputational benefits. Collaboration fairness of the FL framework should ensure a good match between the reward, obtained by each party and its contribution to the learning process. This reward-contribution balance is actively studied in the FL field (e.g., (Wang, Dang, and Zhou, 2019)), but, to the best of our knowledge, was never addressed in the spatiotemporal traffic forecasting domain. This research aims to cover this gap.

In this study, we focus on measuring the party contribution by the valuation of its data. We consider the vertical FL scheme, where data of parties are split spatially – each party manages a relatively isolated spatial fragment of the road network (e.g., a city district). We propose several metrics for measuring the value of the party data for improving forecasting accuracy. Namely, we utilize the federated Shapley value (Wang et al., 2020), an adapted classic indicator of the cooperative game theory, for measuring the value of the party data for network-wide forecasting accuracy. Additionally, we consider the peer-to-peer metrics for pairwise evaluation of the data value between parties(Lyu et al., 2020). A large empirical experiment allowed us to make conclusions on the motivation of parties in collaborative traffic forecasting and potential incentives for this process.

Methodology

We consider an urban transport system network as a graph $G = \{V, E\}$, where V is a set of $|V|$ vertices that correspond to a road segment with observed traffic values, E is a set of edges that connect the vertices. The overall structure of the graph G is represented by the adjacency matrix A, based on travel times between each pair of connected vertices. The traffic flow is observed over the time frames $t = 1, \dots, T$ and includes data $Y_{i,t}$ on several characteristics (speed, volume) for every graph vertex $i = 1, \dots, |V|$.

The transport network is managed by a set of parties P, and the graph G is split into subgraphs $G^p = \{V^p, E^p\}$, managed by parties $p = 1, \dots, |P|$, with a non-overlapping set of vertices V^p and internal edges E^p that connect V^p. Each party own the traffic flow data $Y^p = Y_{j,t}$, where $j \in V^p$, and is interested in the accurate traffic forecast for the managed network $\hat{Y}_{j,T+h}$ for specified horizons $h = 1, \dots, H$. These spatiotemporal settings define the problem of vertical federated learning in the multivariate time series domain, where every party manages its own set of private features (traffic flow characteristics at managed road segments).

Generally, each party can choose its own forecasting model M^p, but the model structure should allow utilization of spatiotemporal relationships for improving forecasting accuracy. This assumption is essential for the participation of the party in the collaborative learning schemes. In this study, we arbitrarily utilized a modern attention-based spatial-temporal graph neural network, ASTGNN (Guo et al., 2022), for all parties. The ASTGNN models include the following components:

— graph convolution layers (Kipf and Welling, 2017) that capture dependencies of the spatial and temporal neighbourhoods;

— spatial and temporal self-attention mechanisms (Veličković et al., 2018) that capture the dynamic structure of spatiotemporal dependencies between data inputs on every GNN layer;

— the general encoder-decoder framework.

The ASTGNN model is known for flexible data-driven learning of spatiotemporal relationships and good forecasting accuracy. In this study, we utilise the conventional R^2-score s a forecasting accuracy metric. Thus, the utility of the model M^p is defined by its accuracy on the testing subset of the traffic flow data Y^p: $v(M^p, Y^p) = R^2_{score}$.

The collaboration process allows forming $2^{|P|}$ coalitions of parties $S \subseteq P$, and each coalition can jointly train its model M^S using the joint data Y^S. The utility of the coalition for every party is also defined by the accuracy of the model of the testing subset of party's data: $v(M^S, Y^p)$.

The primary focus of this study is measuring the potential contribution of each party under two scenarios:

— pairwise sharing of the model and data,

— vertical federated training of the global (network-wide) model.

For measuring the utility of collaboration of the party $p1$ with the party $p2$, we utilise the improvement of the traffic forecasting accuracy on the testing subset of data Y^{p1}, given the joint model $M^{p1 \cup p2}$, trained on the combined data:

$$\delta_{p2 \to p1}(v) = v\left(M^{\{p1\} \cup \{p2\}}, Y^{p1}\right) - v(M^{p1}, Y^{p1}).$$

For measuring the contribution of each party in the second scenario, the asymmetric Shapley value is utilised. The classical formula for the Shapley value is:

$$\phi_p(v) = \frac{1}{|P|} \sum_{S \subseteq P \setminus p} \frac{v\left(M^{S \cup \{p\}}, Y^S\right) - v(M^S, Y^S)}{C^{|S|}_{|P|-1}},$$

where $\phi_p(v)$ is the Shapley value of the party p given the utility function v; P, S, M^S, Y^S are the set of parties, the set of coalitions, the coalition model and data respectively; $C^{|S|}_{|P|-1}$ is number of different coalitions with the excluded party p. The conventional Shapley value satisfies several important properties like symmetry, efficiency, and linearity. In addition to the conventional Shapley value, we consider its asymmetric variation (Frye, Rowat, and Feige, 2020), where the symmetry property is relaxed due to the different utilities of the coalition for the parties (improvement of the forecasting accuracy on the party's data set).

Empirical results

For the experimental study, we utilised the popular Caltrans Performance Measurement System (PeMS) highway traffic flow data in California. A sample of 50 road segments from the centre of Caltrans district 4 data was selected and arbitrarily split into three relatively decoupled graphs that represented different parties (data providers). Then, the ASTGNN model was separately trained for the complete data set, every party and three possible coalitions.

The accuracy values of all models are summarised in Table 1; also, the table contains corresponding symmetric and asymmetric Shapley values.

Table 1. Accuracy of model coalitions and Shapley values

Coalition	R^2 score of the coalition's ASTGNN model			Shapley value	Asymmetric Shapley value
	Party 1	Party 2	Party 3		
Party 1	0.914	0.901	0.91	0.328	0.328
Party 2	0.938	0.899	0.922	0.330	0.326
Party 3	0.935	0.940	0.858	0.307	0.311
Grand coalition	0.965				

Source: Own calculations

The calculated Shapley values allow comparing the contribution of every party to the resulting forecasting accuracy of the global model. The conventional Shapley values indicate the higher contribution of Party 2's data and the lower contribution of Party 3' data. The results of the asymmetric Shapley values are similar to the conventional ones. Summarising the empirical results, we conclude that the mutual utility of weakly coupled spatiotemporal parties is limited, and potential reward schemes should be based not only on the improvement of the local model's forecasting accuracy but other forms of incentives.

Conclusion

This study proposes a novel approach to the valuation of parties' data for collaborative spatiotemporal urban traffic forecasting. The problem of motivation for collaborative learning and fair rewards for different data providers is crucial for multi-party intelligent transportation systems. We consider the federated learning of the traffic forecasting model and propose the measures for the contribution of each party, based on the utility of their data for forecasting accuracy. The empirical experiment illustrates the applicability of the proposed measures. These measures are essential input for the definition of rewards for participation in collaborative learning. The essence, form and volume of the rewards is a perspective subject for further research.

Acknowledgement

The work is financially supported by the specific support objective activity 1.1.1.2. "Post-doctoral Research Aid" (Project id. N. 1.1.1.2/16/I/001) of the Republic of Latvia, funded by the European Regional Development Fund. Dmitry Pavlyuk's research project No. 1.1.1.2/VIAA/1/16/112 "Spatiotemporal urban traffic modelling using big data".

References

Cai, P., Y. Wang, G. Lu, P. Chen, C. Ding, and J. Sun, 'A Spatiotemporal Correlative K-Nearest Neighbor Model for Short-Term Traffic Multistep Forecasting', *Transportation Research Part C: Emerging Technologies*, Vol. 62, January 2016, pp. 21–34.

Ermagun, A., and D. Levinson, 'Spatiotemporal Traffic Forecasting: Review and Proposed Directions', *Transport Reviews*, March 6, 2018, pp. 1–29.

Frye, C., C. Rowat, and I. Feige, 'Asymmetric Shapley Values: Incorporating Causal Knowledge into Model-Agnostic Explainability', *Proceedings of the 34th International Conference on Neural Information Processing Systems*, *NIPS'20*, Curran Associates Inc., Red Hook, NY, USA, 2020.

Guo, S., Y. Lin, H. Wan, X. Li, and G. Cong, 'Learning Dynamics and Heterogeneity of Spatial-Temporal Graph Data for Traffic Forecasting', *IEEE Transactions on Knowledge and Data Engineering*, Vol. 34, No. 11, November 1, 2022, pp. 5415–5428.

Kipf, T.N., and M. Welling, 'Semi-Supervised Classification with Graph Convolutional Networks', 2017.

Liu, Y., J.J.Q. Yu, J. Kang, D. Niyato, and S. Zhang, 'Privacy-Preserving Traffic Flow Prediction: A Federated Learning Approach', *IEEE Internet of Things Journal*, Vol. 7, No. 8, August 2020, pp. 7751–7763.

Lyu, L., J. Yu, K. Nandakumar, Y. Li, X. Ma, J. Jin, H. Yu, and K.S. Ng, 'Towards Fair and Privacy-Preserving Federated Deep Models', arXiv, May 19, 2020.

Meese, C., H. Chen, S.A. Asif, W. Li, C.-C. Shen, and M. Nejad, 'BFRT: Blockchained Federated Learning for Real-Time Traffic Flow Prediction', *2022 22nd IEEE International Symposium on Cluster, Cloud and Internet Computing (CCGrid)*, IEEE, Taormina, Italy, 2022, pp. 317–326.

Pavlyuk, D., 'Short-Term Traffic Forecasting Using Multivariate Autoregressive Models', *Procedia Engineering*, Vol. 178, 2017, pp. 57–66.

Veličković, P., G. Cucurull, A. Casanova, A. Romero, P. Lio, and Y. Bengio, 'Graph Attention Networks', 2018.

Wang, G., C.X. Dang, and Z. Zhou, 'Measure Contribution of Participants in Federated Learning', *2019 IEEE International Conference on Big Data (Big Data)*, IEEE, Los Angeles, CA, USA, 2019, pp. 2597–2604.

Wang, T., J. Rausch, C. Zhang, R. Jia, and D. Song, 'A Principled Approach to Data Valuation for Federated Learning', arXiv, September 14, 2020.

Wang, Y., D. Zhang, Y. Liu, B. Dai, and L.H. Lee, 'Enhancing Transportation Systems via Deep Learning: A Survey', *Transportation Research Part C: Emerging Technologies*, Vol. 99, February 2019, pp. 144–163.

Yang, Q., Y. Liu, T. Chen, and Y. Tong, 'Federated Machine Learning: Concept and Applications', *ACM Transactions on Intelligent Systems and Technology*, Vol. 10, No. 2, March 31, 2019, pp. 1–19.

Zhang, C., S. Zhang, J.J.Q. Yu, and S. Yu, 'FASTGNN: A Topological Information Protected Federated Learning Approach for Traffic Speed Forecasting', *IEEE Transactions on Industrial Informatics*, Vol. 17, No. 12, December 2021, pp. 8464–8474.

The 2020 update of the transport sector in JRC-IDEES - Analysing the past for robust transport and energy policies

J. Tattini[a], M. Rózsai[a]

[a] *European Commission, Joint Research Centre (JRC), Seville, Spain*

Introduction

This study showcases for the first time the 2020 update of the transport sector database within JRC-IDEES (Mantzos et al., 2017). This is the "Integrated Database of the European Energy System", which collects and harmonises statistical data related to the whole energy system in Europe. By collecting, decomposing and processing detailed transport-, energy-and emission-related data, JRC-IDEES constitutes a unique database to analyse past trends and to serve as a solid basis for assessing future transport policies in the European Union (EU). Indeed, policies are desirable to steer the transport sector towards a pathway in line with the Paris Agreement. In the EU, CO_2 emissions from the transport sector have risen constantly from 2012 to 2019 (see Figure 1). After a sharp 14% year-on-year reduction in 2020 due to the Covid-19 pandemic, CO_2 emissions in 2021 have almost rebounded to pre-pandemic levels. Besides, the transport sector's CO_2 emissions as a share of the total from all end-use sectors has been rising (with the exception of the pandemic), which hints the intrinsic difficulty in decarbonising the transport sector. Acknowledging this situation, the European Commission (EC) has proposed a set of additional policies to tackle emissions from the transport sector. In the framework of the Fit for 55 package (European Council, 2023), four policy proposals are specifically targeting transport CO_2 emissions: the stricter CO_2 emission standards for light-duty vehicles, the Alternative Fuel Infrastructure Regulation, the REFUEL-EU Aviation (encouraging the uptake of sustainable aviation fuels) and the FUEL-EU Maritime (supporting the adoption of cleaner maritime fuels).

Figure 6. Historic CO2 emissions by end-use sector in the EU and share of transport emissions out of the total from end-use sectors (on the right axis). Own calculations based on EUROSTAT (2023a)

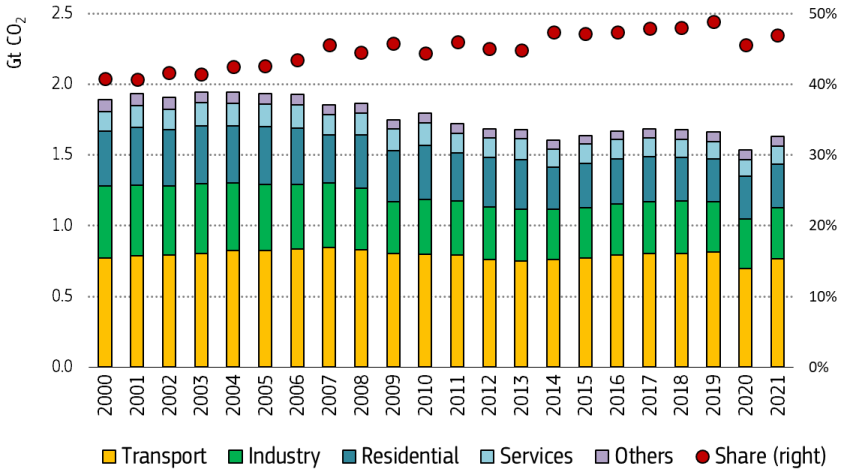

In this context, the differentiation of the factors that influence energy consumption in transport provided by JRC-IDEES offers an adequate basis to assess the scope for improvement that different types of policies may trigger.

The 2020 transport sector update of JRC-IDEES combines in a consistent manner several official statistics in order to provide a plausible decomposition of energy consumption (thus CO_2 emissions) and transport activity by transport technology for each EU member state from year 2000 to 2020. For the EU, the most renowned energy balances (i.e. EUROSTAT (2023a) and International Energy Agency (2023)) split the transport sector's energy consumption only at the level of road transport, rail transport, aviation, domestic navigation and international maritime shipping. The main benefit of the JRC-IDEES transport database lies in its decomposition of energy consumption and transport activity (measured in passenger-kilometre and tonne-kilometre) at a more disaggregated resolution, which covers the transport modes/services shown in Table 2.

Table 2. Structure of the transport sector in JRC-IDEES

Passenger transport	**Freight transport**
Road transport	
Two- and three-wheelers	Light commercial vehicles
Passenger cars	Heavy duty trucks
Buses and coaches	
Rail, metro and tram	
Metro, tram and light rail	Conventional freight rail
Conventional passenger rail	
High speed rail	
Aviation	
Domestic	Domestic
International Intra-EU	International Intra-EU
International Extra-EU	International Extra-EU
Domestic navigation	
Coastal shipping	
Inland waterways	
International maritime shipping	
Intra-EU	
Extra-EU	

Notes: JRC-IDEES assigns all domestic navigation and international maritime shipping activities to freight transport.

Methodology

The decomposition of the energy consumption from the transport sector consists in the following four main steps:

1. **Gathering the necessary data.** This includes: a) Transport final energy consumption by mode/service - mainly obtained from EUROSTAT energy balances (EUROSTAT, 2023); b) Traffic (measured in vehicle-kilometre) statistics – mainly obtained from EUROSTAT (2023b); c) Transport activity (in passenger-kilometre and freight-kilometre) statistics - mainly from the Statistical Pocketbook (EC, 2023) and from EUROSTAT (2023b); d) Vehicle/train/aircraft/vessel registrations and stock – mainly from the Statistical Pocketbook (EC, 2023) and from EUROSTAT (2023b); e) Fuel economies – from European Environment Agency (EEA, 2023a, 2023b) for road transport, from European Maritime Safety Agency (2023) for shipping and from EUROCONTROL (2023) for aviation; f) Annual mileages and occupancy/load factors - collected from various sources to support the decomposition process.
2. **Preparing annual time series.** For each EU member state, complete data series from 2000 to 2020 are prepared with estimations for the missing data.

3. **Identifying for each transport mode/service the relevant technologies on which the macro data is disaggregated.** For road transport modes and rail services, technologies are differentiated solely based on the main input fuel, irrespective of vehicle/train size (i.e. a representative vehicle/train is considered). For aviation, technologies are defined based on their main use - passenger or freight transport; domestic, intra- or extra-EU – to account for different operational profiles in short-, mid- on long-range travels. For maritime shipping, technologies are defined both based on the main input fuel and on the main use. The technology (and fuel) options explicitly represented in JRC-IDEES for each transport sub-sector are shown in Figure 2.

Figure 7. Technology options for the five transport sub-sectors in JRC-IDEES

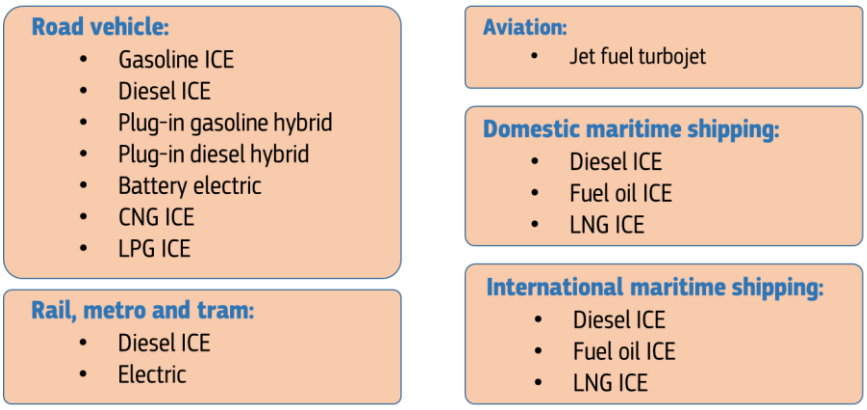

Notes: ICE = internal combustion engine; CNG = compressed natural gas; LPG = liquid petroleum gas; LNG = liquefied natural gas. Hybrid vehicles are reported under ICEs with the corresponding main fuel.

4. **Performing the decomposition.** From 2000 to 2020, for each EU member state and for each transport technology the vehicle/train/vessel/aircraft stock composition, annual mileages, load/occupancy factors and energy efficiencies are determined in order to match the energy balances by fuel and the transport activity statistics without any exception. The procedure to combine the different statistics in a sensible manner consists in a mixture of interdependent bottom-up and top-down calculations specific to each transport sub-sector. While the methodology adopted in JRC-IDEES to carry out the decomposition of the transport sector is not formal (it does not rely on a single mathematical formulation), the rules applied within each sub-sector are the same across countries, ensuring consistency across country-level data.

The rest of this section describes in a bit more detail for each transport sub-sector the procedure to decompose energy consumption and transport activity in the modes/services shown in Table 2 and Figure 1.

Road transport

The decomposition process for the road transport sector implies determining a meaningful set of mode- and technology-specific stock compositions, fuel economies, traffic, annual mileages and load factors that enables to both match the overall fuel-specific energy consumption for road transport (EUROSTAT, 2023a) and the mode-specific transport activity statistics (EC, 2023).

EUROSTAT (2023b) provides the fuel-specific final energy consumption (aggregated across all road transport modes) for all years between 2000 and 2020 and each EU member state. Transport activity and traffic statistics are obtained with the same level of granularity for each road transport mode from the Statistical Pocketbook (EC, 2023).[9]

Initial technology-specific vehicle registration (new sales and second hand registrations) and stock data are collected from EUROSTAT (2023b). Since vehicle stock must match energy consumption, no stock is assumed to exist if the corresponding fuel consumption is not reported. Whenever inconsistencies between vehicle registrations and stock are identified, registrations are modified manually unless substantial modifications are

[9] Transport activity in JRC-IDEES is reported according to the territoriality principle, i.e. the energy consumption of a foreign vehicle on a given territory is allocated to the national vehicle fleet.

needed, in which case a theoretical model of sales is adopted. Retired vehicles are determined via Gompertz survival functions.

Test-cycle fuel economies for new light-duty vehicles are obtained from EEA (2023a, 2023b), while other studies provide fuel economy data for heavy-duty road transport modes (AMF TCP, 2021; Enerdata, 2023). Then, test-cycle fuel economies are scaled to real-word fuel economies via adjustment factors. For each technology, the stock-average fuel economy is based on the vintage-specific composition of its stock and on the real-world fuel economy of new registrations. Since there is not guarantee that such real-world fuel economy and vehicle stock match the energy balances, "effective" fuel economies are then determined to match both transport activity statistics and the energy balance. For all EU member states, the discrepancy between the test-cycle and effective fuel economies lies in a range in line with other studies (e.g. ICCT, 2019).

Load factors are the linking element between vehicle traffic and activity data, while annual mileages bound the vehicle stock to the annual traffic.

Rail transport

The decomposition of the rail sector consists in disaggregating data at the technology level - electricity and diesel (see Figure 2) – while matching transport activity statistics at rail service-level (see Table 2) and the fuel-specific final energy consumption of rail transport. The former is provided by the Statistical Pocketbook (EC, 2023) and the latter by EUROSTAT energy balances (EUROSTAT, (2023b).

The procedure starts by decomposing traffic at the technology level, which is done in an iterative process that combines EUROSTAT traffic statistics, Statistical Pocketbook transport activities and occupancy/load factors estimates.

Stock-average energy efficiencies are initially estimated from previous calculations and then are scaled so that overall energy consumption across rail services and technologies matches the energy balances. The so-determined energy efficiencies are cross checked with other sources (e.g. International Union Of Railways (2023) and EC (2022).

The rolling stock for each rail service and technology type is determined dividing the above-mentioned decomposed traffic by rail service-specific representative annual mileages. Then the new train registrations are calculated considering the rolling stock variations and assuming a step-wise survival function.

Aviation

The decomposition of the aviation sector consists in disaggregating parameters for the services in Table 2 while matching transport activities from the Statistical Pocketbook (EC, 2023) - split in passenger and freight aviation and in domestic and intra-EU transport activity - and the final energy consumption from the energy balances (EUROSTAT, (2023b) – split in domestic and international aviation. Besides, EUROSTAT provides statistics on transport volumes (in terms of number of passengers and tonnes carried) and number of flights that are used in the decomposition.

Commercial data (Sabre, 2023; EUROCONTROL, 2023) are used in combination with the EUROSTAT data in order to split the passenger and freight aviation activities across domestic, international intra-EU and international extra-EU trips. Besides, EUROCONTROL (2023) is used to determine the EU member state-specific split of total transport activity, which the Statistical Pocketbook only provides at EU level (EC, 2023). EUROCONTROL consumption and activity data is also used to estimate an initial technical efficiency of the various aviation services, which is then scaled to match the energy balances.

Finally, a representative aircraft stock is calculated dividing the aviation traffic by an average yearly rotation - i.e. number of flights per year per aircraft, which in turn depends on the average flight distances.

Domestic navigation

EUROSTAT energy balances provide fuel-specific energy consumption statistics for domestic navigation. Inland waterways and coastal shipping transport activities are obtained respectively from the Statistical Pocketbook (EC, 2023) and from EUROSTAT (2023b). Previous calculations are used to obtain the load factors, which are combined with the transport activities to determine traffic.

An initial vessel-fleet average energy efficiency for each shipping service (see Table 2) is determined as a function of the vessel's load and is assumed to be constant across technologies (see Figure 1). Then, such energy efficiency is scaled to match the energy balances. Finally, the size of the vessel fleet is calculated from traffic assuming annual mileages and then new vessel registrations are calculated considering the variation of the vessel fleet over time and a step-wise survival function.

International maritime shipping

EUROSTAT energy balances provide fuel-specific energy consumption statistics for international maritime shipping. EUROSTAT and the Statistical Pocketbook are combined to determine the EU member state specific split of transport activity in intra-EU and extra-EU.

A first estimation of the vessels' load is determined as a function of the vessel fleet's average gross weight tonnage, which in turn is based on EUROSTAT gross tonnage (EUROSTAT, 2023b) using the methodology described in Papanikolaou (2014). Then, the refined vessels' load is determined combining information on annual mileage and traffic. A first estimate of the vessel fleet energy efficiency is determined combining EMSA's Monitoring Reporting and Validation (MRV) (EMSA, 2023) data with the above-mentioned load factor and traffic data, which is then refined in order to match the energy balance.

Finally, the size of the vessel fleet is calculated from traffic assuming annual mileages and new vessel registrations are calculated considering the vessel fleet variation and a step-wise survival function.

Results

The key findings of the transport sector 2020 update in JRC-IDEES will be showcased for the first time at the ninth International Symposium on Transportation Data & Modelling (ISTDM) in June 2023. The authors have decided not to provide any preview of such results beforehand.

After the ISTDM, the entire transport database of JRC-IDEES updated up to 2020 will be made freely available for download on the Joint Research Centre Data Catalogue (JRC, 2023), as it is the case for the latest version of such database (Mantzos et al., 2018). The database consists of a large set of time series - from 2000 to 2020, for each EU member state, for each mode/service in Table 2 and for each technology in Figure 2 - for internally consistent disaggregated transport indicators. The following is a not-exhaustive list of the indicators provided: vehicle/train/aircraft/vessel new registrations[10], stocks, age profiles, annual mileages, activity levels, traffic levels, occupancy/load factors, technical fuel economies/efficiencies, "effective" fuel economies/efficiencies and discrepancies between the latter two parameters.

Conclusions

This study showcases the 2020 update of the transport sector database within JRC-IDEES - the "Integrated Database of the European Energy System". The 2020 transport sector update combines in a consistent manner several transport and energy statistics in order to provide a plausible decomposition of energy consumption and transport activity by mode and technology type for each EU member state from year 2000 up to 2020.

This internally consistent database of disaggregated transport indicators identifies national differences in the structure of the transport sector and defines the vintage-specific composition and operation of the vehicle stock for each transport mode. By identifying the different drivers of total energy consumption from the transport sector and the role of different sectors and technologies in the overall transport energy patterns up to 2020, this study constitutes a robust basis to evaluate the implications of different types of future policies.

JRC-IDEES is fully accessible to the public and the 2020 update of the transport sector is going to be freely downloadable on the Joint Research Centre Data Catalogue. Besides, the transport indicators resulting from this study will be included in the publicly accessible database that the Transport Data Commons Initiative (TDCI) is developing. Being a reliable and cost-free data-box, JRC-IDEES is meant to serve as the reference database for transport and energy system analysis at the EU level, thus avoiding duplication of efforts within this community.

References

Advanced Motor Fuel Technology Collaboration programme (2021), Heavy-Duty Vehicles Performance Evaluation, https://amf-tcp.org/app/webroot/files/file/Annex%20Reports/AMF_Annex_57.pdf

Enerdata (2023), Odyssee-Mure, https://www.odyssee-mure.eu/

EUROCONTROL (2023), Our data, https://www.eurocontrol.int/our-data, accessed on 25.10.2022

European Commission (EC, 2022), Development of a consistent dataset for quantitative analysis, https://transport.ec.europa.eu/transport-themes/sustainable-transport/sustainable-transport-studies_en

[10] For certain road transport modes also second hand registrations are provided.

EC (2023), Statistical pocketbook 2021, https://transport.ec.europa.eu/media-corner/publications/statistical-pocketbook-2021_en

European Council (2023), Fit for 55, https://www.consilium.europa.eu/en/policies/green-deal/fit-for-55-the-eu-plan-for-a-green-transition/

European Environment Agency (EEA, 2023a), Monitoring of CO2 emissions from passenger cars – Regulation (EU) 2019/631, https://www.eea.europa.eu/data-and-maps/data/co2-cars-emission-22, accessed on 09.01.2023

EEA (2023b), Monitoring of CO2 emissions from vans – Regulation 510/2011, https://www.eea.europa.eu/data-and-maps/data/vans-14, accessed on 09.01.2023

European Maritime Safety Agency (2023), THETIS MRV, https://mrv.emsa.europa.eu/#public/eumrv, accessed on 09.01.2023

EUROSTAT (2023a), Complete energy balances (nrg_bal_c), https://ec.europa.eu/eurostat/databrowser/view/nrg_bal_c/, accessed on 25.01.2023

EUROSTAT (2023b), Transport – Main tables, https://ec.europa.eu/eurostat/web/transport/data/main-tables, accessed on 09.01.2023

International Council on Clean transportation (ICCT) (2019), From Laboratory to Road: a 2018 update, https://theicct.org/publication/from-laboratory-to-road-a-2018-update/

International Energy Agency (2023), World Energy Balances, https://www.iea.org/data-and-statistics/data-product/world-energy-balances

International Union of Railways (UIC, 2023), Railisa, https://uic-stats.uic.org/, accessed on 07.02.2023

Joint Research Centre (JRC, 2023), Data catalogue, https://data.jrc.ec.europa.eu/dataset/jrc-10110-10001

Mantzos L., Wiesenthal T., Matei N.A., Tchung-Ming S., Rozsai M. (2017), JRC-IDEES: Integrated Database of the European Energy Sector, https://publications.jrc.ec.europa.eu/repository/bitstream/JRC108244/kjna28773enn.pdf

Mantzos L., Matei N.A., Mulholland E., Rózsai M., Tamba M., Wiesenthal T. (2018), JRC-IDEES 2015. European Commission, Joint Research Centre (JRC) [Dataset] doi: 10.2905/JRC-10110-10001, https://data.jrc.ec.europa.eu/dataset/jrc-10110-10001

Papanikolaou A. (2014), Ship Design – Methodologies of preliminary design, Springer, ISBN 978-94-017-8750-5, doi: 10.1007/978-94-017-8751-2

Sabre (2023), Sabre, https://www.sabre.com/, accessed on 17.05.2022

Design and working principles of NEMO's Nautilus platform for storing, analyzing and classifying high noise and exhaust emitters in traffic

E. van Gils[a], A. Kuijpers[a], B. Peeters[a]

[a]*M+P engineering consultants*

Introduction

In the EU-project NEMO (Noise and Emissions Monitoring and Radical Mitigation), a multi-disciplinary consortium has developed a remote sensing system which monitors air pollutants and noise levels of individual road vehicles and trains in real-time and identifies high emitters. By identifying high emitters, policy makers may in the future be able to enforce limits in low-emission zones, notify drivers of high-emitting vehicles, or even sanction drivers based on their emissions. This paper focuses on road traffic emissions, but most of the methodologies are also applied for trains.

The NEMO-system consists of remote sensing equipment for measuring exhaust and noise emissions, with sensing equipment to obtain vehicle characteristics (vehicle type, speed, acceleration, license plate, etc.), weather conditions. This sensing equipment is employed at various locations (sites) where the assessment of traffic pollutants is wanted. There is a *Synchronizer*, either on site or in the cloud, to time-synchronize the results of all sensors and send them to a centralized cloud system (the *Data Hub*) for storage, enrichment, automated analysis and classification. After classification, the result is communicated back to the driver on site over I2V, by a variable message sign on site or by other means of direct communication (e.g. a text message on a mobile phone). This is done by the so called *Classification Dialog System*.

In this paper we will focus on the design and working principles of *Nautilus*, which is the name for the software infrastructure that facilitates the integration of remote sensing data, data processing and classification of vehicle's emissions. M+P worked together with Kapsch and SINTEF on the design and implementation of the *Nautilus* system.

Methodology

Figure 8. *Nautilus* information flow and interfacing with other systems [3]

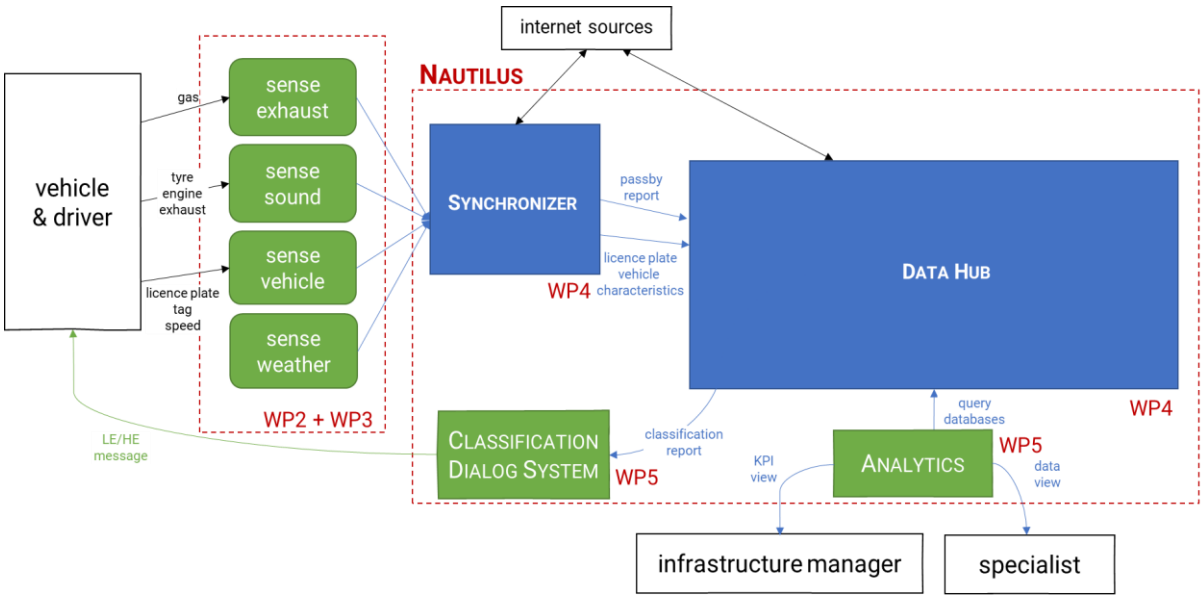

The *Nautilus* system consists of four major components: *Synchronizer*, *Data Hub*, *Classification Dialog System* and *Analytics*. When a vehicle passes a measurement location, the raw data from the different sensors at that site is synchronized based on UTC-time by *Synchronizer.* In addition, it queries a vehicle registration database to obtain additional vehicle characteristics relevant for the classification, such as vehicle type, weight, fuel type, noise emission type approval levels, etc. This data is then transferred in a passby-report to the *Data Hub* cloud system. *Data Hub* stores the report, including information from other internet sources if necessary. Then, based

on vehicle characteristics and noise and gaseous emissions measurements, the passbys are classified. After the classification, the *Classification Dialog System* communicates the result back to the sensing site, and to the vehicle driver or owner. *Analytics* is a data analytics platform for the infrastructure manager to study emissions in detail. An overview of the information flow in the system is outlined in figure 1.

Design considerations

The most important design considerations of the *Nautilus* platform were:

- the system should be flexible; it should support emissions from road and rail vehicles, and should be open to other vehicle types, such as ships;
- the system as a whole should be scalable to support various measurement sites and hence various classification methods and emission limit values;

Synchronizer is specific to the sensing setup. It is operated at the sensing site or optionally in the cloud;

Data Hub is generic to all sites and is operated in the cloud. It should allow for adding new sensor types easily. It should be able to process passby-reports with varying sensor data and be robust to deal with low-quality or missing sensor data;

Data Hub accommodates the use of site-specific classification models, and should be able to communicate classifications back to the site.

An important aspect of the system is that the round trip time (from sensing to informing the driver) should be as short as possible, in order to alert the driver of the vehicle while driving. The round trip time is largely affected by the time needed to distinguish an individual vehicle passby from the traffic stream, the time needed to synchronize the signals, enrich them with vehicle specific data, perform classification and communicate the result back to the site and/or driver of the vehicle. *Data Hub* can be deployed on regional cloud infrastructure, so it is available for different sites with a low latency.

Interfaces and communication

In order to support different sensor setups, the interfaces between the different sub-systems were defined to be as flexible as possible. The communications between the components are done over zeroMQ (pub/sub) for the components on the site. The passby report is compiled by *Synchronizer* and then sent to the *Data Hub Collector*, the component that is responsible for collecting incoming passby reports, see figure 2. Communication is over HTTPS using a REST-interface with the JSON data-format.

The interfaces were defined using the OpenAPI standard. We use a token based authentication scheme and an extra layer of security is added by forcing all communications between the site and the cloud infrastructure over a dedicated VPN-tunnel.

Data Hub

The different sub-components of *Data Hub* are outlined in figure 2. Each component runs as a separate Linux Docker container. Different programming languages may be used here, as long as a component offers a standardized way to either read data from a queue, or can be interacted with over HTTP REST. We use an automated DevOps workflow to build, test and deploy new versions of *Data Hub* minimizing errors and developer time.

Incoming passby reports are collected by *Collector* and a queueing mechanism (supported by a RabbitMQ message broker) is used between different *Data Hub* components. A document based database , based on PostgreSQL was used for the underlying storage, as it offers flexibility with JSON (querying).

Figure 9. Interactions between different *Data Hub* components [3]

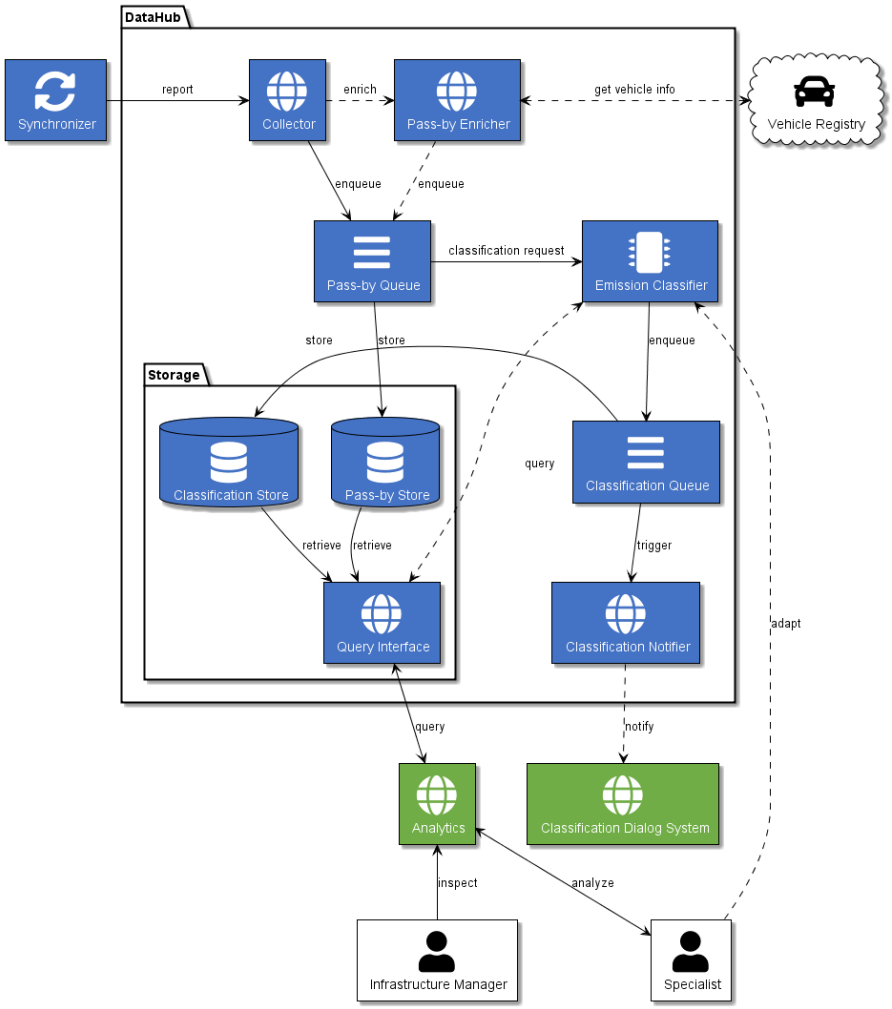

Results

The *Nautilus* platform was first used in a series of tests that were performed in Teesdorf (AT), where Kapsch operates a test site. A series of tests was performed with dedicated vehicles driving under a gantry mounted with measurement equipment. Despite some communication issues between the different measurement systems on site, the system proved to be capable of measuring independently noise and emissions from passing vehicles, synchronize the results, identify the license plate, determining the vehicle category, make an automated request for vehicle registration data and send all results to *Data Hub [4]* . Further testing was done in pilot projects in Madrid (ES) and Florence (IT), and in test projects in Rotterdam (NL) and Munich (DE). Classification was triggered for exhaust and noise.

Classification model

For noise classification we have tested different models, the most extensive one using a machine learning based approach that takes into account the type approval test measurement regulations. This model was trained on the Rotterdam data set. Based on measured noise levels, vehicle properties obtained from the national registry and engine speed (in rpm), the model predicts if a passby is a normal or high emitter. Results of the classification of the Rotterdam data are shown in figure 3. The trained machine learning model could be used in *Data Hub* for near real-time classification of noise emissions. The graph shows that high emitters mainly occur at low vehicle speeds, as engine and exhaust noise are dominant at such speeds. At high engine speeds, vehicles are less likely to be identified as high emitters as the type approval regulations allow more noise at high rpm.

Figure 10. Passby noise levels vs speed (normal and high emitters)

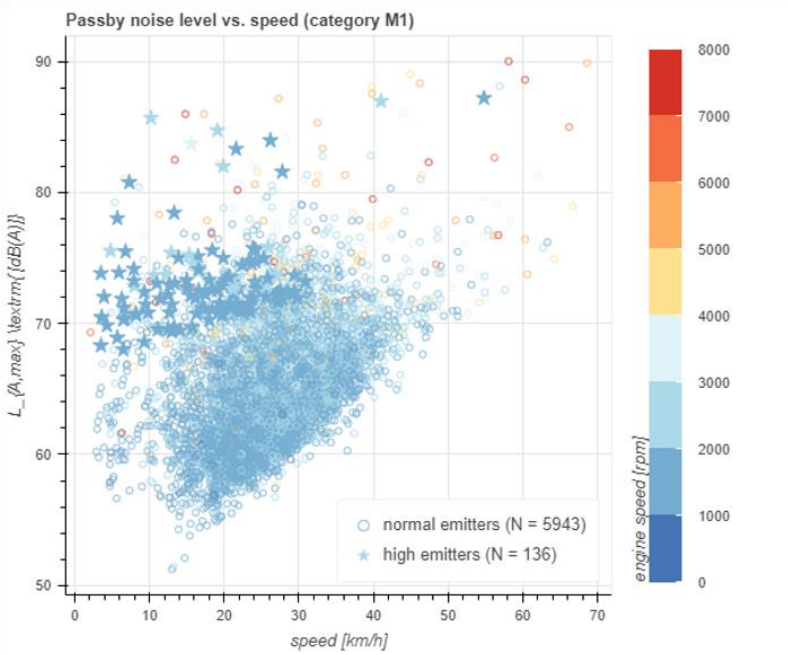

Conclusions

Within the context of the NEMO project, the *Nautilus* system was designed and deployed to store, enrich, analyze and classify noise and exhaust emissions. During a testing phase in Teesdorf and in a few pilot projects in European cities, the *Nautilus* system proved to be rather flexible and robust. By analyzing the data stored in *Data Hub*, a machine learning model was trained to classify normal and high emitters for noise.

Acknowledgment

This work was undertaken as part of the research project NEMO that has received funding from the European Union's Horizon 2020 research and innovation programme under grant agreement No 860441.

References

[1] OUR WORLD IN DATA, https://ourworldindata.org/urbanization

[2] NEMO-project website, https://nemo-cities.eu

[3] Kuijpers. A., Litzinger, P., van Gils, E., *D4.4 – Final description of the Nautilus interface*,2021.

[4] Kahler, P., Kuijpers, A., Litzinger, P., van Gils, E., *D4.2 – Report about integration in Teesdorf*, NEMO WP4, 2022.

Generation of Aggregated Road Network by Vehicle Trajectory Data

Hengyi Zhong[a], Toru Seo[a], Wataru Nakanishi[b], Shohei Yasuda[c], Yasuo Asakura[a], Takamasa Iryo[d]

[a] *Department of Civil and Environmental Engineering, Tokyo Institute of Technology*

[b] *Institute of Science and Engineering, Kanazawa University*

[c] *Faculty of Engineering, The University of Tokyo*

[d] *Department of Human-Social Information Sciences, Tohoku University*

Introduction

Properly aggregated road networks are usually welcomed in traffic network analysis. In those road networks, for example, one intersection area should be represented as only one node. One characteristic of those networks compared to existing road networks is that they may have a significantly smaller number of nodes and links. If there are too much links and nodes even if in a simple network, the calculation time and errors may both increase. To solve this problem, Boeing (2017) introduced a simplification method for OpenStreetMap road network by considering topology of the network. Yasuda et al. (2019) used ETC2.0 data, a set of vehicle trajectory data collected in Japan, to simplify National Digital Road Map (DRM) data by the recorded traffic volume of probe vehicles.

Global Navigation Satellite System (GNSS) trajectories can be considered as a useful data source in geographic data analysis nowadays, and it also can be used for generating road network data. Tang et al. (2019) tried to recognize the structure of intersections by using local features. Huang et al. (2018) introduced graph theory to generate complex road networks. Meanwhile, to generate a part of aggregated road network directly from GNSS trajectories, Zhong et al. (2022) applied spatial scan statistics on different distributions of trajectory dot data to determine intersection areas.

It is efficient to use such trajectory-based road network data in traffic network analysis when there is an absence of proper road network data. However, such a network should contain not only correct geographical positions, but also values which can be used in traffic network analysis. Also, the network should be aggregated, and networks with different aggregate levels can be generated automatically by only adjusting few parameters of the generation method, so that they can be applicated at different scales suitably.

In this paper, we developed a method of generating aggregated road network which is suitable for traffic network analysis directly from vehicle trajectory data. In this method, nodes and links are detected at an aggregated form in advance, and different networks can be generated by considering the traffic volume of probe vehicles. Also, the relationship between the road network generated by proposed method and the real road network was validated.

Methodology

Network generation

The methodology of network generation developed in this study consists of three steps: node detection, link generation, and network reorganization.

A method of detecting nodes by using spatial scan statistics proposed by Zhong et al. (2022) is applied in the node detection step. The area represents a node can be defined as the intersection area where vehicles can select their routes. Considering turning behaviors during route selections, an intersection area can be defined as an area where data dots with large turning angle accumulates.

Once node areas are determined, for each dot of a trajectory, the node or link which it is related to can be determined by checking the node pair $(p_{\mathrm{f}}, p_{\mathrm{b}})$, where p_{f} denotes the last node vehicle passed through before or at that dot and p_b denotes the first node vehicle passed through after or at that dot. We can separate the vehicle trajectory data into each node or link by using the node pair (p_f, p_b) of dots. Dots with the same node pair $(p_{\mathrm{f}}, p_{\mathrm{b}})$ can be considered as the set of fragmental trajectories $D(p_i)$ or $D(e_{ij})$ belong to the node p_i or link e_{ij} of that node pair. If $D(e_{ij}) \neq \emptyset$, then there may exist the link e_{ij}. For each $D(e_{ij})$, traffic characteristic values such as traffic volume q_{ij} of probe vehicles and link length l_{ij} for corresponding link can be easily calculated.

To reorganize the generated road network with different aggregation levels, major links and major nodes are defined by link daily probe traffic volume q (veh/day) and the traffic volume threshold τ_q (veh/day). A major

link is defined as a link with large probe traffic volume, i.e., $q_{ij} > \tau_q$. A major node is defined as a node connected with three or more major links which performs not as an overpass, or a node performs as a dead-end connected with a major link.

Road networks generated by proposed method are called Probe Derived (PD) networks in this paper. Also, we call a PD network which major links and major nodes are defined by τ_q as a PD-τ_q network.

Validation methods

The validation of validity and usefulness of PD road networks are considered from following four aspects: graphical characteristics, correctness of nodes and links, stability of network generation, and the results of shortest path search. Comparison between PD road networks and the real road network is applied for each aspect. We used ETC2.0 data as the real observed trajectory data to generate PD road networks. This vehicle trajectory data was obtained in Tokyo, Japan for three months (July 2021-September 2021). OpenStreetMap (OSM) road network, which was obtained as in September 2022 by using the osmnx module by Boeing (2019), is used as the real road network data.

First, graphical characteristics such as number of nodes and links and link lengths show the level of aggregation in PD networks. In a PD network, which contains only major nodes and major links as well as one intersection appears as only one node, it is expected that it has less nodes and links comparing to existing real road networks. Also, links in PD networks are expected to have a larger length, as small intersections which split roads to several short portions are not expected to exist.

Secondly, the correctness of node means if there is a real intersection geographically or not at where the node exists in PD network. As a node in PD network can also be represented as node areas, it can be checked that whether real road network nodes exist inside the node areas for each node. Meanwhile, the correctness of links can be checked by link lengths from a viewpoint of link performance. The road section between two adjacent intersections always be the shortest path between those two intersections. A link is said to be able to represent real road section if the length of the corresponding shortest path on real road network is the same as the link length on PD network.

Thirdly, if a PD network can represent a real road network uniquely, networks of the same area should be generated in a stable manner even if data is obtained from different dates. That is, the similarity between those two PD networks is expected to be high. The similarity can be evaluated by the Jaccard coefficient. Let E_A and E_B be the sets of links of network A and B respectively. The Jaccard coefficient defined as the size of the intersection divided by the size of the union of E_A and E_B.

Finally, the usefulness of the PD network can be validated by applying shortest path search on the PD network and comparing the results on a real road network. We select origin and destination points randomly from the set of nodes in each PD network, and calculate the shortest path of length by the Dijkstra method. Similarly, on the real road network, the same origin and destination points as in the PD network are used. If the shortest path lengths in the PD network match the corresponding lengths in the real road network, there is a possibility that PD networks are useful for traffic network analysis.

Results

Different PD networks (Figure 1b-1d) perform as different aggregate levels for the real road network (Figure 1a). For PD-10 network, there remains many links which can be considered as aggregations of narrow roads. For PD-100, the shape of the network gets grid-liked, which is more similar to the real road network at normal. Those PD networks with low aggregate level can be used in traffic analysis focus on a part of the road network. As the aggregate level of probe traffic volume gets higher, there only remains links with high traffic volume such as national roads and expressways in the PD-500 network. This kind of PD networks with high aggregate level are suitable for large-scale analysis such as traffic assignment inside a metropolitan area.

Figure 11. Different PD networks and the OSM network

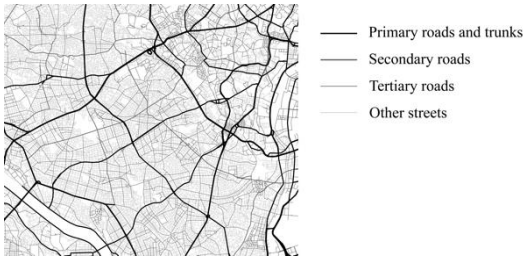

a) *OSM network*

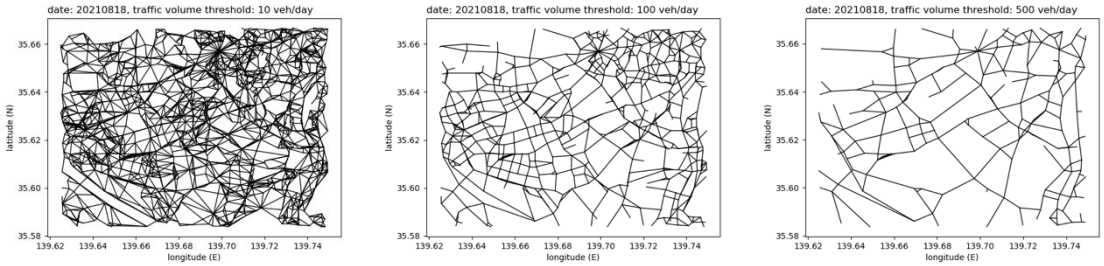

b) *PD-10* ***c)*** *PD-100* ***d)*** *PD-500*

Source: a): OpenStreetMap; b-d): Authors' elaborations.

Table 1. Graphical characteristics of PD and OSM networks

	PD networks			OSM network
	PD-10	PD-100	PD-500	
Number of links	3,136	1,047	319	45,682
Number of nodes	1,025	579	208	30,473
Average link length (m)	417.04	414.87	655.90	58.85

Source: Authors' elaborations.

The graphical characteristics, which includes number of nodes, number of links and link lengths, show that PD networks can be considered as finely aggregated road networks at a viewpoint of nodes and links. The graphical characteristics of PD networks and OSM network are shown in Table 1. There is a large reduction on nodes and links comparing to the OSM network, and the average link length can be considered as the same scale as the length of the road between major intersections in general.

The correctness of nodes and links are confirmed in all generated PD networks. 981 of 1025 (95.7%) nodes in the PD-10 network correspond to intersection nodes of OSM network. And all nodes in PD-100 and PD-500 networks are confirmed to be able to represent real intersections. For most of the links, the lengths on PD networks are close to the lengths of corresponding shortest path on the OSM network. Though the lengths on PD networks tend to be slightly smaller especially on links with curves. This is because link lengths are calculated from the distance of straight line between two data dots, which is smaller than the real travel distance due to the long sampling interval of the ETC2.0 data.

For the stability of network generation, the Jaccard coefficients between two PD networks with same aggregate level can be 0.5-0.6, which means 70-75% of the links are strictly matched when the data is only from one day and obtained from both weekdays or both holidays. The similarity can be a little bit lower otherwise due to the lower traffic volume on holidays than weekdays. A usage of multiple-days data can mitigate this instability. When we use a combined data from more than 5 days, the Jaccard coefficients can be about 0.6-0.8, which means 80-90% of the links are strictly matched.

For the results of the shortest path search (Figure 2), most of the lengths of shortest paths on all PD networks are larger than them on OSM network. The results on PD-10, which includes links represent for narrow roads, however, are closer to the results on OSM network than PD-100 and PD-500. This is mainly because the

searched shortest paths on OSM network including narrow roads which makes a shortcut. PD networks with high aggregate level perform more likely as aggregated networks with only major nodes and links.

Figure 12. Relationship of shortest path lengths between PD and OSM networks

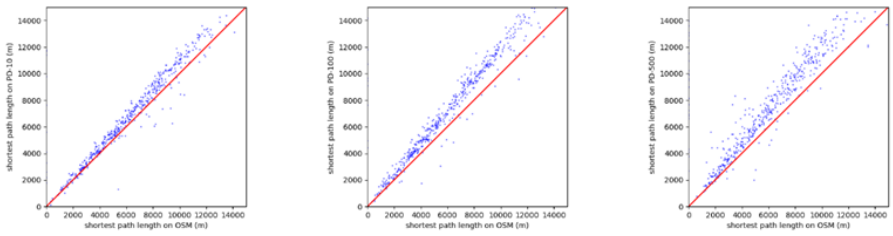

a) *PD-10* ***b)*** *PD-100* ***c)*** *PD-500*

Source: Authors' elaborations.

Conclusion

In this study, we developed a method for generating aggregated road network data from only vehicle trajectory data. As a result of the validations, it was confirmed that PD networks generated by the proposed method are appropriately generated and aggregated. By adjusting the traffic volume threshold, networks with different aggregate levels can be easily generated, which can be applicated in traffic analysis with different scales. A future work of this study is to develop a general method to extract more information. A quantitative method to compare two spatial networks is also expected to be developed for verification.

Acknowledgements

The ETC2.0 data for this study is provided by Tokyo Metropolitan Government through their project called "offering of several datasets on mobility and transportation in Tokyo 2020 Games".

References

Boeing, G., 'Osmnx: New methods for acquiring, constructing, analyzing, and visualizing complex street networks', *Computers, Environment and Urban Systems*, No 65, 2017, pp. 126-139.

Huang, J., Deng, M., Tang, J., Hu, S., Liu, H., Wariyo, S. and He, J., 'Automatic generation of road maps from low quality gps trajectory data via structure learning', In *IEEE Access*, Vol. 6, 2018, pp. 71965–71975.

Tang, J., Deng, M., Huang, J. and Hu, S., 'A novel method for road intersection construction from vehicle trajectory data', In *IEEE Access*, Vol. 7, 2019, pp. 95065–95074.

Yasuda, S., Iryo, T., Sakai, K. and Fukushima, K., 'Data-oriented network aggregation for large-scale network analysis using probe-vehicle trajectories', In *2019 IEEE Intelligent Transportation Systems Conference (ITSC)*, 2019, pp. 1677–1682.

Zhong, H., Nakanishi, W., Yasuda, S. and Iryo, T., 'Extraction of major intersections by only vehicle trajectory data', *Theory and Applications of GIS*, Vol. 30, No 2, 2022, pp.7-18.

The role of the MATSim model in assessing Paratransit performance in a data-scarcity context.

M. Elgohary[a], P. Pucci[a]

[a] *Dipartimento di Architettura e Studi Urbani, Politecnico di Milano*

Introduction

The Multi-Agent Transport Simulation model (MATSim) is an open-source model that simulates population mobility and develops various applications depending on the available data and context. The challenge lies in collecting comprehensive mobility data, especially in developing countries where such data is challenging to create.

Developing countries face more complex mobility patterns. Primarily, public transport cannot meet the mobility demand. Thus, result paratransit. It is a transportation service that supplements public transit systems by providing individualized rides without fixed routes or timetables (Silcock, 1981, p. 152). In Merriam-Webster, Paratransit is a transportation service that supplements larger public transit systems by providing individualized rides without fixed routes or timetables. (Merriam-Webster, 2023).

This study aims to provide a novel approach to modeling Paratransit in Alexandria, Egypt, considering the context of limited data availability. The researcher aims to identify the most pertinent stop-over points required for Paratransit services. By achieving this, they aim to improve Paratransit traffic without significantly altering the inherent nature of self-organized mobility.

Figure 13. Research framework

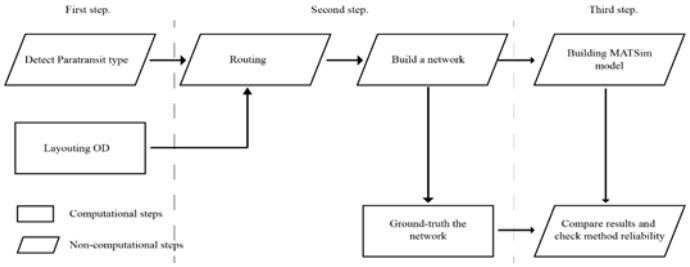

Source: Authors' elaborations.

Methodology

The model of the paratransit will consist of a fine-grained mixture of computational and non-computational steps, where data will be generated consonantly via computational tools and aligned/always justified with different shades of human interventions, as stated in Figure 1.

The methodology employed in this study involves a combination of computational calculations and human calibration to achieve accurate results. Understanding the movement patterns of minibusses in Alexandria and identifying the corresponding Paratransit route patterns are key initial steps in this research.

Minibus Origin-Destination Matrix

The first step in modeling the paratransit network begins with determining the start and end points of the routes, which remain consistent despite the flexibility for drivers to make changes during trips due to traffic conditions and several emerging conditions. The traditional routes primarily follow main corridors, prioritizing areas with high passenger demand for boarding and alighting. The study focuses on mapping the fixed stops and connecting them based on the presence of active buses traveling between

Figure 14. Minibuses OD matrix in Alexandria

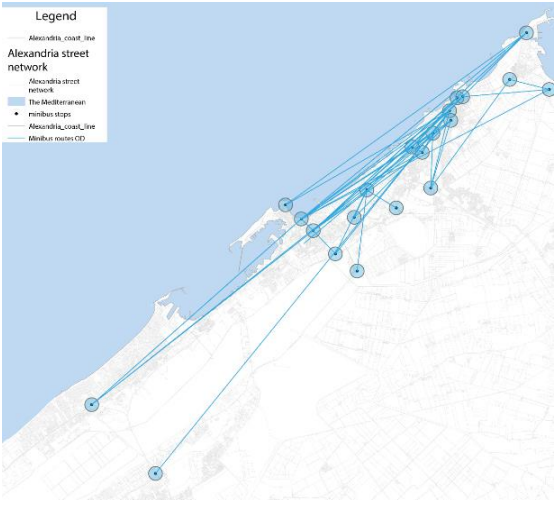

Source: Author elaboration based on OSM data.

the stations, assigning weights to each minibus station based on the number of accessible destinations. Most of the stops are in the eastern part of the city. The hubs serve several destinations. The central hubs have up to 12 destinations, while hubs on the edge of the study are linked to one or two stations, as illustrated in Fig.2.

Routing Alexandria's minibusses

Minibusses' routes are flexible; the driver can change routes before or during the trip. These changes can be due to traffic jams or traffic ambushes. However, the roots' beginning and ending remain unchanged despite the demonstrated flexibility. The traditional routes take place on the main corridors in the city as these roots should not always be the shortest distance in the route network, but drivers tend to take routes where there is a high possibility for passengers to get in and off the vehicle.

Based on this nature and to draw the minibus lines, it was crucial to use a navigation network containing street directions and geometry for this ESRI Streetmap was a helpful base model for minibus routes. However, the network solver understood only the shortest distance between two points, so adding anchor points along that quarter was crucial for the simulation engine to model a close-to-reality route profile.

ESRI Streetmap premium is a navigation network; a Navigation network is a street network with optimized street segmentation; It is used for a quick navigation process. However, the low segmentation triggered an incompatibility between the output routes and the OSM network, as the two networks were created for different reasons. As a result, a manual alignment of the routes was conducted to ensure all future analyses would be based on a route network closer to reality.

Figure 15. Routing Alexandria's minibus routes

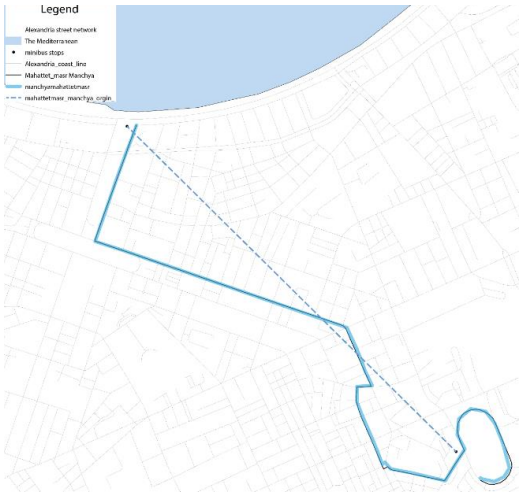

Source: Authors based on ESRI's streetmap premium and OSM data.

Building the network

The result of route modeling is 62 minibus routes connecting 23 main minibus stations with a total length of 934 km in eastern Alexandria. The modeled routes correspond to the OSM network, as the data could be integrated with the OSM platform.

It was crucial to design its Meta data to use best the network(Kitchin & Lauriault, 2018, p. 2). Metadata is data about data that facilitates its use, such as data definitions, provenance, and lineage.

The General Transit Feed Specification (GTFS) is the most standardized mobility data protocol that organizes transit data. The Standards were difficult to be replicated completely to the Paratransit model. Nonetheless, the Paratransit database mimicked the GTFS protocol to facilitate using the data as per indicated in Table 1

Table 3. A sample of Minibus metadata

Start Station	Destination Station	Short name	Long name
Abuquir	Mahattet_Mast	m01	abuquir > mahattet_masr
Mahattet_Mast	Abuquir	m01r	mahattet_masr > abuquir

Source: Authors' elaborations.

Building MATSim model

The model was constructed to measure the demand on Minibuses in the study context; as Alexandria is a data-scarcity context, the model relies primarily on open-source data. Initial demands were constructed based on Meta's OD matrix (Maas et al., 2019), and Street networks were constructed based on OSM data converted later to MATSim-like data through (Neumann & Zilske, 2016) add-in. At the same time, the Minibus data were decoded and integrated manually with the MATSim different files.

The model also pays attention to non-spatial urban mobility attributes like the cost of trips, normal working hours, and waiting time. The model tries to mimic the business-as-usual scenario to mimic the demand on the minibus route. Based on the GPS trajectories, the stop-overs have an average distance of 100 meters between

each other. According to this, the minibus routes were divided into stations every 100 meters inside the MATSim model. This should measure sensitively the boarding in and off behavior in the mobility scenario.

Figure 16. The change of boarding behaviour on route

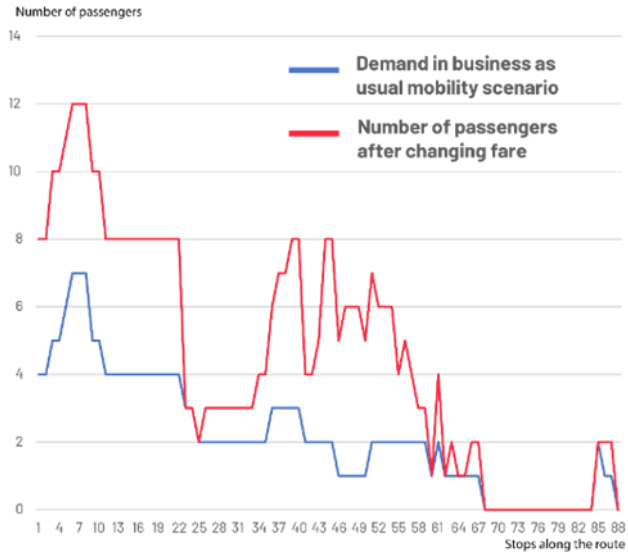

Results

The model aims to spot the most sensitive points along the paratransit routes, and based on an evidence-based methodology, planners can understand where to allocate a proper infrastructure that could correspond to minibus stop-over along routes.

Thanks to the flexibility of the MATSim model, the results will be tested under different Urban mobility changes. For this study case, the authors changed the price of minibus fare and made the price per kilometer ten times cheaper than the car's price/km. The main aim behind this change is to compare the demand on a minibus line and understand where stop-overs could be allocated along the line.

The results underline the mutation of dropping in and off along the minibus route as the demand increases at the beginning of the trip. The station illustrates a sharp decline in the number of passengers. That declination is followed by a short steady supply/demand along the line, followed by a fluctuation till demand decays near the end of the line.

Figure 4 outlines the optionality of designing a permanent stop-over where the change in supply/demand is significant, while more humble stop-overs could be created based on the micro-trends on the microscopic pattern. This evidence-based approach enables planners to test several mobility scenarios and draft mobility policies based on the quality of the data they feed to the model.

Figure 17. Dropping in and off for minibus route Assafrah to- Haddara.

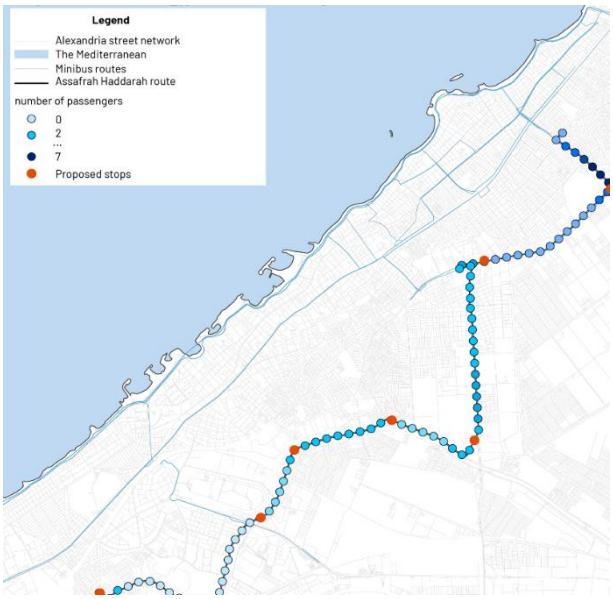

Source: Authors' elaborations based on MATSim Simulation results.

However, the results are very subjective to the case study and focus mainly on the minibus modeling inside the MATSim model; results could correspond more to reality if Public transport supply, detailed census data, and Urban mobility Agenda data were available for public use. Nonetheless, results remain primarily and subject to improvement upon the availability of relevant data.

References

Andreas, N. (2014). *A paratransit-inspired evolutionary process for public transit network design*.

Axhausen, K. W. (2016). *The Multi-Agent Transport Simulation MATSim* (A. Horni & K. Nagel, Eds.). Ubiquity Press. https://doi.org/10.5334/baw

Kitchin, R., & Lauriault, T. (2018). *Digital data and data infrastructures*.

Maas, P., Iyer, S., Gros, A., Park, W., McGorman, L., Nayak, C., & Dow, P. A. (2019). *Facebook Disaster Maps: Aggregate Insights for Crisis Response & Recovery*. KDD, 19(3173).

MATSim.org. (2023). *MATSim's Scenario Gallery*. MATSim.Org. https://www.matsim.org/gallery/

Merriam-Webster. (2023, February 3). *Paratransit Definition & Meaning - Merriam-Webster*. Merriam-Webster. https://www.merriam-webster.com/dictionary/paratransit

Neumann, A., & Zilske, M. (2016). MATSim JOSMNetwork Editor. In *The Multi-Agent Transport Simulation MATSim* (pp. 65–66). Ubiquity Press. https://doi.org/10.5334/baw.8

Silcock, D. T. (1981). Urban paratransit in the developing world: Foreign summaries. *Transport Reviews, 1*(2), 151–168. https://doi.org/10.1080/01441648108716456

A smartphone-based mobility survey feeding the implementation of the Harmony Model Suite in Turin

F. Fermi[a], F. Chirico[a], A. Martino[a], I. Tsouros[b], A. Tsirimpa[c], M. Kamargianni[d]

[a] *TRT Trasporti e Territorio, via Rutilia 10/8, Milan 20141 (Italy)*

[b] *TransDeM Lab, University of the Aegean, Korai 2A, 82100, Chios (Greece)*

[c] *MOBY X Software, Anexartisias & Athinwn Street, Limassol 3040 (Cyprus)*

[d] *MaaSLab, University College London (UCL), 14 Upper Woburn Place, WC1H0NN, London (UK)*

Introduction

With the advent of emerging technology and mobility services aimed at a sustainable transition to a low-carbon and new age of mobility, city authorities are confronted with the task of integrating new mobility services with the existing plans for land use and transport. In regional and urban policy making, the value of integrated spatial and transport planning arises from the profoundly interdependent relationship between land-use, transport demand and transport supply.

The HARMONY Model Suite (HMS) offers a new generation of harmonized spatial and multimodal transport planning tools that comprehensively model the evolving dynamics of the transport and spatial organizations, enabling the authorities of the metropolitan area to sustainably lead the transition to a new age of low-carbon mobility. The HMS is a multi-scale, software-agnostic, integrated activity-based model framework enabling end-users to link independent models and analyse a portfolio of regional and urban interventions[2] for both passenger and freight mobility by integrating land-use models (strategic/long-term), people and freight activity-based models (tactical/mid-term), and multimodal network (operational/short-term) models allowing for vertical planning. The key aim of the model system's architecture is to allow for the assessment of such initiatives in terms of their effect on land use, economic development, transportation networks, electricity, vehicular noise, GHG and air pollutant emissions.

One of the pilot cities where the HMS has been applied is Turin (IT), to test scenarios aimed at rebalancing the demand for transport between collective and individual, in order to reduce congestion and improve the accessibility to the various urban functions.

Methodology and results

The HARMONY Model Suite application in Turin involved several modelling components at different level. The main template applied for the simulations is related to the tactical and operational levels, linked with some models of the strategic level. These models consist of: i) a population model, that generates the total population disaggregated into age-sex cohorts that define the overall size of the city systems in question; ii) a synthetic population model to translate into more disaggregated population the data from population model; iii) a long-term household and individual vehicle choice model, to estimate vehicle ownership and mobility services subscriptions; iv) a tactical activity-based passenger model, that takes inputs from the aggregate economic and demographic forecasting models and estimates passenger' choices on a day-to-day level; v) a passenger network traffic assignment model, to load passenger demand into different types of networks; vi) an energy and emission model, to estimate energy consumption and air pollutant emissions related to passenger mobility patterns in the metropolitan area. These models interact with each other, exchanging data as shown in Figure 1.

The core of the template is the Activity Based Model which consists in the Tactical Passenger Simulator and which requires to collect a multitude of diverse and difficult data, with activity and travel diaries being the most problematic to acquire. Travel and activity diaries, which usually take a significant amount of time and concentration to fill-in, put a significant burden on the survey respondent and are usually costly and prone to errors such as under reporting (Bricka and Bhat, 2006). The approach followed in the Harmony project was to utilize mobile phones to assist in the data collection process (Prelipcean et al., 2018; Pronello and Kumawat (2020). Specifically, the development in technology and data fusion enables close communication to the respondents in surveys, decreased respondent burden, and increased amount and quality of information (Polydoropoulou et al., 2013 or Matyas, M., & Kamargianni, M. 2019).

Figure 18. Template of Strategic-tactical and operational Model Suite for Turin

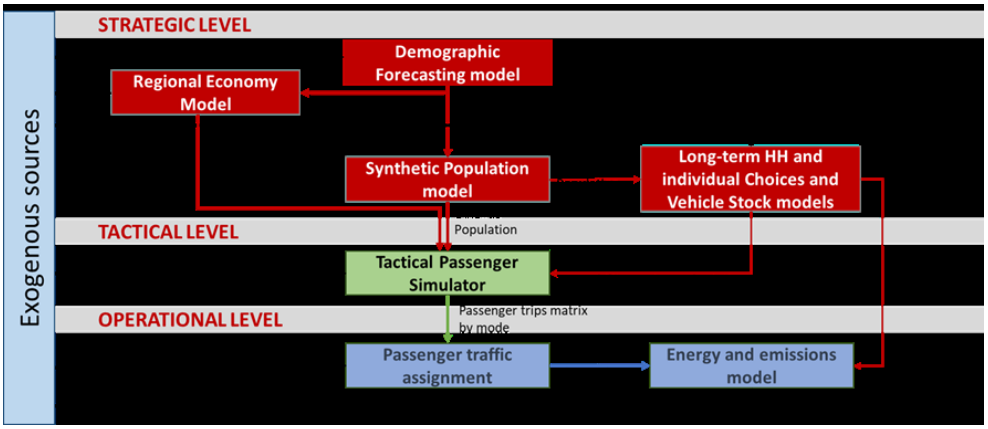

The travel survey making use of MobyApp in Turin Functional Urban Area (which includes the city of Turin as well as other 87 surrounding municipalities) was originally planned for autumn 2020, but the COVID-19 pandemic forced to delay until February 2022. The survey specialist company IPSOS was engaged to select a representative sample (around 600 persons) based on pre-defined criteria. A first criterion was that the sample should consist of individuals distributed throughout the whole Turin FUA, proportionally to population living in different zones. Further criterion was the stratification according to Gender; Age; Occupation and Number of cars available in the household.

The first part of the survey aimed at collecting preliminary information on individuals and on its mobility habits. The second and main part concerned the collection of information on individual daily trips: origin, destination, duration, purpose, mode of transport. In the third part, Stated Preference (SP) questions were asked, based on the mobility behaviour registered in the first section and focused on: Dynamic Travel Behaviour, Mode Choice, Mobility Tool Ownership, and Remote Working. The data collection was managed via the Survey Integrated Platform which consists of four key technology components: i) the Admin App, which creates and sets up all the surveys based on the needs of the client; ii) the Client App, which provides a survey management tool to those who organise the survey (the clients of MOBY X) to supervise the progress of the survey and check key statistics of the collected data via infographics; iii) the Smartphone App (Android and iOS) that collects raw data, such as GPS, GSM, Wi-Fi and accelerometer. Also, it enables users to see their activities/trip diary via the App; and iv) the Server that stores the collected data as well as contextual databases and processes it using machine learning algorithms to detect trips and stops and infer activities.

Figure 19. The smartphone application of the Moby App platform

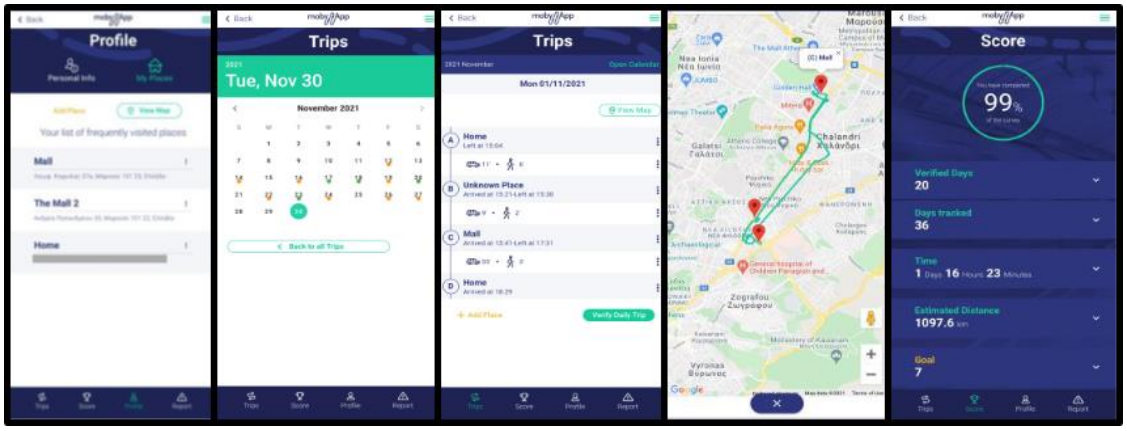

Each participant to the survey had to login and fill in the Introductory Questionnaire (a mandatory step) in order to collect some basic information on the mobility attitude of the users. Once these steps were completed, the MobyApp started to track the trips and the places visited by the user. The application collected time and duration of the trips, transport modes used, and time spent, recording up to 5 different transport modes within the same trip. The application automatically recognized trips, transport modes and visited places by associating travel features (especially speed and acceleration) to a transport mode. Nevertheless, the user' validation was always needed to confirm the transport mode used in those cases where it was not possible for the application to

automatically distinguish, for example, private cars and taxi. Additional information was gathered as well during the validation phase, such as the number of people travelling with the user, the type of vehicle (private or shared), parking information, etc.

Figure 20. Survey results: Modal share in the Functional Urban Area of Turin

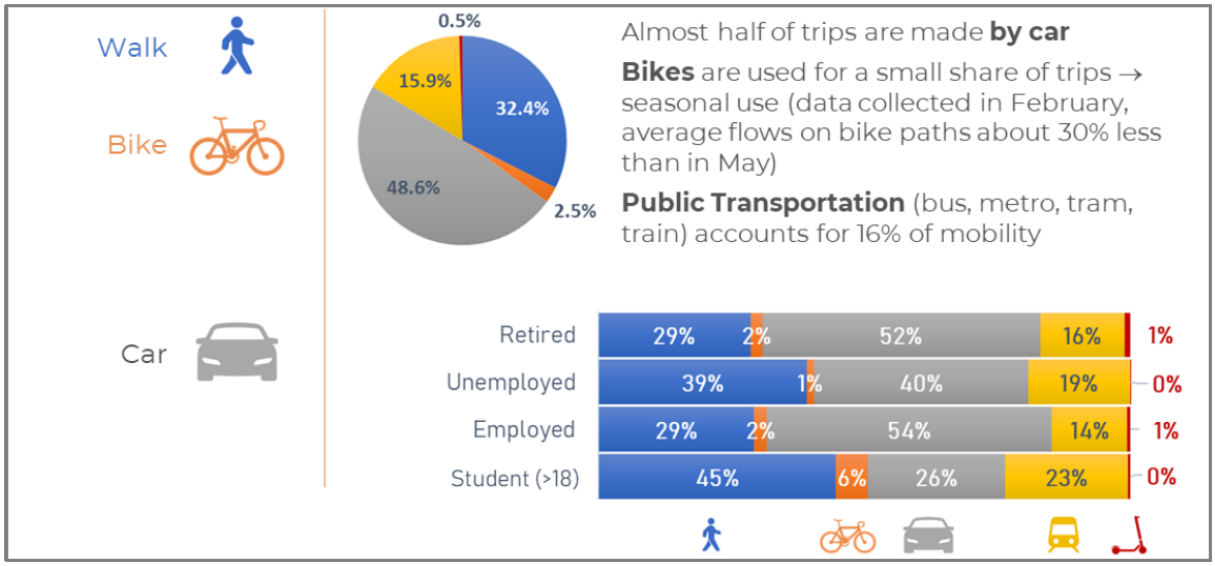

The data provided by the mobility survey were used as key input of the Harmony Model Suite application in the Turin FUA. The different scenarios considered incisive mobility policies, pushing the collective transport use through large infrastructure investments (such as the underground extension and the metropolitan railway service) and through new ITS based mobility services, as well as measures considering remote working and urban vehicle access regulation.

The first use case relied on the SUMP reference scenario and was designed to simulate selected land use developments and new public transport infrastructures planned to be in place at the projection year 2030. This was the basis also for the other three: the second one aimed at promoting the integration of public transport (urban and inter-urban) with shared mobility services (car, bike, e-scooters and mopeds); the third one tested the impacts of changes in mobility patterns of individuals, as a result of the diffusion of remote working and revised activity schedule (albeit less intensely than at the pandemic peak) and eventually the fourth one concerned the introduction of Urban Vehicles Access Regulation measures, considering both traffic calming and Low Emission Zone.

The four use cases were simulated with the modelling components of the HMS. The impacts have been analysed in terms of several output indicators, such as mode split, transport demand, accessibility, GHG and air pollutant emissions, energy consumption.

Conclusions

The integrated usage of the MOBYapp and HARMONY MS demonstrated some significant advantages over traditional ways of integrating travel and activity diary data with model systems but also some barriers and technical difficulties. The streamlining of the MOBY app data to the Activity Based ABM pipeline was smooth, with expected delays in data cleaning and processing. The process is far from automated, apart from regular data cleaning algorithms, specific, human-driven data correction and algorithms need to be put in place to remove GPS errors, duplicates in the database and to improve mode and activity prediction. The effort of the user is imperative to acquiring useful and cleaner data, and it is important to stress the effect of incentives or rewards in the process of data collection and sample recruitment in order to motivate survey respondent to verify their trips and activities.

The modular and flexible deployment of the HARMONY MS ABM proved to be useful for the use-cases investigated in Turin. The use-cases allowed to use several modelling components of the HARMONY MS in an integrated way, providing interesting results through the analysis of key performance indicators ranging from transport to socio-economic and environmental topics.

Acknowledgement

The HARMONY research project (Nº815269) was funded by the H2020 Research and Innovation Programme of the European Commission.

References

Bricka, S., & Bhat, C. R. (2006). Comparative analysis of Global Positioning System–based and travel survey–based data. Transportation Research Record, 1972(1), 9-20.

Matyas, M., & Kamargianni, M. (2019). 'Survey design for exploring demand for Mobility as a Service plans'. Transportation, 46(5), 1525–1558. https://doi.org/10.1007/s11116-018-9938-8

Polydoropoulou, A., Goulias, K. G., Tsirimpa, A., Kamargianni, M., Kourounioti, I., & Tsouros, I. (2013). Innovative data collection for modeling green transport in islands. 17.

Prelipcean, A. C., Susilo, Y. O., & Gidófalvi, G. (2018). 'Collecting travel diaries: Current state of the art, best practices, and future research directions'. Transportation Research Procedia, 32, 155-166.

Pronello, C., & Kumawat, P. (2020, September). 'Smartphone applications developed to collect mobility data: A review and SWOT analysis'. In Proceedings of SAI Intelligent Systems Conference (pp. 449-467). Springer, Cham.

Tsouros I. et al. 'The HARMONY Model Suite application in Turin: activity-based modelling supported by smartphone-based travel survey' submitted to World Conference on Transport Research - WCTR 2023 Montreal 17-21 July 2023.

Using GBFS-Data to identify user behaviour at urban mobility hubs for transport modelling

Jan Weschke[a]

[a]*Institut für Verkehrsforschung Deutsches Zentrum für Luft- und Raumfahrt Rudower Chaussee 7, 12489 Berlin, Germany*

Introduction

To date, most existing transport demand models incorporate only conventional transport modes like driving, public transport, cycling or walking. However, in recent times, multimodal and intermodal behaviour as well as new mobility modes like ridehailing, carsharing or e-scooter sharing changed mobility behaviour, especially in urban areas. Nevertheless, accounting for this behaviour in transport models is still at the beginning. One reason is the missing empirical knowledge on how those new transport modes and opportunities impact user behaviour. This research therefore focusses on gaining knowledge on the usage of bike sharing, and in particular on gaining knowledge on user behaviour at mobility hubs (multimodal stations, placed next to public transport stations that offers various forms of first and last mile mobility options). This is done by using the data source of the General Bikeshare Feed Specification (GBFS) gathered through APIs provided by shared mobility operators for transportation research.

In the following, this paper explains the data acquisition process of this new data source, the data cleaning process and moreover, how this empirical usage data can be analysed and used for transportation research and modelling. For this reason, usage data of a bike sharing system in Berlin is used and analysed with focus on usage at mobility hubs.

Methods and Data

For most bike sharing and also e-scooter sharing systems, live data is available in the GBFS-Format. Those data include information on the vehicles and its characteristics as well as current locations, stations and their availability as well as system pricing (GBFS, 2022). While its main purpose is to make information available for public transport applications or MaaS applications, those data can also be used for transport research to analyse the usage of the system.

When sending a request to a GBFS-API, the GBFS-API used here is from Nextbike in the city of Berlin, Germany (Nextbike, 2022), data on all available vehicles as well as on the stations will be returned. All available vehicles mean that all those vehicles, which are available to rent for a user are displayed. This vehicle information contains a unique id, the bike number, as well as the geolocation of the vehicle and if it is docked to a station. As the bike sharing system in Berlin is a hybrid system, bikes can also be returned outside of station in a free-floating area. Together with the timestamp of the request, this gives a single snapshot on all available vehicles in one city. From this data, it is possible to identify the bike distribution, potential cluster or underserved areas. However, this information is limited to the single time of observation, which cannot give the full picture. Consequently, when regularly sending a request to the GBFS-API, multiple timestamps of observations will be available. By fusing this data together, it can be used to identify usage patterns and bike distributions also over time. One step further, when time between two requests shrinking, it will be even possible to identify movements of vehicles as they disappear, when rented to a user and reappear, when returned. However, identifying movements and especially trips comes with multiple difficulties as not every movement is a user trip (e.g. redistributions) and furthermore, the time between two requests is crucial in order to track the movements correctly. While in recent literature some approaches relied on comparable data requested through APIs, those are either limited by their request interval or their time period of observation, as regularly requesting and saving all information is very data intense (Reck et al., 2021; Radzimski and Dzięcielski, 2021; Li et al. 2022).

For the present paper I collected the data through the GBFS-API over the first nine months of the year 2022 performing a request about every two minutes. From this vehicle location data over the full time period, multiple analysis is done. First, movements of the vehicles are calculated by observing the unique bike id over time as previously explained. To identify which movements counts as trips, the classification shown in table 1 is used here to process the data. Second, to identify the influence of the request interval on the number of trips recorded, movements and trip classification were additionally calculated mocking different longer request intervals. This shows then, the impact of the time interval on the results. Third, the trip data is analysed in terms of the user behaviour at mobility hubs. This is to enrich scare literature on mobility hubs (e.g. Weustenenk and Mingardo, 2023) but also to present a hands-on example for the insights through this data source.

Table 4. Characteristics to identify movements as trips

Variable	Minimum Value	Maximum Value
Distance (great circle)	200 Meter	20,000 Meter
Average speed	3 km/h	20 km/h
Trip duration	1 Minute	60 Minutes

Results

First of all, results on the impact on trip counts depending on the used research interval is presented in figure 1. For the analysis, daily trip counts were calculated over one month with request intervals of 2, 4, 6, 8, and 10 minutes. From this analysis it is striking that the time interval between two requests, linearly reduces the number of trips that are logged by requesting the API. This has a practical implication for the usage of GBFS-data for transport research as it is clearly shown, that trip data accuracy reduces a lot when request intervals are too long.

In terms of insights into mobility behaviour, based on the calculated trip data for the year 2022, general trip demand for bike sharing for different time intervals can be identified. For example, figure 2 shows the number of trips starting at multimodal mobility hubs in Berlin per day over the course of the first nine months of the year 2022. From this, it can be seen that trips are lower in winter and spring but stay pretty much constant over the summer. In addition, the graph shows a maximum of 80 trips per day which translates into less than 2 trips per day per station, given the number of 53 mobility hubs available. From this, it can be very much concluded that the mobility hubs are, at least for bike sharing, not much used. Further analysis gives insights into daily trip patterns at mobility hubs in terms of daily variation of trips starting or ending at stations showed in figure 3 as well as insights into destinations reached from the mobility hubs presented in figure 4. Those can then give information about intermodal usage of bike sharing. Figure 3 with the number of trips starting, summed together for all mobility hubs, shows that bikes are especially rented in the afternoon with the peak in between 18:00 and 19:00. In contrast to overall mobility behaviour, the data shows that there is no real morning peak. Figure 4 presents then the destinations of bike trips starting at four selected mobility hubs. Those hubs are all outside the inner city and are located at an urban rail or metro station. The destination analysis reveals then that most trips are performed into the inner city and not to local destinations around the hubs, indicating that bikes from mobility hubs are not used as last mile but rather as substitute for public transport.

Figure 21. Trips recorded over one month depending on the request interval

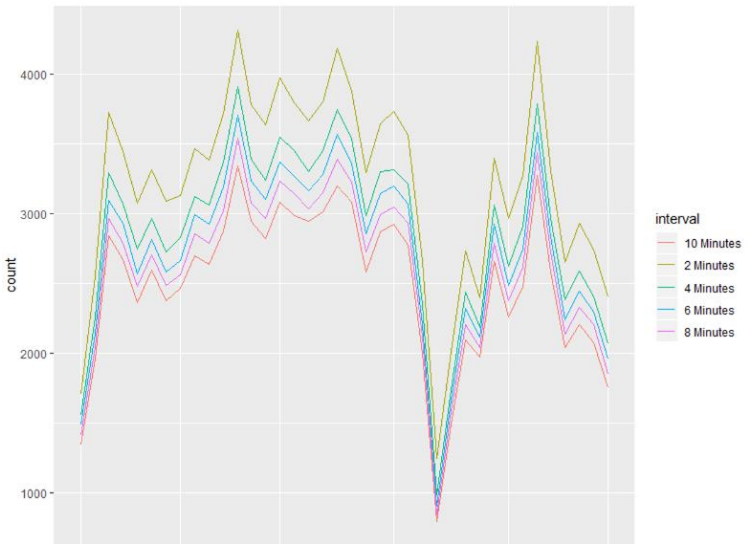

Figure 22. Trips per day in 2022

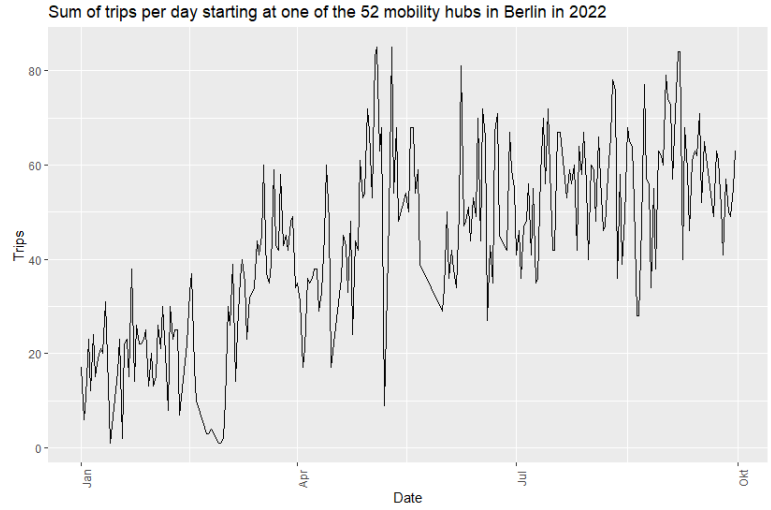

Figure 23. Destinations from trips starting at mobility hubs

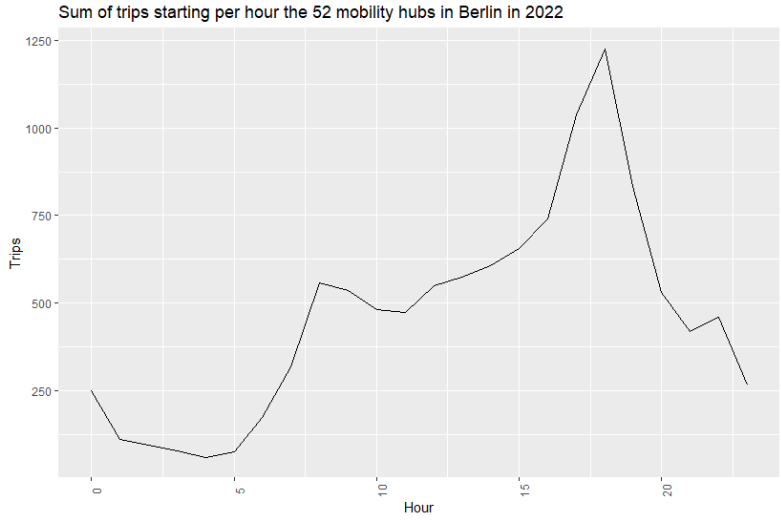

Figure 24. Destinations from trips starting at mobility hubs

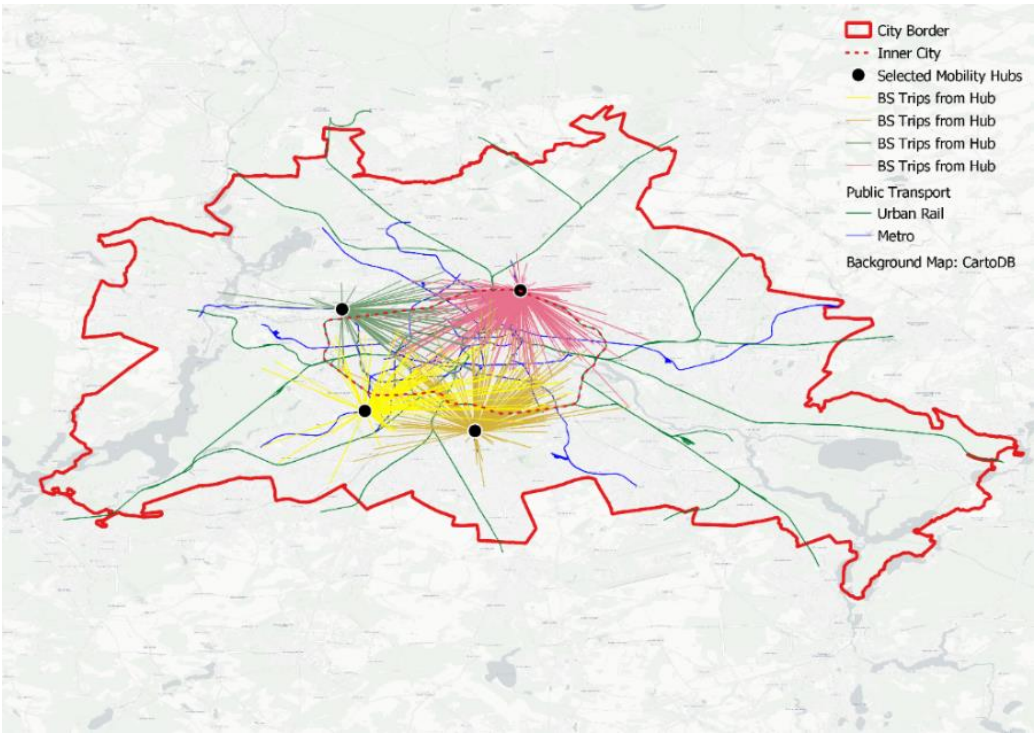

Source: Author's representation, Background Map: CartoDB.

Conclusion

All in all, the presented research presents the opportunities that are given through the usage of GBFS-data in the transport research and transport modelling field. The gathered data give valuable insights into the usage of shared bicycles, user behaviour and, in this case, the impacts of urban mobility hubs. Consequently, this contribution aims at presenting challenges, learnings but in particular the possibilities that new data sources like GBFS-data opens for the field by one the one hand presenting insights from the processing (request interval) but at the other hand gives also an example of the practical usage for mobility research at the example of mobility hubs.

References

GBFS (2022): https://gbfs.mobilitydata.org/

Li, A., Zhao, P., Liu, X., Mansourian, A., Axhausen, K. W., & Qu, X. (2022). Comprehensive comparison of e-scooter sharing mobility: Evidence from 30 European cities. Transportation Research Part D: Transport and Environment, 105, 103229.

Nextbike GBFS-API (2022): https://gbfs.nextbike.net/maps/gbfs/v2/nextbike_bn/gbfs.json

Radzimski, A., & Dzięcielski, M. (2021). Exploring the relationship between bike-sharing and public transport in Poznań, Poland. *Transportation research part A: Policy and Practice*, 145, 189-202.

Reck, D. J., Haitao, H., Guidon, S., & Axhausen, K. W. (2021). Explaining shared micromobility usage, competition and mode choice by modelling empirical data from Zurich, Switzerland. *Transportation Research Part C: Emerging Technologies*, 124, 102947.

Weustenenk, A. G., & Mingardo, G. (2023). Towards a typology of mobility hubs. *Journal of Transport Geography,* 106, 103514.

A deep learning framework to generate synthetic mobility data

E. Arkangil[a], M. Yildirimoglu[a], J. Kima, C. Prato[b]

[a] *The University of Queensland, School of Civil Engineering*

[b] *University of Leeds, School of Civil Engineering*

Synthetic datasets are useful when real-world data is limited or unavailable. They can be used in transport simulation modelsto predict travel behavior or estimate demand for transportation services. However, building these models requires large amounts of data. We propose a novel framework to generate a synthetic population with trip chains using a combination of generative adversarial network (GAN) with recurrent neural network (RNN). Our model is compared with other recent methods, such as Composite Travel Generative Adversarial Networks for Tabular and Sequential Population Synthesis (CTGAN) and shows improved results in predicting trip distributions. The model is evaluated using multiple assessment metrics to gauge its performance and accuracy.

Estimating the impact of traffic congestion on noise emissions using vehicle trajectory data from UAS

M. Barmpounakis[a], J.Espadaler Clapes[a], N. Geroliminis[a]

[a] *LUTS, ENAC, EPFL*

Abstract - In modern cities, excessive noise from traffic has a detrimental effect on people's health since it can lead to physical stress, cardiovascular disorders, and sleep disturbances, among other things. In this paper, we estimate noise emissions in Athens, Greece using detailed trajectory data collected from a swarm of drones. We use a basic sound propagation model and the CNOSSOS-EU model. We first estimate the noise level at bus stops and then measure the contribution of heavy vehicles to the overall noise. Then, we investigate both microscopic and macroscopic noise levels. The results reveal that the mean speed is unable to forecast the aggregated equivalent continuous sound levels, even though they exhibit a distinct pattern with accumulation.

Category 2. Innovative research methodologies

A new methodology for sampling traffic scenarios using *a priori* critical index of functional scenarios

H. Blache[a], P. Laharotte[a], N. El Faouzi[a]

[a] *Univ. Gustave Eiffel, Univ. Lyon, ENTPE, LICIT-ECO7 UMR T9401,F-69675, Lyon (France)*

Introduction

The implementation of Automated and Connected Vehicle systems on the road while ensuring its safety is now a major challenge in the transportation field. Nevertheless, depending on the strategies adopted, their deployment can take a considerable amount of time [1], which challenges their rapid implementation. Thus, the reduction of the number of testing scenarios is one of the major issues today in the context of certification and validation for new intelligent transport systems. Multiple approaches were developed to design testing process for CAV. While the *distance-based* approach [2] remains naive and inefficient, a competitive approach raised in the literature is the scenarios-based approach. The *distance-based* approach consists in driving a vehicle on the road until the validation is reached, i.e., a sufficient variety of situations is met by the vehicle under test. In contrast, the scenarios-based approaches develop methodologies to directly guide the vehicle toward relevant scenarios. Nowadays, it should be noted that some exploratory work has been done to identify and/or reduce the scenarios [3-4]. However, to the best of our knowledge, there is no procedure in the current literature to analyse and drastically reduce a multitude of scenarios in order to evaluate them. The objective is therefore to identify, group and reduce the scenarios to be tested. The innovative approach proposes simultaneously to reduce the abstract layer of scenarios (**functional scenarios**) to be tested and analyse them a priori in order to propose experience plans exhaustively covering the scope of possibilities.

Methodology

The overall methodology is summarized in Fig.1 and broken down into 6 steps:

1. **Step 1 - Generation of functional scenarios by an ontology:** it concerns the process of defining an ontology and the exhaustive set of functional scenarios using this ontology;
2. **Step 2 - Criticality qualification of a subset of Functional Scenarios:** it focuses on the data processing that will assign a criticality distribution to the functional scenarios, then a critical index.
3. **Step 3 - Extraction of underlying and latent relationship between ontology attributes and criticality index of functional scenarios:** based on the Latent Dirichlet Allocation (LDA) [5] clustering process, some underlying topics and clusters are generated and enable to associate criticality index degree to ontology attributes generating functional scenarios.
4. **Step 4 - Generalisation of the underlying features to qualify any functional scenario:** based on a partial least square method, the reconstruction process takes advantage of the formulation of the underlying topics resulting from LDA to predict *a priori* the criticality of any new functional scenario.
5. **Step 5 - Clustering of scenarios between semantic and criticality terms:** based on hierarchical ascendant classification (HAC), the functional scenarios are classified based on the difference between the Euclidean distance of the words versus the a priori criticality difference of the scenarios. For each scenario i and scenario j, the distance equal to:

$$Dist(i,k) = \frac{Dist_{word}\ (i,k)}{Diff_{criticity}(i,k)}$$

   where $Dist_{word}(i,k)$ is the Euclidean distance of the scenario binary vector i and j, and $Diff_{criticity}(i,k)$ is the difference in criticality between scenario i and j.

6. **Step 6 - Reduction of the number of functional scenarios in each cluster:** Selection of representative scenarios for each group in terms of scenario criticality and word representation.

Figure 25. Methodology of reduction of scenarios in 6 steps

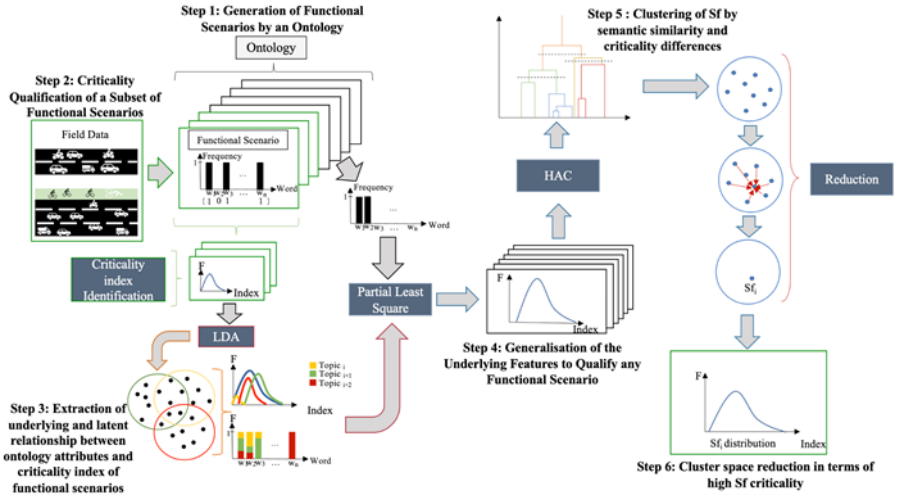

Results

Representation of a functional scenario

Fig.2 shows an example of a scenario generated with the ontology. This ontology generates a scenario in 5 layers (all independent). Layer 5 represents the weather, Layer 4 represents the dynamic and static objects, Layer 3 represents the temporal changes (e.g., road works), Layer 2 represents the road infrastructure and Layer 1 represents the road topology. In addition, the vehicle objective is added to the scenarios that sets up its starting point of arrival and its ending point.

Figure 26. 5-layer representation of functional scenario

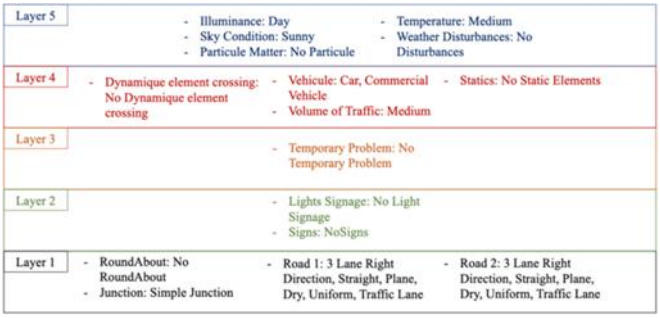

Latent Dirichlet Allocation Results

The results of the LDA can be seen in Fig.3. According to the elbow method, we find an optimal number of topics equal to 5 (for 36 scenarios). Each topic can be interpreted as the distribution of a "typical" functional scenario with its own criticality index. For example, a very critical "Sf" and a less critical one. Another convincing result is the distribution of topics in each Sf, this is interpreted by the contribution of a more or less critical topic in each Sf.

Figure 27. Latent Dirichlet Allocation results:(a) topic distribution (b) topics distribution in each functional scenario

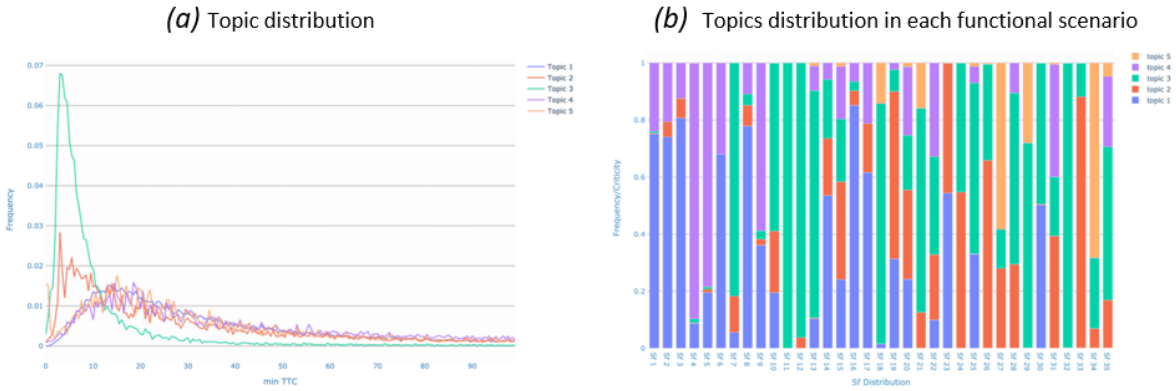

Partial Least Mean Square Results (Reconstruction)

Fig 4 illustrates the gap between a priori estimated criticality indices and observed values drawn from field test data. We compared our model with two other methods, a classical KNN method and a least squares method. In addition, Table I shows the different performance indices. First, using the R2, we notice that the two least squares methods perform better than the KNN method. However, the classical least squares method underestimates the high criticality index scenarios contrary to our model.

Figure 28. Comparison of the reconstructed criticality with the real indices of 3 methods (LDA + Partial Square in red, LDA + Least Square in blue, KNN in green)

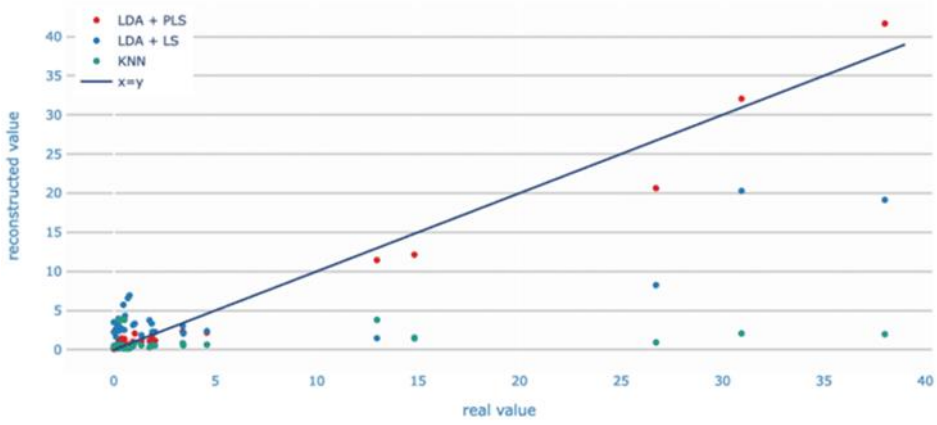

Table 5. Performance index of the reconstruction

Index	LDA+PLS	KNN	LDA+LS
RMSE	1,47	9,34	6,15
Max Error	6,09	36,02	18,86
R2	0,97	0,08	0,53

Clustering and reduction of functional scenario

Fig.5 shows the results of our strategy to select the most critical scenario. This method is compared with two other methods: random drawing of the same number of scenarios and drawing of the most critical scenarios

corresponding to the same number of scenarios drawn in our method. We can see that even though the maximum tragedy allows us to cover a little more overall criticality, our method enables better coverage of all the words of our scenarios, i.e., the scope of possibilities.

Figure 29. Result of clustering and reduction

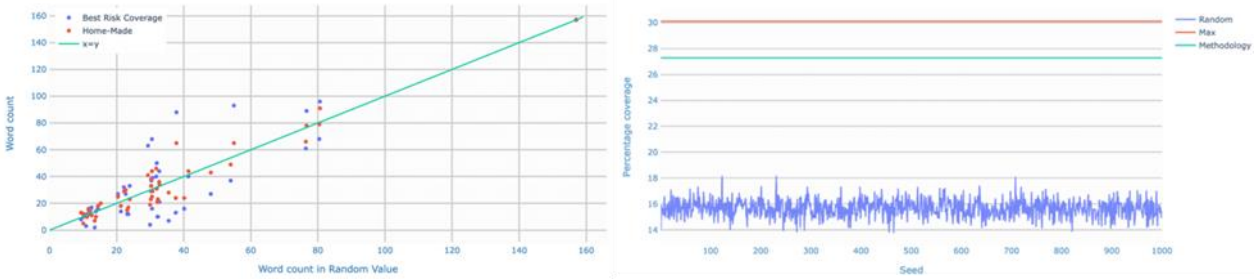

Conclusion

This new reduction methodology has potential in several ways. First, unlike many functional scenario generations, the emphasis is on the stochastic aspect of the words to be more in line with the philosophies of the simulation tools (e.g., the travel demand profile). The a priori generation of new functional scenarios difficult to observe in the field does not emerge in the literature despite its potential. The choice of reducing the most critical scenario of a group seems relevant in view of the diversity of the scenario but also of its potential hazard, compared to other approaches.

Nevertheless, this approach has some limitations, such as the number of data processed in the field and also the actual profile of the "artificially" generated scenarios and the over (or under) estimation of criticality for some scenarios. The next steps will be to process more data to strengthen findings and eventually identify replication abilities in simulations for the validation of CAV systems.

References

[1] N. Kalra and S. M. Paddock, “Driving to safety: How many miles of driving would it take to demonstrate autonomous vehicle reliability?” Transportation Research Part A: Policy and Practice, vol. 94, pp. 182–193, Dec. 2016. [Online]. Available: https://www.sciencedirect.com/science/article/pii/S0965856416302129

[2] S. Riedmaier, T. Ponn, D. Ludwig, B. Schick, and F. Diermeyer, “Survey on Scenario-Based Safety Assessment of Automated Vehicles,” IEEE Access, vol. 8, pp. 87 456–87 477, 2020, conference Name: IEEE Access.

[3] L. Vater, A. Putz, L. Tellis, and L. Eckstein, “Test Case Selection Method for the Verification of Automated Driving Systems,” ATZelectronics worldwide , vol. 16, no. 11, pp. 40–45, Nov. 2021. [Online]. Available: https://doi.org/10.1007/s38314-021-0701-0.

[4] S. Riedmaier, D. Schneider, D. Watzenig, F. Diermeyer, and B. Schick, “Model Validation and Scenario Selection for Virtual-Base Homologation of Automated Vehicles,” Applied Sciences, vol. 11, no. 1, p. 35, Jan. 2021, number: 1 Publisher: Multidisciplinary Digital Publishing Institute. [Online]. Available: https://www.mdpi.com/2076-3417/11/1/35.

[5] D. M. Blei, A. Y. Ng, and M. I. Jordan, “Latent dirichlet allocation,” Journal of machine Learning research, vol. 3, no. Jan, pp. 993–1022, 2003.

A study on the transformation of virtual validation methods in the development of new mobility solutions

J. Freyer[a], T. Düser[a]

[a] *Karlsruhe Institute of Technology (KIT) - Institute of Product Engineering (IPEK)*

Introduction

This contribution analyses the change in the use of virtual validation methods and simulation in the development process of cyber-physical systems. Credibility is identified as an essential characteristic for a reliable validation environment, which does not only describe model accuracy, but depends on many factors in the process. In the analysis of validation environments, particular focus is placed on advanced driver assistance systems (ADAS) and automated driving systems (ADS).

Methodology

Based on exploratory research this effort investigates the use of virtual validation methods in the development process of cyber-physical systems from a holistic product engineering perspective. For this purpose, it is first examined how complex systems-of-systems simulations are built from submodels and how these can be modeled in the context of the XiL framework according to (Albers et al., 2013) and (Riedmaier et al.). Furthermore, it is observed how the roles of the creators and users of the simulation models change and whether new roles emerge. (Düser, 2022) Furthermore, the cycle-oriented processes coming from software development such as CI/CD will be considered and the impact on the classic product development process will be elicited. Finally, new fields of application for simulation are identified.

Results and Findings

Increasing complexity and transformation to systems-of-systems

In the past, modelling and simulations were in general built, executed and evaluated by a simulation engineer with dedicated expert knowledge. The simulation engineer therefore had a very good understanding of the accuracy of the models and what statements could be made with the entire simulation. Today, this approach is no longer feasible due to the increasing complexity of the products towards systems-of-systems and the extended use of virtual methods. This can be illustrated by highly automated vehicles. Validation of the overall function of such a vehicle can only be achieved by holistically mapping the relevant subsystems. For this purpose, the subsystems involved can either be modeled virtually or integrated physically into the validation environment. This applies not only to the systems directly integrated into the vehicle (sensors, perception algorithms, motion control, drivetrain), but also to the systems surrounding as well as all the humans interacting with the vehicle. Especially the modelling and simulation of the environment and the human are major challenges for the validation of these cyber-physical systems. Due to the multi-layered interaction between humans and cyber-physical systems, it is becoming increasingly difficult to model humans realistically. These interactions include, for example, situations during the handover between vehicle and driver, pedestrians in traffic, or the effects of the automated vehicle on the well-being of the occupants. According to Taylor, the realistic representation of human behavior is the greatest challenge in modelling. Both the prediction and the representation of the behavior must be modeled. (Taylor et al., 2015) According to the required fidelity level the representation of humans can for example also be recorded by motion capture and replayed. The modeling of the environment must be carried out as required according to the validation goal. For example, if sensors are to be stimulated with virtual data and the subsequent perception is to be validated, a corresponding (high) model quality of the environment is necessary. In addition to a high resolution of the objects, the physical properties must also be represented. Wallace et al. propose a metric to compare the quality of a modeled environment to reality. (Wallace et al.) Otherwise, if the strategic planning of the ADS is validated, graphically simple environment models may suffice, but with special attention to the traffic model.

Specificities and modularity of validation environments

Traditionally, the XiL validation environments are divided into MiL, SiL, PiL, HiL, DiL and ViL, among others. ASAM e.V. has made a recommendation as to which environment is particularly suitable for which validation use case. (ASAM e.V., 2022) Nowadays the validation of systems-of-systems proves to be challenging, as the complex interactions between the systems have to be considered as well. However, as can be seen in (Dona et al., 2022), realistic modeling of these interactions often requires a combination of XiL environments, which requires a combination of skills and technologies. Therefore, it could be more purposeful to structure the environments

according to the required skills of the users and the technologies used. A structuring into cloud, cyber-physical test bench and proving ground would be feasible. In the cloud cluster all test environments would be usable, which are purely virtual or at least virtualizable. This applies to MiL and SiL in general and can also be extended to PiL or HiL if virtualization or emulation is possible. In general, simulation in the cloud has several advantages over local execution. First and foremost is scalability, which is a basic requirement especially when CI/CD processes are used in development. Parallelization enables a very large number of simulations to be executed in parallel as a consequence. New business models such as simulation-as-a-service are also conceivable here. In contrast, applications that use a physical and virtual component can best be validated on a cyber-physical test bench. For example, validating vehicles equipped with ADAS or AD on a chassis dynamometer with sensor stimulation is a combination of ViL, HiL and a virtual environment component. Tests on a proving ground have the least abstraction but are associated with the greatest effort. The formerly clear separation of the use cases and therefore used test environment is becoming increasingly blurred. For this reason, we recommend a reorganization according to the underlying technology and skills of the stakeholders. Restructuring the test environments would also simplify the assessment of the team experience as mentioned in (United Nations Economic Comission for Europe, 2022).

Reliable process for simulation-based safety argumentation for approval and certification

A comprehensive validation concept is required for the certification and approval of ADAS and ADS. Up to now, virtual simulation environments have primarily served to gain knowledge for the developers and, with the exception of the release of the Electronic Stability Program (ESC) according to UN ECE R140 (R140, 2017), are only permitted to a certain degree for the use in certification. The release of the currently most advanced level 3 systems (e.g. ALKS) is therefore mainly based on proving ground tests and real-world driving. With the increasing degree of automation in the future, this procedure is no longer practical. In order to keep effort and costs low in the future and still achieve the maximum possible gain in knowledge, a combination of virtual tests, cyber-physical test benches, proving ground testing and real-world driving must be used. The challenge here is to use the optimal distribution across the different validation environments throughout the advancing development process. The further development of the system in development results in changing requirements for the validation environment, which must be counteracted by parallel development. At the beginning of the development process, there are often only simple models of the system in development, which can be covered by simple validation environments. It may also be that no physical systems are yet available, which requires purely virtual validation. If, on the other hand, the development process is advanced, the proportion of physical tests can be increased in order to obtain more robust validation results. The process of joint development of the system in development and the accompanying validation system must be designed in a comprehensible manner. This includes the exact validation environment including model and tool versions, input and output data, and scenarios performed. For this purpose, a simulation data management tool must be developed that stores this data in a central location and protects it from manipulation, for example by the use of blockchain technology. (Hildebrand & Driesten, 2020) Once validation results are used for safety argumentation of a system, it must first be shown that the simulation and underlying tool chain is validated. (e.g. in (Dona & Ciuffo, 2022)) Due to the complex nature of the system-of-systems being modeled, this process is associated with a lot of effort. The IAMTS process (International Alliance for Mobility Testing and Standardization [IAMTS], 2021) or the SET Level Credible Simulation process (Heinkel & Steinkirchner, 2022) can assist with this. Liu et al. propose some metrices to evaluate the credibility. (Liu & Yang, 2005)

Extending the range of applications for virtual validation

In the past, simulation models were used analytically and for verification purposes to confirm individual development increments. Today, new processes and technologies open up new application possibilities for simulations, ranging from immersive user experience tests to scenario screenings. Each individual application places special requirements on the simulation which must be fulfilled for credible results. For example, the ever-increasing amount of program code in a vehicle makes regression testing a much needed application for simulation. Furthermore, simulations can be used to determine and identify critical scenarios and edge cases. After virtual screening of a large number of scenarios, these selected scenarios can then be re-run with high credibility on a cyber-physical test bench or proving ground. Another new use case is generating training data for machine learning algorithms. Simulation can be used to specifically represent certain conditions in the data. However, when generating the data, care must be taken to ensure that there is no bias or gaps present (Black Swan Problem (Koopman & Wagner, 2016)) in the data. Furthermore, simulations can be used in combination with VR/AR headsets to test immersive human-machine interactions.

Use of virtual validation in the development process in transition

In the domain of software development, CI/CD or DevOps processes have become established in recent years. In order to be able to use these processes also in the development of cyber-physical systems, the validation environment including models and tool chain must be run in the background. When changes are made to requirements, software or hardware, a predefined set of scenarios can be simulated and evaluated automatically. If a change is made to the system in development, this must therefore also be implemented directly in the model or digital twin in the background. The CI/CD cycle therefore does not only exist for the system under development but also for the development of the validation environment and the set of scenarios and test cases. This approach scales particularly well when using purely virtual validation environments. However, advances in emulation are increasingly making it possible to virtualize HiL or PiL configurations and thus to run them on a scaled server farm. This approach allows the developer to focus on the results and less on the simulation itself.

Personas and roles in the process

Since simulations were formerly used on a much smaller scale in the product development process, it was possible for individual simulation engineers to build the models, run simulations and evaluate the results. This individual expert then had a deep understanding of the problem to be modeled and was therefore able to state very accurately in which areas the simulation had what validity. Today, the problem to be modeled is usually cross-domain and therefore much too complex for a single expert. Submodels of complex systems are therefore built and independently validated by different experts specialized in their respective domains. Still other developers assemble the individual submodels into an overall model and ensure that the interfaces of the models are accurately modeled. If the simulations are to be executed in the cloud, further specialists are required to ensure correct distribution to the nodes of the computing cluster. Creator (simulation engineer), user (validation engineer) and operator (IT administrator or test field operator) are therefore different groups of people, which requires very good coordination among them. Every single person only knows the unique properties or the Operational Design Domain (ODD) of his or her own segment. Nevertheless, they must be able to make clear to each other which requirements apply to the neighboring subsystems. In the end, it must be provable for the emergent overall model, including the implementation in the tool chain, what the simulation is capable of. This is a major challenge for the use of the model for certification.

Result Management

Especially in combination with the before mentioned CI/CD process, a huge number of simulation results are generated in a short period of time. In contrast to the past, it is no longer possible to manually check the large number of results for errors and plausibility. At this point, an automatism is needed that statistically evaluates the results, for example by cascading KPIs, and recognizes critical results. In addition, the results must be managed in a database together with the exact toolchain used. For example, previous results can be checked retroactively in case of model changes.

Conclusion

Product development cycles are becoming increasingly shorter and processes such as CI/CD from software development are also finding their way into the development of cyber-physical systems. This leads to the fact that virtual validation is integrated more and more deeply into the product development process. For this reason, it is essential that a framework is introduced that ensures consistent credibility throughout the entire process. This credibility framework therefore describes not only the correlation of models to reality, but many other factors that must be considered for a trustworthy validation result.

References

Albers, A., Behrendt, M., Schroeter, J., Ott, S., & Klingler, S. (Eds.) (2013). *X-in-the-Loop: A Framework for Supporting Central Engineering Activities and Contracting Complexity in Product Engineering Processes*.

ASAM e.V. (Ed.). (2022, February 2). *Evolving Landscapes of Collaborative Testing for ADAS & AD: ASAM Test Specification Study Group Report 2022.*

Dona, R., & Ciuffo, B. (2022). Virtual Testing of Automated Driving Systems. A Survey on Validation Methods. *IEEE Access*, *10*, 24349–24367. https://doi.org/10.1109/ACCESS.2022.3153722

Dona, R., Vass, S., Mattas, K., Galassi, M. C., & Ciuffo, B. (2022). Virtual Testing in Automated Driving Systems Certification. A Longitudinal Dynamics Validation Example. *IEEE Access*, *10*, 47661–47672. https://doi.org/10.1109/ACCESS.2022.3171180

Düser, T. (2022). Credibility Argumentation - Correlation of virtual and physical testing. *IEEE International Conference on Connected Vehicles and Expo (ICCVE)*.

Heinkel, H.-M., & Steinkirchner, K. (2022, August 19). *Simulation based Decision Process: Simulation-based Engineering and Testing of Automated Driving*.

Hildebrand, N., & Driesten, C. van (2020). *Tezos Deep Dive Deck.* Automotive Solution Center for Simulation (asc (s).

International Alliance for Mobility Testing and Standardization (2021). A Comprehensive Approach for the Validation of Virtual Testing Toolchains.

Koopman, P., & Wagner, M. (2016). Challenges in Autonomous Vehicle Testing and Validation. *SAE International Journal of Transportation Safety*, *4*(1), 15–24. https://doi.org/10.4271/2016-01-0128

Liu, F., & Yang, M. (2005). Study on Simulation Credibility Metrics. *37th Winter Simulation Conference*. Advance online publication. https://doi.org/10.1145/1162708.1163184

Riedmaier, S., Nesensohn, J., Gutenlunst, C., Düser, T., Schick, B., & Abdellatif, H. Validation of X-in-the-Loop Approaches for Virtual Homologation of Automated Driving Functions. In *11. Grazer Symposium VIRTUAL VEHICLE (GSVF) Graz.*

Taylor, S. J. E., Khan, A., Morse, K. L., Tolk, A., Yilmaz, L., Zander, J., & Mosterman, P. J. (2015). Grand challenges for modeling and simulation: simulation everywhere—from cyberinfrastructure to clouds to citizens. *SIMULATION*, *91*(7), 648–665. https://doi.org/10.1177/0037549715590594

Uniform provisions concerning the approval of passenger cars with regard to Electronic Stability Control (ESC) Systems, January 22, 2017.

United Nations Economic Comission for Europe. (2022). *EU ADS Implementing Act Annex.*

Wallace, A., Khastgir, S., Zhang, X., Brewerton, S., Anctil, B., Burns, P., Charlebois, D., & Jennings, P. Validating Simulation Environments for Automated Driving Systems Using 3D Object Comparison Metric, 860–866. https://doi.org/10.1109/IV51971.2022.9827354

Development of a Nowcast Crowd Simulation Framework

H. Hanabusa[a], T. Komiya[a], K. Takahashi[a], K. Ichinose[a], M. Iijima[a], R. Horiguchi[a]

[a] *i-Transport Lab. Co., Ltd.*

Introduction

In the post-pandemic society, this study aims to improve the safety and comfort of citizens using spatiotemporal resources represented by mobility services such as transportation systems and space utilization services (office and urban facilities, etc.), responding to the changes in people's lifestyles. Since 2020, citizens have begun to adopt new lifestyles using ICT such as telework, remote classes, and teleconferences, amidst repeated self-restraint and revitalization of activities to prevent the spread of COVID-19 infection. As a result, the changes in people's life have brought about major changes in public transportation usage, and various service providers have come to accept the current situation. In order to quickly understand and respond to such changes, it is necessary to continuously monitor the people's activities whole of the city and predict events that may occur in the future. Therefore, our goal is the practical use of a framework that understands and predicts people's movements in city-wide in time and space by using various data types and models in real-time, as the "city-scale nowcast simulation framework".

The city-scale nowcast simulation framework consists of macroscale and microscale models by hybrid simulation approach, to reproduce the people's activities in the whole city and the crowd flows in pedestrian spaces. Figure 1 shows the overall structure of the city-scale nowcast simulation framework. For the macroscale, MATSim customized to link with the traffic simulation model "SOUND" is used. MATSim is a large-scale agent-based transport simulation model of an open-source framework, and SOUND is a mesoscopic traffic simulation model to simulate road traffic on large scale. MATSim applies a day-to-day simulation approach of a microscopic traffic model and co-evolutionary algorithms for planning the agent's activity schedule in the simulation loop ("mob sim", "scoring" and "replanning"). SOUND is linked to "mobisim" and reproduces people's movement by using several types of transportation careers (e.g., vehicle, taxi, bus.) on road traffic. For the microscale model, a crowd simulation model "Smart Crowd Model" developed by M. Sarvi et.al is applied. Smart Crowd Model is used for the evaluation of pedestrian space for evacuation in emergencies and crowd flow in normal situations. The macroscale model basically reproduces the traffic flow of the target area, and the microscale model can simulate the crowd flow of the designated space in the target area using the estimated demands from the macroscale model. The microscale model in Figure 1 is the nowcast crowd simulation framework, which is the theme of this paper.

Figure 30. Overall structure of the city-scale nowcast simulation framework

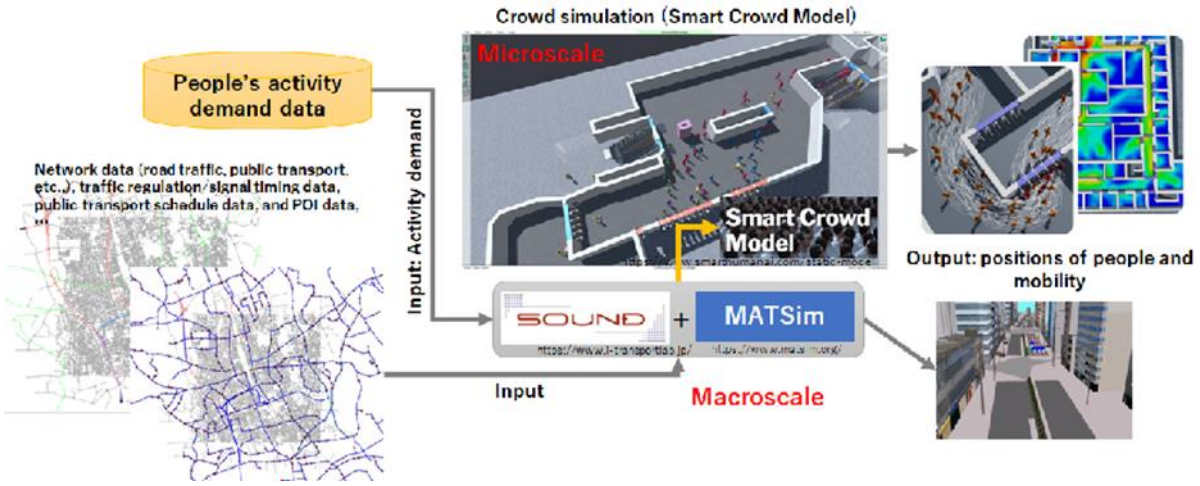

Process of nowcast

Figure 2 shows the real-time process of the nowcast crowd simulation framework. This process consists of a "precast" for the preparation of the crowd simulation model, and a "nowcast" for the real-time estimation of the people flows in the target area. The basic process in the precast process is the following steps.

1. Pedestrian space modelling.
2. Pedestrian survey (OD demand and pedestrian behaviour analysis).

3. Basic model building and calibration.

In the process of pedestrian space modelling, it is necessary to create spatial data such as inside buildings, sidewalks, and squares. In recent years, in Japan, the maintenance of open data has been progressed, and we are working on the utilization of PLATEAU, the 3D city model database released by the Ministry of Land, Infrastructure, Transport and Tourism. Figure 3 shows a demonstration of crowd simulation model using 3D city model PLATEAU.

Figure 31. Real-time process of the nowcast crowd simulation framework

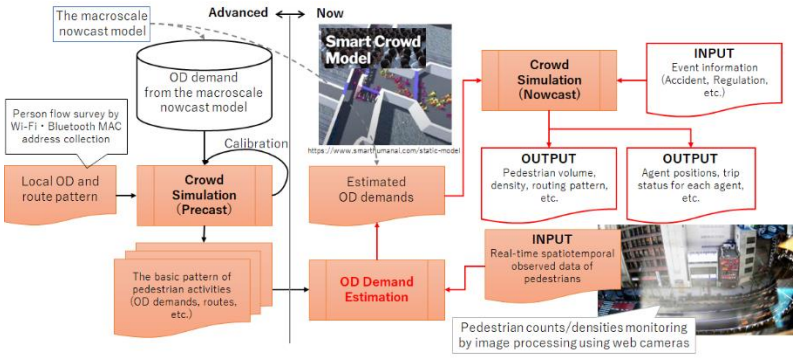

Figure 32. Demonstration of crowd simulation using 3D city model PLATEAU

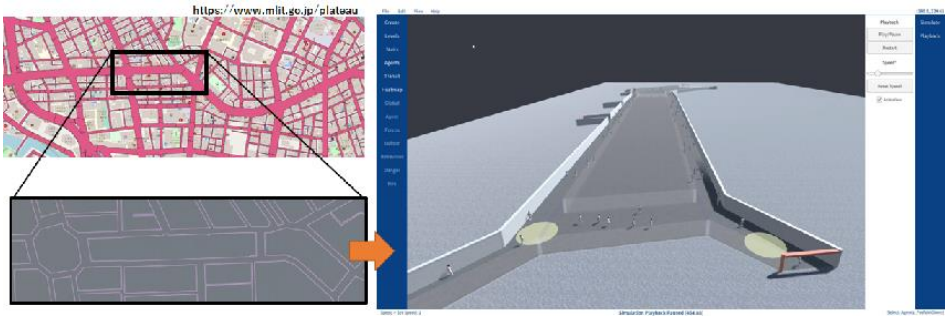

In cooperation with the macroscale nowcast model, the macroscale OD demand related to the target area of the nowcast crowd simulation (called "local area") is shared and used as the input data of crowd simulation. On the other hand, OD and route patterns in the local area should be prepared to compensate for differences in the spatiotemporal resolution of the macroscale model and the microscale model. After the parameter calibration to fit the observed data, the pedestrian behaviours data by the crowd model is used for the od demand estimation model in the nowcast process, to reproduce the present crowd situation.

Methodology of OD Demand Estimation

The nowcast process in this study is a method of updating the OD demand in the local area according to real-time observations. Here a state space model that the relations of OD demand with pedestrian traffic volume is formulated is built. The following equations are the basic model.

$$\boldsymbol{X}(t+1) = \boldsymbol{F}(t)\boldsymbol{X}(t) + \boldsymbol{\omega}(t) \qquad \text{(eq.1)}$$

$$\boldsymbol{Y}(t) = \boldsymbol{H}(t)\left(\boldsymbol{X}(t) + \bar{\boldsymbol{B}}(t)\right) + \boldsymbol{v}(t) \qquad \text{(eq.2)}$$

Where $\boldsymbol{X}(t)$ is state vector, $\boldsymbol{Y}(t)$ is observation vector, $\boldsymbol{F}(t)$ is state transition matrix, $\boldsymbol{H}(t)$ is observation matrix, $\bar{\boldsymbol{B}}(t)$ is basic state vector (known values), $\boldsymbol{\omega}(t)$ is system noise and $\boldsymbol{v}(t)$ is observation noise. Specifically, $\boldsymbol{X}(t)$, $\boldsymbol{F}(t)$, $\boldsymbol{Y}(t)$, $\boldsymbol{H}(t)$ and $\bar{\boldsymbol{B}}(t)$ are defined the below:

$$\boldsymbol{X}(t) = [\boldsymbol{X}^{w}(t) \mid w \in \boldsymbol{W}]^{\mathrm{T}} \qquad \text{(eq.3)}$$

$$\boldsymbol{X}^{w}(t) = \left[x^{w,t}, x^{w,t-1}, \ldots, x^{w,t-n+1}\right]^{\mathrm{T}} \qquad \text{(eq.4)}$$

$$x^{wt} = \hat{q}^{wt} - \bar{q}^{wt} \qquad \text{(eq.5)}$$

$$\boldsymbol{F}(t)=\begin{bmatrix}\boldsymbol{A}^{0}(t) & \cdots & \boldsymbol{O}\\ \vdots & \ddots & \vdots\\ \boldsymbol{O} & \cdots & \boldsymbol{A}^{|\boldsymbol{W}|-1}(t)\end{bmatrix}\quad\text{(eq.6)},\qquad \boldsymbol{A}^{w}(t)=\begin{bmatrix}a^{w,0} & a^{w,1} & \cdots & & a^{w,n-1}\\ 0 & a^{w,0} & \cdots & & a^{w,n-2}\\ \vdots & \ddots & \ddots & \ddots & \ddots\\ 0 & \cdots & 1 & 0 & 0\\ 0 & \cdots & 0 & 1 & 0\end{bmatrix}\quad\text{(eq.7)}$$

$$\boldsymbol{Y}(t)=[\boldsymbol{Y}_{k}(t)\mid k\in\boldsymbol{K}]^{\mathrm{T}}\quad\text{(eq.8)},$$

$$\boldsymbol{Y}_{k}(t)=\left[y_{k,t},\cdots,y_{k,t-n+1}\right]^{\mathrm{T}}\quad\text{(eq.9)}$$

Where, $\boldsymbol{W}$ is full set of OD pair by pedestrian type, $\hat{q}^{wt}$ is od demand of $w$at time t, $\bar{q}^{wt}$ is average od demand at time t (known values) and n is length of time series data and $\boldsymbol{K}$: all sets of observed point by direction. On the other hand, $\boldsymbol{H}(t)$ is composed of submatrices $\boldsymbol{P}_{k}^{w}(t)$ of size $(n\times n)$ that indicate the relationship between the OD demand w and the observed pedestrian traffic volume k in the following.

$$\boldsymbol{H}(t)=\begin{bmatrix}\boldsymbol{P}_{0}^{0}(t) & \cdots & \boldsymbol{P}_{0}^{|\boldsymbol{W}|-1}(t)\\ \vdots & \boldsymbol{P}_{k}^{w}(t) & \vdots\\ \boldsymbol{P}_{|\boldsymbol{K}|-1}^{0}(t) & \cdots & \boldsymbol{P}_{|\boldsymbol{K}|-1}^{|\boldsymbol{W}|-1}(t)\end{bmatrix}\quad\text{(eq.10)},\qquad \boldsymbol{P}_{k}^{w}(t)=\begin{bmatrix}p_{k,t}^{w,t} & p_{k,t}^{w,t-1} & \cdots & p_{k,t}^{w,t-n+1}\\ 0 & p_{k,t-1}^{w,t-1} & \cdots & p_{k,t-1}^{w,t-n+1}\\ \vdots & \vdots & \ddots & \vdots\\ 0 & \cdots & 0 & p_{k,t-n+1}^{w,t-n+1}\end{bmatrix}\text{(eq.11)}$$

$$p_{k\tau}^{wt}=p_{k}^{wt}R_{k}^{wt}(\tau)\quad\text{(eq.12)}$$

Where τ is travel time discretized in the same width of time slot t, $p_{k\tau}^{wt}$ is probability that a pedestrian leaving w at time t arrive k in travel time τ, $R_{k}^{wt}(\tau)$ is provability density of travel time τ from w to k leaving at time t, p_{k}^{wt} is probability that a pedestrian leaving w at time t choose k. In addition, $\bar{\boldsymbol{B}}(t)$ consists of the average OD demand as below:

$$\bar{\boldsymbol{B}}(t)=\left[\bar{q}^{w,t},\bar{q}^{w,t-1},\ldots,\bar{q}^{w,t-n+1}\right]^{\mathrm{T}}$$

Future works

We plan to build a prototype to reproduce the people flow in the demonstration experiment area (The Kashiwa-no-ha Campus station in Kashiwa city, Japan). The survey to collect Wi-Fi and Bluetooth MAC addresses and traffic volumes of pedestrians in the transportation terminal is examined for building the basic patterns of od demands and routes. After the survey, using the survey data, the people flow in the target area will be reproduced by our crowd simulation framework and evaluated some scenario cases based on the forecast information.

Acknowledgment

This study started in 2021 under the project “Research and development of information communication technology that contributes to measures against infectious diseases such as viruses, Issue C: ICT to form a post-corona society “. (Project No.: 222C0201, project title: "Research and development of prediction information sharing type spatiotemporal resource effective utilization technology that supports various urban activities") This project is organized by National Institute of Information and Communications Technology (NICT) in Japan. The authors wish to thank the project members and the NICT people involved.

Scalability Of Power Consumption Of An Autonomous Electric Robo-Car Using Different Adaptive Cruise Control Models

C. Pana, Michel Khoueiry[a], Wissam Sleiman[a], Samer Hamdar[a]

[a] *The George Washington Transportation Program (GWTP), Department of Civil & Environmental Engineering, The George Washington University, Washington DC, USA*

Introduction

The world's growing population and vehicles per capita lead to increased traffic congestion, expenses, and environmental pollution, particularly in densely populated urban areas. The transportation industry is addressing this issue by developing electric vehicles, ride-sharing services, and autonomous driving systems. Clean energy vehicles, specifically electric vehicles, play a pivotal role in creating a more equitable and sustainable transportation system.

Autonomous Electric Vehicles (AEVs) enhance transportation services and reduce maintenance and management expenses. However, accurately modelling their energy consumption is a significant challenge due to limited data availability. Researchers have used a Markov Chain approach to construct Hybrid Electric Vehicles (HEVs) driving cycles and optimize energy consumption.

This aim of this paper is to investigate the autonomous logic characteristics that may reduce power consumption in combined electric and autonomous drive modes. The study hypothesizes that scaled-down less expensive AEVs such as robotic vehicles may be useful for investigating full-scale AEV technology and collecting relevant research data at a laboratory-scaled level. The scalability in power consumption between measured electric robot vehicles and estimated full-scale AEVs power consumption needs to be tested with different drive cycles.

Towards realizing the aforementioned objective while filling the gap in empirical data to highlight the benefits of integrating autonomous features into electric vehicles, the following steps need to be performed: 1) studying the feasibility and the effectiveness of building an autonomous electric driving robot, 2) testing the possibility of applying longitudinal autonomous logics observed in the real-world to a scaled-down driving robot, and 3) analysing the comparability of power consumption between a full-size electric vehicle and a constructed 1/10 proportional Robo-Car.

Methodology

In recent decades, numerous car-following models have been developed to simulate the longitudinal driving behavior of human drivers. This paper investigates three of these models, which are applied to a Robocar to assess power consumption and scalability.

The first model is the Intelligent Driver Model (IDM) - Adaptive Cruise Control (ACC), a widely used approach that prioritizes safety and human-like driving. This model smoothly transitions between speed levels by considering the acceleration and deceleration of the preceding vehicle.

The second model, Nonlinear Model Predictive Control (NMPC), is a predictive model that utilizes a mathematical model of the EV system to optimize future vehicle behavior while considering safety and comfort. The NMPC model is capable of handling complex constraints, such as energy limits, obstacle avoidance, and performance objectives.

The third model, Eco-SDM (Economic and Safe Driving Model), is also widely used and focuses on energy efficiency while maintaining safety and comfort. This model employs a variety of strategies, such as constant speed maintenance, acceleration and deceleration optimization, and idle time reduction, to achieve energy-saving goals.

To mimic realistic driving behavior, a "following" vehicle is tested using these models, with the "leading" vehicle adhering to a specific driving schedule that covers most driving behaviors. The EPA Urban Dynamometer Driving Schedule (UDDS) is utilized to replicate power consumption in an urban driving environment. The UDDS Urban Environment Simulation scenario provides speed fluctuations for city driving conditions. The analysis assumes a zero-slope angle and air density of 1.225 kg/m^3 at 15°C at sea level, and a Kr value of 0.02. The Robocar has a Cd value ranging between 0.6 and 0.8. In this research, the model runs in a laboratory setting, with relative motion with respect to the surroundings being omitted, making Cd close to the lower value of 0.6.

Results and Findings

This study involved significant modifications to the original framework of the F1/10th scaled Robo-Car introduced by the University of Pennsylvania, in order to enable the evaluation of various longitudinal autonomous driving strategies. The revised configuration of the Robo-Car incorporates a Traxxas Slash 4x4 Rally Car, a Vedder Electronic Speed Controller, an NVIDIA Jetson TX2, a ZED 2 Stereo Camera, a Sparkfun IMU, and a Slamtec RPLidar.

The study employed UDDS data to determine the acceleration/deceleration and speed of an electric vehicle, which was pursued by an autonomous ACC-controlled electric vehicle/robot, labelled as the George Washington RoboCar (GWRC). The power consumption for each of the Eco-SDM, IDM, and NMPC ACC models was either measured or estimated for a GWRC or estimated for a full-sized vehicle, respectively. The complete UDDS cycle was executed either in a simulation software or on the GWRC, with a focus on a 33-second section of the UDDS cycle, ranging from the 100th second to the 133rd second for better graphical representation. The vehicle speed was transformed to a motor speed associated with a real vehicle or the GWRC.

Figure 33: Partial UDDS Simulated Power Consumption vs Measured Real Power Consumption for the Leading GWRC

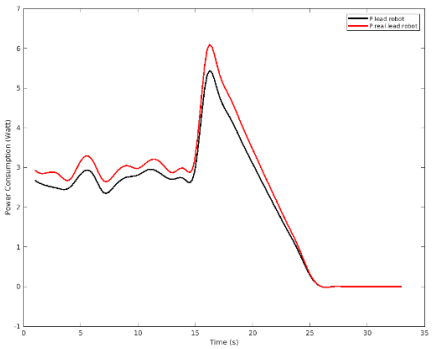

Source: Authors' elaborations.

Figure 34: Relative Error of Simulated and Real Power Comparison for the Leading GWRC

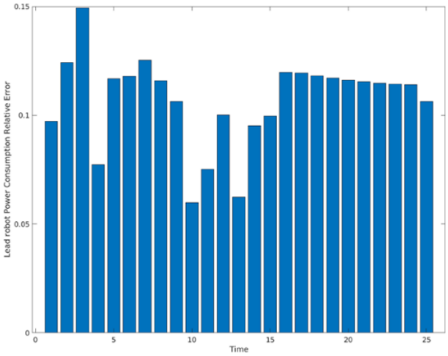

Source: Authors' elaborations.

Using the models described in the methodology section, all ACC methods were applied to a GWRC in a loop setup, following another leading GWRC equipped with UDDS driving behavior. The behavior of the lead vehicle was assumed to be the real behavior to which the follower was being compared. The errors between both behaviors are summarized in Table 1.

Table 6: Error Metrics Comparison for IDM-ACC, Eco-SDM and NMPC Models

Model	Maximum Relative Error	Minimum Relative Error	Average Relative Error
IDM-ACC	15.3 %	6.7%	10.7%
Eco-SDM	12.8 %	6.6%	8.6%
NMPC	13.2 %	1.7%	9.1%

Source: Authors' elaborations.

Furthermore, power consumption measurements recorded from the scaled-down GWRC while operating with the three proposed ACC models were compared against the estimated power consumption of an actual full-sized electric vehicle, the Nissan Leaf, as depicted in Figure 3. In addition, regardless of the specific vehicle under study, the use of the Eco-SDM control method resulted in lower power consumption, as demonstrated by the discernible power consumption difference among the ACC models adopted in Figure 4.

Figure 35: Power Consumption Comparison Between Measured GWRC (Left) and Estimated Nissan Leaf (Right) for IDM-ACC, Eco-SDM & NMPC Models

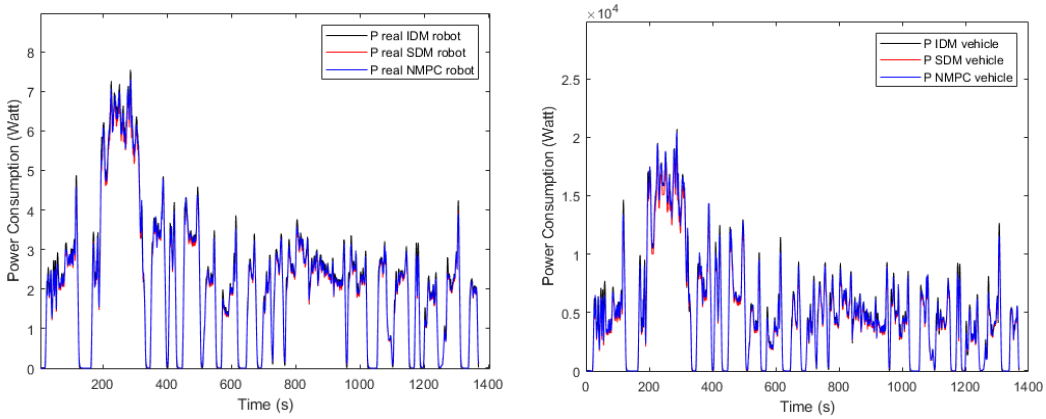

Source: Authors' elaborations.

Figure 36: Power Consumption for GWRC During Partial Cycle Using IDM-ACC, Eco-SDM & NMPC Models

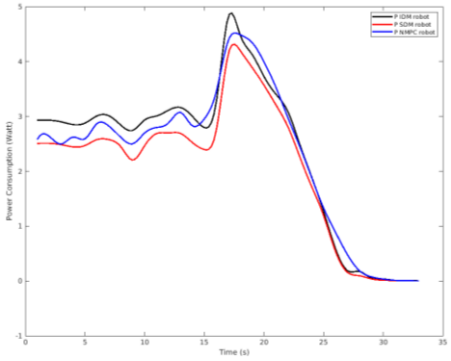

Source: Authors' elaborations.

Conclusion

This study evaluated various longitudinal autonomous driving strategies by modifying the original framework of the F1/10th scaled Robo-Car introduced by the University of Pennsylvania. The revised Robo-Car configuration incorporated several components, including a Traxxas Slash 4x4 Rally Car, a Vedder Electronic Speed Controller, an NVIDIA Jetson TX2, a ZED 2 Stereo Camera, a Sparkfun IMU, and a Slamtec RPLidar, to facilitate the analysis of power consumption and performance of AEVs.

The GWRC platform was utilized to investigate the power consumption of scaled-down AEVs equipped with three ACC models, namely Eco-SDM, IDM-ACC, and NMPC. The results indicated that the power consumption estimation for all implemented ACC models was within an acceptable range, with limited errors (within 10%), and with consistent underestimation of the UDDS issued power across all models. Therefore, it was deemed acceptable to utilize the GWRC platform for analyzing the power consumption of scaled-down electric vehicles.

Furthermore, the Eco-SDM model consistently exhibited the lowest power consumption, while the IDM-ACC and NMPC models each exhibited higher power consumption at distinct times throughout the cycle. The NMPC model also presented a smoother acceleration transition pattern compared to the IDM-ACC and Eco-SDM models. To assess the reliability of the power consumption model, the actual power consumption data from the GWRC was compared with simulation output derived from the power consumption produced by the UDDS cycle. The results confirmed the primary claims of this study, namely that properly designed Robo-Cars controlled by autonomous ACC logics can facilitate the collection of data on AEVs across various longitudinal autonomous driving modes. Distinct autonomous driving models may be implemented within a Robo-Car system, and the associated power consumptions can be extrapolated for use with real AEVs exhibiting varying driving regimes.

These findings have significant implications for the testing and deployment of AEVs, especially given the expensive nature of these technologies and the scarcity of open shared data. The present research faces several

challenges, including the absence of lane changing maneuvers due to the assumption of a single lane road, which necessitates the development of an energy-efficient lane-changing strategy for AEVs that can be integrated with ACC models to mimic realistic driving behavior. Additionally, the simulation model fails to account for varying levels of traffic congestion. Future investigations should explore the effects of communication delays and sensor failure on the performance of CAVs by incorporating communication sensors (emitters and receivers) into the simulation. In conclusion, this study provides valuable insights into the power consumption and performance of AEVs under different autonomous driving modes, and paves the way for further investigations in this field.

References

Yu, L., & Wang, R., Researches on Adaptive Cruise Control system: A state of the art review. *Proceedings of the Institution of Mechanical Engineers, Part D: Journal of Automobile Engineering*, Vol. 236, 2022, pp. 211-240.

Cugurullo, F., Acheampong, R. A., Gueriau, M., & Dusparic, I., The transition to autonomous cars, the redesign of cities and the future of urban sustainability. *Urban Geography*, Vol. 42, 2021, pp. 833-859.

Kesting, Arne, Martin Treiber, and Dirk Helbing. "Enhanced intelligent driver model to access the impact of driving strategies on traffic capacity." *Philosophical Transactions of the Royal Society A: Mathematical, Physical and Engineering Sciences*, Vol. 368, 2010, pp. 4585-4605.

Talebpour, A., Mahmassani, H. S., & Hamdar, S. H. Multiregime sequential risk-taking model of car-following behavior: specification, calibration, and sensitivity analysis. *Transportation research record,* Vol. 2260, 2011, 60-66.

Treiber, M., Hennecke, A., & Helbing, D., Congested traffic states in empirical observations and microscopic simulations. *Physical review E,* Vol. 62, 2000, No. 1805.

Gipps, P. G., A behavioural car-following model for computer simulation. *Transportation Research Part B: Methodological,* Vol. 15, 1981, pp. 105-111.

Talebpour, A., & Mahmassani, H. S., Influence of connected and autonomous vehicles on traffic flow stability and throughput. *Transportation research part C: emerging technologies*, Vol. 71, 2016, pp. 143-163.

Wang, Z., Chen, X., Ouyang, Y., & Li, M., Emission mitigation via longitudinal control of intelligent vehicles in a congested platoon. Computer - Aided Civil and Infrastructure Engineering, Vol. 30, 2015, pp. 490-506.

Beyond Prediction: On-street Parking Recommendation using Heterogeneous Graph-based List-wise Ranking

A. Hanyu Sun[a], B. Xiao Huang[a], C. Wei Ma[a]

[a] *The Hong Kong Polytechnic University*

Introduction

As most on-street parking waste (like energy, time and economic losses) is caused by time consumption in finding a parking space, we thus turn to develop a method that aims to save drivers' time in cruising for parking. On-street parking meters are widely used in cities and can record the parking status in a fine-grained time level. In Hong Kong, there are over 10,000 metered parking spaces covering all main districts of the city and these meters also provide real-time vacancy information of the parking spaces [1]. The latest on-street parking model, such as MePark [2], using the meter data focuses on on-street parking availability prediction. However, an accurate prediction of parking availability is difficult [3]. Besides, only predicting parking availability is not practically interesting for smart parking application because it neither meets the ultimate purpose of saving time consumption nor help drivers make a final decision on where to go. To handle this, we propose a one-step on-street parking recommendation (OPR) task.

Specifically, beyond only predicting on-street parking availability, we recommend a list of ranked parking space candidates so as to help drivers make parking decisions to save time in cruising for parking. To this end, we first define the OPR task formally in the aspect of recommendation. Then a heterogeneous graph is designed to better express the original data in which turnover event (which describe the state switching of parking space between vacant and occupied states) information is included. Following this, an event-then-graph convolutional layer is designed to better aggregate ESGraph features in an efficient way. At last, a score function is learned to extract interdependencies for the final OPR task. We validate the proposed model using real-world data in Hong Kong and San Francisco. In comparison, we considered three kinds of models: prediction-only models; prediction-then-recommendation models; direct-recommendation models like our proposed, then considering their corresponding performance in recommendation metrics like NDCG and MAP as well as saving cruising time for drivers.

Methodology

We first formulate the OPR task in the LTR setting by defining on-street Parking Query (OPQ: $\boldsymbol{Q_{d,t}}$ where $d \in \mathcal{P}$ and $\mathcal{P}$ is the whole set of on-street parking space), relevant Items of OPR (RIO: $\boldsymbol{X_{t'}}$ where $t' = t + \Delta$) and the OPR data set $D = \{(\boldsymbol{Q_{d,t}}, \boldsymbol{X_{t'}}, \boldsymbol{y})\}$ where $\boldsymbol{y}$ is the relevant label. We aims to learn a relevant score function S_θ with θ as its parameter from data set D, such that for an arbitrary OPQ, S_θ takes into $(\boldsymbol{Q_{d,t}}, \boldsymbol{X_{t'}})$ as input and predict a list of relevant scores $\hat{\boldsymbol{y}} = S_\theta(\boldsymbol{Q_{d,t}}, \boldsymbol{X_{t'}})$ with minimized distance from $\boldsymbol{y}$.

Then we build the ORP-LTR model by first designing a heterogeneous graph to represent the historical turnover events and spatiotemporal features for parking vacancy; then a CNN-based event-then-graph network is built to aggregate heterogeneous features; at last, the network output is further forwarded to the final task-based layer for producing the relevant scoring lists for candidate parking spaces. Details are shown in Figure 1.

Figure 37. Overview of the model architecture

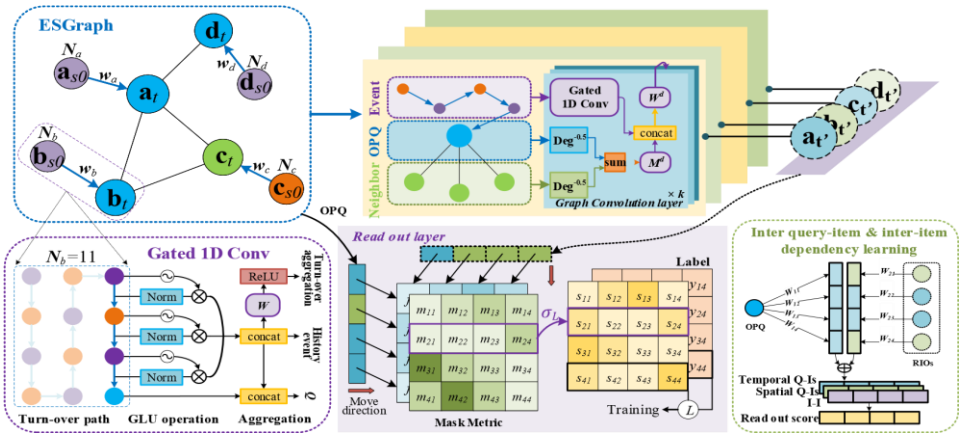

Source: Authors' elaborations.

Graph Construction

Original citywide on-street meter data can be seen as a spatial set of temporal paths which we call it a spatial-temporal Graph (STGraph). When using a STGraph to represent on-street parking meter data, all its temporal paths are represented in fixed time intervals in which we can use an edge-contraction technology to bring in turnover events. The edge-contraction process can be represented by a map function f: $(V_t\ ,\ E_t) \to (U, \mathcal{E}, W_E)$ such that:

$$U = V_t \backslash V_{t'},$$
$$\mathcal{E} = E_t \backslash \{(n_i\ , n_{i+1}) : n_i \in V_{t'}\}_{i=1}^{\|V_{t'}\|},$$
$$W_{\mathcal{E}} = \{coun(u_j) : u_j \in U\}_{j=1}^{\|\mathcal{E}\|}.$$

where $V_{t'}$ is made up of all merged nodes in edge-contraction, $\backslash$ is the removing operation, $\|\cdot\|$ indicates the number of elements in a set, and $coun(\cdot)$ computes the number of contractions that happened in a node of the temporal path. The result is a new-typed path $(U, \mathcal{E}, W_E)$ with fewer nodes and edges than the original temporal path. We call temporal paths after a contraction the turn-over event-based path. By replacing all temporal paths in a STGraph with their corresponding turnover event-based paths, we get a heterogeneous graph with space-based and turnover event-based vertices and edges. We also find that there are several advantages of ESGraph over STGraph: (1) ESGraph data structure is more efficient in both dimensions of space and time. (2) Models based on ESGraph have smaller sizes. (3) ESGraph embeds richer information.

Event-then-graph Convolutional Layer

Following the utility of ESGragh in representing on-street parking meter data, we build a model Z_θ with θ as its parameter, that is able to embed citywide on-street parking meters' spatial features, real-time state, and historical turn-over events together to conduct the following LTR task. Z_θ is an event-then-graph structural network which aggregates turn-over event feature with a gated 1-dimension convolutional layer:

$$X_{U \otimes \mathcal{E}} = \mathrm{GLU}([X_U, W_{\mathcal{E}}]) = W_{\mathcal{E}} \otimes \sigma(X_U),$$
$$\mathbf{H}^n_{:,<T} = \mathrm{ReLU}(X_{U \otimes \mathcal{E}} * W + b).$$

where X_U is the contribution of U and we treat $W_{\mathcal{E}}$ as the contribution of $\mathcal{E}$, $\otimes$ is the point-wise multiplication, gates $\sigma(X_U)$ controls the direction of $W_{\mathcal{E}}$, $*$ is convolution operation, W is a learnable weight, b is the bias.

Then the aggregated event features together with real-time states and spatial relations are aggregated by a GNN-based network to iteratively update the combined representations from event-based convolutional results and local real-time states, then output an updated representation in the final iteration:

$$z_v^{(k)} = \phi(\mathrm{COMBINE}(g(\{z_{v'}^{(k-1)}\}), h_v), z_v^{(k-1)}),$$

where $v' \in \mathcal{N}(v)$ means v' is the neighbor of v, $h_v \in \mathbf{H}^n_{:,<T}$ is the event-based features of vertex v. The function g aggregates local information of v' and function ϕ updates aggregated features in k iterations. $z_v^{(k)}$ is the final representation of vertex v.

Readout Layer and Objection

In this section, we first describe S_θ, then aggregate Z_θ and S_θ for training in a supervised learning manner. Specifically, in order to score RIOs, we consider the following factors in both relevant score function modelling and relevant label-creating processes: (1) Individual features of the query and item; (2) Inter-query-item dependency (Q-Is); (3) Inter-item dependence (I-Is).

Learning-based Score Function. Based on the above discussions, we utilize a learning model to extract the above features, especially, to learn inter-query-item and inter-item dependencies then formulate the model S_θ. Finally, to implement, the proposed model is trained in a supervised-learning manner with a goal to minimize the distance between lists of relevant labels $\boldsymbol{y}$ and predicted scores $\hat{\boldsymbol{y}} = \boldsymbol{s}$, where $\boldsymbol{s}$ is the outcome of S_θ, for citywide OPQ. Recalling that S_θ assigns a score to each item (i.e., parking space), we use a mean square error (MSE) loss function and a Softmax loss to embed listwise relationship:

$$\mathcal{L} = l_m(\boldsymbol{y}, \boldsymbol{s}) + \lambda l_s(\boldsymbol{y}, \boldsymbol{s}) + \| \theta \|^2$$

where λ is a hyperparameter, θ is the model parameter been regularized by L2 and dropout [4] is also applied to avoid over-fitting.

Results

We mainly get the following results when conducting OPR task by conducting extensive experiments:

1. Proposed method outperforms baseline models (from both the prediction and LTR area).
2. Each part (graph and network structures) of our model contribute to the final result.
3. Practically, proposed method saves more citywide on-street parking times than baselines.

Experimental Setup

To validate the mode, we take advantage of two data sets: on-street parking data from Hong Kong Island and San Francisco. We choose state-of-art models from both predicting and recommending areas then made some adoption to OPR. Basically, these baseline models can be categorized into three kinds of tasks: (1) Prediction-only task including T-GCN [5], DCRNN [6], GAMCN [7] and STPGCN [8]; (2) Prediction-then-recommendation task which recommend based on the above prediction-only models; (3) Direct-recommendation task including listMLE [9] and ApproxNDCG [10]. As our proposed model is ranking sensitive, we select NDCG@n and MAP@n as evaluating metrics.

Experimental Results

Our proposed model outperforms all other models in both cities in terms of all the metrics and model sizes which demonstrates the advantage of the proposed model in handling OPR tasks. We also notice both large NDCG improvements of our prosed model from the prediction-only model and other direct-recommendation methods which means both initial feature extraction and later item scoring are important for the final recommendation results, the same conclusion can be gotten from all other metrics. Ablation and sensitivity analysis give explanations of these advantages. Because the ESGrsph uses the turnover events as history features can carry more information in each step, it thus can improve the reprehensive ability of the following model in the same time reduce the model size. We also design two unique metrics to measure the usage and efficiency at a citywide level: Absolute Waiting Time in Parking (AWTP) and Relative Non-waiting Time Ratio (RNWTR) by using which we find the proposed OPR-LTR model has largely decreased the waiting time and increased the parking efficiency of on-street parking.

Conclusions

This paper develops a practical task to directly recommend a parking space to drivers given a specific query, and we have demonstrated that such a task has great potential in saving drivers' on-street searching time in a citywide manner, compared to the prediction-only and prediction-then-recommendation models. In model development, we highlight the importance of turnover events in parking recommendation, and hence an ESGraph-based data representation and an event-then-graph-based convolution network are developed. The ESGraph is proven to have better representation power and lower space&time complexity than the STGraph. Numerical experiments also demonstrate the outperformance of the proposed model, and especially, the proposed model could at most reduce the time in cruising for parking by 95.07% (HK) and 84.02% (SF). Future studies will be focused on designing a real-time parking recommendation system that can be used in the real world. Additionally, ESGraph can be applied to other applications, such as signal timing, system failure, etc, and we plan to develop more generalized graph networks tailored for smart civil infrastructure systems.

Acknowledgements

The research described in this study was supported by the Smart Traffic Fund of the Transport Department of the Hong Kong Special Administrative Region, China (ref. no.: PSRI/07/2108/PR) and a grant from the Research Institute for Sustainable Urban Development (RISUD) at the Hong Kong Polytechnic University (project no. P0038288). The authors thank the Transport Department of the Government of the Hong Kong Special Administrative Region for providing the on-street parking data. The contents of this paper reflect the views of the authors, who are responsible for the facts and the accuracy of the information presented herein.

References

[1] Wu, F., Ma, W., *Clustering Analysis of the Spatio-Temporal On-Street Parking Occupancy Data: A Case Study in Hong Kong*, Sustainability, 14 (2022) 7957.

[2] Zhao, D., Ju, C., Zhu, G., Ning, J., Luo, D., Zhang, D., Ma, H., *MePark: Using meters as sensors for citywide on-street parking availability prediction*, IEEE Transactions on Intelligent Transportation Systems, 23 (2021) 7244-7257.

[3] Rodrigues, F., Pereira, F.C., *Beyond expectation: Deep joint mean and quantile regression for spatiotemporal problems*, IEEE transactions on neural networks learning systems, 31 (2020) 5377-5389.

[4] Srivastava, N., Hinton, G., Krizhevsky, A., Sutskever, I., Salakhutdinov, R., *Dropout: a simple way to prevent neural networks from overfitting*, The journal of machine learning research, 15 (2014) 1929-1958.

[5] Zhao, L., Song, Y., Zhang, C., Liu, Y., Wang, P., Lin, T., Deng, M., Li, H., *T-gcn: A temporal graph convolutional network for traffic prediction*, IEEE transactions on intelligent transportation systems, 21 (2019) 3848-3858.

[6] Li, Y., Yu, R., Shahabi, C., Liu, Y., *Diffusion convolutional recurrent neural network: Data-driven traffic forecasting*, arXiv preprint arXiv:.01926(2017).

[7] Qi, J., Zhao, Z., Tanin, E., Cui, T., Nassir, N., Sarvi, M., Engineering, D., *A Graph and Attentive Multi-Path Convolutional Network for Traffic Prediction*, IEEE Transactions on Knowledge, (2022).

[8] Zhao, Y., Lin, Y., Wen, H., Wei, T., Jin, X., Wan, H., *Spatial-Temporal Position-Aware Graph Convolution Networks for Traffic Flow Forecasting*, IEEE Transactions on Intelligent Transportation Systems, (2022).

[9] Xia, F., Liu, T.Y., Wang, J., Zhang, W., Li, H., *Listwise approach to learning to rank: theory and algorithm*, Proceedings of the 25th international conference on Machine learning, 2008, pp. 1192-1199.

[10] Qin, T., Liu, T.Y., Li, H., *A general approximation framework for direct optimization of information retrieval measures*, Information retrieval, 13 (2010) 375-397.

Exploring Antifragility in Urban Road Network: Learning through Disturbances with Reinforcement Learning

L.Sun[a], A. Genser[a], M. A. Makridis[a]

[a] *Institute for Transport Planning and Systems, ETH Zürich, 8093, Switzerland*

Introduction

With the ever-growing population in the cities and urbanization, traffic systems have gained both in volume and in complexity. The growth of traffic volume also leads to more incidents and more severe peak hour congestions. Therefore, new challenges and requirements have been posed to the urban road networks and particularly to their control strategies to maintain a steady and even increase the overall throughput of the networks. In addition, to enhance the ideas of smart cities and Intelligent Transportation Systems (ITS), modern traffic control methods should be capable of learning towards antifragility against the traffic disturbances as well.

While microscopic simulations and controls are expensive to compute in real time and thus may not be suitable for a large-scale real-time application at this moment, findings in Geroliminis and Daganzo (2008) have proven with empirical data the existence of Macroscopic Fundamental Diagram (MFD), which is a reproducible relationship between average flow and density on a regional level and insensitive to OD information. This makes real-time control strategies computationally affordable on a macroscopic level. Based on MFD and the indicated critical density, multiple control methods targeting a better overall performance of the road network have been proposed since then. Perimeter control is one of the methods that has attracted immense attention. By refraining the incoming vehicles from adjacent regions into a protected region, the traffic density remains below the critical density indicated on MFD for the protected network and thus increasing the trip completion rate. Geroliminis et al. (2013) proposed an optimal perimeter control approach using a Model Predictive Control (MPC) algorithm and proved its effectiveness regarding trip completion within a determined duration in comparison with a greedy controller.

Nowadays, with the abundance of data collected through various approaches, such as loop detectors, video cameras, mobile network, etc., an emerging amount of research work has been shifting towards data-driven approaches in the field of transportation, particularly the application of deep-RL, e.g., traffic light control (Wei et al, 2019), delay management (Zhu et al, 2021), etc. And for perimeter control, there are also some recent works: Zhou and Gayah (2021) and Chen et al. (2022) that illustrate better performance of a RL algorithm. The benefits of RL compared with other classical controllers based on control theories are its flexibility in complex environments and the capability of dealing with multivariate nonlinearities. RL can also be in the form of online training by nature, meaning the algorithm learns and adjusts its decisions with streaming data from the real world.

Category 3. Enhanced demand and traffic management

On integrating large-scale activity-based and traffic assignment models

S. Agriestia,[b], P. Anashin[c], C. Roncoli[a], B.-h. Nahmias-Biran[d]

[a] *Department of Built Environment, School of Engineering, Aalto University, Espoo 02150 Finland*

[b] *FinEst Centre for Smart Cities, Tallinn University of Technology, Tallinn, Estonia*

[c] *Department of Geography - University of Tartu, Estonia*

[d] *Department of Civil Engineering, Ariel University, , Ariel 40700, Israel*

Introduction

Activity-based behavioural models (and more broadly agent-based models) employed for travel demand modelling have gained traction in the last years and the number of dedicated tools and applications is growing accordingly. Still, the inherent complexity and the large amount of input data required are major barriers to their wider adoption by practitioners and researchers [1]. On the other hand, traditional modelling approaches, such as four-step models, are prone to higher aggregation and reliability on historic demand patterns, which makes them less fit to address future challenges and disruptive trends such as teleworking or automation [2], [3]. Yet, a very high number of existing transport models are built with traditional tools and are not easily transferable. Nevertheless, a limitation of existing activity-based models is that they lack sufficient details in modelling the interactions at the supply side, which is problematic while framing how automation and advanced traffic management systems may affect future road network performance. This happens despite advanced traffic simulation models exist and have been widely validated and adopted to simulate scenarios involving automation and advanced traffic management systems [4]. To favour the adoption of disaggregate demand modelling tools while leveraging existing models and extending the capabilities of such models in supply modelling, we propose a methodology to integrate an activity-based model, which is able to produce a disaggregate demand, with a dynamic traffic assignment (DTA) model, capable to produce the resulting multimodal performance from the traffic supply. This way, existing DTA models may be expanded with the addition of an activity-based demand model (and vice-versa). The method is applied to a case study for the city of Tallinn – Estonia, for which two models have been built and calibrated, i.e., SimMobility MT as an activity-based tool and Aimsun as a traffic simulator. This work builds on [5], in which the integration is achieved by employing a simpler and more limited static traffic assignment (STA) tool.

Methodology - The modelling architecture

The proposed method involves the existence of two models: one able to produce daily activity schedules (DAS) for each traveller/agent and one assigning trips to a multimodal transport network, to produce skim (travel time) matrixes. A sketch of this framework, referring to our case study, presented later, is shown in Figure 1. This iterative feedback loop among two large-scale models has been defined as L0 in [6], and, although it has been criticised for its simplicity, our proposed approach allows the integration of existing models ex-post, with no need to build (and calibrate) a whole new modelling architecture.

Figure 38: The integrated framework applied to our case study, consisting of the integration of a demand modelling tool (SimMobility) and a microscopic traffic assignment tool (Aimsun)

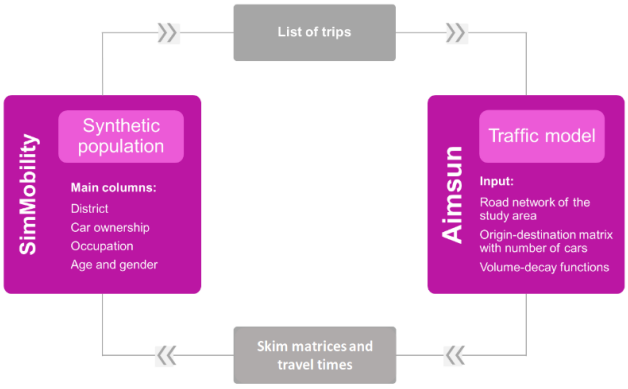

Source: From [5].

Methodology - The iterative algorithm

The proposed method is designed to integrate the two different models, assuming that their parameters, i.e., behavioural parameters in the demand model and the traffic parameters in the supply model, are properly calibrated. This is particularly important as one of the foreseen applications is to expand the applicability of the current traffic assignment model without the need to rebuild them in a different ad-hoc implementation. However, the simple solution of iterating between the two models is expected to almost never reach a stable equilibrium between demand and supply. To understand the goodness of the current equilibrium at each iteration, we introduce a measure of error (MoE) metric defined as the difference between the kernel density areas of the distribution of (travel times multiplied by the number of trips), formulated as

$$\Delta A = \int |k_i - k_{i-1}| \delta(t_{od} \cdot n_{od}) \qquad \forall o, d,$$

where k_i is the kernel density for iteration i corresponding to the distribution of $t_{od} \cdot n_{od}$ for each origin-destination (od) pair, while t and n are, respectively, the travel time and the number of trips for each pair od. This MoE can be visualised as in Figure 2.

Figure 39. Areas whose difference results in the MoE; note that $i + 1$ is the number of the current iteration

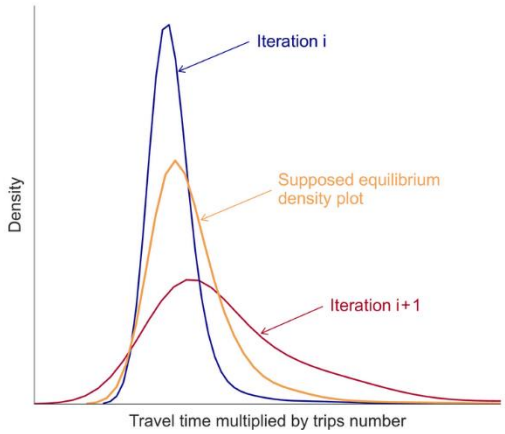

Source: From [5].

The MoE can be employed in an iterative algorithm that perturbs the solutions of each model and steers the overall solution toward an equilibrium. The algorithm consists of the following steps:

- A first round of iterations between the activity-based and the traffic assignment (TA) models defines the bi-dimensional search space, where one dimension is the MoE and the other is the kernel density. The activity-based model produces daily activity schedules that are then fed to the TA model as an OD matrix. The TA in turn produces skims that are fed back to the activity-based model. One run of each model corresponds to one iteration and produces one value of the MoE.
- The search space is discretised through quantiles of the skim matrixes; a finite number of simulations is performed to identify the most promising quantile.
- The surroundings of the identified quantile are evaluated to find the best-performing one (measured via the MoE).
- The skim matrix is perturbed to match the most promising quantile and a few additional iterations are run to assess the equilibrium point and its stability. As per the definition of quantile (i.e. cut points dividing the range of a probability distribution), each cell in the skim matrix assumes the border value between the region within the quantile and the region outside of it, in the area defined by the minimum and maximum t_{od} values from the first round of iterations. To the methodology itself, it does not matter if quantiles or other discretization measures are exploited to explore the defined search space.
- The equilibrium of the found solution is assessed to ensure that the equilibrium reflects an actual correspondence between the generated demand and supply (rather than just a local optimum).

Results

We perform experiments on a case study involving two models calibrated for the city of Tallinn, Estonia. The following two models have been employed.

- The activity-based behavioural model is SimMobility MT (using the pre-day demand module), the theoretical background of which is rooted in nested-logit theory and exploits logsum to relate different levels of the choice tree [7]. SimMobility takes as input a synthetic population [8] and skim matrices for all the modes of transport. The tool then computes the cost of each movement and compares it against the ones of the other alternatives. Further details on such a model, including the calibration procedure, are presented in [9].
- The dynamic traffic assignment is Aimsun [10], using a mesoscopic modelling approach. The calibration was carried out against detector data to perform a value GEH < 5 for 75 % of the entries. Aimsun takes in input aggregated DAS and produces skim matrices (through calibrated volume-delay functions [11]). The experiment involves both an STA (Wardrop's first principle) and a DTA (with stochastic route choice). The methodology has been extensively tested on STA, and the presented results will show how the dynamic component influences equilibrium. Besides, the applicability of DTA in this context will be proved.

Figure 40. Kernel areas whose difference defines the proposed MoE

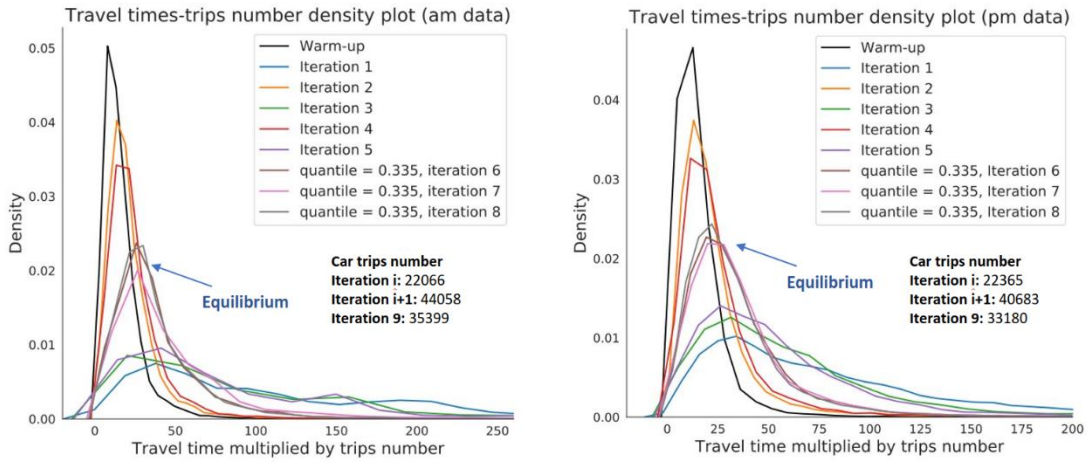

Source: From [5].

The results achieved with our proposed algorithm are illustrated in Figure 3, where the first 5 iterations are run without any perturbation, but then the skim matrix is perturbed to match a 0.335 quantile before running iteration 6. The 0.335 value is chosen after a discrete exploration of the search space bounded by the first 5 iterations' MoE. As it can be seen, the improvement is noticeable and the match between the outputs of the two simulations is very close and fairly stable. While graphically it is easy to see the improvement, The results of the achieved equilibrium have been validated in [5], to ensure that the perturbation of the skim would not result in unrealistic results.

Current work and conclusions

Current developments are focused on the assessment of the DTA model integration, which allows improvements, such as accounting for spillover effects of the queues that an STA cannot frame or framing interactions between single vehicles. The results are expected to allow thorough comparisons between the STA and DTA, highlighting whether the spillover component of traffic congestion is impactful enough to disrupt the proposed methodology or if instead, the proposed approach is applicable as is to the integration of activity-based models and DTA. We will compare the equilibrium points found through STA and DTA and assess their difference, as a way to frame the overall impact of the dynamic component. To further extend the applicability

of this iterative approach shall allow researchers and practitioners alike to expand their current available models by adding "ex-post", with no additional changes, an activity-based component to their DTA (or vice versa).

Acknowledgements

This research was funded by the FINEST Twins Center of Excellence, H2020 European Union funding for Research and Innovation grant number 856602 and the Academy of Finland project ALCOSTO (349327).

References

[1] Kagho G.O., Balac M., Axhausen K.W., 'Agent-Based Models in Transport Planning: Current State, Issues, and Expectations', *Procedia Computer Science*, vol 70, 2020.

[2] Schrank, D., Albert, L., Eisele, B. and Lomax, T., URBAN MOBILITY REPORT, 2021. [Online]. Available online: https://static.tti.tamu.edu/tti.tamu.edu/documents/mobility-report-2021.pdf.

[3] Dadashev, G., Levi, Y. and Nahmias-Biran, B., 'Demand Exploration of Automated Mobility on-Demand Services Using an Innovative Simulation Tool', *IEEE Open Journal of Intelligent Transportation Systems*, vol 3, pp. 580-591, 2022.

[4] Dadashzadeh, N., Elvarsson, A.B., Morshed, G., Agriesti, S., Antoniou, C., Roncoli, C. and Thomopulos, N., 'Autonomous and Connected Transport Scenarios Evaluation Based on Simulation Analysis: WG5 Thematic Report', 2021. [Online]. Available: http://dx.doi.org/10.13140/RG.2.2.36719.92324

[5] Agriesti, S., Anashin, P., Roncoli, C. and Nahmias-Biran, B.-h., 'Integrating activity-based and traffic assignment models: Methodology and case study application', *2023 8th IEEE International Conference on Models and Technologies for Intelligent Transportation Systems (MT-ITS)*, Accepted.

[6] Pendyala, R.M., You, D., Garikapati, V.M., Konduri, K.C. and Zhou, X., 'Paradigms for integrated modelling of activity-travel demand and network dynamics in an era of dynamic mobility management', in *Transportation Research Board 96th Annual Meeting*, 2017.

[7] Lu, Y., Basak, K., Carrion, C., Loganathan, H., Adnan, M., Pereira, F.C., Saber, V.H. and Ben-Akiva, M., 'SimMobility Mid-term simulator: A state of the art integrated agent based demand and supply model', in *Transportation Research Board 94th Annual Meeting*, 2015.

[8] Agriesti, S., Roncoli, C., Nahmias-Biran, B.-h., 'Assignment of a synthetic population for activity-based modelling employing publicly available data', *International Journal of Geo-Information*, vol. 11, 2022.

[9] Agriesti, S., Kuzmanovski, V., Hollmén, J., Roncoli, C. and Nahmias-Biran, B.-h., 'Calibration of large-scale behavioural transport models via bayesian optimization', in *Transportation Research Board 102th Annual Meeting*, 2023.

[10] Aimsun: Simulation and AI for intelligent mobility, 2023. Available online: https://www.aimsun.com/.

[11] Aimsun SLU, Aimsun User Manual, 2022. Available online: https://docs.aimsun.com/next/22.0.1/.

The Impact of Heavy Vehicles on Headway Distributions: A Study Using Naturalistic Urban Expressway Trajectories Extracted From High Resolution Videos Collected in Washington DC., USA.

P. Beigi[a], S. H. Hamdar[a]

[a] *Department of Civil and Environmental Engineering, The George Washington University, Washington, DC 20052, United States*

Introduction and Literature Review

The headway between vehicles is an important traffic flow characteristic affecting safety, level of service, driver behavior, and capacity of a transportation system. Furthermore, it can be used to generate realistic vehicle dynamics in microscopic simulation models, as well as for gap acceptance analysis (1). Research has been conducted on headway distribution for decades, and many models have been proposed to describe their characteristics; however, selecting the most suitable model for a particular traffic condition remains an ongoing research topic (2). In addition, most reported studies on headway concentrate on mixed vehicular flows without examining the variation in headway between different vehicle types (3). Finally, many of the previous studies used headway data collected from a highway without separating data by lane type (4).

This study aims to identify the characteristics of vehicle headways by using naturalistic traffic data separated by vehicle type and lane-position. Four types of headways are analyzed based on different combinations of leading and following vehicles: Car-Car (i.e., passenger car to passenger car – C-C), C-Heavy Vehicle (HV – mainly truck), HV-C, and HV-HV. Comparing each vehicle type's specific headway statistically is undertaken to determine whether there is a significant difference between them. The study focuses on answering the following four questions: (I) what are the differences between the characteristics of the headways if classified by leading/following vehicle types? (II) Which distribution model is most appropriate for a particular type of headway if such headways are made lane-specific? (III) What are the behavioral characteristics of drivers and preferred time headway for different vehicle types? and (IV) Is there a statistical difference between different vehicle types preferred time headway? This paper identifies qualitative differences between vehicle type-specific headways and distributions and provides a base for practical applications, especially to improve microscopic traffic simulation models in a naturalistic congested expressway setting with limited right of way and challenging geometric features.

Methodology and Data Description

The data analyzed in this paper is from the eastbound approach of the I-695 urban freeway (expressway) in Washington, DC, USA. The data is collected through the Third Generation Simulation (TGSIM) trajectory data. Vehicles in this study are classified into two types: Cars (which include sport utility vehicles – SUVs) and Heavy Vehicles (which includes trucks and buses). The headway data is then divided into different groups based on the type of the following and leading vehicles. The median value and standard deviation of the vehicle headways are calculated. The range of mean headway in lanes 1 (right-most lane), 2 (middle), and 3 (left-most merging lane) are 19.2, 20.8, and 21.2 m, respectively. Flow are ranging from 900 passenger's car per hour per lane (pc/h/ln) to 3180 pc/h/ln.

In this study, the Weibull, Gamma, Lognormal, and Inverse Gaussian distributions are applied to fit the observed headway data for each type under different lane positions. It is important to determine which distribution fits the data in an acceptable manner and to what extent the selected distribution "fits" the measured data (feasibility/acceptability of fit and degree of fit). For each lane and each vehicle type combination, the goodness of fit models on the distribution of total headways collected is examined. The most compatible model (degree of fit) to the data is selected for further analysis and discussion and t-tests were utilized to make statistical comparisons between the distributions. In traffic engineering, the chi-square test and the Kolmogorov–Smirnov (K-S) test are commonly used. For each examined sample value x, the K-S test compares the proportion of values less than x with the expected number predicted by the hypothesized distribution. It uses the maximum difference over all x values and its test statistic. In other words, a smaller test statistic indicates a better performance from the examined distribution model. After determining the fittest distribution model for each headway type under all the traffic scenarios, the distribution model with the most traffic scenarios accepted becomes the recommended one for a particular headway type.. In order to find the relation between the time headway and speed, a regression approach is used to estimate coefficients of different regression equations which describe the relationship between one or more independent quantitative variables and a dependent variable. Finally, t-test is applied to compare the average values of the different data sets while determining the corresponding sample origin(s).

Results and Discussions

Table 1 provides Goodness-of-fit statistics comparing different distributions and the results of different tests and estimated parameters. (for summarizing purposes, only Lognormal and Inverse Gaussian for C-C and C-HV headways are presented). When fitting distributions, Kolmogorov-Smirnov statistic, chi-square, Akaike's Information Criterion, and Bayesian Information Criterion statistics are considered. Figures 1 provides four classical goodness-of-fit plots for C-C headway for lane 1.

Figure 41. Four Goodness-of-fit plots for various distributions fitted to C-C for lane 1

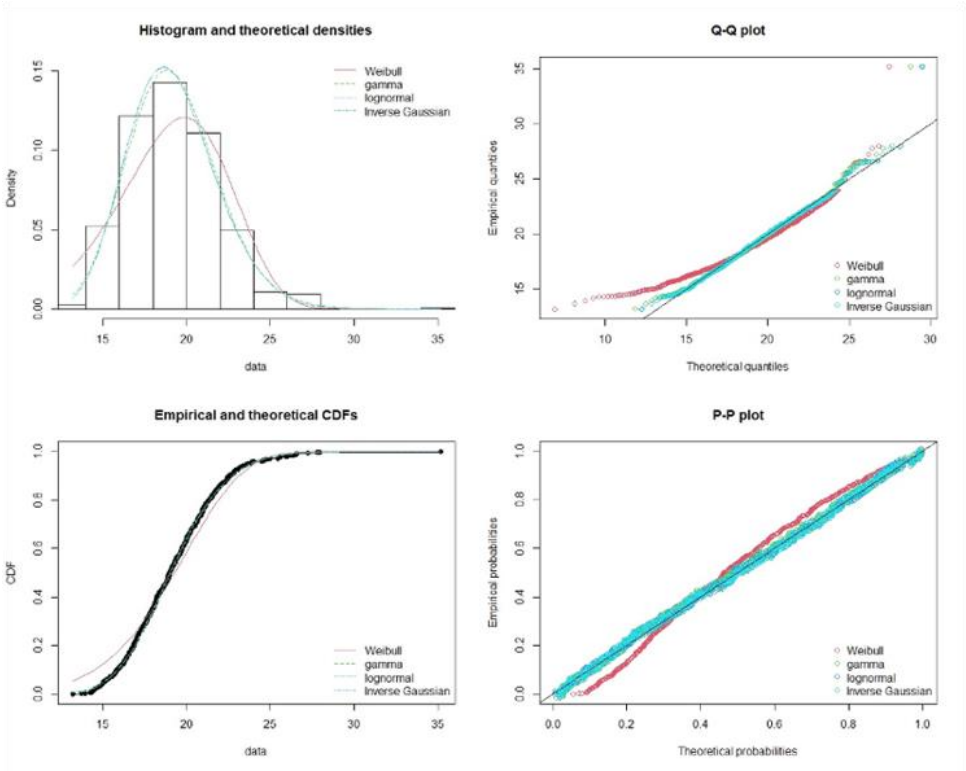

Source: Authors' elaborations.

A statistical hypothesis test used to examine if a variable is likely to come from a given distribution is the Chi-square goodness of fit test. All the goodness-of-fit statistics based on the CDF distance are in favor of the lognormal and Inverse Gaussian distribution. They are characterized by three parameters and supported by "better" AIC and BIC values. Results indicate that the Inverse Gaussian distribution provided better fit to the sample data collected. The K-S test also supports our conclusion drawn from visual comparisons of the curves. The relation between time headway and speed when the acceleration is less than 0.25 and 0.1 m/s^2 are presented. It was observed that most of passenger car drivers choose headway 2s or less while most of heavy vehicle drivers choose more than 2.3s. In order to illustrate the relation between the time headway and speed, the results of a linear regression model is presented in this abstract. The model is applied on actual data and logarithmic data since logarithmic transformation allows dealing with highly skewed variables. There is a relationship between time headway and speed since the p-values from the result are very low. R-value from the result indicates negative correlation between the variables and shows substantial relationship.

Table 2 shows t-test result of comparison between the two data sets and determines if they came from the same population (for summarizing purposes, only C-C vs C-HV for lane 1 is presented). Mean comparison is the central theme of many classical statistical procedures. The independent-sample t-test is used to test the equality of two means from independent populations with equal variances, when these conditions are not met, the Student's t-test can be biased whereas Welch's t-test is generally preferred when the variances are not equal. If the values are large, it indicates that the groups tested are incredibly different. In contrast, a smaller t-score suggests that the groups are similar. The p-value shows we can reject the null hypothesis (H_0) of no difference between the (true) averages of the two groups. Result shows there is a statistical difference between the two means. Here, the word "true" is used to refer to the averages you would get if you had access to all possible samples.

Table 7. Goodness-of-fit statistics comparing different distributions

	Headway Type	C-C			C-HV		
Tests	**Distribution / Lane**	**1**	**2**	**3**	**1**	**2**	**3**
Kolmogorov-Smirnov statistic	Critical values*[11]	0.0535	0.0535	0.0535	0.0842	0.0930	0.1290
	Lognormal	0.022	0.031	**0.064**	**0.105**	0.067	0.069
	Inverse Gaussian	**0.021**	**0.030**	0.065	0.106	**0.064**	**0.067**
Akaike's Information Criterion	Weibull	3255.2	3322.9	3548.6	1761.8	1504.2	748.9
	Lognormal	**3086.2**	3220.6	3382.4	1699.1	1478.9	739.9
	Inverse Gaussian	3086.3	**3220.3**	**3381.9**	**1697.9**	**1478.6**	**739.7**
Bayesian Information Criterion	Gamma	3103.6	3233.7	3407.9	1719.0	1488.2	745.3
	Lognormal	**3095.1**	3229.6	3391.3	1706.3	1485.6	745.3
	Inverse Gaussian	3095.2	**3229.2**	**3390.8**	**1705.1**	**1485.4**	**745.1**
chi-square	Critical values*[2]	11.071	11.071	11.071	11.071	11.071	11.071
	Lognormal	11.57	29.45	43.98	45.75	22.88	9.91
	Inverse Gaussian	**11.52**	**29.22**	**43.63**	**45.38**	**22.53**	**9.79**

Source: Authors' elaborations.

Table 8. Welch Two Sample t-test

Data	t	df	p-value	95% confidence interval	Mean of x	Mean of y
C-C vs C-HV Lane 1	-8.91	256.6	2.2e-16	-1.0418, -0.6643	1.792759	2.645886

Source: Authors' elaborations.

Conclusion

Using video extracted headway data, , it was found that the space and time headways varied according to the follower and leader vehicle types. The headways were therefore divided into four categories (C–C, C–HV, HV–C and HV–HV) and the adaptability of several headway distribution models was examined. This study considered four common distribution models (Weibull, lognormal, inverse Gaussian, Gamma). The results of Maximum likelihood estimation (MLE), K-S, chi-square, AIC, and BIC tests further confirmed that these headway types follow Inverse Gaussian distribution. In addition, it was found that each type of headway can be influenced by the percentage of heavy vehicles and lane position. We quantified the parameters of speed and time headway, differentiating vehicles by type and by lane in order to provide a description of how drivers regulate speed and time-headway. Results show that the average C-C and C-HV, HV-C, HV-HV headways are about 1.84, 2.35, 2.82, and 2.91 seconds, respectively. Result shows drivers prefer to keep a large distance if there is a large vehicle ahead. In order to find a relation between the time headway and speed, a linear regression approach is presented to estimate coefficients of regression equations. It can be concluded from these models that there

([11]) for $\alpha = 0.05$

is a relationship between time headway and speed since p-values from the result are very low. R-value from the result indicates a negative correlation between the time headway and speed. The t-test show that we can reject the null hypothesis (H_0) of no difference since the p-value is less than the usual significance level alpha = 0.05. There is a statistical difference between the means of headways. This result supports the argument that the headway analysis should consider vehicle type and that the mix–flow headway modelling is inadequate. Time headway shows that it is nearly independent of speed for speeds greater than around 10 m/s. In other words, in less congested conditions, when drivers do not tend to be hindered by surrounding disturbances, the time headway is stabilized at uniform values; these values are representative of the desired headways by the drivers following a given leader. Our research provides helpful information in modeling the desired time-gap/headway which may be translated into useful intelligent cruise control vehicle design or calibrated microscopic acceleration models/car-following strategies.

References

Sullivan, D. and R. Troutbeck, 'The use of Cowan's M3 headway distribution for modelling urban traffic flow', *Traffic engineering & control*, Vol. 35, No. 7/8, 1994.

Zhang, G., Y. Wang, H. Wei, and Y. Chen, 'Examining headway distribution models with urban freeway loop event data', *Transportation Research Record*, Vol. 1999, No. 1, 2007, pp. 141–149.

Ye, F. and Y. Zhang, 'Vehicle type–specific headway analysis using freeway traffic data', *Transportation research record*, Vol. 2124, No. 1, 2009, pp. 222–230.

Abtahi, S. M., M. Tamannaei, and H. Haghshenash, 'Analysis and modeling time headway distributions under heavy traffic flow conditions in the urban highways: case of Isfahan', *Transport*, Vol. 26, No. 4, 2011, pp. 375–382.

Modelling road congestion patterns across EU cities

P. Christidis[a]

[a] *European Commission, Joint Research Centre (JRC), Seville, Spain*

Introduction

Road congestion in urban areas has long been a major challenge for transport policy and traffic management (Christodoulou et al., 2020). One of the 'silver linings' of the Covid-19 pandemic was a decrease in transport demand and visibly lower congestion levels in most European cities. Nevertheless, transport activity is already showing a gradual return to year 2019 levels, with the lifestyles and work patterns adopted during the pandemic returning to normality. Some of the behavioural changes –such as remote work- may still partially continue, probably at a lower degree than in the height of the pandemic (but still more commonplace than before). The new patterns may- however- also to increased levels of car ownership and use (Christidis et al., 2022; Lopez Soler et al., 2021), resulting in a rebound in the levels of congestion.

Monitoring congestion levels at urban level can provide insights as regards the evolution of transport demand. Particularly in a post-pandemic context, the analysis of daily congestion patterns can provide useful indicators on how changes in user preferences or the adoption of new policy measures can modify overall demand. From the user side, changes may be due to modified work patterns -such as tele-working- or modal preferences (e.g. increased active mobility choices). From the policy side, measures such pedestrianisation or the introduction of low emission zones can affect both the supply and demand of transport infrastructure.

Data and methods

For the analysis presented here, we used a database of TomTom congestion indicators on a daily level for 178 cities in the EU, from 2019 to 2022 (Christidis and Ibanez Rivas, 2012; Christodoulou and Christidis, 2020). We combine the congestion data with detailed meteorological data at city level from the European Climate Assessment & Dataset (Squintu et al., 2021). The combination of the two datasets allows a direct analysis of the impacts of weekly variance, especially as regards weekdays compared to weekends, as well as an initial exploration of the impact of weather conditions.

Congestion levels in a specific city tend to combine a general trend reflecting the overall evolution of demand, with strong weekly and seasonal effects, sprinkled with unique events that temporarily affect either the demand or the supply of transport infrastructure. These may include extreme weather effect, public transport strikes, or major sport events. A significant part of congestion level can be explained through recurring patterns, but non-recurring events may lead to outliers that are important to monitor.

We apply a hybrid modelling approach that allows us to identify the long-term trends in the evolution of congestion taking into account the factors that affect weekly and seasonal. This involves the combination of two machine learning approaches: a tree based algorithm that estimates the variation caused by specific conditions in the city at a specific time with an informed time series model that allows capturing the underlying trends in total demand. A particularly important variable that is addressed is the change in demand due to teleworking. For this we use the Google indicator, which allows the identification of a trend in each city (Google, 2020). We use different scenarios on how this trend can continue in the future.

Results

Congestion levels were still lower in 2022 compared to those of 2019, for the majority of the cities covered. There is, however, a strong trend towards the recovery of past levels, mainly due to the gradual return to physical presence at work. The impact of remote work is visibly higher than in 2019, but the trend implied in the data suggests that it will be gradually less impactful. Other activities, such as retail and entertainment, appear to have returned to similar –or higher- levels than in 2019 (Figure 1). The observed trends suggest that- unless specific measures are adopted- congestion levels will return to higher levels.

Figure 42. Urban road congestion levels in the EU, change 2019-2022

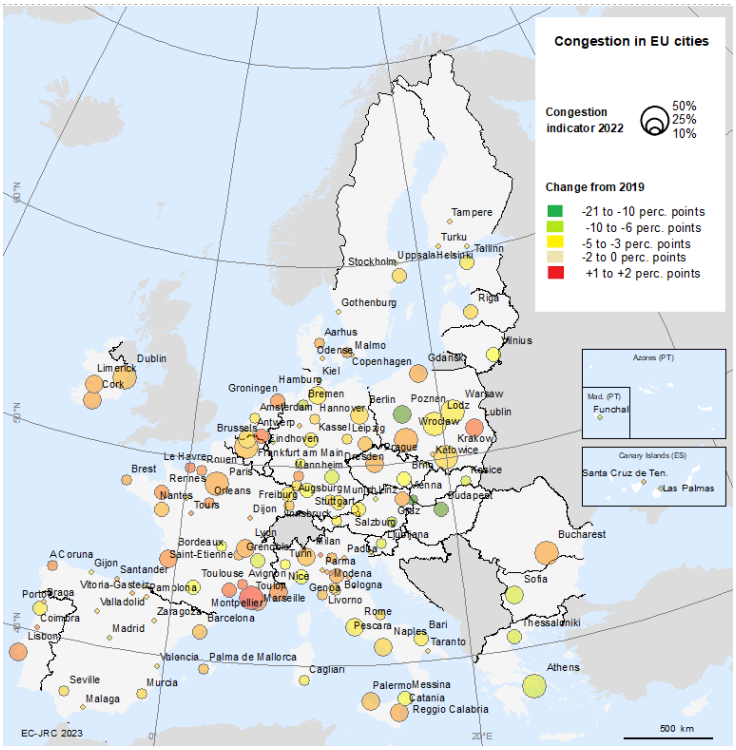

Source: Authors' calculations, based on TomTom data.

The variance of congestion levels across cities is high, but the overall pattern of their evolution reveals a clear trend. Figure 2 compares the average daily congestion level on weekdays (Monday to Friday) by month and year. The indicators reached their minimum in April 2020, at the height of the pandemic, and have been gradually recovering until June 2022. Comparing September-November in 2021 and 2022 shows a new decrease in congestion levels, probably caused by the increased fuel prices and the economic recession in the period.

A main driver for the fluctuations in congestion levels is the presence in the workplace. Comparing the median of the weekly average of congestion on weekdays for the 178 cities covered by TomTom, with the corresponding median for the Google workplace indicator highlights the correlation and suggests that a possible continued increase in workplace presence may lead to higher traffic congestion levels (Figure 3).

Figure 2. Comparison of variance of average monthly congestion across EU cities, 2020-2022

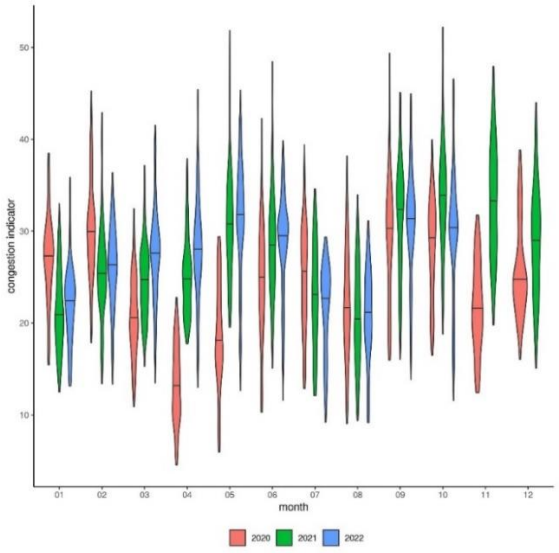

Figure 3. Comparison of evolution of congestion and workplace indicators, 2020-2022

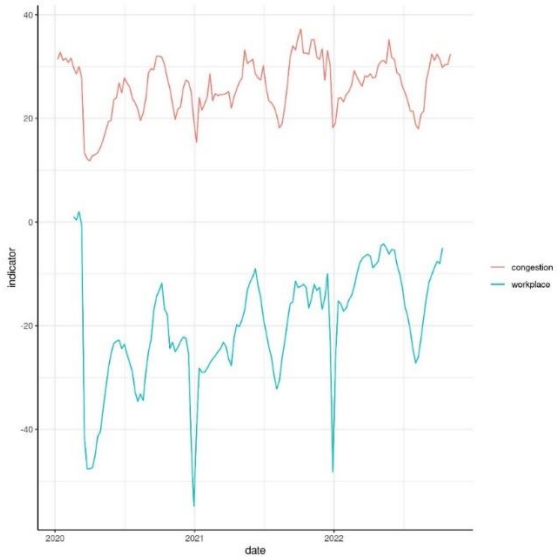

Discussion and conclusions

Congestion levels depends on several factors that may affect both the long-term evolution in time and short-term variability of the daily patterns. The level of congestion depends on the ratio of demand to capacity for a specific time period. A change in the underlying mean congestion level may reflect a shift in demand –through a change in either its total level or its timing- or a change in the capacity (e.g. modifications in the road network or in the alternatives to car use).

From the policy perspective, it is important to be able to identify the underlying trend in the ratio between demand and supply, especially since it can reflect the impact of behavioural changes or the repercussions of policy measures. From the modelling perspective, the hybrid approach presented here permits addressing both long-term trends and short-term variation.

References

Christidis, P., Cawood, E.N., Fiorello, D., 2022. Challenges for urban transport policy after the Covid-19 pandemic: Main findings from a survey in 20 European cities. Transport Policy 129, 105–116. https://doi.org/10.1016/j.tranpol.2022.10.007.

Christidis, P., Ibanez Rivas, J.N., 2012. Measuring road congestion. European Commission, Joint Research Centre (JRC) JRC69961.

Christodoulou, A., Christidis, P., 2020. Evaluating congestion in urban areas: The case of Seville. Research in Transportation Business and Management. https://doi.org/10.1016/j.rtbm.2020.100577.

Christodoulou, A., Dijkstra, L., Christidis, P., Bolsi, P., Poelman, H., 2020. A fine resolution dataset of accessibility under different traffic conditions in European cities. Scientific Data 7. https://doi.org/10.1038/s41597-020-00619-7.

Google, 2020. COVID-19 Community Mobility Reports, https://www.google.com/covid19/mobility/.

Lopez Soler, J.R., Christidis, P., Vassallo, J.M., 2021. Teleworking and online shopping: Socio-economic factors affecting their impact on transport demand. Sustainability (Switzerland) 13. https://doi.org/10.3390/su13137211.

Squintu, A.A., van der Schrier, G., van den Besselaar, E., van der Linden, E., Putrasahan, D., Roberts, C., Roberts, M., Scoccimarro, E., Senan, R., Klein Tank, A., 2021. Evaluation of trends in extreme temperatures simulated by HighResMIP models across Europe. Climate Dynamics 56, 2389–2412. https://doi.org/10.1007/s00382-020-05596-6.

Proposed Methodology for Improving Timetables Using GTFS - A Case Study of Yokohama Municipal Bus

A. Taichi FURUKAWA[a], B. Fumihiko NAKAMURA[b], C. Shinji TANAKA[c]

[a] *Yahoo Japan Corporation*

[b] *Graduate School of Frontier Sciences, The University of Tokyo*

[c] *Graduate School of Urban Innovation, Yokohama National University*

Introduction

In Japan, with the aim of digitization and standardization of data, the spread of General Transit Feed Specification (GTFS) data is advancing among bus operators. While a lot of information is made public as open data, the data is not being utilized much in the operation of bus services. For example, some of the travel time between bus stops to make a timetable is set to uniform throughout the day, and a timetable reflecting the actual operation is not offered. As a result, there are buses that almost always run behind schedule. In response, Ota et al. (2018) have proposed a bus timetable improvement method using actual operation data, targeting a certain bus operator. However, as the timetable is generated based on the percentiles of the required time, it is considered that the improved timetable has a relatively high risk of early departure. Therefore, this research aims to improve the reliability of bus timetables and to reduce the effort required for the improvement of timetables by public transportation operators, proposing a timetable improvement method that can improve reliability without causing early departure as much as possible by using GTFS Real-Time data.

Methodology

Target Bus Operators and Data

In this paper, the Yokohama Municipal Bus operating in Yokohama City, Kanagawa Prefecture, Japan is the target bus operator. The overview of the analyzed data is shown in Table 1. Yokohama Municipal Bus is a bus operator that operates approximately 10,000 buses per day on about 600 routes. Also, since Yokohama City is a municipality with the largest population in Japan, it runs relatively busy roads and has many passengers. In other words, chronic delays are likely to occur at many bus stops, but significant efforts are required to revise the timetable. The Vehicle Position of GTFS Real Time data (GTFS-RT data) used as the target data is collected using the API GET method once every 30 seconds.

Table 9. Summary of Analyzed Data

Target Transportation Operators	Yokohama Municipal Bus
Data Source	Public Transportation Open Data Center
Target Period	2022-10-01 – 2022-11-30
Frequency of GTFS-RT data acquisition	Once every 30 seconds
Record Size	30,783,038

Calculation of departure time results

To begin with, the distance from each starting bus stop to the location of the bus, as specified by the delivered bus location information, was calculated. The location information from the delivered GTFS-RT data was then converted into the distance from the starting point of each route. The conversion was performed using the geodesic algorithm proposed by Karney (2013). Additionally, for convenience, the time was converted into integers representing the elapsed seconds from 00:00am. A part of the results calculated in this manner is presented in Figure 1. In Figure 1, the operational records of 40 buses that were operated during the analyzed period are plotted, focusing on one trip_id. Additionally, Figure 38 shows a map overlay highlighting the chronically delayed section identified in Figure 38.

Figure 43. Yokohama Municipal Bus Route 202

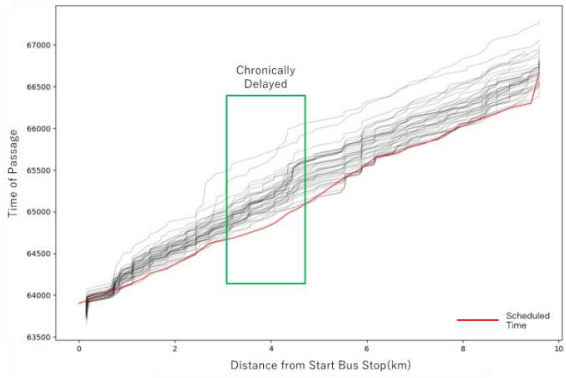

Figure 44. Yokohama Municipal Bus Route 202 Segment of Chronic Delays

Afterward, each bus stop + 20m location was calculated as the departure time of that bus stop, as shown in Table 2. During the calculation, considering that the bus timetable is comprised of minutes, the time was rounded to elapsed minutes from 00:00 am by truncating any seconds.

Table 10. Departure Time Calculation Results (Excerpts)

trip_id	date	route_id	stop_id	stop_sequence	departured_time
20202_03202210011087AC01107	2022/10/26	20202	0826_02	2	583
20202_03202210011087AC01107	2022/10/26	20202	2611_05	3	585
20202_03202210011087AC01107	2022/10/26	20202	0014_02	4	586
20202_03202210011087AC01107	2022/10/26	20202	2610_02	5	587

By utilizing the calculated actual departure times, a new timetable was created. A timetable that is less likely to experience delays can be created by delaying departure times from the current timetable. However, such changes may result in buses arriving earlier than scheduled. In Japan, early departures by buses are prohibited, so buses that arrive early must wait at the bus stop until the scheduled departure time. To consider this trade-off, the Allowable Waiting Occurrence Rate (AWOR) is used as an indicator that shows the maximum occurrence rate of buses requiring time adjustment, which operators can tolerate. Letting r be an arbitrary AWOR, for a route that passes through n bus stops, with $X_1, X_2, X_3, \ldots, X_{n-1}$ representing the set of departure time actuals at each bus stop, the function $Q(X_i, r)$ representing the time that satisfies the AWOR for each bus stop. The function $M(X_i)$ represents the most frequent departure time at each bus stop. The new departure time $T(X_i, r)$ is represented by the following equation:

$$T(X_i, r) = \begin{cases} Q(X_i, r), & M(X_i) > Q(X_i, r) \\ M(X_i), & otherwise \end{cases}$$

Results

The newly calculated timetable, as a result of the calculation, shows a decrease in the number of buses that are generally delayed when comparing the average delay time, as confirmed in Figure 3. Furthermore, even when the AWOR is set to 0%, improvement in delays can be seen, indicating that some buses are not currently operated on schedule.

Figure 45. Top 30 routes with eliminated delays when the AWOR is set to 10%

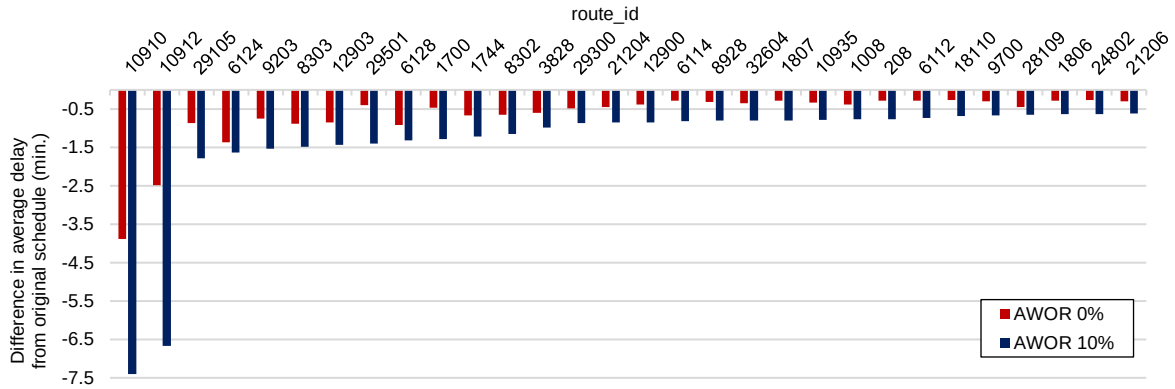

When the AWOR is set to 10%, it is expected that the number of delayed buses, as represented by route_id 10910 in Figure 3, will significantly decrease. However, it should be noted that this decrease may lead to more buses requiring adjustment of their schedules. Nonetheless, Figure 4 shows the frequency of bus schedule adjustment for the route mentioned in Figure 3, and due to the use of the new timetable as the most frequent departure time at many bus stops, schedule adjustments can be controlled with a small number in the low percent range. In addition, Figure 5 shows the percentage reduction in delayed buses on the route mentioned in Figure 3. According to this figure, it is evident that even on routes where the decrease in delay time is small, on-time performance can significantly improve. For example, on route_id 6128, the reduction in average delay time is not significant at about -1 minute with AWOR set to 10%, but the percentage reduction of delayed buses is the highest among other routes, at about -20%.

Conclusions

In this study, a method for creating a schedule that reflects the operating performance of all routes of a targeted operator was presented by using GTFS data. The method demonstrated the ability to significantly reduce the number of delayed buses on some routes. Specifically, the method adopts either the earliest time that satisfies either the most frequent departure time at each stop or the time representing the ratio of buses that allow for permissible time adjustments (AWOR) as the new departure time. With AWOR at 10%, for example, the average delay time was reduced by a maximum of approximately 7 minutes compared to before improvement. Furthermore, even with AWOR at 0%, a decrease in the number of delayed buses was confirmed, revealing that some buses were not operated on time according to the current schedule. This method is considered to be an effective means for revising schedules, especially for bus routes in urban areas with high traffic volume and passenger volume. On the other hand, it is believed that improving the schedule by taking into account the availability of bus bays and other factors that allow for time adjustments can result in a better schedule. Additionally, the method presented in this study does not consider the work system of the drivers. Solving these issues is expected in the future.

Figure 46. The frequencies of bus schedule adjustment when the AWOR is set to 10%

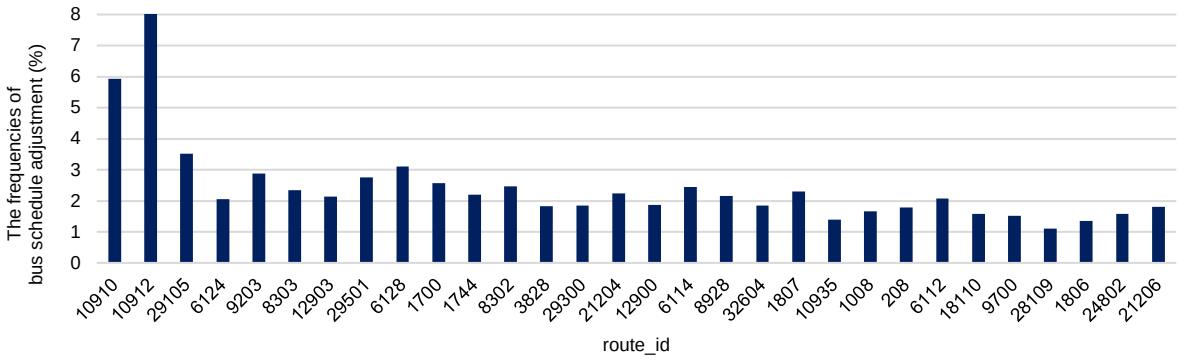

Figure 5. Percentage reduction in delayed buses when the AWOR is set to 0% and 10%

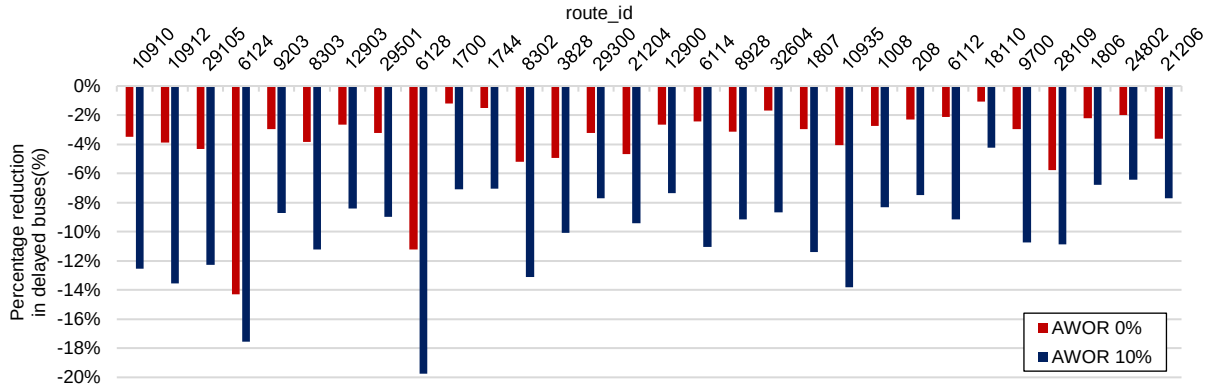

References

Kohei OTA, Keita MORI, Kiyoshi HIRAMOTO, Yusuke MAEKAWA, Masaki ITO, *Improving Bus Schedules Based on Real-Time Bus Arrival Information with Open Innovation in Ryobi Group*, Proceedings of infrastructure planning, 2018.

Bus information of Transportation Bureau, City of Yokohama (https://ckan.odpt.org/dataset/b_bus_gtfs_jp-yokohamamunicipal).

Bus realtime information of Transportation Bureau, City of Yokohama (https://ckan.odpt.org/dataset/b_bus_gtfs_rt-yokohamamunicipal).

Charles F. F. Karney, *Algorithms for geodesics,* Journal of Geodesy, 2013, doi: 10.1007/s00190-012-0578-z.

Reinforcement learning for congestion pricing with day-to-day dynamics

A. Anders Lassen[a], B. Renming Liu[a], C. Ravi Seshadri[a], D. Filipe Rodrigues[a], D. Carlos Lima Azevedo[a]

[a] *DTU Management, Technical University of Denmark, Denmark*

Introduction

The problem of traffic congestion is a growing concern around the world, with traffic networks becoming increasingly congested every year. Despite the decrease in travel during the COVID-19 pandemic, the total distance travelled by vehicles has risen quickly, resulting in further congestion of traffic networks in both Europe and the US (INRIX, 2023). The impacts of traffic congestion extend beyond just delays and frustration for drivers. They also have far-reaching effects on the environment, the economy, and human health (Falcocchio, 2015). These potential impacts highlight the need to research and develop methods to alleviate traffic congestion and mitigate its negative global effects on people and the environment. This serves as the motivation for finding methods to decrease congestion in traffic networks.

Congestion pricing is common approach for mitigating congestion in traffic networks. The concept was introduced by economist Pigou in 1920 (Pigou, 2013) and induces users to change their activity patterns, departure time, mode and route choices by imposing a tax on traffic networks in the form of a toll (de Palma and Lindsey, 2011). Consequently, the behaviour of users can be managed through a pricing scheme, which is typically designed to maximize social welfare.

This paper proposes an adaptive and dynamic congestion pricing system using reinforcement learning (RL) algorithms specifically designed and trained for this purpose. The goal of this system is to reduce congestion and related problems, such as high travel times for users of the traffic network, by optimising the total system travel time. The approach involves first defining a modelling framework and simulating a traffic network environment. Different reinforcement learning algorithms are then applied to train models within this environment. The models will be quantitatively compared against two baselines: one with no toll and one with a toll set using random actions.

Methodology

The overall framework utilizes a simulator for the morning commute problem, which includes a traffic network regulated by an adaptive time of day toll with users who make departure time choices based on network conditions. The users learn and adapt to the traffic network's experienced situations, which will change their mobility choices in a day-to-day manner based on the previous day. The users adapt their mobility choices differently depending on their own value of time as well as their values of schedule delays (early and late). For more details on the simulation framework, we refer the reader to Liu et al. (2022).

Figure 1 shows the overall framework from a high-level perspective. The traffic network is at the centre and is influenced by changes from the regulator that sets the adaptive time-of-day tolls, which in turn affects the mobility choices of the users (modeled using a logit-mixture model). The traffic network simulates network congestion based on the mobility choices made by the users (modeled using a trip-based Macroscopic Fundamental Diagram model). The users pay toll payments to the regulator depending on when and how far they travel and base their own mobility choices on their experience of the realized network conditions. If the toll is more expensive at a certain time than the value of arriving at the desired time for each user, the users will change their departure time accordingly. The control policy, which is learned through reinforcement learning, takes an observation from the traffic network as input and outputs an action consisting of changes to the toll profile parameters which the regulator uses to impose the adaptive time of day tolls for the next day on the traffic network. This means that the policy makes relative changes to the toll profile parameters for each day based on the observation from the previous day.

Figure 47. Overall framework used to train and test models

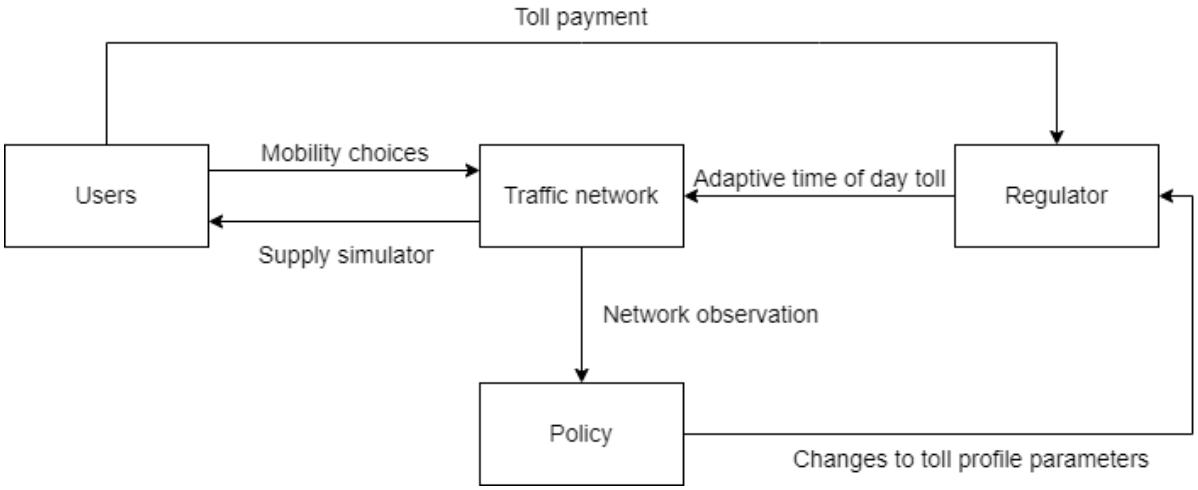

Source: Authors' elaborations.

The time-of-day toll is set by a toll profile, which is a custom Gaussian distribution based on the three toll profile parameters, amplitude, mean and standard deviation. The users have 15 different 15-minute departure time windows to choose from and the toll imposed is based on the departure time window and the distance travelled.

The reinforcement learning algorithms used to learn the policy are Proximal Policy Optimization (PPO), which was introduced by Schulman et al. (2017) and is an on-policy algorithm, and Twin-delayed Deep Deterministic Policy Gradient (TD3), which was introduced by Fujimoto et al. (2018) and is an off-policy algorithm.

The observation space consists of the index of the day (one-hot encoded) and the number of users of the traffic network in each departure time window. The action space is set up to allow relative actions that change the parameters of the toll profile for each day with three dimensions: A change to the amplitude of the toll profile between -2.0 and 2.0, a change to the mean of the toll profile between -3.0 and 3.0 and a change to the standard deviation of the toll profile between -2.0 and 2.0. The reward function is set with the objective of optimising the total system travel time, which Pandey et al. (2020) found utilises the traffic network to full capacity at all times.

The training of models is done in episodes of 30 days, whereafter the simulation environment is reset to the original state with random starting toll profile parameters. The starting departure time choices used when training the models are the departure time choices from the equilibrium state of the simulation environment without a toll. This is done to ensure that training episodes reach the equilibrium state before 30 days. The testing is done across 10 different episodes of 30 days with the mean and standard deviation computed for the last 10 days in each episode to allow the simulation to reach the equilibrium state, where users no longer change their departure time choices significantly.

The metrics used for testing model performance are: travel time, travel time cost, social welfare and consumer surplus for each user.

Results

Experiments are done with no toll, random actions for setting the toll, different observation spaces and a different action space. Table 1 shows the results of testing no toll, random actions and the proposed RL approach described in the previous section.

The RL policies significantly improve the performance measured by travel time and travel time cost per user when compared to the no toll and random actions cases.

Experiments have also been done with different observation spaces, a different action space and a change in capacity of the traffic network from 4500 to 4000. The models are able to achieve comparable performance to the performance reached with the RL algorithms in Table 1. The experiments with a change in capacity of the traffic network further show that the RL policies generalize well to new scenarios.

Figure 48. Results with the basic observation space

Model (mean ± std.)	Travel time [min/user]	Travel time cost [DKK/user]	Social welfare [DKK/user]	Consumer surplus [DKK/user]
No toll	26.66 ± 0.01	26.84 ± 0.01	-24.57 ± 0.01	-24.57 ± 0.01
Random actions	22.93 ± 1.63	23.12 ± 1.63	-23.30 ± 1.15	-34.62 ± 6.47
PPO (225 eps.)	20.17 ± 1.41	20.31 ± 1.44	-23.19 ± 1.12	-38.08 ± 5.21
PPO (300 eps.)	20.49 ± 1.44	20.62 ± 1.46	-23.22 ± 1.23	-37.80 ± 5.55
TD3 (225 eps.)	19.72 ± 0.32	19.82 ± 0.31	-23.72 ± 0.88	-45.03 ± 0.41
TD3 (300 eps.)	19.70 ± 0.44	19.80 ± 0.43	-23.94 ± 0.88	-45.54 ± 0.85
Contextual Bayesian Optimization	19.07 ± 0.03	19.18 ± 0.02	-23.89 ± 0.12	-43.48 ± 0.66

([1]) The performance of models trained with the basic observation space for the final 10 days of each episode across 10 episodes

Source: Authors' elaborations.

Conclusions

The experiments show that the proposed RL approaches are successfully able to achieve significantly better performance than the baseline policies without toll and with random actions. Furthermore, the RL policies learned were empirically shown to be able to adapt to new and unseen scenarios e.g., a change in traffic network capacity.

The improved performance is measured by travel time and travel time cost per user. Future work should investigate the effect of the objective and explore reward functions which include metrics such as social welfare.

References

de Palma, A. and Lindsey, R., 'Traffic congestion pricing methodologies and technologies', *Transportation Research Part C: Emerging Technologies,* Vol. 19, No. 6, Elsevier, 2011, pp. 1377-1399.

Falcocchio, J.C. and Levinson, H.S., 'The Costs and Other Consequences of Traffic Congestion', *Road Traffic Congestion: A Concise Guide*, Springer International Publishing, 2015, pp. 159-182.

Fujimoto, S., Van Hoof, H. and Meger, D., *Addressing Function Approximation Error in Actor-Critic Methods*, arXiv, 2018.

Liu, R., Chen, S., Jiang, Y., Seshadri, R., Ben-Akiva, M. and Azevedo, C.L., 'Managing network congestion with a trip- and area-based tradable credit scheme', *Transportmetrica B: Transport Dynamics,* Vol. 11, No 1, Taylor & Francis, 2022, pp. 434-462.

Pandey, V., Wang, E. and Boyles, S.D., 'Deep reinforcement learning algorithm for dynamic pricing of express lanes with multiple access locations', *Transportation Research Part C: Emerging Technologies,* Vol. 119, Elsevier, 2020, pp. 102715.

Pigou, A.C., *The Economics of Welfare*. Palgrave Macmillan, London, 2013.

Pishue, B., *2022 INRIX Global Traffic Scorecard*, INRIX, 2023.

Schulman, J., Wolski, F., Dhariwal, P., Radford, A. and Klimov, O., *Proximal Policy Optimization Algorithms,* arXiv, 2017.

Generating Traffic Equilibria under Bounded Rationality

S. Lawphongpanich[a], Y. Yin[b]

[a] *Department of Industrial and Systems Engineering, University of Florida, Gainesville, Florida, 32611, USA.*

[b] *Department of Civil and Environmental Engineering, University of Michigan, Ann Arbor, Michigan, 48109, USA.*

Introduction

This presentation addresses user equilibria under bounded rationality (BRty). Under such a behavioural assumption, travellers or users do not always choose fastest or cheapest paths to reach their destinations. Because of personal reasons, ambiguous preferences, perception errors, inaccurate information, etc., they choose paths that are within a threshold of being fastest or cheapest instead. Psychologists and economists have provided evidence and reasons for such behaviour, particularly in the context of day-to-day choices (see Conlisk, 1996, for a review).

In transportation, user-equilibrium (UE) distributions under BRty are called boundedly rational user-equilibrium (BRUE) distributions—see, e.g., Lou et al. (2010). In computer science (see, e.g., Roughgarden, 2005), BRUE distributions are referred to as "approximate Nash equilibria" instead. Generally, the set of all possible BRUE distributions, referred to herein as the "BRUE set", is infinite and shown to be non-convex in Lou et al. (2010). The latter is true even when travel-time functions are well-behaved. To avoid dealing with these two issues, this presentation takes a statistical and computational approach. It is statistical because the approach infers characteristics of BRUE distributions from a finite sample of distributions randomly selected from the BRUE set. In practice, characteristics of interest include performance indicators such as network delays and travel times on individual streets. The approach is also computational because it involves computing or generating random BRUE distributions. This presentation focuses on methods for doing the latter. Such methods involve solving optimization or variational inequality problems with randomly perturbed travel times.

Our Approach

When demands are fixed, there are two equivalent ways of defining BRUE distributions. In one, the rationality thresholds are stated in an additive form. The thresholds are in a multiplicative form in the other. Because these two definitions are equivalent, results based on one definition can typically be derived from those based on the other. This presentation addresses BRUE distributions with additive threshold constants.

For the elastic-demand case, our survey of the literature does not find any definition for BRUE distributions. Under perfect rationality (PRty) and mild assumptions, the travel time at equilibrium for all travellers of an OD pair is unique and, consequently, determines its travel demand. The same is not true under BRty. Boundedly rational (BRal) travellers for the same OD pair typically experience different travel times at equilibrium. Therefore, it is not clear which of these travel time, if any, determines the demand for each OD pair. In our proposed definitions, demands are determined by "de facto" travel prices (or travel prices in effect) instead.

BRUE distributions reduce to perfectly rational user-equilibrium (PRUE) ones (i.e., ones that satisfy Wardrop's first principle) in two ways. One way is by setting all threshold constants to zero. Perturbing path or link travel-times is the second way. To illustrate the latter, consider a 4-node network in Figure 1 that has $(1,4)$ as the sole OD pair with 6 units of demand. In the figure, the travel-time function is next to each link and x represents the link's flow. Three paths, labeled as $p1$, $p2$, and $p3$, connect the OD pair. They correspond to $1 \to 2 \to 4$, $1 \to 3 \to 4$, and $1 \to 2 \to 3 \to 4$, respectively.

Figure 49. 4-node network

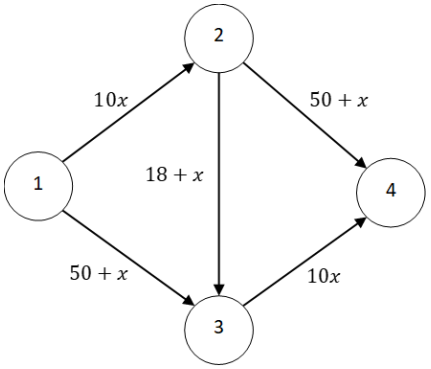

Source: Adapted from Braess (1969).

Let $\boldsymbol{f} = \left(f_{p1}, f_{p2}, f_{p3}\right)$ denote a (flow) distribution. Then, the PRUE distribution for the 4-node network is $\boldsymbol{f}^{PRUE} \sim (2.62, 2.62, 0.76)$, where the travel times of all three paths are the same and approximately equal 86.46 time-units. (The network delay associated with $\boldsymbol{f}^{PRUE}$ is 518.76 time-units.) Let the (additive) threshold constant equal 5 time-units (or, approximately 5.78% of 86.46). Then, one BRUE distribution is $\boldsymbol{f}^{BRUE} \sim (2.78, 2.48, 0.74)$. To verify, let $\boldsymbol{c}(\boldsymbol{f}) = \left(c_{p1}(\boldsymbol{f}), c_{p2}(\boldsymbol{f}), c_{p3}(\boldsymbol{f})\right)$. Then, $(\boldsymbol{f}^{BRUE})$ $\sim (87.99, 84.63, 86.10)$. Observe that $p2$ is the fastest with a travel-time of 84.63. The travel-times for paths $p1$ and $p3$ are, respectively, 3.36 and 1.47 time-units longer. Thus, travel-times of the remaining two (flow-bearing) paths are within 5 time-units of 84.63 and, consequently, $\boldsymbol{f}^{BRUE}$ is a BRUE distribution with an (additive) threshold of 5 time-units.

To perturb path travel-times, let ϵ_p denote the perturbation amount for path p and $\boldsymbol{\epsilon} = \left(\epsilon_{p1}, \epsilon_{p2}, \epsilon_{p3}\right)$. Then, a perturbed travel-time is of the form $\tilde{c}_p(\boldsymbol{f}, \boldsymbol{\epsilon}) = c_p(\boldsymbol{f}) + \epsilon_p$. When $\boldsymbol{\epsilon} = (0.0, 3.36, 1.89)$, $\tilde{c}_p(\boldsymbol{f}^{BRUE}, \boldsymbol{\epsilon}) = 87.99$ for every p, i.e., $\boldsymbol{f}^{BRUE}$ is also a PRUE distribution with respect to $\tilde{\boldsymbol{c}}(\boldsymbol{f}, \boldsymbol{\epsilon})$. Note that the preceding $\boldsymbol{\epsilon}$ is not unique. Also, $\boldsymbol{\epsilon}$ need not be nonnegative. For this case, $\boldsymbol{f}^{BRUE}$ is a PRUE distribution with respect to $\tilde{\boldsymbol{c}}(\boldsymbol{f}, \boldsymbol{\epsilon})$ when $\boldsymbol{\epsilon} = \left(c_{p1}(\boldsymbol{f}^{BRUE}) - \hat{c}, c_{p2}(\boldsymbol{f}^{BRUE}) - \hat{c}, c_{p3}(\boldsymbol{f}^{BRUE}) - \hat{c}\right)$ and $\hat{\boldsymbol{c}} \in [84.63, 87.99]$**.** This is because $\tilde{c}_p(\boldsymbol{f}^{BRUE}, \boldsymbol{\epsilon}) = \hat{c}$ for all three paths.

Sample Results and Findings

For OD pair w, let $c_{mn}^w(\boldsymbol{f}) = \min\left\{c_q^w(\boldsymbol{f}) \middle| q \in \mathcal{P}^w\right\}$ denote the travel time of a quickest path and $\mathcal{P}_+^w(\boldsymbol{f}) = \left\{p \in \mathcal{P}^w \middle| f_p^w > 0\right\}$ be the set of flow-bearing paths. Then, a definition of fixed-demand BRUE (FD-BRUE) distributions with additive threshold constants is below.

FD-BRUE with Additive Constants: A vector $\boldsymbol{f} \in \mathcal{F}(\boldsymbol{d})$ is a FD-BRUE distribution with a vector of additive constants $\boldsymbol{\eta} \geq 0$ if the following hold for all $w \in \mathcal{W}$:

$$c_p^w(\boldsymbol{f}) \leq c_{mn}^w(\boldsymbol{f}) + \eta^w, \forall p \in \mathcal{P}_+^w(\boldsymbol{f}).$$

Given $\boldsymbol{\epsilon}$, let $\epsilon_{mn}^w = \min\left\{\epsilon_p^w \middle| p \in \mathcal{P}^w\right\}$ and $\epsilon_{mx}^w = \max\left\{\epsilon_p^w \middle| p \in \mathcal{P}^w\right\}$ be the minimum and maximum perturbation amount, respectively. Also, $c_{mx+}^w(\boldsymbol{f}) = \max\{c_q^w(\boldsymbol{f}) | q \in \mathcal{P}_+^w(\boldsymbol{f})\}$ denotes the longest or slowest travel time among the flow-bearing paths. Then, the following theorem substantiates the claim made in the 4-node example above. Also, an $\boldsymbol{\epsilon}$ that satisfies the two conditions in the theorem is said to be "compatible" with $\boldsymbol{\eta}$.

Theorem 1: A vector $\boldsymbol{f} \in \mathcal{F}(\boldsymbol{d})$ is a FD-BRUE distribution with $\boldsymbol{\eta}$ if and only if $\boldsymbol{f}$ is a FD-PRUE distribution with respect to $\tilde{c}_p^w(\boldsymbol{f}, \boldsymbol{\epsilon})$ for some $\boldsymbol{\epsilon}$ such that, for every $w \in \mathcal{W}$, (a) $\left|\epsilon_p^w\right| \leq \eta^w, \forall p \in \mathcal{P}^W$, and (b) $\epsilon_{mx}^w - \epsilon_{mn}^W \leq \eta^w$.

Define $\mathcal{FD}\text{-}\mathcal{BRUE}(\boldsymbol{\eta})$ and $\boldsymbol{f}^{UE(\epsilon)}$ as, respectively, the set of all possible FD-BRUE distributions with $\boldsymbol{\eta}$ and a FD-PRUE distribution with respect to $\tilde{\boldsymbol{c}}(\boldsymbol{f}, \boldsymbol{\epsilon})$. Then, the set of all such distributions can be defined as follows:

$$\mathcal{FD}\text{-}\mathcal{PRUE}^{\epsilon}(\boldsymbol{\eta}) = \left\{\boldsymbol{f}^{UE(\epsilon)} \middle| \boldsymbol{\epsilon} \text{ is compatible with } \boldsymbol{\eta}\right\}.$$

Then, the following holds:

Corollary 2: $\mathcal{FD}\text{-}\mathcal{BRUE}(\boldsymbol{\eta}) = \mathcal{FD}\text{-}\mathcal{PRUE}^{\epsilon}(\boldsymbol{\eta})$.

For the two corollaries below, one provides new necessary and sufficient conditions for BRUE distributions. The other associates the latter to variational inequality problems.

Corollary 3: A vector $\boldsymbol{f} \in \mathcal{F}(\boldsymbol{d})$ is a FD-BRUE distribution with $\boldsymbol{\eta}$ if and only if there exists a $\boldsymbol{u} \in \mathbb{R}_+^{|\mathcal{W}|}$ such that the following (path-based) KKT conditions hold for some $\boldsymbol{\epsilon}$ compatible with $\boldsymbol{\eta}$:

$$\begin{aligned} c_p^w(\boldsymbol{f}) + \epsilon_p^w &= u^w, \quad \forall p \in \mathcal{P}_+^w(\boldsymbol{f}), \\ c_p^w(\boldsymbol{f}) + \epsilon_p^w &\geq u^w, \quad \forall p \in \mathcal{P}_0^w(\boldsymbol{f}). \end{aligned}$$

Corollary 4: A vector $\boldsymbol{f} \in \mathcal{F}(\boldsymbol{d})$ is a FD-BRUE distribution with $\boldsymbol{\eta}$ if and only if it solves $VI[\tilde{\boldsymbol{c}}(\boldsymbol{f}, \boldsymbol{\epsilon}), \mathcal{F}(\boldsymbol{d})]$ for some $\boldsymbol{\epsilon}$ compatible with $\boldsymbol{\eta}$, i.e., $\boldsymbol{f}$ satisfies the following inequality:

$$\tilde{\boldsymbol{c}}(\boldsymbol{f}, \boldsymbol{\epsilon})^T\left(\hat{\boldsymbol{f}} - \boldsymbol{f}\right) \geq 0, \forall \hat{\boldsymbol{f}} \in \mathcal{F}(\boldsymbol{d}).$$

Below is a procedure to randomly sample a BRUE distribution from $\mathcal{FD}\text{-}\mathcal{BRUE}(\boldsymbol{\eta})$. It can be repeated many times to generate a random collection of BRUE distributions. In the procedure, $\mathcal{U}[a, b]$ denotes a uniform probability distribution between two real numbers, a and b, where $a < b$, and the notation "$x \sim \mathcal{U}[a, b]$" means that x is a random number with a $\mathcal{U}[a, b]$ distribution.

Procedure

Step 1: For all $w \in \mathcal{W}$, let $\alpha^w \sim \mathcal{U}[-\eta^w, 0]$. Given α^w, let $\epsilon_p^w \sim \mathcal{U}[\alpha^w, \alpha^w + \eta^w], \forall p \in \mathcal{P}^w$.
Step 2: Solve $VI[\tilde{\boldsymbol{c}}(\boldsymbol{f}, \boldsymbol{\epsilon}), \mathcal{F}(\boldsymbol{d})]$ to obtain $\boldsymbol{f}^*$. Then, $\boldsymbol{f}^*$is a FD-BRUE distribution with $\boldsymbol{\eta}$.

To illustrate, consider the 9-node network shown in Figure 2 below. It has four OD pairs: $(1,3)$, $(1,4)$, $(2,3)$, and $(2,4)$. Travel demands for them are $d^{(1,3)} = 12.5, d^{(1,4)} = 25, d^{(3,4)} = 37.5$, and $d^{(2,4)} = 50$. Because of symmetry, every OD pair has 24 acyclic paths from its origin to its destination. For every link, the travel-time function is of the form $t_{ij}(\boldsymbol{x}) = t_{ij}^0\left(1 + 0.15\left(x_{ij}/cap_{ij}\right)^4\right)$, where t_{ij}^0 and cap_{ij} are the free-flow travel-time and capacity, respectively. Values of the two preceding parameters are in Hearn and Yildirim (2002).

Figure 50. 9-node network

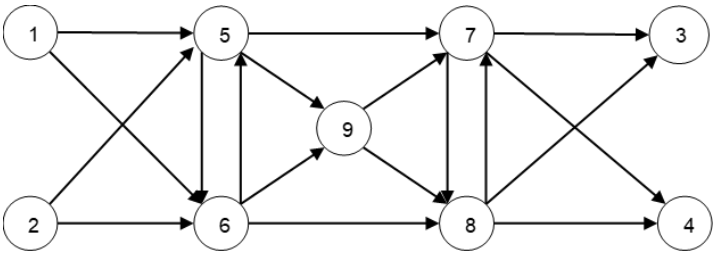

Source: Hearn and Yildirim (2002).

Four vectors of additive constants are used for the tables and figures below. They include $= 0.05\boldsymbol{c}_{mn}\left(\boldsymbol{f}^{UE(\mathbf{0})}\right)$, $0.10\boldsymbol{c}_{mn}\left(\boldsymbol{f}^{UE(\mathbf{0})}\right)$, $0.15\boldsymbol{c}_{mn}\left(\boldsymbol{f}^{UE(\mathbf{0})}\right)$, and $0.20\boldsymbol{c}_{mn}\left(\boldsymbol{f}^{UE(\mathbf{0})}\right)$, where $\boldsymbol{f}^{UE(\mathbf{0})}$ denotes an unperturbed FD-PRUE distribution and $\boldsymbol{c}_{mn}\left(\boldsymbol{f}^{UE(\mathbf{0})}\right)$ is the vector of (equilibrium) travel times for each OD pairs at $\boldsymbol{f}^{UE(\mathbf{0})}$. For convenience, the latter is also referred to as UE(**0**) distribution and the four choices of $\boldsymbol{\eta}$ are denoted as 05%UE(0), 10%UE(0), 15%UE(0), and 20%UE(0), respectively.

Let ND be the network delay associated with a distribution randomly selected from $\mathcal{FD}\text{-}\mathcal{BRUE}(\boldsymbol{\eta})$. Then, ND is a random variable with mean $E[ND] = \mu$ and variance $V[D] = \sigma^2$. To estimate μ, K distributions are sampled from $\mathcal{FD}\text{-}\mathcal{BRUE}(\boldsymbol{\eta})$ using Procedure 1. (Thus, K is the sample size.) Table 1 below provides two estimates of μ, one for $K = 35$ and $K = 100$ for the other. Also provided are the margins of errors at a 95% confidence level or $\alpha = 0.05$. For all four choices of $\boldsymbol{\eta}$ mentioned above, the estimates are similar for both sample sizes. However, the margin of error for $K = 100$ is significantly smaller than the one for $K = 35$ for all four choices of $\boldsymbol{\eta}$. Thus, estimates with larger samples are more reliable.

Table 11. Estimates of μ and margins of errors at 95% confidence level

$\boldsymbol{\eta}$	$K = 35$	$K = 100$
05%UE(**0**)	3904.28 ± 7.87	3899.03 ± 5.15
10%UE(**0**)	3860.68 ± 19.21	3858.57 ± 11.62
15%UE(**0**)	3801.37 ± 29.14	3816.78 ± 18.24
20%UE(**0**)	3835.75 ± 42.23	3814.71 ± 23.15

Source: Lawphongpnich and Yin (2023).

Below, Figure 3 displays two histograms of network delays associated with BRUE distributions with $\boldsymbol{\eta}$ = 20%UE(0), one histogram is constructed with $K = 35$ and the other with $K = 100$. Although they follow a similar pattern, the two histograms in the figure are dissimilar visually in terms of bar heights. As before, it can be argued that the histograms with $K = 100$ are more reliable.—see, e.g., Lawphongpanich and Yin (2023).

Figure 51. Two histograms of network delays associated with BRUE distributions where n = 20%UE (0)

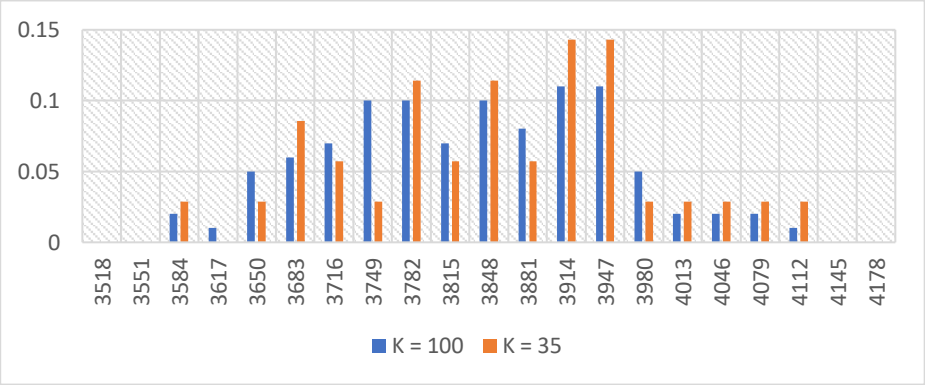

Source: Lawphongpanich and Yin (2023).

References

Braess, D.. "Über ein Paradoxon aus der Verkehrsplanung", Unternehmensforschung. 1969, 12: 258–268.

Conlisk, J., "Why bounded rationality." *Journal of Economic Literature*, 1996, 34(2), 669–700.

Lou, Y., Yin, Y., Lawphongpanich, S., "Robust congestion pricing under boundedly rational user equilibrium," *Transportation Research Part B*, 2010, 44, 15-28.

Hearn, D.W., Yildirim, M.B., "A toll pricing framework for traffic assignment problems with elastic demand," in M. Gendreau and P. Marcotte, Eds., *Transportation and Network Analysis: Current Trend*, Kluwer Academic Publishers, Dordrecht, 2002.

Roughgarden, T., *Selfish Routing and the Price of Anarchy,* The MIT Press, London, 2005.

Lawphongpanich, S, Yin, Y., "Generating Traffic Equilibria under Bounded Rationality," forthcoming technical report, Gainesville, 2023.

Modelling, feasibility analysis, and potential ramp-up of air taxis services in the Rhine-Main region

O. Wohak[a] , J. Erb[a], S. Graf[b], F. Meyer[a]

[a] *d-fine GmbH*

[b] *Fraport AG*

Introduction

Increasing urbanisation, inner-city congestion and growing mobility needs demonstrate the necessity of rethinking existing mobility concepts. Leveraging the advancements in technology, the employment of advanced air mobility (AAM) services presents a promising new mode of transportation. For on-demand inner-city point-to-point services, airport shuttle services, intercity flights (Bauhaus 2022, Shamiyeh 2018, Rajendran 2020) as well as use cases in goods transportation in a medical or agricultural context (Xu 2020), it has become a highly discussed topic. Recently, multiple companies have promised market ready products to be released in the next two years (Lilium 2022, Volocopter 2023) – the first operating air taxi shuttle service is planned for the Olympics in Paris in 2024 (Bloomberg 2022, Stonor 2022). However, besides technical viability the question of economic feasibility for specific operations including potential demand and vertiport locations must be answered, thus enabling a beneficial integration of AAM into pre-existing mobility infrastructure.

Methodology

In a first step, a survey is conducted both on-site at the Frankfurt Airport and online to assess demand, willingness to pay and requirements of potential user groups. Based on the survey results, user groups are defined and corresponding personas are drafted that reflect their preferences and use cases in AAM concepts, such as vacationers or business customers. To quantify the attractiveness of districts which could be integrated into an air taxi service network, a scoring system is developed ranking these for each user group. The scoring considers demographic and economic metrics, information on relevant points of interest, e.g. large company sites, as well as mobility demand data of each district. Potential districts are identified for each of the user groups and visualised with heat maps of the region (see Figures 1 and 2). The resulting districts of interest are thereafter analysed in greater detail. Prospective vertiport locations are evaluated on the basis of a catalogue of requirements, which includes infrastructural and economic criteria. In addition, a traffic simulation model for the Rhine-Main region is being enhanced and complemented by air taxis as an additional mode of transport. For this, the original traffic model data of the region is used within the simulation software PTV Visum (PTV 2023) and a complementing simulation framework is built around this. In order to adequately depict the new mode of transport, a separate network for air taxis is integrated into the simulation model, including intermodal connection points to the existing modes. Based on research and survey data, resistance and utility functions

$$\Sigma_{g} \left[\!\left[\beta * c_{ijmg} \right]\!\right] \qquad (1)$$

with c being the costs per effort (positive)or utility (negative)of using an edge g between two districts (pair i, j) with mode m, are defined. Those functions quantify the time benefits and costs associated with the air taxi service in order to gauge the respective utility. Ultimately, the simulation serves as a complementary tool for the evaluation of potential vertiport locations as the demand distribution and passenger flows can be simulated on a macroscopic level. As a result, multiple future scenarios are evaluated including different vertiport network designs and sizes as well as their economic impact.

Results

Preliminary results of the project indicate that the potential of districts varies depending on the user group. While the Taunus-region to the north-west of Frankfurt displays high scores for most of the persona user groups, vacationer and commuter demand clusters in the Darmstadt-Offenbach metropolitan areas to the south of Frankfurt. In the case of the business client persona, the highest scored districts coincide with the Heidelberg metropolitan area where large industrial companies are located. Under these circumstances, additional emergent use cases can be considered such as a non-public-corporate-case that connects a private, corporate-owned vertiport to an urban vertiport network. Another emergent use case can be considered for the “poorly connected” user group persona that connects areas of further distance to the Frankfurt am Main airport via regional airports in the nearby vicinity, leveraging pre-existing infrastructure to enhance mobility in the region.

Conclusions

Advanced Air Mobility is an innovative and highly discussed topic in the mobility sector. This project provides a data-driven approach towards AAM with the goal of establishing a methodology that can be easily applied to further cities and regions. As described, the first results are promising in identifying specific use cases for AAM in the Rhine-Main-Region, with the next step being the consideration of economic scenarios and business cases. The project will be finalized by the end of August 2023 with a final project report to be published around that time.

Acknowledgement

This work is supported with 79,759.60 EUR by the German Federal Ministry for Digital and Transport (BMDV) under the funding program Innovative Air Mobility. The authors thank the project partners Fraport, DB Digital Ventures, Skyports, and Stadt Frankfurt am Main for the ongoing discussions and contributions to the project.

References

BMDV, Bundesministerium für Digitales und Verkehr, « Flugtaxis in der Rhein-Main-Region – FLAMINGO », https://bmdv.bund.de/SharedDocs/DE/Artikel/DG/UAV-Projekte/flamingo.html.

Bauhaus, Roland Berger, "TechReport", Regional Air Mobility – How to Unlock a New Generation of Mobility, 2022.

Xu E., The future of transportation: White paper on urban air mobility systems, EHang, Guangzhou, China, 2020.

Shamiyeh, M., Rothfeld, R., & Hornung, M., A performance benchmark of recent personal air vehicle concepts for urban air mobility. In Proceedings of the 31st Congress of the International Council of the Aeronautical Sciences, Belo Horizonte, Brazil (Vol. 14, p. 10), 2018, September.

Rajendran, S., & Srinivas, S., Air taxi service for urban mobility: A critical review of recent developments, future challenges, and opportunities. Transportation research part E: logistics and transportation review, 143, 102090, 2020.

Stonor C., "The Countdown Begins: Flying Taxis and the Paris Olympics Games," 2022, [Online]. https://evtolinsights.com/2022/06/the-countdown-begins-flying-taxis-and-the-paris-olympic-games-part-2/ (accessed 05-23-2023).

Bloomberg, Paris Opens Air-Taxi Hub Targeting Flights for 2024 Olympics, 10 November 2022, [Online]. https://www.bloomberg.com/news/articles/2022-11-10/paris-opens-flying-taxi-hub-targeting-flights-for-2024-olympics#xj4y7vzkg (accessed 05-07-2023).

PTV, „PTV Visum", [Online]. Verkehrsplanungssoftware PTV Visum | MyPTV (accessed 05-21-2023).

Lilium, "Technical Blog," 2022. [Online]. https://lilium.com/newsroom-detail/technology-behind-the-lilium-jet (accessed 05-23-2023).

Volocopter, "We aim to launch UAM first," 2023. [Online]. https://www.volocopter.com/urban-air-mobility/ (accessed 05-23-2023).

Development of an Interoperable Traffic Simulation Testbed of the Expressway Network in Tokyo Metropolitan Region

T. Oguchi[a], Y. Suzuki[b], J. Xing[c], R. Horichuki[d]

[a] *Institute of Industrial Science, University of Tokyo, Japan*

[b] *Maintenance and Traffic Management Department, Metropolitan Expressway Co., Ltd., Japan*

[c] *Traffic and Environment Research Department, Nippon Expressway Research Institute Co., Ltd., Japan*

[d] *i-Transport Lab. Co., Ltd. , Japan*

Introduction

Tokyo road network has been drastically changed in the last decade to accommodate traffic demand much more smoothly and efficiently. Especially, the expressways of Tokyo Metropolitan Region (TMR) has been developed three major ring roads and almost completed to form the ring-radial network. The connectivity of expressway network will provide many route choice options for many Origin-Destination (O-D) patterns and the needs for effective and flexible traffic management become much more important.

In practice, the traffic operation on the expressway network in TMR is taken by three expressway companies, Metropolitan Expressway Co., Ltd. (MEX), East Nippon Expressway Co., Ltd (NEXCO-E) and Central Nippon Expressway Co., Ltd (NEXCO-C). As each company covers the part of the ring-radial network, as shown in Figure 1, the cooperative scheme is highly needed to achieve flexible traffic management.

Figure 52. The ring-radial expressway network in TMR

The traffic simulation testbed which covers TMR network and will be continuously updated along the network evolution will be a valuable tool to assist the planning of effective traffic management. So far, MEX and Nippon Expressway Research Institute Co., Ltd. (NEXCO-RI) have separately developed their own traffic simulation testbeds. MEX developed RISE system (Munakata et. al, 2009) which works with the real-time traffic management system and predicts near future conditions for every five minutes. NEXCO-RI developed ENS system (Hirai et. al, 2015) which covers whole inter-urban expressways in Japan to assess the effects of planned network evolution and/or the impacts of traffic regulations.

This research aims to develop the interoperable traffic simulation testbed of TMR expressway network by utilizing RISE and ENS data platform. Since the both RISE and ENS have an affinity by adopting the same traffic simulation model (SOUND, 2023), the main objective of the development is to integrate the data collected by each company and to prepare the cooperative operation scheme over those companies. In this paper, the data flow and the functional components of the testbed are outlined and followed by the description of automatic calibration of time-varying O-D travel demand and bottleneck capacity. Basic studies on typical weekdays and holidays will be demonstrated in the full paper to validate the reproducibility of the simulation model.

Data flow and functional components

Figure 2 illustrates the data flow and the functional components of TMR expressway simulation testbed. The red boxes are the components which work for the 'demand side' while the green works for the 'supply side'.

Figure 2. Data flow and the functional components of the testbed

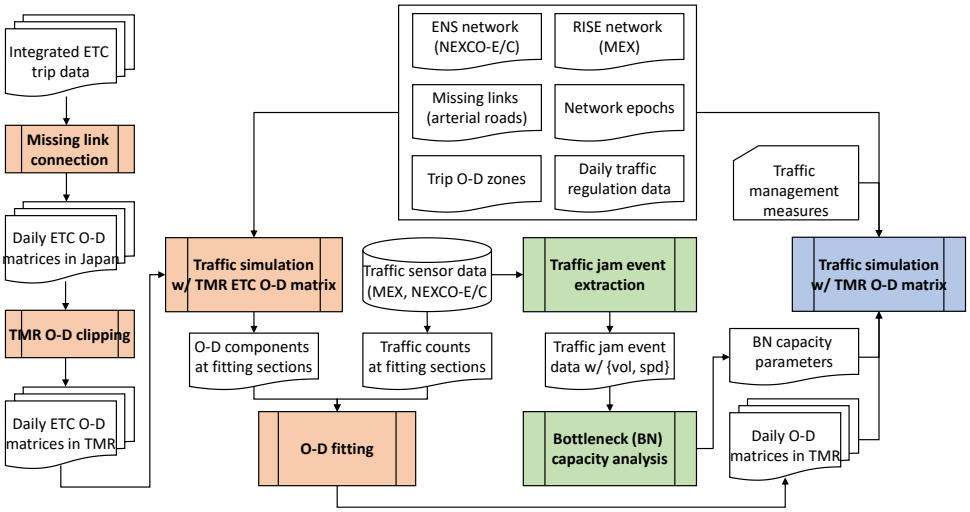

As to the demand side, electric toll collection (ETC) data, which records both entry and exit toll gates with the time stamps, is fully utilized to generate the daily O-D matrices. It is collected by each expressway company and integrated with anonymized ID by NEXCO-RI. The '*missing link connection*' joins two conjunctive ETC trips inferred that the vehicle runs through the surface road sections which are included in the testbed to connect the 'missing links' of TMR expressway network. The ETC trip data is aggregated into daily ETC O-D matrices with 15 minutes time slots.

Since the O-D matrix at this stage spreads over the whole Japan, the '*TMR O-D clipping*' cuts off the sub-matrix at the boundary of TMR (TMR O-D matrix). The boundary assignment ratio and the departure time offset are prepared by using ENS with the whole Japan expressway network.

As the penetration of ETC is rather high but not 100%, it is still needed to expand the ETC O-D matrix into the full. The first '*traffic simulation with TMR ETC O-D matrix*' is executed to obtain the O-D component of each link throughput volume. The O-D component is aggregated and used to calculate the link choice probability for each O-D trip.

The '*O-D fitting*' component imports the ETC O-D matrix and modify it by the numerical search to minimize the square error of the estimated link throughput to the observed throughput from detector data. The link choice probability mentioned above is used for the estimation of throughput with O-D matrix. The details of the numerical search will be explained in the full paper.

Figure 3 is an example of the O-D fitting of one weekday. The plot shows the correlation of 15 minutes throughput at 1053 fitting sections on TMR network. The liner regression of the left plot (before fitting) has 0.977 slope, which is close to the ETC penetration ratio of MEX (0.98 in Dec. 2022), and fairly high correlation determination (R^2=0.942). The right plot (after fitting) shows further improvement of those values as 0.994 and 0.982. The average absolute error reduces 78.6 → 36.2 [vehicle/15min].

Figure 53. Comparison of the traffic volume correlation before/after the O-D fitting

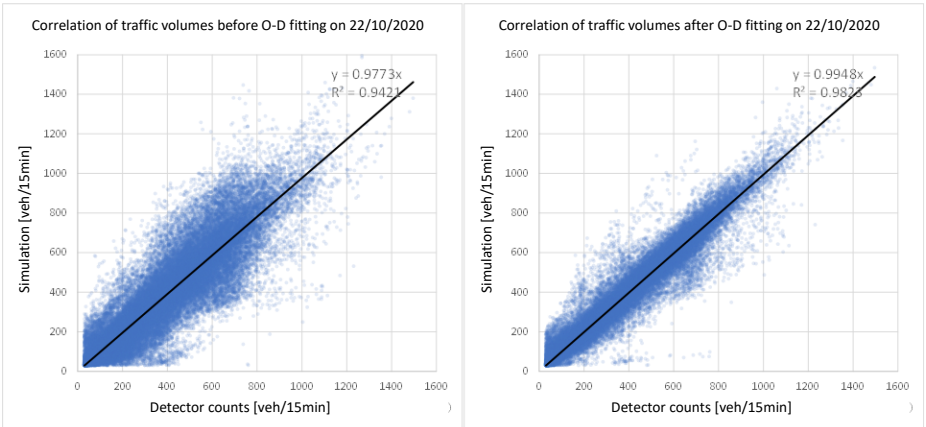

As to the supply side, the historical traffic sensor data is investigated. The '*traffic jam event extraction*' detect a traffic jam event heading to a certain section and lasting for more than 20 minutes. The jam event extracted with its location, duration and the volume and speed for every 5 minutes, as shown in Figure 4.

The '*bottleneck capacity analysis*' calculates the parameters of the bi-level bottleneck capacity model which is implemented in SOUND. The bi-level model has the breakdown flow (BDF) capacity and the queue discharging flow (QDF) capacity. Once the traffic demand higher than BDF arrives at a bottleneck link, a traffic jam forms heading to the downstream of the link. SOUND monitors the jam breakout and gradually reduces the bottleneck capacity from BDF to QDF when the jam lasts for a certain minutes. In this study, BDF is set to the average of maximum flow rate during +/- 15 minutes at the breakdown time of each jam events, and QDF is set to the average flow rate after 30 minutes after the maximum. Those parameters are prepared for weekdays and holidays, as shown in Figure 4.

Figure 54. Discharging flow rate during the jam events at a bottleneck

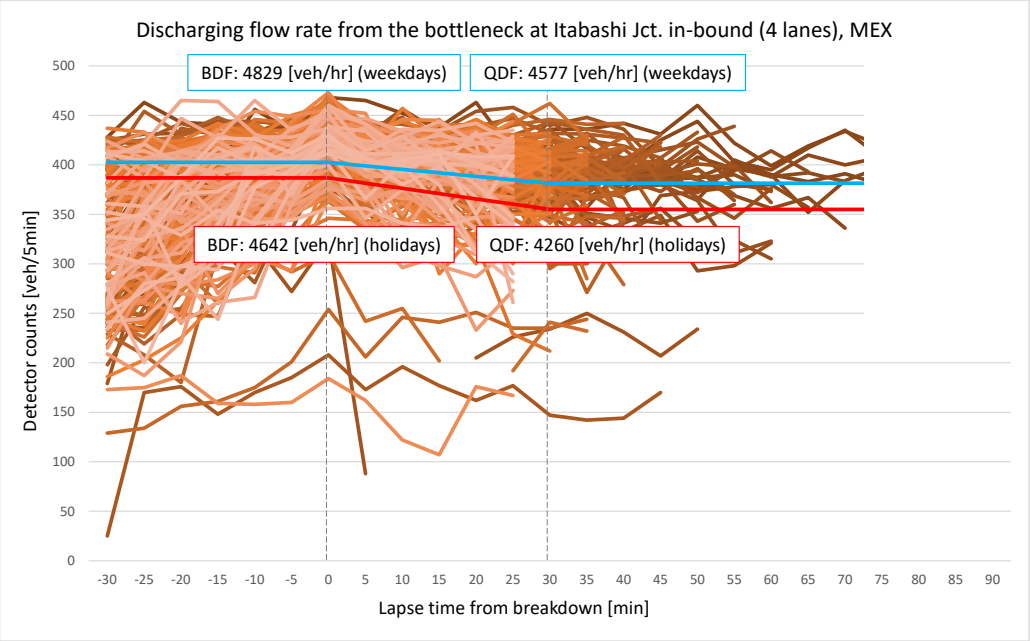

Future works

The basic studies on typical weekdays and holidays will be presented in the full paper.

Acknowledgements

The study is a part of trilateral collaborative research of Metropolitan Expressway Co., Ltd., Nippon Expressway Research Institute Co., Ltd., and the University of Tokyo with supports from East, Central, and West Nippon Expressways Co., Ltd.

References

Hirai, S., Xing, J., Horiguchi, R., Shiraishi, T., Kobayashi, M., Development of a network traffic simulator for the entire inter-urban expressway network in Japan, Transportation Research Procedia, Vol. 6, pp. 285-296, 2015.

Munakata, K., Tamura, Y., Warita, H., Shiraishi, T., A case study about the traffic prediction under accidents using dynamic traffic simulation on Tokyo Metropolitan Expressway, Proceedings of 16th World Congress on Intelligent Transport Systems, Stockholm, 2009.

SOUND product page, https://www.i-transportlab.jp/en/index/products/sound/, visited on 5.3.2023.

Traffic signal optimization of urban arterial network by vehicle-to-infrastructure

B. J. R. Ibonia Rejuso[a] , J. Schweizer[a], C. Poliziani[b]

[a] *Department of Civil, Chemical, Environmental and Materials Engineering, Universita di Bologna, Italy*

[b] *Berkeley Lab, USA*

Introduction

Urbanization has occasionally been linked to negative consequences. An efficient transportation system is a critical component of economic growth and traffic congestion has remained to be one of the most ubiquitous challenges of urbanized cities worldwide. Congestion on road networks is defined as a condition that occurs as the number of road users increases and is characterized by slower speeds, longer travel time, and increased vehicular queuing (Manpreet and Alok, 2020). Mobility within urban road networks has been a complex undertaking of any city. To address this issue, some strategies and sustainable ideas have been implemented, with one of the most successful being the use of "Intelligent Transportation System" (ITS). One of the primary goals of many ITS components, according to the Sustainable Transport and Mobility Handbook, is to improve mobility by reducing delay and travel time (Vanderschuren and Mckune, 2011).

One of the pioneer applications of ITS is in the control of traffic signals. Traffic light system in urban arterial networks plays an essential role to the operation of the transportation systems. The majority of traffic signal studies concentrate on estimating delays and queue lengths caused by the implementation of a signal control strategy at individual intersections as well as a sequence of intersections (Darma, et.al., 2005). As a result, it is understandable that traffic signals receive so much attention (Fusco, et.al., 2017). Traffic control by signals has become a significant traffic management tool in the face of increasing traffic in urban areas to reduce the consequences of this increase: delay, stop, noise, fuel consumption, and so on (Sampson, et. al., 2019). In general, three (3) traffic signal control configurations are currently used in urban areas: pre-timed (or static) based signal control, actuated signal control, and the adaptive-based signal control (Boillot, et.al., 2006). Connectivity has been one of the most recent innovations in ITS and one of its sub-categories is the “vehicle-to-infrastructure (V2I)”. In recent years, the development of V2I communication technologies provides new opportunities to further improve transportation efficiency (Ban, et.al, 2017). GLOSA (or Green Light Optimal Speed Advisory) System is one of the products of V2I. The GLOSA system aims to reduce traffic congestion by reducing average stop time at traffic lights, as well as fuel consumption and harmful CO2 emissions (Vetrano and Fusco, 2018).

This paper emphasizes GLOSA system's potential as a tool for addressing traffic signal optimization. GLOSA serves as an advisory to drivers, informing them of the speed they must maintain to reduce waiting time. Several simulations run in SUMOPy software on each peak-hour period using recent actual traffic count data.

Methodology

Different case scenarios were created to determine which of the traffic signal configurations will produce the optimal results based on traffic parameters such as average waiting time, travel speed, travel time, and fuel consumption. SUMOPy was used to run all the network scenarios. This software is an open-source traffic simulation software which has the capability to run micro-simulation and complex models. SUMOPy includes Python scripts which enable users to direct use of tools that are available as Python scripts. With SUMOPY, users can import maps (from OpenStreetMap), distribute trips, import/model demands (such as traffic counts, OD Matrices), perform modal split (depending on the type of vehicle classification), execute trip assignments, even introduce new transport mode, export simulation results into a schematic map or .csv file, etc.

Meanwhile, Via Aurelio Saffi Corridor in the Metropolitan City of Bologna was selected as the pilot study. The said corridor consists of several signalized intersections that serve as primary link between the City Center of Bologna and its neighboring zones. A traffic count survey was conducted along key intersections along this corridor during morning and afternoon peak-hour. Volume counts were classified as cars, buses, HGV (heavy goods vehicle), motorcycle, and taxi. Existing traffic signal plans were observed also.

Design methodology worked on in this paper starts from creating a scenario, modelling both transport supply and demand, assigning route, and running the simulation. The course of action starts by creating a working directory which will contain all the related files on the scenario. Importing OSM files can be easily done in the SUMOPy that includes all the incorporated attributes of the imported maps. All modification needed for the road network can be done in NetEdit, which is an included package for SUMOPy. Through NetEdit, users have the means to modify the attributes related to the road network (number of lanes, road hierarchy, traffic light signals, etc.). Upon modelling the transport supply, demand was modelled as well. Turnflow modelling was performed

by applying flow on each determined flow based on the gathered actual traffic counts. These turnflows were encoded by getting the *Origin Edge ID, Generating Flow, Destination Edge ID, Turn Flow.* Two time-periods were considered: morning and afternoon peak-hour. In this paper, four (4) different scenarios were considered based on traffic signal plans: static scenario, actuated (baseline) scenario, GLOSA scenario, and modified GLOSA scenario. At the same time, traffic light signals (TLS) were modelled in NetEdit. This can be done by selecting which node contains a signalized intersection and configuring its corresponding traffic signal plan. Figure 1 shows a sample signal plan for an intersection containing an actuated traffic signal. For GLOSA, all vehicles (except for buses) were considered to have a GLOSA device. SUMOPy allows users to modify essential parameters related to GLOSA such as the GLOSA range (distance), GLOSA Min. Speed, and GLOSA Max. Speed Factor. GLOSA range denotes the distance where GLOSA system may be applied to an approaching vehicle meaning at a corresponding GLOSA range drivers will receive information or message through either an on-board unit (OBU) or by a roadside unit (RSU) installed near the traffic light. While GLOSA Min. Speed is the minimum speed GLOSA can advise the driver to lessen its waiting time. Max. Speed Factor is a multiplier to a driver's speed assuming the driver will overspeed to reach the traffic lights before it turns yellow. The only difference between GLOSA and Modified GLOSA situations is the GLOSA range. A GLOSA scenario has a range of 300m, but the Modified GLOSA scenario has a range of 400m. Glastra (2020) mentioned that to further see the potential of GLOSA a minimum range of 300m before the approach of a signalized intersection must be assigned.

Figure 55. Actuated Traffic Signal Plan

```
<?xml version="1.0" encoding="UTF-8"?>

<additional xmlns:xsi="http://www.w3.org/2001/XMLSchema-instance" xsi:noNamespaceSchemaLocation="http://sumo.dlr.de/xsd/additional_file.xsd">
    <tlLogic id="252104549" type="actuated" programID="0" offset="5">
        <phase duration="53" state="rrrrgGggGGGgrrrrgGGrG" minDur="42" maxDur="64"/>
        <phase duration="4" state="rrrryyyyyyyyyrrrryyyry" minDur="4" maxDur="4"/>
        <phase duration="3" state="rrrrrrrrrrrrrrrrrrrrr" minDur="3" maxDur="3"/>
        <phase duration="63" state="GGGGrrrrrrrrgGggrrrGr" minDur="47" maxDur="78"/>
        <phase duration="4" state="yyyyrrrrrrrryyyyrrryr" minDur="4" maxDur="4"/>
        <phase duration="3" state="rrrrrrrrrrrrrrrrrrrr" minDur="3" maxDur="3"/>
    </tlLogic>
</additional>

```

After finishing modelling the supply and demand, route assignment was done based on the turnflows. Routing was done by considering turn probabilities highlighting a greater percentage for through direction since the considered study area is a corridor. With this, a turn flow ratio of 2-96-2 was assigned for right turn – through – left turn direction. Once the route assignment is done, all generated trips with their corresponding route assignment will be displayed and a microscopic simulation can be performed taking note of the time that the traffic flow corresponds and assigning a random integer to seeds to generate random sequences and random decisions during the simulation. To further evaluate the performance of each traffic signal plan, different traffic parameters were evaluated: average waiting time, average speed, and average time loss.

Results

Figure 56. Average velocity of vehicle during afternoon peak-hour for GLOSA Scenario

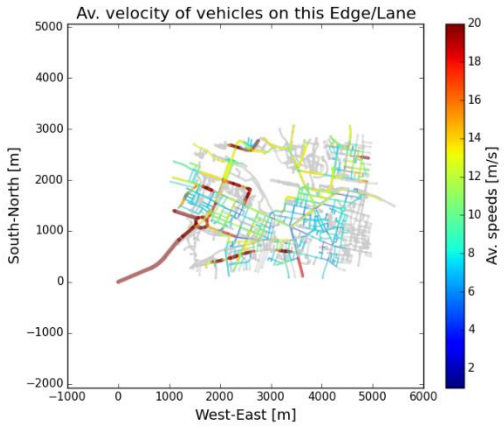

As discussed, visual results of the simulation can be presented by a schematic map. Figure 2 shows the results for average velocity during morning peak hour for GLOSA scenario and slower speed was obtained along the

Via Aurelio Saffi corridor. However, results show improvement for a Modified GLOSA scenario compared with the other three traffic signal plans. Table 1 shows the summary of results for the simulation runs while considering the previously mentioned traffic parameters. Several simulation runs were performed to validate the consistency of results. By performing these simulations, it was also validated that as the GLOSA range increases the performance of signalized intersections improves when it comes to the mentioned traffic parameters.

Table 12. Summary of Simulation Results

	Morning Peak-Hour			***Afternoon Peak-Hour***		
Parameter	*Average waiting time (secs)*	*Average Speed (km/hr)*	*Average time loss (secs)*	*Average waiting time (secs)*	*Average Speed (km/hr)*	*Average time loss (secs)*
Baseline Scenario	84,267	12,539	248,467	86,411	12,651	295,877
Static Scenario	73,642	13,116	250,972	98,240	12,327	295,427
GLOSA Scenario	63,532	13,298	213,429	69,538	12,839	257,266
Modified GLOSA Scenario	57,140	12,604	163,460	62,148	12,886	215,040

Conclusion

A decrease of ~25% with the average waiting time, increase of ~7% in average speed during morning peak hour are remarkably impressive results upon the application of GLOSA in compared with the baseline scenario (actuated). Meanwhile for the afternoon peak-hour, a decrease of ~20% on average waiting time, increase of 2% on average speed for GLOSA. Time loss while performing each trip was also observed in simulation results. During morning peak-hour, ~15% and ~35% in time loss was obtained using GLOSA and Modified GLOSA, respectively, compared with the baseline scenario. During the afternoon peak-hour, a time loss of ~13% and ~28% were observed upon implementing GLOSA and Modified GLOSA respectively. It can be concluded that using GLOSA system will help road users to have an efficient travel and safety as well. With the application of GLOSA, drivers will be notified on what speed can they take to lessen their waiting time in the approach of intersection. It is recommended to use an actuated traffic light system with the application of GLOSA system for urban arterial networks. As observed with the results of simulations, drivers' time loss decreases when using GLOSA and even more when using the Modified GLOSA. It is also worth noting that the greater the GLOSA distance, the more desirable time loss can be achieved.

This paper demonstrated the potential of the GLOSA system as a tool for reducing delays and waiting time at signalized intersections. However, it should be noted that communication between vehicles and infrastructure is a critical factor in achieving GLOSA's goal (or connectivity). During the simulation, it was also observed that the number of vehicles stops decreased, which is due to the vehicle speed becoming a control parameter of the system. Aside from the evaluated traffic parameters, GLOSA also shows a promising result of significantly lowering fuel consumption and CO_2 emissions per vehicle. This is perfectly aligned with the sustainable goals of any city in the world today.

As a recommendation for future work, a city-wide simulation of application GLOSA system can further emphasize its possible impact. Since the majority of road users (or drivers) have their mobile phone with wireless connection, achieving GLOSA in a city-wide setting would be also possible. However, availability of updated traffic-related data is still a concern to achieve this goal.

References

Ban, X., Wang., J., and Bian, Y., 'V2I based cooperation between traffic signal and approaching automated vehicles', *IEEE Intelligent Vehicles Symposium (IV),* Los Angeles, USA, 2017.

Boillot, F., Midenet, F., Pierrelee, J., 'The real-time urban traffic control system CRONOS: Algorithm and experiments', *Transportation Research Part C, Emerging Technologies,* Elsevier, Vol 14, Issue 1, pp. 18-38, 2006.

Darma, Y., Mohamad, J., Karim, M.R., Abdullah, S., 'Control Delay Variability at Signalized Intersection based on HCM Method', *Eastern Asia Society for Transportation Studies,* Vol. 5, pp. 945-958, 2005.

Fusco, G., Gentile, G., Meschini, P, *Urban traffic signal optimization. Intelligent Transport Systems: Past, present, and future directions*, Nova Science Publisher, New York, 2017.

Glastra, T., *Enabling GLOSOA for on-street operating traffic light controllers,* Delft University of Technology, 2020.

Manpreet, B., Alok, A., *Smart Traffic Light System to Control Traffic Congestion, PalArch's Journal of Archaeology of Egypt,* 2020.

Sampson, E., Signor, L., et.al., 'The Role of Intelligent Transport Systems (ITS) in Sustainable Urban Mobility Planning', *European Platform on Sustainable Urban Mobility Plans,* 2019.

Vanderschuren, M., Mckune, A. *The Sustainable Transport and Mobility Handbook, The Essential Guide*, Alive2Green, South Africa, 2011.

Vetrano, E., and Fusco, G., *Road Traffic Signal Setting through V2X Communications,* Sapienza Universita di Roma, 2018.

Contextual data integrations to improve the forecasting accuracy of ST-ED-RMGC with bike-sharing data under atypical situations

R. Rochas[a], A. Furno[a], N. El Faouzi[a]

[a] *Université Gustave Eiffel, LICIT-ECO7*

Introduction

Graph neural networks (GNNs) are considered the cutting-edge technology for traffic forecasting as they can capture spatial dependencies. However, they still have limitations, including when it comes to origin-destination (OD) traffic forecasting. This is particularly challenging as the destination is unknown until the user arrives, and data can be highly sparse (Zhang et al. (2021), (Wang et al.(2019). We decided to work on the ST-ED-RMGC model developed by (Ke et al, 2021) which is the state-of-the-art in OD prediction model. While their work was based on ride-hailing data, we investigated its applicability to bike-sharing data. The integration of contextual data can take many forms. We have chosen to follow the approach of (Tong Liu et al., 2020), who integrated weather data into a traffic forecasting model. Specifically, they concatenated the weather data with historical sequences before passing them through an attention mechanism. We aim to characterize the impacts of atypical scenarios to integrate them into a simulation tool and generate data. Several factors affect the bike sharing demand such as weather conditions, calendar, public transport network and accessibility, or even socio-demographic factor (E. Eren, V.E. Uz, 2020). In this paper, we identify a set of scenarios poorly captured by the algorithm and propose integrating contextual data in the ST-ED-RMGC model to improve the prediction such cases. We also highlight inter-modal patterns between traffic intensity and bike-sharing demand.

To do so, we use multi-source data from various providers of mobility data related to the city of Lyon, France, including Bike-sharing transport data provided by the operator JCDecaux, public socio-economic data from the French Institute of Statistics INSEE, weather data from Meteo France, and traffic data collected via loop detectors, provided by Lyon Metropole. Data from December 1st, 2019, to Mars 15th 2020 have been used as a test dataset. By integrating contextual data into the ST-ED-RMGC model, we aim to address some of the limitations of GNNs and contribute to developing more accurate traffic forecasting models that can be integrated into decision-making tools for transportation planning.

Methodology

We leverage a bike-sharing system (BSS) trip dataset, reporting the trips between pick-up/drop-off bike stations, jointly with departure/arrival timestamps. Since we work by OD defined at the Traffic Analysis Zones (TAZs) level, we needed to group BSS stations and aggregate the related trips in terms of the selected segmentation of the city of Lyon in TAZs. We defined a set of weather-related and traffic-state indicators, detailed below, to identify scenarios of low forecasting accuracy of the considered method. We then propose including, as input features, variables related to the indicators above to improve the forecasting accuracy of the ST-ED-RMGC prediction model.

— Spatial aggregation: BSS stations have been grouped by IRIS zones which is a segmentation in TAZs defined by INSEE allowing to keep homogeneous socio-economic information of buildings and of population within the zone. Then IRIS zones were re-grouped to contain more data in the OD exchanges. Until we have 50 zones, we iteratively aggregate two zones if they represent the minimum of the image of a function f over the set of adjacent zone pairs. The function is :

$$f(zoneA, zoneB) = \frac{surface\ of\ zone\ A + surface\ of\ zone\ B}{common\ perimeter\ between\ zoneA\ and\ zone\ B}$$

— Traffic state indicator: we decided to construct a baseline scenario for training and testing the ST-ED-RMGC in an ideal setup. As rainfall could represent a significant factor of forecasting accuracy decrease, such datasets were built from an external weather data source, filtering out days with precipitations. We propose to establish a link between atypical road traffic and poor prediction of bike-sharing use. To do so, we evaluate the forecasting accuracy of bike-sharing OD demand for which we have recorded atypical road traffic in the origin, and for the same period. Here is how we define atypical road traffic:

  - Considering a zoneA, and the variable “Flow”, we have defined a standard deviation $\sigma_A^{flow}(weekday, hour)$, which computes the standard deviation (std) on the set of flows on the zone for a same ‘weekday’ (from monday to sunday) and a same hour. As for the loop occupancy

rate, we defined $\sigma_A^{loop\ rate}(weekday, hour)$ in the same way. We also define means $\mu_A^{flow}(weekday, hour)$ and $\mu_A^{loop\ rate}(weekday, hour)$ in the same way. For each of these means and standard deviations that we will more simply call σ and μ, we define k-atypical values every value which are out of the range $[\mu - k\sigma; \mu + k\sigma]$, with a k a coefficient. The associated baseline.includes values that are not considered as k-atypical. We define a subset "high" corresponding to values that are above the upper limit of the range. We also define a subset 'low' corresponding to values that are below the lower limit of the range.

For example: Considering the atypical subset with k set to 2. Let the tuple (zone A, Tuesday 2019-02-04 07:00) be identified as atypical because the flow and loop occupancy rate fall outside a 2σ range from the mean value of all Tuesdays at 7am. The associated baseline will be all the OD demand with the origin A and at the date among dates at the same weekday and the same time which are not atypical for zone A: [2020-12-03 07:00, 2019-12-10 07:00, ..., 2020-01-28 07:00, 2020-02-011 07:00, 2020-02-018 07:00, ..., 2020-03-010 07:00]

— *Weather indicators*: we define scenarios of days with 5 classes of daily cumulative rainfall intensity aggregated by hour (dr) in mm per hour per day, and 2 classes of daily cumulative wind intensity aggregated by hour (dw) in m/s per hour per day.

— *Considering contextual data in ST-ED-RMGC:* The original input is a feature vector X composed by N (number of OD selected) rows, and 4 columns. A row represents a sequence of 4 historical data, which are used to forecast the next time-step (eg. the next hour). Let 't' be the period, M(t,d) the OD demand matrix at period t and day d, ki and li respectively the row index and the column index of the i-th OD. Let Si(t,d) be the sequence of historical data used to predict the time step Mk_i,l_i (t,d) of the i-th OD:

$$S_i(t,d) = \left[M_{ki,li}(t,d-7), M_{ki,li}(t,d-1), M_{ki,li}(t-2,d), M_{ki,li}(t-1,d)\right]$$

We propose to concatenate contextual data related to the past to the input sequences. Contextual data are weather data and road traffic data that we can add as inputs of the model. Contextual data are temporally variable as they change every hour, but also spatially variable as the intensity of road traffic metrics such as flow and loop occupancy rate are spatially dependent. By concatenating weather data to the historical sequence, we are considering its temporal variability. By concatenating traffic state metrics of each origin to its associated origin-destination sequences, we are considering its temporal and spatial variability.

Results

MAPE (Mean Average Percentage Error) is the metric used to evaluate the forecasting accuracy.

Table 13. Accuracy prediction on atypical traffic state datasets

dataset	loop occupancy	mape	(date,zones)
std 1.5	high	0,61	427
	low	0,71	1896
	baseline	**0,53**	17985
std 2	high	0,62	125
	low	0,67	294
	baseline	**0,52**	4079
std 2.25	high	0,70	48
	low	0,62	64
	baseline	**0,51**	1103
std 2.5	high	0,62	13
	low	**0,47**	10
	baseline	0,55	222

— *Traffic states indicators* (Table 1): our work highlights a decrease of forecasting accuracy toward baselines when the traffic flow and the occupancy rate on the loop are both atypically high and atypically low. Forecasting accuracy is worse when the flow and occupancy rates are atypical. This result emphasises a link between bike-sharing demand and traffic intensity in a zone and a limit of the ST-ED-RMGC on that type of scenarios. The dataset std 2.5 seems to indicate that a particularly low loop rate occupancy and flow is more easily predictable for the model, However, this could be explained by the fact we have

evaluated only very few data (10 tuples) that would correspond to particularly low flow –which are generally well predicted, or zero flow which are not considered in the MAPE metric.

— *Weather indicators* (Table 2): The table describes the set of considered weather scenarios along with the related performance metrics. As for the 5 classes on the gradation of *dr, t*he accuracy of the model is negatively affected (lower MAPE) as the intensity of *dr* increases. The MAPE increases from 7% for a low dr (dr in]0,1[) to 30% for a high dr (dr>5) compared to the baseline. Additionally, we found that the accuracy of OD demand prediction is worse (MAPE 4% higher) on windy days (*dw* > 100) when using a dataset excluding rainy days compared to the opposite scenario. These results underscore the significance of rain as a major obstacle to accurate forecasting.

Figure 57. Accuracy prediction on weather scenarios

scenarios	mape
dr = 0	**0,54**
dr in]0,1]	0,58
dr in]0,3]	0,6
dr in]3,5]	0,61
dr > 5	0,7
dr = 0 & dw > 100	0,56
dr = 0 & dw < 100	**0,54**

— *Adding contextual and intermodal information on sequences in input:* the production and analysis of results concerning the integration of contextual data are in progress, and we have strong reason to believe that their integration will have a major interest in the improvement of prediction accuracy with respect to atypical situations. These results will be presented at the conference.

Conclusion and future works

This paper proposes integrating contextual information into an ST-ED-RMGC model to improve bike-sharing OD-based travel demand forecasting accuracy. We have defined a library of weather and traffic indicators as proxies to detect perturbation scenarios in a large-scale multi-modal transport dataset and studied their impact on the forecasting accuracy of the initial framework, not integrating any contextual information about the travel demand of other transport modes and weather-related historical data. We have evaluated the impact of these contextual data in terms of decrease of the forecasting accuracy of the initial methodology. The results show potential for improvement by better capturing contextual information through integrating an attention mechanism module. Our study contributes to the ongoing efforts to enhance the accuracy of transport forecasting models by incorporating a wider range of relevant data sources.

Acknowledgments

This research is supported by the French ANR research projects MOBITIC (grant number ANR-19-CE22-0010) and PROMENADE (grant number ANR-18-CE22-0008).

References

Tong Liu, Wenbin Wu, Yanmin Zhu, Weiqin Tong, predicting taxi demands via an attention-based convolutional recurrent neural network, *Knowledge-Based Systems,* 2020.

Ke, J., Qin, X., Yang, H., Zheng, Z., Zhu, Z., and Ye,J, Predicting origin-destination ride-sourcing demand with a spatio-temporal encoder-decoder residual multi-graph convolutional network, *Transportation Research Part C*, 2021.

Zhang, J., Che, H., Chen, F., Ma, W., and He, Z., Short-term origin-destination demand prediction in urban rail transit systems: A channel-wise attentive split convolutional neural network method., 202.

Wang, Y., Yin, H., Chen, H., Wo, T., Xu, J., and Zheng, K, Origin-destination matrix prediction via graph convolution: A new perspective of passenger demand modeling., 2019.

Ezgi Eren, Volkan Emre Uz, A review on bike-sharing: The factors affecting bike-sharing demand, *Sustainable Cities and Society*, 2020.

Understanding large-scale traffic flow using model-based and data-driven dimension reduction: with COVID-19 and Olympic-Paralympic case study

T. Seo[a]

[a] *Department of Civil and Environmental Engineering, Tokyo Institute of Technology*

Introduction

Urban-scale traffic is a very large and complex phenomenon. Typically, vehicular traffic flows occur over large areas of an entire city with resolution on the order of 10 to 100 meters, and occur throughout the year with resolution on the order of minutes to hours. It is difficult to intuitively recognize and interpret the overall state of such a large and detailed phenomenon. This difficulty in interpretation poses challenging issues in traffic science and engineering. This is not only a problem for humans, but also for statistical and machine learning methods in the form of a curse of dimensionality.

In general, dynamic network traffic state can be quantified as a vector of flows, densities, and speeds for all links (or enough locations) at a given time. However, this vector is difficult to interpret due to the high-dimensionality of the vector and non-linearity of traffic phenomena. For example, the Euclidean distance between two vectors does not have essential meaning on traffic because it does not distinguish the direction of traffic. It would be desirable to have a method to compute the intrinsic similarity and distance between traffic states.

To overcome the difficulties caused by this high dimensionality, the Macroscopic Fundamental Diagram (MFD) is used by the transportation research community (Geroliminis and Daganzo, 2007). It represents the state of a road network in terms of two-dimensional state quantities: the network average flow and density. Under idealized conditions, this allows correct and concise recognition of the state of the traffic system and enables simple and efficient traffic control through area inflow control, for example.

However, there are several problems with the low-dimensional representation of traffic phenomena by MFD. First, MFD can represent essentially different traffic phenomena as the same state quantity. For example, a morning peak and an evening peak, during which the direction of traffic flow are completely opposite, may have the same average network flow and density and be indistinguishable on MFD. Furthermore, in order to obtain well-defined MFD, the network should satisfy some homogeneity conditions.

MFD can be interpreted as a model-based dimension reduction method. On the other hand, data-driven dimension reduction methods may provide a more appropriate (in terms of data representation) low-dimensional representation of traffic phenomena. With similar motivations, data-driven clustering methods have been widely applied to traffic phenomena to understand their features (e.g., Wang et al, 2012; Saeedmanesh and Geroliminis, 2017; Zhang et al., 2022). However, to the author's knowledge, continuous dimension reduction methods (e.g., principal component analysis) have not been widely applied to network traffic flows to understand their nature. Because traffic phenomena are inherently continuous, continuous dimension reduction methods may have substantial advantages.

The purpose of this study is to propose a novel approach to intuitively recognize and interpret large-scale traffic phenomena. The approach consists of a model-based dimension reduction method (MFD) and a data-driven method called Uniform Manifold Approximation and Projection (UMAP) (McInnes et al., 2018), a relatively new method. The approach is then applied to actual traffic data obtained in Tokyo in 2019 (ordinally state) and 2021 (with COVID-19 and Olympic-Paralympic Games) to derive some insights on ordinally traffic as well as very special traffic and comparison between these two.

Methodology and Data

UMAP is a non-linear dimension reduction method that computes low-dimensional representation of given data based on manifold learning. It is known that the method is capable of representing global structure of the data while preserving the local structure well. Its computational cost is very low.

The summary of the method is as follows. Let $\boldsymbol{x}_t$ be a vector of traffic data collected on time t, X be a set of $\boldsymbol{x}_t$ for all t. Then, 2-dimensional vector can be obtained as $\boldsymbol{u}_t = UMAP_X(\boldsymbol{x}_t)$ using UMAP (represented as function $UMAP_X$ for dataset X) or $\boldsymbol{m}_t = MFD(\boldsymbol{x}_t)$ using MFD (represented as function MFD which computes the network averages). Finally, the distributions of $\boldsymbol{u}_t$ and $\boldsymbol{m}_t$ are investigated.

We apply MFD and UMAP to traffic data obtained in Tokyo. Specifically, we use the following datasets:

— 5-min flow and density measured by traffic detectors at Tokyo Metropolitan Expressway. The total number of available detectors is 1425.

— 5-min flow measured by traffic detectors at major arterial roads in Tokyo. The total number of available detectors is 626.

— Data collection periods: from July to September in 2019 and 2021. The total number of 5-min time slots (i.e., the size of X) is about 25000. The data in 2021 is thoroughly affected by COVID-19. Olympic Game was conducted from 2021-07-23 to 08-08 and Paralympic Game was conducted from 2021-08-24 to 09-05. The traffic regulation for the Games is summarized at https://www.2020games.metro.tokyo.lg.jp/special/eng/traffic/, but actual impact is not clarified.

See **Figure 44** for the illustration of the traffic data. Unfortunately, speed data is not available in arterial road. Thus, MFD cannot be computed on it; therefore, for arterial road, only UMAP was computed.

Figure 58. Network traffic states on highway (up) and major arterial (bottom) on morning and evening peaks

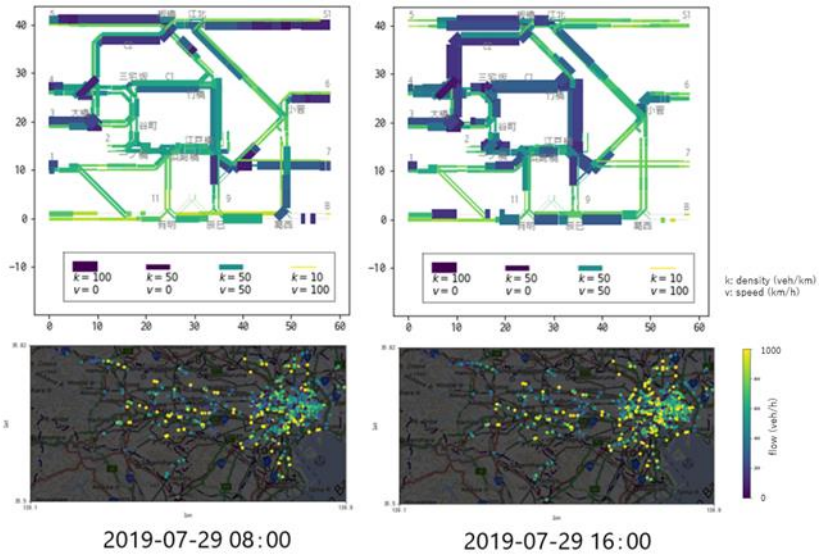

Source: Author elaborations using graphical data provided by Geospatial Information Authority of Japan, Mr. Takara Sakai, and Mr. Yutaro Ishikawa.

Results

MFD and UMAP on the highway are shown in **Figure 2**. Each dot represents $\boldsymbol{m}_t$ or $\boldsymbol{c}_t$ on specific t, and the color represents the time-of-day of t. The shape of MFD can be considered as standard for highways. The shape of UMAP can be expressed as "distorted donut with a gap at 6 o'clock position". In fact, this donut-like shape has very clear physical interpretation. As seen from the color, $\boldsymbol{c}_t$ on a certain (week)day moves on a counterclockwise trajectory on this diagram during the day. Furthermore, on weekend or holiday, a day's trajectory does not pass the lower-right region in the diagram. This means that a qualitative difference exists between traffic patterns in weekdays and weekends, and UMAP is useful to quantify it. This difference was not observed in MFD.

Figure 59. 2-dimentional representations of network traffic state using MFD (left) and UMAP with annotations (right) on the highway

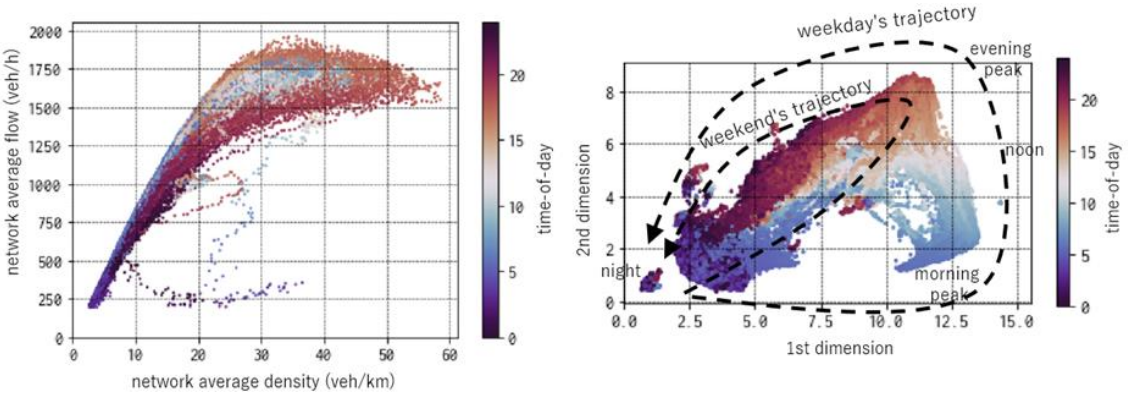

Source: Author's elaborations.

Figure 3 shows further details on UMAP. It was confirmed that MFD's network average density is well correlated to UMAP-representation; it means that the network average density is very useful variable to represent the network state, from both of model-based and data-driven perspectives. On the contrary, no clear relation was observed between average flow and UMAP. By comparing $\boldsymbol{c}_t$ from 2019 and 2021, slight differences were observed before and during COVID-19.

Figure 60. 2-dimentional representations of network traffic state using UMAP and MFD's network average density (left) and UMAP in 2019 and 2021 (right) on the highway

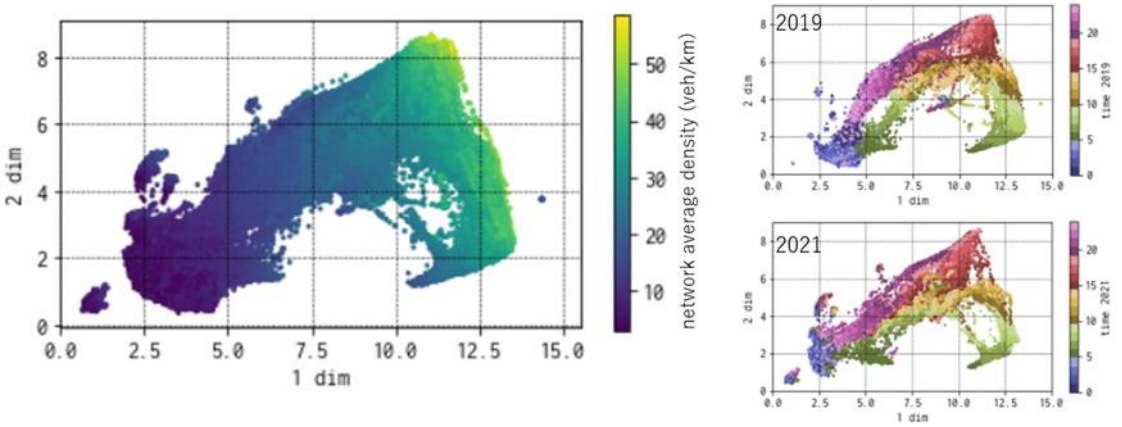

Source: Author's elaborations.

UMAP on the arterial roads is shown in **Figure 4**. You can see a remarkable pattern consists of multiple donut-like shapes. Similar to the highway result, each donut-like shape corresponds to a trajectory of within-day traffic for a certain period: ordinally weekday in 2019, ordinally weekend in 2019, day during COVID-19, and day during the Games. See the bottom of **Figure 4** for trajectories of typical days. These results suggests that UMAP can recognize qualitative differences of traffic patterns in an intuitive way.

Figure 61. 2-dimentional representations of network traffic state using UMAP on the arterial roads (top: all results, bottom: trajectories of typical days)

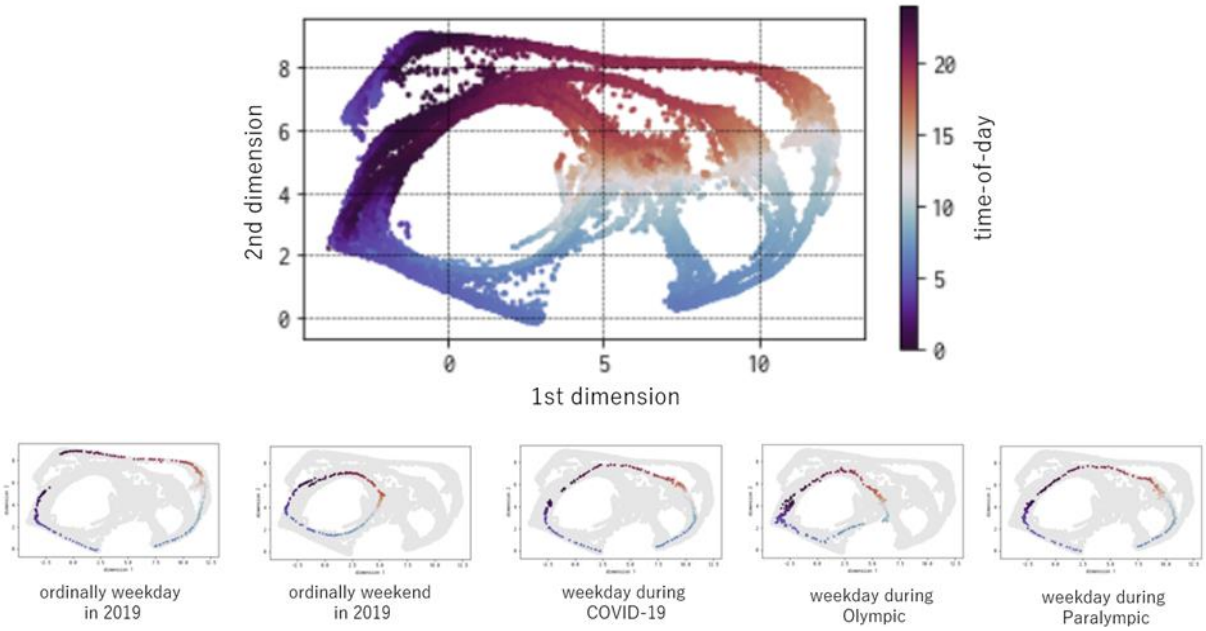

Source: Author's elaborations.

Conclusions

The key insights from this study are as follows. First, the UMAP results showed similar donut-like shapes at the two different locations. We could hypothesize that this is a universal phenomenon in transportation. Second, UMAP is capable of distinguishing and quantifying the qualitative differences in traffic pattens, such as weekday and weekend, before and during COVID-19 pandemic, and with and without the Games. Especially, the results on arterial roads would be remarkable because of its intuitiveness and simpleness; to the authors' knowledge, this kind of results have not been reported in the literature. Third, MFD's network average density is meaningful to represent the network state, from both of model-based and data-driven perspectives. Finally, traffic patterns on highway were not significantly affected by COVID-19 or the Games. On the other hand, ones on arterial were significantly affected by the both of COVID-19 and the Games differently. The future works includes in-depth investigation of the results and application to traffic prediction and control.

Acknowledgements

The data was freely provided by Tokyo Metropolitan Government ("offering of several datasets on mobility and transportation in Tokyo 2020 Games"), JARTIC, Takara Sakai, and Yutaro Ishikawa. Funding was provided by JSPS KAKENHI Grant-in-Aid 20H02267.

References

Geroliminis, N. and Daganzo, C. F.: Macroscopic modelling of traffic in cities, *Transportation Research Board 86th Annual Meeting*, 2007.

McInnes, L., Healy, J., and Melville, J.: UMAP: Uniform manifold approximation and projection for dimension reduction, *arXiv preprint arXiv:1802.03426*, 2018.

Wang, P., Hunter, T., Bayen, A. M., Schechtner, K., González, M. C.: Understanding road usage patterns in urban areas. *Scientific Reports*, Vol. 2, No. 1001, 2012.

Saeedmanesh, M., Geroliminis, N.: Dynamic clustering and propagation of congestion in heterogeneously congested urban traffic networks. *Transportation Research Part B: Methodological* Vol. 105, pp. 193–211, 2017.

Zhang, P., Ma,W., Qian, S.: Cluster analysis of day-to-day traffic data in networks. *Transportation Research Part C: Emerging Technologies*, Vol. 144, 103882, 2022.

Reservation-based Take Off and Landing in Urban Surface and Air Mobility Management

S. Gavric[a], N. Mitrovic[b], A. Stevanovic[a]

[a] *University of Pittsburgh*

[b] *CHA Companies*

Introduction

Traffic congestion is one of the major concerns of modern society because it causes extra delays that not only have negative consequences on the environment but also hinder the ability of high-priority vehicles, such as ambulance vehicles, to travel efficiently. In recent years, technological advances with connected and autonomous vehicles (CAVs) have opened new opportunities to increase both efficiency and safety (Stevanovic and Mitrovic, 2019). Also, the emergence of wireless communications and advanced video and LIDAR sensing technologies has led to the development of flying vehicles, which promise to enable unmanned flying vehicles of the future (Kuru, 2021). Many researchers have worked on the problems of integrating these futuristic technologies into transportation system (Rothfeld et al., 2018; Postorino and Sarné, 2020).

As one of new concepts, urban air mobility (UAM) promises to seize this opportunity by using a new generation of vertical take-off and landing (VTOL) aircraft for urban transportation services. However, before this new UAM is fully introduced into the market these concepts will require further investments in infrastructure (e.g., vertiports – platforms in urban environments where the VTOL aircraft can land, take off, and park), clearly defined flying rules (in an urban environment), and proper integration with the other transportation modes, if they are ever going to be used massively (Dunn, 2018; Vascik and Hansman, 2019). Additionally, while regular long-distance flights follow strict and clearly defined Federal Aviation Administration (FAA) rules, flying VTOL aircraft in urban areas is not currently regulated and this can be a major issue. Our previous work proposed a sub-concept of UAM, Urban Surface and Air Mobility (USaAM) that enables origin-to-destination travel by using the same vehicle for various transportation modes (Gavric et al., 2023). The USaAM utilizes hybrid vehicle that can operate as a regular surface car on the existing road network and as a VTOL aircraft in urban airspace, without the need for communication with conventional cars. Also, our previous research defined rules for low-altitude flights by defining a layered flight-level structure to address the vertical and lateral separations (Gavric et al., 2023).

In this paper, we propose a novel extension of the USaAM concept by incorporating a high-level communication manager that provides priority to Flying Vehicles (FVs), including emergency vehicles and others who deserve higher trip priority. Additionally, we address the downwash effect generated by VTOLs (while taking off and landing), acknowledging need for a larger roadway surface area that must be free of other vehicles during FV landing or take-off operations. Furthermore, we embed the dynamics of FVs with newly proposed reservation system into custom-made simulation environment.

The paper is structured as follows: first, we provide background information on the USaAM concept and its limitations. Next, we detail our proposed methodology for integrating flying operations into surface traffic, including the use of the communication manager and simulation of the downwash effect. Finally, we present our results and engage in a thorough discussion before concluding remarks.

Background of Urban Surface and Air Mobility Management

Our prior research introduced Urban Surface and Air Mobility (USaAM) concept that enables seamless origin-to-destination travel with the same vehicle (Gavric et al., 2023). Specifically, these vehicles, which we refer to as Flying Vehicles (FVs) can operate as a regular surface car on existing road network and as a VTOL aircraft within urban airspace (Gavric et al., 2023). In our earlier work, we detailed the characteristics and components of FVs, as well as our proposal to manage their usage via a system akin to the FAA's regulation of long-distance flights. The USaAM concept requires designation of certain urban corridors, with sufficient space and unobstructed airspace, as take-off and landing segments for urban flight routes. We also introduced a limited number of Street Flight Levels (SFLs) to facilitate the vertical separation of potentially conflicting FVs.

To further explain USaAM, a representative USaAM trip is shown in Figure 1. For example, a FV starts driving from a parking lot, followed by a drive through a residential area (where it is not allowed to fly). Then, once it reaches an FV-eligible road, the FV drives shortly on a surface road before taking off, once certain conditions are met. Once the FV starts flying above the eligible arterial, it flies between urban waypoints at high speeds, and then descend above another FV-eligible arterial road, where it can land too. The landing usually happens in front of a traffic signal, if there is a gap on the surface street that is large enough. Alternatively, the signal

controller can be actuated to enable a special phase that assists with the landing, as explained previously (Gavric et al., 2023). After landing, the FV drives again through residential streets to its final destination. It is worth noting that not every trip will have all of these segments. Some trips will have origin and destination on arterial streets, thus, their driving time could be significantly shorter.

Figure 62. Overview of Urban Surface and Air Mobility Concept

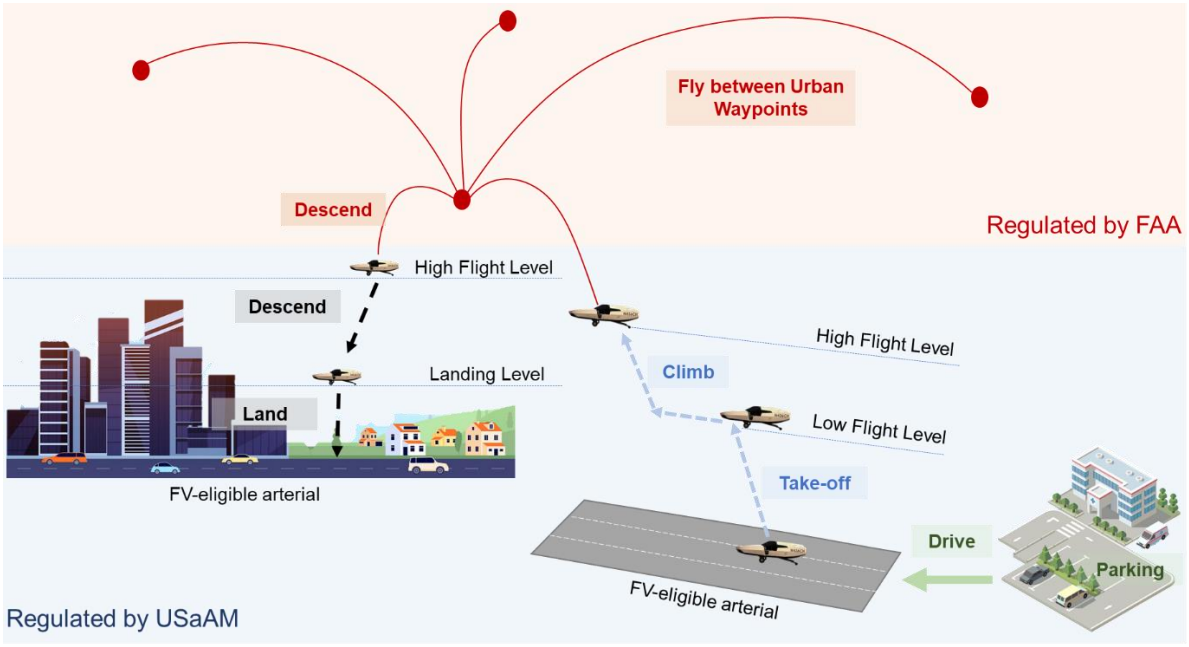

Source: Authors' elaborations.

Methodology of Autonomous Urban Surface and Air Mobility Management

A multiagent mobility system proposed in this research utilizes a reservation-based strategy wherein FVs (agents) seeking to perform landing or take-off contact FV Operations Manager (FVOM) responsible for the relevant link to reserve a trajectory that ensures their safe take-off or landing among other surface vehicles.

Reservation-based flying operations

Landing and take-off operations in autonomous USaAM are solved in reservation-based fashion similar to one that was originally introduced by others, for the purpose of controlling traffic at surface intersections (Dresner and Stone, 2008). The FVOM decides whether a FV will be granted the reservation to land or take off or not. A typical interaction of FV and FVOM is as follows:

- A FV announces its impending take-off/land intention to the FVOM. The FV communicates its intended/predicted climbing/descending time, velocity, acceleration, and destination.
- The FVOM then 'simulates' the FV landing/take-off trajectory, checking for conflicts with the paths with any surface vehicles. If any of the nearby surface vehicles are about to enter the area reserved by the FV, their requests are denied and they are instructed either to slow down or make a complete stop, if necessary. In that way, the area reserved for the FV is kept clear of all surface vehicles. Also, a similar procedure is used to keep any surface vehicles away from FVs trying to take-off.
- The FV can only take-off/land once its request for such an operation has been approved by the FVOM.

Figure 63. Diagram of the FV landing/taking off reservation system

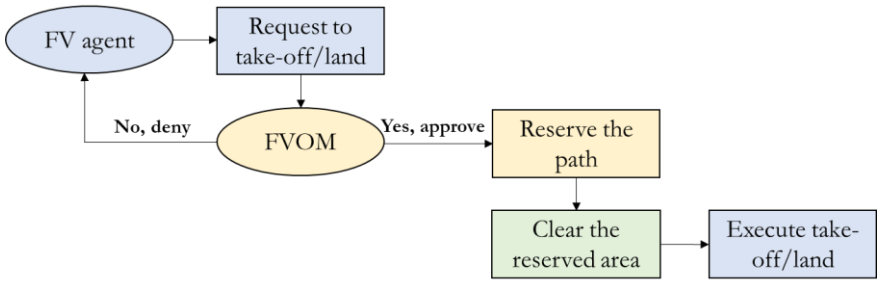

Source: Authors' elaborations.

Surface Operations

Traffic management at the street level includes a set of control algorithms for lane changing, car-following, and intersection control. The following text provides a brief overview of these operations. To maintain consistency with traditional driving principles, we suggest keeping right-side driving and traditional lane assignment. At the upper, flying levels, we recommend limiting each direction to a single 'lane' or path per flying level, which will decrease the number of conflict points and potentially hazardous situations. To minimize the risks of collisions, all vehicles can change their paths only at the surface level, and outside of intersections. The utilized lane changing procedure is explained elsewhere (Stevanovic and Mitrovic, 2019). Furthermore, conflicts at the intersection are resolved by utilizing fixed signal timings.

Simulation Platform

For this study, we propose extension of our previous work (Gavric et al., 2023) by developing a modelling platform, within the NetLogo, that allows the simulation of vehicle operations both on the urban surface and in the air. The developed platform, coded within NetLogo environment through a series of custom-made codes written in Scala (Java-compatible language), is shown in Figure 3.

Experiments

Experiments are conducted by using the three-intersection network shown in Figure 3. Three levels of surface traffic demand and five levels of FV penetration rates, ranging from 1% to 5% of the total traffic demand, were used. It should be noted that each scenario is simulated for multiple random seeds and a full hour of simulation time, resulting in a total of 75 runs. The first part of the performance assessment is based on conventional traffic metrics, such as the average vehicle delay and the number of stops and the analysis includes two distinct groups of vehicles: regular vehicles and FVs. In addition, to assess the effectiveness of flying operations in the USaAM, a comprehensive evaluation is conducted by utilizing newly developed performance metrics for this purpose.

Figure 64. Developed simulation platform

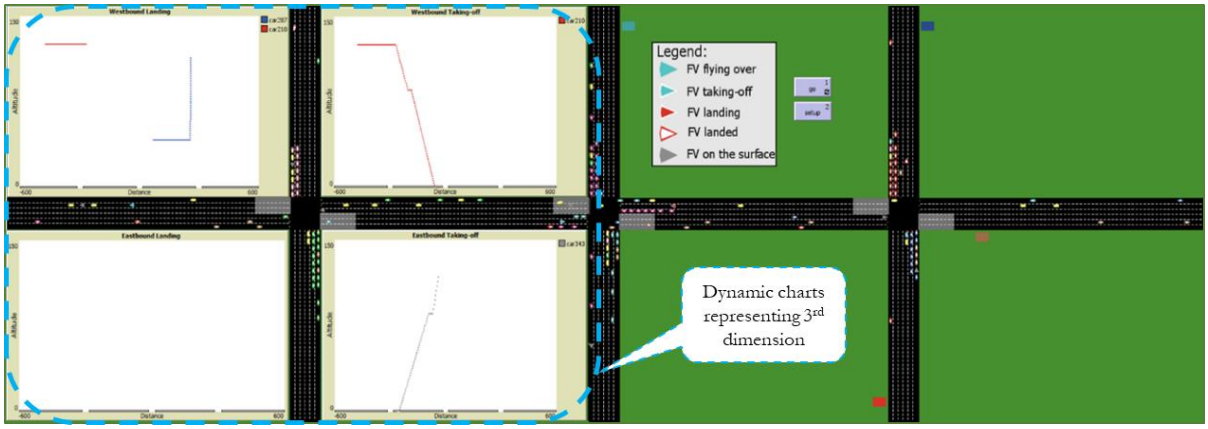

Source: Authors' elaborations.

Results

The application of our simulation model through numerous experiments is expected to yield interesting results demonstrating that the number of denied requests to take-off are reduced (when compared to our previous study) as priority is given to FVs. Also, the results are expected to show that traffic demand on surface is highly influenced by implementing reservation-based flying operations on the surface traffic.

Conclusions

The goal of this research is to present an upgrade to a novel concept, called Urban Surface and Air Mobility (USaAM), which proposes the use of FVs both on urban surface streets and airspace in reservation-based fashion. In this research we upgrade the first-of-its-kind modelling platform to implement reservation-based flying operations into the USaAM simulation environment. We introduce reservation-based take-off and landing operations to increase the efficiency for FVs, such as emergency FVs and other high-priority FVs (e.g., delivery of medical supplies or other high-value goods).

References

Dresner, K., and P. Stone, 'A Multiagent Approach to Autonomous Intersection Management', *Journal of Artificial Intelligence Research*, Vol. 31, March 31, 2008, pp. 591–656.

Dunn, N. (Nicholas S.), 'Analysis of Urban Air Transportation Operational Constraints and Customer Value Attributes', Thesis, Massachusetts Institute of Technology, 2018.

Gavric, S., A. Stevanovic, N. Mitrovic, F. Netjasov, and J. Rakas, 'Introduction and Preliminary Evaluation of Urban Surface and Air Mobility Management', *Transportation Research Board 102nd Annual Meeting*, Washington, DC, 2023.

Kuru, K., 'Planning the Future of Smart Cities With Swarms of Fully Autonomous Unmanned Aerial Vehicles Using a Novel Framework', *IEEE Access*, Vol. 9, 2021, pp. 6571–6595.

Postorino, M.N., and G.M.L. Sarné, 'Reinventing Mobility Paradigms: Flying Car Scenarios and Challenges for Urban Mobility', *Sustainability*, Vol. 12, No. 9, January 2020, p. 3581.

Rothfeld, R., M. Balać, K. Ploetner, and C. Antoniou, 'Agent-Based Simulation of Urban Air Mobility', *2018 Modeling and Simulation Technologies Conference*, 2018.

Stevanovic, A., and N. Mitrovic, 'Traffic Microsimulation for Flexible Utilization of Urban Roadways', *Transportation Research Record*, Vol. 2673, No. 10, October 1, 2019, pp. 92–104.

Vascik, P.D., and R.J. Hansman, 'Development of Vertiport Capacity Envelopes and Analysis of Their Sensitivity to Topological and Operational Factors', January 8, 2019.

Dynamic network loading based on link travel times

O. Mansour[a], T. Toledo[a]

[a] *Technion – Israel Institute of Technology*

Introduction

Dynamic network loading (DNL) models have been widely used in transportation planning and operations to evaluate long-term and short-term traffic states in urban areas. More recently, DNLs are also used in real-time to predict traffic conditions in support of making control actions. Most DNL models formulate and solve the problem using densities and flows as the variables of interest.

DNL models express the propagation of travel demands in the network using traffic flow models. Macroscopic DNL models commonly describe the aggregate traffic dynamics on a link using variables of density and flow rate in a continuous stream. These models are often based on the Lighthill, Whitham and Richards (LWR) kinematic wave theory. Examples include the cell transmission model (Daganzo, 1994) and its modifications (e.g., Gomes et al., 2006; Srivastava et al., 2015), the link transmission model (Newell, 1993; Yperman, 2007; Himpe et al., 2016; Raadsen et al., 2016), dynamic programming methods (Daganzo, 2005), the Lax-Hopf algorithm (Mazaré et al., 2011) or wave tracking (Henn, 2005). These approaches require triangular or concave fundamental diagram (FD) functional forms, suffer from discretization errors (Raadsen et al., 2016) or are not applicable to large scale networks. Whereas their solution is defined in terms of density and flow, in some applications, travel times may be of primary interest. However, their calculation requires tracing densities and speeds in the network, which is not trivial.

To facilitate travel time calculations, this study explores their dynamics in the network. The theoretical foundations for a traffic model based on link travel time dynamics are presented and its equivalence to the LWR density-based model is established. Based on this theory, a DNL model that uses travel time as independent variable is proposed and implemented. The DNL describes the traffic states at the link boundaries using the travel time dynamics and a spillback model. It does not require tracking the states within the link. A node model describes the flow distribution at interactions.

Methodology

We begin the derivation of the model by defining the travel time dynamics for a single link. Let $N(x,t)$ be the cumulative flow at point x and time t. Figure 65 shows the cumulative flow curves at two points: the entrance and exit of a link, which are denoted with – and + signs, respectively. In the figure, travel times on the link are the time difference between points of equal cumulative flow on the two curves. These travel times are time dependent and may be defined based on the entry time to the link (forward travel time, $\tau^+(t)$) or the exit time (backward travel times, $\tau^-(t)$).

The link inflow and outflow are expressed by the time derivatives of the cumulative curves. We denote these as $f^-(t)$ and $f^+(t)$, respectively. Finally, we note that link travel times are bounded from below by τ^{min}, which is the travel time achieved with the free flow speed. Using these variables, the forward travel times dynamics is given by:

$$\tau^+(t+dt) = \max\left\{\tau^+(t) + \left(\frac{f^-(t)}{f^+\left(t+\tau^+(t)\right)} - 1\right)dt, \quad \tau^{\min}(t)\right\} \tag{1}$$

This forward travel time dynamic was used in delay-function models. However, its use within a DNL is difficult because it depends on the future unknown outflow $f^+\left(t+\tau^+(t)\right)$.

Figure 65 Cumulative flow curves and travel times on a single link

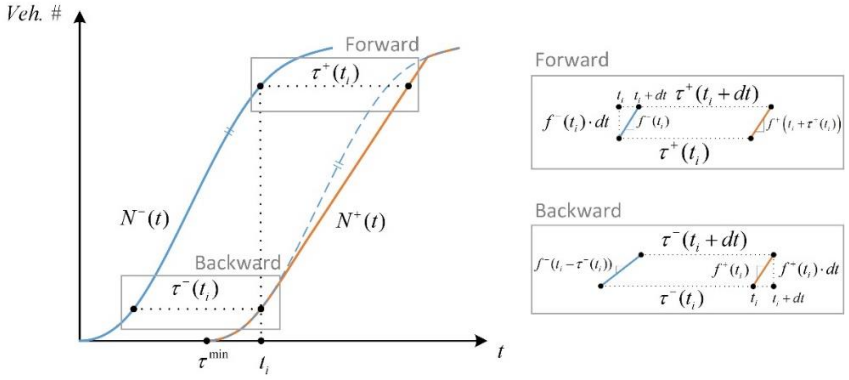

We now focus on the backward travel times. In this case, the travel times dynamics are given by:

$$\tau^-\left(t+dt\right)=\max\left\{\tau^-\left(t\right)+\left(1-\frac{f^+\left(t\right)}{f^-\left(t-\tau^-\left(t\right)\right)}\right)dt,\quad \tau^{\min}\left(t\right)\right\} \tag{2}$$

Equation (2) above holds as long as $f^-\left(t-\tau^-(t)\right)>0$. If the entry flow $f^-\left(t-\tau^-(t)\right)=0$, then, the outflow $f^+(t)$ entered the link later, at the moment that again $f^-\left(t-\tau^-(t)\right)>0$ is again positive. In the case that downstream traffic conditions do not affect inflows.

Flows are transferred between links by nodes that represent bottlenecks and are the source of delays in the network. Each node maintains sets of its incoming and outgoing links, and similar sets of routes. These are defined by:

$$\mathbf{f_n^-}=\begin{bmatrix} f_1^+ \\ \vdots \\ f_i^+ \\ \vdots \\ f_I^+ \end{bmatrix},\quad \mathbf{f_n^+}=\begin{bmatrix} f_1^- \\ \vdots \\ f_j^- \\ \vdots \\ f_J^- \end{bmatrix},\quad \mathbf{f_n^{r-}}=\begin{bmatrix} \mathbf{f_1^{r+}} \\ \vdots \\ \mathbf{f_i^{r+}} \\ \vdots \\ \mathbf{f_I^{r+}} \end{bmatrix},\quad \mathbf{f_n^{r+}}=\begin{bmatrix} \mathbf{f_1^{r-}} \\ \vdots \\ \mathbf{f_j^{r-}} \\ \vdots \\ \mathbf{f_J^{r-}} \end{bmatrix},\quad i\in L_n^-,\quad j\in L_n^+,\quad n\in N$$

Where, L_n^-/L_n^+ are the sets of upstream and downstream links for node n, respectively. $\mathbf{f_i^+}$ and $\mathbf{f_n^-}$ are vectors of the flows entering and exiting the node, respectively. That is, they are the outflows on the links entering the node and the inflows on the links that exit the node. f_i^+ is exit flow on link i that enters the node. f_j^- is the entry flow to link j that exits from the node.

$\mathbf{f_n^{r-}}$ and $\mathbf{f_n^{r+}}$ are the corresponding vectors or flows on routes entering and exiting the node. Without loss of generality, we assume that they are ordered by the entry or exit links that they use through the node. Thus, $\mathbf{f_i^{r+}}$ and $\mathbf{f_j^{r+}}$ are vectors of the routes that enter the node through link i, and those that exit the node through node j, respectively.

The mapping of flows on links entering the node to flows on links exiting the node is given by:

$$\boldsymbol{\beta}=\begin{bmatrix} \mathbf{1}_{1\times K1} & \cdots & 0 \\ \vdots & \ddots & \vdots \\ 0 & \cdots & \mathbf{1}_{1\times KJ} \end{bmatrix}^T\begin{bmatrix} \mathbf{T_{11}} & \cdots & \mathbf{T_{1I}} \\ \vdots & \ddots & \vdots \\ \mathbf{T_{J1}} & \cdots & \mathbf{T_{JI}} \end{bmatrix}\begin{bmatrix} diag(\mathbf{p_1})_{M1\times M1} & \cdots & 0 \\ \vdots & \ddots & \vdots \\ 0 & \cdots & diag(\mathbf{p_I})_{MI\times MI} \end{bmatrix}\begin{bmatrix} \mathbf{1}_{1\times M1} & \cdots & 0 \\ \vdots & \ddots & \vdots \\ 0 & \cdots & \mathbf{1}_{1\times MI} \end{bmatrix} \tag{3}$$

Where, the first matrix in the multiplication is the link-route incidence matrix for the links exiting from the node. Similarly, the last matrix is a link-route incidence matrix for the links entering the node. The dimensions $K1$ through KJ are the numbers of routes that use the exiting links. Similarly, $M1$ through MI are the numbers of

routes that use the entering links. The matrices T are mapping from the routes on links that enter the nodes to those that exit the nodes. P are the fractions of the flows on links that stem from the relevant routes, such that for every entering link, the values of p for all routes that pass through it sum to 1.

The relationship between the links' inflows and outflows in a node is given by:

$$\mathbf{f_n^+} = \boldsymbol{\beta} \cdot \mathbf{f_n^-} \tag{4}$$

The corresponding relation among route flows is given by:

$$\mathbf{f_n^{r+}} = \mathbf{T_n} \cdot \mathbf{f_n^{r-}} \tag{5}$$

We assume that entry capacities are associated with links in the network. In some cases, the flows calculated for these links may exceed their entry capacities. Then, the exit flows on the links entering the node need to be adjusted so that the capacity constraints are respected. This may be done by multiplying them by a factors α that captures the priority policy for these links. For example, the factor may reflect a policy where the proportion of vehicles on the various routes are kept. With the priority policy, the node updates as follow:

$$\begin{aligned} f_j^- &= \min\left(f_j^{\max}(t), \quad \beta \cdot f_i^+ \right) \quad \forall i \in L_n^-, \\ f_i^+ &= \alpha_i \cdot f_i^+ \qquad\qquad\qquad\quad \forall j \in L_n^+ \end{aligned} \tag{6}$$

If the priority factors do not maintain the proportions of flows on the various routes, these proportions P are adjust accordingly for the next time step. These proportions are also shared with downstream nodes so that they can also update their routes proportions accordingly.

Results

The model was calibrated, against the Transmodeler (TSM) microscopic traffic simulation model on a section of the Ayalon Highway through the Tel Aviv metropolitan area in Israel, through minimization of the difference in counts and route travel times between the two models during the AM peak period. Calibration variables are the fundamental diagrams, link entry capacities and priorities. Calibrated RMSE values are 18.3 veh./5-min and 1.752 min. RMSPE values are 0.103 and 0.168, respectively.

The model was tested in three experiments showing various scenarios. In the first and second tests, the demand matrix was scaled and re-structured (keeping the total demand constant), randomly. In the third experiment, traffic incidents were introduced during the simulation. The experiments are summarized in **Table 14**. In each case the model results are compared with those of TSM.

The experiments results are presented in

Table 15. The model's fit to TSM are similar in most cases, which indicate to the explanatory power of the proposed model, which is robust to the demand level and distribution and the capacity reductions due to incidents.

Table 14. Preformed Experiments

	Factor	**Levels**
Experiment 1	OD scale	60%, 65%, 70%, 75%, 80%, 85%, 90%, 95%
Experiment 2	Random OD change (by a uniform term α)	U[$1 \pm \alpha \mid \alpha = 0.05, 0.1, 0.15, 0.2$]
Experiment 3	Incident (capacity reduction)	1, 2, 3, 4, 5 blocked lanes out of 5

Table 15. Performance measures of each scenario in case 1

Experiment 1								
Demands scale	100%	95%	90%	85%	80%	75%	70%	60%
RMSE – Counts	18.3	6.5	5.6	5.4	5.2	5.0	4.8	4.4
RMSPE – Counts	10.3%	4.5%	4.4%	4.6%	4.3%	4.4%	4.6%	4.3%
RMSE – Travel times	1.754	1.266	0.942	0.378	0.312	0.300	0.330	0.360
RMSPE – Travel times	16.8%	13.9%	12.6%	6.1%	5.2%	5.1%	5.6%	6.2%

Experiment 2				
Perturbation factor α	0.05	0.1	0.15	0.2
RMSE – Counts	14.7	16.0	16.2	18.8
RMSPE – Counts	0.070	0.080	0.083	0.091
RMSE – Travel times	1.7	2.0	2.3	2.4
RMSPE – Travel times	0.158	0.178	0.193	0.215

Experiment 3					
Blocked lanes N	1	2	3	4	5
RMSE – Counts	16.1	15.5	19.4	26.6	24.0
RMSPE – Counts	0.066	0.069	0.091	0.141	0.139
RMSE – Travel times	1.3	1.7	1.7	1.8	2.6
RMSPE – Travel times	0.129	0.151	0.153	0.174	0.199

Conclusions

This paper sets a theoretical foundation for the travel time dynamics in traffic networks. Travel time dynamics in space and time are established and Equal Travel Time curves are derived. The relations between the classical dynamic models that are based on density and travel time dynamics were presented. Then, a simulation model based on link's travel times dynamics was developed.

References

Daganzo, C.F., 'A Variational Formulation of Kinematic Waves: Solution Methods', *Transportation Research Part B: Methodological*, Vol. 39, No. 10, 2005, pp. 934–950.

'The Cell Transmission Model: A Dynamic Representation of Highway Traffic Consistent with the Hydrodynamic Theory', *Transportation Research Part B*, Vol. 28, No. 4, 1994, pp. 269–287.

Gomes, G., and R. Horowitz, 'Optimal Freeway Ramp Metering Using the Asymmetric Cell Transmission Model', *Transportation Research Part C: Emerging Technologies*, Vol. 14, No. 4, 2006, pp. 244–262.

Henn, V., 'A Wave-Based Resolution Scheme for the Hydrodynamic LWR Traffic Flow Model', *Traffic and Granular Flow'03*, Springer, 2005, pp. 105–124.

Himpe, W., R. Corthout, and M.J.C. Tampère, 'An Efficient Iterative Link Transmission Model', *Transportation Research Part B: Methodological*, Vol. 92, 2016, pp. 170–190.

Mazaré, P.E., A.H. Dehwah, C.G. Claudel, and A.M. Bayen, 'Analytical and Grid-Free Solutions to the Lighthill-Whitham-Richards Traffic Flow Model', *Transportation Research Part B: Methodological*, Vol. 45, No. 10, 2011, pp. 1727–1748.

Newell, G.F., 'A Simplified Theory of Kinematic Waves in Highway Traffic, Part Ii: Queueing At Freeway Bottlenecks', *Transpn. Res.-B*, Vol. 27, No. 4, 1993, pp. 289–303.

Raadsen, M.P.H., M.C.J. Bliemer, and M.G.H. Bell, 'An Efficient and Exact Event-Based Algorithm for Solving Simplified First Order Dynamic Network Loading Problems in Continuous Time', *Transportation Research Part B: Methodological*, Vol. 92, 2016, pp. 191–210.

Srivastava, A., W.L. Jin, and J.P. Lebacque, 'A Modified Cell Transmission Model with Realistic Queue Discharge Features at Signalized Intersections', *Transportation Research Part B: Methodological*, Vol. 81, 2015, pp. 302–315.

Yperman, I., *The Link Transmission Model for Dynamic Network Loading*, *Open Access Publications from Katholieke Universiteit Leuven*, 2007.

Does a livable city profit from a shared CCAM Shuttle Bus on demand?

Galia Weidl[a], Stefan Berres[a], J. Raiyn[a]

Connected Urban Mobility, Faculty of Engineering, Technical University of Applied Sciences, Aschaffenburg, Germany

Introduction

There are various levels of autonomous shuttle buses (AS) as a concept of shared CCAM (Connected Cooperative Autonomous Mobility). Depended on the degree of autonomy, an autonomous shuttle bus with low degree of autonomy (SAE level 3) is supposed to travels in a special lane (a.k.a segregated lane). A highly automated shuttle bus (SAE level 4) is expected to have full control over all functions and travel in mixed traffic which shared the road with other road users (motorized and vulnerable ones. The ASs can communicate with each other and share information about the surrounding environment. Communication is neither limited to be only between cars, nor between cars and infrastructure (Bucchiarone et al., 2020) (Ainsalu, 2018) and it can involve communication between all traffic participants in order to reach the highest level of service as well as of safty. Our motivation to introduce at the Technical Hochschule an autonomous shuttle bus (TH-AS) is inspired by a preliminary survey of citizen participation in the city life, revealing the students' opinion at the university of applied sciences Aschaffenburg. The preliminary results show that a shuttle bus that connects all three campuses leads to safer roads, less congestion, saving time for search of parking slots and less stress for the students to attend the education units on time. TH-AS challenges are divided in social and research challenges. TH-AS will travel through the city and sharing the same road with public transportations and taxi drivers which consider the TH-AS as a competitor. Some people will less trust the AS and have anxiety sceptical attitudes towards the new installed technologies (Salonen & Haavisto, 2019). To collect the citizens' opinion a questionnaire will be distributed and interviews performed in order to find the real attitude towards the new technologies. The research challenges are focused on TH-AS response time to anomalies in rea-time (Raiyn, 2022). The process of anomaly detection faces many challenges. It is needed to discover patterns which are not conform to a normal expected behaviour in the traffic data. Anomalies cause discomfort to both TH-AS and users, thus they lead to a negative impact on traffic efficiency. In case traffic accidents occur or if there is a congestion, the traffic flow is abnormal. The anomalies are caused by traffic accidents, bad weather, construction work, special events, rush hours, parking/ recharge search, traffic light phase. Furthermore, there are a number of other challenges faced by TH-AS, such as noise and interference, which are further sources of anomalies in traffic flow. The deep learning approach is proposed to find these patterns and can be applied to all roads with usually normally traffic. Since TH-AS is traveling in mixed traffic, manoeuvre recognition is proposed in order to take into account on the behaviour of all surrounding vehicles (Weidl et al., 2018). Adaptive decision support is proposed to resolve the arising changes of identified abnormalities and to ensure safe driving of the TH-AS.

Related work

In smart cities, an autonomous shuttle buses are becoming a part of everyday life with goal to improve the public transportation. Esterwood et al. (2021) conducted a survey on how individual differences can influence trust, attitude, and the intention to ride AV buses. Tsigdinos et al. (2022) proposed identified transforming concepts of the future urban road, which can be categorized into five categories, namely, efficiency, safety, liveability, accessibility, and smart technology. To understand the driving behavior, Flötteröd et al. (2021) analyzed real autonomous shuttle bus data. Our contribution in this study is creating smart infrastructure to establish communication between smart intersections, autonomous shuttle buses and drones to improve the traffic flow efficiency and safety. The novelty lies in their potential to transform the way of human thinking to navigate their surroundings and make rea-time decision based on dynamic Bayesian networks.

Methodology

The technical university of applied sciences (TH) Aschaffenburg plan to introduce TH-autonomous shuttle bus (TH-AS) to serve the students that travel between the three university campuses as illustrated by Figure 1. The TH-AS will also serve on demand, outside the daily lecture breaks, by offering an alternative to public transportation for both people and goods. It will provide bus stops on demand for the local residents and especially the elderly citizens to simplify their daily life. Additional benefit of the TH-AS is in reducing the urban road congestion in Aschaffenburg, where the traffic demand exceeds the road capacity in rush hours, which is often characterized by slower speeds, longer trip times, delays and increased queuing. Reducing the road congestion has strong impact on the noise reduction and on climate change, such as better air quality by reducing the carbon dioxide emissions. The smart intersection at TH-AS is already equipped and recently

updated with various internet of thing devices, such as smart cameras, Lidars, GPS, and sensors to sense the environment (Hetzel et al. 2021). The road segments between the two roundabouts (2.1 km in each direction) will be equipped with Road Site Units (RSU) for continuous monitoring of the traffic flow. The received data is analyzed by monitoring and control unit (MCU). MCU is processing various format of data based on deep learning scheme (DL). Complimentary to the RSU, an unmanned aerial vehicle (UAV), also known as (a.k.a) drone, plays a significant role for the planned TH-AS to ensure redundancy of data for traffic safety reasons. Moreover, drones have been used to map and measure the smart intersection. Drone technologies can help to reduce the risks of weather made errors while guaranteeing the safety of operation. Besides the drone's safety monitoring of the road in a designed air corridor and the TH-AS's designated optimal lane for vulnerable road users (VRU. i.e. pedestrian, bicycles and scooter), drones have been considered as the large moving step toward the smart city's sustained growth.

Figure 66. TH-AS concept

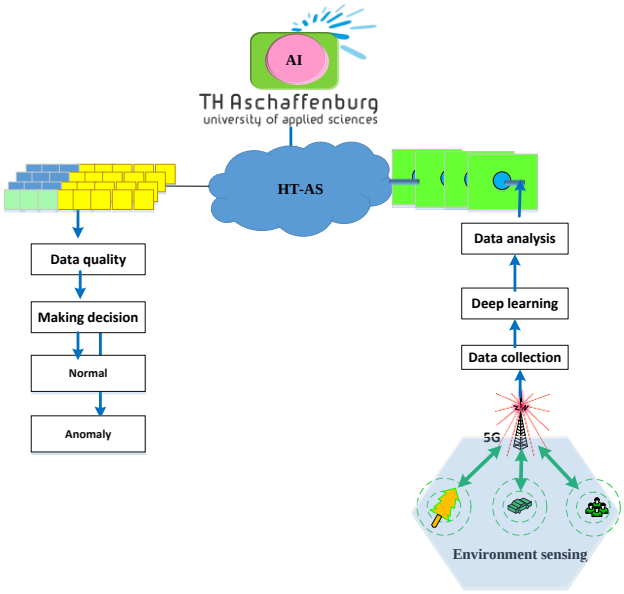

Data Collection

TH-AS operates and performs tasks under its own power on an operations' platform. Some features of TH-AS are sensing the surrounding environment, collecting information, and managing communication with other traffic participants. TH-AS uses a combination of cameras, sensors, GPS, radar, LiDAR, and an on-board computer. These technologies work together to map the vehicle's position and its proximity to everything around it. TH-AS support various types of communication, such as, vehicle-to-vehicle, vehicle-to-infrastructure, and vehicle–to-mobile device communication. The overall system intelligence utilizes advanced deep learning model (DL) in machine learning for the classification and visibility detection of the fog weather. The use of DL is to provide better accuracy in terms of an image dataset and performs multiple iterations of layers, such as convolution, max pooling and flattening, on the images to classify them correctly for the needs of maneuver recognition and route's safety.

Data preparation

TH-AS receives data from various devices in different formats, and this can lead to problems with data quality. In the preparation phase on the cloud operation platform, data are converted to a desired format, then the dataset is cleaned, and inconsistent, invalid, and corrupt data are removed. Our algorithms can deal robustly with up to 10% missing data.

Data Processing

These raw data have been processed using various techniques to extract relevant features, machine-learning algorithms have been applied to recognize road anomalies and cognitive models have been developed to recognize maneuvers of the surrounding objects, which behavior might have an impact on a possible collision risk, hazard avoidance and safety. Moreover, for trustworthy systems, explanations will be provided, which are feasible due to the qualitative structure of the developed cognitive hierarchical models (Weidl et al., 2018). The

proposed deep learning model is supposed to deal with the quality of raw data. The quality of raw GNSS measurements (also called observables) is affected by several factors that originate from satellites, signal propagation and receivers. The signal transmitted by a satellite propagates through the atmosphere, where it is subject to delays caused by ionospheric and tropospheric media. At ground level, a multipath effect, namely, the multiple reception of signals that are reflected from obstacles such as buildings surrounding the receiver, can occur, causing one of the largest sorts of errors. Furthermore, weather conditions, such as fog, cloud, heavy rain and snow reduce the quality of raw data that are received by camera or GNSS.

Data evaluation

The multiple statistical measures, such as the mean and the standard deviation of a variable, variance, mean absolute error (MAE), root mean squared error (RMSE), relative absolute error (RAE) and their interactions with other features, help to distinguish between normal and abnormal traffic flow and to explain the reasons for any differences.

Discussion and conclusions

The dataset has been collected at a public intelligent intersection (i.e. equipped with sensors) at TH Aschaffenburg, Germany, which is located between the three campuses of the University of Applied Sciences Aschaffenburg (Goldhammer et al. 2012). The dataset describes the transition between waiting and starting movements of cyclists (see Figure 2). To reduce the waiting time, it is proposed to manage the intersection by dynamically changing the traffic light to green based on demand dependent on traffic flow density. Additionally, the traffic light can be removed at the intersection to prioritize the performance of the TH-AB shuttle bus. For this purpose, we want to explore the potential of using Reinforcement Learning in the context of traffic flow optimization with traffic lights or instead of traffic lights (in the simulation) based on the exchanged information between communicating vehicles & infrastructure (C2X). It is important to note that any changes made to the intersection's management should be carefully planned and executed to ensure the safety of all road users. We will design and conduct further studies and analysis before implementing any changes to the intersection's management. Additionally, it may be beneficial to consider the potential impacts of these changes on the surrounding area and its residents.

Figure 67. Transition between waiting time and start movement

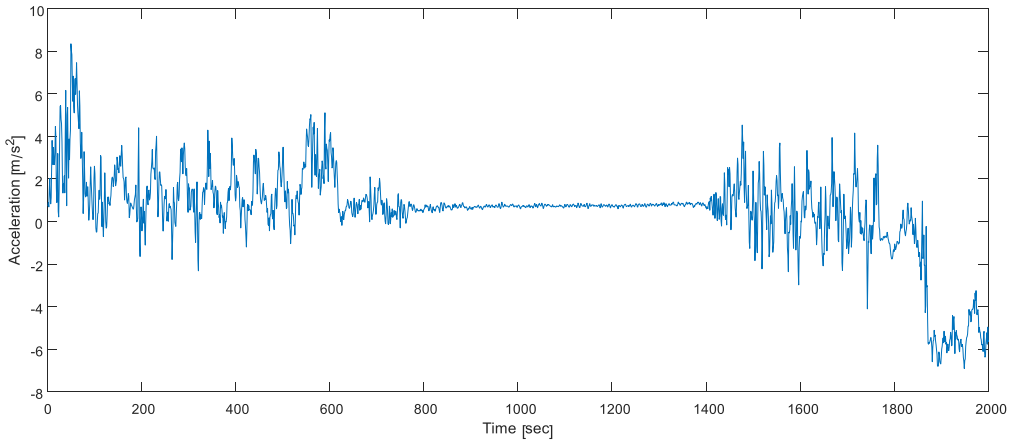

Acknowledgments

This study has been supported by the Project 101076165 — i4Driving within Horizon Europe under the call HORIZON-CL5-2022-D6-18 01-03, which is programmed by the European Partnership on 'Connected, Cooperative and Automated Mobility' (CCAM).

References

Inlodean, C., Cordos, N. and Varga, O. Autonomous Shuttle Bus for Public Transportation: A Review, *energies*, 13, 2917. doi:10.3390/en13112917.

Raiyn, J. Detection of Road Traffic Anomalies Based on Computational Data Science, *Discover Internet of things,* 2,6, 2022. https://doi.org/10.1007/s43926-022-00025-y.

Salonen, O.A. and Haavisto, N. Towards Autonomous Transportation. Passengers' Experiences, Perceptions and Feelings in a Driverless Shuttle Bus in Finland, *sustainability,* 2019, 11, 588; doi:10.3390/su11030588.

Bucchiarone, A., Battisti, S, Marconi, A. and Ponce, C. D. Autonomous Shuttle-as-a-Service (ASaaS):Challenges, Opportunities, and Social Implications, IEEE Transactions on Intelligent Transportation Systems. PP(99). DOI: 10.1109/TITS.2020.3025670.

Weidl, G., Madsen, A. L., Wang, S. R., Kasper, D., Karlsen, M. „Early and Accurate Recognition of Highway.

Traffic Maneuvers Considering Real-World Application: A Novel Framework Using Bayesian Networks", *June 2018 IEEE Intelligent Transportation Systems Magazine* 10(3):146 – 158, DOI: 10.1109/MITS.2018.2842049.

Ainsalu, J., Arffman, V., Bellone, M., Ellner, M., Haapamäki, T., Haavisto, N., Josefson, E., Ismailogullari, A., Lee, B., Madland, O., Madžulis, R., Müür, J., Mäkinen, S., Nousiainen, V., Pilli-Sihvola, E., Rutanen, E., Sahala, S., Schønfeldt, B., Smolnicki, P.M. Soe, R.-M. Sääski, J. Szymańska, M. Vaskinn, I. Åman, M. State of the Art of Automated Buses. Sustainability 2018, 10, 3118. https://doi.org/10.3390/su10093118.

Goldhammer, M., Strigel, E., Meissner, D., Brunsmann, U., Doll, K., Dietmayer, K. Cooperative Multi Sensor

Network for Traffic Safety Applications at Intersections, 15th International IEEE Conference on Intelligent Transportation Systems Anchorage, Alaska, USA, September 16-19, 2012.

Hetzel, M., Reichert, H., Doll K., Sick, B. Smart Infrastructure: A Research Junction, 9/2021, 2021 IEEE International Smart Cities Conference (ISC2), DOI: 10.1109/ISC253183.2021.9562809.

Esterwood, C., Yang, X. J., & Robert, L. P. (2021). Barriers to AV Bus Acceptance: A National Survey and Research Agenda. International Journal of Human–Computer Interaction, 37(15), 1391-1403. https://doi.org/10.1080/10447318.2021.1886485.

Flötteröd, Y.-P., Bieker-Walz, L., & Olstam, J. (2021). Towards safe and efficient shared-space oriented DRT Service : someinsights with real case study in Linköping. Intelligent Transport Systems World Congress, ITS 2021. Presented at the ITS World Congress 2021, 11.-15. Okt. 2021, Hamburg, Germany. Retrieved from http://urn.kb.se/resolve?urn=urn:nbn:se:vti:diva-18523.

Tsigdinos, S., Tzouras, P. G., Bakogiannis, E., Kepaptsoglou, K., & Nikitas, A. (2022). The future urban road: A systematic literature review-enhanced Q-method study with experts. Transportation Research Part D: Transport and Environment, 102, 103158. https://doi.org/10.1016/j.trd.2021.103158.

A Queue Length Distribution Estimation Method for Signalized Intersections Using Multi-Section License Plate Recognition Data

Hao WU[a], J. YAO[b], K. Tang[a]

[a] *Key Laboratory of Road and Traffic Engineering of the Ministry of Education, College of Transportation Engineering, Tongji University, China*

[b] *School of Electrical and Electronic Engineering, Nanyang Technological University, College of Transportation Engineering, Tongji University, Singapore*

Introduction

Different from the actuated and adaptive signal control, the fixed-time signal control often partitions an entire day into several time-of-day (TOD) periods according to traffic flow fluctuations and signal timing plan of each TOD period remains unchanged. The TOD-based fixed-time control is considered as a cost-effective means and is thus widely used to adapt to traffic demand variations within the day in many countries. Identification of TOD breakpoints play an important role in the overall performance of fixed-time controlled intersections.

TOD breakpoints identification has motivated many research efforts. Conventionally, TOD breakpoints were identified solely using single performance index such as traffic volume, velocity *(1 - 2)*. Later, multiple indices were studied to achieve a better TOD scheme to make up for the one-sidedness of single performance index especially under oversaturated conditions *(3 - 4)*. There are mainly two categories of breakpoint identification methods, i.e., heuristic search approach *(5)* and clustering approach (*6 - 7*). The former requires a lot of validation works on various parameters such as window size for greedy search method, while the latter are not capable of incorporating the temporal information of operational indices.

In recent years, License Plate Recognition (LPR) systems have been used increasingly in many Chinese cities to ensure public security and enforce traffic law. LPR cameras are often installed at the stop-lines of signalized intersections to record individual vehicles' license plate numbers and stop-line crossing time on a basis of lane. Therefore, LPR data are ideal sources to provide refined performance measures for TOD breakpoints identification.

Hence, by taking advantage of rich information provided by the LPR data, this study proposes a Change Point Analysis (CPA) method for TOD breakpoints identification to overcome the drawbacks of the existing methods. First, we choose traffic volume and control delay as operational indicators to avoid the one-sidedness of single performance index; then, the TOD breakpoints identification problem is transformed into a change-point identification problem relating to time-series. A statistical method, the E-Divisive with Medians (EDM) method, is first adopted for change-point analysis to TOD breakpoints identification. The proposed method was validated with empirical data and the results indicate that the proposed method can properly identify the TOD breakpoints.

Methodology

The proposed approach mainly includes two steps, i.e., calculation of operational indicators and identification of TOD breakpoints based on EDM method. In the first step, two operational indicators including control delay and traffic volume are calculated based on LPR data. In the second step, the TOD breakpoints can be identified based on the time-series datasets of the calculated control delay and traffic volume in the first step.

Calculation of operational indicators

Suppose T is the objective time period of a day (e.g., 7:00~24:00) and t is the analysis period (e.g., 15 min), the whole objective time period can be divided into n parts, where $n = \lceil T/t \rceil$; then, traffic volume series $\{Q^1, Q^2, \dots, Q^n\}$ can be calculated by aggregating the vehicles of each analysis period; moreover, intersection control delay series $\{d_I^1, d_I^2, \dots, d_I^n\}$ can be obtained based on traffic volume and original signal timing parameters, using the model of Highway Capacity Manual (2010). Hence, two time series $\{Q^1, Q^2, \dots, Q^n\}$, $\{d_I^1, d_I^2, \dots, d_I^n\}$ can be obtained, which indicate intersection traffic flow and intersection control delay, respectively.

Identification of TOD breakpoints based on CPA method

Given the two time series $\{Q^1, Q^2, \dots, Q^n\}$, $\{d_I^1, d_I^2, \dots, d_I^n\}$, a E-divisive median (EDM) method is applied to each time series dataset. two subsets of traffic flow, $A_Q^\tau = \{Q^1, Q^2, \dots, Q^\tau\}$, $B_Q^{\tau-n} = \{Q^{\tau+1}, Q^{\tau+2}, \dots, Q^n\}$ and two

subsets of control delay, $A_d^\tau = \{d^1, d^2, \dots, d^\tau\}$, $B_d^{\tau-n} = \{d^{\tau+1}, d^{\tau+2}, \dots, d^n\}$ can be divided by the τ-th analysis period.

The inner difference between subsets given a candidate breakpoint is calculated and the inter-group difference for two datasets of flow and delay is also calculated to represent the statistical divergence on both sides of the breakpoints, which is denoted by the Distance Components (DISCO) statistic. Thus, for any analysis period, the change point can be identified as period, $\hat{\tau}$, with the maximal DISCO statistics, as shown in Eq. (1),

$$(\hat{\tau}|s) = argmax\ \frac{pq}{p+q}\left[2D_{A_\tau B_{\tau-N}} - D_{A_\tau} - D_{B_{\tau-N}}\right], \quad (1)$$

To accurately identify the change points, a permutation test is then adopted to test the change point obtained. Both traffic volume series and control delay series are verified by permutation test, and the change point is valid only when both traffic volume series and control delay series meet the required significance level of the permutation test. Here, the significance level is set as 5%, and the times of permutations is set as 10000.

In the case that the change point meets the significance level demand, each of the two sub-sequence divided by the first change point, can be used to identify change points iteratively. Change points can be obtained based on the same method mentioned above, and this iteration stops when the specific change point can't meet the significance level demand of the permutation test. Then, a final change point collection can be obtained, which indicate the TOD breakpoints of the time period of a day.

Evaluation of the proposed method

The proposed method was validated using an empirical case. In this study, the intersection of Middle Tongjiang Road and Hanjiang Road of Changzhou City, China, is selected as the test site, and LPR detectors are installed at each lane. Empirical data from 7:00 to 21:00 on a weekday (January 9, 2019) and a weekend (January 12, 2019) were used in the empirical evaluation; The analysis period is set as 0.15 hour, and the original TOD scheme is illustrated in FIGURE 1 as a comparison.

Figure 68. Original TOD schemes of the empirical case

	Weekday (January 9, 2019)	Weekend (January 12, 2019)
7:00~9:00	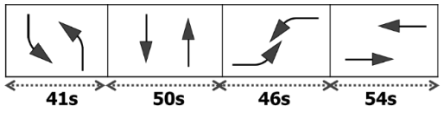	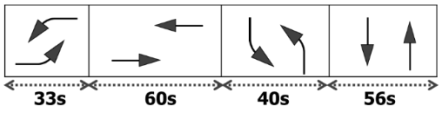
9:00~16:30		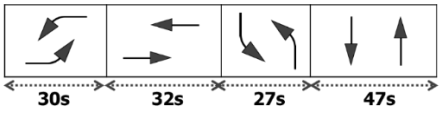
16:30~19:00	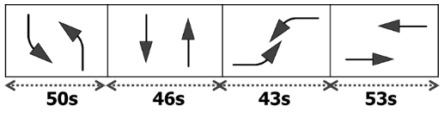	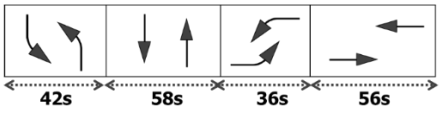
19:00~21:00	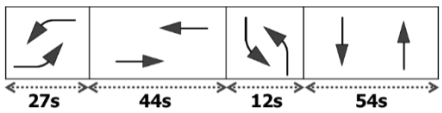	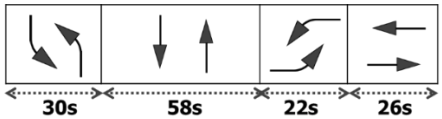

Here, we choose variation coefficient as the performance indicators to describe the similarities between TOD periods, and calculated as,

$$c_{d,mean} = \frac{\sum_{i=1}^{n} c_{d,i}}{n}, \qquad c_{Q,mean} = \frac{\sum_{i=1}^{n} c_{Q,i}}{n} \tag{2}$$

where, $c_{d,mean}, c_{Q,mean}$ indicates the average variation coefficient of control delay, traffic flow, respectively; and $c_{d,i}, c_{Q,i}$ is the variation coefficient of control delay and traffic flow of TOD period $i, (1 \le i \le n)$, respectively.

Figure 69. Verification results

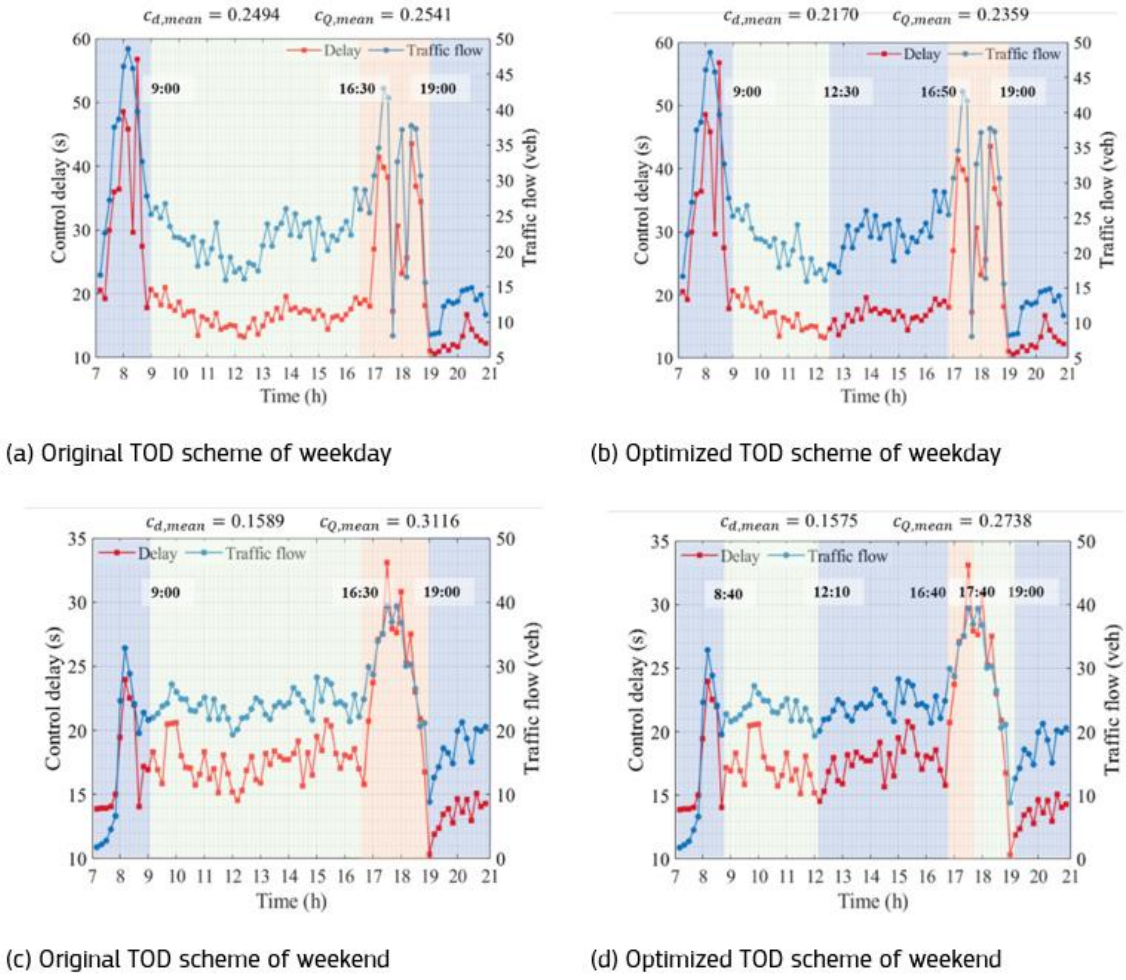

As shown in FIGURE 2, the proposed method can achieve a TOD scheme which close to the original one. Hence, TOD scheme can be estimated when original TOD scheme is not available. Besides, the proposed method achieves better results in weekday, as the $c_{d,mean}$ value is decreased from 0.2494 to 0.2170 and the value of $c_{Q,mean}$ decreased from 0.2541 to 0.2359, which indicates that the operation evaluation indexes are more homogenous. Moreover, there is no significant difference for weekend considering control delay as the gap is around 0.001, while the value of $c_{Q,mean}$ declined 0.0378. The case of weekend also proves the necessity of multiple indices as single index cannot evaluate the differences in many cases.

CONCLUSION

This paper proposes a change point analysis method for TOD breakpoints identification solely using LPR data. The performance of the proposed method is tested using an empirical case and the results indicate it can properly identify the TOD breakpoints, which can be further applied in signal control optimization.

For future research, firstly, various validation through simulation test, e.g., oversaturated condition, are required to evaluate the performance of the proposed method, using traffic performance indicators such as control delay, queue length. Furthermore, it is also necessary to compare the method with classic heuristic search approach and clustering approach, to evaluate the accuracy and calculation speed.

REFERENCES

[1] Yao, J., Xu, J., and Han, Y. TOD optimal control method of urban traffic based on clustering analysis. *Journal of Traffic and Transportation Engineering*, 2014, (06), pp.110-116.

[2] Zheng, J., Henry L., and Steve M. Fine-Tuning Time-of-Day Transitions for Arterial Traffic Signals. Transportation Research Record: Journal of the Transportation Research Board, 2015, 2488 (1), pp.32-40.

[3] Lee J., Kim J., and Park B. A genetic algorithm based procedure for determining optimal time of day break points for coordinated actuated traffic signal systems. KSCE Journal of Civil Engineering, 2011, 15(1), pp.197-203.

[4] Chen, P., Zheng, N., and Sun, W., et al. Fine-tuning time-of-day partitions for signal timing plan development: revisiting clustering approaches. *Transportmetrica A: Transport Science*, 2019, 15 (2), pp.1195-1213.

[5] Park, B., Lee, J. A procedure for determining time of day break points for coordinated actuated traffic signal systems. *KSCE Journal of Civil Engineering*, 2008, 12(1), pp.37-44.

[6] Ratrout, N. T. Developing optimal timing plans for cyclic traffic along arterials using pre-timed controllers. *Intersections Control and Safety*, 2013, 66 (29).

[7] Ma, D., Li, W., and Song, X., et al. Time-of-day breakpoints optimization through recursive time series partitioning. *IET Intelligent Transport Systems*, 2018, 13(4), pp.683-692.

Privacy-Preserving Adaptive Traffic Signal Control Based on Partially Connected Vehicles

C. Tan[a], K. Yang[a]

[a] *Department of Civil and Environmental Engineering, National University of Singapore*

Introduction

Connected Vehicles (CVs) have enjoyed increasing popularity in transportation thanks to their benefits in improving traffic operations, particularly traffic signal control [1-3]. However, detailed vehicle trajectory data can contain sensitive information about personal driving behaviors and human mobility patterns [4, 5]. For example, driving behavior data may be used for discriminatory pricing in insurance. Moreover, human mobility patterns are highly unique and can be used to accurately infer travelers' identities, personal profiles, and social relationships [6, 7].

Privacy research in transportation aims to protect location privacy. Most existing works concentrate on privacy-preserving trajectory data publishing, which assumes a central trusted party that owns the trajectory data of users. To the best of our knowledge, very few works have investigated privacy-preserving traffic operations using data from individual CVs distributed across the transportation network. For example, Qin et al. [8], Sun et al. [9], Tsao et al. [10] developed privacy-preserving transportation operation algorithms with a minimum reduction of system performance. However, these studies mainly focus on protecting vehicle path information at the network level. In contrast, detailed vehicle trajectories at intersections are rarely considered when being used for traffic signal control. Indeed, with the aid of traffic flow theory, vehicle path information can be easily reconstructed from trajectory data at local intersections, even though the data is unlinked and anonymized. To the best of our knowledge, only a few studies have considered the privacy issue of CVs for traffic control at the intersection level, e.g., PrivacySignal for intelligent transportation system proposed by Ying et al. [11] and privacy-preserving digital twin-based traffic control proposed by Lai et al. [12]. Although these methods can be effective in protecting privacy, they fail to consider specific requirements of transportation modeling and thus may sacrifice control performance when applied to traffic operations.

To fill these gaps, we propose a privacy-preserving traffic signal control method using data provided by connected vehicles with various penetration rates. The contribution of this study is three-fold. First, we propose a privacy-preserving data-aggregation mechanism that aggregates CV data to calculate key traffic quantities in a privacy-preserving manner with triple protection. Second, we develop a simple but effective linear optimization model for CV-based real-time traffic signal control, which utilizes only the aggregated information as the outcome of the data-aggregation mechanism. Third, we implement a two-stage stochastic optimization model to handle the noises brought by differential privacy, which has been shown to improve the trade-off between privacy and control performance.

Methodology

Scenario, Parties, and Adversary Model

We consider an isolated signalized intersection with four links. As shown in Fig. 1(a), there are four parties of the CV-based real-time traffic control system: 1) *Connected vehicles (CVs)* that can transmit their data at a specific frequency or upon request. 2) *CV data center (CV-DC)* that can aggregate and store data shared by CVs. 3) *Traffic signal control center (TSCC)* that optimizes signal timings with data sent by CV-DC. 4) *Traffic signal light (TSL)* that executes the signal timings sent from TSCC.

We consider an adversary model with three types of attack: 1) *Collusion*. A group of CVs may collude to infer the sensitive information of the other CVs during vehicle-to-vehicle communication. 2) *Data leakage*. The CV-DC is untrusted and may be subject to an attack leading to data leakage. 3) *Result inference*. The TSCC may also be attacked, and the aggregated data transmitted to the TSCC may be intercepted to infer sensitive information about individual CVs.

Figure 70. Framework of Privacy-Preserving CV Data-Aggregation Mechanism for Traffic Control System

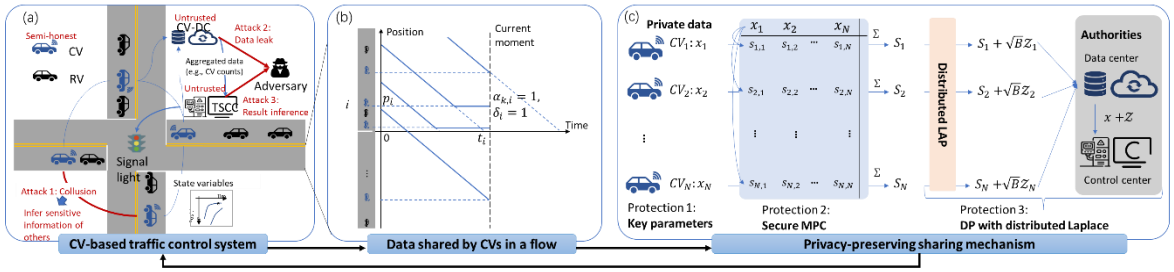

CV information preprocessing

The state of CV *i* at the studied intersection can be described by $\left\{\{\alpha_{k,i}\}_{k\in K}, \delta_i, p_i, t_i\right\}$ (Fig. 1b), where $\alpha_{k,i} = 1$ indicates the CV is in stream k and 0 otherwise. Variable $\delta_i = 1$ indicates the vehicle is stopped and 0 otherwise. Variable p_i is the current position (veh) measured from the stopline, which can take a negative value if a CV passes through the stopline. Variable t_i is the (expected) arrival time to stopline (s). Given the above state variables, each CV will leverage the privacy-preserving aggregation mechanism to share the following private data on request for calculation: $\{\eta_{k,i}, P_{k,i}, T_{k,i}\}_{k\in K}$, where $\eta_{k,i,j} = \alpha_{k,i}\delta_i$, $P_{k,i} = \alpha_{k,i}\delta_i p_i$, and $T_{k,i} = \alpha_{k,i}\delta_i t_i$. Note that we allow all CVs to participate in the aggregation in each stream, which enhances privacy without affecting the calculation results.

Privacy-Preserving CV data aggregation mechanism

In this mechanism (Fig. 1c), we aggregate individual CV data to obtain key traffic variables. We implement *triple* protections to ensure privacy. **Protection 1** is via sharing only key parameters. We only require CVs to share key parameters of their trajectories upon request rather than real-time locations and speeds (i.e., complete trajectories). Therefore, the travel path and OD at the macro level, as well as the detailed spatiotemporal trajectories at the micro level, cannot be reconstructed as long as key parameters are protected. **Protection 2** is secure multi-party computation (SMPC) [10]. The SMPC enables data owners to jointly compute a public function in the absence of a trusted third party, while keeping data private with data owners. We implement SMPC via additive data sharing, whereby CV i randomly divides its data y_i into N shares $y_i = \sum_j s_{ij}$ and transmits s_{ij} to CV j. CV j collects all messages from other CVs and send $S_j = \sum_{i'} s_{i'j}$ to the CV-DC. Such a mechanism ensures that both other CVs and the CV-DC will not be able to reconstruct the data of CV i even if they collude. **Protection 3** is via differential privacy (DP). Existing studies have demonstrated that an adversary may obtain private information by analyzing the changes in the query results [13]. To address this issue, we adopt differential privacy (see Definition 1) to provide a strong and provable privacy guarantee such that modifying one data element would result in statistically indistinguishable changes in the query results.

Definition 1 (ϵ-Differential privacy [13]). A randomized mechanism $\mathcal{A}: \mathcal{D} \to \mathcal{X}$ satisfies ϵ-differential privacy, if for any neighboring databases D and D' that differ on one record (e.g., adding or removing one record), and any possible output set $S \in \mathcal{X}$, $Pr[\mathcal{A}(D) \in S] \leq e^{\epsilon} Pr[\mathcal{A}(D') \in S]$ holds.

We adopt a commonly used Laplace perturbation (LAP) mechanism to achieve ϵ-Differential privacy, whereby all CVs jointly add noises following Laplace distribution to the aggregated traffic variables. Specifically, we obtain $\mathcal{G}_k = \sum_i e^T \eta_{k,i} + Z_{G,k}$, $P_k = \sum_i e^T P_{k,i} + Z_{P,k}$, and $T_k = \sum_i e^T T_{k,i} + Z_{T,k}$, where $e = [1,1,\cdots,1]^T$ with the appropriate dimension, and $Z_{G,k}$, $Z_{P,k}$, $Z_{T,k}$ are Laplace noises.

Traffic Signal Control Optimization

We consider a four-phase signalized intersection as an example. We adopt a rolling-horizon optimization scheme for real-time signal control (Fig. 2a). We solve an optimization model at the end of each phase group (i.e., every half cycle) to optimize the signal timings over the entire cycle.

Objective: We aim to minimize the total delay of all CVs. We use g_k^s and g_k^e (decision variables) to denote the green start time and green end time of stream *k*, respectively. Then, the expected delay of a queued CV_i ($i \in I_k$) is $d_i = \tau_i - t_i$, where τ_i is the expected stopline through time. By Fig. 2(b), we can get $\tau_i = g_k^s + l_k^s + p_i h_k$, where l_k^s is the start-up lost time of stream *k*; h_k the average queue discharging headway of stream *k* at stopline. Thus, the total delay of queued CVs of stream *k* reads as

$$\sum_{i\in I_k} d_i = (g_k^s + l_k^s)\sum_{i\in I_k} 1 + h_k \sum_{i\in I_k} p_i - \sum_{i\in I_k} t_i = (g_k^s + l_k^s)\eta_k + h_k P_k - T_k$$

where η_k, P_k, T_k are the aggregated variables (stochastic due to DP) as the outputs of the privacy-preserving data aggregation mechanism. Hence, our objective function can be written as

$$\min \sum_{k\in K}\sum_{i\in I_k} d_i = \sum_{k\in K} (\eta_k (g_k^s + l_k^s) + h_k P_k - T_k)$$

Figure 71. Rolling optimization scheme and calculation of the objective

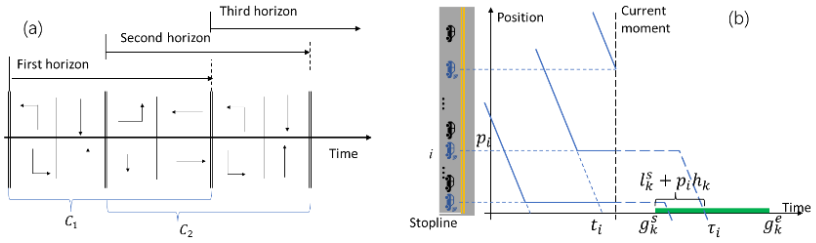

Constraints: In addition to the phase sequence constraints required by NEMA, here we add the following constraint to ensure no residual queues, $g_k^e - g_k^s + y_k - l_k^s - l_k^y \geq \lambda_k (g_k^s - r_k^s) h_k, k \in \mathrm{K}$, in which λ_k can be estimated by a maximum likelihood estimator [14], $\lambda_{MLE} = \sum_{i\in I_k} p_i / \sum_{i\in I_k} t_i = P_k / T_k$. The λ_k is calculated at the last green start time of stream *k*. Thus, we have

$$\left(g_k^e - g_k^s + y_k - l_k^s - l_k^y\right)/h_k \geq (g_k^s - r_k^s)\, P_k / T_k \,, k \in \mathrm{K}$$

Solution: The optimization model is a linear programming problem with uncertain parameters, which can be formulated into a scenario-based stochastic programming problem and solved efficiently.

$$\min \textstyle\sum_{k\in K} (\mathcal{G}_k g_k^s + C_{max} r_k) + \frac{\xi C_{max}}{M} \sum_{k=K} \sum_{m=1}^{M} q_{k,m},$$

$$subject\ to \quad 1)\ \text{phase sequence constraints}\ 2)\ r_k \geq \frac{\mathcal{P}_k}{\mathcal{T}_k}(g_k^s - r_k^s) - \frac{(g_k^e - g_k^s + y_k - l_k^s - l_k^y)}{h_k},\ k \in \mathrm{K}$$

$$3)\ q_{k,m} \geq \frac{P_{k,m}}{T_{k,m}}(g_k^s - r_k^s) - \frac{(g_k^e - g_k^s + y_k - l_k^s - l_k^y)}{h_k}, \qquad 4)\ q_{k,m} \geq 0, k \in \mathrm{K} \text{ and } m = 1,2,\ldots M$$

Findings

The proposed method is evaluated via a SUMO simulation with a four-leg intersection. Each link has one left-turning lane, two through lanes, and one uncontrolled right-turning lane. The demand ranges from 3360 to 6360 veh/hour for the entire intersection. Four different control methods are tested: *actuated control* (embedded in SUMO), *Linear programming with SMPC* (proposed SMPC-LP), *Linear programming with SMPC and DP* (proposed SMPC&DP-LP), and *stochastic linear programming with SPC and DP* (proposed SMPC&DP-SLP). Fig. 3 shows the performance of the four methods.

We obtain the following findings from Fig. 3: 1) The proposed methods all outperform actuated control with penetration rates above 40%, which demonstrates the superiority of the optimization model. 2) The SMPC&DP-LP and SMPC&DP-SLP perform worse than SMPC-LP due to the random noise of model parameters introduced by DP. 3) SMPC&DP-SLP considers the uncertainty of parameters via stochastic programming and achieves fewer stops and residual vehicles compared to SMPC&DP-LP. Overall, these methods provide an efficient trade-off between privacy and control performance.

Significance

This work is among the few pioneering works that address real-time traffic signal control based on CVs while achieving privacy guarantees, which provides a paradigm of the privacy-preserving utilization of CV data in the transportation field. The proposed privacy-preserving CV data aggregation mechanism is not limited to signal control but is also expected to advance the research on traffic state estimation and traffic/transportation network modeling.

Figure 72. Performance of four methods: vehicle delay, stops, and residual vehicles

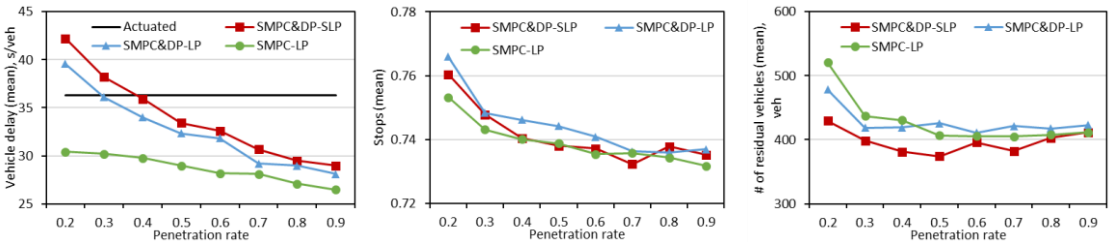

Acknowledgment

We would like to acknowledge the support from the Singapore Ministry of Education under its Academic Research Fund Tier I.

Reference

[1] Q. Guo, L. Li, and X. J. Ban, "Urban traffic signal control with connected and automated vehicles: A survey," *Transportation research part C: emerging technologies,* vol. 101, pp. 313-334, 2019.

[2] K. Yang, S. I. Guler, and M. Menendez, "Isolated intersection control for various levels of vehicle technology: Conventional, connected, and automated vehicles," *Transportation Research Part C: Emerging Technologies,* vol. 72, pp. 109-129, 2016.

[3] C. Tan, Y. Cao, X. Ban, and K. Tang, "Cumulative Flow Diagram-Based Fixed-Time Signal Timing Optimization at Isolated Intersections Using Connected Vehicle Trajectory Data," *arXiv preprint arXiv:2210.10508,* 2022.

[4] H. Eren, S. Makinist, E. Akin, and A. Yilmaz, "Estimating driving behavior by a smartphone," in *2012 IEEE Intelligent Vehicles Symposium*, 2012, pp. 234-239: IEEE.

[5] Y. Huang, Z. Xiao, D. Wang, H. Jiang, and D. Wu, "Exploring individual travel patterns across private car trajectory data," *IEEE Transactions on Intelligent Transportation Systems,* vol. 21, no. 12, pp. 5036-5050, 2019.

[6] C. Wan, Y. Zhu, J. Yu, and Y. Shen, "SMOPAT: Mining semantic mobility patterns from trajectories of private vehicles," *Information Sciences,* vol. 429, pp. 12-25, 2018.

[7] J. Li, F. Zeng, Z. Xiao, Z. Zheng, H. Jiang, and Z. Li, "Social relationship inference over private vehicle mobility data," *IEEE Transactions on Vehicular Technology,* vol. 70, no. 6, pp. 5221-5233, 2021.

[8] G. Qin, S. Deng, Q. Luo, J. Sun, and H. Kerivin, "Toward Privacy-Aware Multimodal Transportation: Convergence to Network Equilibrium under Differential Privacy," *Available at SSRN 4244002,* 2022.

[9] Z. Sun, B. Zan, X. J. Ban, and M. Gruteser, "Privacy protection method for fine-grained urban traffic modeling using mobile sensors," *Transportation Research Part B: Methodological,* vol. 56, pp. 50-69, 2013.

[10] M. Tsao, K. Yang, K. Gopalakrishnan, and M. Pavone, "Private location sharing for decentralized routing services," in *2022 IEEE 25th International Conference on Intelligent Transportation Systems (ITSC)*, 2022, pp. 2479-2486: IEEE.

[11] Z. Ying, S. Cao, X. Liu, Z. Ma, J. Ma, and R. H. Deng, "PrivacySignal: Privacy-Preserving Traffic Signal Control for Intelligent Transportation System," *IEEE Transactions on Intelligent Transportation Systems,* 2022.

[12] C. Lai, M. Wang, and D. Zheng, "SPDT: Secure and Privacy-Preserving Scheme for Digital Twin-based Traffic Control," in *2022 IEEE/CIC International Conference on Communications in China (ICCC)*, 2022, pp. 144-149: IEEE.

[13] C. Dwork, "Differential privacy: A survey of results," in Theory and Applications of Models of Computation: 5th International Conference, TAMC 2008, Xi'an, China, April 25-29, 2008. Proceedings 5, 2008, pp. 1-19: Springer.

[14] S. Goryczka and L. Xiong, "A comprehensive comparison of multiparty secure additions with differential privacy," *IEEE transactions on dependable and secure computing,* vol. 14, no. 5, pp. 463-477, 2015.

[15] C. Tan, J. Yao, X. Ban, and K. Tang, "Joint estimation of multi-phase traffic demands at signalized intersections based on connected vehicle trajectories," *arXiv preprint arXiv:2210.10516,* 2022.

Unmanned aerial vehicle (UAV) service network design for urban monitoring

B. Zhou[a], W. Liu[b], H. Yang[a]

[a] Department of Civil and Environmental Engineering, The Hong Kong University of Science and Technology, Hong Kong, China

[b] Department of Aeronautical and Aviation Engineering, The Hong Kong Polytechnic University, Hong Kong, China

This study examines the multi-depot location-routing problems of UAVs for urban monitoring (MDLRP-UM). MDLRP-UM appears in several service networks in urban environments, such as daily security patrols or monitoring the operation of infrastructures. The problem can be modelled as a mixed integer quadratically constrained problem (MIQCP), where we jointly optimize the service routes of the UAVs, the service intensity or frequency on each route, and the location of the depots to minimize the total cost. We propose an adaptive large neighborhood search (ALNS) heuristic to solve real-world large-scale problems, of which the efficiency and effectiveness are demonstrated by extensive numerical experiment.

Surrogate Model-based Framework for Urban Traffic Signal Optimization Considering Model Uncertainty

Zhixian Tang[a], Edward Chung[a]

[a] *Department of Electrical Engineering, The Hong Kong Polytechnic University, Hung Hom, Kowloon, Hong Kong, China*

Traffic signal optimization is important for urban traffic efficiency. Surrogate model (SM)-based optimization has become a popular approach for signal optimization. Existing studies mainly adopt a greedy strategy to exploit the optimal areas. However, misidentifying optimal areas caused by model uncertainty can mislead the searching algorithm to suboptimal areas. In this study, an SM-based framework is proposed considering model uncertainty. An active learning strategy is applied to adaptively select the infill samples at both optimal and uncertain areas of the SM. Four uncertainty measurement methods are proposed, whose uncertainty error is validated. Case studies on an arterial proved the efficiency of the proposed framework considering model uncertainty.

Including fairness considerations in traffic assignment models using linear programming

V. Morandi[a]

[a] *University of Brescia*

Road congestion is one of the major problems in the modern era as it causes queuing, pollution, higher logistic costs and increases road maintenance costs. At the same time, recent advances in sat-nav technologies are changing the way people drive. Alongside giving precious information about the network status in real-time, they could enhance the implementation of coordination mechanisms, called coordinated traffic assignment, aiming at suggesting paths to drivers to eliminate, or least reduce, congestion and, consequently, to reduce the total travel time in vehicular traffic networks. According to Morandi(2023), among possible congestion avoidance methods, coordinated traffic assignment is a valuable choice since it does not involve huge investments to expand the road network. Traffic assignments have been traditionally divided into to two main, based on the well-known Wardropian principles, perspectives: the user equilibrium and the system optimum. User equilibrium is a natural traffic assignment in which each user chooses the most convenient path in a selfish way. It guarantees fairness among users as, at equilibrium, all users with the same origin and destination will experience the same travel time. The main drawback that the whole network total travel time is not minimized paying the so-called Price of Anarchy is paid. Conversely, the system optimum is an efficient system-wide traffic assignment where drivers are routed on the network minimizing the total travel time. Unfortunately, here users might experience travel times that are much higher than the others, affecting the compliance. Drawbacks in implementing one of the two assignments can be kept under control by hybridizing the two approaches, i.e. aiming at bridging users' fairness to system-wide efficiency. In the last years, a significant number of attempts have been done to bridge fairness among users and system efficiency in traffic assignments. In the talk, we will go through the latest advances in terms of static coordinated traffic assignment models, as described in Morandi(2023), and in particular through linear programming models bridging user equilibrium and system optimum traffic assignment.

Category 4. Transport electrification

An agent-based electric vehicle charging demand modelling framework to assess the needs for the energy transition in transport

S. Girgin[a], M. B. Ulak[b], O. A. L. Eikenbroek[b]

[a] *Centre of Expertise in Big Geodata Science, Faculty of Geo-Information Science and Earth Observation, University of Twente, The Netherlands*

[b] *Transport Engineering and Management Group, Department of Civil Engineering, Faculty of Engineering Technology, University of Twente, The Netherlands*

Introduction

The transport systems are being electrified: from infrastructure management to intelligent transportation systems to electric vehicles, including heavy trucks, personal cars, and bikes. Electric vehicles (EVs) do not still have a very high market share; however, there is up to a 40% year-on-year increase in the registered EVs (International Energy Agency, 2020), and many countries are in the process of designing policies to phase out vehicles that use fossil fuels (Netherlands Enterprise Agency, 2022). The feasibility of the widespread use of EVs highly depends on the capacity of the charging infrastructure and the ubiquity of charging stations. However, to a large extent, the current charging infrastructure is not adequate to satisfy future demand, indicating the need for technical improvements and financial investments (Muratori, 2018; Gilleran et al., 2021). For cost-effective and efficient investments, the setup of charging infrastructure (e.g., location and capacity of charging stations) should be based on the expected demand considering local conditions such as population, income level, socio-demographics, and travel behaviour. For a realistic assessment, temporal (e.g., preferred time of charging, day or night charging) and spatial (e.g., preferred charging location, residence or workplace) aspects should also be taken into consideration. On the other hand, the adoption of EVs and the availability of the infrastructure may influence the travel behaviour of individuals. Current technology does not allow for successive long-range trips with limited charging time. Consequently, individuals may need to reconsider their daily activities and travel choices, e.g., by changing routes considering the availability of charging stations in congested electricity grids.

Current models and frameworks for transportation fall short to address such complex situations and dependencies on other systems, such as the electric power infrastructure. Considering the steps taken by the European Union towards phasing out fossil fuel use and promoting a shift to electric transport (EEA, 2016), the need for models and frameworks capable of estimating spatiotemporal charging demand taking socio-economic conditions and travel behaviour into consideration becomes even more imperative. It is especially important to make easy-to-use and openly accessible tools available, which can be used by public and private stakeholders to assess different scenarios for data-driven decision-making processes. To address these needs, the objectives of this study are: 1) developing an analysis framework that can determine spatiotemporal EV charging demand considering the travel and charging behaviours of individuals; and 2) making the developed framework accessible to public and private stakeholders as open-source software. The developed framework and software are novel in terms of enabling the estimation of EV charging demand by utilizing an agent-based modelling approach, which provides a detailed spatiotemporal distribution of the demand and allows various scenarios to be analysed at scale.

Methodology

The framework, which is designed to allow a detailed analysis even with limited data, is based on agents mimicking the behaviour of individuals commuting between home and work daily. Each agent has a home location, a workplace location, a commuting behaviour (i.e., time to work and time to home), an EV with certain characteristics (e.g., charge capacity, maximum range, etc.), a location indicating its current spatial position and a state that is dynamically updated during an analysis based on various state transition rules.

There are three states defined by the framework that roughly correspond to different states of an EV:

- *Idle state* indicates that the agent is located at a specific location (e.g., home, workplace) and the car is parked and not recharging; hence, subject to idle discharge.
- *Driving state* indicates that the agent is travelling between two specific locations (e.g., from home to work) and the car is consuming the charge of its battery in driving mode.
- *Recharging state* indicates that the agent is located at a specific location and the car is parked similar to the idle state, but it is connected to a charging station; hence, its battery is recharged.

The framework follows the state transition mechanism illustrated in Figure 1 to model the actions of an agent. From midnight to the time to leave home for work (i.e., time to work), an agent can be either in idle or in recharge state at home. This state is either assigned as the initial state at the beginning of the analysis if the analysis start time is within this period, or otherwise relayed from the previous day. Then, a state transition occurs to a driving state from home to work for a duration that corresponds to the required travel time. Once the agent arrives at work, it enters either an idle or a recharge state and stays in this state until the time to leave work for home (i.e., time to home). To decide which state to select, the framework first checks if the agent *can recharge*, i.e., if there is a recharge station available to use. If it is possible to recharge, then the framework checks if the agent *wants to recharge*. If the outcome is positive, then a recharge state is started. Otherwise, the state is set as idle. The selected state changes into a driving state when the analysis time reaches the time to home, and the agent travels back to home, where it can enter again either an idle or a recharge state following the same probabilistic logic that is applied when it arrived at work. This state continues until the time to work the next day, which completes a full transition cycle.

Figure 73. Example state transition workflow for an agent

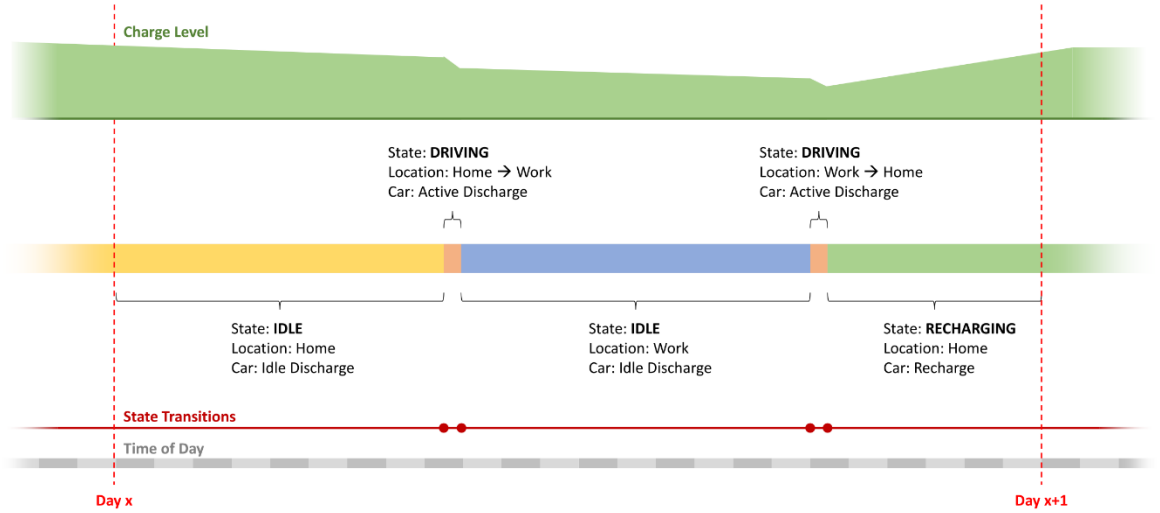

Source: Authors' elaborations (2023).

Implementation

An open-source research software is developed that implements the framework to enable the analysis of user-defined EV charging demand scenarios and to produce detailed as well as aggregated reports of the analysis results. The software, *EVDemand*, has an object-oriented architecture that facilitates modification of the existing methodology and further development of additional features easily. The self-documented source code, which is written in PHP, is available at https://github.com/ITC-CRIB/EVDemand.

To simplify the analysis, the software defines home and workplace locations by using regions (e.g., postcode zones). The number of agents commuting between the regions and the average commuting distance between the regions are required as input. To determine the time to work and time to home of each agent, a discrete intra-day commuting volume pattern is used for each commute direction. For each agent, first, discrete time periods (e.g., 08:00-10:00 and 16:00-18:00) are determined randomly for time to work and time to home considering the respective volume patterns, and then specific times within these periods are assigned randomly. This ensures a variation in the commuting behaviour of different agents, even if they commute the same route. For a more realistic analysis, the software also allows time to work and time to home of each agent to be modified slightly for each day by a small random delta time. At present, the travel duration is calculated by using the average commuting distance between the locations and a constant average speed.

A set of car models can be provided as input and for each car model, charge capacity (kWh), maximum travel range at full charge (km), recharge time from zero charge to full charge (h), and idle discharge rate (%/h) can be specified. A car of an agent is based on a car model, but the software allows these parameters to be customised for each car. For example, a car can have a charge capacity different from its base model, e.g., to simulate long-term fatigue. For the designation of car models, three different options are provided: 1) a single car model for all agents, 2) random distribution of car models to the agents, and 3) random distribution of car

models to the agents based on a predefined probability for each car model (e.g., 50% for Model A and 50% for Model B). The software keeps track of the battery charge level of each car. The initial charge capacity can be specified either as a constant value for all cars (e.g., 100%) or can be assigned randomly. A minimum charge percentage can be specified in case of random distribution to guarantee that the assigned values are greater.

The software implements the logic illustrated in Figure 1. The location and state of each agent are updated regularly during an analysis period (e.g., 120 hours), which is divided into smaller time steps (e.g., 5 mins). The software allows each state to have a definite duration (e.g., idle at work *for 8 hours*) at the end of which a state transition occurs, or an indefinite duration which requires a temporal trigger to initiate a state transition (e.g., idle at work *until time to home*). Indefinite duration states are checked for state transition *at the beginning* of each time step; hence, their temporal resolution is equal to the analysis time step. In contrast, the state transition is checked *during* a time step for each state with a definite duration, and a new state is assigned to the agent if the elapsed time of the state reaches its defined duration within the time step. The software iteratively performs this check enabling multiple consecutive state transitions during a single time step, which results in an improved temporal resolution. Each agent has a state history, and the software keeps track of previous states in addition to the current state, which can be utilised to define complex state transition rules.

An initial state is assigned to each agent based on the start time of the analysis. For this purpose, the software considers the time periods an agent is expected to be at home, at work, or commuting. For example, if the start time is later than the time to work of an agent, but earlier than the agent is expected to be at the workplace, then the initial state is set as driving from home to work. The elapsed duration of the state is also calculated, and the state variables are set accordingly. For example, if the start time is 5 mins after the time to work of an agent and if the total commute duration is 15 mins, then the elapsed duration of the initial driving state is set as 5 mins and the distance travelled is set as 1/3 of the travel distance. While assigning the initial state, the initial battery charge level is also controlled to ensure that it is sufficient to complete the assigned state.

Currently, it is assumed that sufficient charging points are available at home and workplace locations, as these locations are only known as regions (e.g., postcode zones) that prevent the assignment of specific capacities. To describe different recharge behaviours, recharge behaviour functions are utilized that define the willingness of an agent to recharge given the current charge level of the car. Each behaviour function is defined by a list of charge percentage vs recharge probability values that are interpolated for intermediate charge percentages. This allows non-linear rechange behaviours to be described easily. The software has the following options to assign recharge behaviours to agents: 1) a single behaviour for all agents, 2) random distribution of behaviours to the agents, and 3) random distribution of behaviours based on a predefined probability for each behaviour.

Conclusions and Discussion

The developed framework to simulate the commuting and recharge behaviours of EV owners allows estimation of the spatiotemporal distribution of EV recharge needs, hence the required charging capacity. Because the framework allows alteration of physical (e.g., charge capacity) as well as physiological (e.g., willingness to recharge) parameters, it can facilitate the planning and development of local or regional infrastructure to serve the needs in an effective and cost-efficient manner. Various scenarios, including socio-economic incentives to motivate people to follow certain recharging behaviour (e.g., the low cost during night time, high cost in case of extended recharge at the workplace), can be easily tested by using the developed open-source software.

The agent-based approach of the framework allows detailed analysis of the recharge needs of individuals but also enables the calculation of aggregated results for designated regions. The software implementing the framework can simulate a high number of agents and can scale up easily provided that sufficient computing resources are available. Therefore, it is suitable to perform simulations not only at a small scale (e.g., city level) but also at a large scale (e.g., country level). Depending on the precision required, the time step of the analysis can be altered to speed up the computation. The capability to simulate state transitions within each time step for states with definite durations helps to improve the accuracy in the case of large time steps.

Although it is currently not utilised for analysis, the framework also allows all parameters related to agents (e.g., commute times, car properties, recharge behaviour, etc.) to be altered dynamically during an analysis. This capability, together with the state history of the agents, can be exploited to generate more complex simulations, during which the agent states can be altered based on previous actions of the agent, as well as the actions of other agents (e.g., commuting the same route). Because the framework is time-aware (i.e., knows the day of the week and time of the day), it can also be extended to simulate not only commuting during workdays but also travelling during the weekends and other holiday periods. The modular and object-oriented architecture of the software allows easy modification of the analysis logic by introducing additional actions (e.g., shopping) and

locations (e.g., shopping malls). Hence, it can be enhanced through additional analysis components in the future, also through the involvement and collaboration of all interested parties thanks to the open-source approach.

Currently, we are working on two case studies to demonstrate the capabilities of the framework. The first case study is a regional study in the Overijssel province of the Netherlands located in the eastern part of the country with a population of 1.2 million people. The second case study, which is larger in extent, includes all provinces of the Netherlands that correspond to about 17.5 million people. For estimating the number of EV trips within these networks (i.e., the number of agents), we use a four-stage travel demand model (de Dios Ortuzar and Willumsen, 2011) based on MobiSurround (Tutert and Thomas, 2012). The four-stage transport model partitions the network into different postal code zones (neighbourhood level, so-called PC4 level), using land-use and socio-economic data to estimate the motive-dependent trip volume originating in each zone. Using a so-called deterrence function that aims to reflect an increased resistance to travel longer distances in general (de Dios Ortuzar and Willumsen, 2011), a gravity-based model determines the total commuter trips between all pairs of zones (origin-destination matrix) (Thomas and Tutert, 2013). We estimate, per origin-destination pair, the shares for cars, active modes (mostly cycling), and public transport (train); and utilise the shares for cars. These case studies will allow us to test the scalability of the framework and fine-tune the performance of the software implementation.

References

de Dios Ortuzar, J. and Willumsen, L. G., *Modelling Transport*, 4th edition, Wiley, Sussex, 2011.

European Environment Agency, *Electric vehicles in Europe*, EEA Report No 20/2016, Publications Office of the European Union, Luxembourg, 2016, doi:10.2800/1002.

Gilleran, M., Bonnema, E., Woods, J., Partha, M., Doebber, I., Hunter, C., Mitchell, M., and Mann, M., 'Impact of electric vehicle charging on the power demand of retail buildings', *Advances in Applied Energy*, Vol. 4, 2021, 100062, doi:10.1016/j.adapen.2021.100062.

International Energy Agency, *Global EV Outlook 2020: Entering the decade of electric drive?*, IEA Publications, France, 2020, https://www.iea.org/reports/global-ev-outlook-2020.

Muratori, M., 'Impact of uncoordinated plug-in electric vehicle charging on residential power demand', *Nature Energy*, Vol. 3, 2018, pp. 193-201, doi:10.1038/s41560-017-0074-z.

Netherlands Enterprise Agency, *Electric driving policy*, The Netherlands, 2022, https://www.rvo.nl/onderwerpen/elektrisch-rijden/beleid.

Thomas, T. and Tutert, S. I. A., 'An empirical model for trip distribution of commuters in the Netherlands: transferability in time and space reconsidered', *Journal of Transport Geography*, Vol. 26, 2013, pp. 158-165, doi:10.1016/j.jtrangeo.2012.09.005.

Tutert, B. and Thomas, T., 'Open source quickscan verkeersmodel Mobi Surround: simplificatie kan samengaan met kwaliteitsverhoging', Verkeer in beeld, Vol. 6, No 1, 2012, pp. 30-32.

A prospective analysis of vehicles electrification based on floating car data: application to the urban area of Lyon, France

B. Othman[a], G. De Nunzio[a]

[a] *IFP Energies nouvelles, Rond-point de l'échangeur de Solaize, BP 3, 69360 Solaize, France.*

Introduction

Local and regional authorities make a point of evaluating the impact and effectiveness of certain policy measures. A subject of public interest today is the modal shift towards more eco-friendly modes of transport, including vehicle electrification. It is essential to understand the extent to which today's mobility would be compatible with electric vehicles (EVs), and what adjustments need to be made to ensure a smooth transition to an increasingly low-carbon mobility.

The use of Floating car data (FCD) is gradually spreading in mobility research. It provides valuable information and is therefore often used in addition to magnetic loop detectors or cameras to measure the flow and average speed of road traffic. Today, work is beginning on the adjustment of these data to predict traffic flows using machine learning models. However, these data could be used to go further in the analysis and understanding of mobility patterns on a given territory. Such data-based approaches are particularly promising to try and understand people's behavior and traffic demand over a long period. They have the undeniable advantage of using real data, unlike studies based on traffic simulators data.

It is clear that FCD present a bias as the tracked agents do not necessarily depict the mobility habits of the entire population on the analyzed territory. Yet, these approaches open the door to the characterization of the behavior of a non-negligible part of the population in a very precise and reliable way. This offers promising prospects for the analysis of the mobility of a pool of agents, even without statistical adjustment of our sample population. In our case, we will focus on the compatibility of agents to the possible adoption of EVs.

The objective of this study is to predict the impact of a massive adoption of EVs on a given territory. To do so, we propose to use FCD as a proxy for mobility. A fleet of selected agents are tracked over a period of one month. The data recorded on their trips are then given as input to a microscopic mobility model to conclude on the compatibility of the agents with electromobility. An underlying question is what changes need to be made to the infrastructure, particularly in terms of number and distribution of charging stations to facilitate and encourage the transition to electromobility.

Methodology

The mobility data of more than 7000 agents is collected in March 2022 in the urban area of Lyon, France. These data are provided by Autoroutes Trafic[12]. They contain information on each stop such as its coordinates, its duration, the identifier of the agent who made the stop, the length and duration of the previous and next trips. To analyze the data in a consistent way, each agent is associated with a unique identifier. The study area is represented on the figure below. The red dots represent the public charging stations. Each agent resides in the study area, i.e., each agent spends the most time over the month in the study area.

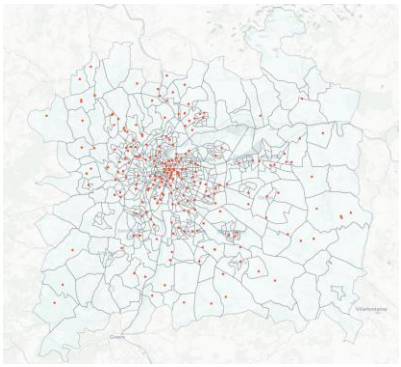

Source: Authors' elaborations.

[12] Autoroutes Trafic is a French company that develops connected vehicle travel data analysis solutions.

A first insight into the behavior of the agents corresponds to their monthly traveled distances. As represented on the figure below, all tracked agents travel between 50 km and 4000 km per month.

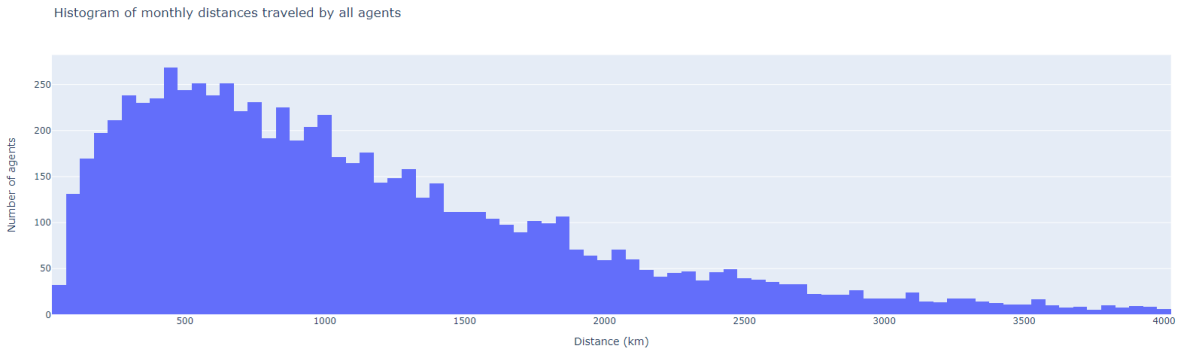

Source: Authors' elaborations.

In this study, the following types of charging are possible for EVs:

- Public charging stations (PCS): in one of the charging stations represented on the map above. The positions and electric powers of each charging point is available in the French national database[13].
- Home charging stations (HCS): hypotheses are made on the number of home charging stations and their distribution among agents. Each agent is assigned as home the area in which he/she spends the most time.
- Workplace charging stations (WCS): Similar hypotheses are made concerning the number and distribution of charging stations in workplaces. Each agent is assigned the second zone in which he/she spends the most time as his/her workplace.

Assumptions are also made about battery capacity, the threshold batteries states of charges (SOCs) at which agents seek to recharge their vehicles, and an average coefficient of electricity consumption per distance traveled.

The mobility of each agent is then simulated according to the trips recorded in the FCD database, and it is assumed that each agent has adopted electromobility and is using an EV. A trip is allowed and completed only if the battery SOC is sufficient. In cases where the agent stops more than 30 minutes and wishes to recharge, he/she can do so in the following cases:

- If the agent stops in an area where a public charging station is available.
- If the agent is in his home area and has a home charging station.
- If the agent is in his workplace area and has a workplace charging station.

All agents who are unable to complete a trip assigned to them by the FCD due to insufficient battery SOC are then labeled as incompatible with electromobility, for the chosen set of hypotheses. As a result, an overall incompatibility rate for the simulation is defined as follows:

$$\varepsilon = \frac{Number\ of\ agents\ incompatible\ with\ EVs}{Total\ number\ of\ agents}$$

Results

For a given set of parameters and hypotheses, different simulations are run for various numbers of HCS and WCS. As represented in the Figure below, the minimum incompatibility rate ε is naturally reached for maximum values of HCS and WCS.

[13] https://www.data.gouv.fr/fr/datasets/fichier-consolide-des-bornes-de-recharge-pour-vehicules-electriques/

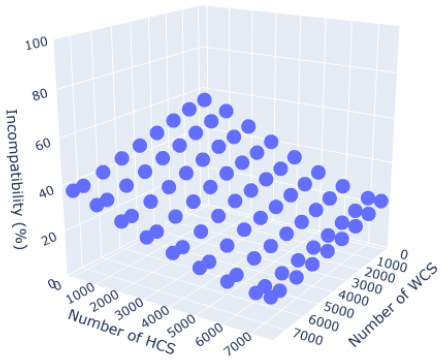

Source: Authors' elaborations.

If our entire agent fleet switches to EVs, this incompatibility rate does not go below 15% with our simulation parameters. The reason is that very long-distance drivers would need customized solutions: alternative engine type, higher battery capacity, additional PCS, etc.

As it is and with individual HCS and WCS (only PCS are shared), we notice that HCS seem to have a more percussive impact on the decrease of the incompatibility rate. This can be explained by the fact that agents park more often in their home area than in their workplace area. Today, with the current infrastructure, the incompatibility rate would probably be around 20% for the selected agents.

For the following, we assume the current network infrastructure. The analysis of the charging stations usage leads to the electrical power demand. It is detailed for each type of charging on the figure below. It appears that the highest power demand corresponds to home charging, although we assume 3 kW HCS and 7 kW WCS. The electric power of PCS is given by the French national database. As expected, there is a daily phase shift between the peak power demand on HCS and WCS. For all types of charging, the power demand on weekends is lower than on weekdays. This is even more striking for WCS.

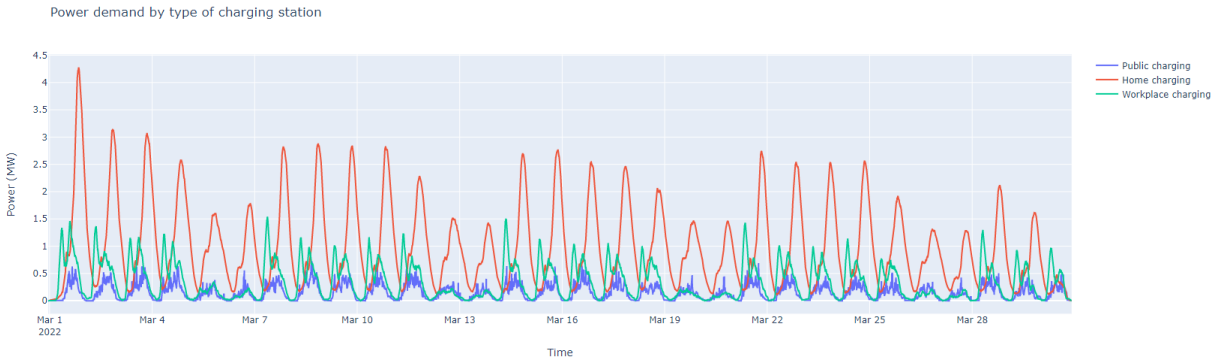

Source: Authors' elaborations.

Conclusions

This study proposes to use actual travel data from a fleet of agents to conclude on their compatibility with electric mobility. Different hypotheses are made regarding the network charging infrastructure, the recharging behavior of the agents and the capacity of their EVs. An overall metric, the incompatibility rate, is introduced to track the number of agents that would need additional efforts to be compatible with EVs. To understand the behavior of agents from the perspective of the charging infrastructure, the power demand of the different types of charging stations is monitored over time.

The following steps of this work are:

— A sensitivity analysis on the parameters to understand which ones have the most impact on the incompatibility rate.

— A transposition of these results in terms of incompatibility rate as a function of the EV penetration rate.

— An analysis of the results in the context of a mutualization of charging stations, especially at work.

References

Othman, B., et al., 'A Novel Approach to Traffic Flow Estimation based on Floating Car Data and Road Topography: Experimental Validation in Lyon, France', IEEE 25th International Conference on Intelligent Transportation Systems (ITSC), 2022, pp. 2571-2576.

Laraki, M., et al., 'A large-scale and data-based road traffic flow estimation method leveraging topography information and population statistics', IEEE 25th International Conference on Intelligent Transportation Systems (ITSC), 2022, pp. 2343-2349.

Nigro, M., et al., 'Exploiting floating car data to derive the shifting potential to electric micromobility', Transportation Research Part A: Policy and Practice, Vol. 157, 2022, pp. 78-93.

Acknowledgments

This research was funded by ADEME (French Environment and Energy Management Agency); MOUVEMENT project, APRED 2020/2021, grant number 2266D0005.

Virtual testbed for the planning of urban battery electric buses

S. Würtz[a], Jonas Rossa[a], K. Bogenberger[b], U. Göhner[a]

[a] *University of Applied Sciences Kempten*

[b] *Technical University of Munich (TUM)*

Introduction

The planning of battery electric buses (BEB) for urban public transport is a crucial topic for many cities around the world. The local bus operators are experts in the planning process of daily operations, but the BEBs have very different requirements and constraints for their operation. And although many cities have transitioned a fair number of vehicles to electric drives, the know-how for optimal energy-efficient planning is still limited.

There are a multitude of approaches to simulate energy demand for electric vehicles based on traffic simulations (Papa et al. 2022). Many researchers choose the open-source solution SUMO (Validi et al.) to generate trajectories. The authors of (Maia et al.) implemented an energy model for SUMO and integrated it into the codebase. In (Koch et al. 2021) a model is proposed which can predict the energy demand based on the *Worldwide harmonized Light vehicles Test Cycle* (WLTC). (J. Macedo et al. 2013) proposed an architecture to couple SUMO and MATLAB to model energy demand of electric vehicles. (Sagaama et al.) propose a more accurate energy model for EVs with focus on recuperation. Other investigations for private vehicles where done in (Schlote et al. 2012), (Kurczveil et al. 2014) and (Topić et al. 2020), but all the mentioned approaches rely on the speed profiles provided by the traffic simulation tool.

With the detailed analysis of tracking data for battery electric buses (BEB) in this paper we saw major differences in the acceleration patterns. And since the energy consumption from the simulations can only correspond to the actual energy demand of a bus if the speed profile has the same characteristics as the actual bus, it is worthwhile to optimize the acceleration behavior in the simulation (Ranta et al. 2016). Due to the randomness of the traffic, the speed curve generated in the simulation tool will never be the same as in real life as was found in (Ranta et al. 2016), but the goal is to achieve a speed profile that is as realistic as possible. (Validi et al.) also found that some major differences in the energy prediction stem from inaccurate modelling of acceleration and deceleration. In (Xu et al. 2021) and (Zhang et al. 2020) improved movement patterns for electric vehicles are developed.

Those findings motivated the presented methodology to calibrate the SUMO traffic simulation for realistic movement patterns and calculate the energy demand with a powertrain model. The powertrain model is described in (Würtz et al. 2023), which enables a very detailed prediction of the energy demand for all vehicles during the whole day operation. In this paper, an approach is presented which enables the validation of new routes for battery electric buses in a traffic simulation environment (SUMO). This allows the optimization of battery sizes and charging infrastructure for new bus networks as described in (Würtz et al. 2022).

Methodology

The described approach of this paper consists of a feedback loop between the traffic simulation and the evaluation against tracking data from real buses. For this paper the Open-Source Traffic Simulation SUMO (Behrisch et al. 2014) was chosen. As shown in Fig. 1 the speed values from the tracking data obtained from electric buses operated in Göttingen, Germany is used to calibrate the vehicles parameters like acceleration and deceleration as well as the driver behavior represented by a car-following model. We chose the EIDIM Model developed in (Salles et al. 2022), since it provides the best customizability from the available built-in models. For the calculation of the powertrain energy demand the model developed in (Würtz S. 2023) is used since it allows for accurate energy values and can incorporate detailed information about passenger load, vehicle types and the topology.

Figure 74. Overview of the Methodology. Tracking Data is used to calibrate the vehicles and driver behavior within SUMO. The Output is used to predict the energy demand for specific bus routes.

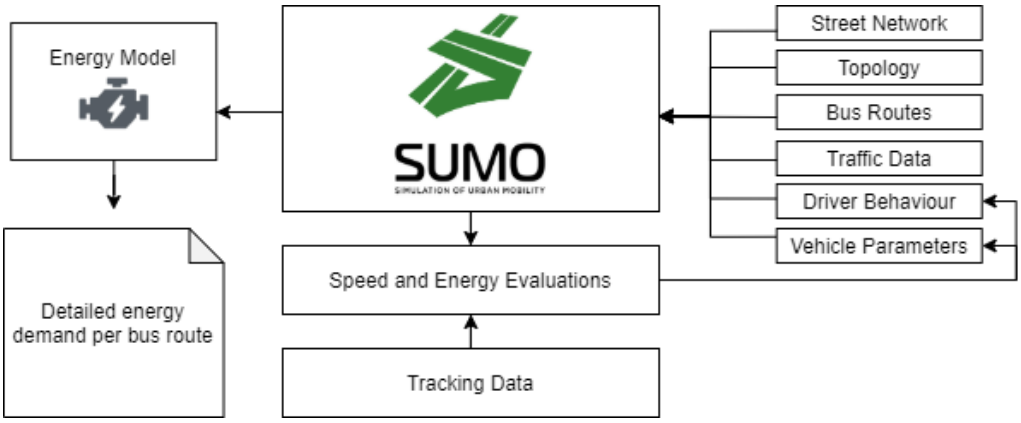

This approach forms the basis for the virtual testbed for BEB planning, since it enables the planner to setup new bus routes and get reliable data about the required energy demand on a second-by-second basis, which enables the planning of battery size as well as location and dimensioning of charging infrastructure.

Results

To evaluate this virtual testbed for BEBs we chose an existing route in Göttingen, where we have tracking data for the bus as well-as the actual energy demand.

Figure 75. Analyzed bus line with the color indicating the vehicle speed. Left: Speed profile from SUMO simulation. Right: Speed profile from the actual bus

In Fig. 2 the route is shown on a map indicating the speed throughout the route after the proposed optimization. Except for a deviation on the upper right part where the simulated bus strictly adheres to the speed limit of 10km/h the speed profile is very similar. In Fig. 3 we show the different histograms of speed values for the simulation runs. In blue the data from the tracked bus is shown the other histograms show different stages of the optimized vehicle behavior.

The default vehicle behavior has two major peaks around 30km/h and 50km/h which correspond to the speed limits on most streets, this is still true when we adjusted the acceleration and deceleration parameters for the electric buses. This shows that the default SUMO model has an extreme driving behavior with very fast acceleration and deceleration. One major improvement was possible by calibrating the EIDIM car-following model, which mostly eliminated those peaks in the histogram, further improvements can be achieved by optimizing the behavior around traffic lights (GLOSA) and the speed at turns and junctions (junction_speed).

Figure 76. Left: Histogram of the different simulated bus trips and the actual measured bus trip. Right: The energy demand according to the energy prediction model for the tracking data, default behavior of sumo and the final optimized version of the simulation

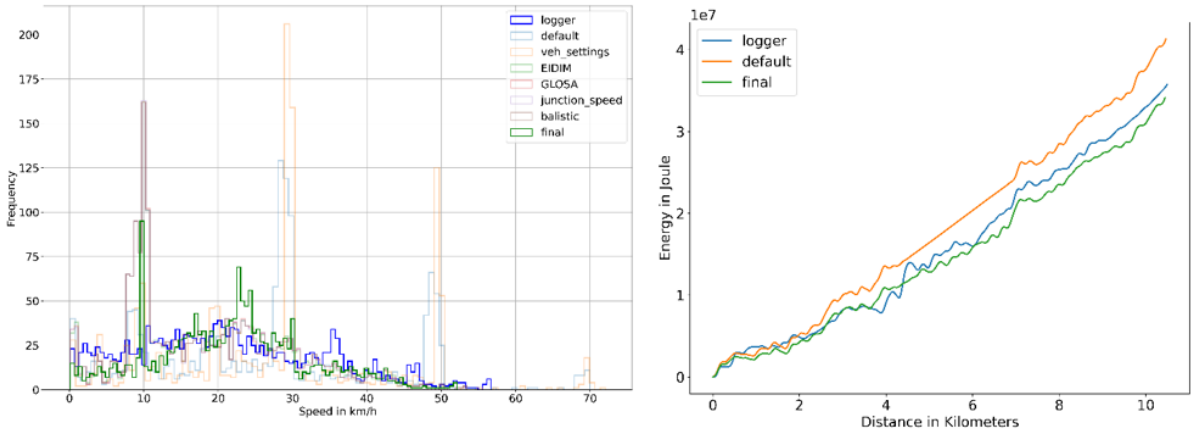

A final improvement which also improves the computability is the usage of ballistic calculation of the vehicle trajectories compared to the Euler method implemented within SUMO.

To put all of this into perspective it is important to understand the impact of this on the energy demand. In Fig. 3 on the right side the computed energy demand is shown for the tracking data (35,748 Kilojoule), the default SUMO model (41,285 Kilojoule) and the described optimized vehicle model (34,120 Kilojoule). The default model produces an error of 15% while the improved model has an error of 4.5% which is a significant improvement.

Conclusion and Outlook

This paper has the goal to propose an approach to enable reliable planning of BEBs in a traffic simulation which acts as the virtual environment. It was shown that the defaults for the vehicle trajectories from the traffic simulation SUMO, introduce significant errors. With some fine tuning and optimization of the vehicle behavior, reasonable results can be obtained from the traffic simulation. This can be used for planning of new bus networks considering many aspects, like energy demand, impact of traffic on delays and the resulting charging times at terminal stations.

In future works we want to investigate the impact of traffic within the virtual environment and consider a custom Car-Following model to address the needs for accurate energy prediction better. Another improvement can be expected by applying the optimization to the whole bus network instead of a single route.

References

Behrisch, M.; Krajzewicz, D.; Weber, M. (2014): Simulation of Urban Mobility. Springer Berlin Heidelberg.

J. Macedo; G. Soares; Z. Kokkinogenis; D. Perrotta; F. RosaldoJ.; Rossetti (2013): A Framework for Electric Bus Powertrain Simulation in Urban Mobility Settings : coupling SUMO with a Matlab / Simulink nanoscopic model.

Koch, L.; Buse, Dominik S.; Wegener, M.; Schoenberg, S.; Badalian, K.; Dressler, F.; Andert, J. (2021): Accurate physics-based modeling of electric vehicle energy consumption in the SUMO traffic microsimulator. In *2021 IEEE Intelligent Transportation Systems Conference*.

Kurczveil, T.; López, P.; Schnieder, E. (2014): Implementation of an Energy Model and a Charging Infrastructure in SUMO. In *Behrisch, Krajzewicz et al. (Hg.) 2014 – Simulation of urban mobility*.

Maia, R.; Silva, M.; Araujo, R.; Nunes, U.: Electric vehicle simulator for energy consumption studies in electric mobility systems.

Papa, G.; Santo Z., Marina; Vukašinović, V. (2022): Electric-bus routes in hilly urban areas: Overview and challenges. In *Renewable and Sustainable Energy Reviews.*

Ranta, M.; Karvonen, V.; Potter, J. J.; Pasonen, R.; Pursiheimo, E.; Halmeaho, T. et al. (2016): Method Including Power Grid Model and Route Simulation to Aid Planning and Operation of an Electric Bus Fleet. 2016 IEEE Vehicle Power and Propulsion Conference (VPPC). Hangzhou, China.

Sagaama, I.; Kchiche, A.; Trojet, W.; Kamoun, F.: Evaluation of the Energy Consumption Model Performance for Electric Vehicles in SUMO. In, pp. 1–8.

Salles, D.; Kaufmann, S.; Reuss, H. (2022): Extending the Intelligent Driver Model in SUMO and Verifying the Drive Off Trajectories with Aerial Measurements. In *SUMO Conf Proc* 1.

Schlote, A.; Crisostomi, E.; Kirkland, S.; Shorten, R. (2012): Traffic modelling framework for electric vehicles. In *International Journal of Control* 85.

Topić, J.; Soldo, J.; Maletić, F.; Škugor, B.; Deur, J. (2020): Virtual Simulation of Electric Bus Fleets for City Bus Transport Electrification Planning. In *Energies* 13.

Validi, Aso; Morales-Alvarez, Walter; Olaverri-Monreal, Cristina: Analysis of the Battery Energy Estimation Model in SUMO Compared with Actual Analysis of Battery Energy Consumption.

Würtz, S.; Bogenberger, K.; Göhner, U. (2022): Big Data and Discrete Optimization for Electric Urban Bus Operations. In *Transportation Research Record.*

Würtz S., et al. (2023): Energy Prediction Model Development and Parameter Estimation for Urban Battery Electric Buses with Real-World Data. https://annualmeeting.mytrb.org/OnlineProgram/Details/19446.

Xu, Y.; Zheng, Y.; Yang, Y. (2021): On the movement simulations of electric vehicles: A behavioral model-based approach. In *Applied Energy* 283.

Zhang, Z.; He, H.; Guo, J.; Han, R. (2020): Velocity prediction and profile optimization based real-time energy management strategy for Plug-in hybrid electric buses. In *Applied Energy* 280.

Optimal planning of electric vehicle fast-charging stations considering uncertain charging demands via Dantzig-Wolfe decomposition

B. Zhou[a], R. Liu[a]

[a] *Institute for Transport Studies, University of Leeds, Leeds LS2 9JT, United Kingdom*

Introduction

Electric vehicles (EVs) have been widely recognized as an auspicious way to curtail the green house gas emissions produced by road transportation. As a result, many governments have promulgated incentive policies to promote the mass adoption of EVs. International Energy Agency (2021) reports that EVs on the world's roads at the end of 2020 have reached 10 million, following a decade of rapid growth, and simultaneously, electric car registrations have increased by 41% in 2020, despite the pandemic-related worldwide downturn in car sales dropped by 16%.

However, there are several obstacles that hinder the adoption of EVs on a larger scale. Among them, the range anxiety maybe the most momentous challenge, which reflect the fear of running out of energy before reaching the destinations or charging stations, since the driving range of EVs is often unstable, which can be affected by multi-factors (Xu et al. 2020). In practice, an efficient way to popularize the EVs, especially for the long inter-city trips, is to reasonably plan fast-charging stations over the traffic network. This motivates us to investigate the optimal planning problem of fast-charging stations, that is, determing where to build the fast-charging stations and how many charging plies to be installed in each fast-charging station.

The planning problem of fast-charging stations have been studied in several context, in which the charging demands of EVs are the crucial ingredients. In practice, the distribution of uncertain charging demands is often unknown, which has posed challenges to the stochastic modeling approach. Instead, massive amount of data is routinely available in transportation networks, for which the distributionally robust optimization and chance-constrained programming approach are more suitable. Wu and Sioshansi 2017 employs the sample average approximation approach to deal with the uncertain charging demands, where the distribution of the charging demands is no longer required. Instead, it only uses the data of charging demands to formulate the planning model. Zhou et al. 2020 develops a distributionally robust optimization planning model based on Φ-divergence, where the potential distributions of uncertain charging demands are estimated using their available data.

In this study, we leverage a data-driven paradigm to establish a chance-constrained programming model for the planning of fast-charging stations on the basis of the multicommodity flow mode. We separate the original planning model into multiple disjoint sub-components corresponding to the O-D pairs in the transportation network, which are facilitate to be implemented in a decentralized manner using parallel machines. We apply a scenario-based approach as well as a big-M coefficients generation algorithm to reformulate the programming model into tractable one, then use the Dantzig-Wolfe decomposition method to find its optimal solution, where the master problems and subproblems are one-to-one. Each possesses a moderate scale of decision variables, which makes it conducive to improve the computational performances.

Methodology

We consider a traffic network $G(V,A)$, where V is the set of nodes and A is the set of edges. We denote Q be the set of O-D pairs, which is indexed by q. For an O-D pair q, we denote its origin and destination by s^q and t^q, respectively. We denote the set of edges between O-D pair q be $\overline{A^q}$. It should be mentioned that $\overline{A^q}$ includes not only the edges in A, but also the virtual edges generated by accounting for the limited driving ranges using the expanded network approach (MirHassani and Ebrazi 2013). Based on the multicommodity flow model, we formulate the following model for the planning problem of fast-charging stations

$$\min \quad \sum_{i \in V} (c_{1,i} u_i + c_{2,i} y_i) \tag{1}$$

$$s.t. \quad \sum_{j \in N_i^-} x_{ij}^q - \sum_{j \in N_i^+} x_{ji}^q = \begin{cases} 1, & \text{if } i = s^q, \\ -1, & \text{if } i = t^q, \\ 0, & \text{if } i \neq s^q, i \neq t^q, \end{cases} \quad \forall\, q \in Q, \tag{2}$$

$$\mathbb{P}\left(\sum_{q\in Q}\tilde{F}^{q}\sum_{j\in N_i^+}x_{ji}^{q}\le y_i\right)\ge\alpha,\ \forall\ i\in V, \tag{3}$$

$$y_i\le\Upsilon u_i,\forall\ i\in V, \tag{4}$$

$$u_i\in\{0,1\},\ \forall\ i\in V, \tag{5}$$

$$y_i\in\mathbb{Z}_+,\forall\ i\in V, \tag{6}$$

$$x_{ij}^{q}\ge 0,\ \forall\ (i,j)\in\bar{A}^{q},\ q\in Q, \tag{7}$$

where $c_{1,i}$ and $c_{2,i}$ are the cost for building fast-charging station and installing charing piles, respectively; $\tilde{F}^{q}$ is the uncertain charging demand between O-D pair q; Υ is the upper bound for the charging plies in each fast-charging station; u_i is a binary variable that represents whether a fast-charging station is built at node i; y_i is a integer variable that represents how many charging piles are installed in each fast-charging station; x_{ij}^{q} is a continuous variable that represents the proportion of charging demands between O-D pair q allocated from node i to node j. This model aims to minimize the total cost for planning the fast-charging stations. Constraint (2) is the flow-conservation conststraint; Constraint (3) is the chance-constraint which guarantees the probability that the EVs successfully get charged in a fast-charging station at least reaches a specified service level α. Constraint (4) bounds the number of charging piles installed in each fast-charging station; Constraints (5)-(7) restrict the decision variables.

The uncertain charging demands between O-D pairs are difficult to be accurately evaluated in reality. Thus, we resort to a scenario based reformulation. We denote Ω be the finite set of all possible scenarios of $\tilde{F}^{q}$, which can be obtained by applying the sample average approximation to the available data of uncertain charging demands. We denote the realizations of $\tilde{F}^{q}$ by $\left\{\hat{F}_1^{q},\hat{F}_2^{q},\ldots,\hat{F}_{|\Omega|}^{q}\right\}$. We further introduce an auxiliary binary variables $z_{i\omega}$ to reformulate Constraints (3) into their linear counterparts, where $z_{i\omega}=1$ if fast-charging station at node i satisfies the allocated charging demands in scenario ω, that is, the ith chance constraint is satisfied, and $z_{i\omega}=0$ otherwise. Then, a tractable reformulation can be expressed as follows:

$$\min\ \sum_{i\in V}(c_{1,i}u_i+c_{2,i}y_i)$$

$$s.t.\quad (2),\ (4)-(7),$$

$$\sum_{q\in Q}F_{\omega}^{q}\sum_{j\in N_i^+}x_{ji}^{q}\le y_i+M_{i\omega}(1-z_{i\omega}),\forall\ i\in V,\omega\in\Omega,$$

$$\sum_{\omega\in\Omega}z_{i\omega}\geqslant\lceil\alpha|\Omega|\rceil,\forall i\in V,$$

$$z_{i\omega}\in\{0,1\},\ \forall\ i\in V,\omega\in\Omega,$$

where $M_{i\omega}$ is a big-M coefficient that is obtained by a generation algorithm used in Zhang et al. 2020.

In order to improve the computational efficiency, we separate the problem into Q sub-components with respect to to the Q O-D pairs, then apply the Dantzig-Wolfe decomposition to find the optimal solution of each sub-component. At last, we obtain the optimal solution of original problem by synthesizing the optimal solutions of the sub-components. Our method is different form the existing works, in which the master problem and the sub-problem is one-to-one for each sub-component, while the existing works employs one master problem and several subproblems.

Results

We test the proposed model in a hypothetical 25-node network shown in Figure 1. The number labelled in each edge represents its length. Every node is considered as origin, destination and candidate site for the fast-charging stations, yielding totally 600 O-D pairs and 25 candidate sites. We suppose that the EVs start their trips with fully charged batteries. We investigate 10 scenarios of charging demands between O-D pairs. In each scenario, the charging demands between each O-D pair are equal, that is, $F_{\omega}^{q} = 5 + \omega, \ \ \forall q \in Q$

Figure 77. The 25-node network

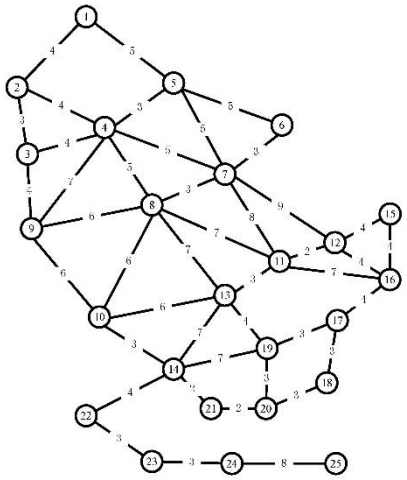

Source: Authors' elaborations.

The solving algorithms are coded in Matlab R2017b calling YALMIP (version: R20210331) using CPLEX 12.10 on a Windows machine with Intel(R) Core(TM) i9-11950H and 64 GB RAM. The building cost of the fast-charging stations and the installing cost of the charging piles are set to be 100 and 10, respectively. The upper bound for the charging plies is set to be 800.

To evaluate the performance of Dantzig-Wolfe decomposition, we consider one service levels 0.4, four driving ranges 8, 9, 10 and 11. We compare the cpu time between the CPLEX solver and our Dantzig-Wolfe decomspotion. Note that there are totally 600 subcomponents in our model, it is impossible to put all of the runtime in one table. Thus, we perform four curcial indexes of the runtime for the 600 componments, which include the maximum, the median, the average and the minimum.

Figure 78. Results of scenario-based reformulation in 25-node network with α=40%

	Performance of CPLEX				Performance of Dantzig-Wolfe decomposition							
Driving Range	Runtime (in Sec.)				Runtime of MP (in Sec.)				Runtime of SP (in Sec.)			
	Max.	Med.	Ave.	Min.	Max.	Med.	Ave.	Min.	Max.	Med.	Ave.	Min.
8	42.14	12.90	15.40	0.09	0.21	0.14	0.15	0.12	0.32	0.20	0.21	0.14
9	48.81	10.72	14.36	0.11	0.29	0.19	0.19	0.16	0.33	0.25	0.25	0.18
10	52.84	10.45	13.77	0.10	0.73	0.23	0.23	0.20	0.62	0.29	0.29	0.22
11	57.13	9.07	10.92	0.14	0.37	0.27	0.27	0.24	0.47	0.33	0.34	0.27

Source: Authors' elaborations.

Table 1 illustrates the simulation results. We observe that Dantzig-Wolfe decomposition significantly reduces the runtime for the planning model when compared with the CPLEX solver. We can also observed from Table 1 that for the driving range impacts the runtime of CPLEX significantly. The reason is that longer driving range can induce more virtual edges in the expanded network, which means that more decision variables are encountered in the planning model. On the contray, the Dantzig-Wolfe decomposition method is insensitive to the increase of decision variables, because we decompose the original planning model into Q sub-componments, each of them has a moderate size, which increases the computational efficiency of Dantzig-Wolfe decomposition.

Conclusions

We establishes a chance-constrained programming model for the planning problem of fast-charging stations. By applying the sample average approximation to the available data of uncertain charging demands, we get several scenarios of the charging demands. Then, we propose a scenario-based tractable reformulation of the chance-constrained programming model. We then utilize the Dantzig-Wolfe decomposition to find the optimal solution. At last, we present a numerical example to test the efficiency of the proposed methods. By comparing the runtime, we show that our method is more efficient than the CPLEX solver.

References

International Energy Agency. *Global EV outlook 2021*. https://www.iea.org/reports/global-ev-outlook-2021, 2021.

Xu, M., Yang, H., Wang, S.A., Mitigate the range anxiety: siting battery charging stations for electric vehicle drivers, *Transportation Research Part C: Emerging Technologies*, vol. 114, 2020, pp. 164-188.

Wu, F., Soishansi, R., A stochastic flow-capturing model to optimize the location of fast-charging stations with uncertain electric vehicle flows, *Transportation Research Part D: Transport and Environment*, vol. 53, 2017, pp. 354-376.

Zhou, B., Chen, G., Huang, T.W., Song, Q.K., Yuan, Y.F., Planning PEV fast-charging stations using data-driven distributionally robust optimization approach based on Φ-divergence, *IEEE Transactions on Transportation Electrification*, vol. 6, no. 1, 2020, pp. 170-180.

MirHassani, S.A., Ebrazi, R., A flexible reformulation of the refueling station location problem, *Transportation Science*, vol. 47, no. 4, 2013, pp. 617-628.

Zhang, Z., Dention, B.T., Xie, X.L., Branch and price for chance-constrained bin packing, *INFORM Journal on Computing*, vol. 32, no. 3, 2020, pp. 547-564.

An analytical model to evaluate city-wide waiting and detour time for electric vehicle public charging

A. Yichan An[a], B. Jinwoo Lee[a]

[a] *Korea Advanced Institute of Science and Technology, Daejeon, Republic of Korea*

In this study, we propose an analytical model based on queuing theory and the continuous approximation method to efficiently estimate waiting and detour times associated with public charging for electric vehicles in a city-wide context, which directly influences the level of service of charging infrastructure system. The model considers spatial heterogeneity and evaluates three different scenarios for assigning electric vehicles to charging stations: (i) nearest station assignment; (ii) optimal station assignment within a search area; and (iii) optimal station assignment within the entire area. We verify the adequacy of the model through a comparison with Monte Carlo simulation results. In addition, we identify optimal scenarios under various circumstances through sensitivity analyses.

Category 5. Travel demand in the future mobility landscape

Online demand forecasting with spatial-temporal graph attention networks: a proof of concept

M. Dominguez[a], A. Tympakianakia, F. Torrent-Fontbona[a], T. Hayman[d], J. Perarnau[a], J. Casas[a]

[a] *Aimsun SLU*

[d] *Aimsun Ltd.*

Introduction

The demand estimation and prediction problems have been studied intensively in the literature for several decades. However, due to the complexity and difficulty to observe directly the (origin-destination) OD flows along all possible routes in the network, the problem still entails significant challenges. Dynamic OD estimation methods are usually categorized as offline, which refer to the manual estimation (or calibration) of a set of time-dependent OD matrices given a set of available time-series of link traffic counts, and online approaches, used in the context of real-time traffic management and route guidance. Online approaches aim at predicting future OD flows given real-time traffic information from the network as it becomes available, providing fast estimates for recent time intervals with predictions for future time intervals (Antoniou et al., 2016).

Online dynamic OD demand estimation is a very challenging problem due to the non-linearity and observability issues associated with the demand estimation problem (Castiglione et al., 2021). The Kalman filter (KF) algorithm (Kalman, 1960) has been commonly used to estimate online dynamic demand (e.g., Antoniou et al., 2007; Liu et al., 2020). The algorithm solves a least-square problem in an incremental way, allowing for the update of the unknown time-dependent OD flows as additional traffic data become available. Krishnakumari et al. (2020) propose a data-driven method to estimate OD flows without the need for an iterative dynamic network loading using link speed and flow measurements and deriving path travel times.

Current advances in data-driven methodologies using deep neural networks have been tested at large in traffic supply forecasting (cf. among others, Yu et al., 2017; Cheng et al., 2018; Fang et al., 2022) seeking to explore spatial-temporal dependencies inherent to traffic. Yet graph neural networks (GNNs), which seem to be the most suitable representation of a traffic network, have not been as extensively investigated for demand forecasting (cf., Jiang & Luo, 2021). When real-time intelligent transport systems (ITS) systems require the use of simulators to test ad-hoc response plans for traffic control centre[14] to swiftly react to an unplanned event, demand prediction tasks are still addressed using traditional methodologies, such as KF. Hence, a big gap is faced between advances in deep learning (DL) and real-world real-time implementations in ITS involving data-driven demand forecasting.

In this paper, a preliminary proof of concept is presented where a GNN architecture is used to predict aggregated demand generated at origins (in the OD pair matrix). Synthetic data, created offline in simulation, has been used to test several configurations in a controlled experimental DL setting. Based on Zhang et al (2019) good results in traffic supply forecasting, a spatial-temporal graph attention network (ST-GAT) architecture is used for our experiments. This type of GNN architecture has been adapted to predict in a supervised way the demand at time *t* (in all origins generating vehicles) using traffic data from the previous hour (*t-1*) from all sections aggregated in 15-minute intervals and modelling centroids as part of the graph adjacency.

The data used for the DL experiments comes from a network[15] with around 3000 sections and 500 centroids developed and calibrated at mesoscopic traffic flow resolution. A three-hour peak afternoon period (from 15:15 to 18:15) with a total demand of 213,859 vehicles was selected from the network, and a demand warm-up of 30 minutes was included. The original time-dependent origin-destination (OD) matrix based on 15-minute intervals is considered as the base demand matrix (with a total of 27,787 OD variables along all the time intervals) for the experiments. Demand perturbations were then applied by changing the vehicle generation modifying an exponential random seed. As a result, twenty-three perturbations were generated, and simulations were run in Aimsun Next (Aimsun, 2022) to extract traffic counts (vehicles/15min.) and travel times at all sections to be further used as input to the supervised ST-GAT experiments.

[15] We cannot disclose the name of the network used due to privacy related issues.

The data was processed by adding all demands generated at each origin and time and the formats were converted to the requirements of the GNN (built on PyTorch Geometric[16]). The graph dataset composed of 184 samples was split into train, validation, and test sets as described below for each experiment. In our experiments, 'true' demand is the aggregated demand per origin at time *t* used in the test samples of the dataset[17]. Note that supervised DL algorithms need a test set with 'true' (or reference) labels to evaluate their task performance. As we are testing the adequacy of the DL approach and not its applicability in simulation, our evaluation reports the results from the DL experiment.

The ST-GAT architecture proposed by Zhang et al. (2019), cf. **Figure 79** has been adapted to the demand prediction task. Zhang's architecture consists of two main blocks: 1) the spatial block comprises the GAT to model the geometry of the network; and 2) the temporal block uses a Recurrent Neural Network (RNN) block with two layers of Long-Short Term Memory (LSTMs) to model the flow as a vector of time features from the previous hour in 15-minute intervals (i.e., *t-60, t-45, t-30, t-15* as a time feature vector and *t* as the class to be predicted) across the whole network.

Figure 79. ST-GAT architecture used in the experiments

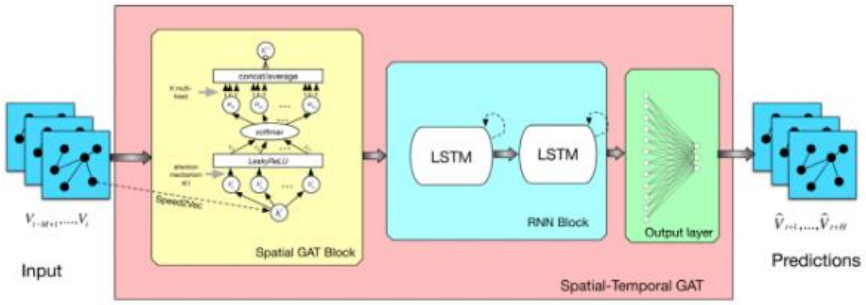

Source: Zhang et al. (2019).

Our experimental design varies from Zhang's in the geometry of the network which includes centroids and all sections as nodes (instead of only sections with detectors), and their adjacency as edges of each graph. We furthermore model the type of nodes (sections, origins, destinations) as a one-hot encoded vector, and include travel times and base demand in the last experiment.

Three experiments were run to explore the potential of this architecture for the demand prediction problem. In all experiments, a supervised transductive learning methodology for node regression is deployed.

- Experiment 1: flow information from the previous hour is used at sections to predict demand at centroids modelling the type of node (i.e., section, origin, and destination) as a one-hot encoded vector of features. Train, validation, and test sets were extracted from the total 184 samples (23 replications by 8 time intervals) using all (i.e., 8) time intervals in the last replication for testing and shuffling the rest for training (160 samples) and validation (16 samples).
- Experiment 2: the same setup as in experiment 1 is used. Train, validation, and test sets are split in this experiment according to timestamps. Therefore, 23 samples corresponding to the first timestamp in the timeseries is used for testing, 23 samples from the last timestamp for validation, and the rest 138 samples for training.
- Experiment 3: the same experimental design as in experiment 2 is used, changing the graph geometry to model travel time between sections, and using base demand from the previous hour in the feature vector of origin nodes.

Scatter plots depicted in **Figure 80** show the correlation between 'true' or reference demand (x-axis) and predicted demand[18] (y-axis) in all experiments. The dots in these figures represent the total demand generated

[16] https://pytorch-geometric.readthedocs.io
[17] 'True' demand in the context of this paper should not be confused with base demand or real demand in the context of simulation or calibration of a transport model.
[18] 'True' demand is the class to be predicted from the test dataset, and predicted demand is the algorithm's estimation using the model trained on the rest of the data.

at a given origin and time interval. Root mean squared error (RMSE) was computed for each experiment and results are presented in **Table 16**.

Figure 80. Results comparing gold (x-axis) and predicted (y-axis) values in each experiment

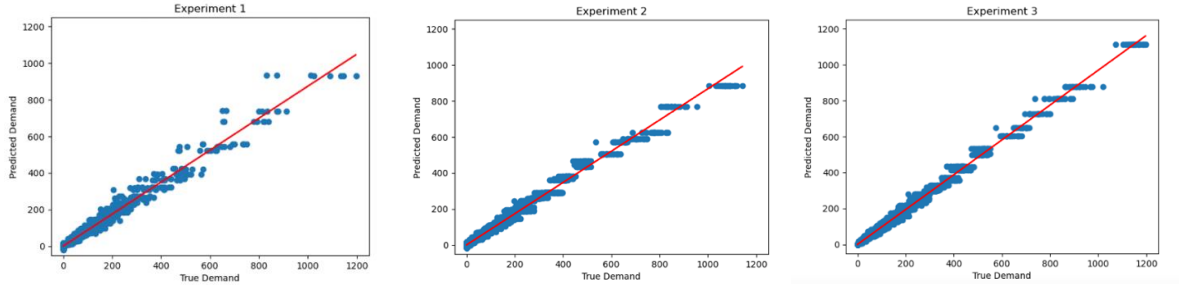

Source: Authors' elaborations.

Table 16. Root Mean Squared Error (RMSE) of experiments (in %)

Experiment 1	Experiment 2	Experiment 3
1.0%	1.0%	0.4%

Source: Authors' elaborations.

Results show that RMSE improves from the first to the last experiment, which implies that proposed modelling and ST-GAT architecture have a considerable potential for predicting aggregated demand at origins in 15-minute time intervals when simulated data is used for training. We need to bear in mind, though, that the experimental setting uses quasi-perfect data with a full coverage over the network, i.e., we have counts at all sections, as well as travel times, and base demand which may certainly not be available in a real online dynamic OD prediction setup. Given the perfect nature of the data, we must admit were expecting that results showed even better performance. However, it can be observed in the plots that, even though the scale of the predicted values is in line with what could be expected, the model keeps predicting the same value within specific ranges. For example, experiment 3 and 4 show that all reference values ('true' demand) between 1,000 and 1,200 are always predicted as 1,000 regardless of the replication and/or time interval used for testing. Such limitation may be due to the inherent difficulty of the demand prediction task, very low number of training samples, or deficiencies in the architecture that need to be further explored.

Future work will include modelling directionality of OD pairs as path information in the GAT block of the ST-GAT architecture to be able to predict demand at each time interval and OD pair. We will also carry out a proof of concept in the context of TANGENT H2020 project with data from the pilot use cases.

Acknowledgements

This work has received funding from the European Union´s Horizon 2020 research and innovation programme under grant agreement No 955273 (TANGENT – Enhanced data processing techniques for dynamic management of multimodal traffic).

References

Aimsun, *Aimsun Next 22 User's Manual*, Aimsun Next Version 22.0.1, Barcelona, Spain. Accessed on: May. 26, 2022. [Online]. Available: https://docs.aimsun.com/next/22.0.1/

Antoniou, C., Barceló, J., Breen, M., Bullejos, M., Casas, J., Cipriani, E., Ciuffo, B., Djukic, T., Hoogendoorn, S., Marzano, V., Montero, L., Nigro, M., Perarnau, J., Punzo, V., Toledo, T., & van Lint, H., 'Towards a generic benchmarking platform for origin–destination flows estimation/updating algorithms: Design, demonstration and validation', *Transportation Research Part C: Emerging Technologies*, Vol. 66, 2016, pp. 79–98.

Antoniou, C., Ben-Akiva, M., & Koutsopoulos, H. N., 'Nonlinear Kalman Filtering Algorithms for On-Line Calibration of Dynamic Traffic Assignment Models'. *IEEE Transactions on Intelligent Transportation Systems*, Vol. 8, No 4, 2007, pp. 661–670.

Castiglione, M., Cantelmo, G., Qurashi, M., Nigro, M., & Antoniou, C., 'Assignment Matrix Free Algorithms for On-line Estimation of Dynamic Origin-Destination Matrices', *Frontiers in Future Transportation*, Vol. 2, 2021, pp. 640570, doi: 10.3389/ffutr.2021.640570.

Cheng, X., Zhang, R., Zhou, J., & Xu, W., 'DeepTransport: Learning Spatial-Temporal Dependency for Traffic Condition Forecasting', *Proceedings of the International Joint Conference on Neural Networks* (IJCNN), Rio de Janeiro, Brazil, 2018, pp. 1-8, doi: 10.1109/IJCNN.2018.8489600.

Fang, W., Zhuo, W., Yan, J., Song, Y., Jiang, D., & Zhou, T., 'Attention meets long short-term memory: A deep learning network for traffic flow forecasting'. *Physica A: Statistical Mechanics and Its Applications*, Vol. 587, 2022, pp. 126485, doi: 10.1016/j.physa.2021.126485.

Jiang, W., & Luo, J., 'Graph Neural Network for Traffic Forecasting: A Survey', in *Arxiv*, 2021, http://arxiv.org/abs/2101.11174

Kalman, R. E., & Bucy, R. S., New Results in Linear Filtering and Prediction Theory. *Journal of Basic Engineering*, Vol. 83, No 1, 1961, pp. 95–108.

Krishnakumari, P., van Lint, H., Djukic, T., & Cats, O., 'A data driven method for OD matrix estimation', *Transportation Research Part C: Emerging Technologies*, Vol. 113, 2020, pp. 38–56.

Liu, J., Zheng, F., van Zuylen, H. J., & Li, J., 'A dynamic OD prediction approach for urban networks based on automatic number plate recognition data', *Transportation Research Procedia*, Vol. 47, 2020, pp. 601–608.

Yu, H., Wu, Z., Wang, S., Wang, Y., & Ma, X., 'Spatiotemporal Recurrent Convolutional Networks for Traffic Prediction in Transportation Networks', *Sensors*, Vol. 17, No 7, 2017, pp. 1501, doi: 10.3390/s17071501.

Zhang, C., Yu, J. & Liu, Y., 'Spatial-Temporal Graph Attention Networks: A Deep Learning Approach for Traffic Forecasting', *IEEE Access*, Vol. 7, 2019, pp. 166246-166256, doi: 10.1109/ACCESS.2019.2953888.

Estimating the environmental and societal impact of new mobility services

A. Garus[ab], B. Alonso Oreña[b], B.Ciuffo[a]

[a] *European Commission – Joint Research Centre, Via E. Fermi, 2749 – 21027 Ispra (VA), Italy*

[b] *Department of Transportation and Projects and Processes Technology - University of Cantabria, Santander, Av. de los Castros s/n, 39005 Cantabria, Spain*

Introduction

We all need transportation and its infrastructure not only to manage our daily tasks but also because few economic resources are located just where we would want them. However, transport is also a source of numerous negative externalities, such as road accidents, congestion in urban areas and lacking air quality. Transport is also a sector substantially contributing to climate crisis with more than 16% of global greenhouse gas emissions being a result of transport activities (Ritchie et al., 2020). Nevertheless, even though transport might be a necessity, its negative impacts could be limited or, some of them with a right approach, could even be avoided entirely.

Like in numerous other sectors we can turn to innovation to secure better efficiency of the overall system, and while transport has been stable for the second part of the XXth century, today there are numerous new mobility solutions enabled by connectivity, automation, and electrification (Alonso Raposo et al., 2019). Electrification of the transport solutions coupled with development of renewable energy sources could result in lower greenhouse gas emissions as well as better air quality (Alonso Raposo et al., 2019). While connectivity and automation could lead to a safer and more efficient road environment, reducing number of accidents and lowering congestion in urban areas (Litman, 2023). The most awaited transport innovation is of course an autonomous vehicle (AV), which would have the automation connectivity and electrification at its core.

Nevertheless, with each introduction of a new mobility service we can observe factors that could negatively contribute to the sustainability of the transport system – a chain of behavioural changes caused by introduction of entirely new possibilities. The literature review performed for the purpose of the study showed that introduction AVs could have a substantial impact on the way we behave (Garus et al., 2022). The identified behavioural changes caused by AVs are presented in a graphical manner on Figure 1 hereunder.

As transport system is heavily integrated with various other systems in urban areas and results in numerous negative implications there is a need to anticipate the possible triggered behavioural changes before, they arise causing a further depletion in overall urban sustainability. Such anticipation is usually done via transport modelling. Nevertheless, the today's modelling tools are often not agile enough and highly aggregated which complicates representation of new mobility services and the reaction to their deployment. Hence, for all reasons mentioned previously the first objective of the study is to identify how the introduction of new mobility services can impact the societal and environmental transport externalities. In particular, the objective is to develop and validate a modelling framework able to capture the complexity of the transport system and to apply it to assess the potential impact of a shared autonomous vehicle – SAV. However, preparation of the model led to discovery of an unexplored component, namely the personal parking preferences of a privately owned AV. Uncovering those preferences became a second objective of the study.

Figure 81. Categorization of behavioural changes triggered by SAVs

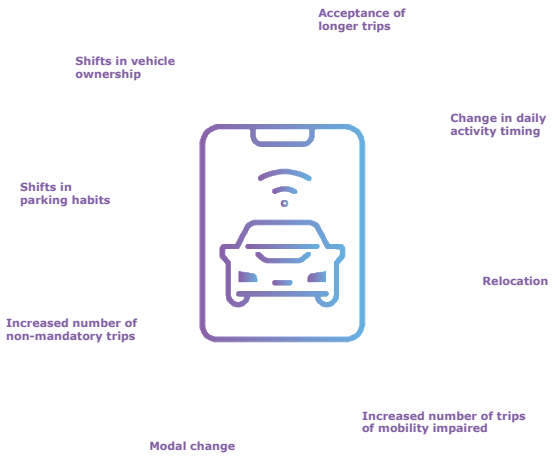

Methodology

In achieving the first objective a focus was put on an environmental rebound effect – environmental implications of introduction of SAV based service. The research mainly focused on investigating how the sizing of the fleet could impact the environmental rebound effect, as well as, which of the identified behavioural changes (Figure 1) would have the highest contribution to the negative externality. In the research we chose to use an agent-based demand estimation coupled with traffic microsimulation to investigate the performance of SAV-based systems in the context of a case study in Santander, Spain. An activity-based model allows to represent decisions of individuals based on their socioeconomic profile. By doing so, agent-based models are used to capture short and medium effects of transport policies. The activity-based demand estimation was employed in SimMobility - an open-source activity-based simulation platform (Adnan et al., 2016). In the study a fraction of SimMobility was used - a Pre-day simulator. The Pre-day module is an ABM, used to obtain daily activity schedules of the entire synthetic population, including the timing (arrival time and departure time) of each activity at a resolution of 30 min, the destination at zonal level and the travel mode for each tour (Oh et al., 2020). The Pre-day simulation generated activity schedules for everyone in the population. The information was then processed using a Python script to represent the trip-chains of individuals in OD matrixes accepted as a demand input by the used traffic simulator – Aimsun Next (Aimsun, 2023). The traffic in Aimsun was simulated using microscopic traffic simulation with static path assignment combined with dynamic path reassignment for 40% of all vehicles.

For the second objective – to provide empirical evidence on the preferences of parking in the future, once new parking strategies, enabled by vehicle automation, emerge a stated preference survey was used. The respondents were confronted with four parking strategies: i) on-street parking nearby ii) dedicated parking area on the outskirts of the city iii) cruising and iv) sending AV back home with changing wait time for the AV and a parking pricing policy. The results of the survey were analysed through a mixed logit with latent variables.

Results

The results of the study show that the deployment of a SAV based service could be environmentally beneficial due to fleet electrification and sharing of rides. Nevertheless, behavioural changes could indeed lead to a significant rebound effect. The maximum obtained rebound effect resulted in 42% higher CO_2 emissions. The behavioural change that resulted in the highest magnitude of environmental rebound effect was the induced demand caused by citizens participating in more nonmandatory trips. However, the negative environmental rebound effect could be minimised by an optimal fleet size. Such fleet size should facilitate that users willing to switch from private modes towards shared rides do so, while those opting for sustainable modes remain using them. Those results are illustraded on the figure 2 hereunder. Moreover, further land use policies could be used to support a sustainable uptake of SAVs. For instance, if cities were to follow the 15-minute city trend, which aims to secure all required services in a proximity to the residential area, the usage of SAVs for induced demand would be lower, as citizens would rather opt for an active mode on short trips as they do nowadays.

Figure 82. Daily CO2 emissions in grams for analysed scenarios

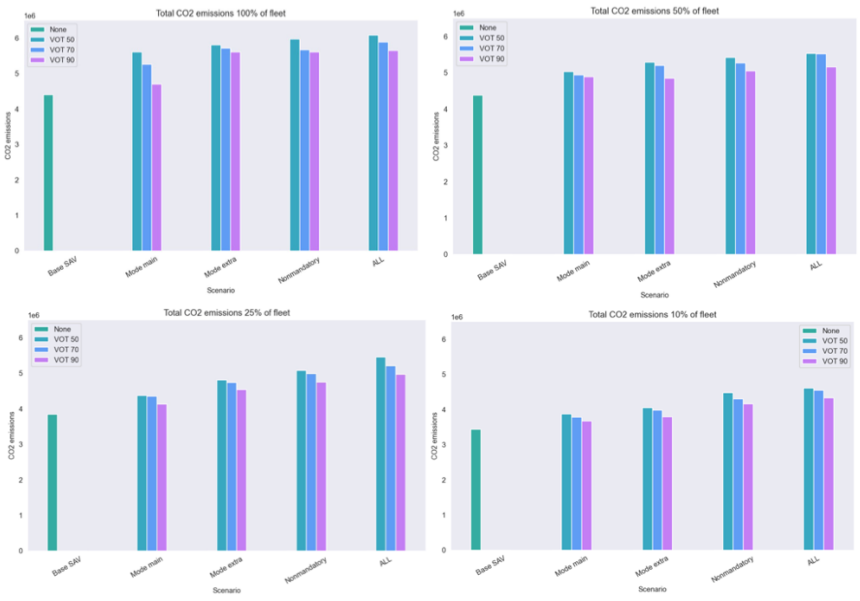

As per the future of parking preferences four latent variables were found to significantly impact the decision about the preferred parking option: environmental concern, innovativeness, AV acceptance and support for sustainable car-free cities. The results suggest that trusts towards AVs and innovativeness increase the probability of choice of unconventional parking strategies like allowing the vehicle to cruise or sending it back home. Therefore, whilst the massive deployment of AVs may still be a long way ahead, it is important to already encourage sustainable attitudes towards mobility in order to mitigate the risk of future negative externalities related to the uptake of those vehicles.

Conclusions

Overall, the main purpose of this research was to investigate how the introduction of new mobility services could impact the negative externalities of transportation. The results suggest that technology in this case could not solve all issues arising from transportation but could only support a sustainable transition. Along, the technological development a citizen and sustainability focused policy making is needed. However, if the deployment of transport services is to seriously lower the negative externalities a collaboration between service providers, regulators, citizens and academia is needed. In that way the services could be codesigned in living laboratories, where citizens could have a say in their development. Such procedure could be the most effective in terms of securing the sustainable transport sector in the future.

References

Adnan, M., Pereira, F., Lima Azevedo, C., Basak, K., Lovric, M., Raveau, S., Zhu, Y., Ferreira, J., Zegras, C., & Ben-Akiva, M. (2016, January 11). SimMobility: A Multi-Scale Integrated Agent-based Simulation Platform.

Aimsun. (2023). Aimsun Next Users Manual (Aimsun Next 22.0.1). https://docs.aimsun.com/next/22.0.1/.

Alonso Raposo, M., Ciuffo, B., Ardente, F., Aurambout, J.-P., Baldini, G., Braun, R., Christidis, P., Christodoulou, A., Duboz, A., Felici, S., Ferragut, J., Georgakaki, A., Gkoumas, K., Grosso, M., Portela, M., Julea, A., Krause, J., Martens, B., Mathieux, F., & Vandecasteele, I. (2019). The future of road transport—Implications of automated, connected, low-carbon and shared mobility. https://doi.org/10.2760/668964.

Garus, A., Alonso, B., Alonso Raposo, M., Ciuffo, B., & dell'Olio, L. (2022). Impact of New Mobility Solutions on Travel Behaviour and Its Incorporation into Travel Demand Models. Journal of Advanced Transportation, 2022, e7293909. https://doi.org/10.1155/2022/7293909.

Litman, T. (2023). Autonomous Vehicle Implementation Predictions: Implications for Transport Planning.

Oh, S., Seshadri, R., Azevedo, C. L., Kumar, N., Basak, K., & Ben-Akiva, M. (2020). Assessing the impacts of automated mobility-on-demand through agent-based simulation: A study of Singapore. Transportation Research Part A: Policy and Practice, 138, 367–388. https://doi.org/10.1016/j.tra.2020.06.004.

Ritchie, H., Roser, M., & Rosado, P. (2020). CO_2 and Greenhouse Gas Emissions. Our World in Data. https://ourworldindata.org/co2-emissions.

Identifying group travellers for modelling on-demand mobility

G. O. Kagho[a], M. Balac[a]

[a] *Institute of Transport Planning and Systems, ETH Zurich*

Introduction

Group travel is where more than one person travels together for a specific purpose. Group travellers are involved in interpersonal interactions and need to coordinate their schedules and preferences; they can be from the same or different households. Understanding group travel can inform the design and deployment of transport infrastructure and services. In particular to emerging on-demand mobility such as ridesharing, or shared autonomous vehicles (SAV), the correct estimation of group travellers is crucial for understanding their impacts on the transport infrastructure, e.g., in sizing fleet of vehicles or pricing and subsidy schemes. Also, SAVs would disrupt how people currently travel together. Newer group travel patterns may form as specific trips that usually facilitate group travel may change, for example, a person that may have required an escort may no longer need it, or friends may find it much more convenient to use an SAV.

Even with the growing importance of on-demand mobility, group travel is barely considered when modelling existing ridesharing services, even though these services have been shown to occur majorly during the weekends and for leisure trips where persons are more likely to travel in groups (Gehrke et al., 2021). The Swiss 2015 household travel survey (HTS)[19] shows that most weekend trips have a higher percentage of car passenger trips (about 19%) compared to weekdays (9%). The richer 2008 French National HTS data[20], shows that 64% of group trips are made within households, out of which 80% were made by car, 16% by walk and 3% by public transport (PT). For non-household group trips, 70% by car, 19% by walking and 8% by PT. Clearly, families or groups of friends tend to travel together and carpool. This makes it crucial to consider group travels when considering ridesharing services in travel demand models.

Agent-based models, have proven to be a powerful tool for modelling complex problems related to travel behaviour at the microscopic scale. With these models, policies and operational decisions for on-demand mobility that could directly impact travellers can be modelled to manage travel demand. However, the representation of group travel in these models is limited. This is because of the difficulty in identifying group travellers from most HTS data, resulting in agent-based and activity-based transport models where group travellers are separately modelled. In the past, there have been travel demand models related to group travel which focus on the household as the basic unit of analysis (Axhausen & Gärling, 1992; Arentze & Timmermans, 2009; Kang & Scott, 2008). However, these models address the interrelationship between individuals' travel behaviour with little focus on group travellers. Group travel has been studied from the aspect of familiar strangers, where smart card data from transit trips are used to identify social encounters (Sun et al., 2013) or those travelling together (Zhang et al., 2018). However, these studies are either limited in their focus on PT or have not been translated to modelling emerging mobility scenarios. Carpooling, considered a form of group travel, has been well-studied with a rise in models that match passengers to carpool drivers (Liu et al., 2020). These carpooling models place importance on the car driver's needs which decide pooling. Only a few implementations of agent-based models have started to feature group travel (Mallig & Vortisch, 2015).

Therefore, this study focuses on identifying group travellers for a given region where data on group travel is limited. The Swiss synthetic travel demand is used to identify potential group travellers, i.e., car drivers and passengers. A heuristic approach based on mixed integer linear programming is implemented to match car drivers and passengers while considering vehicle capacity constraints, and overall vehicle occupancy distribution of the region. Furthermore, an agent-based simulation model is set up to simulate ridesharing while considering group travel. This is to reveal the impact group travel can have on ride-sharing operational policies and the potential changes to group travel patterns with the use of SAVs.

Methodology

Group travel can be classified based on Furuhata et al. (2013)'s four patterns of ridesharing: identical, inclusive, partial, and detour ridesharing. For example, in identical ridesharing, both the origin and destination of the driver

---

([19]) BFS, Mikrozensus Mobilitat und Verkehr. https://www.bfs.admin.ch/bfs/de/home/statistiken/mobilitaet-verkehr/erhebungen/mzmv.html, 2015.

([20]) Ministry of Ecology, Enquête nationale transports et déplacements (ENTD) 2008, Publié le 05/12/2018 https://www.statistiques.developpement-durable.gouv.fr/enquete-nationale-transports-et-deplacements-entd-2008

and passenger are the same. In partial ridesharing, the pick-up and drop-off locations of the passenger are on the way of the driver's original route, but either the origin or the destination is not on the way. In this study, we first explore the problem of identifying group travellers as travellers with the same origin and destination and the similar departure time, using a car as their mode of travel, i.e., identical group travellers. The Swiss HTS surveys only one person per household and only captures when a person has taken a trip within a group, either as an accompanying person or as a car driver, including the number of people in the car. Information on whether they are from the same household or just friends is not captured. Using this information, car passenger trips have been identified and treated as their own distinct modes when generating the Swiss synthetic population for travel demand (Tchervenkov et al., 2022). In this study, we enrich a subset of the Swiss synthetic travel demand with information about group travellers based on the HTS. The focus is on Zurich city, extended by a buffer of 5km. The aim is to identify group travellers by matching car drivers and passengers using the Swiss synthetic travel demand for an average working day. The travel demand for Zurich is converted to a trip-based model, and only car and car passenger trips that start and end within the region are considered, leaving about 500,000 trips with a ratio of car drivers to passengers of 1.51 for an average weekday.

Matching

Matching problems are not new, as they occur wherever there is a need for a proper allocation of resources. Online matchmaking, network flows, and uber/taxi pickup problems are a few examples. They are sometimes described as classical assignment problems or graph problems. In this context of driver-passenger matching to identify group travellers, the problem follows a minimum weight matching in a bipartite graph problem, where we can represent each driver and passenger as a node, and draw an edge between a driver and a passenger if they can be matched. The weight of each edge represents the cost of the matching, which could be based on factors such as the distance between the origins and destinations of the driver and passenger or the departure time required for the trip. The following are assumptions for the matching:

- A travel group is made up of two or more persons, depending on the vehicle capacity, with only one person as a driver
- Persons in a travel group may be within the same household or among friends
- A travel group consist of persons whose trips have approximately the same departure time, point of origin, and destination

Therefore, given two subsets, N and M, representing car passengers and drivers, respectively, the problem instance is described by an *n X m* matrix *C,* where each c_{ij} represents the cost of matching node *i* of the first subset, car passengers, and node *j* of the second subset of car drivers. The goal is to find a complete matching of the drivers and passengers at a minimal cost while also satisfying certain constraints. These constraints include limits on the number of passengers matched to a single driver and requirements on the occupancy distribution of the vehicles in the region. The cost, in Equation 1, is defined as the sum of the weighted difference in departure time and weighted distance cost (derived from the sum of the distance between origin of the driver and the origin of the passenger and the distance between the destination of the driver and the destination of the passenger).

$$c_{ij} = \sum \alpha t_{ij} + (1 - \alpha) d_{ij} \quad (1)$$

where t_{ij} is the absolute difference in departure time between passenger *i* and driver *j*, and d_{ij} is the distance cost between passenger *i* and driver *j*. α is a weight applied to the departure time differences and the distance cost. An α value of 0.8 has been chosen to place more weight on time. The linear problem is thus formulated as follows:

Minimize

$min \sum_{i=1}^{n} \sum_{j=1}^{m} c_{ij} x_{ij}$, (x_{ij} = 1 if passenger i is matched with driver j otherwise 0)

Subject to:

Each passenger is assigned one driver: $\mathrm{i} = 1, \ldots, n \sum_{j=1}^{m} x_{ij} = 1$

Each driver is assigned at most k passengers, $\mathrm{j} = 1, \ldots, \mathrm{m} \sum_{j=1}^{n} x_{ij} \leq k$

The problem can be seen as a variant of the classical assignment problem studied by researchers using various methods, including mixed-integer linear programming (MILP) and solvers such as Gurobi or CPLEX. However, the problem formulated above is not a standard matching problem, given that N and M can be as large as 500,000 elements; solving this problem using a MILP solver can be computationally expensive and may not

scale well. Therefore, a heuristic method is proposed to solve the problem. The algorithm implements a greedy approach to find the minimum cost pairing between drivers and passengers by iteratively choosing the next best match. A match is considered best if it meets the following conditions:

1. The driver has not reached the maximum number of matches.
2. The cost of pairing with the current driver is lower than with any other driver.
3. The number of matches for the current driver is within the specified vehicle occupancy distribution range.
4. The number of drivers with the current number of matches is less than the occupancy distribution value for that number of matches.

The code's efficiency depends on the size of the cost matrix and the specific input data. The algorithm has a time complexity of O(n^2), where n is the number of passengers and drivers. To account for the size of the cost matrix, time bins are used to select driver candidates for matching. A minimum threshold for the number of candidates is set to ensure that there are adequate candidates for efficient matching. In this study, the threshold is at 30 for a 10 minutes time bin whereby drivers before and after the selected time bin are also considered. When the threshold value is not met, the time bin is expanded. In the results, we show validation of the matching model.

Simulation Framework

The multi-agent transport simulation framework MATSim (Horni et al., 2016) is used for this study and extended to include the capability for ridesharing and group travel. MATSim provides the ability to model large-scale transport systems realistically. To represent a fleet managing system for shared autonomous vehicles (SAVs) that allows for pooling and group travel, the MATSim demand-responsive transit (DRT) extension is used (Bischoff et al., 2017). A constraint for group travel is added to the dispatching algorithm to check the number of passengers in the vehicles to ensure enough seats to accommodate group travel requests.

Findings

Here are the initial findings from validating the matching algorithm and simulation of the ridesharing scenario with group travel behaviour.

Figure 1 shows the validation of the matching algorithm in terms of how well the vehicle occupancies are represented and their distribution by distance. It compares the vehicle occupancy and distance distribution of trips obtained from the HTS, to the matching results. Although, as the vehicle occupancy increases, the difference between the distribution from the current matching algorithm and the Swiss HTS increases. This is possibly due to the more weight applied to departure time; the next step is a sensitivity analysis to test how different α values weighing on the distance or departure time affects the results. Overall, the algorithm shows promising results.

Figure 83. Distribution of vehicle occupancy by distance (Sim: synthetic population, HTS: Swiss HTS)

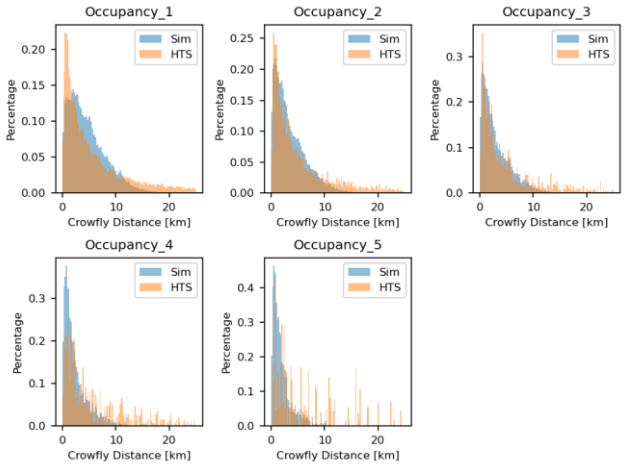

Further results from the initial ridesharing simulation reveal a reduction in ridesharing requests, as expected when group travel is considered. This inadvertently translates to the lower wait and detour times for the riders. On average, the vehicles in the "group" scenarios pooled more passengers than in non-group scenarios with a relative difference of up to 38%. Effect on group travel patterns is the next step in the analysis.

Conclusion

This study is a first step to open discussion and research on the inclusion of group travel behaviour in ridesharing simulations and provides several opportunities for future work. The study proposes a methodology for modelling group travel in cases whereby, in the transport model, typically agent-based and activity-based models, car drivers and passengers are modelled separately, and there is available data on distributions of vehicle occupancy.

References

Arentze, T. A., & Timmermans, H. J. (2009). A need-based model of multi-day, multi-person activity generation. Transportation Research Part B: Methodological, 43(2), 251-265.

Axhausen, K. W., & Gärling, T. (1992). Activity-based approaches to travel analysis: conceptual frameworks, models, and research problems. Transport reviews, 12(4), 323-341.

Bischoff, J., M. Maciejewski, and K. Nagel, City-wide shared taxis: A simulation study in Berlin. In 2017 IEEE 20th international conference on intelligent transportation systems (ITSC), IEEE, 2017, pp. 275–280.

Gehrke, S. R., Huff, M. P., & Reardon, T. G. (2021). Social and trip-level predictors of pooled ride-hailing service adoption in the Greater Boston region. Case Studies on Transport Policy, 9(3), 1026-1034.

Furuhata, M., Dessouky, M., Ordóñez, F., Brunet, M. E., Wang, X., & Koenig, S. (2013). Ridesharing: The state-of-the-art and future directions. Transportation Research Part B: Methodological, 57, 28-46.

Tchervenkov, C., Kagho, G. O., Sallard, A., Hörl, S., Balać, M., & Axhausen, K. W. (2022). The Switzerland agent-based scenario. Arbeitsberichte Verkehrs-und Raumplanung, 1802.

Horni, A., K. Nagel, and K. W. Axhausen, Introducing MATSim. Ubiquity Press, 2016.

Mallig, N., & Vortisch, P. (2015). Modeling car passenger trips in mobiTopp. Procedia Computer Science, 52, 938-943.

Liu, X., Titheridge, H., Yan, X., Wang, R., Tan, W., Chen, D., & Zhang, J. (2020). A passenger-to-driver matching model for commuter carpooling: Case study and sensitivity analysis. Transportation Research Part C: Emerging Technologies, 117, 102702.

Kang, H., & Scott, D. M. (2008). An integrated spatio-temporal GIS toolkit for exploring intra-household interactions. Transportation, 35, 253-268.

Sun, L., Axhausen, K. W., Lee, D. H., & Huang, X. (2013). Understanding metropolitan patterns of daily encounters. Proceedings of the National Academy of Sciences, 110(34), 13774-13779.

Zhang, Y., Martens, K., & Long, Y. (2018). Revealing group travel behavior patterns with public transit smart card data. Travel Behavior and Society, 10, 42-52.

A hierarchical approach to solve p-Mobility hub location problems to reduce carbonization

M. Bencekri[a], D. Kim[a], Donggyun Ku[b], D. Lee[c], S. Lee[d], S. Lee[b]

[a] *Department of Transportation Engineering / Smart Cities, University of Seoul, Korea*

[b] *Department of Transportation Engineering, University of Seoul, Korea*

[c] *Graduate School of Environmental Studies, Seoul National University, Korea*

[d] *Department of Transportation, Seoul Institute, Korea*

Abstract

This research investigates the optimal placement of mobility hubs in Seoul to mitigate greenhouse gas emissions by reducing travel time, energy consumption, and carbon emissions while enhancing coverage. A hierarchical approach is adopted for the hub location problem (HLP) to identify the most efficient locations. Initially, a coverage maximization strategy is employed using a sorting algorithm, resulting in a list of potential hub sites. Next, the genetic algorithm (GA) is applied to this list to minimize travel time, carbon emissions, and energy consumption, aligning with the principles of the uncapacitated single allocation p-median HLP. Finally, GIS location-allocation analysis is employed to maximize the market share through a gravity model that allocates demand to each hub site, considering the potential competition. This comprehensive methodology led to the selection of mobility hub sites situated in dense and dynamic regions of Seoul, replete with business offices, markets, transit stations, and employment centers, bolstering the study's validity and reliability.

Introduction

Amid rising climate change concerns, the transportation sector's contribution to carbon emissions necessitates efficient solutions. Mobility hubs, which integrate various transport modes, are seen as a key decarbonization strategy. However, the Hub Location Problem (HLP), which involves selecting optimal hub locations to optimize various objectives, is complex. While greener transportation models have emerged, integrating environmental costs into optimization processes, a gap exists in considering socioeconomic factors influencing travel patterns.

Addressing this, our study innovatively expands on existing models by integrating travel time, environmental factors, and socioeconomic elements in optimizing mobility hub locations in Seoul, a city known for its high traffic congestion. Through a hierarchical approach to HLP, our research first maximizes fixed-cost coverage, factoring in population, employment densities, parking capacity, and land use mix index. The second stage minimizes travel time, energy consumption, and carbon emissions, utilizing a new objective function for the uncapacitated single allocation p-median HLP.

Thus, our research presents a novel, comprehensive solution to optimizing mobility hub locations, emphasizing sustainability and efficiency while being responsive to local population needs, filling a crucial gap in the current landscape of transportation optimization models.

Methodology

This research employs a hierarchical three-stage hub location optimization modeling to select the best subdistricts to implement mobility hubs (**Figure 84**). For stage-1, the optimization was formulated using the sorting algorithm with a summation-based cost function of a set of predetermined criteria. These criteria include population and employment densities, parking capacity, public transit station number, bike station number, and land use mix index. For stage-2, the uncapacitated single p-median HLP is implemented, while developing a new cost equation that includes travel time, carbon emissions, and energy consumption. Finally, stage-3 consists of a GIS location-allocation optimization based on maximizing the market share method and using the traffic volume as a wight.

Figure 84 Research Flow Chart

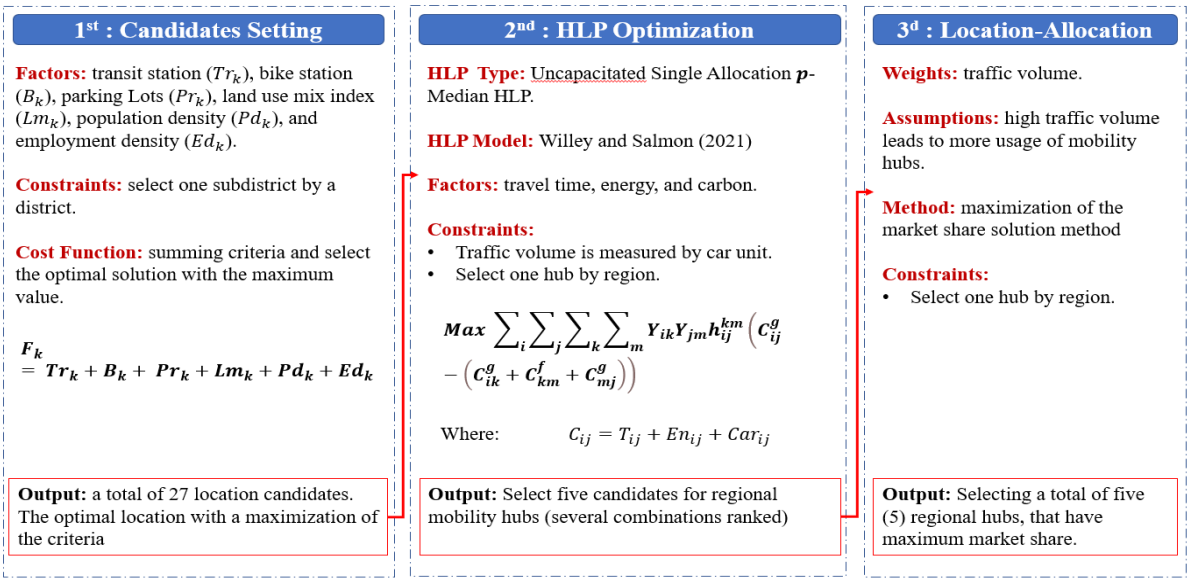

First, the study formulated a sorting algorithm to choose optimal hub locations. The model evaluates city subdistricts based on set criteria and picks high-performing ones from different districts to balance geographic distribution, ultimately boosting demand and coverage. These criteria include: the transit station number (Tr_k), bike station number (B_k), parking capacity (Pr_k), land use mix index (Lm_k), population density (Pd_k), and employment density (Ed_k). The sorting algorithm model's cost function F_k (1) is a summation of these criteria. The goal is to find the optimal candidate solution, maximizing the selected parameters' total values while selecting only one by the corresponding district.

For the second stage, the study adopted the Hub Location Problem (HLP) to select the best mobility hub sites. The HLP involves choosing p hubs from potential candidates, with each non-hub node assigned to one hub, considering the lesser cost of hub-to-hub connections. This study enriches the problem formulation with works by O'Kelly (1987), Wiley and Salmon (2021), Farahani et al. (2013), and Contreras et al. (2011). The latter offered a model for incomplete hub networks, contributing to a more realistic HLP optimization.

A Genetic Algorithm (GA) is employed in this study, proven for its effectiveness in solving similar integer and non-convex optimization problems. GA, inspired by natural evolution, seeks near-optimal solutions for NP-hard problems. It has successfully been applied in diverse fields, including electric vehicle charging stations' location and transportation network configuration.

Diverging from prior research, this study uses GA to determine hub locations that minimize both travel costs and environmental impacts, such as carbon emissions and energy consumption. This strategy selects sites that reduce travel time and environmental pollutants most effectively. Cost in this context includes travel time, energy consumption, and carbon emissions, assumed as linear functions of travel speed. GA's primary steps include initialization, selection, and crossover mutation, aiming to find the global solution to the mobility hubs' location problem. The algorithm's performance is assessed through mutation rate and generation number, identified through trials.

As a third step, this study exploited the GIS location-allocation method, which can identify optimal facility locations for different purposes. This method, used in studies like Mix et al. (2022), factors in demand points, potential locations, travel time, and capacity constraints. The location-allocation tool in ArcGIS optimizes objectives like cost minimization, coverage maximization, supply-demand balance, and impedance minimization. For an effective application, the problem should be accurately defined, including the number of facilities, potential and customer locations, capacities, costs, and demand levels. The study at hand uses the market share maximization method to find locations with maximum potential ridership, capturing customer behavior, facility attractiveness, and competitive dynamics accurately.

Results and Discussion

This study aims to optimize the location of regional mobility hubs in Seoul's five key regions: central, east-north, west-north, east-south, and west-south, with one hub per region. The first stage of optimization employs a personalized sorting algorithm to select high-performance subdistricts based on predetermined criteria: transit

and bike station numbers, parking capacity, land use mix index, population, and employment density. This process results in an initial set of 27 candidate locations, which are then further refined through a genetic algorithm in the study's second stage, adopting the HLP optimization.

According to GA, several neighborhoods were selected by each region. The algorithm's objective function was to minimize total transportation costs of travel time, carbon emissions, and energy consumption. The chosen areas for mobility hubs in Seoul's central, east-north, west-north, west-south, and east-south regions are predominantly business districts, shopping areas, and neighborhoods with high commuter activity. These areas contain significant transfer stations, universities, and densely populated zones handling intra and intercity commutes. The GA results, which showed a good fitness function (**Figure 85**), indicate a strong focus on travel volume, but this approach lacks consideration for other important factors like socioeconomic conditions and geographical indicators.

Addressing existing research gaps, this study uses the location-allocation method in ArcGIS to optimize Seoul's mobility hub locations. The strategy integrates travel time, GPS demand data, and gravity models to balance demand allocation. It considers subway station impact and hub competition, ultimately identifying the optimal sites for hubs.

Figure 85. Results of GA Optimization and Location-Allocation

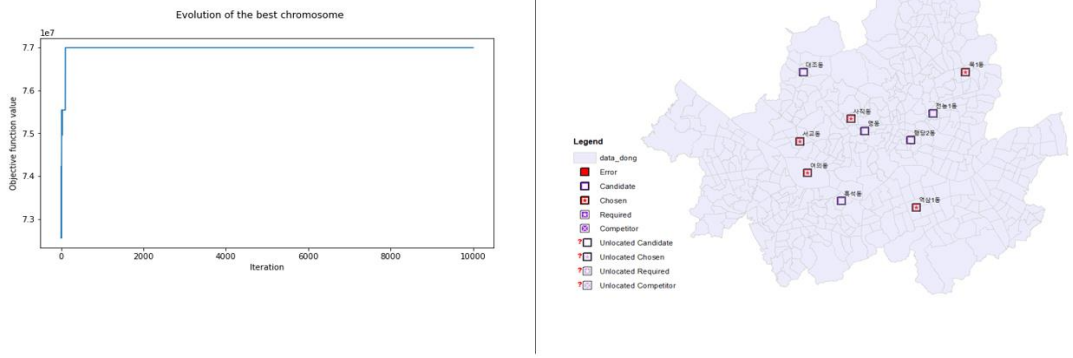

The selection of optimal mobility hub locations in this study has considered the unique characteristics and demands of different regions in Seoul. By strategically placing hubs in bustling central areas with business offices, shopping centers, and tourist attractions, the mobility hubs can serve both office workers and tourists, maximizing their potential usage. The placement of hubs in west-south and east-south districts, known for their dynamic business environments, allows them to effectively cater to the needs of city commuters. In the east-north region, the selection of hubs near multiple transit stations enables them to accommodate commuters traveling from outside the city, providing a convenient transfer point. Lastly, the choice of the west-north region, which is densely populated with universities and shopping areas, ensures that the mobility hubs can efficiently serve the transportation needs of numerous students. By considering these factors, the study aims to enhance the convenience and accessibility of the mobility hub network, benefiting a wide range of users throughout Seoul.

Conclusion

This study introduces an innovative methodology that addresses the optimization of mobility hub locations in Seoul, aligning with the city's long-term vision outlined in the 2040 Plan. The plan's key objectives revolve around creating pedestrian-friendly environments, enhancing public and shared transit networks, and strategically implementing mobility hubs. The selection of optimal hub locations is crucial for maximizing their service areas and overall potential impact. Policymakers can utilize the findings and recommendations from this research to consider various socioeconomic and transportation factors when making decisions on mobility hub placement. By incorporating regional characteristics, such as the presence of commuters, students, or tourists, policymakers can ensure efficient utilization of resources and meet the diverse needs of different user groups. This study serves as a solid foundation for future mobility hub initiatives within Seoul, offering valuable insights and guidance for sustainable and effective urban development.

Acknowledgment

This work was supported by the Architecture & Urban Development Research Program in the Ministry of Land, Infrastructure, and Transport of the Korean government (19TLRPB148659-02).

References

Contreras, I., Cordeau, J. F., & Laporte, G. (2011). Stochastic uncapacitated hub location. European Journal of Operational Research, 212(3), 518-528. https://doi.org/10.1016/j.ejor.2011.02.018.

Farahani, R. Z., Hekmatfar, M., Arabani, A. B., & Nikbakhsh, E. (2013). Hub location problems: A review of models, classification, solution techniques, and applications. Computers & Industrial Engineering, 64(4), 1096–1109. https://doi.org/10.1016/j.cie.2013.01.012.

Mix, R., Hurtubia, R., & Raveau, S. (2022). Optimal location of bike-sharing stations: A built environment and accessibility approach. Transportation Research Part A: Policy and Practice, 160, 126–142. https://doi.org/10.1016/j.tra.2022.03.022.

O'Kelly, M. E. (1986). The Location of Interacting Hub Facilities. Transportation Science, 20(2), 92–106. https://doi.org/10.1287/trsc.20.2.92.

Willey, L. C., & Salmon, J. L. (2021). A method for urban air mobility network design using hub location and subgraph isomorphism. Transportation Research Part C: Emerging Technologies, 125(January), 102997. https://doi.org/10.1016/j.trc.2021.102997.

Gaps in Accessibility Levels and Potential Travel Demand in Public Transport Services: A Case Study of Porto Metropolitan Area

A. Mudassar Shafiq[ab], B. Hudeyron Rocha[ab], C. Sara Ferreira[ab], D. António Couto[ab]

[a] *Faculdade de Engenharia da Universidade do Porto, Porto, Portugal*

[b] *CITTA - Centro de Investigação do Territórios dos Transportes e Ambiente, Porto, Portugal*

Introduction

The development and expansion of the urban areas have led to increase in the demographics and the socioeconomic activities, creating a need for various modes of transportation. Public transportation (PT) plays a crucial role in providing sustainable alternative modes to private vehicles, and its availability and accessibility are of utmost importance in cities. PT systems are becoming a significant mode of transportation because the increase in car dependence and larger share of trips by car are damaging the physical well-being, health, and the environment. Another important aspect is the social aspect that there is a large segment of the population who do not own private cars are dependent on the availability and access to the PT services Litman, (2005). The provision of PT services and changes in the demographics and travel patterns over time have resulted serious spatial and social gaps the in accessibility to these services, with many travellers with not enough access to them Mavoa et al., (2012).

Accessibility is defined as the ability or the ease to reach the desired destinations by the available transport services by Hansen, (1959); Stępniak et al., (2019). The key is to reduce the mobility gap between travellers and the available services Welch, (2013) so that people would have more access to daily activities. Therefore, there is a need to analyse the accessibility to the existing PT systems and the potential demand for these services and identify and overcome the gaps for future travel demand. In the methodology section, we discuss and define suitable measures for accessibility and potential demand for this study.

Methodology

The aim of this study is to develop a methodology on the lowest possible spatial scale to accurately assess the existing levels of accessibility to rail and metro services in the PT system and measure the demand for these services. The case study for this analysis is the Porto Metropolitan Area (AMP), which comprises of 17 municipalities in the northern part of Portugal. The AMP region is served by 8 metro and rail lines with a total 152 stops represented by Figure 1.

Figure 86. Porto Metropolitan Area (AMP)

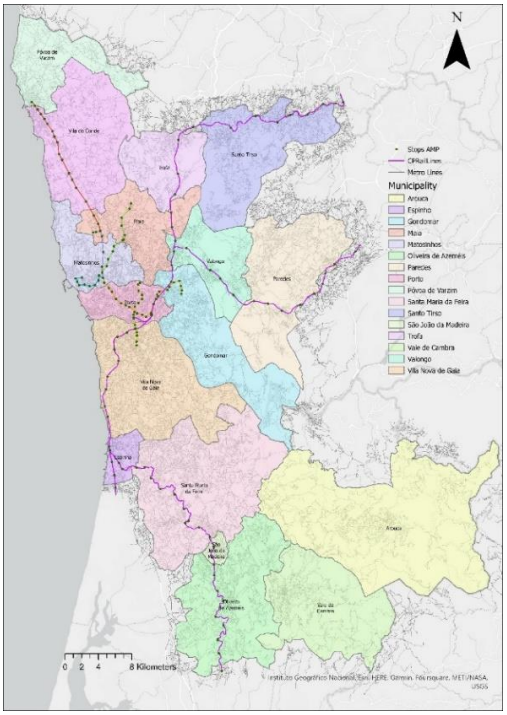

To evaluate the potential demand and calculate the accessibility index gravity measures were used for active modes (i.e., walking, cycling) and motorized modes including private cars and buses using travel distances. Gravity measures provide more composite results as it can incorporate the minimum travel distances between origins and destinations, distance decay parameters associated with the modes and the attraction at the destinations as a sum of opportunities available Neutens et al., (2010) and Vale & Pereira, (2017). To calculate the accessibility index A_i, we start by calculating the minimum travel distances from every subsection (lowest level of geographical scale) to the nearest station using a geographical information system tool ArcGIS. In the gravity measure used also incorporates a distance decay parameter λ and the supply (attraction) at the station in terms of frequency as presented below by Eq. 1.

$$A_i = a_j * e^{-\lambda d_{ij}} \qquad \text{Eq. 1}$$

Where λ is the mode decay parameter, d_{ij} is the minimum travel distance and a_j is the attractiveness at station j.

Additionally, to calculate the potential demand, we use the mobility survey conducted in 2017 in the AMP which provides a detailed information about the travel patterns including the trips by modes, travel distances and the origin of the trips. The potential travel demand index for active and motorized modes is calculated using the number of trips and average trip distances by the considered modes in every subsection and the total population that is the potential of that subsection to generate demand is given by Eq. 2.

$$D_i = Pop_i * e^{-\lambda d_{ij}} \qquad \text{Eq. 2}$$

The comparison of the accessibility index and the demand index provides results about the gaps that exists in the accessibility of the PT services by the modes and the potential travel demand at the subsections. As it is important to identify the areas where people either don't have the access or lack the access available to fulfil the need of the demand for PT services and therefore, the potentiality to invest and promote the PT services.

Findings

The findings indicate that there exists a demand for the use of PT services but however many people in the AMP are unable to use the PT services effectively mainly due to limited access to the stations and low levels of supply (i.e., frequency of rail and metro services). It can also be concluded that incorporation of better bus services can increase the mode share of the public transportation in the region. It is important to consider the demand effect for various modes and evaluate the demand-sustainability of the system in terms of modal shift in an equitable PT network.

Conclusions

In a sustainable urban environment, it is important that public services such as PT to fulfil the very purpose they are built for, which should be ensured by planners, designers, policy makers and decision makers. The social and physical structures of the urban society are critical in the context of the problem. There is a need to improve the traditional design and planning approaches by promoting more accessible and sustainable PT systems, and avoiding solutions that result to social exclusion. In this study, the developed methodology will help to assess and evaluate PT systems, with a focus on the solutions to make them more:

- accessible: in a way that people can easily reach and have access to PT services.
- demand sustainable: by improving the current and integrating new services in a way that make the services more demand sustainable and accessible, so that more and more people benefit from the services provided, resulting in a shift of commuters previously using private cars to public transport.

Acknowledgments

This work is funded by:

- The Portuguese Foundation for Science and Technology (FCT) through the grant agreement 2020.05098.BD.
- The project DynamiCITY: Fostering Dynamic Adaptation of Smart Cities to Cope with Crises and Disruptions, with reference NORTE-01-0145- FEDER000073, supported by Norte Portugal Regional Operational Programme (NORTE 2020), under the PORTUGAL 2020 Partnership Agreement, through the European Regional Development Fund (ERDF).

References

Hansen, W. G. (1959). How Accessibility Shapes Land Use. *Journal of the American Planning Association*, *25*(2), 73–76. https://doi.org/10.1080/01944365908978307.

Litman, T. (2005). Evaluating Transportation Equity: Guidance for Incorporating Distributional Impacts in Transportation Planning. *Victoria Transport Policy Institute, Victoria, British …*, *8*(2), 50–65. http://scholar.google.com/scholar?hl=en&btnG=Search&q=intitle:Evaluating+Transportation+Equity+Guidance+For+Incorporating+Distributional+Impacts+in+Transportation+Planning+by#2.

Mavoa, S., Witten, K., McCreanor, T., & O'Sullivan, D. (2012). GIS based destination accessibility via public transit and walking in Auckland, New Zealand. *Journal of Transport Geography*, *20*(1), 15–22. https://doi.org/10.1016/j.jtrangeo.2011.10.001.

Neutens, T., Schwanen, T., Witlox, F., & de Maeyer, P. (2010). Equity of urban service delivery: A comparison of different accessibility measures. *Environment and Planning A*, *42*(7), 1613–1635. https://doi.org/10.1068/a4230.

Stępniak, M., Pritchard, J. P., Geurs, K. T., & Goliszek, S. (2019). The impact of temporal resolution on public transport accessibility measurement: Review and case study in Poland. *Journal of Transport Geography*, *75*(July 2018), 8–24. https://doi.org/10.1016/j.jtrangeo.2019.01.007.

Vale, D. S., & Pereira, M. (2017). The influence of the impedance function on gravity-based pedestrian accessibility measures: A comparative analysis. *Environment and Planning B: Urban Analytics and City Science*, *44*(4), 740–763. https://doi.org/10.1177/0265813516641685.

Welch, T. F. (2013). Equity in transport: The distribution of transit access and connectivity among affordable housing units. *Transport Policy*, *30*, 283–293. https://doi.org/10.1016/j.tranpol.2013.09.020.

Exploring the Multi-modal Demand Dynamics During Transport System Disruptions

A. A. Shateri Benam[a], B. A. Furno[a], C. N. El Faouzi[a]

[a] *LICIT-ECO7, ENTPE, Univ. Gustave Eiffel*

Introduction

Human mobility in the urban context follows specific patterns and cycles [1]. These patterns are prone to short-term divergences or long-term changes. Disruptive events such as extreme weather conditions, road or public transport accidents, or large-scale events can disrupt the usual flow of urban travel. In response to such events, passengers exhibit heterogeneous responses depending on various factors, including their original mode of choice and the nature and timing of the disruption [2]. While these responses may include the cancellation or delay of trips, this study seeks to investigate the inter-modal shifts that occur during such disruptive events.

Previous research has examined the passenger responses to disruptions in transport systems using surveys [3,4] and mobile or public transport ticketing data to analyse the demand dynamics between two specific modes during certain events [5,6]. However, current literature lacks an integrated, automated approach that goes beyond single-kind disruption events and accounts for multiple urban transport modes. This study aims to follow that approach in identifying disruptions and exploring the associated multi- and inter-modal demand dynamics.

Utilising multi-source data from various entities, we have developed methods for detecting and classifying anomalous multi-modal travel demand using machine learning techniques. By leveraging urban mobility data related to the city of Lyon, France, we have identified several forms of passenger response to disruptions through travel demand anomalies. Our approach is innovative in its data-driven analysis of complex multi-modal demand dynamics during disruptive events. This study aims to inform the development of more effective strategies for mitigating the negative impacts of transport network disruptions.

Data and Methodology

We present a methodological framework for exploring the multi-modal dynamics through anomalous demand detection. We use road traffic, public transport and shared-bike data at our disposal. Our road data comes from a Floating Car Dataset (FCD), which provides timestamped geo-localised data collected via GPS from moving vehicles. Each observation in the FCD data captures information such as the corresponding vehicle ID's speed, direction, and map-matched link identifier with an average observation frequency of 30 seconds. The public transport data is obtained from Lyon's public transport provider and includes ticket validation data for trams, metro, and bus lines. Each validation record in the dataset includes temporal information of said validation with its corresponding line. Finally, we incorporate the shared-bike data from Lyon's Velo'V bike-sharing service, which contains information about bike retractions and returns and their stations. We follow our methodology through 4 steps, shown in Figure 1.

Figure 87. Methodology flowchart

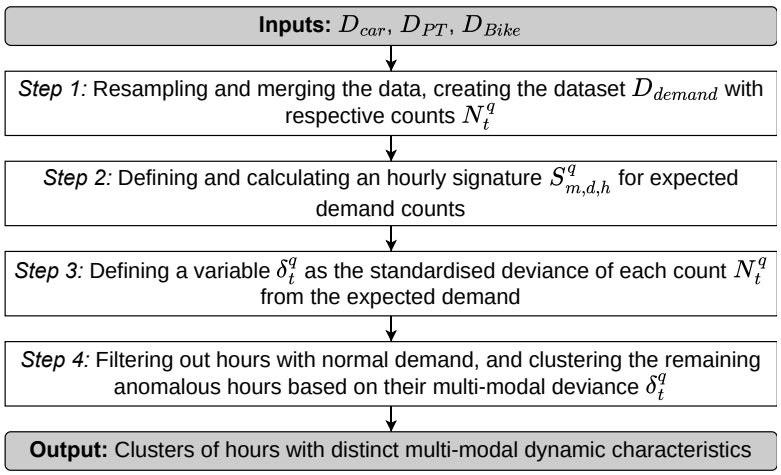

Step 1: First, we constructed a compressed representation of the typical demand for each transport mode by unifying our multi-source datasets. By aggregating observations hourly, we combined three datasets (D_{car}, D_{PT},

and D_{Bike}) into one unified dataset, D_{demand}. The hourly number of observations in the FCD dataset is related to the city-wide number of moving cars on the road network and is thus assimilated to an hourly count for car demand. The number of hourly ticketing validations for public transport modes is associated with the hourly demand for the respective mode. The hourly number of shared-bike retractions is used to indicate shared-bike demand. The final pre-processed dataset is denoted as $D_{demand} = \{N_t^q\}$. N_t^q represents the observed demand count for mode *q* on the generic 1-hour time slot *t* from the data availability period, and *q* ∈ **Q** = {*bus, tram, metro, bike, car*}.

Step 2: We adapt and extend the approach initially proposed in [7] by defining a rolling signature describing the expected demand on each mode for a given reference period (one week). Such a signature, defined on 24*7 hourly time period, is a compressed representation computed from previous and future observations of demand counts. Specifically, the expected behaviour for a given week *m*, is computed over a temporal support (W_m^K, *d, h*). $W_m^K \subset$ **M** represents the subset of weeks, of size K (a hyper-parameter of our approach), from the available set of weeks (**M),** related to a specific temporal reference point (a given week number *m*), with the reference point itself excluded from the subset of weeks. *d* ∈ **Δ**, represents the weekday variable from an ordered set of selected weekdays **Δ**. *h* ∈ **H**, represents the hour of the day variable from an ordered set of selected hours **H**. It is worth noting that the (W_m^K, *d, h*) support identifies a set of time slots that will be considered for aggregation during the computation of the signature. Based on the temporal support (W_m^K, *d, h*) and transport mode ∈ **Q**, the signature element $S^q_{(m,d,h)}$ is defined as Equation 1.

$$S^q_{(m,d,h)} = \mu^q_{(W_m^K,d,h)} \pm \lambda^q_{(W_m^K,d,h)} \qquad \text{Equation 1}$$

Setting the number of weeks *K* for our temporal support to 4, $\mu^{q}_{(W^{4}_{m},d,h)}$ represents the average demand counts for the mode *q*, hour *h*, and weeks *m-2, m-1, m+1, and m+2*. The standard deviation for the same set of hours is denoted as $\sigma^q_{(W^K_m,d,h)}$, and the range amplitude of the signature $\lambda^{q}_{(W^K_m,d,h)}$ is defined as the product of a coefficient α and the hourly standard deviation $\sigma^q_{(W^K_m,d,h)}$. Through a sensitivity analysis based on the knee curve method [8], we determined the standard deviation hyper-parameter α for the range amplitude to be 4, therefore $\lambda^{q}_{(W^K_m,d,h)} = 4 \times \sigma^q_{(W^K_m,d,h)}$. Around 15% of the hours in 2019 and 2020 fall outside the expected signature produced by this range amplitude.

Step 3: To assess the distance of observed demand from the expected average demand for a particular mode at a given hour, a continuous variable δ_t^q is defined as formulated in Equation 2. By pivoting the data on the deviance variable δ_t^q, we produce a dataset $D_{deviance}$ with transport modes for columns, hours for rows, and standardised deviance of expected demand for values.

$$\delta_t^q = \frac{N_t^q - \mu^q_{(W_m^K,d,h)}}{\sigma^q_{(W_m^K,d,h)}} \qquad \text{Equation 2}$$

Step 4: As we are solely looking through anomalous hours for their categorisation, we omit hours in which demand in all modes falls inside the expected signature in a new dataset denoted as $D_{anomaly}$. This dataset is produced by filtering out regular hours; thus, it only includes hours where at least one mode's absolute value of deviance $|\delta_t^q|$ is bigger than the range amplitude of the signature $\lambda^{q}_{(W^K_m,d,h)}$. We then apply clustering to this dataset to categorise various anomaly forms regarding multi-modal demand dynamics.

Results

Following our previous study, we hypothesised to observe distinct types of multi-modal dynamics in disruptions, and we applied agglomerative clustering with a cosine distance to our $D_{anomaly}$ dataset. As our research focuses on discrete forms of multi-modal passenger response, we adopt the Davies-Bouldin method for obtaining an optimal number of clusters [9]. The method indicates 11 as the optimal number for clusters to be as non-identical as possible.

We conducted clustering and labelled each hour with the cluster number. We selected all hours belonging to each cluster to exhibit how each cluster manifested a particular multi-modal dynamic. We averaged the

deviance δ_t^q for each mode and produced a demand dynamic profile for each cluster. We then used radar plots to illustrate these multi-modal dynamic profiles. Additionally, we labelled the dates and the hours of anomalies belonging to each cluster to explore their temporal correspondence to traceable events.

The multi-modal dynamics of clusters were adequately explainable by ground truth (news and weather data). We present three clusters of anomalous data and their interpretation (other clusters are not reported due to space limitations). The radar plot for each cluster displays different modes' deviance δ_t^q averaged among the hours belonging to the corresponding cluster. For example, a value of +1 on the plot indicates that, on average, demand counts belonging to the cluster's hours have been one standard deviation above the temporal support's average demand.

Figure 88. Left: Average multi-modal demand deviance in Cluster 1; Middle: Average multi-modal demand deviance in Cluster 2; Right: Average multi-modal demand deviance in Cluster 3

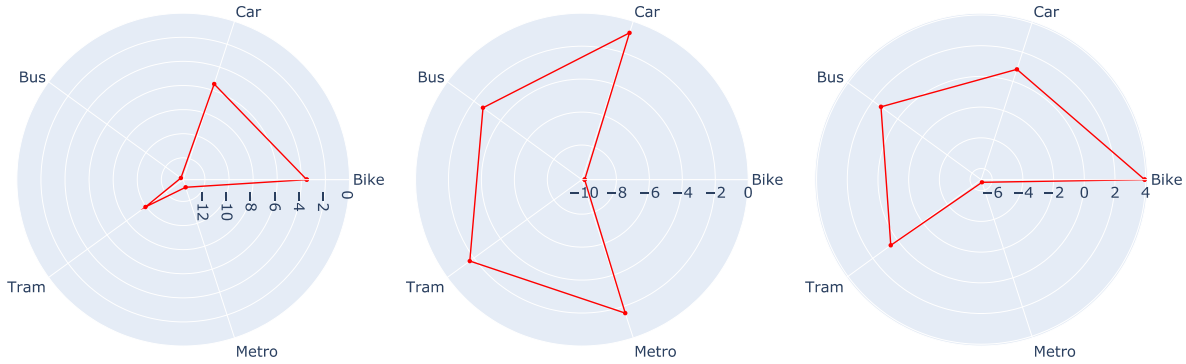

The radar plot representing the average deviance of each mode in *Cluster 1* is exhibited in Figure 2. The plot indicates negative deviance from the expected average demand in all modes. However, the demand for public transport modes is much lower than the expected average demand. *Cluster 1* covered around 36% of all anomalous hours through 2019 and 2020. The hours of *Cluster 1* were not scattered and were mostly continuous for several hours. Using France's holiday calendar for 2019 and 2020, we verified that the hours belonging to this cluster were mainly affiliated with national holidays, such as Christmas, New Year's, and Easter holidays.

Figure 3 illustrates the average deviance of each mode in *Cluster 2,* which covers 17.5% of all anomalous hours through 2019 and 2020. This plot shows the demand dynamics of anomalous hours in which a slight decrease in demand for all modes and a sharp decrease in shared-bike use are observed. Building from our previous study, we hypothesised that this cluster might represent instances of anomaly where the use of shared bikes has been negatively affected by precipitation. We made use of Lyon's meteorological data to test this hypothesis. The meteorological data at our disposal consists of hourly recorded information on precipitation, wind and their properties. To put our hypothesis to the test, we employed a one-sample student's t-test (a reference here) to determine if the precipitation rate is significantly higher during the hours marked with *Cluster 2's* label. The t-test results prove that the precipitation during Cluster 2 hours is significantly higher than the entire hours, with a t-value of 5.03 and a P-value of $7.29*10^{-7}$.

Cluster 3 covers around 1% of all anomalous hours, and as shown in Figure 4, the hours in this cluster exhibit metro validations with an average negative deviance of -6. At the same time, other public transport modes and road traffic exhibit slight positive average deviance, while shared bikes demonstrate significant positive deviance. Such dynamics may reflect disruptions in the metro service, leading passengers to shift to other modes. Our hypothesis was verified by investigating the news articles through calendar hours labelled with Cluster 3. These hours corresponded to metro closure events where some metro lines or stations were closed (such as terrorist attacks, bomb suspicions, and human accidents). Another point in the calendar belonging to this cluster was Lyon's festival of lights, where metro service was announced free for the afternoon, resulting in zero metro validations.

Conclusion

This study explores the complex network-wide multi-modal demand dynamics under disruptions. Specifically, we examined the case of Lyon by unifying multi-source data and defining a normal/expected range of hourly demand for each mode of transportation. By identifying anomalous instances where demand fell outside this

range, we applied clustering techniques to investigate the various distinct multi-modal passenger responses to these disruptions. The clusters formed from the abovementioned method revealed significant variations in their multi-modal dynamics. These dynamics were analysed on ground truth, three examples were presented, and their interpretations were explained. We plan to continue this study by diving more deeply into a more predictive approach by training machine-learning regression models over larger instances of historical multi-modal demand datasets. A decision-maker could leverage the latter to determine, in advance, the expected travel demand increase/decrease of one mode when one or multiple other modes are expected to be disrupted.

References

[1] W. Burgholzer, G. Bauer, M. Posset, and W. Jammernegg, "Analysing the impact of disruptions in intermodal transport networks: A micro simulation-based model," in Decision Support Systems, Mar. 2013, vol. 54, no. 4, pp. 1580–1586. doi: 10.1016/j.dss.2012.05.060.

[2] A. Consilvio, A. di Febbraro, V. Moretti, and N. Sacco, "Design of collaborative multimodal strategies for disruption management in urban railway systems," in 2020 IEEE 23rd International Conference on Intelligent Transportation Systems, ITSC 2020, Sep. 2020. doi: 10.1109/ITSC45102.2020.9294329.

[3] S. Zhu, H. Masud, C. Xiong, Z. Yang, Y. Pan, and L. Zhang, "Travel behavior reactions to transit service disruptions: Study of metro safetrack projects in Washington, D.C.," Transp Res Rec, vol. 2649, no. 1, pp. 79–88, 2017, doi: 10.3141/2649-09.

[4] Budnitz Hannah, Champan Lee, and Tranos Emmanouil, "Better by bus? Insights into public transport travel behaviour during Storm Doris in Reading, UK," 2017.

[5] X. Zhang and N. Li, "Characterising individual mobility perturbations in cities during extreme weather events," International Journal of Disaster Risk Reduction, vol. 72, p. 102849, Apr. 2022, doi: 10.1016/j.ijdrr.2022.102849.

[6] H. Li, X. Ma, X. Zhang, X. Li, and W. Xu, "Measuring the Spatial Spillover Effects of Multimodel Transit System in Beijing: A Structural Spatial Vector Autoregressive Approach," J Adv Transp, vol. 2020, 2020, doi: 10.1155/2020/8870449.

[7] A. Furno, M. Fiore, R. Stanica, C. Ziemlicki, and Z. Smoreda, "A Tale of Ten Cities: Characterizing Signatures of Mobile Traffic in Urban Areas," IEEE Trans Mob Comput, vol. 16, no. 10, pp. 2682–2696, Oct. 2017, doi: 10.1109/TMC.2016.2637901.

[8] V. Satopää, J. Albrecht, D. Irwin, and B. Raghavan, "Finding a 'kneedle' in a haystack: Detecting knee points in system behavior," in Proceedings - International Conference on Distributed Computing Systems, 2011, pp. 166–171. doi: 10.1109/ICDCSW.2011.20.

[9] D. L. Davies and D. W. Bouldin, "A Cluster Separation Measure," IEEE Trans Pattern Anal Mach Intell, vol. PAMI-1, no. 2, pp. 224–227, 1979, doi: 10.1109/TPAMI.1979.4766909.

A Unified Framework for End-to-End Transportation Network Equilibrium Modeling

Zhichen Liu[a], Yafeng Yin[a], Fan Bai[b], Donald K Grimm[b]

[a] *Department of Civil and Environmental Engineering, University of Michigan, United States*

[b] *General Motors Research and Development, United States*

Introduction

Transportation network equilibrium modeling plays an essential role in the planning and operations of transportation networks. This framework models the interaction between the road network (i.e., supply) and travelers (i.e., demand) and estimate the flow distribution at an equilibrium state where no travelers can be better off by unilaterally changing their travel choices (Wardrop, 1952). This equilibrium flow distribution is then used as a benchmark against which improvement plans can be designed and compared. To improve the generalizability and accuracy of the equilibrium modeling framework, continued efforts have been devoted for over half a century to enhancing the representation of the supply- or demand-side components in a network equilibrium model. See, e.g., Xu et al. (2011) and Kitthamkesorn and Chen (2013) for recent reviews of previous attempts on improving the behavioral realism of equilibrium models, and Zhou et al. (2022) for recent efforts on deriving and calibrating link performance functions. To improve the empirical consistency of the framework, substantial efforts have also been made to develop better techniques to calibrate equilibrium models against empirical data. The calibration task has been formulated as a mathematical program with equilibrium constraints (MPEC), with the objective of minimizing the differences between estimated and observed link flows (Yang et al., 2001). Recent efforts have explored the use of computational graphs and automated differentiation to take advantage of multi-source, large volumes of data to enable scalable calibration on large networks (Wu et al., 2018).

Despite the modeling and calibration improvements over the past sixty years, previous network equilibrium models have been constructed via a **"bottom-up" assembly approach**. The model-building process starts with adopting a particular assumption, rule or theory on how travelers make their travel choices over a congestible network. Modelers then conceptualize the resulting equilibrium state and derive the corresponding equilibrium conditions. The conditions are subsequently formulated as an equivalent mathematical program or variational inequality (alternatively fixed point or nonlinear complementarity problem). In a formulation for static network equilibrium analysis, there are typically three major components: 1) demand functions that describe how the demands between origin-destination (OD) pairs change with respect to travel costs; 2) link performance functions that yield the link travel times given link flows; and 3) generalized cost functions that represent travelers' choice preferences. The latter can be determined once a behavior model is adopted, while the former two are typically calibrated separately against empirical data beforehand.

The bottom-up assembly approach is justified when each of these modeling components can be properly calibrated or determined individually, which, unfortunately, is not the case. For one thing, it is difficult to obtain empirical OD demand data and even more so to properly calibrate a demand function due to the endogeneity problem. It is also very challenging to properly specify and calibrate a link performance function because congestion does not persist as a steady state in practice. The appropriate specification of a link performance function depends on the underlying dynamics, which is often unobservable to modelers (Small and Chu, 2003; Cheng et al., 2022). Lastly, the behavior models adopted in the literature are far from being perfect for representing travel choice preferences. The selection of a behavior model reflects modelers' belief or judgments rather than being the outcome of a calibration process against empirical data. Recall that a different behavior model yields different equilibrium conditions that would produce a different traffic flow distribution. Therefore, observed flows should play a role in selecting the behavior model. However, we have never done so, due to the lack of a selection methodology and empirical data.

Overall, the limitation of the bottom-up assembly approach is that the specification and calibration of individual components in a network equilibrium model are divorced from the end goal of the model building, i.e., prescribing an equilibrium flow distribution that matches observations as closely as possible. To overcome this limitation, we recently propose **an "end-to-end" framework** that directly learns route choice preferences from empirical data (Liu et al. 2023). Assuming that OD demands are available, we approximated the generalized cost functions with neural networks and let the learning process automatically discover a good functional specification from empirical data. This aligns the behavior model selection with the ultimate goal of replicating flow distributions. Moreover, the end-to-end framework learns the equilibrium state of the network even though real systems never settle into equilibrium and observed flows are not equilibrium flows. It yields an equilibrium state that matches all the observations as closely as possible.

This study advances the end-to-end framework by relaxing the assumption that OD demands are observable and integrating the learning of both supply and demand components from empirical data. The proposed framework also unifies the use of model-based and model-free approaches for specifying supply or demand components, thereby leveraging both domain knowledge and the representation power of neural networks. This unified framework offers more flexibility and interpretability for handling the complexities of real-world transportation networks. More specifically, it uses computational graphs with learnable parameters to approximate the unknown supply or demand components (either model-based or model-free) and embeds them in a variational inequality (VI) that enforces user equilibrium conditions. By minimizing the differences between estimated and observed travel times, the parameters for both sides are simultaneously estimated. To the best of our knowledge, it is the first paper to validate a unified end-to-end network equilibrium model with both theoretical analysis and real-world case study.

Computational-graph-based VI formulation of elastic user equilibrium

We consider a case where partial link travel times at peak periods are observable for a long period of time. Suppose that a planning agency is interested in developing a static network equilibrium model to analyze the network for peak periods. The learning task is to learn the OD demands, travelers' route choice preferences, and link performance functions from multi-day observations. Mathematically, consider a network $\mathcal{G} = (\mathcal{N}, \mathcal{A})$, where $\mathcal{N}$ and $\mathcal{A}$ are the set of nodes and links. Let $\mathcal{R}$ denote the set of OD pairs. Each OD pair $r \in \mathcal{R}$ is connected by paths that form a finite and nonempty feasible path set $\mathcal{P}_r$. $\mathcal{P}$ represents the set of feasible paths for all OD pairs.

We propose three continuous functions to approximate the unknown supply and demand modeling components. Input features $x \in \mathcal{X}$ include road network features, traveler features, and contextual features (e.g., weather and gas price). The learnable parameters of three components will be jointly learned and thus are all represented as $\theta \in \Theta$. Each component is encoded with computational graphs and can be either model-based, model-free (e.g. neural networks), or the integration of both (e.g. physics-informed neural networks).

On the supply side, the **link performance function $\boldsymbol{\tau_\theta}$** outputs the link travel time $t \in \mathcal{T}$ as a function of path flow $h \in \mathcal{H}$, defined as $\tau_\theta: \mathcal{H} \times \mathcal{X} \to \mathcal{T}$, where input features $x \in \mathcal{X}$ include road network features, such as link capacity and free flow time, and contextual features; $\mathcal{H} \subseteq \mathbb{R}_+^{|\mathcal{P}|}$ and $\mathcal{T} \subseteq \mathbb{R}_+^{|\mathcal{A}|}$ require the path flow and link time to be nonnegative.

On the demand side, travelers are free to switch paths to improve their utility. Findings from travel behavior research suggest travel choice behaviors are much more complicated than just choosing the shortest paths. We use **genialized cost function $\boldsymbol{\pi_\theta}$** to describe the perceived path cost $c \in \mathcal{C}$ as a continuous function of link time $t \in \mathcal{T}$ and input features $x \in \mathcal{X}$, defined as $\pi_\theta: \mathcal{T} \times \mathcal{X} \to \mathcal{C}$, where $\mathcal{C} \subseteq \mathbb{R}_+^{|\mathcal{P}|}$ requires the path cost to be nonnegative. Input features include traveler characteristics (e.g., income and travel purpose), route features (e.g., number of left turns along the way) as well as contextual features.

In addition to route choice, travelers have the freedom to choose travel or not and switch origin and/or destination to improve their utility. We assume the demand function is upper-bounded and introduce the excess demand function to model travel choice. We define the excess demand as $e = \bar{q} - q$, where q is OD demand and $\bar{q}$ is the maximum possible OD demand. The **excess demand function $\boldsymbol{\mu_\theta}$** describes the equilibrium path utility $u \in \mathcal{U}$ as a function of excess demand $e \in \mathcal{E}$ and input features, i.e., $\mu_\theta: \mathcal{E} \times \mathcal{X} \to \mathcal{U}$. The feasible regions of excess demand and equilibrium path cost are $\mathcal{E} = \{e \in \mathbb{R}^{|\mathcal{R}|}: 0 \le e \le \bar{q}\}$ and $\mathcal{U} \subseteq \mathbb{R}_+^{|\mathcal{R}|}$ respectively.

Assuming rational travelers try to maximize their own travel utilities, the **multi-class user equilibrium with elastic demand** is formulated as a parametric VI in Eq.(1), the solution to which is the equilibrium flow h^* and equilibrium excess demand e^*.

$$\langle F_\theta(z^*, x), z - z^* \rangle \geqslant 0, \qquad \forall z \in \mathcal{Z}, \tag{1}$$

where $F_\theta(z, x) = [\pi_\theta(h, x), \mu_\theta(e, x)]^\top$ denotes equilibrium function; $z = (h, e)$ represents the response variable; $\mathcal{Z} = \{(h, e) \in \mathbb{R}^{|\mathcal{P}|+|\mathcal{R}|}: h \geq 0, e \geq 0, \Gamma^T h + e = \bar{q}\}$ and Γ is the path-OD incidence matrix.

Framework formulation

Assume a subset of link travel times are observed over a number of days (sample set) $\mathcal{M}$. Let $\bar{t} \in \overline{\mathcal{T}}$ represent observed link times and every training sample $m \in \mathcal{M}$ is $\left(x^{[m]}, \bar{t}^{[m]}\right)$. We consider a smooth loss function $\mathcal{L}: \mathcal{T} \times \overline{\mathcal{T}} \to \mathbb{R}$ that measures the distance between estimated equilibrium link times and observations. The

learning problem can be formulated as the following Mathematical Program with Equilibrium Constraints (MPEC).

$$\begin{aligned} &\min_{\theta} \quad E_x\left[\mathcal{L}\left(t^{\star[m]}, \bar{t}^{[m]}\right)\right] \\ &s.t. \quad z^{\star[m]} \in VI\left(F_\theta\left(z, x^{[m]}\right), \mathcal{Z}\right), \quad \forall m \in \mathcal{M} \\ &\qquad t^{\star[m]} = \tau_\theta\left(h^{\star[m]}, x^{[m]}\right) \end{aligned} \tag{2}$$

We adopt an iterative gradient-based algorithm to solve the MPEC (see Figure 1). Each iteration first (i) finds a near-optimal solution of the lower-level VI by solving a sequence of auxiliary optimization problems and then (ii) updates θ by approximating the gradient of the loss function with respect to the learnable parameters with backpropagation. Each auxiliary optimization problem is designed to update the response variables with closed-form rules (Li et al., 2022). This closed-form solution process of VI is encoded with computational graphs, enabling automated differentiation through the equilibrium points t^* with respect to θ during backpropagation.

Figure 89. Illustration of the unified end-to-end network equilibrium modeling framework

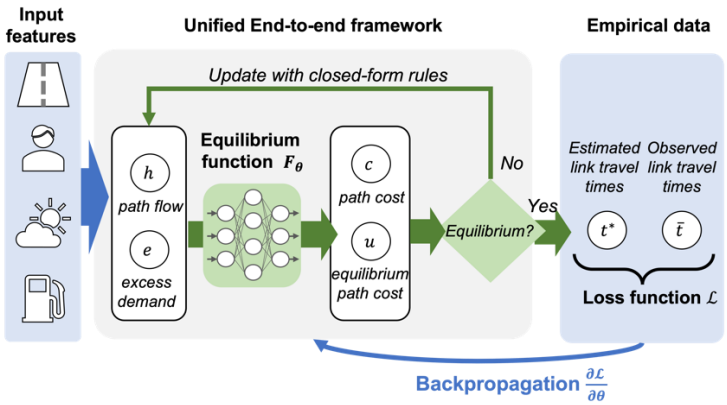

Framework analysis

This section analyzes the model and data requirements to guarantee framework. In real life, the observed flows may indeed not be equilibrium flows. Consequently, we consider a target equilibrium state that matches all the observations as closely as possible and will then serve as a consistent benchmark for comparing improvement plans. Theorem 1 shows with unlimited training samples and well-posed VI in Eq.(1), the proposed framework can jointly learn both supply and demand components and approximate the target equilibrium path flows infinitely close.

Theorem 1 (Performance guarantee) Suppose the link performance function, generalized cost function, and inversed demand function in Eq.(1) are strong monotonicity and Lipschitz continuity and there exists an estimated equilibrium function $F(z,\theta)$ that approximates the target function $F(z,\bar{\theta})$ within a sufficiently small approximation error ϵ, i.e., $\| F(z,\theta) - F(z,\bar{\theta}) \| \leq \epsilon$. Then both the equilibrium path flows h^* and excess demand e^* can approximate the target flow and excess demand within a constant φ of ϵ, i.e., $\| z(\theta) - z(\bar{\theta}) \| \leq \varphi\, \epsilon$.

The Universal Representation Theorem states that any continuous function can be approximated with a narrow, infinite-depth deep neural network within infinite small error (Kidger and Lyons, 2020). This suggests that the condition in Theorem 1 always holds when the equilibrium function is parametrized with neural networks.

Conclusions

This paper presents a unified end-to-end network equilibrium modeling framework that jointly learns the supply and demand components from empirical data and provides a performance guarantee for such a framework We demonstrate and validate the proposed framework using using synthesized data for the Sioux Falls network.

References

Cheng, Q., Liu, Z., Guo, J., Wu, X., Pendyala, R., Belezamo, B., Zhou, X.S., 2022. 'Estimating key traffic state parameters through parsimonious spatial queue models'. *Transportation Research Part C: Emerging Technologies* 137, 103596.

Kidger, P., Lyons, T., 2020. 'Universal approximation with deep narrow networks', in: *Conference on* learning theory, PMLR. pp. 2306–2327.

Kitthamkesorn, S. and Chen, A., 2013. 'A path-size weibit stochastic user equilibrium model'. Transportation Research Part B: Methodological, 57(C), pp.378-397.

Li, J., Yu, J., Wang, Q., Liu, B., Wang, Z., Nie, Y.M., 2022. 'Differentiable bilevel programming for stackelberg congestion games'. *arXiv preprint* arXiv:2209.07618.

Liu, Z., Yin, Y., Bai, F. and Grimm, D.K., 2023. 'End-to-end learning of user equilibrium with implicit neural networks'. *Transportation Research Part C: Emerging Technologies*, *150*, 104085.

Small, K.A., Chu, X., 2003. Hypercongestion. *Journal of Transport Economics and Policy* 37, 319–352.

Wardrop, J.G., 1952. 'Road paper. some theoretical aspects of road traffic research'. *Proceedings of the institution of civil engineers* 1, 325–362.

Wu, X., Guo, J., Xian, K., Zhou, X., 2018. 'Hierarchical travel demand estimation using multiple data sources: A forward and backward propagation algorithmic framework on a layered computational graph'. *Transportation Research Part C: Emerging Technologies* 96, 321–346.

Xu, H., Lou, Y., Yin, Y., Zhou, J., 2011. 'A prospect-based user equilibrium model with endogenous reference points and its application in congestion pricing'. *Transportation Research Part B: Methodological* 45, 311–328.

Yang, H., Meng, Q., Bell, M.G., 2001. 'Simultaneous estimation of the origin-destination matrices and travel-cost coefficient for congested networks in a stochastic user equilibrium'. *Transportation science* 35, 107–123.

Zhou, X., Cheng, Q., Wu, X., Li, P., Belezamo, B., Lu, J., Abbasi, M., 2022. A meso-to-macro crossresolution performance approach for connecting polynomial arrival queue model to volume-delay function with inflow demand-to-capacity ratio. *Multimodal Transportation* 1, 100017.

Bayesian Networks for travel demand generation: An application to Switzerland

A. Aurore SALLARD[a], B. Milos BALAC[a]

[a] *ETH Zürich, Stefano-Franscini Platz 5, 8093 Zürich, Switzerland*

Bayesian Networks (BNs) are probabilistic graphical models representing conditional dependencies existing between variables of interest. Recent studies have employed BNs for population synthesis and daily activity plan generation. Those studies highlight the ability of BNs to efficiently detect the causality links between variables in an easily interpretable way. This short paper aims to propose a further application of BNs for both population and daily activity plan synthesis in Switzerland. We show that understanding the dependency structure linking the population characteristics and its mobility behaviour is key to generating representative synthetic activity patterns. Furthermore, we lay the foundations for the development of temporally transferable travel demand models.

Category 6. Urban logistic

Automated delivery droids – results from real life experiments

A. Garus[a], L. Bonamini[b], L. Duboz[a], E.Silani[b], B.Ciuffo[a]

[a] *European Commission – Joint Research Centre, Via E. Fermi, 2749 – 21027 Ispra (VA), Italy*

[b] *Yape Srl Via San Martino 12, 20122 Milan (MI), Italy*

Introduction

The e-commerce industry is rapidly expanding, resulting in the transportation of small packages in high volumes, with varying frequency, which presents significant challenges for logistics providers (Ghajargar et al., 2016). The shift towards business-to-consumer (B2C) e-commerce is further increasing the demand for logistic services in cities. In 2020, e-commerce grew two to five times faster than before in countries such as the United States, China, United Kingdom, Spain, Germany, India, France, and Japan (Lund et al., 2021). Compared to traditional markets, e-commerce poses new challenges for companies and stakeholders, particularly in the complexity of logistics, especially the last-mile delivery, which involves delivering products from transportation hubs to final customers (Allen et al., 2018). The last-mile is the least efficient and most expensive stage of the delivery process due to challenging service levels, small orders, and a high dispersal of destinations (Macioszek, 2018). Additionally, last-mile delivery has various environmental and social externalities, such as air pollution, greenhouse gas emissions, noise pollution, infrastructure wear and tear, congestion, and road accidents (Ranieri et al., 2018). Therefore, innovative, efficient, and automated delivery methods are necessary to handle increasing delivery volumes, rising customer expectations, and conventional delivery challenges.

To improve efficiency and support environmentally friendly practices, companies are implementing various solutions for last mile logistics, which is part of a complex freight transport system that interacts with different urban ecosystems. These solutions include tricycles, bicycles (known as cargo bicycles), alternatively fuelled vehicles (such as electric or hybrid LCVs), and even vehicles typically used for passenger transport, like trams (Pietrzak & Pietrzak, 2021). Companies such as Amazon, DHL, Google, and start-ups like Starship and Yape are also testing innovative solutions like unmanned aerial vehicles (drones) and autonomous ground robots known as Autonomous Delivery Robots (ADRs). ADRs fall into one of three categories based on their design and operational capabilities: Sidewalk Automated or Autonomous Delivery Robots (SADRs), Road Automatic or Autonomous Delivery Robots (RADRs), and Autonomous Delivery Vehicles (ADVs) (Ionita, 2017; Jennings & Figliozzi, 2019). ADR-based deliveries may also depend on infrastructures such as robot depots and stations and conventional vehicles like motherships.

In recent years, drones and ADRs have gained increasing attention as potential delivery options due to their numerous benefits. However, while they share some advantages, they also have their own strengths and weaknesses (Simoni et al., 2020). Aerial drones, for instance, have the advantage of traveling at higher speeds and in direct Euclidean paths compared to ADRs, which can put ADRs at a disadvantage (Hong et al., 2018; Simoni et al., 2020). On the other hand, ADRs are superior to drones in various aspects, such as having multiple compartments, higher payload capacity, and extended operational range, which allow for multiple deliveries in a single trip (Figliozzi & Jennings, 2020; Jennings & Figliozzi, 2019; Simoni et al., 2020). Another important consideration is the energy consumption of both delivery options. Drones consume significantly more energy than electric ground vehicles (applicable to ADRs) in medium to high wind conditions and can consume more energy than diesel delivery vehicles in scenarios with increased stops and customers, such as dense urban settings (Kirschstein, 2020). In addition to design and operational benefits, regulatory frameworks also favor ADRs over drones due to the latter's higher perceived threats to public infrastructure and civilians (Simoni et al., 2020). Furthermore, drones can contribute to noise pollution, which may soon become a public health issue, while ADRs are both safer and quieter (Ostermeier et al., 2022; Torija & Clark, 2021). For further studies on ADRs, a full review is available in (Srinivas et al., 2022).

To fully assess the potential impact of drones and ADRs on urban structures, it is crucial to conduct more studies on their effects. While there have been several studies on the sustainable use of drones for last-mile delivery (Chung et al., 2020; Otto et al., 2018; Rojas Viloria et al., 2021) research on the impact of ADR-based delivery is still in the early stages. Jennings and Figlozzi (2020, 2019) have attempted to estimate the impact of ADRs on freight efficiency, total energy consumption, and emissions. Garus et al. (2022) have proposed an operational and sustainability assessment of delivery droids compared to other popular last-mile delivery systems. However, previous studies have relied on modeling to predict the energy consumption of these vehicles, whereas this study seeks to understand the real energy consumption based on experimental data and identify the factors that could affect it.

ADRs experiments

The real-life experiments were conducted in the Future Mobility Solutions Living Lab of the Joint Research Centre of the European Commission. As a representative ADR a Yape robot was used. Yape is a small autonomous delivery robot designed to carry goods over short distances. It is manufactured by e-Novia, an Italian engineering company known for developing innovative solutions for various industries. The Yape robot is approximately one-meter-tall and weighs around 54 kg. It can carry up to 10 kg of goods in its cargo compartment. The compartment is secured with a lock that can be opened with a smartphone app, ensuring safe and secure deliveries. Yape is equipped with various sensors, including cameras, 3D sensors, LiDAR sensors, and ultrasonic sensors, which enable it to navigate through urban environments safely and efficiently. The robot is also equipped with GPS and other positioning technologies, which allow it to accurately navigate to its destination. The Yape robot is powered by an advanced software system that uses artificial intelligence algorithms to optimize its route and maximize efficiency. The software can analyse traffic patterns and other data to determine the most efficient route for the robot to take. It can also automatically reschedule deliveries in case of unexpected events or traffic congestion.

The experiment conducted over a six-day period in November was designed to assess the efficacy of the Yape delivery robot as a means of delivering stationary goods to employees of the JRC. The experiment involved 27 participants who were required to navigate the Yape app to request deliveries. The Yape robot was in full autonomous mode and was capable of delivering goods from the base to seven buildings within close proximity, covering a distance of 100 to 300 meters.

The test involved 38 successful deliveries, while seven failed due to issues such as connection problems and interaction with the environment. To evaluate the performance of the Yape, various metrics were recorded, including the weight of the parcel (0.5kg to 10kg), temperature and humidity, the time it took for the robot to reach the recipient, the time the robot was idle while waiting for the recipient or for the parcel to be placed, and the time it took for the robot to return to the base. The total state of charge was also recorded to understand how those metrics impact the energy consumed by the ADR. In addition to the metrics mentioned earlier, the experiment also involved testing the Yape robot's performance at two different velocities: 1m/s and 2m/s. During the experiment, the Yape was operated in full autonomous mode, and if there was an occurrence, it was switched to manual mode and controlled from a control room in the base. The test was considered a pilot study with potential users of the technology and the app that operates it. The results of these tests were recorded and analysed to evaluate the robot's energy consumption and efficiency in delivering goods. This additional data provides further insight into the capabilities of the Yape robot and can help inform decisions about its potential use in real-world scenarios.

The impact that the measured metrics have on energy consumption is presented on the figure 1. The experiment showed that the Yape ADR consumes on average 0.10 Wh/m and 0.04 Wh/s. The outside temperature, humidity and velocity did not have an impact on the electricity consumption. Interestingly neither did the weight of the parcel, the average electricity consumption per meter for Yape carrying 10 kg was in fact lower (0.05 Wh/m average from three experiments). Those results show that the energy consumed by the ADR could not be determined by the vehicle dynamics, which is the measure often used to estimate the consumption of cars. Which means that the electric power is not used to drive the vehicle but is rather transformed to the hardware and software of the ADR that enable the automation of the vehicle. Moreover, Yape consumed more electricity when it experienced connection issues. In fact, in two experiments the connection issues were severe and the average electricity consumed per meter increased to 0.27 Wh/m and 0.24 Wh/m. Those preliminary results from a series of tests show that the hope that autonomous vehicles might be able to lower energy consumption is premature and that the energy required to power the hardware and software that supports automation might be substantial in the end.

Figure 90. Impact of various factors on the average electricity consumption per meter for each experiment

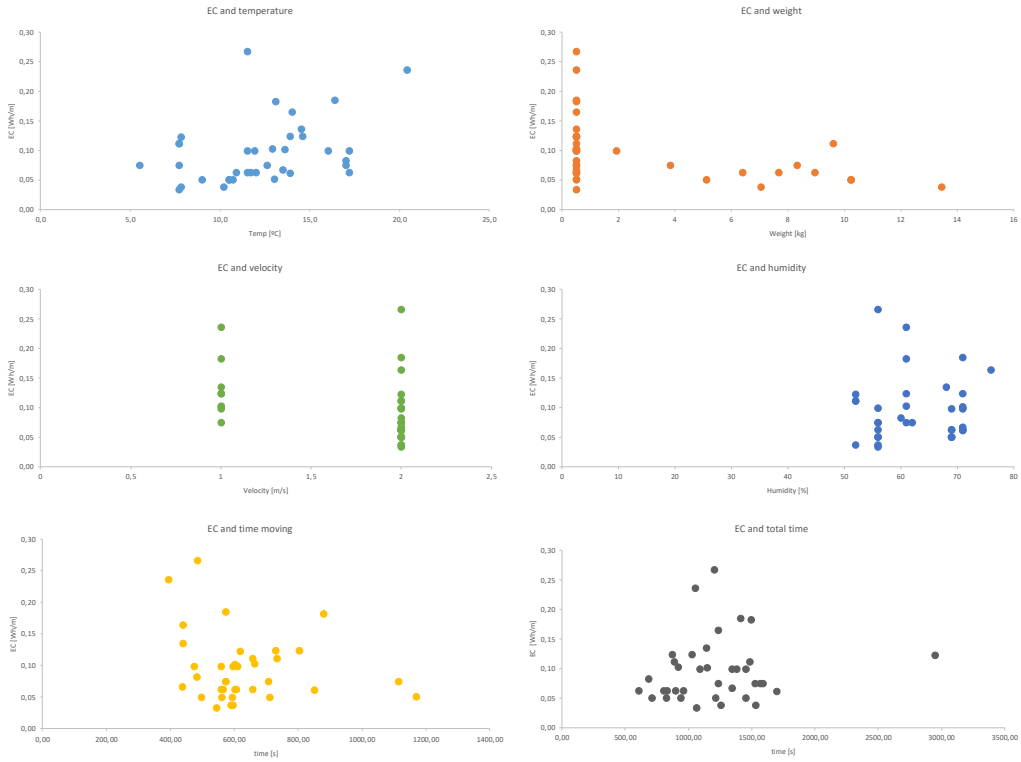

Conclusions

This study presents the results of real-life experiments with an automated delivery robot - Yape. The 38 experiments were carried out on the Ispra site of the Joint Research Centre of the European Commission. Our goal was to evaluate Yape's performance in a real-world setting and to assess its potential for improving logistics operations. We collected data on Yape's delivery times, electricity consumed and various factors that could have an impact on the electricity consumption. According to the results, the electric power is not used for vehicle propulsion but for the hardware and software of the ADR to enable automation. These initial findings indicate that the notion of autonomous vehicles reducing energy consumption may be premature, as the energy requirements for the hardware and software supporting automation could be significant.

References

Allen, J., Piecyk, M., Piotrowska, M., McLeod, F., Cherrett, T., Ghali, K., Nguyen, T., Bektas, T., Bates, O., Friday, A., Wise, S., & Austwick, M. (2018). Understanding the impact of e-commerce on last-mile light goods vehicle activity in urban areas: The case of London. Transportation Research Part D: Transport and Environment, 61, 325–338. https://doi.org/10.1016/j.trd.2017.07.020.

Chung, S. H., Sah, B., & Lee, J. (2020). Optimization for drone and drone-truck combined operations: A review of the state of the art and future directions. Computers & Operations Research, 123, 105004. https://doi.org/10.1016/j.cor.2020.105004.

Figliozzi, M., & Jennings, D. (2020). Autonomous delivery robots and their potential impacts on urban freight energy consumption and emissions. Transportation Research Procedia, 46, 21–28. https://doi.org/10.1016/j.trpro.2020.03.159.

Garus, A., Alonso, B., Raposo, M. A., Grosso, M., Krause, J., Mourtzouchou, A., & Ciuffo, B. (2022). Last-mile delivery by automated droids. Sustainability assessment on a real-world case study. Sustainable Cities and Society, 79, 103728. https://doi.org/10.1016/j.scs.2022.103728.

Ghajargar, M., Zenezini, G., & Montanaro, T. (2016). Home delivery services: innovations and emerging needs. IFAC-PapersOnLine, 49(12), 1371–1376. https://doi.org/10.1016/j.ifacol.2016.07.755.

Hong, I., Kuby, M., & Murray, A. T. (2018). A range-restricted recharging station coverage model for drone delivery service planning. Transportation Research Part C: Emerging Technologies, 90, 198–212. https://doi.org/10.1016/j.trc.2018.02.017.

Ionita, S. (2017). Autonomous vehicles: from paradigms to technology. IOP Conference Series: Materials Science and Engineering, 252(1), 012098. https://doi.org/10.1088/1757-899X/252/1/012098.

Jennings, D., & Figliozzi, M. (2019). Study of Sidewalk Autonomous Delivery Robots and Their Potential Impacts on Freight Efficiency and Travel. Transportation Research Record, 2673(6), 317–326. https://doi.org/10.1177/0361198119849398.

Kirschstein, T. (2020). Comparison of energy demands of drone-based and ground-based parcel delivery services. Transportation Research Part D: Transport and Environment, 78, 102209. https://doi.org/10.1016/j.trd.2019.102209.

Lund, S., Madgavkar, A., Manyika, J., Smit, S., Ellingrud, K., Meaney, M., & Robinson, O. (2021). The future of work after COVID-19 [Technical Report]. McKinsey Global Institute. https://www.mckinsey.com/featured-insights/future-of-work/the-future-of-work-after-covid-19#/.

Macioszek, E. (2018). First and Last Mile Delivery – Problems and Issues. In G. Sierpiński (Ed.), Advanced Solutions of Transport Systems for Growing Mobility (pp. 147–154). Springer International Publishing. https://doi.org/10.1007/978-3-319-62316-0_12.

Ostermeier, M., Heimfarth, A., & Hübner, A. (2022). Cost-optimal truck-and-robot routing for last-mile delivery. Networks, 79(3), 364–389. https://doi.org/10.1002/net.22030.

Otto, A., Agatz, N., Campbell, J., Golden, B., & Pesch, E. (2018). Optimization approaches for civil applications of unmanned aerial vehicles (UAVs) or aerial drones: A survey. Networks, 72(4), 411–458. https://doi.org/10.1002/net.21818.

Pietrzak, O., & Pietrzak, K. (2021). Cargo tram in freight handling in urban areas in Poland. Sustainable Cities and Society, 70, 102902. https://doi.org/10.1016/j.scs.2021.102902.

Ranieri, L., Digiesi, S., Silvestri, B., & Roccotelli, M. (2018). A Review of Last Mile Logistics Innovations in an Externalities Cost Reduction Vision. Sustainability, 10(3), 782. https://doi.org/10.3390/su10030782.

Rojas Viloria, D., Solano-Charris, E. L., Muñoz-Villamizar, A., & Montoya-Torres, J. R. (2021). Unmanned aerial vehicles/drones in vehicle routing problems: a literature review. International Transactions in Operational Research, 28(4), 1626–1657. https://doi.org/10.1111/itor.12783.

Simoni, M. D., Kutanoglu, E., & Claudel, C. G. (2020). Optimization and analysis of a robot-assisted last mile delivery system. Transportation Research Part E: Logistics and Transportation Review, 142, 102049. https://doi.org/10.1016/j.tre.2020.102049.

Srinivas, S., Ramachandiran, S., & Rajendran, S. (2022). Autonomous robot-driven deliveries: A review of recent developments and future directions. Transportation Research Part E: Logistics and Transportation Review, 165, 102834. https://doi.org/10.1016/j.tre.2022.102834.

Torija, A. J., & Clark, C. (2021). A Psychoacoustic Approach to Building Knowledge about Human Response to Noise of Unmanned Aerial Vehicles. International Journal of Environmental Research and Public Health, 18(2), 682. https://doi.org/10.3390/ijerph18020682.

Enhancing the Co-modality of Passengers and Freights in Train Systems

A. Yanyan Ding[a], B. Xiaoshu Ding[a], C. Wentao Huang[a], D. Sisi Jian[a]

[a]*Department of Civil and Environmental Engineering, The Hong Kong University of Science and Technology, Clear Water Bay, Kowloon, Hong Kong SAR*

Introduction

In the mobility system, mobility service providers (MSPs) are mainly selfish entities that aim to maximize their own profits using pricing instruments and operation strategies. For example, ride-sourcing operators and bike-sharing operators allocate different numbers of vehicles to different zones and set discriminatory prices for different groups of customers (Bennaceur et al. 2020, Duran-Rodas et al. 2020). Their resource allocation and pricing strategies are designed to maximize their own profits. This may lead to a situation where low-income customers are less likely to be allocated to desired mobility services, especially during congested periods. Meanwhile, travelers living in remote areas (often low-income people) may incur higher prices, while travelers in urban districts (often high-income people) may be charged lower prices as a result of profit-oriented resource allocation and pricing strategies. Such inequity can harm the welfare of some traveler groups and undermine the sustainable development of the transport service market. For example, there may exist some equilibrium states in which no MSPs are willing to take trip orders from weak minorities, while MSPs may compete to serve customers with a high income, resulting in an unbalanced distribution and utilization of mobility resources. Motivated by these realistic challenges, we discuss the optimal resource allocation and pricing strategies of MSPs under not only the capacity constraint but th 额 equity constraint as well. In previous studies, researchers explored the equity problem by only considering either resource allocation (Jiang and Zografos, 2021, Yin et al. 2022) or pricing strategies (Holguín-Veras et al. 2020, Zhu et al. 2022). Different from prior studies, we examine the impacts of joint resource and price decisions under both equity and capacity constraints.

The general model

We consider an MSP providing mobility services for travelers with unit operational cost c. Travelers are categorized into multiple groups based on their socio-demographics, such as income, spatial location, gender, race, age, etc. We index these groups by 1,2, ... and include in a set I. The potential number of travelers (i.e., the market size) in group i is denoted as $N_i, \forall\, i \in I$. The travelers from group i have valuation v_i for the mobility service provided by the MSP, which is a random variable that is uniformly distributed on $[0, \overline{V}_i]$. The corresponding surplus is given by $u_i = v_i - \tau_i$. In comparison, we consider an outside option under which the surplus of travelers will be zero, i.e., $u_0 = 0$. Then, travelers compare the outside option and the MSP to determine their options, i.e., travelers in group i will choose the MSP if their valuation is no less than the offered price; otherwise, they will choose the outside option. Formally, the number of travelers choosing the MSP is $d_i = N_i\, P(v_i | v_i \geq \tau_i)$ and the number of travelers choosing the outside option is $d_0 = N_i P(v_i | v_i < \tau_i)$.

The MSP needs to first determine the long-term decision, i.e., the amount of mobility resources s_i (e.g., the number of vehicles if the MSP is a ridesourcing operator, service frequency if the MSP is a bus operator, etc.) and the short-term decision, i.e., the service price τ_i for each group i. When making the joint price and resource strategy, the MSP needs to consider two realistic constraints. The first constraint is known as the *capacity constraint*, i.e., the total number of resources allocated to all groups of travelers shall be no greater than the cap of its own resources, $\overline{s}$. The second constraint is the *equity constraint*. In practice, policy makers would allocate equity constraints that requires the MSP to satisfy, i.e., the MSP needs to determine the mobility resources and the service prices equitably among different groups. To capture the equity constraint, we let $R_i(s_i, \tau_i)$ represent the equity measure for group i. For simplicity, we denote it as R_i in the following discussion. In comparison, we use R_j to represent the equity measure for any other group j except of group i. Then, $|R_i - R_j|$represents the equity gap between two different groups. In addition, we use a superscript ``$*$" to represent the result under the optimal joint resource-pricing strategy. $|R_i^* - R_j^*|$ represents the equity gap in the without-equity-constraint case by taking the optimal join resource-pricing strategy. Under the mobility resource capacity constraint and the equity constraint, the MSP aims to maximize its profit by setting the number of allocated resources s_i to group i and the corresponding service price τ_i. The profit maximization problem of MSP is formulated as follows:

$$\max_{\tau_i, s_i} \pi_M = \sum_{i \in I} (\tau_i - c) \min(d_i, s_i) \tag{1}$$

s.t.

$$\sum_{i \in I} s_i \leq \overline{s} \tag{2}$$

$$\left|\tau_i - \tau_j\right| \leq (1-\alpha)\left|\tau_i^* - \tau_j^*\right|, \quad i,j \in I \tag{3}$$

$$s_i \geq 0, \qquad i \in I \tag{4}$$

Eq. (2) is the capacity constraint and Eq. (3) is the equity constraint, where $\alpha \in [0,1]$ represents the level of the equity and it is predetermined by the MSP, in order to satisfy regulatory requirements or internal goals. As α increases, the equity level raises. In light of this, $\alpha = 0$ corresponds to the without-equity-constraint case and $\alpha = 1$ corresponds to fully-equity case. To keep consistency, we denote it as α-equity constraint. In Eq. (3), we introduce the price equity constraint which is initiated by different dimensions (Cohen et al. 2021, 2022), i.e., the price discrimination shall not surpass that in the without-equity constraint situation. Eq. (4) guarantees the non-negativity of resources allocated to group i.

To ease the exposition, we consider that there exist two groups of travelers and the MSP determines the joint price and resource strategy under equity and capacity constraint in the following discussion. In comparison, we take the without-equity-constraint case (i.e., $\alpha = 0$) as the benchmark case, which compares with the with-equity constraint case (i.e., $\alpha > 0$).

The joint resource and price strategies between H- and L-income travellers

We consider that there are two groups of travelers: high-income Group (H-travelers) and low-income Group (L-travelers). To distinguish the two groups of travelers, we denote the highest intrinsic value of H-travelers as $\overline{V}$ and the highest intrinsic value of L-travelers as $\gamma\overline{V}$, where $\gamma \in (0,1)$. Then, the intrinsic value of H-travelers is uniformly distributed in $[0,\overline{V}]$ and the intrinsic value of L-travelers is uniformly distributed in $[0,\gamma\overline{V}]$. By comparing the relative value of surplus by choosing the MSP (i.e., $u_i = v - \tau_i, i \in \{H,L\}$ with the surplus by choosing the outside option (i.e., $U_0 = 0$), we can derive the numbers of H-travelers and L-travelers choosing the MSP and the outside option below:

$$d_H = \left(1 - \frac{\tau_H}{\overline{V}}\right) N_H \tag{5}$$

$$d_L = \left(1 - \frac{\tau_L}{\gamma\overline{V}}\right) N_L \tag{6}$$

$$d_0 = \frac{\tau_H}{\overline{V}} N_H + \frac{\tau_L}{\gamma\overline{V}} N_L \tag{7}$$

where d_H represents the number of H-travelers choosing the MSP and d_L represents the number of L-travelers choosing the MSP. The first part of d_0 represents the number of H-travelers choosing the outside option and the second part of d_0 represents the number of L-travelers choosing the outside option. From Eqs.(5-6), we observe that the travel demand decreases in the service prices. For clarity, we can write $d_H(\tau_H)$, $d_L(\tau_L)$, and $d_0(\tau_H,\tau_L)$ as the demand functions of travelers in terms of τ_H and τ_L. The maximal travel demand achieves when the service prices reduce to the marginal cost, i.e., the maximal number of H-travelers choosing the MSP is $\left(1 - \frac{c}{\overline{V}}\right) N_H$ and the maximal number of H-travelers choosing the MSP is $\left(1 - \frac{c}{\gamma\overline{V}}\right) N_L$.

In reality, there is no need to discuss the capacity and equity constraints, if the capacity is sufficient, e.g., it has already been greater than the total potential number of travelers, and all travelers will be satisfied. In light of this, we focus on the setting that resources are scarce and the MSP needs to strategically make pricing and resource allocation decisions to satisfy the capacity and equity constraints as well as maximization its own profit. In fact, the MSP will not determine a service price lower than the marginal cost, because it cannot gain positive benefit. We can rewrite the optimization program of the MSP below:

$$\max_{\tau_H,\tau_L,s_H,s_L} \pi_M = \min(d_H, s_H)(\tau_H - c) + \min(d_L, s_L)(\tau_L - c) \tag{8}$$

s.t.

$$d_H = \left(1 - \frac{\tau_H}{\overline{V}}\right) N_H, d_L = \left(1 - \frac{\tau_L}{\gamma\overline{V}}\right) N_L \tag{9}$$

$$s_H + s_L \leq \overline{s} \tag{10}$$

$$|\tau_H - \tau_L| \le (1-\alpha)|\tau_H^* - \tau_L^*|, \quad i,j \in I \tag{11}$$

$$s_H \ge 0, \qquad s_L \ge 0 \tag{12}$$

In the following discussion, we first analyze the without-equity-constraint case, and then analyze the with-equity-constraint case under the aforementioned three equity constraints.

Analysis and discussion

In this section, we compare the two situations: the without-equity-constraint situation and the with-equity constraint situation. To distinguish with the without-equity-constraint case, we use superscript "**" to represent the optimal solutions in the with-equity constraint case. In this section, we consider the price equity situation.

In the without-equity-constraint situation, we can solve that the optimal solutions below:

There shall exist a unique optimal price solution $\tau_H^* = \frac{\overline{V}+t}{2}$ and $\tau_L^* = \frac{\gamma\overline{V}+t}{2}$, where we have $t = \max\left(\frac{\overline{V}(N_H+N_L-2\overline{s})}{N_H+\frac{N_L}{\gamma}}, c\right)$.

When $c \le \frac{\overline{V}(N_H+N_L-2\overline{s})}{N_H+\frac{N_L}{\gamma}}$, the capacity constraint is binding and there shall exist a unique optimal resource solution $d_H(\tau_H^*) = s_H$ and $d_L(\tau_L^*) = s_L$. When $c > \frac{\overline{V}(N_H+N_L-2\overline{s})}{N_H+\frac{N_L}{\gamma}}$, the capacity constraint is unbinding and there are multiple resource solutions, where $d_H(\tau_H^*) \le s_H$, $d_L(\tau_L^*) \le s_L$, and $s_H + s_L < \overline{s}$.

In the with-equity-constraint situation, we can derive the following results:

The MSP cannot be better off by determining price and resource decisions which induce that demand exceeds supply.

When $d_H \le s_H$ and $d_L \le s_L$, we obtain the following results: $\tau_H^{**} = \frac{\overline{V}+t}{2} - \frac{\mu\overline{V}}{2N_H}$ and $\tau_L^{**} = \frac{\gamma\overline{V}+t}{2} + \frac{\mu\gamma\overline{V}}{2N_L}$, where $t \equiv \max\left(\frac{\overline{V}(N_H+N_L-2\overline{s})}{N_H+\frac{N_L}{\gamma}}, c\right)$ and $\mu = \frac{\alpha(1-\gamma)}{\frac{1}{N_H}+\frac{\gamma}{N_L}}$.

To have a better explanation of the above results, we present Figure 1 below to illustrate the changes of price and resource decisions on the travel demand and MSP's profits. Figure 1(a) presents the results when capacity constraint is binding and Figure 1(b) presents the results when capacity constraint is unbinding. Red lines and regions (Y_1) represent the optimal results in the without-equity-constraint situation. Blue lines and regions (Y_2) represent the optimal results in the with-equity-constraint situation when demand does not surpass supply, whereas black lines and regions (Y_3) represent the results when demand surpass supply. It is evident that when $d_H + d_L < \overline{s}$, multiple resource solutions can be achieved due to redundant capacities, which are floating green lines. When $d_H + d_L = \overline{s}$, there shall exist a unique solution. Moreover, we can theoretically prove that the area follows $Y_1 > Y_2 > Y_3$. This indicates that the MSP gains the highest profit without equity constraints. Otherwise, it gains the highest profit when demand does not surpass supply.

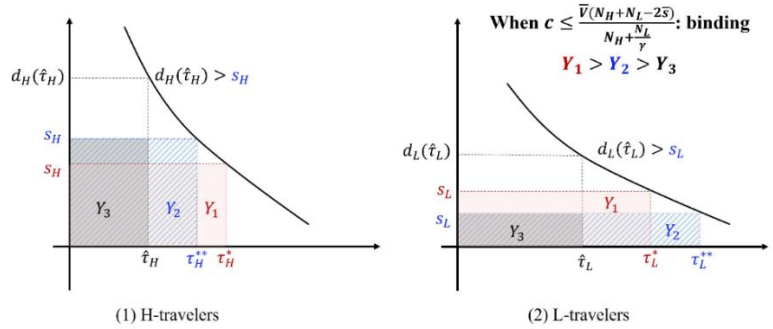

(a)When $d_H + d_L = \overline{s}$

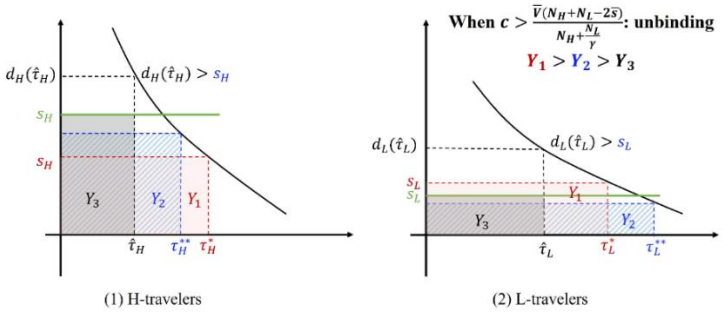

(a)When $d_H + d_L < \bar{s}$

References

Bennaceur, M., Delmas, R., & Hamadi, Y. (2022). Passenger-centric Urban Air Mobility: Fairness trade-offs and operational efficiency. Transportation Research Part C: Emerging Technologies, 136, 103519.

Cohen, M. C., Miao, S., & Wang, Y. (2021). Dynamic pricing with fairness constraints. Available at SSRN 3930622.

Cohen, M. C., Elmachtoub, A. N., & Lei, X. (2022). Price discrimination with fairness constraints. Management Science, 68(12), 8536-8552.

Duran-Rodas, D., Villeneuve, D., Pereira, F. C., & Wulfhorst, G. (2020). How fair is the allocation of bike-sharing infrastructure? Framework for a qualitative and quantitative spatial fairness assessment. Transportation Research Part A: Policy and Practice, 140, 299-319.

Holguín-Veras, J., Encarnación, T., & González-Calderón, C. A. (2020). User perception of fairness of time-of-day pricing and other typical toll discounts. Transportation Research Part A: Policy and Practice, 137, 560-581.

Jiang, Y., & Zografos, K. G. (2021). A decision making framework for incorporating fairness in allocating slots at capacity-constrained airports. Transportation Research Part C: Emerging Technologies, 126, 103039.

Yin, Y., Li, D., Han, Z., Dong, X., & Liu, H. (2022). Maximizing network utility while considering proportional fairness for rail transit systems: Jointly optimizing passenger allocation and vehicle schedules. Transportation Research Part C: Emerging Technologies, 143, 103812.

Zhu, G., Zhang, J., Xing, E., & Han, D. (2022). Pricing and quality decisions with conspicuous consumers. Transportation Research Part E: Logistics and Transportation Review, 165, 102857.

Comparing a conventional urban logistics chain with an airborne-supplied concept

M. Klatte[a], F. Kuehnel[a], E. Feldhoff[b], J. Roesing[b], I. Lima[b]

[a] *RWTH Aachen University, Chair and Institute of Urban and Transport Planning, Mies-van-der-Rohe-Straße 1, 52074, Aachen, Germany*

[b] *RWTH Aachen University, Institute of Transport Science, Mies-van-der-Rohe-Straße 1, 52074, Aachen, Germany*

Introduction and objectives

Urbanization and the need for faster delivery services have put significant strain on metropolitan road transportation networks leading to increased congestion and poor air quality. While the use of cargo pedelecs has increased, the conventional logistic chain still requires delivery trucks to enter cities in order to deliver parcels to either transshipment points inside the city (so called city hubs) or customers, causing additional congestion. With technological advances in Urban Air Mobility (UAM) driven by progress in distributed electric propulsion and battery performance, cargo drones have become a solution for this problem in urban logistics. Cargo drones can be used on the first and last mile or to supply city hubs. To date, however, drones are mainly explored in this context for the last mile, often delivering directly to the costumer a with small drone carrying one parcel at a time (Kim, J. et al., 2020). While some manufacturers have developed heavy-duty drones, corresponding concepts for cargo transportation to city hubs or transshipment centres have been less in focus (Roesing, J. et al., 2023). Considering the potential and growth in the industry, our study thus addresses the logistics of air-borne supplied city hubs in parcel delivery.

Effectively exploring benefits and shortcomings of the logistics chain, many studies have already simulated air cargo and last mile parcel delivery processes, e.g. for air cargo handling (Nsakanda, A. et al., 2004; Ou, J. et al., 2007; Yan, S. et al., 2006) and for parcel delivery in the last mile segment (Kim, J. et al., 2020; Moshref-Javadi, M. et al., 2020). Similar to the method applied by Cokyasar, T. et al. (2023) for energy impacts, we compare in this work the throughput performance of a conventional ground-supplied urban logistics chain against the introduction of an airborne-supplied and city hub centred logistics chain for parcel delivery and discuss the potential benefits and drawbacks of both concepts. Our focus is on cargo process simulation starting at an international airport, going through a regional airfield and a city hub before delivering the cargo to the customer. We determine the percentage of successfully delivered shipments and the delivery time difference between the two logistics chains while taking the local environmental impact into account.

Boundary Conditions

The logistics chain under consideration is a 3-stage distribution of B2C express cargo shipments from the Courier, Express and Parcel (CEP) sector, leading from an international commercial airport via a regional airfield and city hubs to the customers. The goods are transported in containers that are loaded at the international airport with all the parcels for a particular city hub and used throughout the logistics chain. In this way, only complete containers need to be handled at the transshipment hubs, making it easy and time-saving to handle deliveries. Between the international commercial airport and the regional airfield, containers are transported by a light airplane that is powered by alternative fuels. At the regional airfield, containers are transferred to fully electric heavy-lift drones, each of which transports one container to an urban city hub close to the final customer's location. Arriving at the city hub, containers are loaded into electric transporters and cargo pedelecs to be delivered to the customer (last mile). In the context of the study, only one direction of the logistics chain is considered, since goods are to be delivered as quickly as possible. Our case study for the logistics chain is the area of the municipal region of Aachen. The international commercial airport considered is the Cologne/Bonn Airport (CGN) and the regional airfield is the Aachen-Merzbrueck Airfield (AAH). The customers are located in the municipal region of Aachen. In preparation for the simulation of the logistics chain, various input parameters were generated and assumptions made. These are described below, starting with the identification of the requirements and the layout of an airborne supplied city hub.

While the airport and the regional airfield are existing infrastructure that can be used for the logistics chain with some adjustments, the city hub will be a new transshipment point. It requires a completely new design, based on the legal framework and the requirements to the infrastructure and the operation of take-off and landing areas for autonomous eVTOLs (Feldhoff, E.; Metzner, N., 2021). Additionally, the layout of the city hub is adapted to the local conditions on the one hand, and to the size of the specific drones and ground vehicles on the other hand. Essential components such as operational areas, landing and parking areas for the drone and the ground vehicles and areas for cargo handling, security and energy elements form the basis for the

design of a city hub. Other individually designed elements can be added and planned according to the necessity at each location (e.g. parcel station).

For the **location of the city hubs**, we apply a three-stage process based on the combination of the aforementioned with legal requirements formulated by Roesing, J. et al. (2023). In the macroscopic stage we evaluate the local zoning law. We exclude residential areas, air exclusion zones and maintain a minimum distance to interference-prone (e.g. schools) and security-relevant structures (e.g. military facilities). In the mesoscopic stage we search aerial photographs of not excluded areas for potential landing sites. We perform a location-based accessibility analysis to rank the sites by the number of potential customers. Finally, the top-ranked locations are analysed in more detail in the microscopic stage by evaluating obstacle clearance, the landing and logistics space on-site and compliance with minimum distances from high-traffic areas. After the installation of each location, we return to the mesoscopic stage. We evaluate the accessibility of the vacant locations, accounting for customers already served. We identify six city hub locations with sufficient customer demand.

Another necessary input for the simulation of the logistics chain is the **forecast of the parcel demand** on the considered route. We developed an estimate of demand for express cargo on a certain route, in our case between the international airport and the customer (see Roesing, J. et al., 2023). As a result, we obtain, on the one hand, the average parcel weight and volume. On the other hand, we obtain the total number of parcels for the route considered in this work. In order to transfer a part of this parcel volume to the new type of logistics chain, the willingness-to-pay is varied in three different demand scenarios.

Finally, we run multiple Monte Carlo simulations to determine the **number of drone flights and vehicles** needed for an economically feasible use case in each demand scenario. Using a synthetic population, we apply weighted random sampling to distribute the parcels at the address level and assign the parcels to city hubs through catchment areas. We then evaluate the utilization of city hubs and vehicles to determine the most economically feasible number and location of city hubs and vehicles for each demand scenario.

Methodology

Considering the goals context and structure of our study, **Figure 91** below provides an overview of the logistics chain as well as simulation methods, inputs and outputs. The simulative study can be divided into two parts, which refer to different spatial areas of the logistics chain. The DES model considers the logistics chain from the international commercial airport to the urban city hub, taking into account airside delivery processes as well as ground handling processes. The VRP model starts there and examines the last mile from the urban city hub to the customer with ground-based delivery vehicles.

Starting with the DES model, the framework includes logistic processes at CGN, at AAH and at the city hub. The modelled logistics chain starts with the loading process of containers into the small airplane at Cologne Bonn Airport. The final process of the logistic modelled in the DES simulation is the unloading process of a container at the city hub. We use the boundary conditions of the logistics chain as simulation input for our model. The total cargo volume is based on the forecast of parcel demand and different demand scenarios corresponding to varying utilization rates. The specific city hub locations that were selected for this use case are another simulation input. These inputs indicate the number of containers delivered from each city hub and the flight time to the airfield. Process times such as for taxiing, transshipment, and charging were obtained from the literature. We varied the number of operating vehicles to examine their influence on the system and investigated the influence of stochastic processing times as opposed to deterministic processing times. We focused on the following simulation output parameters: time of drone arrival at the city hub, utilization rate of drones, and waiting time of containers.

Figure 91. Schematic representation of the airborne-supplied logistics chain

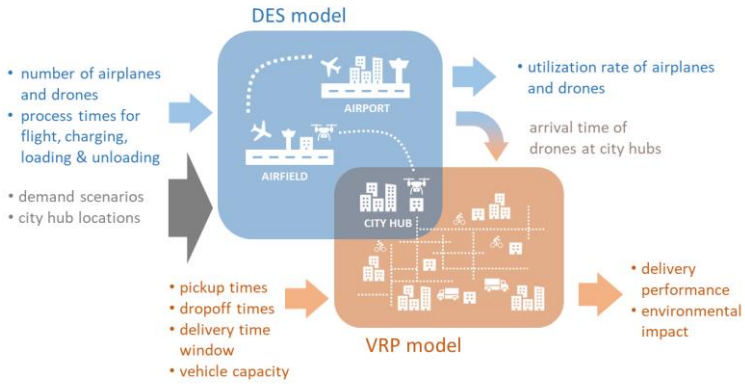

The VRP model of the logistics chain is based on the study area and is considered comparatively for the conventional and airborne logistics chain. To simulate last-mile delivery, parcels are distributed at the address level using weighted random sampling. We assign the parcels to the various city hubs based on the demand scenario's defined city hubs, ground vehicles, and catchment areas. The conventional logistics chain is solved by using the Vehicle-Routing-Problem (VRP) for a logistics center, from which a diesel-powered delivery truck delivers to customers. For the airborne-supplied logistics chain, the optimal delivery sequence from city hubs to customers is determined. Therefore, the VRP is solved for each demand scenario with varying parcel volumes and delivery addresses. A cargo pedelec or an electric van is used depending on the demand of the delivery areas. In the second step, we added a constraint to the jsprit simulation to accommodate the single container system. Due to the "FullPickupConstraint," the delivery vehicle does not start the delivery tour until a certain number of containers are delivered to the city hub, and new containers are only picked up after all loaded parcels have been delivered. Following the first step of determining the order of delivery, the delivery tours are assigned to container availability, determining the earliest start time of the respective delivery tour. The parcels distributed in this manner can then be delivered by the VRP in optimized delivery tours from the city hub or logistics distribution center with a focus on cost minimization. This methodology allows for the evaluation of both logistics chains, taking factors such as delivery times, delivery time windows, and emissions into account. The calculation for local pollutant emissions is based on the HBEFA key figures. The local emissions were calculated for the entire logistics chain based on the distances traveled by the corresponding vehicles.

Results and Discussion

The DES model shows that the containers' transportation time until arriving at the city hubs can be partly reduced by using more airplanes and drones. However, the time reduction stagnates at a specific number of operating aircraft. As expected, using more drones leads to lower container waiting times at the airfield. Using more small airplanes while maintaining the number of drones leads to higher container waiting times at the airfield, but not necessarily to later arrival times at the city hubs. The availability of drones at the airfield was found to be one bottleneck of the logistics chain; the container waiting time for the transshipment by forklifts is lower than the waiting time for an available drone.

For the VRP model, the results show that the airborne logistics chain was able to make 88% of deliveries, while the conventional logistics chain was able to make 100% of deliveries. In the airborne logistics chain, not all parcels can be delivered even in the medium scenario, whereas in the conventional logistics chain, all parcels are delivered by 5:40 p.m. even in the maximum scenario. This results from the drones arriving too late at the city hub for the parcels to be successfully delivered within the delivery time window. However, the results show that the local particulate matter emissions were three times higher for the conventional logistics chain. These findings highlight the trade-off between delivery efficiency and environmental impact and suggest that further research is needed to identify sustainable logistics solutions.

Many observations can be made under further analysis of the models. A trade-off between time-efficiency and utilization of the logistics chain is necessary for the volume of operating vehicles. Transportation times tend to be overall long and dividing deliveries into types of service products to be sold at different prices ranges could be beneficial. Also, an increased value could possibly be added to the proposed logistics chain in the case of longer distances between the international airport and the airfield, as aircraft range was not used to its full potential. There is further room for improvement in the data exchange between the models so that the VRP does not have to be run twice, and more data is required regarding delivery times on the last mile (e.g. pick-up

and parking lot search times, walking distances for delivery agents). A missing comprehensive legal framework (Roesing, J. et al., 2023) and data lead to uncertainties in the city hub design and the inputs for the simulation models. A more accurate assessment and the inclusion of other aspects, e.g. public acceptance and costs, are relevant for the introduction of the logistics concept using airborne-supplied city hubs in an urban environment and should be explored in future studies.

Acknowledgments

This work was supported by the Federal Ministry of Economy, Innovation, Digitalization and Energy of the federal state of North Rhine-Westphalia in the project URAF in the framework of the European Regional Development Fund (ERDF) (EFRE-0801699).

References

Cokyasar, T., Stinson, M., Sahin, O., Prabhakar, N. and Karbowski, D., *´Comparing Regional Energy Consumption for Direct Drone and Truck Deliveries´,* Transportation Research Record: Journal of the Transportation Research Board, Sage Publicatons inc, 2023, 1-18.

Feldhoff, E. and Metzner, N., *´Examining legal requirements for a ground infrastructure at airfields as part of an automated, emission-free airfreight transport chain´,* Transportation Research Procedia 00 special issue: 23rd Euro Working Group on Transportation Meeting (EWGT 2020), Pafos, 16.09.2020-18.09.2020, Vol. 52, Elsevier Procedia, Amsterdam, 2021, 461-468.

Kim, J., Moon, H. and Jung, H., *´Drone-Based Parcel Delivery Using the Rooftops of City Buildings: Model and Solution´,* Applied Sciences, Vol. 10, No 12, mdpi, Basel, 2020, 4362.

Moshref-Javadi, M., Hemmati, A. and Winkenbach, M., *´A truck and drones model for last-mile delivery: A mathematical model and heuristic approach´,* Applied Mathematical Modelling, Vol. 80, Elsevier, New York, 2020, 290-318.

Nsakanda, A., Turcotte, M. and Diaby, M., *´Air Cargo Operations Evaluation and Analysis through Simulation´*, Proceedings of the 2004 Winter Simulation Conference. New York, 2004, 711-719.

Ou, J., Zhou, H. and Li, Z., *´A Simulation Study of Logistics Operations at an Air Cargo Terminal´*, 2007 International Conference on Wireless Communications, Networking and Mobile Computing. IEEE-Inst Electrical Electronics Engineers Inc, Piscataway, 2007, 4398-4402.

Roesing, J., Lima, I., Feldhoff, E., Hoenen, S., Kuehnel, F. and Theissen, A., *´Identifying requirements for airborne-supplied city hubs´,* Journal of Air Transport Management, Vol. 107, Elsevier, Oxford, 2023, 102326.

Yan, S., Chen, C.-K. and Chen, C.-H., *´CARGO TERMINAL SHIFT SETTING AND MANPOWER SUPPLYING IN SHORT-TERM OPERATIONS´,* Journal of Marine Science and Technology, Vol. 14, No 2, Elsevier, Tokyo, 2006.

Towards multi-scale modelling and multiple effect estimation of a logistics hub in a large city with large scale simulation

G.A. Klunder[a], A. Rondaij[a], R. Sterkenburg[a], N. Deschle[a], K. Adjenughwure[a], S.L. Veldman[a]

[a] *TNO, The Netherlands*

Introduction

Cities are working on measures such as environmental zones, emission-free zones, car-free city centres and hubs. Guided by customer demand, recommendations often focus on a single location and a single indicator i.e. safety, environment, accessibility or liveability, while an integral view is often missing. In addition, there is a risk of issuing contradictory recommendations from different studies and perspectives, due to insufficient familiarity with other research areas and failure to take interactions into account. In order to decide about the most effective measures, it would be preferred to determine the effects, on large scale but also in detail to find out who benefits and who is hindered. If only few indicators are used at one level, it will give a one-sided perspective, while an integral view at all levels provides a more complete view.

To create an integral view onsocietal/traffic problems which cities, provinces and countries are facing and to improve the assessment of interventions in the mobility and logistic system, a study was carried out that aimed to integrate different traffic and transport models at different levels. Combining knowledge and models at multiple scale levels, starting at the micro level up to the meso/macro models, makes it possible to determine the impacts of phenomena that are understood at one level also at the other levels.

Logistics use case

A logistics use case has been defined that requires integral multiscale assessment and involves a hub at the edge of the city in order to improve efficiency and environment. For the selected use case, some aspects require microscopic modelling (e.g. calculation of detailed emissions, traffic congestion and spillback), while macroscopic modelling suffices for other aspects (e.g. how routes changes due to the hub and how much traffic exists on each link). The city of Amsterdam has been involved in defining this use case.

Figure 92. Hub location (A) and destination area '"9 Straatjes"' (red plane, B) shown on the map. Source: Google Maps

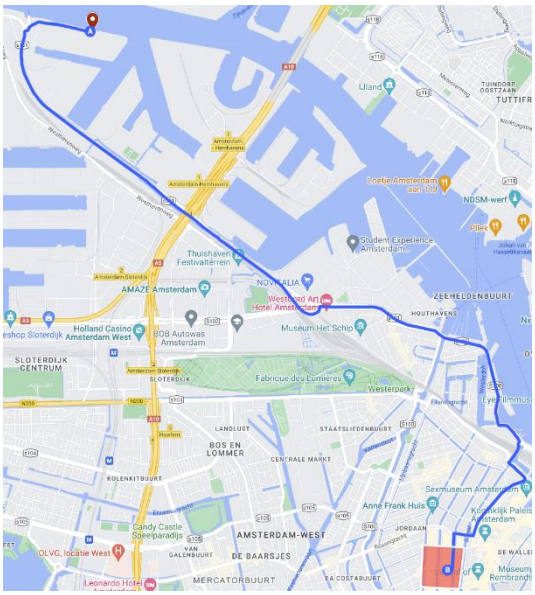

The logistics use case focuses on the implementation of a city logistics hub for the distribution of goods in the city centre of Amsterdam. The destination area is the neighbourhood '"9 Straatjes"', which is a touristic area with narrow streets and small retail, cafés and restaurants. Every day, a significant amount of vehicles enters the area to distribute goods and to deliver services. Though these transport movements are essential for the city to function successfully, it also brings negative impacts such as congestion in the narrow streets, nuisance, air pollution and CO_2 emissions. The hub facilitates bundling of goods and a shift to zero emission vehicles.

For the purpose of the use case, the soon to be opened ctPark Amsterdam Cityhub is chosen as the location of the hub. This is a strategic location on the west side of the city, easily accessible from the highway and within close reach of the city.

Microscopic modelling

As main model on the microscopic level, a novel agent-based microscopic traffic model under development by TNO called, the Large Scale Micro Simulator (LSMS) is used. The LSMS uses parallel computing on the graphical card (GPU) using CUDA. In this way, the model is capable of simulating larger networks with more agents than conventional microsimulation models. Since it is an agent-based model, modelling can be done on the individual vehicle level, which makes it more accurate than macroscopic traffic models. For example, for calculating emissions, individual vehicle speeds and accelerations and cold starts can be taken into account, which significantly increases the accuracy of emission calculations.

Since the microsimulation model LSMS is in early stage of development, new developments were needed in order to be able to simulate the logistic use case. These new developments concern agent models for intersections in urban environments, but also more basic developments of the core of the model. Other developments for the LSMS in this study were an emission model with separated cold start emissions, incorporation of a hub in the OD matrix, adding heterogeneity to the vehicle agents, agent models for trucks and editing/formatting small and large road networks for this use case. For the network modelling, a conversion model has been developed to transform a macro-level road network to a micro-level road network using the OpenDRIVE standard.

Inclusion of heterogeneity in the vehicle fleet, which incorporates a variety of properties of the vehicles, allow for a detailed and realistic modelling for e.g. congestion propagation and emission calculations. The specific impact of fleets with different vehicle euro class composition will let the stakeholders take decisions based in quantitative detailed analysis. Therefore, several properties such as weight and vehicle type were added to the vehicle agents. Although the heterogeneity in the fleet is currently mainly used in the emission module, these properties can be further included into the vehicle behaviour in later developments.

Cold start emissions

To the best of our knowledge, this implementation is the first microscale emission model that incorporates cold start contributions. Cold start emissions have been in the spotlight for years but there are only few studies on their impact on urban areas. With a large scale micro simulation model that incorporates cold start emissions their true scope and impact can be assessed.

In the current work the approach was to follow a data driven methodology, using monitoring data from the Smart Emissions Measurement System (SEMS) developed by TNO. (see for example [Vermeulen et al. 2012], [Kadijk et al. 2015] and [Kadijk et al. 2017]. This system acquires measurements of pollutants, including NO_x and CO_2. By means of these measurements, an equation for CO_2 as a function of kinematic variables is determined, given a principle-based data-fitted equation for the CO_2.

For the NO_x, the approach is slightly different: it is a fully data driven approach. After identifying the main dependencies of NO_x these were binned according to the amount of data available to map vales of NO_x dependencies to NO_x levels on a very detailed fashion. These Augmented Emission Maps (AEM) have been under development and improvement at TNO for several years. Currently, the cold start emission model adds the cold start contribution to the start of the trip using an exponential function to smooth the emission function.

Intersection models

For micro-level modelling of traffic through intersections, an inventory of intersection types has been made. For two of those types a specification of how to model car (driver) behaviour has been formulated in terms of a State (Transition) Diagram and textual documentation of the behaviour in each state. These two types are the signalized intersection and unprioritized intersections.

For the signalized intersection the model has also been implemented and tested (albeit only on small scale) in the LSMS. For the unprioritized intersection only the tactical layer has been implemented, and so far without gap detection. Also deceleration for approaching a traffic light is implemented based on earlier models developed at TNO.

Macroscopic modelling

For the macroscopic approach, the same OD and hub location were used and implemented into a macroscopic traffic model from TNO, called Urban Strategy (US) [Borst, 2022]. A simulation run was performed and first results were obtained as comparison to the microscopic approach.

The initial results of the logistics use case at macroscopic level showed that the traffic effect was localized in the destination area and at the hub location. There was a positive effect on the truck traffic going to the area. This means that as expected, the hub could help reduce truck traffic going into the area. However, there was a negative effect on other locations. Specifically, the roads leading to the hub location were faced with increased truck traffic. The effect of the hub on trips going to the "9 Straatjes" was visible in the traffic intensities of Euro 6 Trucks. As expected, there was a decrease in the Euro 6 truck traffic in that area while there was an increase in traffic for other surrounding areas. This indicates that there was an expected positive effect on the truck traffic on those streets if the hub is introduced. As expected, for the hub location, there is an increase in traffic towards the hub. This is because all Euro 6 trucks going to the destination area are redirected to the hub location. Furthermore note that on the flip side, for the hybrid/ZEEV matrix, the emission-free traffic going to the destination area will increase due to new hybrid trucks coming from the hub to the area.

Due to a lack of data on the use case, a generic approach was required. this had an impact on the accuracy and reliability of the results. However, the use case was useful as a hands-on approach to explore what is required to make a macroscopic traffic model suitable for logistics questions. From this exploration it follows that it is essential to have a clear picture on the composition of logistics in urban areas to be able to compose the Origin Destination matrices and to expand knowledge on the potential effect of logistics measures such as the use of hubs.

Conclusions

Many core developments have been implemented for the new large scale microscopic model LSMS. These concern e.g. curve driving, basic intersection objects (including traffic lights with basic traffic state) and traffic assignment. These were necessary for urban traffic simulation on microscopic level. Though the model was not yet far enough developed to already simulate the use case on microscopic level, the developments and early results are promising to continue these developments.

To date, the implementation of a cold start emission model into a microscale emission model has not often been reported. Although the total amount of the cold start emissions is accurate, the smoothing creates an artificial distribution in a small area that might not be accurate. The behaviour of cold start emissions should be further investigated and properly implemented. Overall, the model should be periodically updated using monitoring data, to add accuracy and also adjust to the new fleet composition.

Besides the development of the microscopic model, this study has also explored how the macroscopic tool Urban Strategy can be used for showing the impact of logistics. The exploration of a logistics use case using Urban Strategy demonstrated that Urban Strategy can be valuable to show the (negative) impact on the surroundings of logistics hubs or other locations where logistics movements concentrate (such as construction sites). Additionally, it can be used to show the potential of logistics and technical measures on city level. It is necessary to further research the composition of urban logistics: the number of trips, kilometres and vehicles in urban areas per vehicle type and logistics segment.

References

Kadijk, G., Ligterink, N. and Spreen, J., 2015. On-road NO_x and CO_2 investigations of Euro 5 light commercial vehicles (p. 30). Delft: TNO.

Vermeulen, R.J., Ligterink, N.E., Vonk, W.A. and Baarbé, H.L., 2012. A smart and robust NO_x emission evaluation tool for the environmental screening of heavy-duty vehicles.

Kadijk, G., Vermeulen, R., Buskermolen, e.a., 2017. NO_x emissions of eighteen diesel Light Commercial Vehicles: Results of the Dutch Light-Duty road vehicle emission testing programme 2017. Delft: TNO.

J. Borst (2022) The healthy city: accessible, safe and vital. https://www.tno.nl/en/digital/smart-traffic-transport/societal-impact/healthy-city-accessible-safe-vital.

Category 7. The interaction of different modes (including safety aspects)

Drivers' heterogeneity, vehicle hetereogeneity, driving behaviour, independent driver style

A. L. Marin[a] ,J. Suarez [b], A, Tansini[b], D. Komnos[b], M.J. Ramírez-Quintana[a], F. Martínez-Plumed[a], G. Fontaras[b],

[a] *Universitat Politècnica de València, VRAIN, Valencia 46022, Spain*

[b] *European Comission's Joint Research Centre (JRC), Ispra 21027, Italy*

This paper proposes a new methodology for exploring the impact of heterogeneity on longitudinal vehicle movement due to the variation in driver behaviours. Driver heterogeneity affects traffic flow, safety and energy efficiency. We propose a methodology that analyses the acceleration behaviour of drivers to enable inter-driver and intra-driver characterisation. The comparison of different drivers in different vehicles becomes possible through a standardisation process that transforms observed accelerations into so-called Independent Driver Style (IDS) distributions. The dynamics of powertrain technologies are considered when acceleration values are observed to enable a fair driver comparison. The results demonstrate that the IDS methodology effectively captures the heterogeneity of driver behaviour and powertrain technologies and can identify areas for improvement in driving behaviour.

Train delay propagation analysis, train delay reason attribution, data mining, Ggraph neural network

R. Tang[a], R. Liu[a], Z. Lin[a]

[a] *Institute for Transport Studies, University of Leeds*

Complex interactions between trains lead to delay propagation determined by many factors. In-depth insights are required to better understand how a delay at a location affects the wider network. In this study we investigate the cause-effect relations between the incidents and causes of initial delays using a GNN-based method. First, we use data mining to analyse the connectivity structure of the existing delay instances occurred in part of the GB rail network, based on their temporal-spatial sequence and cause-effect relations. Then we train a link prediction model, where each event/delay is modelled as a node and given any two nodes, we can predict whether they are linked, i.e., they have cause-effect relations using GraphSAGE neural network.

Category 8. Mobility as a Service and complex trip-chains including micromobility

Verification of the possibility of transportation conversion through the introduction of MaaS at the University of the Ryukyus

Y. Kikuchi[a], H. Sugawara[a], A. Ishii[a], D. Kamiya[b], A. Uechi[c]

[a] *Yachiyo Engineering CO., LTD., Research Institute for Infrastructure Paradigm Shift*

[b] *University of the Ryukyus, Faculty of Engineering*

[c] *University of the Ryukyus, Graduate School of Engineering and Science*

Introduction

The share of public transportation in Japan has been declining in recent years as more people use private vehicles as their primary mode of transportation, especially in regional metropolitan areas (Ministry of Land, Infrastructure, Transport and Tourism, 2017). If private vehicle use exceeds parking capacity, traffic congestion caused by waiting for parking will reduce the convenience of public transportation, triggering further decline in the number of public transportation users. Specifically, in Okinawa Prefecture –the target of this study– public transportation is limited to one railroad line, the monorail, and buses. Buses have been identified as having problems, such as "few services" and "late arrivals," resulting in low levels of public transportation convenience and use awareness (Ishii et al., 2019). Japan's public transportation policy is based on a maximum fare approval system subject to price-cap regulations, thus it is not sufficiently flexible for fare changes due to legal restrictions. Therefore, service improvements that actively utilize public transportation, such as park-and-ride and school bus systems to ease traffic congestion in urban areas, have not progressed as well as expected. Furthermore, many students who travel to their part-time jobs after classes commute to the university using their own vehicles because of the travel time of public transportation and lack of a regular schedule. There is concern that the influx of students commuting to universities using private vehicles will cause traffic accidents on campus and traffic congestion in the surrounding area, as well as increase greenhouse gas emissions from private vehicles. Therefore, the challenge is to provide such students with multiple means of transportation other than their own vehicles and to change their attitudes, so that they will use alternative means of transportation is required.

A new mobility service concept called mobility-as-a-service (MaaS) was launched in Finland in 2014, aiming to increase the convenience of mobility by combining various mobility services for door-to-door travel. The idea is to increase the convenience of mobility by combining various mobility services, such as bicycles, car sharing, and on-demand bus services, as well as public transportation, such as railways, subways, street cars/trams, and buses. Currently, the MaaS model is mainly operating in Europe, while in Japan, various MaaS models, including those of transportation operators, have been verified for introduction and considered for implementation since 2018. Most MaaS models being tested are specialized for transportation in sightseeing areas or for completing reservations for demand transportation in depopulated areas via mobile apps, among others. However, few aim to maintain public transportation as a means of transportation in the community.

Therefore, this study proposes a transportation demand management (TDM) approach that aims to shift university commuting from private cars to public transportation, and to maintain public transportation in the region. To do so, we propose a campus MaaS model that introduces shared bicycle services, carpooling to and from schools, and a parking lot use system. Campus MaaS is built on a blockchain-based platform, and a demonstration experiment was conducted using a mobile app that implements some of the proposed functions, targeting students and faculty members at the University of the Ryukyus in Okinawa Prefecture, Japan, where many students commute to school by private vehicles.

Methodology

Figure 1a shows the current commuting method to the University of the Ryukyus. Most students commute to the University of the Ryukyus via private vehicles, partly because parking on campus is free. Other means of commuting to the university include direct route buses and a combination of buses running on the main road, approximately 2 km from the university, and shared bicycles as a last-mile service. However, direct buses to the university are infrequent and can be delayed by 10 minutes or more on some days, causing students to be late for class (Ishii et al., 2019). In addition, reservations for the use of shared bicycles in Japan can only be made 30 minutes before use, and it is not clear whether bicycles will actually be available until just before using them, which does not ensure a reliable means of daily commuting to school.

Figure 93. Left picture: Current method for university commuting; Right picture: Example of MaaS model for university commuting

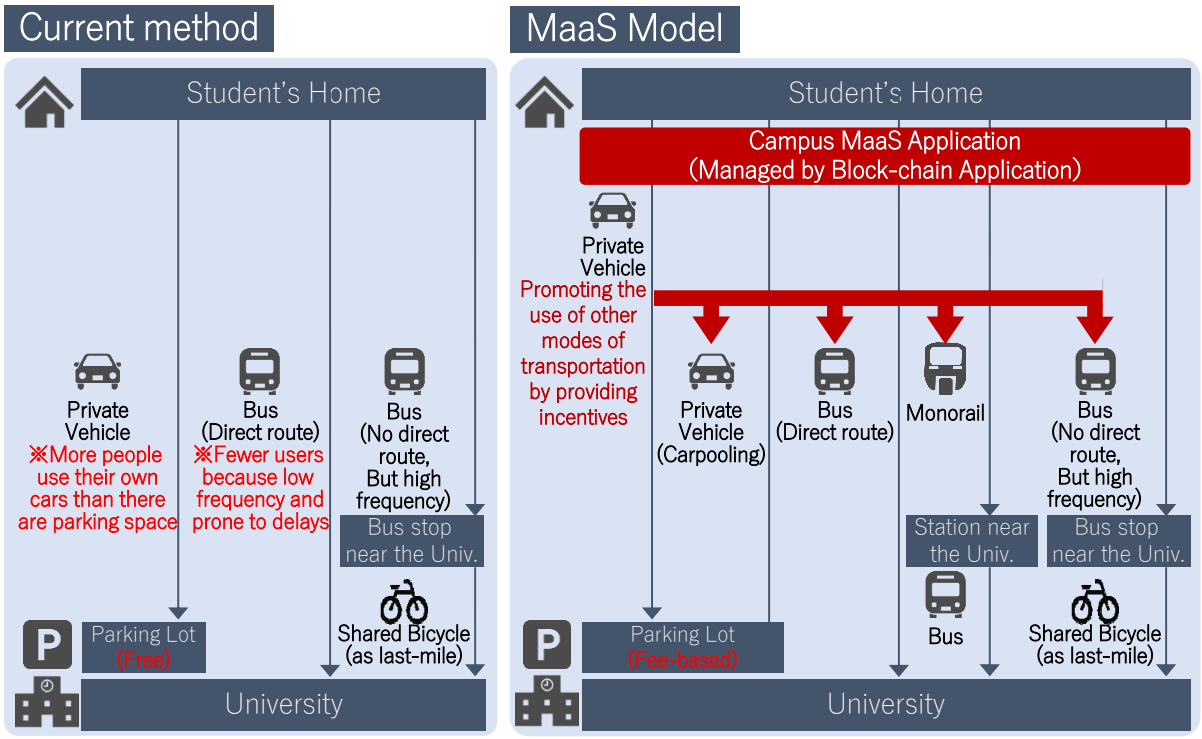

Source: Prepared by the authors.

To solve this problem, our proposed campus MaaS model provides "parking lot sharing", "advance shared bicycle reservation", and "reservation and payment integration" for parking and each means of transportation, as shown on Figure 1b. This model aims to optimize the use of parking spaces, promote the use of public transportation, and improve services. Specifically, for the campus MaaS model shown in Figure 1b, we propose an economic model that integrates transportation behavior and incentivization in a TDM measure to promote public transportation use. Currently, parking at the University of the Ryukyus is free; however, this model aims to reduce the use of private cars by charging parking fees. The parking fees can then be used as a source of funds, redistributed to students and faculty members who discourage the use of private cars and as a last-mile measure to encourage shifting to the use of public transportation. Figure 2 illustrates the economic model of campus MaaS.

Figure 94. Campus MaaS Economic Model

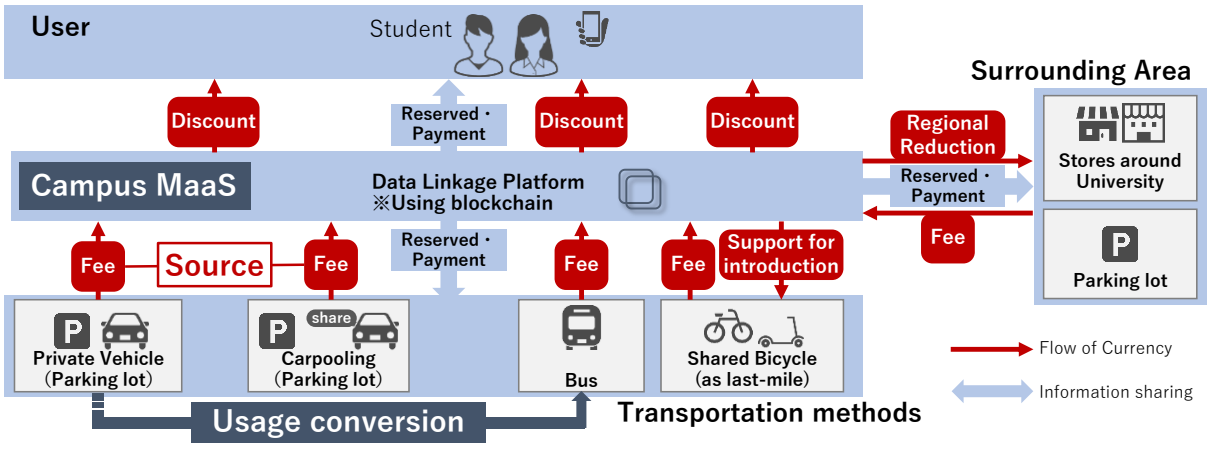

Source: Prepared by the authors.

To create a sustainable autonomous economic model, blockchain technology was used to provide a data collaboration platform. In applying blockchain technology, we evaluated it based on the indicators of necessity in the "Blockchain Technology Overview" flowchart provided by the U.S. National Institute of Standards and

Technology (Dylan et al., 2018). The results, it was determined that the application of blockchain was desirable given the need to provide multiple pieces of information for this demonstration experiment (publicizing the reservation status of parking, carpooling, and shared mobility), preventing falsification of reservation status, and eliminating the need to appoint an administrator for continuous and efficient management.

The demonstration experiment was conducted over 10 weekdays, from December 5 (Monday) to December 16 (Friday) 2022, at the University of the Ryukyus, in Nishihara Town, Okinawa Prefecture, Japan, and targeted the commuting behaviors of 25 people (16 students and 9 faculty members). At the University of the Ryukyus, approximately 1.5 times as many students (approximately 5,000) commute by vehicle as the number of parking spaces available (Kikuchi et al., 2022) and problems, such as "traffic congestion caused by waiting to enter parking lots," have become apparent. Since there was concern that students who did not commute to school using private vehicles would be reluctant to use public transportation due to the increased time and cost burden (bus fares, etc.), we considered those who chose a means that led to public transportation use as contributing to "reducing traffic congestion" and "maintaining regional public transportation." Therefore, we rewarded them with points as an incentive for choosing public transportation instead of private vehicles. To verify the effectiveness of the shift in transportation mode, we implemented the following two functions, which are part of the proposed model, on a blockchain platform:

1. Shared bicycle as last-mile service (registration can be made one week in advance).

   Shared bicycles were introduced as a means of access (last-mile) to the university from bus stops in the vicinity that are operated by high-frequency buses, thereby increasing the university transportation options.

2. Carpooling assist system.

   To reduce the number of private vehicles commuting to the university, a carpooling system was established in which several people ride together to the university. Carpool matching was implemented by issuing and acquiring tickets through blockchain-based smart contracts.

Results

Based on the analysis of the data posted on the platform, Figure 3 shows the results of the reservations and registrations for means of commuting during the experimental period. Overall, the largest number of participants used private vehicles (alone) at 71 (43%), while 38 (23%) used public transportation. There were four (2%) carpool drivers and passengers, and one (1%) shared bicycle user. In follow-up interviews regarding the reasons for the low use of carpooling, participants cited "resistance to riding in someone else's car" and "resistance to the increased time required" as reasons for the low use of carpooling. Thus, it is necessary to consider changes to the use system in the future. Regarding why only a few participants used the shared bicycle, some respondents stated that "the roads around the university are narrow and dangerous for bicycles," "the university is located on hilly terrain, making it difficult to use bicycles", and 23 of the 25 participants in the experiment did not consider using the shared bicycle because they could take the bus that goes directly to the university. Therefore, it is necessary to consider changing the shared bicycle use system in the future, as well as expanding the range of participants' residences in subsequent experiments. Regarding mode of transportation, 46 participants (28%) chose "other;" however, according to the interviews, they chose "walking" as their mode of transportation. It should be noted that some of the participants in the experiment are students who may be willing to use public transportation, and the results confirm that the redistribution of parking fees to public transportation users may convert approximately 20% of participants from private cars to public transportation. Though used infrequently, we were also able to establish the use of carpooling systems and shared bicycle, thus confirming the possibility that these can be used as a means of commuting to the university.

Figure 95. Reservations and registrations of means of transportation (experimental period)

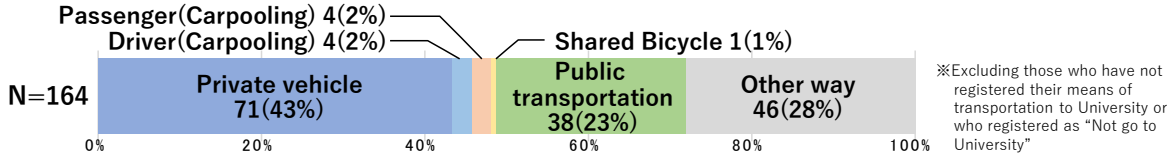

Source: authors' elaborations.

Conclusion

By introducing an advanced last-mile reservation system, a carpooling support system, and incentives when using public transportation, we were able to confirm the possibility of shifting from private vehicles to public transportation when commuting to the university. However, most of the participants in this experiment live in locations with high accessibility to the university. In future studies, the relationship between student residences, the required commute time, and the number of public transportation connections from their residences to the university must be analyzed to identify measures to optimize the commuting method. Moreover, when the number of people shifting away from private vehicles increases, the current public transportation infrastructure and other services may not be sufficient to handle the increase. Therefore, it is necessary to consider the scale of use conversion through the amount of incentives and other measures. Finally, because the platform constructed for the current experiment has not yet been linked to the data owned by each transportation administrator, a technical verification of the blockchain system must be conducted and rules for data linkages established in the future.

Acknowledgements

A total of 25 people, including staff at the University of the Ryukyus and students at the Kamiya Laboratory of the Department of Engineering, Faculty of Engineering, cooperated in the implementation of the demonstration experiment. We would like to express our gratitude to them.

References

Ministry of Land, Infrastructure, Transport and Tourism (2017), Movement of people in cities and its changes, City Planning Division of Ministry of Land, Infrastructure, Transport and Tourism, Tokyo.

Ishii A., Amakata Y., Sugawara H. and Ozasa K. (2019), Demonstration experiment for an integral approach of parking lot management and public transportation use pro-motion by using blockchain technology, Papers of research meeting on civil engineering planning, Vol. 59.

Dylan Y., Peter M., Nik R. and Karen S. (2018), Blockchain Technology Overview, National Institute of Standards and Technology, U.S. Department of Commerce, Washington, D.C.

Kikuchi Y., Sugawara H., Horii D., Kamiya D. and Uechi A. (2022), Research on pre-verification of Campus MaaS demonstration experiment system, Papers of research meeting on civil engineering planning, Vol. 66.

An approach based on simulation and optimization to integrate ride-pooling with public transport for a cooperative approach

Ester Lorente[ab], Jaume Barceló[a], Esteve Codina[a], Klaus Nökel[b]

[a] *Universitat Politècnica de Catalunya, Statistics and Operational Research Depart. Jordi Girona 1, Campus Nord, C5, 08034 Barcelona, Spain*

[b] *PTV Group, Haid-und-Neu-Str. 15, 76131 Karlsruhe, Germany*

Introduction

Mobility uses change, the way we travel to overcome the spatial separation of activities, the consequence of the urban spatial structure determined by the land use, and the physical connectivity provided by the transport infrastructure, changes over time due to technological and societal changes. Mobility as a Service (MaaS) emerged as a new form of combining both factors expected to improve mobility, especially in large urban areas. After a few years, the experience shows that has not always been the case, not only the expectancies have not been met, but the new mode has hindered public transport. The International Union of Public Transport (UITP) and the International Transport Forum (ITF) have made proposals and conducted exploratory studies aimed at defining policies to use these services as feeders of public transport to achieve a win-to-win strategy. This raises the problem of how to combine both modes in an intermodal system to achieve such objectives, especially in those areas of large metropolitan conurbations that, as a consequence of urban sprawl, cannot be efficiently served by conventional public transport. Ride-pooling, a form of Demand Responsive Transport, coordinated with multimodal public transport could be a solution. This paper explores how to model such systems, based on a simulation-based intermodal assignment approach, where an agent-based simulator manages service requests, accounting for the locations and capabilities of the vehicles in the fleet, and the schedules of the public transport, and the time constraints in a dialogue with an intermodal dispatcher defined by an optimization model, that proposes the best-combined solution.

Since the present system accounts for an intermodal scenario in which the ride-pooling serves as a feeder of the public transport, it makes sense to account for five different intermodal types of journeys: a 1-leg trip of either ride-pooling (RP) or public transport (PT), a 2-leg combined one of either RP+PT or PT+RP and a 3-leg combined one of RP+PT+RP. While the first four possibilities would be more common in areas with short routes, the latter one would be more suitable in lengthy interurban journeys since the additional transfer times may be absorbed into the overall journey duration.

This topic has lately been gaining some interest in the research community. Yet, based on our findings, the intermodality appears to be oversimplified. The majority simply assess the combination resulting from the nearest vehicle and stop, with only Hickman and Blume (2001) considering more than one stop. Moreover, studies such as Liang et al. (2016) and Stiglic et al. (2018) evaluate their approaches on artificial or small PT networks, as well as with a limited set of trip requests. Pinto et al. (2020), on the other hand, employ a larger test area but do not evaluate all intermodal types of journeys. In contrast, our research relies on a simulated approach that accounts for all the intermodal types, not only the nearest vehicle and stop, and is tested in a large realistic transportation network.

Figure 96. Intermodal system architecture

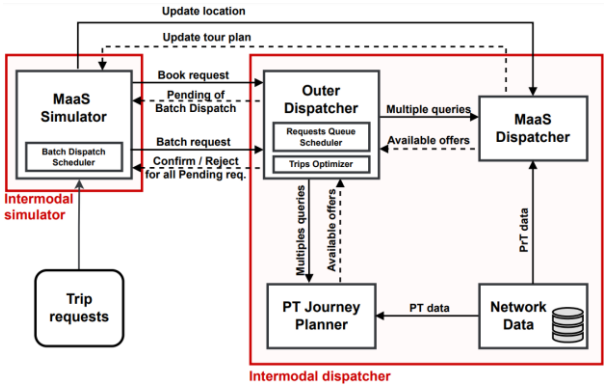

Figure 97. Relationships in the optimization model

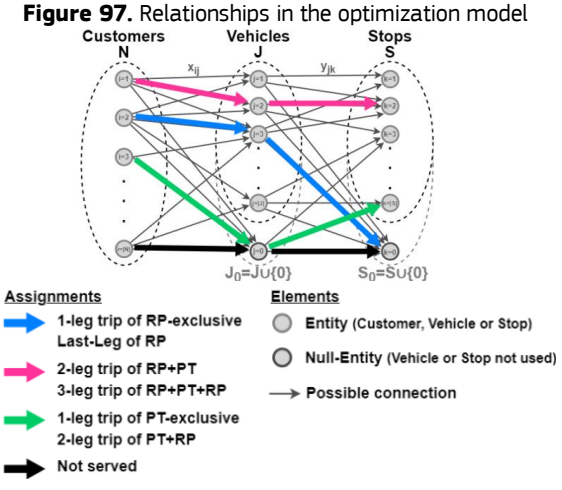

Figure 1 below depicts the proposed intermodal system. It consists of a simulator that evaluates the new use case based on simulation, and a dispatcher that, among other functions, calculates the new intermodal routes. The methodology of the present system is as the follow. When a request's booking time is reached, the simulator sends the request to the dispatcher, who responds with the proposed intermodal route. The simulator then updates the new tour plan and begins its simulation. Vehicle location updates are given to the dispatcher on a regular basis in accordance with these tour plans, ensuring that every component in the system is informed and up to date for future booking requests.

The intermodal simulator

The intermodal simulator, introduced in Lorente et al. (2021), is an event-scheduling and agent-based simulator that originally covered a ride-pooling exclusive scenario. However, for this research, it has been extended to account for the integration with the public transport. It has two type of agents: vehicles and customers. The vehicle represents a vehicle moving between pick-up and drop-off locations. A customer, on the other hand, represents a customer who books and performs a trip. Its behavior has been extended so that his journey consists of various legs of ride-pooling and public transportation modes, and may transfer between modes. It has also been enhanced with a batch dispatching strategy, which groups and solves requests that arrive in a short period of time (a batch) together to maximize the system's resources (fleet of vehicles and system performance).

The intermodal dispatcher

The intermodal dispatcher, introduced in Lorente et al. (2022), is made up of various components. The core, the Outer Dispatcher, determines the intermodal tour plans based on the information supplied by the other two components that handle each transport mode to combine: MaaS Dispatcher, a ride-pooling dispatcher, and PT Journey Planner, a route planner based on rRAPTOR (Delling et al. (2012).

Due to the batch dispatching strategy, the booking requests, when received by the dispatcher, are queued in the dispatcher's queue and kept unanswered until a batch request arrives and responds with a solution for every pending request in the queue. Furthermore, because it is difficult to accurately determine the best ride-pooling vehicle for long trips containing a last-leg of ride-pooling that far in advance, a delay-dispatching strategy has been adopted, which separates the dispatching procedure of these kinds of trips into two batch iterations: in the first, the first part of the trip is determined (until the transit leg) with an estimation of the last-leg of ride-pooling. Then, in a second iteration, when the time-window of this last-leg approaches, the ride-pooling vehicle is finally determined. This makes it necessary to consider the so-called LL request types referring to Last-Leg requests.

The intermodal dispatching algorithm consists of a three-step algorithm. First, the candidate vehicles and stops that could be potentially combined to form these combined trips are heuristically determined by restricting the search space from the origin and destination areas. Then, the tour plans options are determined using the MaaS Dispatcher and PT Journey Planner, finding suitable combinations from the set of candidate found before. And lastly, the best-combined solution is determined by means of an optimization model explained below.

The model assumes that there is a set of customer requests N, a set of ride-pooling vehicles J and a set of transit stops S. Each customer will be assigned to a vehicle and a stop. Figure 2 depicts the possible decisions. For convenience, a "null-vehicle" and a "null-stop" represent not using a vehicle or a stop. Hence, two additional sets are defined: $J_0 = J \cup \{0\}$ and $S_0 = S \cup \{0\}$.This suggests the use of model using binary variables x_{ij} and $y_{jk}, i \in N, j \in J_0, k \in S_0$, representing the customer-to-vehicle and vehicle-to-stop assignment, which admit a representation as binary network flow on the graph. Additionally, variable z_{ijk} represents the customer-to-vehicle-and-stop assignment. The optimization model (c1) to (c6') below yields the modal trip composition. Constraints (c1) to (c2''') verify the flow restrictions, while (c3) to (c5) (omitted due to abstract space limitations) express the time-constraints of the assignments. (c6) to (c6') impose the fulfillment of the customer's intermodal preference (N^a wants RP-exclusive and N^b the PT included. Requests not in these sets do not impose a preference). The model seeks to minimize the overall cost of the assignments denoted by c_{ijk} considering their travel time and fare (based on reported fares from equivalent enterprises already operating in the experiment's test area), while also penalize requests not served with T_1 to T_4, which applies a 4-level request prioritization that prioritizes LL requests with the highest priority, followed by requests that could not be solved in a previous dispatch, and a priority distinction to encourage requests to be booked in advance rather than at the last minute.

$$\mathrm{Min}_{x,y,z,T} \sum_{i\in N} \sum_{j\in J_0} \sum_{k\in S_0} c_{ijk} z_{ijk} + T_1 + T_2 + T_3 + T_4$$

$$\sum_{j\in J_0} x_{ij} = 1, \mathrm{i} \in N \ (c1)$$

$$\sum_{i\in N} x_{ij} \leq 1, \ j \in J (c1')$$

$$\sum_{i\in N} x_{ij} = \sum_{k\in S_0} y_{jk}, \ \ j \in J \ (c1'')$$

$$z_{ijk} \geq x_{ij} + y_{jk} - 1, \ i \in N, j \in J, \ k \in S_0 (c2)$$

$$z_{ijk} \leq x_{ij}, \ \ z_{ijk} \leq y_{jk}, i \in N, j \in J_0, \ k \in S_0 \ (c2')$$

$$x_{i0} \leq \sum_{k\in S_0} z_{i0k} \ \ i \in N \ (c2'')$$

$$y_{0k} \leq \sum_{i\in N} z_{i0k}, k \in S_0 \ (c2''')$$

$$\sum_{j\in J} z_{ij0} = 1 - x_{i0}, \mathrm{i} \in N^a \cup N_{LL}, (c6)$$

$$\sum_{j\in J} \sum_{k\in S} z_{ijk} = 1 - x_{i0}, \ i \in N^b \ (c6')$$

$$x_{ij} \in \{0,1\}, \ y_{jk} \in \{0,1\}, \ z_{ijk} \in \{0,1\}, \ i \in N, \ j \in J_0, \ k \in S_0$$

$$T_i \geq 0, i \in N$$

It is assumed that for each stop, the most convenient stop near the destination location has been established in a prior step of the dispatching algorithm. Depending on how close it is to the destination, the customer may be able to walk there, but if not, a ride-pooling last-leg would be estimated.

Results

The proposed approach has been computationally tested in the close to reality large real transport system of the main part of the First Crown of the Metropolitan Area of Barcelona, with an extension of 20x15 kilometers and a high urban density. The required data has been obtained from the Barcelona Virtual Mobility Lab model (Montero et al. (2018)), which is depicted in Figure 3. The public transport network includes bus, metro, railways and trams, with about 3,000 stops, nearly 300 distinct bus lines, 10 metro lines, 16 railways lines and 2 tramways and providing more than 6,000 services during the operational horizon assumed in the tests (from 9 am to 13 pm). Moreover, the private traffic network is constituted of 114,000 links and 87,300 nodes. The experiments were carried out using a collection of 10,031 trip requests, with departures spread over a 4-hour period (from 9 am to 12 pm). Table 1 shows an example of three experiments that assess if the LL is not delayed, if it is dispatched 40 minutes before the customer leaves the PT system, or if a vehicle reservation strategy is employed 60 minutes in advance. These findings show how not delaying the LL dispatch is the most reliable option and delaying it may result in some being left at the stop (the LL could not be dispatched).

Figure 98. Test area showing the transit network

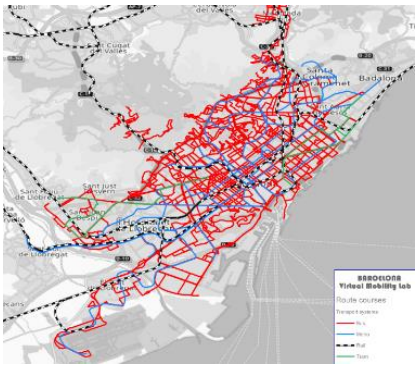

Test area showing the transit network However, if a vehicle reservation strategy is used, the system serves slightly more requests, completes all trips while also producing more profitable results.

Table 17. Results summary, including number of trips, average travel time and fare per intermodal type, number of customers left at stop (LL could not be dispatched), and system's profit (deducting salaries and fuel costs)

LL configuration	Served demand					Left at stop	Profit
	RP	PT	RP+PT	PT+RP	3-leg		
Dispatch not delayed	1,216 58.5min 10,4€	5,540 26.5min 1,1€	574 40.8min 4,4€	501 56.6min 5,1€	113 68.1min 8,8€	0	5,543.6€
Dispatch 40 min adv. No reservation	1,144 62.9min 10,9€	5,418 26.0min 1,1€	443 40.5min 4,3€	774 52.5min 5,0€	123 59.5min 8,6€	27	5,882.3€
Dispatch 40 min adv. Reservation 60 min adv.	1,206 58.7min 10,3€	5,497 26.4min 1,1€	545 40.7min 4,3€	570 54.9min 5,4€	136 62.7min 8,8€	0	5,747.9€

Conclusions

The simulations show that travel times and user fares are competitive, especially for 2- and 3-leg trips and that the system is appealing as it may not only act as a feeder for the central PT system, but also for the RP system, since commuters in the surrounding areas may become its clients.

Acknowledgements

This work was supported by an Industrial PhD of the Generalitat de Catalunya and PTV-AG under Grant DI-071 2019; and a research project of the Spanish R+D Programs under Grant PID2020-112967GB-C31. Also, many thanks to inLabFIB-UPC for allowing us to use one of their machines for the experiments.

References

Delling, D.; Pajor, T. and Werneck, R. Round-Based Public Transit Routing. In Proceedings of the Proceedings of the 14th Meeting on Algorithm Engineering and Experiments (ALENEX' 12), 2012.

Hickman, M. and Blume, K., Modeling Cost and Passenger Level of Service for Integrated Transit Service. In Computer-Aided Scheduling of Public Transport; Vos, S.; Daduna, J.R., Eds.; Springer Berlin Heidelberg: Berlin, Heidelberg, 2001; pp. 233–251.

Liang, X.; de Almeida Correia, G.H. and van Arem, B., Optimizing the service area and trip selection of an electric automated taxi system used for the last mile of train trips. Transportation Research Part E: Logistics and Transportation Review, 2016, 93, 115–129.

Lorente, E.; Barcelo, J.; Codina, E. and Noekel, K., An Agent-based Simulation Model for Intermodal Assignment of Public Transport and Ride Pooling Services. Presented at 2021 International Symposium on Transportation Data and Modelling (ISTDM 2021), 21st - 24th June 2021, Virtual due to COVID-19.

Lorente, E., Barceló, J., Codina, E., and Noekel, K., An Intermodal Dispatcher for the Assignment of Public Transport and Ride Pooling Services. 24th Euro Working Group on Transportation Meeting. Transportation Research Procedia, 2022, 62, 450–458.

Montero, L., Linares, P., Salmerón, J., Recio, G., Lorente, E., and Vázquez, J.J. Barcelona Virtual Mobility Lab: The multimodal transport simulation testbed for emerging mobility concepts evaluation, ADAPTIVE 2018.

Pinto, H.K.; Hyland, M.F.; Mahmassani, H.S. and Omer Verbas, I., Joint design of multimodal transit networks and shared autonomous mobility fleets. Transportation Research Part C: Emerging Technologies, 2020, 113, 2–20.

Stiglic, M.; Agatz, N.; Savelsbergh, M. and Gradisar, M., Enhancing urban mobility: Integrating ride-sharing and public transit. Computers & Operations Research, 2018, 90, 12–21.

Mobility as a Service for commuters. Estimation of environmental impacts in a medium-sized city

Riccardo Ceccato[a], Andrea Baldassa[a], Federico Orsini[a], Riccardo Rossi[a], Massimiliano Gastaldi[ab]

[a] *Department of Civil, Architectural and Environmental Engineering, University of Padua, Padua 35131, Italy*

[b] *Department of General Psychology, University of Padua, Padua 35131, Italy*

The evaluation of impacts of Mobility as a Service (MaaS) on environment has received little attention. This study aims to forecast the diffusion of MaaS in a medium-sized city and quantify the consequent reduction in pollutant emissions for commuting trips. Results of a mobility survey administered to employees of the Municipality of Padova (Italy) were used to calibrate a model predicting MaaS adoption, that was applied to real working trips to estimate vehicle emissions in scenarios with different bundles. A reduction in the range of 4-41% was quantified, depending on the proposed scenario, if compared with the current situation, indicating that MaaS can contribute to reach sustainable goals even in medium-sized cities, however the extent of these benefits depends on its design.

Category 9. Pricing strategy

A tradable credit scheme to manage the morning commute problem in a multimodal network

G. Albano [a], M. Mattas[b], A. Mourtzouchou[a], B. Ciuffo[b]

[a] *Piksel SRL*

[b] *European Commission – Joint Research Centre*

Introduction

Traffic congestion negatively affects the quality-of-life of the people, causing significant costs at individual, social, and economic levels (Rahman et al., 2021). Generally, there are two ways to alleviate traffic congestion: enhancing the supply or acting on the demand. In the first case, the objective is to expand the road capacity by building new roads and facilities or adding lanes to existing roads. The second approach, called demand management, consists in reducing and/or fairly distributing the traffic demand. Congestion pricing schemes and car rationing policies are examples of demand management strategies.

In the last decade, a new type of demand management strategy has attracted much interest in the transportation community: the tradable credits scheme (TCS) (Yang and Wang, 2011). In a TCS, a central authority (CA) aims to decrease the congestion on a transportation network. The CA designs a charging scheme and sets the traffic demand to be served by allocating a certain number of credits. The users of the network are the recipients of this allocation. They make their mobility choices taking into account their personal credits budget. In fact, users have to pay an amount of credits to the CA that varies depending on how much the choice made is in line with the CA's objective. If the budget is not enough to afford the charge, the user can buy additional credits from other users whose mobility choices led them to save credits. This buy/sell mechanism takes place on a market monitored by the CA.

Since the pioneering paper of (Yang and Wang, 2011), many TCSs have been proposed to either reallocate the traffic demand in space and time or discourage car usage in favor of alternative modes of transport (Balzer and Leclercq, 2022; Bao et al., 2019; Liu et al., 2022; Nie, 2012; Nie and Yin, 2013). Furthermore, game and field experiments have been carried out to study the effectiveness of TCS and the response of people to such technology (Aziz et al., 2015; Brands et al., 2021, 2020). However, no full-scale TCS has been implemented yet. The main difficulties lie in the complexity of the problems and the high transaction costs related to monitoring the vehicles and trading the credits. In fact, the majority of the works consider link-specific or distance-based charging schemes, which imply knowing the path chosen, and so the position of the vehicles. Moreover, the most adopted credits market is a peer-to-peer negotiated market, with the CA only ensuring the transparency of the transactions. This type of market may give space to speculators and presupposes a constant update of the credit price.

In the present paper, we propose a TCS with a mode-based and time-varying charging scheme, with the users trading the credits directly with the CA. The network considered is formed by M origins and a single destination. The latter is assumed to be a limited area with one gate entrance representing a bottleneck. The scope of the CA is twofold: decrease the number of vehicles accessing the area every day and spread the vehicle demand in time to reduce the waiting time at the entrance.

Methodology

We considered a traffic demand consisting of N homogeneous users coming from M different origins. All the users have the same destination, which is the gate entrance of the limited area. Each user commutes from his/her origin to the destination on a daily basis and has four mode alternatives to complete the trip: car, bus, bike, or on foot. Users arriving by car contribute to the formation of the queue at the entrance. A CA implements a TCS to decrease the number of vehicles accessing the area every day, and spread the vehicle demand in time to reduce the waiting time at the entrance. As a first step, the CA allocates a certain amount of free credits every week, according to a uniform strategy. The credits expire after one week, so none can gain by banking them, and speculations are limited.

Then, the CA introduces the following charging scheme: users who arrive by bus, bike, and on foot are not charged; vice versa, users who commute by car have to pay a tariff in credits to compensate for the emission/congestion caused. The tariffs vary depending on the arrival time window. We considered four different arrival time intervals: 7.30 AM - 8.00 AM, 8.00 AM - 8.30 AM, 8.30 AM - 9.00 AM, 9.00 AM – to the rest of the day. We assumed that 8.00 AM - 8.30 AM is the desired arrival window for all the drivers, and the related tariff is the highest one. Drivers who arrive before/after the desired time window experience an early/late arrival cost. In general, the travel costs for each mode are the following:

$$\begin{cases} C_{car}^{Wi} = MC_{car} + \alpha * TT_{car} + \alpha * WT_{Wi} + AC_{Wi} + \tau_{Wi} * p \\ C_{bus} = MC_{bus} + \alpha * TT_{bus} \\ C_{bike} = MC_{bike} + \alpha * TT_{bike} \\ C_{on\ foot} = MC_{on\ foot} + \alpha * TT_{on\ foot} \end{cases} \quad (1)$$

where: *MC* is the mode cost which includes the mode preference and the fixed cost associated with the mode. *TT* is the travel time, calculated as the O-D distance divided by the average speed of the mode, whereas α is the Value of *Time*. WT_{Wi} is the waiting time experienced by a driver arriving at the gate entrance at the time window *Wi*. This waiting time is a function of the number of vehicles registered the previous day during the same time window. AC_{Wi} and τ_{Wi} are the arrival cost and the credit cost associated to the arrival time window *Wi*. Finally, p represents the credit price.

The decision process follows a nested logit model. The users choose the mode of transport, and in case it is the car, they have to decide the arrival time window, as depicted in Figure 1. The probability to choose the car and the arrival time window Wi is given by:

$$Pr_{car}^{Wi} = \frac{e^{\frac{-C_{car}^{Wi}}{\lambda_{car}}} \left(\sum_j e^{\frac{-C_j}{\lambda_{car}}} \right)^{\lambda_{car}-1}}{\sum_l \left(\sum_j e^{\frac{-C_j}{\lambda_j}} \right)^{\lambda_l}} \quad (2)$$

where *j* are the different alternatives in the nest *l*, whereas λ_{car} is a parameter that measures the degree of independence among the alternatives in the nest car.

Figure 99. Decision process via nested logit

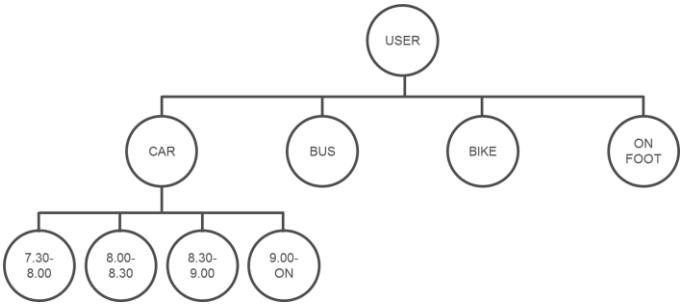

Source: Authors' elaborations.

In the present scheme, the CA acts as a virtual bank. Users can trade the credits directly with the CA. The latter sets an initial credit price and then adjusts the price on a daily basis. We adopted the same price adjustment mechanism proposed by (Liu et al., 2022). According to this mechanism, the credit price for the day d+1 is based on the previous credit price and the expected excess credit consumption Z as:

$$p(d+1) = p(d) + Q(p(d), Z) \quad (3)$$

Results

We carried out a simulation with 200 users randomly assigned to 5 different origins. Each origin has a different distance from the destination: 2, 7, 15, 25, 40 km. The CA allocates 8 credits per week and sets the following credit tariffs: $\tau_{7.30-8.00} = 3$, $\tau_{8.00-8.30} = 5$, $\tau_{8.30-9.00} = 4$, $\tau_{9.00-on} = 2$. The initial credit price is set to 0.01€. The results are presented in Figure2. Under the TCS, the number of users arriving by car starts decreasing, whereas the number of users choosing alternative modes increases. At the same time, the cars are uniformly spread over the time windows, as shown in figure 2b. The credit price becomes stable, and the difference between the credits allocated and the credits consumed tends to zero after a transition period. These two last outputs confirm the robustness of the model and how it converges to an equilibrium condition.

Figure 100. Simulation results

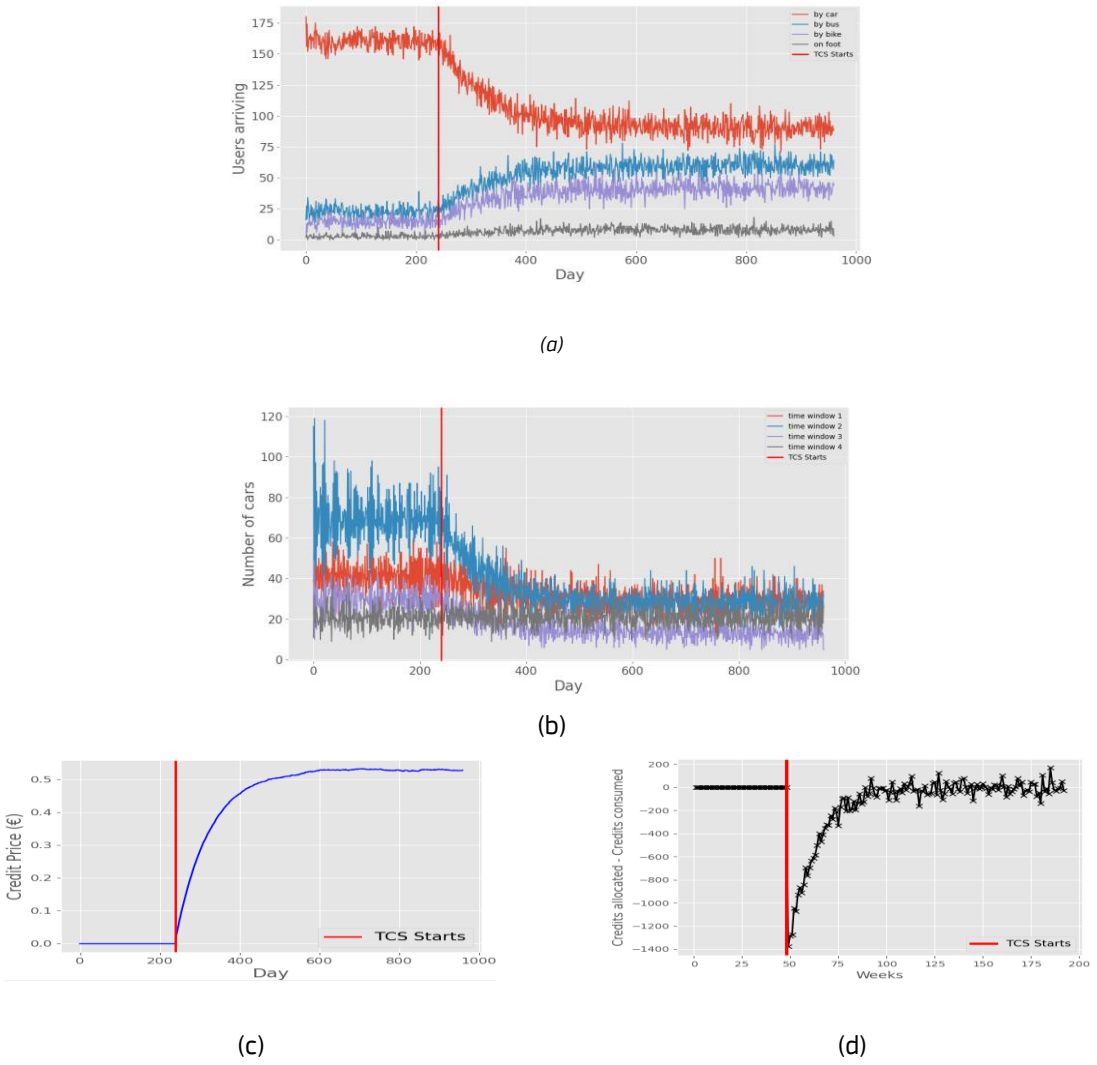

Source: Authors' elaborations.

Conclusions

Although the TCSs have been recognized as a promising instrument to decrease traffic congestion and the literature is dense of models, no full-scale TCS has been implemented yet. Most of the proposed models adopt link-specific or distance-based charging schemes, which imply knowing the position of the vehicles and generate issues in terms of complexity and privacy. Morerover, the majority of the works consider a peer-to-peer negotiated market for the credits. This type of market presupposes a constant update of the credit price and may leave space for speculators. In the present paper, we propose a practical TCS with a mode-based and time-varying charging scheme to reduce and spread in time the vehicle demand. The users can trade the credits directly with the CA, which acts as a virtual bank. The results show the effectiveness and robustness of the

model. For further research, the heterogeneity of the users and their behavioral response have to be investigated.

References

Aziz, H.M.A., Ukkusuri, S.V., Romero, J., 2015. Understanding short-term travel behavior under personal mobility credit allowance scheme using experimental economics. Transportation Research Part D: Transport and Environment 36, 121–137. https://doi.org/10.1016/j.trd.2015.02.015.

Balzer, L., Leclercq, L., 2022. Modal equilibrium of a tradable credit scheme with a trip-based MFD and logit-based decision-making. Transportation Research Part C: Emerging Technologies 139, 103642. https://doi.org/10.1016/j.trc.2022.103642.

Bao, Y., Verhoef, E.T., Koster, P., 2019. Regulating dynamic congestion externalities with tradable credit schemes: Does a unique equilibrium exist? Transportation Research Part B: Methodological 127, 225–236. https://doi.org/10.1016/j.trb.2019.07.012

Brands, D., Verhoef, E., Knockaert, J., 2021. Pcoins for parking: a field experiment with tradable mobility permits. SSRN Journal. https://doi.org/10.2139/ssrn.3819842.

Brands, D.K., Verhoef, E.T., Knockaert, J., Koster, P.R., 2020. Tradable permits to manage urban mobility: Market design and experimental implementation. Transportation Research Part A: Policy and Practice 137, 34–46. https://doi.org/10.1016/j.tra.2020.04.008.

Hansen, M., Huang, Y., 1997. Road supply and traffic in California urban areas. Transportation Research Part A: Policy and Practice 31, 205–218. https://doi.org/10.1016/S0965-8564(96)00019-5.

Liu, R., Chen, S., Jiang, Y., Seshadri, R., Ben-Akiva, M., Lima Azevedo, C., 2022. Managing network congestion with a trip- and area-based tradable credit scheme. Transportmetrica B: Transport Dynamics 0, 1–29. https://doi.org/10.1080/21680566.2022.2083034.

Nie, Y. (Marco), 2012. Transaction costs and tradable mobility credits. Transportation Research Part B: Methodological 46, 189–203. https://doi.org/10.1016/j.trb.2011.10.002.

Nie, Y. (Marco), Yin, Y., 2013. Managing rush hour travel choices with tradable credit scheme. Transportation Research Part B: Methodological 50, 1–19. https://doi.org/10.1016/j.trb.2013.01.004.

Rahman, Md.M., Najaf, P., Fields, M., Thill, J.-C., 2021. Traffic congestion and its urban scale factors: Empirical evidence from American urban areas. International Journal of Sustainable Transportation 15. https://doi.org/10.1080/15568318.2021.1885085.

Yang, H., Wang, X., 2011. Managing network mobility with tradable credits. Transportation Research Part B: Methodological 45, 580–594. https://doi.org/10.1016/j.trb.2010.10.002.

Joint price and resource strategy under equity constraints

A. Yanyan Ding[a], B. Xiaoshu Ding[a], C. Wentao Huang[a], D. Sisi Jian[a]

aDepartment of Civil and Environmental Engineering, The Hong Kong University of Science and Technology, Clear Water Bay, Kowloon, Hong Kong SAR

Introduction

In the mobility system, mobility service providers (MSPs) are mainly selfish entities that aim to maximize their own profits using pricing instruments and operation strategies. For example, ride-sourcing operators and bike-sharing operators allocate different numbers of vehicles to different zones and set discriminatory prices for different groups of customers (Bennaceur et al. 2020, Duran-Rodas et al. 2020). Their resource allocation and pricing strategies are designed to maximize their own profits. This may lead to a situation where low-income customers are less likely to be allocated to desired mobility services, especially during congested periods. Meanwhile, travelers living in remote areas (often low-income people) may incur higher prices, while travelers in urban districts (often high-income people) may be charged lower prices as a result of profit-oriented resource allocation and pricing strategies. Such inequity can harm the welfare of some traveler groups and undermine the sustainable development of the transport service market. For example, there may exist some equilibrium states in which no MSPs are willing to take trip orders from weak minorities, while MSPs may compete to serve customers with a high income, resulting in an unbalanced distribution and utilization of mobility resources. Motivated by these realistic challenges, we discuss the optimal resource allocation and pricing strategies of MSPs under not only the capacity constraint but th 额 equity constraint as well. In previous studies, researchers explored the equity problem by only considering either resource allocation (Jiang and Zografos, 2021, Yin et al. 2022) or pricing strategies (Holguín-Veras et al. 2020, Zhu et al. 2022). Different from prior studies, we examine the impacts of joint resource and price decisions under both equity and capacity constraints.

The general model

We consider an MSP providing mobility services for travelers with unit operational cost c. Travelers are categorized into multiple groups based on their socio-demographics, such as income, spatial location, gender, race, age, etc. We index these groups by 1,2, ... and include in a set I. The potential number of travelers (i.e., the market size) in group i is denoted as $N_i, \forall\, i \in I$. The travelers from group i have valuation v_i for the mobility service provided by the MSP, which is a random variable that is uniformly distributed on $[0, \overline{V}_i]$. The corresponding surplus is given by $u_i = v_i - \tau_i$. In comparison, we consider an outside option under which the surplus of travelers will be zero, i.e., $u_0 = 0$. Then, travelers compare the outside option and the MSP to determine their options, i.e., travelers in group i will choose the MSP if their valuation is no less than the offered price; otherwise, they will choose the outside option. Formally, the number of travelers choosing the MSP is $d_i = N_i\, P(v_i | v_i \geq \tau_i)$ and the number of travelers choosing the outside option is $d_0 = N_i P(v_i | v_i < \tau_i)$.

The MSP needs to first determine the long-term decision, i.e., the amount of mobility resources s_i (e.g., the number of vehicles if the MSP is a ridesourcing operator, service frequency if the MSP is a bus operator, etc.) and the short-term decision, i.e., the service price τ_i for each group i. When making the joint price and resource strategy, the MSP needs to consider two realistic constraints. The first constraint is known as the *capacity constraint*, i.e., the total number of resources allocated to all groups of travelers shall be no greater than the cap of its own resources, $\overline{s}$. The second constraint is the *equity constraint*. In practice, policy makers would allocate equity constraints that requires the MSP to satisfy, i.e., the MSP needs to determine the mobility resources and the service prices equitably among different groups. To capture the equity constraint, we let $R_i(s_i, \tau_i)$ represent the equity measure for group i. For simplicity, we denote it as R_i in the following discussion. In comparison, we use R_j to represent the equity measure for any other group j except of group i. Then, $|R_i - R_j|$represents the equity gap between two different groups. In addition, we use a superscript ``$*$" to represent the result under the optimal joint resource-pricing strategy. $|R_i^* - R_j^*|$ represents the equity gap in the without-equity-constraint case by taking the optimal join resource-pricing strategy. Under the mobility resource capacity constraint and the equity constraint, the MSP aims to maximize its profit by setting the number of allocated resources s_i to group i and the corresponding service price τ_i. The profit maximization problem of MSP is formulated as follows:

$$\max_{\tau_i, s_i} \pi_M = \sum_{i \in I} (\tau_i - c) \min(d_i, s_i) \tag{1}$$

s.t.

$$\sum_{i \in I} s_i \leq \overline{s} \tag{2}$$

$$\left|\tau_i - \tau_j\right| \leq (1-\alpha)\left|\tau_i^* - \tau_j^*\right|, \quad i,j \in I \tag{3}$$

$$s_i \geq 0, \qquad i \in I \tag{4}$$

Eq. (2) is the capacity constraint and Eq. (3) is the equity constraint, where $\alpha \in [0,1]$ represents the level of the equity and it is predetermined by the MSP, in order to satisfy regulatory requirements or internal goals. As α increases, the equity level raises. In light of this, $\alpha = 0$ corresponds to the without-equity-constraint case and $\alpha = 1$ corresponds to fully-equity case. To keep consistency, we denote it as α-equity constraint. In Eq. (3), we introduce the price equity constraint which is initiated by different dimensions (Cohen et al. 2021, 2022), i.e., the price discrimination shall not surpass that in the without-equity constraint situation. Eq. (4) guarantees the non-negativity of resources allocated to group i.

To ease the exposition, we consider that there exist two groups of travelers and the MSP determines the joint price and resource strategy under equity and capacity constraint in the following discussion. In comparison, we take the without-equity-constraint case (i.e., $\alpha = 0$) as the benchmark case, which compares with the with-equity constraint case (i.e., $\alpha > 0$).

The joint resource and price strategies between H- and L-income travellers

We consider that there are two groups of travelers: high-income Group (H-travelers) and low-income Group (L-travelers). To distinguish the two groups of travelers, we denote the highest intrinsic value of H-travelers as $\overline{V}$ and the highest intrinsic value of L-travelers as $\gamma\overline{V}$, where $\gamma \in (0,1)$. Then, the intrinsic value of H-travelers is uniformly distributed in $[0,\overline{V}]$ and the intrinsic value of L-travelers is uniformly distributed in $[0,\gamma\overline{V}]$. By comparing the relative value of surplus by choosing the MSP (i.e., $u_i = v - \tau_i$, $i \in \{H,L\}$ with the surplus by choosing the outside option (i.e., $U_0 = 0$), we can derive the numbers of H-travelers and L-travelers choosing the MSP and the outside option below:

$$d_H = \left(1 - \frac{\tau_H}{\overline{V}}\right) N_H \tag{5}$$

$$d_L = \left(1 - \frac{\tau_L}{\gamma\overline{V}}\right) N_L \tag{6}$$

$$d_0 = \frac{\tau_H}{\overline{V}} N_H + \frac{\tau_L}{\gamma\overline{V}} N_L \tag{7}$$

where d_H represents the number of H-travelers choosing the MSP and d_L represents the number of L-travelers choosing the MSP. The first part of d_0 represents the number of H-travelers choosing the outside option and the second part of d_0 represents the number of L-travelers choosing the outside option. From Eqs.(5-6), we observe that the travel demand decreases in the service prices. For clarity, we can write $d_H(\tau_H)$, $d_L(\tau_L)$, and $d_0(\tau_H,\tau_L)$ as the demand functions of travelers in terms of τ_H and τ_L. The maximal travel demand achieves when the service prices reduce to the marginal cost, i.e., the maximal number of H-travelers choosing the MSP is $\left(1 - \frac{c}{\overline{V}}\right) N_H$ and the maximal number of H-travelers choosing the MSP is $\left(1 - \frac{c}{\gamma\overline{V}}\right) N_L$.

In reality, there is no need to discuss the capacity and equity constraints, if the capacity is sufficient, e.g., it has already been greater than the total potential number of travelers, and all travelers will be satisfied. In light of this, we focus on the setting that resources are scarce and the MSP needs to strategically make pricing and resource allocation decisions to satisfy the capacity and equity constraints as well as maximization its own

profit. In fact, the MSP will not determine a service price lower than the marginal cost, because it cannot gain positive benefit. We can rewrite the optimization program of the MSP below:

$$\max_{\tau_H,\tau_L,s_H,s_L} \pi_M = \min(d_H, s_H)(\tau_H - c) + \min(d_L, s_L)(\tau_L - c) \tag{8}$$

s.t.

$$d_H = \left(1 - \frac{\tau_H}{\overline{V}}\right) N_H, d_L = \left(1 - \frac{\tau_L}{\gamma\overline{V}}\right) N_L \tag{9}$$

$$s_H + s_L \leq \overline{s} \tag{10}$$

$$|\tau_H - \tau_L| \leq (1-\alpha)|\tau_H^* - \tau_L^*|, \quad i, j \in I \tag{11}$$

$$s_H \geq 0, \qquad s_L \geq 0 \tag{12}$$

In the following discussion, we first analyze the without-equity-constraint case, and then analyze the with-equity-constraint case under the aforementioned three equity constraints.

Analysis and discussion

In this section, we compare the two situations: the without-equity-constraint situation and the with-equity constraint situation. To distinguish with the without-equity-constraint case, we use superscript "**" to represent the optimal solutions in the with-equity constraint case. In this section, we consider the price equity situation.

In the without-equity-constraint situation, we can solve that the optimal solutions below:

(i) There shall exist a unique optimal price solution $\tau_H^* = \frac{\overline{V}+t}{2}$ and $\tau_L^* = \frac{\gamma\overline{V}+t}{2}$, where we have $t = \max\left(\frac{\overline{V}(N_H+N_L-2\overline{s})}{N_H+\frac{N_L}{\gamma}}, c\right)$.

(ii) When $c \leq \frac{\overline{V}(N_H+N_L-2\overline{s})}{N_H+\frac{N_L}{\gamma}}$, the capacity constraint is binding and there shall exist a unique optimal resource solution $d_H(\tau_H^*) = s_H$ and $d_L(\tau_L^*) = s_L$. When $c > \frac{\overline{V}(N_H+N_L-2\overline{s})}{N_H+\frac{N_L}{\gamma}}$, the capacity constraint is unbinding and there are multiple resource solutions, where $d_H(\tau_H^*) \leq s_H$, $d_L(\tau_L^*) \leq s_L$, and $s_H + s_L < \overline{s}$.

In the with-equity-constraint situation, we can derive the following results:

(i) The MSP cannot be better off by determining price and resource decisions which induce that demand exceeds supply.

(ii) When $d_H \leq s_H$ and $d_L \leq s_L$, we obtain the following results: $\tau_H^{**} = \frac{\overline{V}+t}{2} - \frac{\mu\overline{V}}{2N_H}$ and $\tau_L^{**} = \frac{\gamma\overline{V}+t}{2} + \frac{\mu\gamma\overline{V}}{2N_L}$, where $t \equiv \max\left(\frac{\overline{V}(N_H+N_L-2\overline{s})}{N_H+\frac{N_L}{\gamma}}, c\right)$ and $\mu = \frac{\alpha(1-\gamma)}{\frac{1}{N_H}+\frac{\gamma}{N_L}}$.

To have a better explanation of the above results, we present Figure 1 below to illustrate the changes of price and resource decisions on the travel demand and MSP's profits. Figure 1(a) presents the results when capacity constraint is binding and Figure 1(b) presents the results when capacity constraint is unbinding. Red lines and regions (Y_1) represent the optimal results in the without-equity-constraint situation. Blue lines and regions (Y_2) represent the optimal results in the with-equity-constraint situation when demand does not surpass supply, whereas black lines and regions (Y_3) represent the results when demand surpass supply. It is evident that when $d_H + d_L < \overline{s}$, multiple resource solutions can be achieved due to redundant capacities, which are floating green lines. When $d_H + d_L = \overline{s}$, there shall exist a unique solution. Moreover, we can theoretically prove that the area follows $Y_1 > Y_2 > Y_3$. This indicates that the MSP gains the highest profit without equity constraints. Otherwise, it gains the highest profit when demand does not surpass supply.

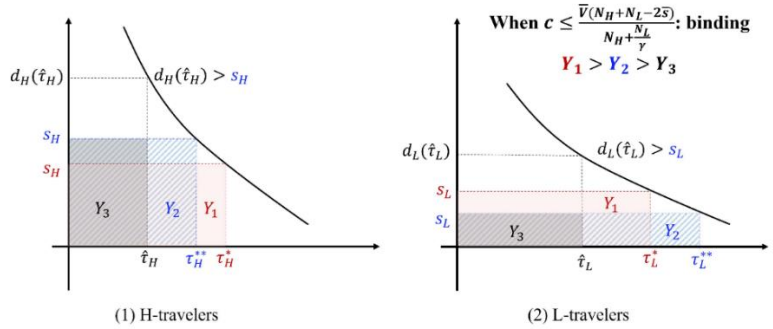

(a)When $d_H + d_L = \bar{s}$

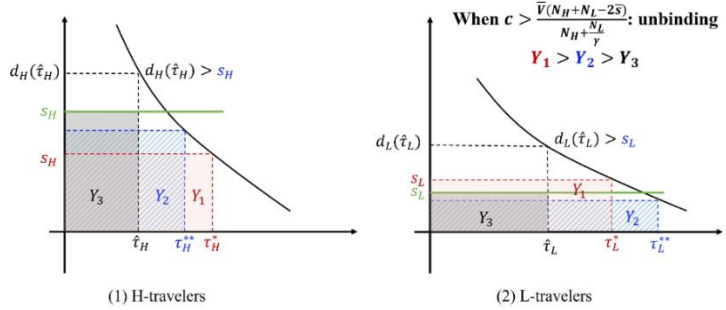

(a)When $d_H + d_L < \bar{s}$

References

Bennaceur, M., Delmas, R., & Hamadi, Y. (2022). Passenger-centric Urban Air Mobility: Fairness trade-offs and operational efficiency. Transportation Research Part C: Emerging Technologies, 136, 103519.

Cohen, M. C., Miao, S., & Wang, Y. (2021). Dynamic pricing with fairness constraints. Available at SSRN 3930622.

Cohen, M. C., Elmachtoub, A. N., & Lei, X. (2022). Price discrimination with fairness constraints. Management Science, 68(12), 8536-8552.

Duran-Rodas, D., Villeneuve, D., Pereira, F. C., & Wulfhorst, G. (2020). How fair is the allocation of bike-sharing infrastructure? Framework for a qualitative and quantitative spatial fairness assessment. Transportation Research Part A: Policy and Practice, 140, 299-319.

Holguín-Veras, J., Encarnación, T., & González-Calderón, C. A. (2020). User perception of fairness of time-of-day pricing and other typical toll discounts. Transportation Research Part A: Policy and Practice, 137, 560-581.

Jiang, Y., & Zografos, K. G. (2021). A decision making framework for incorporating fairness in allocating slots at capacity-constrained airports. Transportation Research Part C: Emerging Technologies, 126, 103039.

Yin, Y., Li, D., Han, Z., Dong, X., & Liu, H. (2022). Maximizing network utility while considering proportional fairness for rail transit systems: Jointly optimizing passenger allocation and vehicle schedules. Transportation Research Part C: Emerging Technologies, 143, 103812.

Zhu, G., Zhang, J., Xing, E., & Han, D. (2022). Pricing and quality decisions with conspicuous consumers. Transportation Research Part E: Logistics and Transportation Review, 165, 102857.

MobilityCoin system design– modelling challenges and opportunities

A. Loder[a], K. Bogenberger

[a] *Chair of Traffic Engineering and Control, Technical University of Munich, Germany*

Introduction

Tradable mobility credits (TMC) are currently discussed as a promising alternative to existing road user charging schemes, e.g., fuel excise taxes or congestion charges. TMC schemes do not follow the idea of Pigouvian pricing, i.e., marginal social cost pricing; contrary, TMC schemes are cap-and-trade schemes that define an upper limit to a to-be-regulated quantity, e.g., external costs, which is then linked to the credit volume. Credits are distributed among participants and schemes then usually requires credit redemption upon using or creating of the to-be-regulated quantity. Participants can trade credits based on supply and demand, while the resulting market price factors into the economic decisions of individuals and companies. In transport, the use of such credits has been proposed almost thirty years ago by Verhoef, Nijkamp, and Rietveld (1997), with increasing interest ever since especially on understanding the public's response to such policy proposal (Kockelman and Kalmanje, 2005; Krabbenborg, van Langevelde-van Bergen, and Molin, 2021). While textbook TMC schemes focuses on private transport and imposes charges, the idea can be generalized to imposing charges and providing incentives (negative charges) to all modes of transport. This idea has been proposed under the MobilityCoin framework by Blum et al. (2022). This framework is used in the following. In addition to studying the public's response, research on TMCs also focused on understanding experimentally how users interact on the market, e.g., Tian, Chui and Sun (2019) and Brands et al. (2020), as well as developing first integrated models to understand system design, responses and outcomes, e.g., Balzer and Leclercq (2022) and Tian and Chiu (Tian and Chiu, 2015). However, no policy model exists that studies the policy design of MobilityCoins schemes as a generalization of TMCs.

The introduction of policy instruments affecting entire nations means that a deep understanding is required of how a policy design affects individuals, the economy, and the environment. Especially for such radical innovations like TMC schemes the design problem is very complex as plenty of aspects must be considered and design decisions must be made (Provoost, Cats, and Hoogendoorn, 2023). Here, it can be considered that the core policy challenge is the definition of the overall system's objective, e.g., reduction of congestion and emissions or maximization of accessibility, and the derivation of suitable market volume, initial allocation to all travellers and the charging scheme. With the plethora of dimensions to be analysed, tools are required that can identify feasible, reasonable, and efficient parameter contributions. While agent-based approaches generally allow to investigate many of the mentioned aspects at an individual level, their large computation time especially for larger metropolitan areas or even nations, basically precludes any larger global parameter optimization. In. this paper we present our research on developing a macroscopic integrated transport model to investigate the policy design problem of MobilityCoin and TMC schemes.

Policy design problem

To investigate the outcomes of a particular MobilityCoin or TMC design, let us consider a transportation system with a network of nodes $\mathcal{N}$ and arcs $\mathcal{A}$. Nodes are referenced by $i, j, k \in \mathcal{N}$ and arcs are referenced by their start-end pair $(i,j) \in \mathcal{A}$. The system has modes of transport $\mathcal{M}$ that are referenced by $m \in \mathcal{M}$. The transportation system has origin-destination pairs $\mathcal{O}$, which are referenced by $(o,d) \in \mathcal{O}$. The set of origins and destinations $\mathcal{O}$ is a subset of the set of nodes $\mathcal{N}$. We consider three modes of transport: car, public transport, and bicycle, where only the first mode sees congestion effects, while the other two have fixed origin-destination travel times. We let X_{odm} being the share of travellers on origin-destination pair (o,d) using mode m, where W_{odm} describes the minimal travel costs on origin-destination pair (o,d) using mode m. Further, let T_{ij} be the travel time, Q_{ij} the flow of vehicles, and C_{ij} the total cost including charges and incentives on link (i,j). M_{ij} is the minimum travel cost from node i to j using the car. Further, consider that Y_{ijk} describes the flow of vehicles on link (i,j) towards node k and P the MobilityCoin/TMC market price. The policy design parameters are the individual initial allocation of credits, γ, origin-destination charges and incentives for each mode, λ_{odm}, and link-specific charges and incentives for each mode, κ_{ijm}.

The share of travellers X_{odm} is obtained using a logit-based assignment as a function of W_{odm}.

$$X_{odm} = \frac{\exp(-\mu W_{odm})}{\sum_{m' \in \mathcal{M}} \exp(-\mu W_{odm'})}$$

Where μ is a logit scale parameter. We obtain W_{odm} for cars and the other modes separately as defined below, where τ_{odm} is the exogenous and constant travel time.

$$W_{odm} = \begin{cases} M_{od}, & m = \{"car"\} \\ \tau_{odm} + P \cdot \lambda_{odm}, & else \end{cases}$$

The minimal travel costs M_{od} results from the link travel cost C_{ij}

$$C_{ij} = T_{ij} + P \cdot \kappa_{ij,\text{car}}$$

where T_{ij} is modelled by using the Bureau of Public Roads (BPR) function, computing link travel times T_{ij} as a function of flow Q_{ij}, and the arbitrage condition that describes Wardrop's user equilibrium. It states that an equilibrium is reached when no road user can reduce her or his travel costs anymore by unilateral action, where $\perp$ indicates complementarity (Ferris, Meeraus, and Rutherford, 1999)

$$C_{ij} + M_{jk} \geq M_{ik} \quad \perp \quad Y_{ijk} \geq 0$$

The flow on link (i,j) towards node k is positive only if the travel costs from i to k via j are equal to the minimum travel costs between i and k. Then, the total link flow Q_{ij} is obtained as follows.

$$Q_{ij} = \sum_{k} Y_{ijk}$$

Importantly, we must ensure that the in- and outflows at each node are balanced. This is ensured by the following constraint, where n_{od} is the total travel demand between origin-destination pair (o,d).

$$X_{od,\text{car}} \cdot n_{od} = \sum_{(o,j)\in\mathcal{A}} Y_{ojd} - \sum_{(j,o)\in\mathcal{A}} Y_{jod}$$

Last, the market clearing of the MobilityCoin/TMC scheme must be formulated. Here, only if the demand exceeds or is equal to the supply of MobilityCoins or credits, the market price P becomes non-zero and then results in an economic signal to individuals and companies (Yang and Wang, 2011).

$$\gamma \sum_{(o,d)\in\mathcal{O}} n_{od} \geq \sum_{m\in\mathcal{M}} \sum_{(i,j)\in\mathcal{A}} Q_{ij}\kappa_{ijm} + \sum_{m\in\mathcal{M}} \sum_{(o,d)\in\mathcal{O}} n_{od} X_{odm} \lambda_{odm} \quad \perp \quad P \geq 0$$

All listed constraints are then formulated as a single mixed-complementarity problem (MCP) (Ferris, Meeraus, and Rutherford, 1999). The key policy parameters γ, λ_{odm}, and κ_{ijm} can then be varied and the MCP be solved subsequently to assess the macroscopic outcomes of interest, e.g., mode choice, travel time and traffic externalities, and in particular the gap towards the set objective. Here, as emphasized by Balzer and Leclercq (2022), a starting point for defining a scheme's objective function for the identification of policy parameters are total travel times and carbon emission.

Case study

We illustrate the proposed policy design problem for MobilityCoin schemes using the simple network shown in Figure 1. For simplicity, we assume that cars have only link-specific charges and public transport, and bicycles have only origin-destination-specific charges. The network has 17 nodes of which 13 are origins and destinations of the travel demand. The origin-destination travel times τ_{odm} of public transport and bicycles are

set to a multiple of the free-flow travel times of cars, i.e., 1.35 and 1.4 respectively. All parameters of the network are available in the full paper.

Figure 101. The case-study network (own illustration)

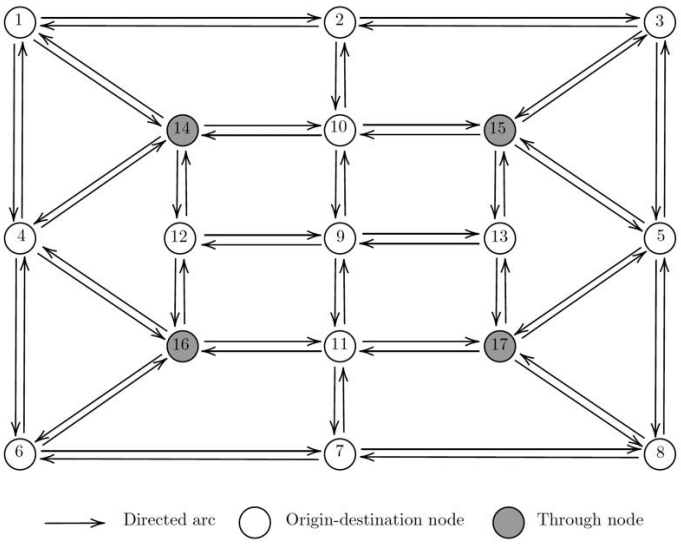

For the initial analysis, we set $\gamma = 1$ MoCo and $\kappa_{ij,\text{car}} = 0.5$ MoCo, and all other policy parameters to zero. We then incrementally impose a "central-business district" (CBD) charge for cars on all links from and to node "9" ranging from 1 to 16 MoCos as well as incrementally provide flat incentives for cyclists on all origin-destination pairs of 1 to 16 MoCos. We then solve the MCP and compute the total car travel production as a measure of externalities and the benefit each cyclist receives that computed as $|P \cdot \lambda_{odm}|$. Figure 2 shows the results. With higher CBD charges, car travel is reduced as less MoCos are available and the costs of alternative modes are cheaper. However, providing more MoCos as an incentive, i.e., increasing the market volume, slightly weakens the impact of increasing CBD taxes. Considering the benefits cyclists receive we find that at low CBD charge levels the market is oversupplied as the market price is zero, leading to zero benefit. Generally, we see that the benefit is increasing with the incentive provided, but it is larger when CBD charges are high.

Discussion

Already the simple example provided highlights complexity of MobilityCoin/TMC schemes and emphasizes that a throughout analysis of the interactions of system design parameters is required. A starting point would be the integration of the proposed macroscopic policy model into a mathematical problem with equilibrium constraints (MPEC) that has been previously been applied to transport-policy problems (Loder, Bliemer, and Axhausen, 2022). However, it is unlikely that this algorithm identifies a global optimum, but when using the status quo of a transportation system as the starting point, it can be expected that the solver identifies an optimal solution in the area around this starting point. Consequently, it can be argued that although a global optimum is not guaranteed, an optimum is found that is most policy relevant. In closing, the proposed model is clearly just a starting point. The next steps are the application to a real-world network and adding more details, e.g., socio-economic status of travellers. Further, adding better parameters on the behavioural responses to TMC/MobilityCoins supports the discovery of feasible, reasonable, and efficient policy parameters.

Figure 102. Simulation results (own illustration)

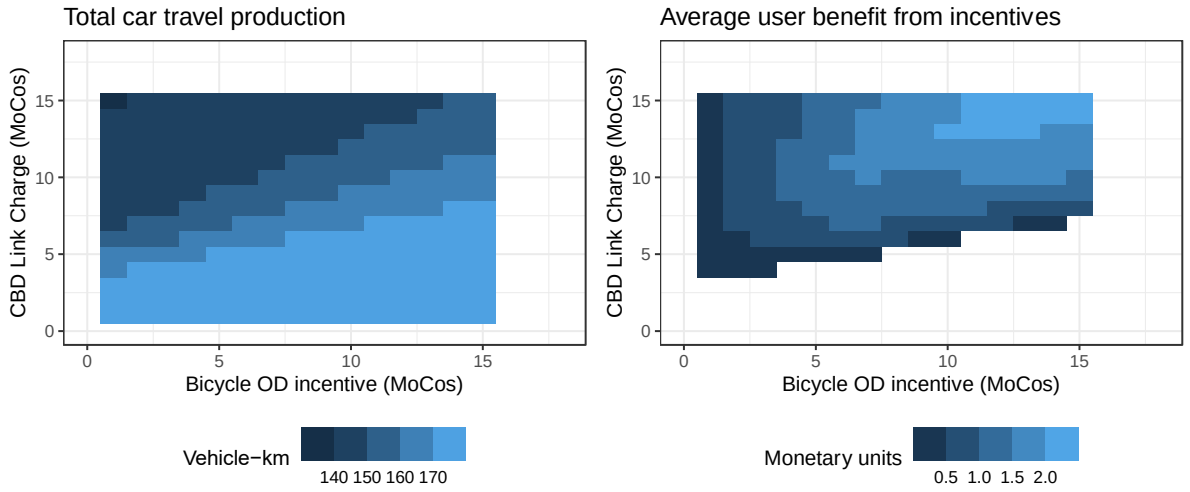

References

Balzer, L., and L. Leclercq, 'Modal Equilibrium of a Tradable Credit Scheme with a Trip-Based MFD and Logit-Based Decision-Making', Transportation Research Part C: Emerging Technologies, Vol. 139, June 2022, p. 103642.

Blum, P., L. Hamm, A. Loder, and K. Bogenberger, 'Conceptualizing an Individual Full-Trip Tradable Credit Scheme for Multi-Modal Demand and Supply Management: The MobilityCoin System', Frontiers in Future Transportation, Vol. 3, August 9, 2022, p. 914496.

Brands, D.K., E.T. Verhoef, J. Knockaert, and P.R. Koster, 'Tradable Permits to Manage Urban Mobility: Market Design and Experimental Implementation', Transportation Research Part A: Policy and Practice, Vol. 137, July 1, 2020, pp. 34–46.

Ferris, M.C., A. Meeraus, and T.F. Rutherford, 'Computing Wardropian Equilibria in a Complementarity Framework', Optimization Methods and Software, Vol. 10, No. 5, 1999, pp. 669–685.

Kockelman, K.M., and S. Kalmanje, 'Credit-Based Congestion Pricing: A Policy Proposal and the Public's Response', Transportation Research Part A: Policy and Practice, Vol. 39, No. 7–9, August 1, 2005, pp. 671–690.

Krabbenborg, L., C. van Langevelde-van Bergen, and E. Molin, 'Public Support for Tradable Peak Credit Schemes', Transportation Research Part A: Policy and Practice, Vol. 145, March 1, 2021, pp. 243–259.

Loder, A., M.C.J. Bliemer, and K.W. Axhausen, 'Optimal Pricing and Investment in a Multi-Modal City — Introducing a Macroscopic Network Design Problem Based on the MFD', Transportation Research Part A: Policy and Practice, Vol. 156, No. January, 2022, pp. 113–132.

Provoost, J., O. Cats, and S.P. Hoogendoorn, 'Design and Classification of Tradable Mobility Credit Schemes', Washington D.C., 2023.

Tian, Y., and Y.C. Chiu, 'Day-to-Day Market Power and Efficiency in Tradable Mobility Credits', International Journal of Transportation Science and Technology, Vol. 4, No. 3, 2015, pp. 209–227.

Tian, Y., Y.C. Chiu, and J. Sun, 'Understanding Behavioral Effects of Tradable Mobility Credit Scheme: An Experimental Economics Approach', Transport Policy, Vol. 81, September 1, 2019, pp. 1–11.

Verhoef, E., P. Nijkamp, and P. Rietveld, 'Tradeable Permits: Their Potential in the Regulation of Road Transport Externalities', Environment and Planning B: Planning and Design, Vol. 24, No. 4, August 1, 1997, pp. 527–548.

Yang, H., and X. Wang, 'Managing Network Mobility with Tradable Credits', Transportation Research Part B: Methodological, Vol. 45, No. 3, 2011, pp. 580–594.

Credit Charge-cum-reward Scheme for Green Multi-modal Mobility

Hongxing Ding[a], Hai Yang[a,b], Xiaoran Qin[a] , Hongli Xu[c]

[a] *Department of Civil and Environmental Engineering, The Hong Kong University of Science and Technology, Hong Kong, China.*

[b] *Intelligent Transportation Thrust, The Hong Kong University of Science and Technology (Guangzhou), Guangzhou, China.*

[c] *School of Engineering and Management, Nanjing University, Nanjing, 210000, China.*

To promote green mobility, we propose a credit charge-cum-reward (CCR) scheme where the government determines mode-specific credit charging/rewarding rates and redemption/charging prices. Over a CCR scheme period, travelers choose driving by consuming credits or taking transit to cumulate credits to minimize individual travel costs. In the end, the individual credit balance will be settled by the government at a charging (redemption) price for credit deficits (surpluses). We formulate the travelers' periodic mode usage equilibrium as a decision optimization problem. Based on the analysis of travelers' behavior, we further investigate the Pareto-improving and revenue-neutral CCR scheme and examine the relationship between credit prices and the government's credit-related budgets.

Category 10. Evolving transport impact on energy consumption

Comparison of different methods to identify high-emitting vehicles through real-world measurements in Florence using a novel Remote Sensing Device

L. J. Kramer[a], H. Walker[a], J. Buhigas[b]

[a] *Ricardo Energy and Environment*

[b] *Opus RS Europe SL*

Introduction

Road transport emissions have a significant harmful impact on the population. These emissions include pollutants such as nitrogen oxides (NOx) and particulate matter (PM), which can lead to a range of health issues (Anenberg et al., 2019). To tackle this problem, it is critical to monitor vehicle emissions in the real-world, to know the actual contribution of each type of vehicle to total emissions, to assess what are the discrepancies between theory and reality, to use the data to update emission inventories (and subsequently air quality models), and to regulate vehicles in circulation so that they emit within acceptable limits. Monitoring vehicle emissions can be performed through remote sensing technology, for real-time measurements under real-world conditions. This technology was first used to monitor CO from vehicle exhausts (Bishop et al., 1989) and has since developed to measure other pollutants (e.g. Bishop et al., 2012, Carslaw et al., 2013, Ropkins et al., 2017, Chen et al., 2020). Remote sensing can be used to identify individual HE vehicles and to enforce emissions regulations. The identification and regulation of HE vehicles, after detection by RSD has been applied on a large scale and for decades in the USA, China, South Korea and some other countries, but in Europe there is still no common regulation that would allow this solution to be deployed in a unified manner. Although several approaches have been proposed (e.g. Rushton et al., 2021, Kang et al, 2021, Buhigas et al., 2022, Qiu et al., 2022, Ghaffarpasand et al., 2023), the results from different methods have never been compared with each other. Therefore, in this study, we compare four different methodologies for the identification of high emitters (HEs) using data collected from a new remote sensing instrument, called 'LRSD' developed under the EU-funded H2020 NEMO project. The LRSD has been recently matured and validated (Buhigas et al. 2022). and the system has been used in Florence to monitor the actual emissions of the circulating fleet in various parts of the city.

Methodology

The methodology can be divided into two parts: 1) on the measurement campaign in Florence, 2) on the analysis of the collected data and the application of the four different methods of HEs identification and their subsequent analysis.

1) The measurement campaign was conducted between June 6 and June 22, 2022 at seven different sites in the municipality of Florence, using the LRSD in a world-first manner, deployed in its portable configuration. The LRSD individually measures free circulating vehicles' tailpipe emissions non-intrusively using Interband and Quantum Cascade Lasers (ICL and QCL) for the precise and highly sensitive detection of several pollutants (CO, CO_2, NO, NO_2, hydrocarbons and NH_3) using a spectroscopic approach. The system was used in this campaign just after validation tests were performed at the Joint Research Centre (JRC) facilities at Ispra. The system was deployed at the roadside of the measurement sites, to measure in an open-path cross-road manner. 45,790 vehicle measurements were collected as vehicles passed through the sensor. Due to the project budget restrictions, it was only possible to request technical data from 8,625 different vehicles (this data is subject to a fee in Italy). Thanks to repeated measurements of some of these vehicles, a dataset of 17,017 measurements was consolidated with associated technical data: fuel type, UNECE category, make, model, etc. The Euro standard was not provided, so it was estimated based on other parameters of each vehicle, including the registration date.

2) When applying an approach for identifying HEs, it is important to consider the reason a vehicle may be flagged as a HE - is it due to an issue with something on the vehicle which has stopped working correctly or has it been deliberately tampered with? These are issues that may be fixed in order to reduce their emissions. However, there are other factors that can result in high emissions such as, older vehicles, cold ambient temperatures and heavy vehicle loads. Average emissions also vary greatly across different vehicle manufacturers. These variables cannot be fixed, therefore is it correct to flag the vehicle in these cases as a HE? Another important consideration when using remote sensing is that only a short period ("snapshot") of the emissions under specific conditions is measured for each vehicle. As such a vehicle may be flagged as a high emitter, even if the average emissions over a typical drive cycle may be much lower. Therefore, using a method that incorporates multiple measurements of potential high emitters can reduce false positives.

Using the dataset from part 1, four different methodologies were applied to identify potential HEs in the fleet. All four methods described below are applied to each pollutant individually (NOx, CO, PM and HC), therefore, it may be possible that a vehicle is flagged as a HE in more than one pollutant. However, the vehicle is only counted once for the comparison.

Method A - Gumball distribution: Rushton et al. (2021) found that the distribution of NOx emissions from vehicles measured by an RSD during their study could be explained in the most part by a Gumball distribution (an extreme value Type I distribution). Quantile-quantile plots (Q-Q plots) are used to determine the relationship between theoretical and observed distributions. A maximum likelihood estimation (MLE) method is then applied to find the best estimate of the fit parameters. Measurements that deviate from the model are hypothesised as high emitter candidates. Rushton et al. applied their method to pairs of Euro class and fuel type to identify high emitters in each group. The focus for this study is to identify HEs relative to the whole fleet. Therefore, the approach taken here is to group all vehicles together and apply the methodology once, for each pollutant of interest. A further filter is used where only those vehicles that have more than one valid measurement for at least one pollutant are flagged as high emitters.

Method B - On-Road High Emitter (ORHE) limit: In this method, vehicles are identified as potential high emitter candidates if their emissions exceed predefined high-emitting limits (Buhigas et., 2022). For each pollutant of interest there are two limits defined based on the data from a wider monitoring campaign: the ORHE limit, calculated as the 98th percentile (P_{98}), and the 80th percentile (P_{80}) limit. A vehicle is flagged as a high emitter if the following criteria are met: 1) The vehicle has a vehicle specific power (VSP) range between 0 and 30 kW/Ton during the measurement and 2) The emissions exceed P_{98} and P_{80} at least once each during different measurements or 70% of the time the vehicle is measured the emissions are above P_{80} (when there are at least 4 measurements of the same vehicle).

Method C – Type-Approval exceedance: One of the simplest methods for identifying high emitters is to compare the emissions with the EU type-approved emission standard for the given vehicle class, EURO class and fuel type. The RSD measures emissions as ratios to CO_2, therefore, the data is first converted to the same units as the type-approval standards (either gKm or gkWh). As emissions can vary greatly over a vehicles' drive cycle, to be conservative the high emitter limit is defined as 10 times the corresponding type-approval standard. For mixed fuelled vehicles (LPG-Petrol and CNG-Petrol) the equivalent petrol type-approval limit is applied. A vehicle is flagged as a high emitter if it meets the following criteria: 1) The vehicle has a VSP range between 0 and 30 kW/Ton during the measurement, 2) Emissions exceed 10 times the type-approval limit on 3 or more occasions for at least one pollutant.

Method D – Combined assessment of repeated records: This method is similar to the Type-Approval exceedance (Method C), however, proposes a very conservative combined evaluation. Vehicles susceptible to HE identification must be measured at least 3 times by the sensor and both maximum emission values (an extreme single emission event) and average values of all measurements of the same vehicle (consistently high emission levels) are evaluated. The highest measurement must be at least 100 times its corresponding type-approval limit and, in addition, the average emission value of all observations of the vehicle must be at least 4 times its type-approval limit.

Results

The methods described above were applied to all measurements of passenger cars and light duty vehicles with valid data. The majority of the fleet sampled were Euro 6 vehicles (53%), followed by Euro 5 (22%), Euro 4 (19%) and Euro 3 (6%). Euro's 0, 1 and 2 collectively made up less than 1 % of the fleet sampled. It should be noted that the Gumbel method could not be applied to the CO data effectively, due to a number of negative emission ratios present in the dataset. Negative values can arise when vehicles are driving close together during sampling by the RSD resulting in elevated background levels. Table 1 presents a pairwise comparison matrix for HEs across all four methods. There is a wide range in the number of vehicles flagged as HEs across the four methods. The results show that Method D is the most conservative method, with only 34 vehicles in total identified as HEs, whereas Method A (the least conservative method) flagged 690 vehicles. The vehicles flagged as HEs in the more conservative methods were not always the same ones in the other methods. This result suggests that some HEs may be missed when using methods that are less conservative. There is also the possibility of false positives. Only a detailed inspection of all these vehicles could assess how many of all these vehicles had an obvious defect. Further analysis of the data found that 9 vehicles in total were commonly flagged by all four methods.

Figure 103. Matrix showing the number of HE emitters flagged by pairs of methods. Values in red represent the total number of vehicles sampled that were flagged as high emitters by each method

	Method A	**Method B**	**Method C**	**Method D**
Method A	690	235	107	26
Method B		353	100	29
Method C			249	13
Method D				34

Source: Authors' elaborations.

Figure 104. Bar chart illustrating the number of vehicles flagged as HEs with each method. Numbers above the bars represent the percentage of HEs flagged within the fleet, in each Euro class.

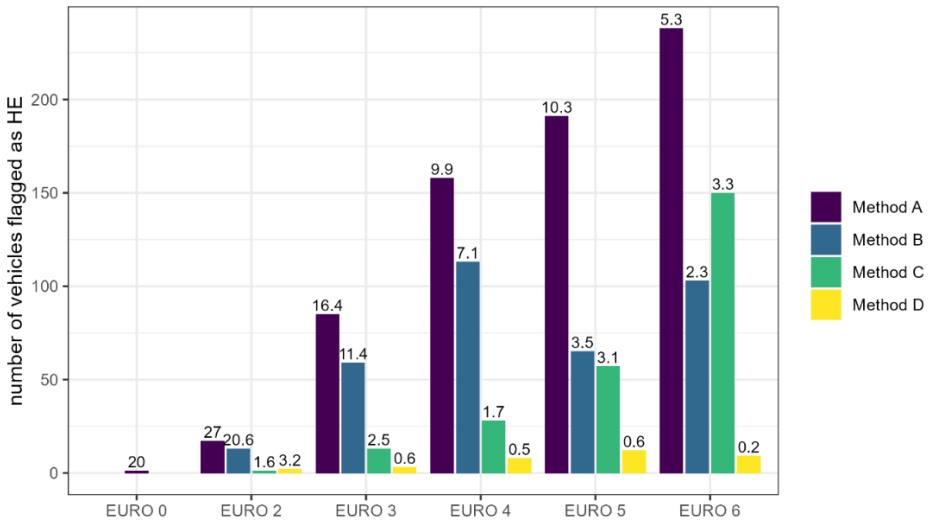

Source: Authors' elaborations.

Figure 1 shows a summary of the number of vehicles flagged as high emitters in each Euro class. Although there were very few Euro 1 vehicles sampled, none of these were flagged as high emitters in any of the methods, and only Method A (Gumball distribution) flagged Euro 0 as a high emitter. Euro 6 vehicles were typically flagged more times than the other Euro standards, however, as a percentage of the fleet sampled, less than 5.3% of Euro 6 vehicles were identified as HEs.

Conclusions

The results show that, as a percentage of the fleet, older vehicles were more likely to be identified as HEs than newer Euro 6 vehicles, however, the methods varied greatly in the number of vehicles identified. Further work will investigate whether high emitter identification should consider multiple pollutants together, to increase the likelihood of identifying a problematic vehicle. Identifying high emitting vehicles is an important issue for air quality policymakers. As part of the NEMO project an atmospheric dispersion model of Florence is under development and incorporates the data collected during the measurement campaign. The model will be used to simulate different mitigation scenarios associated with the removal of HEs from the fleet.

Acknowledgements

This study is part of the H2020 NEMO project (https://nemo-cities.eu/), funded by the European Commission within the Horizon 2020 research and innovation programme under the Grant Agreement n° 860441. The authors thank David Carslaw and Rebecca Rose for their input into the analysis.

References

Anenberg, S., Miller, J., Henze, D.A.V.E.N. and Minjares, R., 'A global snapshot of the air pollution-related health impacts of transportation sector emissions in 2010 and 2015', *International Council on Clean Transportation: Washington, DC, USA*, 2019.

Bishop, G.A.; Starkey, J.R.; Ihlenfeldt, A.; Williams, W.J.; Stedman, D.H., 'IR long-path photometry: A remote sensing tool for automobile emissions', Anal. Chem. 1989, 61, 671A–677A.

Rushton, C. E., Tate, J. E. and Shepherd, S. P., 'A novel method for comparing passenger car fleets and identifying high-chance gross emitting vehicles using kerbside remote sensing data', Sci. Total Environ., vol. 750, 2021, p. 142088.

Buhigas, J., Fleire, M., and Pujadas, M., 'Design of a program for the identification and correction of high emitting vehicles in Europe using remote sensing devices', Transport and Air Pollution (TAP) Conference, 2022, p. 107.

Ghaffarpasand, O., Ropkins, K., Beddows, D.C. and Pope, F.D., 'Detecting high emitting vehicle subsets using emission remote sensing systems'. *Sci. Total Environ.*, 858, 2023, p.159814.

Qiu, M. and Borken-Kleefeld, J., 'Using snapshot measurements to identify high-emitting vehicles', Environ. Res. Lett., 17(4), 2022, p.044045.

Kang, Y., Li, Z., Lv, W., Xu, Z., Zheng, W.X. and Chang, J., 'High-emitting vehicle identification by on-road emission remote sensing with scarce positive labels '. Atmos. Environ., 244, 2021, p.117877.

Bishop, G.A., Schuchmann, B.G., Stedman, D.H. and Lawson, D.R., 'Multispecies remote sensing measurements of vehicle emissions on Sherman Way in Van Nuys, California', J Air Waste Manag Assoc., 62:10, 1127-1133, 2012, DOI: 10.1080/10962247.2012.699015

Carslaw, D.C. and Rhys-Tyler, G., 'New insights from comprehensive on-road measurements of NOx, NO_2 and NH_3 from vehicle emission remote sensing in London, UK', Atmos. Environ., 81, 2013, pp.339-347.

Ropkins, K., DeFries, T.H., Pope, F., Green, D.C., Kemper, J., Kishan, S., Fuller, G.W., Li, H., Sidebottom, J., Crilley, L.R. and Kramer, L., 'Evaluation of EDAR vehicle emissions remote sensing technology', Sci. Total Environ, 609, 2017, pp.1464-1474.

Chen, Y., Sun, R. and Borken-Kleefeld, J., 'On-Road NOx and smoke emissions of Diesel light commercial vehicles–combining remote sensing measurements from across Europe '. Environ. Sci. Technol., 54(19), 2020, pp.11744-11752.

Buhigas J., A. Alonso de Lomas and J. Muñoz. 'Performance of a remote sensing device based on a spectroscopic approach for the remote measurement of vehicle emissions', Transport Research Arena (TRA) Conference 2022.

Kenya Transport-Energy Futures: building transport pathways to support climate-compatible

J. Dixon[a], E. Pierard [b], P. Mwanzia [c], J. Onjala [d], W. Ondanje [e], C. Brand [a], S. Hirmer [f], H. Dalkmann [g].

[a] *Transport Studies Unit, University of Oxford, Oxford, UK*

[b] *Smith School of Enterprise and the Environment, University of Oxford, Oxford, UK*

[c] *Strathmore Energy Research Centre, Strathmore University, Nairobi, Kenya*

[d] *Institute for Development Studies, University of Nairobi, Nairobi, Kenya*

[e] *African E-mobility Alliance (AFEMA), Nairobi, Kenya*

[f] *Energy and Power Group, University of Oxford, Oxford, UK*

[g] *Sustain2030, Berlin, Germany*

Introduction

The Kenya Transport-Energy Futures (KTEF) project aims to develop decision support tools to assist policymakers at county, national and international scales in testing out credible futures of the transport-energy system given different policy and scenario pathways. KTEF is part of the UK FCDO-funded Climate Compatible Growth (CCG) research programme.

The future of the transport system, and that of the wider energy system in which it is enveloped, will determine Kenya's ability to meet its targets in economic development (Government of Kenya, 2008) and climate mitigation (Government of Kenya, 2021). These transport-energy futures are outcomes of a complex web of systems; they are driven by policy in the transport-energy sector and across the wider economy, and wider changes in society that cannot directly be controlled (including socio-economic changes, such as changes in a population's age distribution, and broader shifts in travel demand, such as a population's propensity for leisure travel).

In developing decision support tools, a strategic transport-energy systems model, the Transport Energy Air pollution Model (TEAM) (Brand et al., 2019b), has been adapted to the Kenyan case.

Re-introducing TEAM: Transport Energy Air pollution Model

TEAM is a strategic transport, energy, emissions and environmental impacts systems model, covering a range of transport-energy-environment issues from socio-economic and policy influences on energy demand reduction through to lifecycle carbon and local air pollutant emissions and external costs. It is built around exogenous and quantified scenarios, covering passenger and freight transport across all modes of transport (road, rail, shipping, air). It provides annual projections up to 2100, is technology rich with endogenous modelling of more than 1,200 vehicle technologies, and covers a wide range of output indicators, including travel demand, vehicle ownership and use, energy demand, life cycle emissions of 26 pollutants, environmental impacts, government tax revenues, and external costs. For more information on TEAM, see (Anable et al., 2012; Brand et al., 2017, 2019a, 2020).

TEAM quantifies the likely impact of policy pathways – given a background context – on transport system energy demand, GHG emissions and air pollutants. TEAM requires various inputs that come from the development of narrative scenarios (a.k.a. 'storylines'). The inputs from these storylines cover the following three types of variables:

- *Context* variables, broadly defined as those that are beyond direct government control, such as fuel prices before tax, demographics and GDP per capita;
- *Policy* variables, broadly defined as those that are within direct government control, such as taxation (e.g. on fuel and vehicle purchase), vehicle purchasing (dis)incentives or scrappage rebates (e.g. tax exemption for EV purchase), and regulations (e.g. air pollution);
- *Demand* variables, broadly defined as changes to travel demand that may result from a combination of policy and context changes, such as reductions in commuter trip passenger-km amongst the working-age population due to growth in teleworking.

This is the first time the TEAM framework is being used in a country with i) limited data on travel demand and vehicle stocks and ii) a sizeable second-hand imports market.

TEAM-Kenya: a transport-energy system model for the Kenyan context

The major updates carried out as part of this adaptation, which were made in January-March 2023, are detailed in Table 1.

Table 18. Major updates as part of the adaptation of TEAM-Kenya (from TEAM-UK)

Change title	Details
Second-hand import technologies	The majority (~85%) of cars and minivans bought in Kenya are second-hand imports (SHI), mostly from the Japanese and UK markets. Therefore, TEAM-Kenya models separate markets for SHI and new technologies; in the present version, SHI technologies have been made for all car and minivan types, and they are offset by a fixed number of years. Presently, as Kenyan law stipulates that no vehicle over 8 years old is allowed to be imported into the country, SHI vehicles in TEAM-Kenya are 8 year-delayed versions of their new counterparts.
Changes to vehicle stock data (baseline year)	Data for the Kenyan vehicle fleet for the base year (2015) were generated from a report from GIZ and the University of Nairobi (Ogot et al., 2018). Data were processed from the format as provided in the report into the format as required by TEAM-Kenya according to a set of assumptions as described in (Giki & Dixon, 2023).
Changes to travel demand (baseline year)	Concurrent CCG work is currently (at the time of writing in May 2023) collecting travel survey data from approx. 1000 participants in Kenya. However, these data are not yet available. As a working version, travel demand data (trips and distance by modes and purpose) were input based on data from a 2013 World Bank study as published in (Salon & Gulyani, 2019). As data in the latter only covers commuting travel, a set of assumptions based on the literature were made to translate travel demand for commuting trips into other trip types (Dixon et al., 2023).
Changes to background demographic data and projections to 2050	The population, GDP, number of households and urban/rural split, the share of households with more than 1 person, and the share of the population of driving age, for the base year (2015) were taken from a set of online sources. Projections were made, either from online sources or by using assumptions based on proxies. For a list of data sources and assumptions, see (Dixon et al., 2023).

A graphical user interface (GUI) was developed for TEAM-Kenya to allow effective communication of model results (Figure 1). TEAM-Kenya modelling results are still in development and are due for release in July 2023. However, the next section covers the development of scenarios used for modelling.

Figure 105. Web-based graphical user interface for communication of results (Ziarkowski & Dixon, 2023)

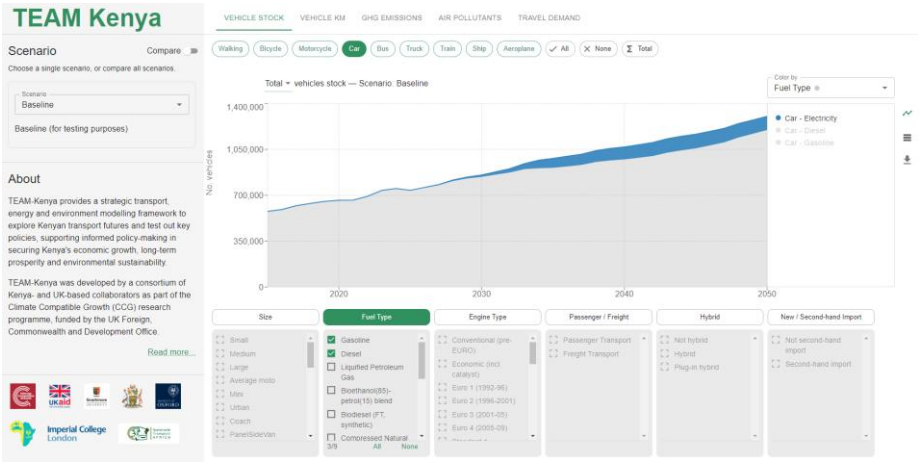

Scenario development

Whilst both Global North and Global South transport transformations appear to be similar in aspiring to cleaner, just and modern transport, the futures in which both transformations are occurring and their plausible outcomes are strikingly particular to the place where they are planned and executed. Taking this difference as a basis, this study was designed to identify narratives from the point of view of the experts and decision-makers based

in and currently key to the planning and implementation of transport and energy in Kenya. Modellable scenarios, pertaining to the three points above (context; policy; demand), were developed for the TEAM-Kenya model through (i) interviews with local experts and (ii) a scenario development workshop.

41 key experts were first identified and then interviewed to provide insights from the current state of transport in the country and the key areas of transformation in the sector but also in wider social and economic dynamics. The key experts covered the central actors engaged both in the planning, regulation, implementation, service provision, manufacturing, and financing of transport. As such it covered civil servants in the Kenyan national and local government of Nairobi, manufacturers, start-ups and transport service providers, NGOs and financing institutions (Figure 2). The interviews, each lasting approx. 1 hour, were formulated around a set of semi-structured questions around the current state of Kenya and visions of Kenya in the future. The questions are available in the appendix.

Figure 106. Breakdown of experts and decision-makers engaged for scenario development for interviews (left) and workshop attendees (right)

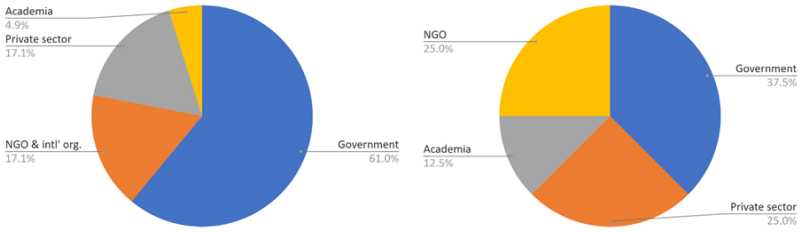

The full-day workshop was attended by 32 stakeholders on 28 March 2023 in Nairobi. The workshop was planned and executed following methodologies for scenario-making that place the identification of narratives from the central actors –or users– as the core-basis of scenario building (Ramírez & Wilkinson, 2016). In this sense, the purpose of the workshop was not to extract knowledge from participants, nor to give them instructions of a preconceived outcome. Rather, it consisted of a collaborative process of unstructured exercises to prompt both their expertise and imagination for understanding their present setting and plausible future events to occur in their environment.

The workshop was structured around three main sessions.

1. The first session consisted on the identification of the factors that influenced decision-making (e.g. fiscal policy), as well as wider actors in the sector (e.g. ministry of transport) influenced or impacted by such factors.
2. In the second session, the participants were asked to identify plausible outcomes of those factors, and choose the two most definitive for the sector to work over a four-quadrant chart. This builds the core of the scenario-making exercise, and sets how particular factors interact and impact outcomes. The result gave a chart of four scenarios to which participants had to discuss within their groups to find fitting names to what was plausible to occur in each pane. An example chart is shown inFigure 3, which used the axes of ‘strength of legislation’ and ‘availability of finance’ to produce four separate scenarios. The scenarios’ names are references to Kenyan popular culture.
3. Finally, in the third and last sessions, participants were asked to provide the storyline of how the most likely or most interesting scenario to them would have to unfold. The starting point was chosen depending of the first crucial step taken towards that scenario, or the event setting the scenario in motion. Such point could be located in the past, as well as starting in the present. Equally, the previous outcome identified of the scenario in the quadrant could be considered the end of the story as well as the middle point of it. Thus, the participants within their teams had to decide how to arrange the narrative to fit a causal chain of events and their progression across time.

Figure 107. Example quadrant of four scenarios: Omoka, Wash-Wash, Fuliza and Kujinauo

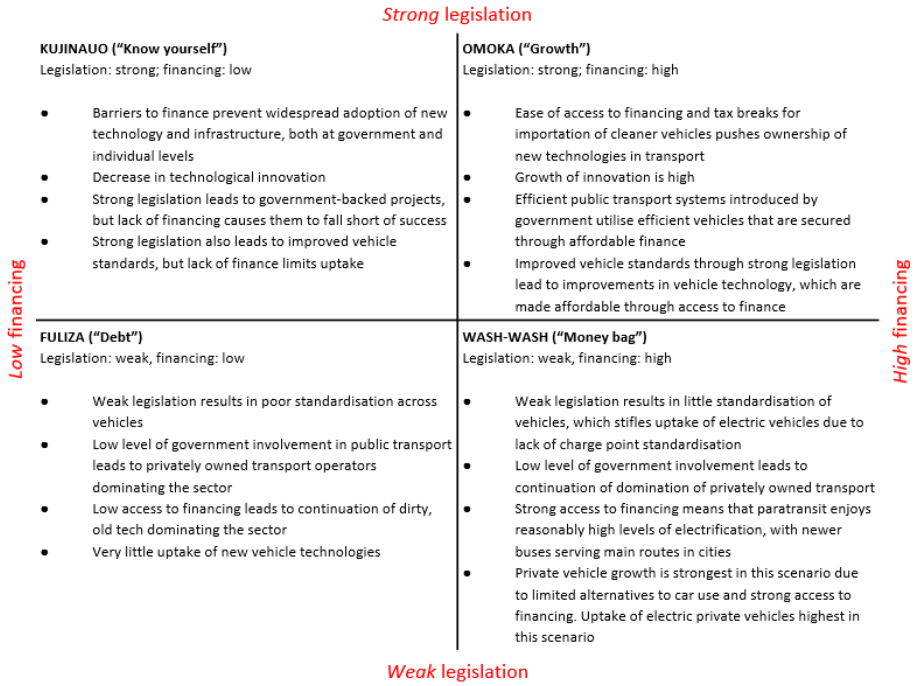

Conclusion

The KTEF project represents, to the authors' knowledge, a vanguard effort to develop decision support tools in a data-poor context to assist policymakers in trialling policies to support low-carbon economic growth. Whilst the project is still underway – at the time of writing, data is still being collected and efforts are ongoing to translate the scenarios developed from the workshop into modellable scenarios in TEAM-Kenya – there have been many lessons learnt from the project, in terms of the availability of data and the cumbersome nature of translating transport models from one context to another.

In comparison to many other sub-Saharan African economies, availability of data on the transport system in Kenya is relatively good: there are datasets on travel behaviour and vehicle fleet datasets (albeit some of these are at least partially from modelled results, such as (Ogot et al., 2018)). That being said, developing a model with sufficient detail for the TEAM framework in Kenya was challenging and required significant resources in data collection and model development.

Ultimately, transport systems across the world are highly diverse and, as such, pathways for their evolution in meeting climate mitigation and economic development goals must be context-specific. Renewed effort is required in developing modular, open-source tools that can be easily adapted according to different transport contexts and levels of data availability; in order to do that, in-country stakeholders must be engaged from the start. Investment in the development of these tools is necessary, but will act to promote climate finance being assigned to the right projects in securing climate-compatible transport pathways for the world.

References

Anable, J., Brand, C., Tran, M., & Eyre, N. (2012). Modelling transport energy demand: A socio-technical approach. Energy Policy, 41, 125–138. https://doi.org/10.1016/j.enpol.2010.08.020.

Brand, C., Anable, J., Ketsopoulou, I., & Watson, J. (2020). Road to zero or road to nowhere? Disrupting transport and energy in a zero carbon world. Energy Policy, 139(January). https://doi.org/10.1016/j.enpol.2020.111334.

Brand, C., Anable, J., & Morton, C. (2019a). Lifestyle, efficiency and limits: modelling transport energy and emissions using a socio-technical approach. Energy Efficiency, 12(1), 187–207. https://doi.org/10.1007/s12053-018-9678-9.

Brand, C., Anable, J., & Morton, C. (2019b). Transport Energy and Air pollution Model (TEAM). https://ukerc.ac.uk/project/team-model/.

Brand, C., Cluzel, C., & Anable, J. (2017). Modeling the uptake of plug-in vehicles in a heterogeneous car market using a consumer segmentation approach. Transportation Research Part A: Policy and Practice, 97, 121–136. https://doi.org/10.1016/j.tra.2017.01.017.

Dixon, J., Brand, C., & Zhou, Z. (2023). TEAM-Kenya data inputs. Zenodo. https://doi.org/10.5281/zenodo.7892446.

Giki, P., & Dixon, J. (2023). TEAM-Kenya data processing. Zenodo. https://doi.org/10.5281/zenodo.7892126.

Government of Kenya. (2008). Vision 2030.

Government of Kenya. (2021). Updated NDC.

Ogot, M., Nyang'aya, J., & Muriuki, R. (2018). Characteristics of the in-service vehicle fleet in Kenya. https://changing-transport.org/publications/characteristics-in-service-vehicle-fleet-kenya/.

Ramírez, R., & Wilkinson, A. (2016). Strategic Reframing: The Oxford Scenario Planning Approach. Oxford University Press. https://doi.org/10.1093/acprof:oso/9780198745693.001.0001.

Salon, D., & Gulyani, S. (2019). Commuting in Urban Kenya: Unpacking Travel Demand in Large and Small Kenyan Cities. Sustainability, 11(14). https://doi.org/10.3390/su11143823.

Ziarkowski, M., & Dixon, J. (2023). TEAM Kenya (GUI). https://climatecompatiblegrowth.github.io/team-kenya.

A comprehensive methodology for CO2 savings assessment in MAC and other eco-innovative technologies applied to PHEVs

S. Gil-Sayas[a], G. Di Pierro[b], D. Currò[c], A. Tansini[b], A. Broatch[a], G. Fontaras[b]

[a] *CMT-Motores Térmicos. Universitat Politècnica de València*

[b] *European Commission's Joint Research Centre*

[c] *Piksel s.r.l., Italy*

Introduction

The European Union adopted the target of achieving net-zero greenhouse gas (GHG) emissions by 2050 (European Commission, 2021) and the transportation sector is one of the most significant contributors (European Environment Agency, 2022). Fleet electrification has gained momentum in this regard, but electric range anxiety and insufficient charging infrastructure have become important issues. For this reason, plug-in electric vehicles (PHEV) appear in the market as a middle-way choice, including the benefits of electric and internal combustion engine vehicles. Numerous studies show that auxiliary systems consume a significant share of a vehicle's energy. And vehicle heating, ventilation and air-conditioning (also known as mobile air-conditioning, MAC) systems play an essential role in overall energy consumption. Hence, the automotive sector is interested in making them more efficient, so the electric range increases. From 2025, EU law will consider these efficient systems to contribute to reducing CO2 emissions, as part of the Eco-innovation scheme (EC, n.d.). The standard CO_2 measurement methods used to evaluate technologies that generate electrical energy (i.e., reducing CO2 emissions in real-world driving) may not accurately quantify the amount of CO2 savings in PHEV. The Eco-innovation scheme has been in place since 2009 (Malfettani et al., 2016); nevertheless, the industry has not applied for any technology installed in PHEVs. For this reason, the present study introduces a methodology aimed at determining the CO_2 emissions reductions coming from innovative technologies installed in PHEVs, both in Charge-Depleting (CD) and Charge-Sustaining (CS) mode, as well as the additional CO2 emissions to due extra electrical loads. This activity will be used as a basis to update the Technical Guidelines governing the Eco-innovation scheme (EC, 2018).

Methodology

The main challenge when studying the CO_2 emissions and energy consumed in PHEVs is finding and developing an approach that combines CD and CS modes. Eco-innovative technologies (so-called eco-innovations, EI) consume energy in a more efficient way, thus, the overall battery consumption is affected, together with the number of cycles driven in CD and its electric range. According to Regulation (EU) 2017/1151, the utility factor (UF) calculation is influenced by the vehicle's electric capabilities, hence this aspect needs to be considered when calculating the new combined CO2 from an eco-innovative vehicle. As mentioned in the Introduction, the prompt irruption in EU markets as a CO_2-reducing component (Frieske et al., 2013) and being the largest auxiliary consumer, as seen in literature (Mamikoglu et al., 2017; Mebarki et al., 2013; Suarez-Bertoa et al., 2019; Zhang et al., 2017), make MAC systems suitable for the study.

The PHEV methodology addresses separately the CD and CS modes to represent all ways of exploiting the powertrain energy management system. The CS mode represents a regular Hybrid mode where the internal combustion engine (ICE) and the electric motor work simultaneously to conserve the HV battery's State of Charge (SOC). In this case, the already-in-place approach to calculate CO_2 savings in Hybrid Electric Vehicles can be adopted. As defined in Appendix 2 to Sub-Annex 8 to Annex XXI to Regulation 2017/1151, these savings can be calculated by the eco-innovation's power difference and the K_CO_2 factor, as shown in Equation 1.

$$C_{CO2} = \frac{K_{CO2} \cdot \Delta P \cdot Usage\ factor}{\mathrm{v} \cdot \eta_{DCDC}}$$

Equation 1

Where K_CO_2 is the CO_2 correction factor [(gCO_2/km)/(Wh/km)], as defined in paragraph 2.2 of Appendix 2 to Sub-Annex 8 to Annex XXI to Regulation (EU) 2017/1151, *Usage factor* defines the usage of the technology in real-world conditions [-], ΔP is the technology's power increment between the eco-innovative and the baseline vehicle [W], v is the mean driving speed of the WLTC, 46.5 [km/h], and nDCDC is the efficiency of the DC/DC converter. This term shall be neglected if the eco-innovative technology is powered by the high-voltage system of the vehicle.

As for the CD mode, this study introduces a model-based approach to run a sensitivity analysis on the impact of an eco-innovative technology. The aim is to determine the effect of the eco-innovations energy saved, thanks to the higher efficiency, through an in-house 0D vehicle simulator. The model is developed in Python and it is adopted to simulate an average C-segment passenger car with a generic technology on board. Generally speaking, the model can simulate the presence of an energy-providing device and an extra electric load that consumes energy. The model can simulate the entire type approval campaign for a PHEV, giving as output the most relevant information such as CO_2 emissions in CD, CS and combined, and CD range and the Equivalent All-Electric Range (EAER). These two ranges are defined in Regulation 2017/1151.

The same baseline vehicle has been scaled up and down to simulate vehicles with different characteristics, thus, enlarging the applicability of the methodology to a wider range of PHEV models. The scaling was done by playing with its electric capability, i.e. the HV battery capacity, and its driving resistance, i.e. its road loads. As a result, each virtually-tested vehicle was defined by a dimensionless parameter as in Equation 2.

$$ratio = \frac{HV\ Batt\ Nominal\ Capacity\ [kWh]}{Vehicle\ Cycle\ Energy\ [kWh]}$$

Equation 2

Where *Vehicle Cycle Energy* is calculated as described in SAE J2951 ("J2951_201401," n.d.). Nine ratios were investigated, meaning that nine different versions of the baseline vehicle were simulated. More in detail, the model simulates a technology whose power ranges from -4 to 4 kW on the HV side: negative power stands for additional electric loads, while positive power stands for generated energy. This being said, the Eco-innovation saved energy due to higher efficiency can be treated as positive electrical energy given to the HV vehicle network. This wide range was chosen to accommodate multiple power consumption. Innovative MAC systems could consume up to 4 kW in cold temperatures during a WLTC (i.e., without solar radiation) and with controlled temperatures.

Results

As already mentioned, nine vehicle versions were simulated under five conditions of power demand, i.e., +4, +2, 0, -2, and -4 kW; this means simulating 45 scenarios based on a C-segment PHEV. Positive power demand indicates energy provided (saved in case of EI) while negative power demand refers to energy consumption requested to the vehicle network as an extra load.

Figure 108. Dependency of CO2 emissions (CS, CD and combined) and EAER with technology's power contribution

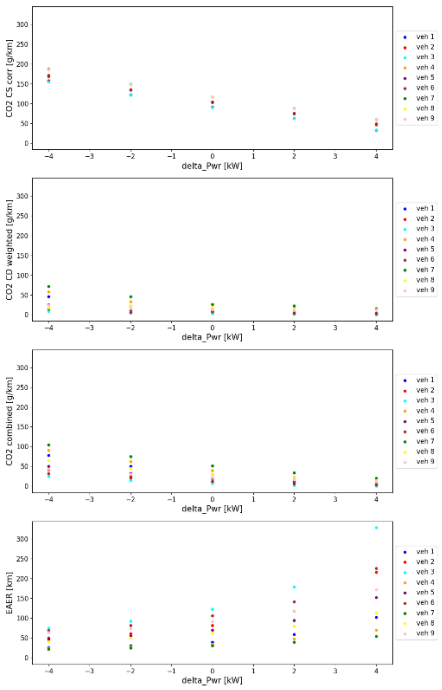

Source: Authors' elaborations.

Figure 1 shows the output of the analysis performed via the model-based approach for nine vehicle versions, where each dot represents a model variant. The plots share the same x-axis, i.e. the sweep of power demand from the installed technology that goes from -4 kW to +4 kW. The first subplot shows the simulated CO_2 emissions in CS mode for the 45 different scenarios, where a linear relationship exists between CO_2 in CS mode and on-board power demand. Additionally, three linear groupings can be detected by observing the mentioned subplot. Hence, the cases are grouped by the different road loads since vehicle 1 to 3, 4 to 6 and 7 to 9 share the same RL parameters. This means that the relevant parameter in CS mode is the vehicle resistance to motion, while the battery size can be neglected. This occurs because the battery SOC in CS mode is kept almost constant and this technology does not work to propel the vehicle in electric mode. The linear relationship highlighted by the model validates the assumption made in the Methodology section: a K_CO_2 factor can be applied to transform energy into CO_2. In the second and third subplots, the CO_2 emissions in CD mode, and the combined CO_2 emissions are displayed, respectively. In this case no linear relationship is found because other parameters such as the UFs play a role in the CO_2 emissions calculation. This is also reflected in the calculation of the vehicle's EAER (last subplot). Moreover, .

Figure **109.** 3D correlation between CD electric range (z-axis), vehicle dimensionless ratio (x-axis) and with technology's power contribution (y-axis)

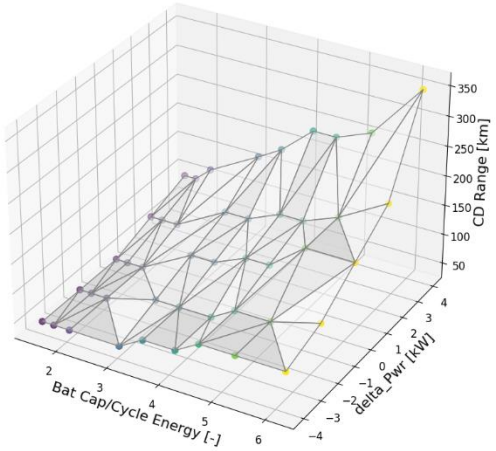

summarizes all the above findings in one single 3D plot. Generally, a higher ratio between HV Battery Capacity and Cycle Energy, and a higher energy saved from a eco-innovation, leads to a higher the CD range.

Table 19. CO2 savings calculated with Equation 1 for different eco-innovation energy consumptions. A usage factor of 0.2 has been used as dummy value to apply the Equation 1

EI Energy [W]	CO_2 emissions(1) [g/km]	K_{CO2} factor [(g/km)/(Wh/km)]	CO_2 savings [g/km]
4000	4.72	0.946	16.28
2000	10.32	0.959	8.25
0	19.56	0.976	0.00

(1) Combined CO_2 emissions from the CD sequence plus the CS cycle.

Source: Authors' elaborations.

Figure 109. 3D correlation between CD electric range (z-axis), vehicle dimensionless ratio (x-axis) and with technology's power contribution (y-axis)

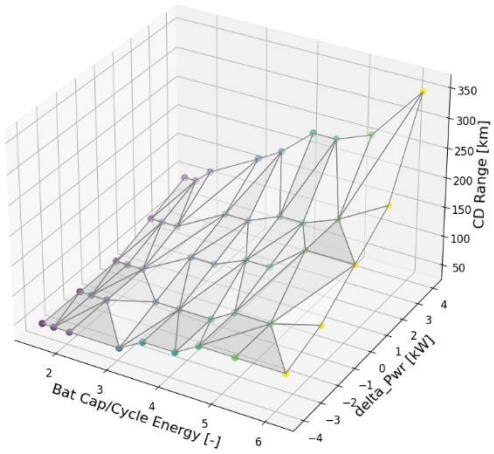

Conclusions

Findings show that charge-sustaining cycles have a linear dependency between the technology's consumed or provided energy and the cycle CO_2 emissions and, hence, potential CO_2 savings and it is strongly dependant on the vehicle road loads. As for the CD sequence, the method proposed relates the MAC electric energy and CO_2 emissions with the vehicle's battery capacity and road loads, and both electric range and equivalent all-electric range (EAER). The tendency shows that increasing the MAC efficiency, the electric range and EAER increase with a non-linear dependency. Moreover, higher battery capacities have a positive impact in the ranges.

Currently, the authors are working on expanding the database used for the synthetic analysis in order to retrieve an empirical relationship between EI saved energy and combined CO_2 emissions that can be integrated in the updated Technical Guidelines.

References

EC, 2018. Technical Guidelines for the preparation of applications for the approval of innovative technologies pursuant to Regulation (EC) No 443/2009 and Regulation (EU) No 510/2011 - Revision: July 2018.

EC, n.d. Regulation (EU) 2019/631 of the European Parliament and of the Council of 17 April 2019 setting CO2 emission performance standards for new passenger cars and for new light commercial vehicles, and repealing Regulations (EC) No 443/2009 and (EU) No 510/2011 (recast).

European Commission, 2021. European Climate Law.

European Environment Agency, 2022. Decarbonising road transport: the role of vehicles, fuels and transport demand. Publications Office of the European Union, LU.

Frieske, B., Kloetzke, M., Mauser, F., 2013. Trends in vehicle concept and key technology development for hybrid and battery electric vehicles, in: 2013 World Electric Vehicle Symposium and Exhibition (EVS27). Presented at the 2013 World Electric Vehicle Symposium and Exhibition (EVS27), pp. 1–12. https://doi.org/10.1109/EVS.2013.6914783.

J2951_201401: Drive Quality Evaluation for Chassis Dynamometer Testing - SAE International [WWW Document], n.d. URL https://www.sae.org/standards/content/j2951_201401/ (accessed 3.7.23).

Malfettani, S., Lodi, C., Huld, T., Bonnel, P., 2016. Latest Developments on the European Eco-innovation Scheme for Reducing CO2 Emissions from Vehicles: Average Input Data for Simplified Calculations. Transportation Research Procedia 14, 4113–4121. https://doi.org/10.1016/j.trpro.2016.05.382.

Mamikoglu, S., Andric, J., Dahlander, P., 2017. Impact of Conventional and Electrified Powertrains on Fuel Economy in Various Driving Cycles (SAE Technical Paper No. 2017- 01–0903). SAE International, Warrendale, PA. https://doi.org/10.4271/2017-01-0903.

Mebarki, B., Draoui, B., Allaou, B., Rahmani, L., Benachour, E., 2013. Impact of the Air-Conditioning System on the Power Consumption of an Electric Vehicle Powered by Lithium-Ion Battery. Modelling and Simulation in Engineering 2013, 1–6. https://doi.org/10.1155/2013/935784.

Suarez-Bertoa, R., Pavlovic, J., Trentadue, G., Otura-Garcia, M., Tansini, A., Ciuffo, B., Astorga, C., 2019. Effect of Low Ambient Temperature on Emissions and Electric Range of Plug-In Hybrid Electric Vehicles. ACS Omega 4, 3159–3168. https://doi.org/10.1021/acsomega.8b02459.

Zhang, Q., Meng, Y., Greiner, C., Soto, C., Schwartz, W., Jennings, M., 2017. Air Conditioning System Performance and Vehicle Fuel Economy Trade-Offs for a Hybrid Electric Vehicle (SAE Technical Paper No. 2017- 01–0171). SAE International, Warrendale, PA. https://doi.org/10.4271/2017-01-0171.

The role of Europe's heavy-duty vehicle CO2 standards in complying with climate neutrality

E. Mulholland[1]

[1] *The International Council on Clean Transportation, Berlin, Germany*

Heavy-duty vehicles (HDV), defined as trucks and buses with gross vehicle weights above 3.5 tonnes, are responsible for over one quarter of transport-related CO_2 emission across the 27 Member States of the European Union (EU-27), despite accounting for only 2.5% of road vehicle annual sales. The combat this growing disparity, on February the 14th 2023, the European Commission released a proposal to amend the existing CO_2 standards for HDVs (European Commission 2023b). Currently, the regulation mandates emissions reductions in new vehicles of 15% in 2025, and 30% in 2030, compared to a 2019-2020 baseline (European Commission 2019). The CO_2 standards are currently only applicable to some of the highest-emitting vehicle segments that together accounted for 66% of total HDV sales in 2022.[21] The proposed amendment increases the 2030 target to 45% and introduces targets of 65% in 2035 and 90% in 2040. It also extends the scope of the standards to cover more varieties of trucks, buses, coaches, and trailers which when combined comprise over 90% of annual heavy-duty sales.

To accurately model the impact of these newly proposed standards, it is critical to have a detailed representation of the vehicle stock, including age profiles and energy consumption by vehicle type. Data on HDVs in Europe is normally aggregated to a high degree, however the truck market is highly heterogenous with a wide variety of vehicle classes. We apply an optimization framework to use sales data to conform registration data by Member State. We apply this methodology to split heavy-duty vehicles from aggregated data into 48 vehicle categories, following the current VECTO vehicle groups (the characterization by with the CO_2 standards are applied), and model their future stock, activity, and emissions. This process is shown below in Figure 1. The process also enables for trucks to be categorized under new and used vehicles.

Figure 110. Calculation of HDV stock by age profile and VECTO grouping

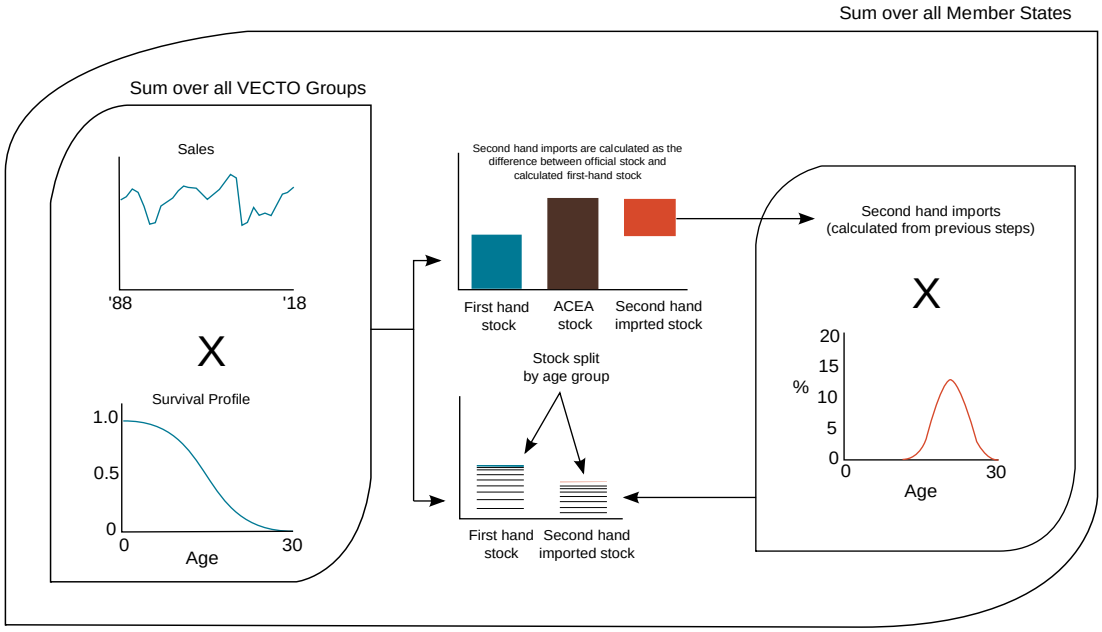

We evaluate the tailpipe CO_2 emissions from HDVs between 2020 and 2050 using the ICCT's Roadmap model. Applying the European Commission's proposed CO2 standards sees a reduction in overall HDV emissions by 77% by 2050 relative to 2020. By contrast, the overall target of the European Commission is to reduce road transport by 90% by the same year. These results are shown below in Figure 2.

[21] Based on annual sales data supplied by IHS Global SA; Copyright © IHS Global SA, 2022.

Figure 111. Emissions reductions under the newly proposed CO2 standards

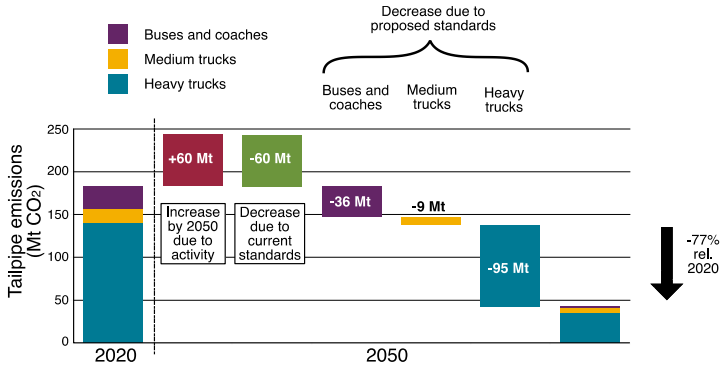

References

European Commission. (2019). Regulation (EU) 2019/1242 of the European Parliament and of the Council of 20 June 2019 Setting CO2 Emission Performance Standards for New Heavy-Duty Vehicles and Amending Regulations (EC) No 595/2009 and (EU) 2018/956 of the European Parliament and of the Council and Council Directive 96/53/EC. Official Journal of the European Union, L 198. https://eur-lex.europa.eu/eli/reg/2019/1242/oj#d1e1921-202-1.

European Commission. (2023). Proposal for a regulation of the European Parliament and of the Council amending Regulation (EU) 2019/1242 as regards strengthening the CO_2 emission performance standards for new heavy-duty vehicles and integrating reporting obligations, and repealing Regulation (EU) 2018/956. Official Journal of the European Union. https://climate.ec.europa.eu/system/files/2023-02/policy_transport_hdv_20230214_proposal_en_0.pdf.

Sustainable automated mobility on-demand strategies in dense urban areas

B.Nahmias-Biran[a]; G. Dadashev[a]; Y. Levi[a], J. B. Oke[b]

[a]*Department of Civil Engineering, Ariel University, Ariel 40700, Israel*
[b]*Department of Civil and Environmental Engineering, University of Massachusetts, Amherst, MA 01003, United States*

Introduction

The prospect of automated mobility on-demand (AMoD) services has garnered significant research, policy and economic interest. However, the prognosis on AMoD availability is mixed, while its interaction with current mobility pattern types and impacts on system performance has yet to be fully determined. Optimistic studies project that AMoD will potentially reduce costs (Pavone, 2015), VKT (Alonso- Mora et al., 2017; Vazifeh et al., 2018) and parking demand (Zhang and Guhathakurta, 2017). AMoD, under environmentally conscious regulation, has also been demonstrated to reduce energy usage and greenhouse gas (GHG) emissions (Greenblatt and Shaheen, 2015). Yet, the expected efficiencies of AMoD could further exacerbate cannibalization and even active modes (Le Vine and Polak, 2014). Bleaker outlooks suggest that any energy gains from AMoD could be negatively moderated by increased demand for travel (Wadud et al., 2016). In some instances, AMoD is also expected to worsen congestion (Hensher, 2018). A comprehensive review of recent and important AMoD studies can be found in Zhao and Malikopoulos (2019).

Various experiments have demonstrated how AMoD could impact urban mobility under various cost, demand, supply (fleet control and management) and policy scenarios. These studies have however been modeled on either specific cities (Azevedo et al., 2016; Vazifeh et al., 2018; Alonso-Mora et al., 2017; Santi et al., 2014) or on virtual cities (Basu et al., 2018; Wen et al., 2018; Zhang and Guhathakurta, 2017; Gross et al., 2019) under idealized conditions. The result is that the implications of these studies are neither readily nor broadly applicable to a wide range of cities. These limitations highlight the importance of understanding how differences in urban form and behavior affect moderate the impacts of new modes such as AMoD. Insights from consequent investigations could consequently dictate the optimal implementation of AMoD strategies in relevant cities. To address this knowledge gap, Oke et al. (2019) embarked on a typologization of cities based on mobility-relevant indicators. Subsequently, AMoD scenario simulations were conducted on two prototypes of auto-dependent cities generated to represent their respective typologies Oke et al. (2020) and equity analyses are performed in Nahmias-Biran et al. (2020). This paper further contributes to the prototype-city simulation approach by developing and simulating AMoD scenarios in two dense, transit-oriented city type.

Methods

Our objective is to examine the environmental impacts of future AMoD strategies in dense transit-oriented cities, in order to provide insights for sustainable implementation. Given the infeasibility of modeling and simulating all cities of interest due to time and data constraints, we classified cities on a global scale, based on network topology, socio-economic indicators and mobility factors (Oke et al., 2019). From these groups, which we call *urban typologies*, we then developed broadly representative *prototype cities* (Oke et al., 2020) that can be used to analyze scenarios with outcomes that are relevant to the cities in that typology.

Urban typologies

Based on data from over 300 cities worldwide , Oke et al. (2019) uncovered 9 urban dimensions and 12 typologies. These 9 factors are composed of: metro propensity, bus rapid transit (BRT) propensity, bikeshare propensity, development, population, sustainability, congestion, sprawl and network density. The reader is referred to (Oke et al., 2019) for an explanation of the typology approach and detailed descriptions of each typology. In this paper, our simulation experiments are performed on a prototype city representing the MassTransit Heavyweight and a futuristic Tel Aviv for 2040. Tel Aviv is expected to become MassTransit Heavyweight once the massive investments in public transportation will be realized by 2040. MassTransit Heavyweight is a group of highly developed and densely-populated cities with robust mass transit availability and usage. Examples of MassTransit Heavyweight member cities include Madrid, Seoul, Berlin, Paris and Singapore.

Simulation environment

The MassTransit Heavyweight city was modeled using SimMobility Mid-Term (SimMobility-MT) is an agent-based simulator that models a given population's daily decision-making and movement, capturing supply-demand interactions (Adnan et al., 2016). SimMobility-MT has been extended to include various fuel types,

costs, and energy consumption and emissions models (Oke et al., 2020; Chen et al., 2018), including on-demand modes in a flexible framework (Nahmias-Biran et al., 2019). Further details on the SimMobility-MT framework are provided in Oke et al. (2020). Tel Aviv metropolitan area was modeled using a simulation framework which is a hybridization of SimMobility MT and Aimsun next. Aimsun Next is a commercial software provides multi-resolution model for large-scale networks (Aimsun, 2018). Further details on the SimMobility-Aimsun framework are provided in (Nahmias-Biran et al., 2022).

City Generation

We created two cities: one is a prototype city to represent the characteristics of the *MassTransit Heavyweight* typology and a futuristic Tel Aviv which is expected to expected to belong to the same topology by 2040. Both are a high-fidelity testbed in which we develop AMoD scenarios for agent-based simulation.

Population and land-use synthesis: We synthesize *MassTransit Heavyweight* population using the hierarchical iterative proportional fitting (HIPF) approach (Müller and Axhausen, 2012). On the individual level, age, income and educational status are controlled for, while income and vehicle ownership are controlled for on the household level. After the population was synthesized, the prototype city was gridded into cells. Based on the land-use category (residential, commercial, education) of each cell, households, employment locations and schools were randomly allocated in order to match totals in each SAL. Workers and students were then assigned to their respective workplaces and schools via a gravity model.

Demand modeling: The *PreDay* ABM was initially estimated for Boston (de Lima et al., 2018). We then calibrated it to fit the average mode shares, activity shares and trip generation rate of the MassTransit Heavyweight typology and Tel-Aviv typology. This was accomplished by manually adjusting alternative-specific constants, scale parameters (Chen et al., 2018) and variable coefficients to coincide with the MassTransit Heavyweight and Tel-Aviv activity shares and mode. Simultaneously, using the same adjustment procedure, we also fit the model to European fuel price elasticities. We also performed checks on temporal patterns, mode-activity proportions, trip and tour distributions.

Supply modeling: We modeled the supply network by obtaining the archetype road network and mass transit (bus and rail) data from OpenStreetMaps and General Transit Feed Specification sources, respectively. We then calibrated the network parameters (lane capacities and speeds) to match highway and arterial peak period speeds for the archetype city. After the supply model was specified, path sets for the road and transit network were generated prior to simulation. Passenger route choices are modeled in the *WithinDay* module, while the *Supply* module of SimMobility-MT provides trajectories of person and vehicle agents in the simulation. From these, the travel times, which were link-based for *WithinDay* iterations, were aggregated by zone and feedback to equilibrate traffic assignments. Similar feedback mechanizem was created for SimMobility-Aimsun framework, were for Tel-Aviv network the supply was modeled via Aimsun (Nahmias-Biran et al., 2022).

Energy and emissions considerations: For each vehicle the energy is computed during the simulation based on speeds and accelerations in successive timeframes. This was accomplished using a powertrain- specific energy model for internal combustion engines (conventional vehicles), hybrid- electric vehicles, battery-electric vehicles, diesel buses and electric trains (Rakha et al., 2011; Fiori et al., 2016; Wang and Rakha, 2017a,b) for the MassTransit Heavyweight Gross et al. (2019). For Tel-Aviv 2040, the emissions were calculated according to emission factors that link pollution to activity based on the HBEFA methodology (Dadashev et al., 2022).

Scenario Design

To analyze the impacts of AMoD across the two cities under consideration, we consider four scenarios. Through these, we explore plausible AMoD futures in which passive or active strategies are employed to manage AMoD across the cities. In these scenarios, the AMoD fleet is assumed to be fully electrified while MoD vehicles, if presents, are gasoline-powered hybrids. With such an imposed regulation, this can be seen to represent a future characterized by environmental- friendliness and optimism.

Base Case: The Base Case represents current conditions for MassTransit Heavyweight and Tel-Aviv in terms of mode availability and choice, and network performance. Available modes are Private Car (single and pooled), Mobility on-Demand (taxis and ride-hailing), Mass Transit (bus and rail), Active Mobility (bicycle and walk) and Other (motorcycle and private bus). Taxi and ride-hailing fares are modeled according to city regulations and Grab, respectively.

AMoD Intro: These conditions describe a future in which AMoD services are introduced in replacement of MoD at a 50% discount from regular taxi fares, but without further policy interventions or strategies. Earlier studies investigating the cost implications of AMoD provide context for this cost starting point (Pavone, 2015; B¨osch

et al., 2018). The AMoD service offers both single and shared ride (pooling) options to allow for additional fare and energy consumption reductions. Shared AMoD rides are 30% cheaper than single AMoD rides. The demand models assume that consumer preference—modeled via coefficients—for AMoD is the same as for MoD.

AMoD Transit Integration: Rather than allow a passive and transit-competitive introduction of AMoD, governments could intervene by subsidizing the integration of AMoD with mass transit. The potential of the integration of on-demand with transit to improve connectivity has received considerable attention (Scheltes and de Almeida Correia, 2017; Shen et al., 2018; Wen et al., 2018) as a viable urban policy. Therefore, we explore this strategy via the AMoD Transit Integration scenario, whereby AMoD is subsidized by 20% for shared access-and-egress connectivity to rail stops.

AMoD + Car Reduction: Another intervention that can be imposed by governments is the reduction in car ownership through the increase in costs or other instrument. Recent studies have indicated that AMoD could encourage a reduction in car ownership (Firnkorn and Müller, 2015; Giesel and Nobis, 2016). We thus test such an approach under the scenario AMoD + Car Reduction. Here, we simulate the effects of restricted car ownership along with the use of a low- cost AMOD service in lieu of traditional MoD. The ownership restriction is actualized by a reduction of 25% in household car ownership.

Results

In this section, preliminary results of the AMoD scenario simulations are presented. We plan to analyze the impacts on demand, VKT, congestion, energy and emissions in the full paper for both cities and compare the results.

Demand impacts

AMoD introduction does not appreciably increase the number of trips (0.2%) demanded relative to *Base Case*. Under both *AMoD Transit Integration* (0.2%) and AMoD *+ Car Reduction* (~ 0%), similar effects are observed. These results indicate that there is no existing latent demand in *MassTransit Heavyweight*. We show the mode shares across all scenarios in Figure 1.

Figure 112. Summary of mode shares and trip impacts

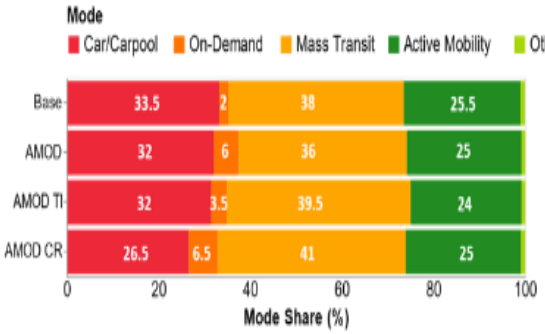

Trip type	Percentage change w.r.t. Base Case		
	AMOD	AMOD TI	AMOD CR
On-Demand	+180%	+75%	+225%
Private Car	-3%	+5%	-28%
Mass Transit	-4%	+4%	+7%

Under *AMoD Intro*, there is an increase of 180% for on-demand trips, while for private car trips there is a decrease of 3%. In addition, Transit use decreases by 4%. Integrating AMoD with transit (*AMoD Transit Integration*) reverses cannibalization, as transit ridership increases by 4%. In this scenario, there is an increase of 75% for on-demand trips and a decrease of 5% for private car trips. Shifts from AMoD and mass transit make up the largest portion of the integrated AMoD.

Vehicle kilometers traveled

We calculate the passenger vehicle kilometers traveled (VKT) as the distance covered by all passenger vehicles during a 24-hour day. Passenger vehicles comprise both private cars and on- demand fleet (MoD or AMoD). Under *AMoD Intro*, passenger vehicle kilometers traveled (VKT) significantly increase by 29% (Figure 2). Notably, on-demand VKT increases by 380% (from 4 million km to 19.4 million km) under this scenario. Private car VKT, however, only reduces by 3%. Transit integration significantly moderates the impact of AMoD in *MassTransit Heavyweight*. While VKT increases by 29% under *AMoD Intro*, it only increases by 8% under *AMoD Transit Integration*. Reducing car ownership also mitigates the VKT impacts of AMoD. Under *AMoD + Car Reduction*, VKT only increases by 13% (compared to the 29% under *AMoD Intro*), as shown in Figure 2. The private VKT

share is much lower, decreasing by 29% (compared to 3% under *AMoD Intro*). Notably, this strategy is the most successful in *MassTransit Heavyweight* at significantly reducing private car VKT.

Figure 113. Passenger vehicle kilometers traveler

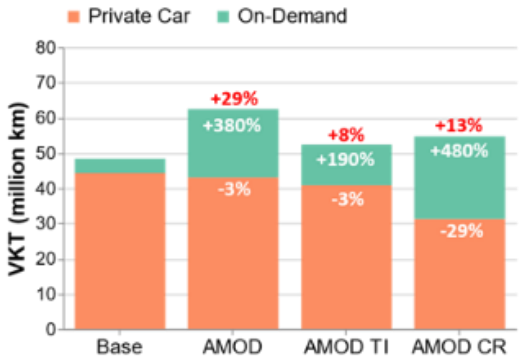

Conclusion

We developed and calibrated two large scale cities: one is a prototype city representing the *MassTransit Heavyweight* typology and the other is the future city of Tel-Aviv which will belong to the same typology. This typology is characterized by a high level of development coupled with a significant mass transit availability and usage. We investigated the effects of Automated Mobility on-Demand services in these transit-oriented cities. The goal was to understand which strategies would lead to the most sustainable outcomes in these types of cities. From the *Base Case*, three scenarios were simulated and compared, namely: *AMoD Intro*, *AMoD Transit Integration* and *AMoD + Car Reduction*. We expect the results will indicate that even with high levels of AMoD transit integration and massive reduction in car ownership, AMoD still increases VKT and congestion. Thus, infrastructure and demand-based pricing are likely to be more effective in tackling the congestion problem. However, we expect that both the integration and car reduction strategies will reverse the cannibalization of mass transit. We expect these simulation results to provide valuable insights to policymakers and other researchers in the continuing exploration of AMoD implementation and AMoD regulation. Furthermore, they would be of immediate value to cities in the *MassTransit Heavyweight* typology.

References

Adnan, M., Pereira, F.C., Lima Azevedo, C.M., Basak, K., Lovric, M., Raveau, S., Zhu, Y., Ferreira, J., Zegras, C., Ben-Akiva, M.E., 2016. Simmobility: A multi-scale integrated agent- based simulation platform, in: Transportation Research Board 95th Annual Meeting.

Alonso-Mora, J., Samaranayake, S., Wallar, A., Frazzoli, E., Rus, D., 2017. On-demand high- capacity ride-sharing via dynamic trip-vehicle assignment. Proceedings of the National Academy of Sciences 114, 462–467.

Azevedo, C.L., Marczuk, K., Raveau, S., Soh, H., Adnan, M., Basak, K., Loganathan, H., Desh- munkh, N., Lee, D.H., Frazzoli, E., et al., 2016. Microsimulation of demand and supply of autonomous mobility on demand. Transportation Research Record: Journal of the Transporta- tion Research Board , 21–30.

Basu, R., Araldo, A., Akkinepally, A.P., Biran, B.H.N., Basak, K., Seshadri, R., Deshmukh, N., Kumar, N., Azevedo, C.L., Ben-Akiva, M., 2018. Automated mobility-on-demand vs. mass transit: A multi-modal activity-driven agent-based simulation approach. Transportation Research Record 0, 0361198118758630.

Bösch, P.M., Becker, F., Becker, H., Axhausen, K.W., 2018. Cost-based analysis of autonomous mobility services. Transport Policy 64, 76–91.

Chen, S., de Lima, I.H.V., Needell, Z., Araldo, A., Akkinepally, A., Trancik, J., Ben-Akiva, M., Fournier, N., Deliali, A., Christofa, E., et al., 2018. Integrated simulation of activity-based de- mand and multi-modal dynamic supply for energy assessment, in: ITSC 2018: 21st International IEEE Conference on Intelligent Transportation Systems, Maui, Hawaii, USA.

Dadashev, G., Levi, Y., Nahmias-Biran, B. (forthcoming). Implications of de-carbonization policies using an innovative simulation tool. Transportation Research Part D: Transport and Environment.

Fiori, C., Ahn, K., Rakha, H.A., 2016. Power-based electric vehicle energy con- sumption model: Model development and validation. Applied Energy 168, 257–268.

Firnkorn, J., Müller, M., 2015. Free-floating electric carsharing-fleets in smart cities: The dawn- ing of a post-private car era in urban environments? Environmental Science & Policy 45, 30 – 40.

Giesel, F., Nobis, C., 2016. The impact of carsharing on car ownership in ger- man cities. Transportation Research Procedia 19, 215 – 224.

Greenblatt, J.B., Shaheen, S., 2015. Automated vehicles, on-demand mobility, and environmental impacts. Current Sustainable/Renewable Energy Reports 2, 74–81.

Gross, E., Oke, J., Akkinepally, A., Nahmias-Biran, B.h., Azevedo, C.L., Zegras, P.C., Ferreira, J., Ben-Akiva, M., 2019. Accessibility and energy consumption evaluation under different strategies of mobility on-demand deployment, in: 98th Annual Meeting of the Transportation Research Board.

Hensher, D.A., 2018. Tackling road congestion – what might it look like in the future under a collaborative and connected mobility model? Transport Policy 66, A1 – A8.

Le Vine, S., Polak, J., 2014. Automated Cars: A smooth ride ahead? ITC Occasional Paper. Independent Transport Commission. London, UK.

de Lima, I.V., Danaf, M., Akkinepally, A., Azevedo, C.L.D., Ben-Akiva, M., 2018. Model- ing framework and implementation of activity- and agent-based simulation: An applica- tion to the greater boston area. Transportation Research Record 0, 0361198118798970.

Müller, K., Axhausen, K.W., 2012. Multi-level fitting algorithms for population synthesis. Arbeits- berichte Verkehrs- und Raumplanung 821.

Nahmias-Biran, B., Oke, J.B., Kumar, N., Akkinepally, A.P., Azevedo, C.L., Ferreira, J., Zegras, P.C., Ben-Akiva, M., 2020. Who benefits from AVs? equity aspects of autonomous vehicles policies in full-scale prototype cities, in: 99th Annual Meeting of the Transportation Research Board. In review.

Nahmias-Biran, B., Oke, J.B., Kumar, N., Basak, K., Araldo, A., Seshadri, R., Akkinepally, A., Azevedo, C.L., Ben-Akiva, M., 2019. From traditional to automated mobility on demand: A comprehensive framework for modeling on-demand services in simmobility. Transportation Research Record 0, 0361198119853553.

Nahmias-Biran, B., Dadashev, G., Levi, Y. (2022). Demand Exploration of Automated Mobility on-Demand Services Using an Innovative Simulation Tool. IEEE Open Journal of Intelligent Transportation Systems. vol. 3, pp. 580-591, 2022, doi: 10.1109/OJITS.2022.3197709.

Oke, J.B., Aboutaleb, Y.M., Akkinepally, A., Azevedo, C.L., Han, Y., Zegras, P.C., Ferreira, J., Ben-Akiva, M.E., 2019. A novel global urban typology framework for sustainable mobility futures. Environmental Research Letters 14, 095006.

Oke, J.B., Akkinepally, A.P., Chen, S., Xie, Y., Aboutaleb, Y.M., Azevedo, C.L., Zegras, P.C., Fer- reira, J., Ben-Akiva, M., 2020. Evaluating the systemic effects of automated mobility-on-demand services via large-scale agent-based simulation of auto-dependent prototype cities. Transportation Research Part A: Policy and Practice 140, 98 – 126.

Pavone, M., 2015. Autonomous mobility-on-demand systems for future urban mobility, in: Au- tonomes Fahren. Springer, pp. 399–416.

Rakha, H.A., Ahn, K., Moran, K., Saerens, B., den Bulck, E.V., 2011. Virginia tech compre- hensive power-based fuel consumption model: Model development and testing. Transportation Research Part D: Transport and Environment 16, 492–503.

Santi, P., Resta, G., Szell, M., Sobolevsky, S., Strogatz, S.H., Ratti, C., 2014. Quantifying the benefits of vehicle pooling with shareability networks. Proceedings of the National Academy of Sciences 111, 13290–13294.

Scheltes, A., de Almeida Correia, G.H., 2017. Exploring the use of automated vehicles as last mile connection of train trips through an agent-based simulation model: An applica- tion to elft, Netherlands. International Journal of Transportation Science and Technology 6, 28 – 41.

Shen, Y., Zhang, H., Zhao, J., 2018. Integrating shared autonomous vehicle in public transportation system: A supply-side simulation of the first-mile service in Singapore. Transportation Research Part A: Policy and Practice 113, 125–136.

Vazifeh, M.M., Santi, P., Resta, G., Strogatz, S., Ratti, C., 2018. Addressing the minimum fleet problem in on-demand urban mobility. Nature 557, 534.

Wadud, Z., MacKenzie, D., Leiby, P., 2016. Help or hindrance? the travel, energy and carbon impacts of highly automated vehicles. Transportation Research Part A: Policy and Practice 86, 1 – 18.

Wang, J., Rakha, H.A., 2017a. Convex fuel consumption model for diesel and hybrid buses. Trans- portation Research Record: Journal of the Transportation Research Board , 50–60.

Wang, J., Rakha, H.A., 2017b. Electric train energy consumption modeling. Applied Energy 193, 346–355.

Wen, J., Chen, Y.X., Nassir, N., Zhao, J., 2018. Transit-oriented autonomous vehicle oper- ation with integrated demand-supply interaction. Transportation Research Part C: Emerg- ing Technologies 97, 216–234.

Zhang, W., Guhathakurta, S., 2017. Parking spaces in the age of shared autonomous vehicles. Transportation Research Record: Journal of the Transportation Research Board 2651, 80–91.

Zhao, L., Malikopoulos, A.A., 2019. Enhanced mobility with connectivity and automation: A review of shared autonomous vehicle systems. arXiv preprint arXiv:1905.12.

Modelling the effects of mobility hubs using a Predictive Digital Twin

M.S. van der Tuin[a], L.P. Oirbans[a], T. van Rooijen[a]

[a] *TNO, The Netherlands*

Introduction

MOVE21 is a four-year European Horizon 2020 Innovation project started in 2021, aiming to transition European cities and their surroundings such that a 30% transport-related emission reduction is achieved by the year 2030 (MOVE21, 2021). Mobility measures enabling this transition, such as public transportation hubs, shared modes and zero emission zones are explored on both people and freight transport with an integrated approach. Living labs in the cities of Oslo, Gothenburg and Hamburg with replicator cities in Munich, Bologna and Rome form a central part of the approach within MOVE21.

Within the project, upscaled variants of the living labs are explored for both people and freight transport in these six urban areas across the Scandinavian-Mediterranean (Scan-Med) corridor of the Trans-European Transport Network (TEN-T). The aim is to learn from the living labs to identify and harness successful interventions which contribute to transport-related emission reductions and to validate the effectiveness beyond the so-called urban nodes to the entire Scan-med TEN-T corridor. In this way, MOVE21 delivers new, (close to) market ready solutions that have proofed to be effective in different regulatory and governance settings.

One of the proposed solutions explored within MOVE21 is the notion of mobility hubs for both people and freight. Mobility hubs can be defined as "*physical locations where different shared transport options are offered at permanent, dedicated and well-visible locations and public or collective transport is available at walking distance.*" (SmartHubs, 2021). Successful hub designs have the potential to positively impact efficiency, quality, environment and health within the mobility system (Heezen et al., 2022). When designing the living labs in MOVE21, ex ante analyses are made of potential mobility hub implementations and supporting policies in a digital simulation environment representing characteristics of the real world cities.

Methodology

The simulation environment applied within MOVE21 is built using the by TNO developed Urban Strategy platform. Urban Strategy is a unique set of GPU-accelerated simulation models integrated trough a scalable and fast communication framework (Lohman et al., 2023). Given these unique capabilities, Urban Strategy allows to construct so called Predictive Digital Twins, which allow to perform exploratory 'what-if' scenarios to estimate the potential impact on both traffic, noise and air quality of individual and combined policy measures. These measures can consist of urban development (e.g. addition of housing, workplaces or other facilities), transportation policies (e.g. pricing strategies and the introduction of new modes) and traffic management (e.g. mode specifically limit street access or alteration of the speed and capacity of roads) (Borst, 2010).

The simulation of mobility hubs within MOVE21 is achieved through the appliance and continuous development of the Urban Strategy multi modal mode choice and two assignment models as shown in Figure 1.

The multi modal mode choice model, referred to as the 'New Mobility Modeller' (NMM), re-estimates (based on a multinomial logit-model) the mode choice for each population group after an intervention is applied by computing new utilities for every origin-destination (OD) pair in the network (Snelder et al., 2019). Input data of the NMM consist of both population data (e.g. car possession and drivers' licenses) and the original trips between the OD-pars as input. Given the aforementioned speed of Urban Strategy, the NMM allows to interactively explore the impact of pricing strategies and the introduction of new modes to the mode choice on a city scale. This is used within MOVE21 to explore different micro-mobility hub configurations and geographical integration.

The assignment models utilizes the results from the NMM by recalculating the new route choices in this alternated scenario. Within the Digital Twin applied in MOVE21, both an assignment model for traffic is used, as well as a separate assignment model for public transport. The Urban Strategy traffic assignment model handles the assignment of trips by car, truck and bicycle on the road networks. Additionally, trips performed by new (shared) modes like shared bikes, kickscooters and shared cars are also assigned by the same module. The model utilizes an all-or-nothing algorithm for trips by truck and bicycle, this means that route-choice of these modes are not influenced by congestion on individual roads or routes. The muti-user class assignment volume averaging algorithm is utilized to assign trips by car (and shared car), implying route choice of car trips are influenced by intensities on a road from other car trips. The resulting car and freight trips are then used as an input for environmental calculations, computing the noise and air emissions related to road traffic. The

assignment model for public transport assigns public transport trips to the public transport network (van der Tuin et al., 2022). The module incorporates both line choice (e.g. bus, light rail and inter-city trains), stop choice and the choice for access and egress mode (i.e. first mile/last mile).

Figure 114. Overview of modules for computing effects of mobility hubs in Urban Strategy

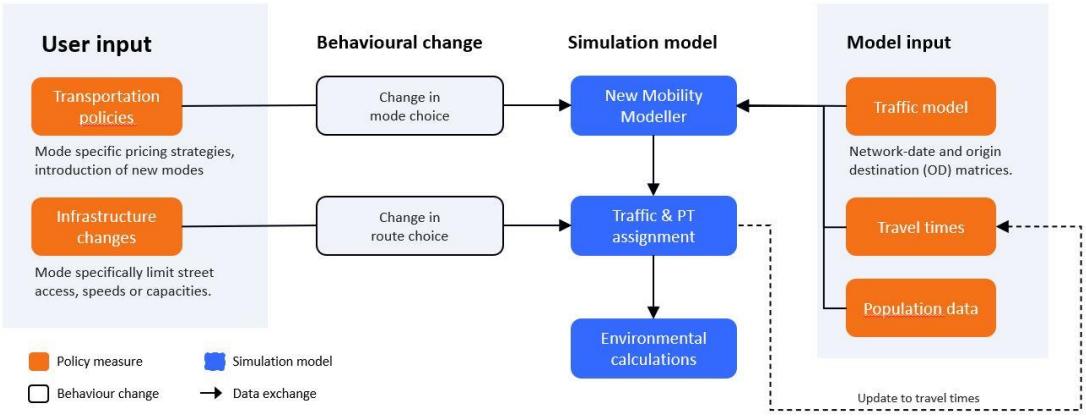

A visualisation model of Urban Strategy allows to visualise the impact of interventions in different indicators such as modal split, road intensities and intensity/capacity ratios (i.e. congestion levels) which is utilized within interactive simulation sessions with stakeholders from the different cities. The interactive sessions consisted of a common exploration of model specific parameter values, impact assessment and (re)formulation of policy measures in additional scenario's.

Results

The described methodology has been implemented for the city of Hamburg. First a digital twin in Urban Strategy has been created based on the traffic model of the city of Hamburg (Hamburg, 2020) for the future year scenario 2030. Next, the several modules (New Mobility Modeller, Traffic assignment, Public Transport assignment, Environment) have been calibrated and set-up. This makes it possible to run various scenarios related to mobility hubs.

The scenarios for upscaling mobility hubs have been designed in collaboration with the city of Hamburg. This resulted in three scenarios each involving 10 mobility hubs in the district of Altona, shown in Figure 2. In the base hub scenario travellers can pick-up various shared modes at the mobility hub: shared cars, shared kick scooters and shared bikes. It is assumed that the maximum walking distance toward the hub is 800 meters. The second scenario is identical, but includes parking costs for cars around the hub to encourage usage of shared modes instead of the own car. The third scenario focusses on a situation where only shared bikes are available at the hubs (i.e., no shared cars and shared kick scooters), encouraging active forms of mobility.

Figure 115. 10 mobility hubs are positioned in district Altona in Hamburg

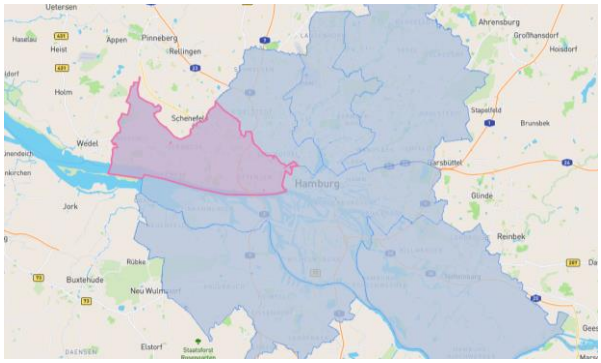

The New Mobility Modeller computed the resulting modal split for the district of Altona for each of the aforementioned scenarios. It can be seen in Table 1 that the introduction of mobility hubs, lead to replacing trips originally performed by public transport, bike or car by shared modes via the hub. In total, more people use a car (combination of car and shared car), which is usually an undesirable effect in terms of mobility transitions. By increasing the parking costs this problem is mitigated. The third scenario only focussing on shared

bikes shows that mainly shorter distance trips by public transport and bike are being replaced by shared bike trips.

Table 20. Modal split in district Altona for each scenario

Scenario	Car	Public transport	Bike	Shared car	Shared bike	Shared kick scooter
Base	49.2%	37.5%	13.3%	0.0%	0.0%	0.0%
Mobility hubs	48.5%	34.9%	12.9%	1.7%	1.8%	0.1%
Mobility hubs and parking cost	46.2%	35.1%	13.5%	2.4%	2.5%	0.2%
Mobility hubs shared bike only	49.1%	34.8%	13.1%	0.0%	3.0%	0.0%

Figure 116. Road intensities (left) and accompanying NO2 emissions (right)

The resulting trips have been assigned to the network. This provides traffic flows, used as an input for environmental calculation modules as shown in Figure 3. It should be noted that the shared cars are assumed to be electric, zero-emission, cars. Thereby an increase in overall car usage (scenario 1) results in an improvement of air and noise quality as shown in Table 2. It can be concluded that the introduction of mobility hubs result in a higher usage of shared modes as well as improved environmental conditions. However, the results also show that introducing shared cars may lead to more car trips in total being performed (in favour of public transport), which is an undesirable effect. This effect can be mitigated by introducing flanking policies like increase of parking costs.

Table 21. Difference in air (NO2 , PM10) and noise (Lden) emission levels within Hamburg for each scenario compared to base

Scenario	NO_2 change	PM_{10} change	L_{den} change
Mobility hubs	-0,002%	0,000%	-0,008%
Mobility hubs and parking const	-0,013%	-0,003%	-0,076%
Mobility hubs shared bike only	-0,001%	0,000%	-0,002%

Conclusion

This paper provides a brief overview of the EU H2020 MOVE21 project, aiming to transition European cities and their surroundings such that a 30% transport-related emission reduction is achieved by the year 2030. The contribution of TNO is embedded in the realisation of Predictive Digital Twins with Urban Strategy of the cities Oslo, Gothenburg and Hamburg, as well within the guidance and advice when constructing, exploring and assessing different upscaled mobility scenario's in these digital replicas.

Exploring different mobility interventions or alternative policies can be challenging due to risks, costs and time constraints (Borst, 2010). Simulation within a Predictive Digital Twin provides an efficient and effective alternative for examining upscaled scenario's of mobility hubs or when comparing the effectiveness of different policy variants. The approach within MOVE21 of combining Predictive Digital Twins with the living labs adds value to the living lab due to the ability to experiment with small set-ups including flanking policies that give promising results in simulations.

The interplay between the several Urban Strategy models within the digital twin have been demonstrated in this paper in the instance of the city of Hamburg, Germany. Results indicate that the implementation of a mobility hub in the district of Altona results in a modal shift, resulting in less car, public transport and bike trips in favour of trips by shared modes offered at the hub. Due to the reduced use of cars also emission levels are affected positively. Further exploration of additional policy measures alongside the hub show that pricing measures, such as parking pricing for cars, can further stimulate the use of shared modes at the expense of, among others, cars.

This use case demonstrates the added value and potential of utilizing Predictive Digital Twins when exploring the required (combination of) policies in order to transform towards a sustainable city wide mobility system.

Acknowledgements

The research reported in this paper has been funded by the MOVE21 project, which has received funding from the European union's Horizon 2020 research and innovation programme under grant agreement No 953939.

References

Borst, J. (2010). "Urban Strategy: Interactive spatial planning for sustainable cities". *Next generation infrastructure systems for eco-cities, IEEE (pp. 1-5).*

Hamburg (2020). Gesamtstädtisches verkehrsmodel für Hamburg und das Umland.

Heezen, M.J.M., Bouma, G.K., & Vonk Noordegraaf, D.M. (2022). "Hubs for People and Goods: nodes to achieve societal goals". *Transport Research Arena (TRA) Conference 2022, Lisbon.*

Lohman, W., Cornelissen, H., Borst, J., Klerkx, R., Araghi, Y. & Walraven, E. (2023). "Building digital twins of cities using the Inter Model Broker framework". *Future Generation Computer Systems. (under review).*

MOVE21 (2021). "Deliverable 6.1: Reflective monitoring guide."

SmartHubs. (2021). "A multidimensional mobility hub typology and inventory" https://www.smartmobilityhubs.eu/_files/ugd/c54b12_819c85702a6442c6bebb18538fb93516.pdf.

Snelder, M., Wilmink, I., van der Gun, J., Bergveld, H. J., Hoseini, P., & van Arem, B. (2019). "Mobility impacts of automated driving and shared mobility: Explorative model and case study of the province of north Holland". *European Journal of Transport and Infrastructure Research, 19(4).*

van der Tuin, M.S., Zhou, H., Walraven, E.M.P. (2022). "Simultaneous modelling of access, egress & transit line choice for public transport". *Transport Research Arena (TRA) Conference 2022, Lisbon.*

Path-based Network signal coordination control optimization: Multi-agent system modeling

J. Yao[a], C. Tan[b], K. Tang[c]

[a] *School of Electrical and Electronic Engineering, Nanyang Technological University, 50 Nanyang Avenue, Singapore, 639798*

[b] *Department of Civil and Environmental Engineering, National University of Singapore, 21 Lower Kent Ridge Road, Singapore, 119077*

[c] *College of Transportation Engineering, Tongji University, No.4800, Cao'an road, Shanghai, China 201804*

Current network coordination control in practice is mainly realized by control subarea partitioning, which fails to describe the intrinsic property of urbanite trip reflected by vehicle paths, while some path-based network coordination control methods depend strongly on given critical paths derived from subjective experience. In this paper, a path-based coordination control optimization model is proposed under a multi-agent control modelling framework. Aiming at minimizing the total delay, network coordination control is realized through agent self-optimization and an optimization iterator describing the interaction between neighbouring agents. Evaluation was done through a simulation case with satisfactory results outperforming Synchro and MULTIBAND model by 29.4% and 27.2%, respectively.

Category 11. Discrete choice model

Urban Air Mobility in the future mobility landscape: differences in users' approach to airport shuttle and city taxi services

P. Coppola[a], F. Silvestri[a], F. De Fabiis[a]

[a] *Politecnico di Milano, Department of Mechanical Engineering, Via G. La Masa 1, 20156 Milano, Italy*

Introduction

After exploiting both ground and underground urban mobility, the idea of adding the "third dimension" to urban transportation networks has been receiving increasing attention, making the Urban Air Mobility (UAM) concept more and more popular. However, this is not new: first examples of UAM services using helicopters are dated to the 1940s and operated for more than two decades, ceasing their activities only due to several incidents of mechanical failures, highlighting safety concerns (Thipphavong et al., 2018). The list of direct and indirect enabling technologies related to the nowadays renewed idea of introducing UAM services is wide (Pons-Prats et al., 2022), but progresses in sensor and communication systems, together with recent advances in electric batteries (Li et al., 2021; Yang et al., 2021), have been identified as crucial for developing new aerial vehicles, the so called electric Vertical Take-Off and Landing (eVTOL) aircrafts (Rezende et al., 2018). Many vehicle manufacturers, such as Joby Aviation, Airbus, Volocopter and Lilium, are competing to bring advanced eVTOL technologies to market for UAM commercially operating services, while national and regional administrative and political bodies are preparing roadmaps for a sustainable UAM adoption. Integration of these new services within the existing mobility system is one of the main challenges and a well-designed ground infrastructure system is fundamental to this aim (Wu and Zhang, 2021): UAM services need vertiports, i.e., eVTOL take-off and landing infrastructures, whose location should be optimally identified to maximize potential passenger demand from the service operator perspective.

There is still uncertainty about what kind of use cases (e.g., airport shuttles or city taxis) should be prioritized at an early implementation stage and what will be perceived as the most appealing one from a user perspective. To this aim, this study investigates passengers value of travel time (or users' willingness to pay) for UAM services, comparatively exploring the differences between two potential business models, i.e. airport shuttle and city taxi services. Data from a large-scale Revealed and Stated Preference (RP/SP) survey in the Milan metropolitan area (Italy) have been collected in the period 2021-2022 and these have been subsequently analysed by means of discrete choice models. The goal is to provide policy indications to both public and private transport planner interested in deploying and developing a sustainable UAM ecosystem.

Methodology

A mixed RP/SP survey was designed and on-site distributed to interviewees randomly approached at the major transport nodes and points of interest of the Milan metropolitan area, including airports, railway stations, huge bus stations and other important urban attraction poles. The data collection campaign lasted 3 months, from November 2021 till to January 2022, collecting a total of 4'174 complete interviews.

The aim of the RP section was twofold: collecting socio-economic data of the interviewee and profiling respondents with respect to their travel habits. At the end of the RP section, a video describing the UAM service and travel experience was proposed: this has shown all the journey steps, starting from the UAM service booking to the vertiport access, from the check-in and security checks to the boarding, from the flight to the deboarding, and concluding with the egress from vertiport till to destination. Finally, interviewees were asked to participate in an SP choice experiment (with a maximum of six choice situations per person), designed following the optimal, or statistically efficient, approach (Hensher et al., 2015; Rose and Bliemer, 2009). Respondents were asked to implicitly compare and choose among four mobility solutions (using Car, Public Transport, Taxi or UAM) to carry out the same travel typology they were doing when interviewed, considering level of service attributes such as access/egress time, waiting/boarding time, in-vehicle time and monetary cost.

Data gathered have been analyzed through Mixed Multinomial Logit (MMNL) (McFadden and Train, 2000) discrete choice models: these allow to consider systematic and random components for each alternative included in users' choice sets differing among respondents; thus, the assumption of constant marginal utilities across all individuals is relaxed and heterogeneity in travelers' tastes can be identified. Moreover, panel data have been used to consider the non-independence of the observations associated with the same interviewee, while choices of different individuals have been still assumed independent.

It has been considered that an individual n has preferences on each transport mode j, in the different choice situations s, which can be measured through the perceived utility function U_{nsj} (see Equation below). The U_{nsj} function is set equal to the sum of the systematic utility function V_{nsj} plus random residuals ε_{nsj}, where V_{nsj}

is assumed as a weighted by β_{nk} linear combination of k explanatory variables x_{nsjk} (i.e. level of service and socio-economic variables).

$$U_{nsj} = V_{nsj} + \varepsilon_{nsj} = \sum_{k} (\beta_{nk} \cdot x_{nsjk}) + \varepsilon_{nsj}$$

The probability of choosing a transport mode j among those available is expressed as:

$$Prob(choiche_{ns} = j) = \int \left(\frac{exp(V_{nsj}/\theta)}{\sum_{j=1}^{J_{ns}} exp(V_{nsj}/\theta)} \right) f(\beta) d\beta$$

The above reported Equation means that the probability of choice is a weighted average of the Multinomial Logit formula evaluated for different values of β, with weights given by the mixture of distributions $f(\beta)$. Parameters estimation has been performed by means of the Maximum Simulated Likelihood Estimation (MLSE) method.

Results

To comparatively explore differences between passengers' value of travel time related to two potential UAM use cases (i.e. airport shuttle and city taxi services), dataset where split in two sub-datasets depending on the interviewee trip pattern. Particularly, it turned out that the sub-dataset related to access/egress trips to/from airports has a sample size $N = 1127$, while the one related to city trips has a sample size $N = 1018$.

Therefore, two different MMNL models have been considered, estimating β parameters for each of the variable included in the systematic utility specifications, i.e., in-vehicle time, monetary cost, access/egress time, waiting/boarding time, and socio-economic dummies. Note that the β associated to the monetary cost variable have been considered as random (i.e., assuming them to be distributed as a normal random variable with μ mean and σ standard deviation); moreover, interactions with the trip purpose variable (i.e., a dummy equal to 1 if the interviewee was traveling for business purpose) have been introduced in the specifications.

Starting from the estimated coefficients and following suggestions by (Hess et al., 2005) in the case of MMNL models, the population of the ratios between in-vehicle travel time and monetary cost coefficients (i.e., Values of Travel Time - VoTT) was simulated, subsequently analysing distribution properties. Particularly, a Monte Carlo simulation have been run generating 1000 samples, each of size 1000, and for each resulting distribution, the central tendency was estimated by the sample median. Simulation results for in-vehicle VoTT, classified by service type (from/to airports or within city), by transport mode (Car, Public Transport, Taxi and UAM) and trip purpose (business and non-business) are reported in Table 1.

Table 22. Simulation results for in-vehicle Value of Travel Time (VoTT) [€/h]

Trip purpose	VoTTs - From/to airports trips				VoTTs - City trips			
	Car	PT	Taxi	UAM	Car	PT	Taxi	UAM
Business	20	4	62	65	4	6	20	50
Non-Business	17	4	51	52	4	6	19	46

Source: Authors' elaborations.

Conclusions

Results shown in Table 1 highlight how the in-vehicle VoTT for UAM airport shuttle services is in a range of 65-52 €/h, where higher values are related to those travelling for business purpose. Likewise, the estimated value for UAM city taxi services is in the range of 50-46 €/h. Depending on the trip purpose, VoTTs for UAM airport shuttle services are about 29-14% higher than those for city taxis. Therefore, looking at these values and reading them as (potential) users' willingness to pay for UAM, this suggests how the implementation of UAM airport shuttle services should be prioritized over within-city UAM taxi ones, especially in a first phase which will be probably characterized by high fares, gradually decreasing over time.

Furthermore, focusing on trips from/to airports and looking at the competition between transport modes, users' willingness to pay for UAM services (65-52 €/h) resulted to be at maximum 5% higher than those related to

taxis (62-51 €/h), suggesting how differences between the two mode of transport pricing policies should be reduced at minimum to promote a significant modal shift from taxi to UAM services accessing/egressing airports.

Future research could deepen the analysis by investigating the impact of individuals' latent traits, such as personal attitudes (e.g., aversion to fly, vocation for technology) and perceptions (e.g., expectations and safety concerns), on VoTTs for UAM services.

References

Hensher, D.A., Rose, J.M., Greene, W.H., 2015. Applied Choice Analysis, 2nd ed. Cambridge University Press, Cambridge. https://doi.org/10.1017/CBO9781316136232.

Hess, S., Bierlaire, M., Polak, J.W., 2005. Estimation of value of travel-time savings using mixed logit models. Transp. Res. Part Policy Pract., Positive Utility of Travel 39, 221–236. https://doi.org/10.1016/j.tra.2004.09.007.

Li, C., Wang, Z., He, Z., Li, Y., Mao, J., Dai, K., Yan, C., Zheng, J., 2021. An advance review of solid-state battery: Challenges, progress and prospects. Sustain. Mater. Technol. 29, e00297. https://doi.org/10.1016/j.susmat.2021.e00297.

McFadden, D., Train, K., 2000. Mixed MNL models for discrete response. J. Appl. Econom. 15, 447–470. https://doi.org/10.1002/1099-1255(200009/10)15:5<447::AID-JAE570>3.0.CO;2-1.

Pons-Prats, J., Živojinović, T., Kuljanin, J., 2022. On the understanding of the current status of urban air mobility development and its future prospects: Commuting in a flying vehicle as a new paradigm. Transp. Res. Part E Logist. Transp. Rev. 166, 102868. https://doi.org/10.1016/j.tre.2022.102868.

Rezende, R.N., Barros, E., Perez, V., 2018. General Aviation 2025 - A study for electric propulsion, in: 2018 Joint Propulsion Conference, AIAA Propulsion and Energy Forum. American Institute of Aeronautics and Astronautics. https://doi.org/10.2514/6.2018-4900.

Rose, J.M., Bliemer, M.C.J., 2009. Constructing Efficient Stated Choice Experimental Designs. Transp. Rev. 29, 587–617. https://doi.org/10.1080/01441640902827623.

Thipphavong, D.P., Apaza, R., Barmore, B., Battiste, V., Burian, B., Dao, Q., Feary, M., Go, S., Goodrich, K.H., Homola, J., Idris, H.R., Kopardekar, P.H., Lachter, J.B., Neogi, N.A., Ng, H.K., Oseguera-Lohr, R.M., Patterson, M.D., Verma, S.A., 2018. Urban Air Mobility Airspace Integration Concepts and Considerations, in: 2018 Aviation Technology, Integration, and Operations Conference, AIAA AVIATION Forum. American Institute of Aeronautics and Astronautics. https://doi.org/10.2514/6.2018-3676.

Wu, Z., Zhang, Y., 2021. Integrated Network Design and Demand Forecast for On-Demand Urban Air Mobility. Engineering 7, 473–487. https://doi.org/10.1016/j.eng.2020.11.007.

Yang, X.-G., Liu, T., Ge, S., Rountree, E., Wang, C.-Y., 2021. Challenges and key requirements of batteries for electric vertical takeoff and landing aircraft. Joule 5, 1644–1659. https://doi.org/10.1016/j.joule.2021.05.001.

Towards replicable mode choice models for transport simulations in France

S. Hörl[a]

[a] *IRT SystemX, F-91120, Palaiseau, France*

Introduction

Transport models play a crucial role in understanding the impact of new technologies, services, and policies on the transportation system. Their impact can be studied through simulations of entire territories. The simulations incorporate these new elements with the aim of evaluating their effects on economic, ecological, and social indicators.

Recently, a framework for creating synthetic travel demand data sets in France was developed by (Hörl and Balac, 2021). It creates households, persons, and their daily activities with times and locations in a replicable way. Since the input data sets are standardized in France and the framework is open source, it has been applied for various additional cases such as Nantes (Le Bescond et al., 2021), Lille (Diallo et al., 2021), Lyon (Hörl and Puchinger, 2022), or Rennes (Leblond, Desbureaux, and Bielecki, 2020).

Various modelling frameworks, such as MATSim (Horni, Nagel, and Axhausen, 2016) or SUMO (Lopez et al., 2018) exist which make use of the trips connecting the activities in travel demand data sets. The trips are simulated all at once, leading to phenomena such as congestion and crowding. The experienced travel characteristics can then be used to obtain updated choices for each trip's mode of transport. The choices are mandated by a behavioural model, the Multinomial Logit model (Train, 2009) being the most commonly applied approach in transportation. Extending the logic from (Hörl and Balac, 2021), in this paper, we take another step towards a fully replicable simulation of French territories by focusing on the mode choice component.

Methodology

We propose a data preparation pipeline in six steps leading to semi-standardized mode choice models for French use cases. The first step is the **cleaning** of the **Household Travel Survey** (HTS) data. They provide the daily activities and connecting tips for a specific sample of the population in a study area. In France, several formats of such data sets exist and they are partly standardized. They are available for most of the cities and regions in France and generally available for research. Some of them are available as open data, for instance, for Nantes and Lille. Often, the surveys are spatially anonymized. However, Euclidean distances between trip origins and destinations are known, and zone identifiers (municipalities or specifically designed shapes) are provided. Based on this information, it has been shown that it is possible to synthesize representative origin and destination coordinates from which choice models with high quality can be estimated (Balac, Hörl, and Schmid, 2022). The goal of the cleaning process is to obtain origins and destinations of all trips in the HTS along with additional attributes on the trips and the decision-makers.

The second step is the **generation of car alternatives**, i.e., for each trip in the HTS data, we obtain a representative travel time when using the car. Our goal being to develop an easily adaptable and replicable pipeline, we don't make use of the common approach of using a commercial routing API. Instead, we propose to use data from OpenStreetMap (OSM) which is available anywhere in France to obtain travel times based on the speed limit. The routing is based on the Dijkstra algorithm and is performed using the *osmnx* package (Boeing, 2017). After, the travel times need to be corrected to represent realistic speeds. The correction is performed in two steps. In order to consider congestion, we make use of the TomTom Congestion Index (Cohn, Kools, and Mieth, 2012) which is available online and describes the inflation of travel times by hour of the day with respect to free-flow conditions in a region. On top of these hourly factors, we add another global factor that (1) corrects for the difference between maximum speeds according to the speed limit and regular free-flow speeds and (2) potential shifts in travel times between the HTS survey period and today. This global correction factor is obtained by performing a line search with the objective of minimizing the offset between the reported travel times of HTS trips that have been performed by using the car and the routed values. For validation, the resulting statistical deviation can be examined.

Third, we **generate transit alternatives** giving information on the number of transfers, in-vehicle times for individual transit modes (metro, tram, bus, ...), access times, and connection frequencies when using public transport. For that purpose, we make use of digital transit schedules in GTFS format that are generally available in France. While for some regions, like Île-de-France, consolidated GTFS data sets with all operators are available, they need to be collected and merged for other use cases. We provide the respective tools in our framework. After, the routing is performed using the RAPTOR algorithm (Delling, Pajor, and Werneck, 2015) with a specific implementation in Java that is part of the MATSim framework. During routing, waiting times and

travel times for the individual transit modes can be weighted differently to represent differing levels of comfort and reliability across the transit modes. For that purpose, we use as ground truth those HTS trips for which public transport was chosen. We perform a black-box optimization using the CMA-ES algorithm (Hansen, Müller, and Koumoutsakos, 2003) to obtain routing weights that minimize the offset between the distribution of transit modes and the distribution of transfers between the HTS and the routed trips. We have found that the resulting itineraries are more realistic than bare time-minimizing routes and that they provide a better model fit in the final choice model.

As the fourth step, a **cost model** needs to be defined, which will be specific to each individual use case. While the car costs may be fixed to a general rate per distance, we also include parking costs that can be defined on a spatial zoning system and may depend on the duration of the activity following the trip. Public transport pricing systems are usually more complex and need to be modelled for every use case.

Fifth, we impute **contextual information** to the data sets. Specifically, for the current version of the generic model, we include an indicator on *parking pressure* which is the quotient of the number of cars registered in a statistical area (available for any place in France) and the total length of the road network in that area (obtained from OSM). The indicator greatly increases the explanatory power of the resulting choice model.

Finally, a **choice model** for the *chosen alternative* in the HTS can be estimated making use of trip attributes for the *car* and *transit* modes. Additional attributes for *walking* and *bicycle* are obtained, but they are modelled simplistically (for the current state of the pipeline) based on Euclidean distances. As an additional feature, we include the *car passenger* mode, which, in the downstream simulations is often a requirement to realistically simulate activity chains, especially for persons without car access (because of age) and limited public transport supply (in rural and suburban areas). The model is a standard Multinomial Logit Model with mode availabilities based on per-person attributes such as whether the person has a driving license.

Results

The described pipeline has been applied to the case of Paris and the Île-de-France region. The *Enquête Globale Transport* survey (Île-de-France Mobilités, OMNIL, and DRIEA, 2010) has been used which provides detailed origin and destination coordinates for research purposes. Table 1 shows the choice dimensions for the five defined transport modes. While a full documentation of the model equations and the estimated model parameters exceeds the scope of the present abstract, they will be presented at the symposium. We have obtained a promising R^2 of 0.54 and Values of Time (10.50 EUR/h for car) that are in line with previous research (Meunier and Quinet, 2015).

For Île-de-France, specific developments have been performed to clean the HTS data and define the cost models for the car and public transport modes. All other steps of the pipeline are sufficiently generic so that they can directly be applied to other use cases. Furthermore, during the selection of variables, it was verified that the same choice attributes are available in other relevant HTS data sets.

Table 23. Attributes and Value of Time (VOT) for the estimated model for the Île-de-France region

Transport mode	**Attributes**
Private car	Travel time (min), Monetary cost (EUR), Parking pressure (veh/km)
Car passenger	Driving permit (Y/N), Travel time (min), Parking pressure (veh/km)
Public transport	Driving permit (Y/N), Headway (min), In-vehicle time (min), Only Bus (Y/N), Access/Egress time (min), Transfers (discrete), Monetary cost (EUR)
Bicycle	Travel time (min)
Walking	Travel time (min)

Source: Authors' elaborations.

Conclusion

In conclusion, we have set up a pipeline to estimate a discrete choice model for mode choice in French territories. The pipeline provides a clean basis for future improvements with a successful application to the case of Paris and Île-de-France. We have available most of the necessary data for other cities, including cleaned HTS for

Nantes, Lyon, and Lille, which are based on the above-referenced synthetic population implementations. The only pieces that are missing so far are the pricing structures for these cities.

There are two interesting avenues for future research on the model itself. The first is to estimate the same or a similar model for all available French cities and compare the results. The second is to estimate a pooled model for these use cases to have a general model for France, which could have high potential for generalization.

We, furthermore, have combined the model for Île-de-France with our synthetic travel demand data for the region and integrated both into an agent-based simulation based on the MATSim framwork. This activity has already provided fruitful results, although further optimization steps for network optimization will be necessary. The final goal in this line of research will be to publish a fully replicable and reproducible agent-based transport simulation for a large territory like Île-de-France in a future publication.

Acknowledgements

This work has been supported by the French government under the "France 2030" program, as part of the SystemX Technological Research Institute.

Reference

Balac, M., S. Hörl, and B. Schmid, 'Discrete Choice Modeling with Anonymized Data', Transportation, September 15, 2022.

Boeing, G., 'OSMnx: New Methods for Acquiring, Constructing, Analyzing, and Visualizing Complex Street Networks', Computers, Environment and Urban Systems, Vol. 65, September 1, 2017, pp. 126–139.

Cohn, N., E. Kools, and P. Mieth, 'The TomTom Congestion Index', 19th ITS World Congress, 2012.

Delling, D., T. Pajor, and R.F. Werneck, 'Round-Based Public Transit Routing', Transportation Science, Vol. 49, No. 3, August 2015, pp. 591–604.

Diallo, A.O., A. Doniec, G. Lozenguez, and R. Mandiau, 'Agent-Based Simulation from Anonymized Data: An Application to Lille Metropolis', Procedia Computer Science, Vol. 184, 2021, pp. 164–171.

Hansen, N., S.D. Müller, and P. Koumoutsakos, 'Reducing the Time Complexity of the Derandomized Evolution Strategy with Covariance Matrix Adaptation (CMA-ES)', Evolutionary Computation, Vol. 11, No. 1, March 2003, pp. 1–18.

Hörl, S., and M. Balac, 'Synthetic Population and Travel Demand for Paris and Île-de-France Based on Open and Publicly Available Data', Transportation Research Part C: Emerging Technologies, Vol. 130, September 1, 2021, p. 103291.

Hörl, S., and J. Puchinger, 'From Synthetic Population to Parcel Demand: Modeling Pipeline and Case Study for Last-Mile Deliveries in Lyon', Lisbon, 2022.

Horni, Andreas, Kai Nagel, and Kay W. Axhausen, eds., The Multi-Agent Transport Simulation MATSim, Ubiquity Press, 2016.

Île-de-France Mobilités, OMNIL, and DRIEA, Enquéte Globale Transport (2010), 2010.

Le Bescond, V., A. Can, P. Aumond, and P. Gastineau, 'Open-Source Modeling Chain for the Dynamic Assessment of Road Traffic Noise Exposure', Transportation Research Part D: Transport and Environment, Vol. 94, May 2021, p. 102793.

Leblond, V., L. Desbureaux, and V. Bielecki, 'A New Agent-Based Software for Designing and Optimizing Emerging Mobility Services : Application to City of Rennes', European Transport Conference 2020, 2020, p. 17.

Lopez, P.A., E. Wiessner, M. Behrisch, L. Bieker-Walz, J. Erdmann, Y.-P. Flotterod, R. Hilbrich, L. Lucken, J. Rummel, and P. Wagner, 'Microscopic Traffic Simulation Using SUMO', 2018 21st International Conference on Intelligent Transportation Systems (ITSC), IEEE, Maui, HI, 2018, pp. 2575–2582.

Meunier, D., and E. Quinet, 'Value of Time Estimations in Cost Benefit Analysis: The French Experience', Transportation Research Procedia, Vol. 8, 2015, pp. 62–71.

Train, K., Discrete Choice Methods with Simulation, 2nd ed., Cambridge University Press, Cambridge ; New York, 2009

Using digital twins & simulation to aid operational planning & disaster recovery responses

A. Naik[a]

[a] *Amazon Web Services*

Spatial Simulations will help us make better decisions about the roadways we construct, dealing with large crowds, and how we respond to disasters. With spatial simulation, we can peer into the future to see the impacts of our efforts, running "what-if" scenarios that answer our questions without having to wait and see what the impact might be years down the line. While the problems that spatial simulations can solve are significant, the difficulty of building and running simulations is a barrier for all. Learn how AWS SimSpace Weaver has been enabling our customers for large-scale city modelling, crowd simulation and disaster recovery.

In this session we walk through the opportunities and challenges that exist in scaling spatial simulation, and talk through how our lead lighthouse customers and research organisations have been using this technology for transportation data and modelling.

Developing an estimation algorithm for generalizing the parameters of the network-gev model in destination choice

J. Urata[a], Y. Kaneda[a], R. Ishii[a]

[a] *the University of Tokyo, Japan*

Introduction

State-of-the-art model estimation techniques in the deep learning (DL) field enable to obtain models that fit large amounts of data. Models used to fit data exhibit high predictive performance. The more oriented the fit is to the data, the more the model is overfitted, and the lower the generalisation performance. Accordingly, various algorithms have been developed to avoid overfitting. There are methods to choose a model that is a good fit, such as AIC or cross-validation. Regularisation can also avoid overfitting by appropriately varying the objective function. Currently, in the transportation field, GPS positioning in smartphones, automobiles, and other devices allows for the collection of a vast amount of passive data and observation of human behaviour. Therefore, algorithm development to fit the data is necessary to obtain generalisable parameters for models in the transportation field.

The development of point-based observation techniques and service systems, such as demand-response e-hailing and micro-transit, have necessitated higher-resolution destination choice models. In the 20th century, it was sufficient to forecast major rail and car trips over relatively large zones but new transportation services require forecasts at greater resolution in both time and space. For high-resolution prediction, the smaller is the spatiotemporal scale, the fewer are the number of observations tied to each spatiotemporal zone. Even in the era of Big Data, it is only possible to observe the behaviour of some people. The smaller is the sample, the greater the risk of overfitting an out-of-representative sample becomes. Algorithms developed in the DL field avoid overfitting and obtain generalised parameters considering the flatness of the objective function (Hochreiter & Schmidhuber (1997)), such as stochastic gradient descent (SGD) (Keskar et al. (2016)). Meanwhile, discrete choice models, such as the network-GEV model (Daly & Bierlaire (2006)), have improved the representativeness of the correlation structure but their parameter estimation algorithms aim to simply maximise the likelihood. Therefore, the predictability of a discrete choice model is lower than that of the deep/machine-learning models; however, discrete choice models have the advantage of explaining behavioural reasoning (Zhao et al. (2020)). There is room for further development of discrete choice models by introducing parameter estimation algorithms that can increase their generalisability.

The network-GEV model requires an algorithm to obtain highly generalisable parameters. The model is highly expressive owing to using scale and allocation parameters to define the network structure. The richness of these parameters is similar to that of the DL models. Indeed, they can encapsulate the spatially correlated logit model structure (Bekhor & Prashker (2008)) and effectively address destination-choice problems. However, the likelihood function of network-GEV models is multimodal and likely to yield locally optimal parameters. In addition, parameter estimation of the constant terms of the zone pairs increases the prediction accuracy of destination choice (Zhu & Ye (2018)). Naturally, as the number of parameters increases, the likelihood of overfitting and difficulty of parameter estimation increase. Therefore, an effective parameter estimation algorithm is needed to apply the network-GEV model to the destination choice problem. The algorithm must solve overfitting and multimodality problems.

In this study, we propose an algorithm to estimate parameters with respect to the generalisability of the network-GEV model. This study improves the sharpness-aware minimisation algorithm (SAM) (Foret et al. (2020)), which evaluates the flatness of the likelihood function. Our numerical examples validate the performance of the proposed algorithm in a destination choice problem.

Proposed Estimation Algorithm

A highly generalisable model can be constructed by obtaining the model parameters from the flat part of the objective function. The objective function to be optimised in the parameter estimation considers the model, parameters, and data. In other words, each parameter changes as the data changes. Figure 1 shows the relationship between the objective function for each dataset regarding sharp and flat parameters. Suppose that the parameter minimising the objective function is obtained for the (observed) training data but the shape of the objective function around the parameter is sharp. In such cases, the obtained parameters may not yield a good objective value for slightly different (unobserved) population data. However, if a parameter with a sufficiently small objective value is employed as an estimator in a flat objective function shape, a good objective value can be maintained for slightly different population data. Figure 1 illustrates this relationship.

Figure 117. Example of network structure

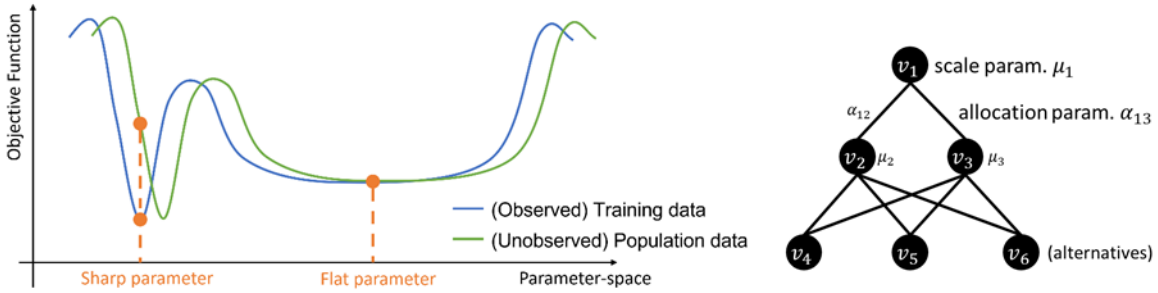

SGD, which is used as a parameter estimation algorithm in DL, has been proven empirically to converge to flatter solutions when the batch size is sufficiently small compared to the training data size (Keskar et al. (2016)). Foret et al. (2020) proposed an SAM algorithm that directly obtained a flat solution. The flatness of the solution neighbourhood is defined as the maximum value $L(\boldsymbol{\theta}+\hat{\boldsymbol{\varepsilon}})$ of the objective function L that should be minimised in the neighbourhood space ρ around a parameter $\boldsymbol{\theta}$:

$$\max_{\|\boldsymbol{\varepsilon}\|_p \le \rho} L(\boldsymbol{\theta}+\boldsymbol{\varepsilon}),$$

where is $\|\cdot\|_p$ denotes the p-order norm. The gradient of $\boldsymbol{\theta}+\hat{\boldsymbol{\varepsilon}}(\boldsymbol{\theta})$ in the direction of the smaller value is used to update $\boldsymbol{\theta}$.

To apply the SAM algorithm to the network-GEV model, we allow exploration under constrained conditions. First, the G-function is defined as follows:

$$G_i = \sum_{v_j \in S(v_i)} \alpha_{ij} G_j^{\mu_i/\mu_j},$$

where is $S(v_i)$ is the set of lower nodes of node v_i. The G-function introduces the choice probability of the alternatives (Daly & Bierlaire (2006)). The network-GEV model requires a circuit-free network, as shown in Figure 2, and each node v_i has a scale parameter μ_i. The scale parameters must satisfy the condition for upper node v_i and all its lower nodes v_j ($\in S(v_i)$): $0 \le \mu_i \le \mu_j \le 1$. The proposed modified SAM algorithm obtains parameters that satisfy the constraints by introducing an exterior penalty approach. The penalty function $EP(\mu_i)$ is defined as follows:

$$EP(\mu_i) = \begin{cases} |\mu_i|^2 & if\ \mu_i \le 0, \\ 0 & if\ 0 \le \mu_i \le \forall \mu_j\ (v_j \in S(v_i)), \\ \left|\mu_i - \min \mu_j\right|^2 & if\ \exists \mu_j < \mu_i\ \left(v_j \in S(v_i)\right). \end{cases}$$

Using the probability $P_h(d)$ that and individual h will choose the destination d, which can be calculated using the G-function, the proposed likelihood function LL' is defined as follows:

$$LL' = \sum_{\forall h} \delta_{hd} \log P_h(d) + \lambda \sum_{T(v_i)} EP(\mu_i),$$

where δ_{hd} is an indicator that equals 1 if the individual h chooses the destination d and 0 otherwise, λ is a hyperparameter for penalty terms, and $T(v_i)$ is a node set different from the bottom layer. The first term is the usual log-likelihood LL on the right-hand side.

In likelihood maximisation, in addition to the scale and allocation parameters, the parameters for the explanatory variables are estimated by setting the deterministic utility as $V = \sum \beta X$. If the GEV network has multiple nests, the probability $P_h(d)$ includes the μ-square of V. The sensitivity of μ is usually not equivalent to β in the likelihood function. In the maximisation process of LL', the partial differentiation with respect to μ is larger than that with respect to β, and then μ is prone to exhibit large changes. We introduce the momentum approach (Qian (1999)), which reflects the previous parameter-updating direction, to the SAM-based algorithm for reducing variability.

Numerical Examples

The experiment used artificial trip data generated in a virtual urban space based on the model developed by Bekhor and Prashker (2008). The total number of trips taken was 40,000. The experiment regards this total trip data as "population data". Next, we randomly extracted 40, 400, and 4000 (observed) sample data from the population data. We used the sample data for training and estimated the parameters with the following estimation algorithms: proposed SAM, SGD, and differential evolution (DE). DE optimises the usual log-likelihood function and obtain the parameters; however, SAM and SGD optimises the proposed LL'. Each algorithm was executed 100 times. We compared the obtained log-likelihood values against the population data to evaluate the predictability and flatness of the estimated parameters. The log-likelihood value in the population data is defined as follows:

$$\sum_{h=1}^{40000} \delta_{hd} \log P_h(d|\widehat{\boldsymbol{\theta}})$$

using the estimated parameters $\widehat{\boldsymbol{\theta}}$ and population data. We evaluated the flatness through

$$\max_{\|\epsilon\|<\rho} LL(\widehat{\boldsymbol{\theta}}) - LL(\widehat{\boldsymbol{\theta}} + \boldsymbol{\epsilon})/1 + LL(\widehat{\boldsymbol{\theta}})$$

using sample data. A smaller value denotes greater flatness.

Figure 3 shows that the proposed SAM and SGD attain excellent prediction performances over small samples (N=40). The results validate the flatness characteristics regarding predictability, especially for small-sample cases. Figure 4 with N = 40 demonstrates that our proposed algorithm obtains flat parameters in a stable manner; however, the algorithm may have room for improvement regarding the results obtained with N = 400 and higher. In addition, we compared the distribution of each parameter and (artificial) true value to evaluate estimability. Although space is limited and results cannot be displayed here, the proposed SAM yielded parameter distributions with true values for all parameters, as did SGD, but not DE, which did not consider flatness. For N=40, the proposed SAM estimates of the scale parameters were superior to the SGD results.

Next, we evaluate the algorithm that combines the momentum method with SAM. The results for N = 40 and 400 reported in Table 1 indicate that the SAM with momentum is superior to that without momentum. By reducing the variation in the estimates of the scale parameter search process, we obtained parameters with a better generalisation performance.

Figure 118. Log-likelihood value in population data with each sample size (N =40, 400, 4000)

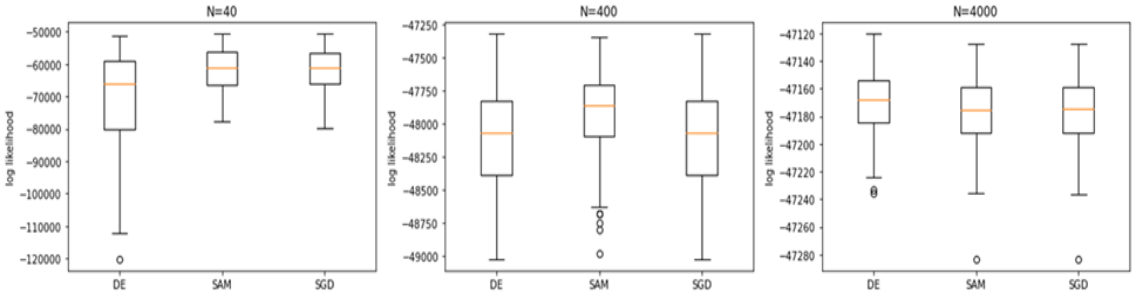

Figure 119. Flatness with each sample size (N =40, 400, 4000)

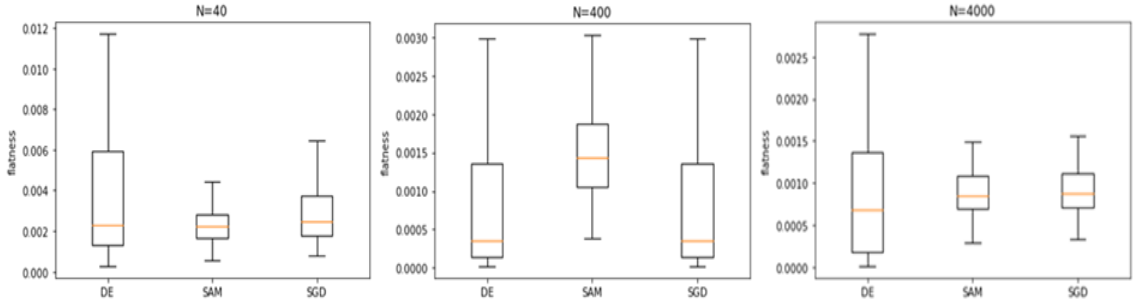

Table 24. Log-likelihood value in population data to compare the results obtained with/without Momentum

Algorithm	N=40	N=400	N=4000
SAM	-61286	-47937	-47175
SAM + Momentum	-59868	-47915	-47915

Conclusions

This study proposed an algorithm to estimate parameters considered the generalisability of the network-GEV model by improving the SAM algorithm used in the deep learning field. The algorithm was mainly used to evaluate the flatness of the likelihood function. The parameter around the flat objective function provided a good objective value when the training data were slightly different from the test data. Our numerical examples validated the proposed algorithm in a destination choice problem, particularly with a small sample size.

References

Bekhor, Shlomo, and Joseph N. Prashker. "GEV-based destination choice models that account for unobserved similarities among alternatives." Transportation Research Part B: Methodological 42.3 (2008): 243-262.

Daly, Andrew, and Michel Bierlaire. "A general and operational representation of generalised extreme value models." Transportation Research Part B: Methodological 40.4 (2006): 285-305.

Foret, Pierre, et al. "Sharpness-aware minimization for efficiently improving generalization." arXiv preprint arXiv:2010.01412 (2020).

Keskar, Nitish Shirish, et al. "On large-batch training for deep learning: Generalization gap and sharp minima." arXiv preprint arXiv:1609.04836 (2016).

Hochreiter, Sepp, and Jürgen Schmidhuber. "Flat minima." Neural computation 9.1 (1997): 1-42.

Qian, Ning. "On the momentum term in gradient descent learning algorithms." Neural networks 12.1 (1999): 145-151.

Zhao, Xilei, et al. "Prediction and behavioral analysis of travel mode choice: A comparison of machine learning and logit models." *Travel behaviour and society* 20 (2020): 22-35.

Zhu, Jiayu, and Xin Ye. "Development of destination choice model with pairwise district-level constants using taxi GPS data." Transportation Research Part C: Emerging Technologies 93 (2018): 410-424.

A preliminary study for exploring ML algorithms to understand the mode choice preferences with a special focus on access mode choice to train stations

L. Cheraitia[ab], R. Chevrier[b], N. van Oort[c], L. Leclercq[a]

[a] *University Gustave Eiffel, ENTPE, LICIT-ECO7, Lyon, France*

[b] *SNCF DTIPG – 1-3 avenue François Mitterrand, F-93210 Saint-Denis, France*

[c] *Dept. of Transport and Planning, Delft University of Technology, Stevinweg 1, 2628CN, Delft, The Netherlands*

Travel mode choice has become a complex problem with the increasing number of transport modes. The early research has used discrete choice models to predict and model travel mode choice (Barff et al. 1982, Hensher et al, 1993). However, recent studies have used Machine learning algorithms to predict travel mode choice which have proven to give better results (Cheng et al. 2019, Nam et al. 2017). Access mode choice to railway had also its fair share of studies by applying mostly discrete choice models. The goal of this study is to fill the gaps by using machine learning to model and predict the combined modes choice (all the modes taken by the traveller to make their trip) with a special focus on railway trips and eventually compare the performances of the two modelling approaches.

Category 12. Traffic flow theory in the presence of different levels of vehicles' connectivity and automation

Road-Side Units location optimization: a Mixed Integer Linear Program approach

E. Fauchet[a], M. Guillot[a], P.-A. Laharotte[a], N.-E. El Faouzi[a], M. Guériau[b]

[a] *Univ. Gustave Eiffel, Univ. Lyon, ENTPE, LICIT-ECO7*

[b] *Normandie Univ., INSA Rouen, UNIROUEN, UNIHAVRE, LITIS*

Introduction

The deployment of Cooperative-Intelligent Transport Systems (C-ITS) and Connected Vehicles (CVs) in traffic is only possible in parallel with the development of the communication infrastructures as RSUs to ensure vehicle-to-infrastructure (V2I), infrastructure-to-vehicle (I2V), or infrastructure-to-infrastructure (I2I) communications through Dedicated Short-Range Communication (DSRC) devices. Like any other type of sensor (e.g. Loop Detectors or LDs), RSUs are expensive to install and maintain. Thus, their installation places have to be chosen carefully. Therefore, our problem is a Traffic Sensor Location Problem (TSLP).

Owais presents in [1] a review and a categorization of TSLP studies. A distinction is made between them based, among others, on: their objective, the type of the studied sensor (passive or active), the location of the sensor (node or link), the mathematical formulation and the solution method. Different objectives are distinguished as the O/D estimation/updating, Path reconstruction, or the Travel Time estimation (TME) [2]. A lot of different mathematical formulations were used. Among them, the ones that come up most often are Systems of Linear Equation (SLE), Binary Integer Programming (BIP) and Binary Integer Non-Linear Programming (BINLP).

Mixed Integer Linear Program (MILP) formulation is not listed in [1]. Yet, MILPs are widely used, especially in transportation problems as transport network downsizing to adjust its offer to the demand,which can both suddenly vary as seen during the COVID-19 crisis, by selecting an optimal sub-network [3]. In [4], Ahmed et al adress the TSLP by focusing on RSUs with a specific objective and therefore not mentioned above. The aim is to locate RSUs to minimize transmission and propagation delays and ensure optimal communication between vehicles and the infrastructure. The problem is modelled as an Integer Linear Program (ILP).

In this study, we also focus on RSUs i.e. passive detectors, which will be located on the network nodes. Thus, we propose a new formulation of TSLP by modelling it as a MILP with a new objective: to provide the most accurate speed profile of the network with a limited number of RSUs. We assume that the speed of road sections on routes can only be captured if a sensor is nearby. If not, the value of its speed is set to the speed limit. Thus, we want to install RSUs in locations where they will be able to capture the greatest differences between actual speeds and speed limits on the road routes around. Furthermore, we formulate the constraints to avoid overlapping between RSUs coverage but to enable a partial coverage of some road sections by RSUs.

This paper is organized as follows: section 2 presents the methodology, section 3 exposes the case studies and the performances achieved, and section 4 discusses the conclusions and perspectives from this work.

Methodology

This section introduces the problem definition and the MILP formulation. The generic framework is introduced in Figure 1.

Figure 120. Generic Framework

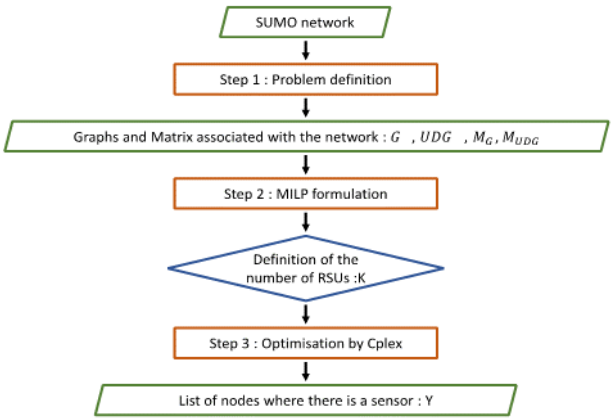

Step 1: Problem definition

This step aims to build Graphs G and DG of the considered network.

Let $G = (V, A)$ be a directed graph representing the road network with A the set of arcs representing all the network route roads and V the set on $|V| = N$ vertices representing all the intersections between the network road routes.

We introduce:

- K the maximum number of RSUs available;
- d_{v_1,v_2} the Euclidean distance between two vertices, $v_1, v_2 \in V$;
- $d_{coverage}$ the coverage distance of a RSU, representing the detection's radius of the RSU;
- $v_{max}(a)$ the speed limit on arc a. We have $v_{max}: A \rightarrow \mathbb{R}$

$$a \mapsto v_{max}(a)$$

- $v_{actual}(a)$ the actual speed on arc a. We have $v_{actual}: A \rightarrow \mathbb{R}$

$$a \mapsto v_{actual}(a)$$

A solution to our problem is a subset $V' \subseteq V$ with $|V'| \leq K$ in which we place the RSUs.

Let $DG = (V, E)$ (DG for DiskGraph) be an undirected graph where neighbours of each vertex in the road network are connected to it. In this graph, two vertices are connected if and only if the Euclidean distance between them is smaller than the detection radius of a RSU. We have:

$$E = \left\{(v_1, v_2) \in V^2 \;\middle|\; d_{v_1,v_2} \leq d_{coverage}\right\}$$

We also define N_{UG} the set of neighbours of vertex i:

$$N_{UG}(i) = \{j \in V \mid \exists e \in E, e = (i, j)\}$$

We call "detected" a vertex that is within the detection radius of a RSU. In particular, if $i \in V'$, all vertices of $N_{UG}(i)$ are said to be detected. Similarly, an arc $a = (v_1, v_2) \in A$ is said to be detected if both vertices v_1 and v_2 are detected.

We call $Adet(V')$ the set of arcs detected for the RSUs location choice V'.

We assume that we know the actual speed on the detected arcs, and that for the others we will consider their speed as the arc's speed limit. The aim is to detect arcs whose actual speed is far from the speed limit, that is to say:

$$\triangle(V') = \sum_{a \in Adet(V')} (v_{max}(a) - v_{actual}(a))$$

The problem which consists in finding V'which maximizes $\triangle(V')$ is called the Traffic Sensor Location Problem (TSLP).

Step 2: MILP formulation

We decided on the following formulation:

1) The decision variables are:

$$\forall i \in N, \quad Y(i) = \begin{cases} 1, & if\ we\ place\ one\ RSU\ at\ vertex\ i \\ 0, & otherwise \end{cases}$$

$$\forall i \in N, \quad \tilde{Y}(i) = \begin{cases} 1, & if\ i\ is\ detected \\ 0, & otherwise \end{cases}$$

$$\forall e \in E, \quad z(e = (i,j)) = \begin{cases} 1, & if\ e\ is\ detected \\ 0, & otherwise \end{cases}$$

Note that the use of z(e) could be avoided, but it eases the formulation's writing.

2) The objective function is: $\forall e \in E, f_{obj} = \min \sum_e \big((1 - z(e)) * (v_{max}(e) - v_{actual}(e)) \big)$

Thus, to minimize this sum, a maximum number of arcs e has to be observed.

3) The constraints are:

(a) $\sum_{i \in N} Y(i) \leq K$ We have a limited number of RSUs.

(b) $\sum_{i \in N} \tilde{Y}(i) \leq \sum_{j \in N_{DG}} Y(j)$ This constraint ensures that $\tilde{Y}(i) = 0$ if no RSU is located near i.

(c) $z(e = (i,j)) \leq \frac{1}{2} * (\tilde{Y}(i) + \tilde{Y}(j))$ This constraint ensures that $z(e = (i,j)) = 0$ if no RSU is located near i and j.

Then, let us consider the mathematical Program (P):

$$min \quad \sum_e \big((1 - z(e)) * (v_{max}(e) - v_{actual}(e)) \big)$$

$$st \quad \sum_{i \in N} Y(i) \leq K \qquad \forall i,\ Y(i) \in \{0,1\} \qquad (1)$$

$$\sum_{i \in N} \tilde{Y}(i) \leq \sum_{j \in N_{DG}} Y(j) \qquad \forall i,\ \tilde{Y}(i) \in \{0,1\} \qquad (2)$$

$$z(e = (i,j)) \leq \frac{1}{2} * (\tilde{Y}(i) + \tilde{Y}(j)) \qquad \forall e,\ z(e) \in \{0,1\} \qquad (3)$$

The decision variables are binary and the three constraints are linear. Thus, (P) is a MILP. Thus, an optimal solution can be found using a standard MILP-solver as CPLEX.

Test case and Results

Figure 121. Reference Speed Profile and Observed ones according to K (for one seed)

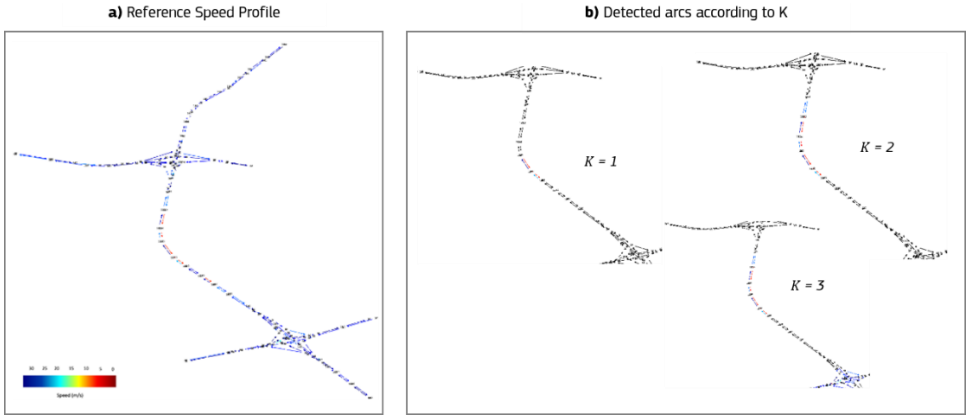

We apply the formulation above on a sandbox example based on the M50 network in Dublin introduced in [5]. We build a simple case where we define the graphs $G = (V, A)$ and $DG = (V, E)$ according to the M50 SUMO network with N the number of road vertex.Then, we define:

- $d_{coverage} = 250\ m$ and $\forall a \in A, v_{max}(a) = 33\ m/s$;
- $\forall a \in A, v_{actual}(a)$ is artificially built to control the congestion location. $v_{actual}(a)$ follows a normal distribution with mean μ and standard deviation σ, $v_{actual}(a) \sim \mathrm{N}(\mu, \sigma^2)$. As shown in Figure 2a, where the reference speed profile is shown for one seed (of normal distribution), speeds are close to the maximum speed in all the network (all section roads in dark blue) except in one part of one of the principal axes called the congested area (in red). Thus, in the congested area, we have $v_{actual}(a) \sim \mathrm{N}(5, 0.5)$. And, in the rest of the network, we have $v_{actual}(a) \sim \mathrm{N}(33, 3.3)$.
- K the maximum number of RSUs available on the road network vertex. It varies with the scenarios under consideration from 1 to 50 with the following discrete values {1, 2 ,3, 5, 10, 20, 50}.

Figure 122. Variability of the predicted value compared to the reference one according to K

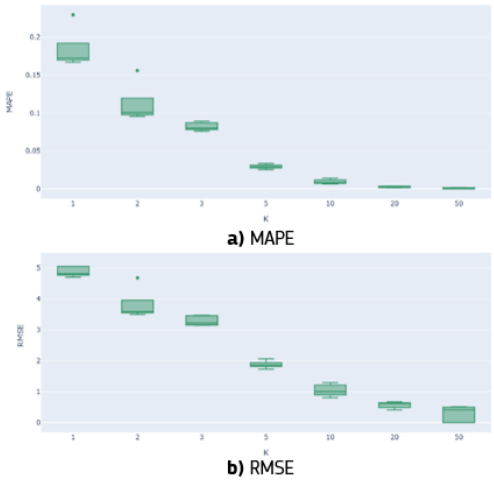

In Figure 2b, only edges detected by a RSU (red nodes) are colored as a function of the observed speed with one, two, or three RSUs, for one seed. When K = 1 and K = 2, RSUs are located in the congested area as expected. Two RSUs are enough to detect the entire congested area. Thus, the third one is located on one of the road interchanges, and it seems to be the one that presented the most variability to the maximum speed allowed.

In Figure 3, indicators MAPE and RMSE are displayed for five seeds as a function of the number of RSUs K. They both summarize the variability of the predicted value compared to the reference ones. As expected in this sandbox test case, error values are low even with only one RSU. However, there is an expected trend: the error values tend to be 0 when K (number of RSUs) tends to N (number of nodes on the network).

Discussion

The aim was to obtain speed tricolours as close as possible to the reference profile with as few RSUs as possible by defining the problem as a MILP. We validate here a Proof of concept with results showing that RSUs are located in the only congested area of the network. Future work will test our formulation on more complex network before applying the methodology on real instances. Supplementary perspectives lie in a new formulation with the objective of placing RSUs in the optimal locations of the network to apply control strategies such as a Variable Speed Limit Systems.

References

[1] Owai, M., 'Traffic sensor location problem: Three decades of research', *Expert Systems with Application*, 2022, pp. 118134.

[2] Gentili, M. and Mirchandani P.B., 'Review of optimal sensor location models for travel time estimation', *Transportation Research Part C: Emerging Technologies*, Vol. 90, 2018, pp. 74-96.

[3] Guillot, M., Furno, A., Aghezzaf, E.-H. and El Faouzi, N.-E., 'Transport network downsizing based on optimal sub-network', Communications *in Transportation Research*, Vol. 2, 2022, pp. 100079.

[4] Ahmed, Z., Naz, S. and Ahmed, J., 'Minimizing transmission delays in vehicular ad hoc networks by optimized placement of road-side unit', *Wireless Networks*, Vol. 26, 2020, pp. 2905-2914.

[5] Gueriau, M. and Dusrapic, I., 'Quantifying the impact of connected and autonomous vehicles on traffic efficiency and safety in mixed traffic', *in 2020 IEEE 23rd International Conference on Intelligent Transportation Systems (ITSC)*, 2020, pp. 1-8.

Estimating traffic capacity in sag sections using continuum traffic flow theory

S.KAI[a], K. WADA[b], R. HORIGUCHI[a], J. XING[c]

[a] *i-Transport Lab. Co., Ltd., Japan*

[b] *Institute of Systems and Information Engineering, University of Tsukuba., Japan*

[c] *Nippon Expressway Research Institute Co., Ltd., Japan*

Introduction

As Koshi et al. (1992) point out, traffic congestion caused by sags has long been a problem in Japan, and road administrators are implementing various congestion countermeasures (e.g., Sato et al., 2021). However, there is no established method for identifying precise bottleneck section, while the bottleneck is determined (as a point) using rules of thumb such as speed criteria and the starting point of speed recovery in practice. This study discusses the spatial heterogeneity of the traffic capacity inside sag sections using the continuum traffic flow theory which treats the bottleneck as a continuous section rather than a point.

Methodology

In the continuum traffic flow theory for sag bottlenecks proposed by Jin (2018) and Wada et al. (2020), it is assumed that the capacity continuously decreases inside the bottleneck section due to the increase in the safety time gap. Let $0 \le x \le L$ denote the section and $\tau(x)$ denote the time gap at position x where $\frac{d\tau(x)}{dx} > 0$. With the triangular fundamental diagram, the traffic capacity $C(x)$ at position x can be shown in the following equation.

$$C(x) = \frac{u\kappa}{1 + u\kappa\tau(x)} \qquad 0 \le x \le L \tag{1}$$

where u is the free-flow speed and κ is the jam density. In short, $C(0)$ represents the traffic capacity before the bottleneck section, and $C(L)$ represents the traffic capacity at the downstream end of the bottleneck section, namely "bottleneck capacity."

During persistent congestion, the capacity drop is observed and traffic states such as the flow and speed are almost stationary and stable (Koshi et al., 1992; Ozaki, 2003). We refer to this state as "capacity drop stationary state." Let C_d be the dropped capacity (or queue discharge flow rate) in the stationary state, then the stationary speed $v(x)$ at position x in the bottleneck section can be expressed as follows (Jin, 2018).

$$v(x) = \frac{1}{\{1/C_d - \tau(x)\}\kappa} \qquad 0 \le x \le L \tag{2}$$

The basic idea of estimating the capacity using the above theory is very simple. Once C_d and $v(x)$ during the capacity drop stationary state are given by observation, the time gap $\tau(x)$ can be uniquely determined by solving equation (2) for $\tau(x)$. Also, assuming that free flow speed u and jam density κ are given, the traffic capacity $C(x)$ can be calculated from equation (1). If $C(x)$ is calculated continuously at the bottleneck section ($0 \le x \le L$), it can represent the change in traffic capacity from the upstream end to the downstream end of a bottleneck section. Note that we used the calibration method of the continuum traffic flow theory presented by Wada et al. (2022) to determine the bottleneck section ($0 \le x \le L$) appropriately by using the detector data and probe data.

Results

We examine four Japanese highway sag sections shown in Table 1. These are selected from the heavily congested sections, emphasizing the following points.

- The queue length is long enough to cover the sag section.
- The head of the traffic congestion is in the sag in question.
- Traffic congestion is not affected by other bottlenecks.
- Traffic congestion continues for several hours.

— Sufficient probe samples are obtained.

Figure 1 shows the spatial heterogeneity of the estimated traffic capacity and longitudinal gradient inside each bottleneck section. These box plots are calculated by the estimated traffic capacities of 10 congestion events per section. Figure 2 shows the average spatial heterogeneity of the normalized traffic capacity (i.e., $C(x)/C(L)$) with respect to the bottleneck capacity for comparison. These are calculated only for those locations where traffic capacities are estimated for all 10 events.

Table 123. Target expressway sections

No.	Expressway Name	Direction	Bottleneck Name	Num of lane (by direction)	Longitudinal gradient
A	Tomei	east bound	Nisshin	2	-2.7% ~ 1.1%
B	Meishin	east bound	Semimaru	2	-3.5% ~ 2.7%
C	Kan-etsu	south bound	Takasaka	3	-0.4% ~ 1.1%
D	Kan-etsu	north bound	Komagawa	3	-1.2% ~ 1.0%

Source: Authors' elaborations.

Figure 124. Spatial heterogeneity of traffic capacity

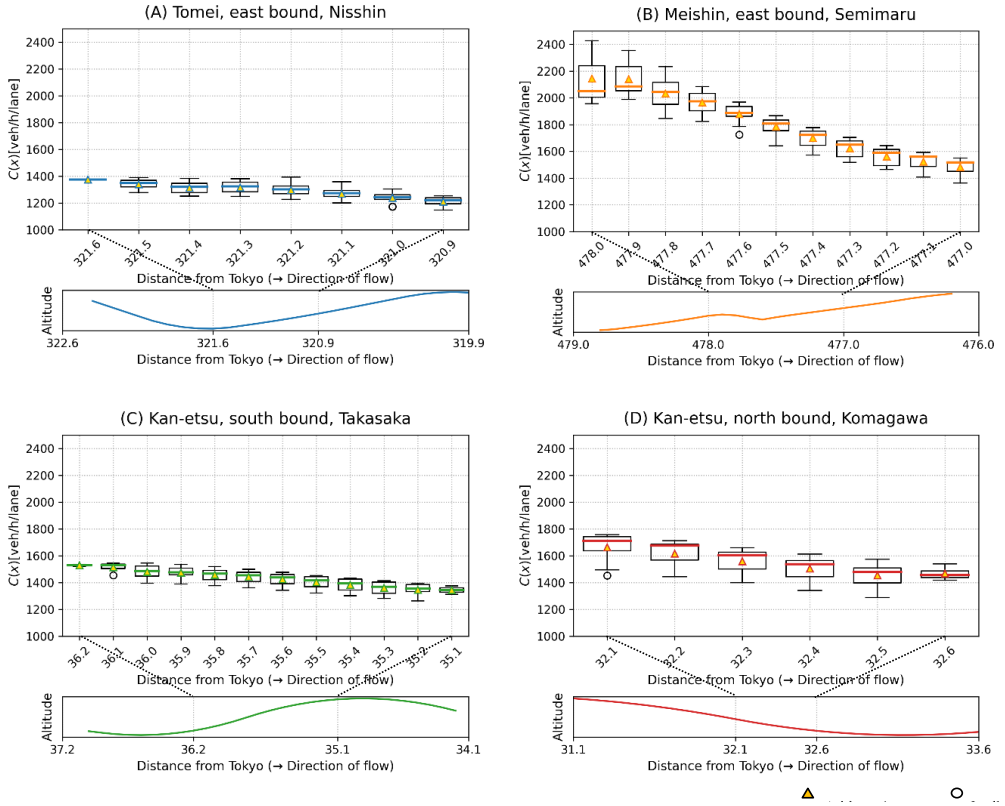

Source: Authors' elaborations.

Figure 125. Normalized traffic capacity with respect to the bottleneck capacity

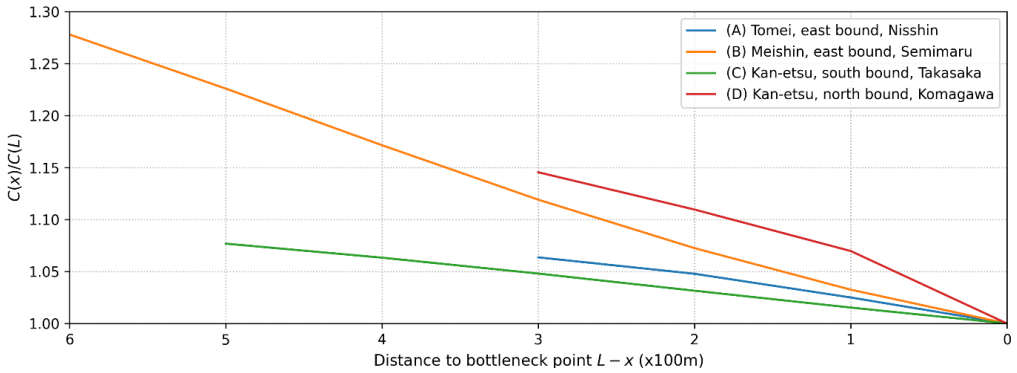

Source: Authors' elaborations.

Discussion

From Figure 1, we can see that the position of the decrease in the capacity inside the sag section varies significantly across locations. Specifically, the estimated capacity decreases (A) at Nisshin, from the bottom of the sag to the middle of the upgrade; (B) at Semimaru, from the beginning of the downgrade to the middle of the upgrade; (C) at Takasaka, from the middle of the upgrade to near the crest; (D) at Komagawa, along the downgrade-to-downgrade section located upstream of the bottom of the sag.

Figure 2 shows that the spatial decreasing rate in the traffic capacity also differs across locations, and that longer [shorter] bottleneck sections do not necessarily result in a more gradual [sudden] degree of capacity reduction. Another interesting finding is that (D) at Komagawa, which is downgrade-to-downgrade bottleneck among target sections, exhibits the largest spatial decreasing rate in traffic capacity. According to the theory (Wada et al., 2020), it can be interpreted as the speed adjustment to the vehicle ahead during the speed recovery process is delayed more at (D) at Komagawa than others. This might be because drivers drive more carefully by taking into account the increase in acceleration on a downgrade.

The above results suggest that the relationship between longitudinal gradient change and bottleneck section is not simple, indicating the importance of properly identifying bottleneck section at each sag. The analysis and results in this study will help to more effective spatial placement of congestion measures. Furthermore, although the measures may have been focused on downgrade-to-upgrade sags where it is easy to imagine speed reductions, if the spatial decreasing rate in traffic capacity is generally greater for downgrade-to-downgrade bottleneck it will call for revisiting the priority of sag bottlenecks for introducing congestion measures.

Acknowledgements

This work was supported by JSPS KAKENHI Grant Number JP19K04637.

References

Koshi, M., Kuwahara, M., Akahane, H., Capacity of sags and tunnels on Japanese motorways. ITE Journal. Vol.62, pp.17–22, 1992.

Sato, H., Nishida, T., Kashiwagi, Y., Sakurai, M. and Aoki, T.: Analysis of the effectiveness of voice guidance utilizing speakers for the provision of speed recovery information, Journal of Japan Society of Civil Engineers, Ser. D3 (Infrastructure Planning and Management), Vol.77, No.1, pp.1-11, 2021. (in Japanese).

Ozaki, H., Modeling of vehicular behavior from road traffic engineering perspectives. In: Traffic and Granular Flow'01. Springer, Berlin Heidelberg, pp.281–292, 2003.

Jin, W.-L.: Kinematic wave models of sag and tunnel bottlenecks, Transportation Research Part B: Methodological, Vol.107, pp.41–56, 2018.

Wada, K., Martínez, I., Jin, W.-L.: Continuum car following model of capacity drop at sag and tunnel bottlenecks, Transportation Research Part C: Emerging Technologies, Vol.113, pp.260–276, 2020.

Wada, K., Xing, J. and Oguchi, T.: On the mechanism of capacity drop at freeway sag and tunnel bottlenecks, JSTE Journal of Traffic Engineering, Vol.8, No.3, pp.1-10, 2022. (in Japanese).

A novel model of Inertia-Oriented Driving Technique

K. Mattas[a], R. Donà[a], G. Albano[a], B. Ciuffo[a]

[a] *European Commission – Joint Research Centre*

[a] *Piksel SRL*

Introduction

Road transportation is a vital part of our communities, even if transportation externalities include environmental damage, accidents, congestion, and oil dependence. The carbon emissions from road transport are increasing (IEA, 2022). Road traffic injuries are the leading cause of death for children and young adults aged 5-29 years according to the WHO (WHO, 2022). Additional costs include the time wasted in traffic congestion. The rise of automation and connectivity provides an important opportunity to change that trend (European Commission. Joint Research Centre, 2019). However, automation alone may not be sufficient, to make road traffic networks more efficient and sustainable, and connectivity could be required (Mattas et al., 2018). Indeed, automated driving systems that are commercially available have been shown to be potentially harmful to traffic flow (Ciuffo et al., 2021). Connectivity solutions are not yet available in the market, and since there are several problems to be overcome before this is possible, alternative solutions are being investigated (Donà et al., 2022).

In recent years, a new idea promises to improve the way we are driving. It is assumed that human drivers tend to "Drive to keep Distance" (DD), meaning that human drivers have an interpretation of what is a safe distance to a preceding vehicle, and their behaviour is based on keeping this distance. However, human drivers could alternatively "Driving to keep Inertia" (DI) (Blanch Micó et al., 2018). Frequently, human drivers can be string unstable in their driving behaviour, meaning that speed perturbations coming from preceding vehicles are amplified when travelling upstream (Wilson and Ward, 2011). This has been also witnessed with commercially available Adaptive Cruise Control (ACC) systems (Makridis et al., 2020), which represent automation level 1 or 2 according to the SAE taxonomy (SAE, 2021). Those novel inertia-oriented driving techniques suggest that a driver can be conscious of the traffic shockwaves in order to attenuate their magnitude (Lucas-Alba et al., 2020). The effectiveness of this approach has been investigated in driving simulator experiments (Tenenboim et al., 2022). Both young and experienced drivers were able to change their driving style after following a short course. Moreover, they were able to decrease the energy consumption, also for the vehicles upstream, by keeping larger distances be able to absorb some of the traffic oscillations.

Two possible questions arise. Firstly, if this is a tactic that human drivers can easily follow, is it possible that also automated driving systems can replicate this behaviour, bringing benefits to the traffic flow? Secondly, influencing traffic flow can be challenging. Changing drastically the driving behaviour can induce the emergence or strengthening of phenomena such as traffic hysteresis and capacity drop (Laval, 2011), and alter macroscopic characteristics of the traffic flow in ways that are not obvious a-priori. Further investigation is required to understand the effects of DI on capacity, flow and throughput, and possible interactions with vehicle dynamics that are not always considered (Makridis et al., 2019).

In the present paper, we explore the possibility to model DI in microscopic simulation. Such a model can allow a thorough investigation of DI for different conditions and different penetration rates. Moreover, the DI model is designed to be similar to traditional car-following models, which can represent the DD behaviour, using similar inputs, assuming the same information is known to drivers of both types. In this way, it is possible to compare the two driving styles. The model is based on Fuzzy logic (Zadeh, 1965), to replicate fairly the different suggestions that are given to human drivers in the aforementioned driving simulator experiments (Tenenboim et al., 2022).

Methodology

Two microscopic car-following models are used in the current work. To represent the DD driving behaviour, a simple linear model is used, which has already been investigated in terms of string stability (Wang et al., 2017). For the alternative inertia-oriented technique, a new Fuzzy DI model is developed.

Linear model. The linear model, with some adjustments, has been used to simulate both human drivers and ACC systems (Gunter et al., 2021; Shladover et al., 2012). The control mechanism is presented in equation 1.

$$\dot{u}_i = k_v(u_{i-1} - u_i) + k_s(s_i - u_i t_d - s_0), \quad (1)$$

where k_v and k_s are gain factors for the speed error and the spacing error respectively; t_d is the desired time gap; s_i the leader-follower instantaneous spacing; s_0 is the standstill spacing. There is no perception or actuation delay. Two different parameter combinations are considered in the present work, one denoted linear S, which corresponds to a string stable parametrization, and linear U which corresponds to an unstable one. For Linear S, k_v is equal to 1 and k_s is 0.25, while the respective values for the linear U are 0.13 and 0.4. For the present work, the two cases serve as a qualitative comparison of the different behaviours, and additional calibration efforts are omitted.

Fuzzy DI model. The DI driving behaviour is based on a few simple rules. The DI driver should not allow the preceding vehicle to be too far away. Moreover, the inter-vehicle distance should not be shorter than the safety distance. Up to this point, the behaviour is not different to a simple DD driver behaviour. The most important rule is that the driver should keep additional space, termed the anti-jam distance, that can be used to attenuate perturbations in the leader's speed. Moreover, examples of the behaviour presented in the aforementioned papers show an indifference of the DI driver behaviour to small perturbations in the leader's speed (Blanch Micó et al., 2018). This indifference in the DI distance is not common in traditional car-following models, for which there is a specific desired distance for each steady state speed. Models including indifference have been proposed, such as the application of the three-phase theory (Kerner et al., 2007), however, this is commonly a simulation of the uncertainty of the estimation of distance and not a wide anti-jam distance.

To simulate the behaviour, a Fuzzy controller is developed. Fuzzy controllers are based on 'If…then…" rules, in which both the antecedent and the consequent can be fuzzy linguistic variables. A fuzzy linguistic variable can represent the expression "too long" in a robust way, that is similar to the intuitive understanding of humans. Thus, the simple suggestions given to DI drivers can be formalized.

For the formalization, three linguistic variables have to be defined, using fuzzy sets. Firstly, the safety distance can be fuzzified using the Proactive Fuzzy surrogate Safety metric (PFS) (Mattas et al., 2020). When the PFS membership value is 1, the situation is unsafe, and the value 0 corresponds to a safe distance. However, the PFS membership value can take any value between 0 and one, representing a situation that is unsafe with a degree of truth. Similarly, the anti-wave space is represented by a trapezoidal fuzzy set. Finally, another trapezoidal fuzzy set represents the linguistic variable "too long".

The fuzzy controller is of the Takagi-Sugeno type (Scherer, 2012), where the consequent is not fuzzy. The rules defined are: 1) **If** the distance is unsafe (PFS) T**hen** decelerate (6 m/s2), 2) **If** the distance is on the Anti-wave space T**hen** do nothing, 3) **If** the distance is Too Long T**hen** accelerate (2 m/s2). The final acceleration is calculated as a weighted average of the consequent accelerations.

Results

A simple simulation experiment of two vehicles car following is carried out. The preceding vehicle is following a predefined speed profile, while the follower vehicle uses one of the three car-following models. The results are presented in Figure 1. The speed drops and increases for the Linear U are more extreme that the leader's while there is also an overshoot in the initial acceleration. For the Linear S, the oscillation is dampened, but the effect of the Fuzzy DI is distinctively different, with the oscillation being completely absorbed, on the cost of keeping a larger constant distance.

This is an important advantage of the DI approach, as the following vehicles would not experience a perturbation. Additionally, the speed of the DI vehicle is constant for most of the simulation, while the intervehicle distance is oscillating, with a decreasing trend. This shows the indifference, that can lead to multiple different equilibrium conditions. Finally, in the acceleration phase, the DI takes more time to achieve the steady state speed. This can be influential to the throughput after bottlenecks in real world conditions and has to be further investigated. Additional rules could be established to correct this, in case it presents negative impacts.

Figure 126. Resulting speed profiles for (a) Linear S, (b) Linear U, (c) Fuzzy DI models

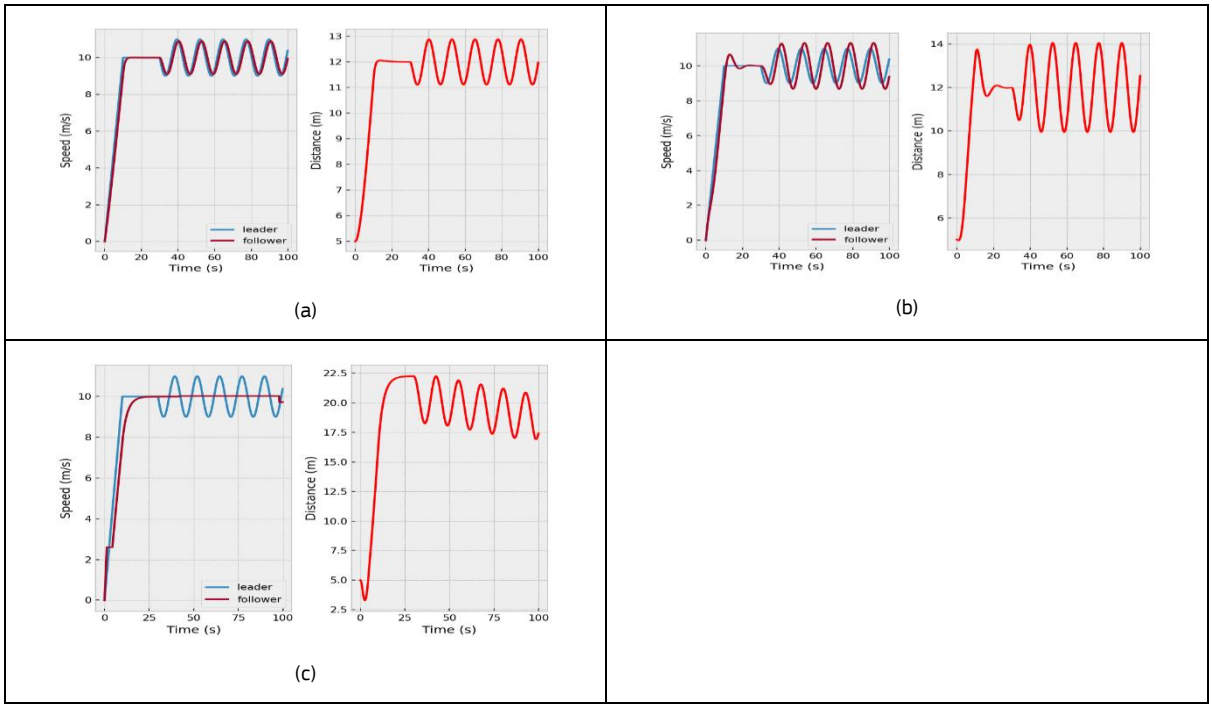

Source: Authors' elaborations.

Conclusions

In the present paper, a modelling framework is presented to simulate an inertia-oriented driving technique in micro simulation. The results show that this technique can be reproduced in simulation using a Fuzzy model.

The effect of DI is evident and different to string stable parameterizations of traditional car-following models. Based on this, the effects of such an approach can be investigated, for the relevant effects on traffic flow. For further research, the model's parameters have to be calibrated on DI human drivers, or optimized if they can be applied to ACC systems. Moreover, the current Fuzzy DI model includes only the most necessary rules. Additional rules, coming from observing results of simulation experiments, or from experienced DI drivers, may further improve the model's simulation. Finally, realistic vehicle dynamics can also be added, to further support relevant results.

References

Blanch Micó, M.T., Lucas Alba, A., Bellés Rivera, T., Ferruz Gracia, A.M., Melchor Galán, Ó.M., Delgado Pastor, L.C., Ruíz Jiménez, F., Chóliz Montañés, M., 2018. Car following: Comparing distance-oriented vs. inertia-oriented driving techniques. Transport Policy, Efficient, Safe and Intelligent Transport. Selected papers from the XII Conference on Transport Engineering 67, 13–22. https://doi.org/10.1016/j.tranpol.2017.05.008.

Ciuffo, B., Mattas, K., Makridis, M., Albano, G., Anesiadou, A., He, Y., Josvai, S., Komnos, D., Pataki, M., Vass, S., Szalay, Z., 2021. Requiem on the positive effects of commercial adaptive cruise control on motorway traffic and recommendations for future automated driving systems. Transportation Research Part C: Emerging Technologies 130, 103305. https://doi.org/10.1016/j.trc.2021.103305.

Donà, R., Mattas, K., He, Y., Albano, G., Ciuffo, B., 2022. Multianticipation for string stable Adaptive Cruise Control and increased motorway capacity without vehicle-to-vehicle communication. Transportation Research Part C: Emerging Technologies 140, 103687. https://doi.org/10.1016/j.trc.2022.103687.

European Commission. Joint Research Centre, 2019. The future of road transport : implications of automated, connected, low-carbon and shared mobility, EUR (Luxembourg). Publications Office, LU.

Gunter, G., Gloudemans, D., Stern, R.E., McQuade, S.T., Bhadani, R., Bunting, M., Delle Monache, M.L., Lysecky, R., Seibold, B., Sprinkle, J., Piccoli, B., Work, D.B., 2021. Are commercially implemented adaptive cruise control systems string stable? IEEE Transactions on Intelligent Transportation Systems 1–12. https://doi.org/10.1109/TITS.2020.3000682.

IEA, 2022. Transport.

Kerner, B.S., Klenov, S.L., Hiller, A., 2007. Empirical test of a microscopic three-phase traffic theory. Nonlinear Dyn 49, 525–553. https://doi.org/10.1007/s11071-006-9113-1.

Laval, J.A., 2011. Hysteresis in traffic flow revisited: An improved measurement method. Transportation Research Part B: Methodological 45, 385–391. https://doi.org/10.1016/j.trb.2010.07.006.

Lucas-Alba, A., Melchor, Ó.M., Hernando, A., Fernández-Martín, A., Blanch-Micó, M.T., Lombas, A.S., 2020. Distressed in the queue? Psychophysiological and behavioral evidence for two alternative car-following techniques. Transportation Research Part F: Traffic Psychology and Behaviour 74, 418–432. https://doi.org/10.1016/j.trf.2020.09.011.

Makridis, M., Fontaras, G., Ciuffo, B., Mattas, K., 2019. MFC Free-Flow Model: Introducing Vehicle Dynamics in Microsimulation. Transportation Research Record: Journal of the Transportation Research Board 036119811983851. https://doi.org/10.1177/0361198119838515.

Makridis, M., Mattas, K., Ciuffo, B., Re, F., Kriston, A., Minarini, F., Rognelund, G., 2020. Empirical Study on the Properties of Adaptive Cruise Control Systems and Their Impact on Traffic Flow and String Stability. Transportation Research Record 2674, 471–484. https://doi.org/10.1177/0361198120911047.

Mattas, K., Makridis, M., Botzoris, G., Kriston, A., Minarini, F., Papadopoulos, B., Re, F., Rognelund, G., Ciuffo, B., 2020. Fuzzy Surrogate Safety Metrics for real-time assessment of rear-end collision risk. A study based on empirical observations. Accident Analysis & Prevention 148, 105794. https://doi.org/10.1016/j.aap.2020.105794.

Mattas, K., Makridis, M., Hallac, P., Raposo, M.A., Thiel, C., Toledo, T., Ciuffo, B., 2018. Simulating deployment of connectivity and automation on the Antwerp ring road. IET Intelligent Transport Systems 12, 1036–1044. https://doi.org/10.1049/iet-its.2018.5287.

SAE, 2021. J3016C: Taxonomy and Definitions for Terms Related to Driving Automation Systems for On-Road Motor Vehicles - SAE International [WWW Document]. URL https://www.sae.org/standards/content/j3016_202104/ (accessed 1.4.22).

Scherer, R., 2012. Takagi-Sugeno Fuzzy Systems, in: Scherer, R. (Ed.), Multiple Fuzzy Classification Systems, Studies in Fuzziness and Soft Computing. Springer, Berlin, Heidelberg, pp. 73–79. https://doi.org/10.1007/978-3-642-30604-4_7

Shladover, S., Su, D., Lu, X.-Y., 2012. Impacts of Cooperative Adaptive Cruise Control on Freeway Traffic Flow. Transportation Research Record: Journal of the Transportation Research Board 2324, 63–70. https://doi.org/10.3141/2324-08.

Tenenboim, E., Lucas-Alba, A., Melchor, Ó.M., Toledo, T., Bekhor, S., 2022. Car following with an inertia-oriented driving technique: A driving simulator experiment. Transportation Research Part F: Traffic Psychology and Behaviour 89, 72–83. https://doi.org/10.1016/j.trf.2022.06.003.

Wang, M., Li, H., Gao, J., Huang, Z., Li, B., van Arem, B., 2017. String stability of heterogeneous platoons with non-connected automated vehicles, in: 2017 IEEE 20th International Conference on Intelligent Transportation Systems (ITSC). Presented at the 2017 IEEE 20th International Conference on Intelligent Transportation Systems (ITSC), pp. 1–8. https://doi.org/10.1109/ITSC.2017.8317792.

WHO, 2022. Road traffic injuries [WWW Document]. URL https://www.who.int/news-room/fact-sheets/detail/road-traffic-injuries (accessed 3.5.23).

Wilson, R.E., Ward, J.A., 2011. Car-following models: fifty years of linear stability analysis – a mathematical perspective. Transportation Planning and Technology 34, 3–18. https://doi.org/10.1080/03081060.2011.530826.

Zadeh, L.A., 1965. Fuzzy sets. Information and Control 8, 338–353. https://doi.org/10.1016/S0019-9958(65)90241-X.

Dynamic model-enhanced reinforcement learning for mixed-fleet mobility-on-demand systems

A. Ruining Yang[a], B. Longhao Yan[b], C. Kaidi Yang[c]

[a] *Department of Civil and Environmental Engineering, National University of Singapore*

Introduction

One key operational challenge associated with mobility-on-demand (MoD) systems can be characterized by vehicle imbalances due to asymmetric travel demand. Recent advances in automated vehicles (AVs) provide an excellent opportunity to address such a challenge by allowing MOD operators to coordinate their fleets in a centralized manner. Despite the benefits of AVs, it is evident that the development and deployment of AVs can only happen gradually. In the near future, MoD systems will be operating a mixed fleet of human-driven vehicles (HVs) and AVs, whereby HVs could strategically respond to the actions of AVs, making global coordination computationally challenging.

Several studies have explored control strategies for managing mixed-fleet MoD. Afeche et al. (2018) analyzed the steady-state system equilibria under different control regimes, taking into account of HVs' profit-oriented behavior. Yang et al. (2020) proposed a bi-level Stackelberg framework to control mixed-fleet MoD, developing a game-theoretic HV behavioral model at a lower level and model predictive control at a higher level. Xie et al. (2022) proposed a two-sided multi-agent (i.e., the operator and HVs) deep reinforcement learning (RL)-based approach to address the challenge of spatial-temporal uncertainty in demand considering the interactions between HVs and AVs. Although these methods have succeeded in improving mixed-fleet MoD operations, they may not scale well to large transportation networks due to computation complexity and sample efficiency. To address this issue, we propose an RL-based control framework for AVs that integrates a model-free advantage actor-critic approach and mode-based components, including a dynamic model of the system and prior knowledge of HV behavior (e.g., Feinberg et al., 2018). The proposed method can improve the computation efficiency in operating a mixed-fleet MoD while being sample efficient.

Our contributions are summarized as follows. First, we devise a dynamic model-enhanced RL-based algorithm for rebalancing AVs in mixed-fleet MoD systems, whereby a dynamic model simulating the MoD system is integrated into the model-free RL framework to improve sample efficiency. Second, we employ a Wasserstein loss function for training the dynamic model to align the prediction accuracy of the next state with the control objective of the RL framework. The Wasserstein loss can mimic the rebalancing process. Third, we incorporate prior knowledge (i.e., theoretical model) about HV cruising behavior into the neural network-based dynamic model in a physics-informed manner. Such behavioral models can help improve sample efficiency and ensure that the trained dynamic model is physically meaningful.

Methodology

We consider a city with a transportation network described as a directed graph $\mathcal{G} = (\mathcal{V}, \mathcal{E})$, where each vertex $i \in \mathcal{V}$ represents a station (i.e., pickup/dropoff locations), and each edge $(i,j) \in \mathcal{E}$ represents a connecting path between station i and station j. The considered time horizon is discretized as a set $\mathcal{T} = \{0, 1, 2, \cdots, T\}$. Here we consider the scenario where the MoD fleet takes a small percentage of the entire vehicle population on the road network, and therefore the travel time is independent of operational algorithms. The system operates as follows. After receiving a batch of requests, the MoD operator will perform order dispatching to assign each request to a vehicle (AV or HV). AVs will always accept the assigned passengers, while HVs can choose to reject passengers with low profits. Vehicles without passengers will either stay at the same station or move to another station. Specifically, AV rebalancing decisions are made by the MoD operator, whereas HV cruising decisions are made by themselves.

We focus on AV rebalancing. Our dynamic model-enhanced RL builds on a state-of-the-art RL-based approach, which formulates a bi-level problem. The lower level problem at time step t is formulated as Eq.(1)-Eq.(4).

$$\min_{\{f_{ijt}\}_{(i,j)\in\mathcal{E}}} \beta \sum_{(i,j)\in\mathcal{E}} \tau_{ijt} f_{ijt} \qquad (1)$$

$$s.t. \qquad \sum_{j\in\mathcal{V}} (f_{jit} - f_{ijt}) + m_{it} \geq o_{it}, \forall i \in \mathcal{V} \qquad (2)$$

$$\sum_j f_{ijt} \leq m_{it}, \forall i \in \mathcal{V} \qquad (3)$$

$$f_{ijt} \geq 0, \forall (i,j) \in \mathcal{V} \qquad (4)$$

where τ_{ijt} is the travel time from station i to station j at time t; f_{ijt} represents the AV rebalancing flow from station i to station j at time t; m_{it} represents the number of AVs in station i at time t; o_{it} is the desired number of AVs in station i at time t, which is given by the RL agent at the upper level.

The upper-level problem is formulated as a Markov decision process (MDP) (S, A, P, r, γ) with state space S, action space A, process P, reward function r, and discounted factor γ. The state ($\boldsymbol{s_t} \in \boldsymbol{S}$) contains the information needed by the rebalancing strategies, including (1) attributes of the transportation network (i.e., adjacency matrix and travel times), (2) passenger demand and trip prices in current and past time steps, (3) current availability and predicted arrivals of AVs and HVs. The action ($\boldsymbol{a_t} \in \boldsymbol{A}$) is defined as the desired number of idle AVs over all stations, which can be calculated using the probability sampled from a Dirichlet distribution, denoted by z_{it}, $\forall i \in \mathcal{V}$. Naturally, we have $\sum_{i \in \mathcal{V}} z_{it} = 1$ and $z_{it} \geq 0$, $\forall v \in \mathcal{V}$. Note that the desired number of vehicles o_{it} used in Eq.(2) can be written as $o_{it} = z_{it} \sum_{i \in \mathcal{V}} m_{it}$. The round reward ($\boldsymbol{r_t}$) is defined as the profit at each time step, i.e., the difference between the total revenue and cost (i.e., cost from order dispatching and rebalancing). The dynamics ($\boldsymbol{P}(\boldsymbol{s_{t+1}}|\boldsymbol{s_t}, \boldsymbol{a_t})$) describe the transition of the system state $\boldsymbol{s_t}$ in the current time step t to the state $\boldsymbol{s_{t+1}}$ in the next time step, given the rebalancing decisions. The attributes of the transportation network are directly obtained from real data. Passenger demand is assumed to follow a time-dependent Poisson process with the Poisson rate obtained from real data. The vehicle availability is updated every time step with vehicle conservation equations. The RL is based on advantage actor-critic (A2C), whereby the policy ($\pi_\theta(a_t|s_t)$), i.e., a mapping from a state to the probability of selecting an action, is defined as a Dirichlet distribution with a concentration parameter θ calculated from a graph neural network with the current state as input. The actor takes the current state as input and outputs the concentration parameter for the Dirichlet distribution. The critic takes the current state and action as input and outputs the estimation of the future state value ($V_{\pi_\theta}(s_t)$).

We improve the sample efficiency of the RL using a dynamic model-enhanced approach. Specifically, we train a dynamic model $\widehat{\boldsymbol{P}}(\boldsymbol{s_{t+1}}|\boldsymbol{s_t}, \boldsymbol{a_t})$ to approximate the dynamic process $\boldsymbol{P}$ in an online manner, i.e., to simulate the dynamics of the MoD system to enhance the RL agent. The dynamic model is leveraged to "imagine" the future transition states resulting from the current policy $\pi_\theta(a_t|s_t)$. It has been theoretically proved by Feinberg et al. (2018) that such a framework can provide a more accurate estimation of the future state value $V_{\pi_\theta}(s_t)$, and thus improve the sample efficiency of the proposed RL framework. Our dynamic model is based on graph neural networks to exploit the topology of transportation networks. Our dynamic model-enhanced RL includes a critic-enhanced module and an actor-enhanced module (see Figure 1). In the critic-enhanced module, the dynamic model is leveraged to generate multiple state transition paths to better estimate the future state value $V_{\pi_\theta}(s_t)$, which is further used to update the critic network. The actor-enhanced module uses the dynamic model to predict the distribution of HVs at the next time step, which is further incorporated into the actor to inform the potential response of HVs.

Moreover, we integrate our prior knowledge about the HV cruising behavior with the dynamic model in a physics-informed manner (Mo et al., 2021). The physics-informed dynamic model is implemented by incorporating the predictions made by HV behavioral models into the loss function in the training of the dynamic model. Examples of such HV behavioral models can include logit models with utility functions considering the revenue and cost of rebalancing to a region. The benefits of the physics-informed process include: (i) further improving sample efficiency using prior knowledge about HV cruising behavior and (ii) ensuring that the trained model is more physically meaningful, such as satisfying certain monotonicity conditions (e.g., higher demand will attract more HVs).

Finally, in order to align the prediction accuracy of HVs' distribution with the control objective of the RL framework, we employ the Wasserstein loss function (Goodfellow et al., 2014) in the training of the prediction model to mimic the rebalancing process. Inspired by the optimal transport theory, Wasserstein loss measures the minimum effort of changing one distribution to another, which is mathematically similar to the rebalancing problem.

Figure 127. Relationship between different models

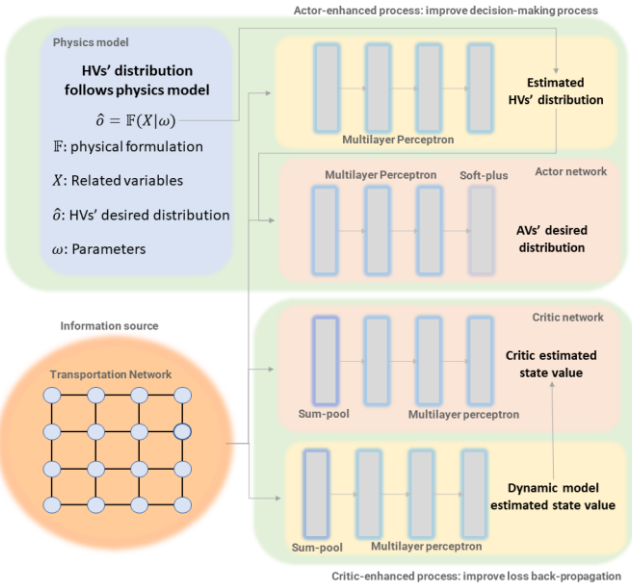

Results

The demand, travel time, and trip price are converted from the trip record data provided by the NYC Taxi and Limousine Commission (March 2013). Due to the space limit, we only demonstrate the results for scenarios with an AV penetration rate of 50%. The trend is similar for scenarios with other penetration rates.

Figure 128. Value of the proposed dynamic model-enhanced RL

a) value of the dynamic model

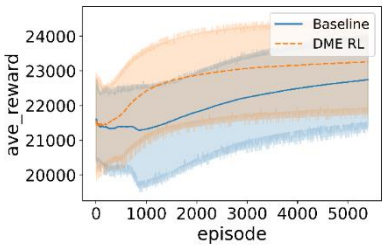

b) value of using Wasserstein loss

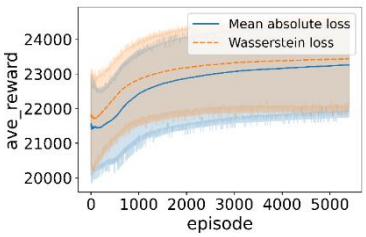

c) value of phyics-informed model

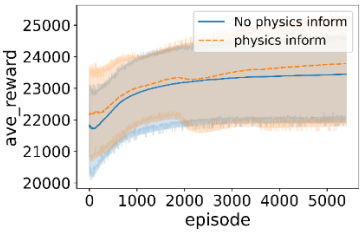

Figure 2a) shows the value of enhancing the RL agent with the dynamic model. The result suggests that the imaginary state transitions provided by the dynamic model can help the RL converge faster and gain a higher final average reward. Figure 2 b) validate the value of adopting Wasserstein loss instead of using other pointwise losses such as mean absolute loss. The results suggest that adopting Wasserstein loss can improve both data efficiency and control performance. Figure 2c) indicates the value of the physics-informed process in facilitating the convergence of the RL framework.

Figure 129. Sensitivity analysis

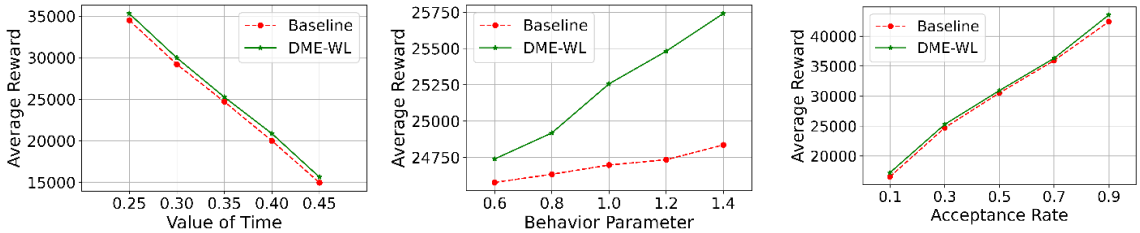

We further perform sensitivity analysis to important parameters used in the simulation. The sensitivity analysis results in Figure 3 confirm that our proposed framework performs well (i.e., outperforms the baseline RL model)

under different scenarios with various values of time, HV cruising patterns (i.e., behavior parameters), and HVs' passenger acceptance behavior (note that we allow HVs to decline passengers).

Conclusion

In this paper, we develop a dynamic model-enhanced RL for coordinating AVs in a mixed-fleet MoD system, which integrates the benefits of model-free RL and model-based RL. We build our work on an RL agent based on an A2C framework and enhance it by incorporating a dynamic model that simulates the dynamics of the MoD system. This dynamic model can predict future state transitions and the corresponding future state values, which are leveraged to enhance the training of both the actor and the critic. Moreover, we enhance the dynamic model by incorporating prior knowledge about HV cruising behavior to improve the sample efficiency and fidelity of the dynamic model. Finally, we leverage Wasserstein loss for training the dynamic model to align the prediction accuracy of future states and the RL objective. Simulations show that the proposed method can improve both the sample efficiency and the control performance.

This paper opens several directions for future work. First, the dynamic model-enhanced RL can be extended to integrate with other incentive-based strategies (i.e., dynamic pricing, carpooling, and subsidies) in mixed-fleet MoD systems. Second, it would be interesting to extend the proposed method to consider the interactions with public transport and competitive MoD systems would be interesting. Third, the proposed framework can be incorporated with the co-design framework for the joint optimization of mobility services, vehicle parameters, and infrastructure design.

Acknowledgment

We would like to acknowledge the support from the Singapore Ministry of Education under its Academic Research Fund Tier I.

Reference

Afeche, P., Liu, Z., Maglaras, C., Ride-hailing networks with strategic drivers: The impact of platform control capabilities on performance. *Rotman School of Management Working Paper*, 2018. 18–19.

Feinberg, V., Wan, A., Stoica, I., Jordan, M.I., Gonzalez, J.E., Levine, S.. Model-based value expansion for efficient model-free reinforcement learning*, in: Proceedings of the 35th International Conference on Machine Learning (ICML 2018)* , 2018.

Gammelli, D., Yang, K., Harrison, J., Rodrigues, F., Pereira, F.C., Pavone, M.. Graph neural network reinforcement learning for autonomous mobility-on-demand systems, *in: 2021 60th IEEE Conference on Decision and Control (CDC)* , IEEE, 2021, pp. 2996–3003.

Goodfellow, Ian, et al. "Advances in neural information processing systems." *Curran Associates, Inc*, 2014, 27: 2672-2680.

Mo, Z., Shi, R., Di, X., A physics-informed deep learning paradigm for car-following models. *Transportation research part C: emerging technologies,* 2021. 130, 103240.

Xie, J., Liu, Y., & Chen, N. Two-Sided Deep Reinforcement Learning for Dynamic Mobility-on-Demand Management with Mixed Autonomy. *Transportation Science*, 2023.

Yang, K., Tsao, M.W., Xu, X., Pavone, M., 2020. Planning and operations of mixed fleets in mobility-on-demand systems. arXiv preprint arXiv:2008.08131.

Zardini, G., Lanzetti, N., Censi, A., Frazzoli, E., & Pavone, M. (2022). Co-Design to Enable User-Friendly Tools to Assess the Impact of Future Mobility Solutions. *IEEE Transactions on Network Science and Engineering*, 2022.

Non-survey methodology to build a multi-regional input-output model

P. Delle Site[a], Q. Zhang[a],

[a] *Niccolò Cusano University, Rome, Italy*

Introduction

This paper deals with non-urban freight transport. The demand of freight transport is the inevitable result of economic activities. The Input-Output model (IO model) can capture the economic impacts of a sector's changes in the system, but it fails to investigate the inter-regional effects when the study area has economic interchanges with other areas. To overcome such shortage of the basic IO model, the Inter-regional Input-Output (IRIO) model and the Multi-Regional Input-Output (MRIO) model are often used to perform the analysis of inter-regional economy, tracing the relations between various economic sectors in different regions with a set of trade coefficients (Kim, 1974; Round, 1978; Hewings and Jensen, 1986; Cascetta, et al., 1996; Isard, et al., 1998; Oosterhaven and Stelder, 2007; Kanemoto and Murray, 2013).

Different from the IRIO model, the MRIO assumes that the supply of a generic product from one origin zone in the destination region is uniform to all consumption sectors, and the consumption sector is then ignored to simplify the model and reduce the data requirement. The concerned information that is used to estimate the trade coefficients usually comes from origin-to-destination commodity shipment information. The commodity shipment information and the data in the IO models should be uniform somehow (e.g. the categorisation of industries and products, the value unit, et cet.).

The regional IO tables and commodity shipment information are often not available. Due to the complexity of the freight transport sector, building the MRIO from disaggregated data via survey requires an important amount of resources and efforts. Therefore, we build the MRIO model on the basis of national IO tables and other statistical data. The Flegg's Location Quotients, and the Bi-proportional apportionment are used.

In the next section, building local IO tables and trade flows matrices using the data-driven methodology is reported. The subsequent section illustrates the expected results of the MRIO model in a case study related to the Decision Support System (DSS) under development for one regional government in Italy.

Methodology

The national IO table of "activity by activity" is the accounting of national economy; it tells the value of sectoral productions used by national business and consumers. These sectoral productions come from both national activities and foreign suppliers. For each national sector of activity, it uses these sectoral productions as input; the national supply of this activity is the sum of these intermediate uses, its tax and added value. Adding the value of imports, we get the total supply from this sector. On the other hand, for each sectoral production, the total use is equal to the sum of all intermediate uses by different national activities and final consumers, as well as the exports abroad. For each sector, the total supply is equal to the total use.

By subtracting the IO table of imported resources from that of all resources, we have obtained the IO table of national resources. Then the table of national and imported resources are proportioned to the regional level according to the statistical data of the population and the employment. The 4 constraints from the Regional Accounts (regional added value per sector, regional total expenditure of families, regional total expenditure of public administrations, and total regional gross fixed investment) are used to calibrate the proportioned data. The sum of regional uses of a sectoral production should equal the correspondent value in the national table. Then these regionally proportioned tables are brought down to the sub-regional level. They represent the value of sectoral productions with national and foreign origin used by local activities and consumers.

The Location Quotients (LQ) methods are among the most common "non-survey" tools to assess the degree of regional self-sufficiency. LQ methods consider the specialization of production in the region, the relative size of the activities and of the region (Round, 1978). The Flegg's Location Quotients (FLQ) is developed by Flegg et al., (1995) to overcome the shortcoming of the Cross-Industry Location Quotients (CILQ) of not taking into consideration the relative size of the study area, and the shortcoming of the Simple Location Quotients (SLQ) of not considering the relative size of the consumer sector, and it is reformulated by Flegg and Webber (1997):

$$q_{ms}^R = \begin{cases} 1, & FLQ_{ms}^R \geq 1 \\ FLQ_{ms}^R, & otherwise \end{cases}, \quad \lambda^* = \left[log_2\left(1 + {E^R}/{E^{IT}}\right)\right]^\delta$$

$$FLQ_{ms}^R = \begin{cases} \lambda^* \cdot \dfrac{E_m^R/E_m^{IT}}{E_s^R/E_s^{IT}}, & m \neq s \\ \lambda^* \cdot \dfrac{E_m^R/E_m^{IT}}{E^R/E^{IT}}, & m = s \end{cases}$$

where q_{ms}^R is the degree of self-sufficiency that indicates in the region *R* the share of the intermediate demand from sector *s* for the production of sector *m* satisfied by the local production. E_m^R, E_m^N, E^R, E^N are the employment of the sector *m*, and the total employment on the regional and national level, respectively.

The local IO tables show the local supplies and uses as well as the exchanges with other areas in terms of sectoral production value. Based on the international trade data from EUROSTAT, the import and export value in the national IO table are allocated to all other countries in the world. These data are used as the total value of every column and row in the matrix of national trade, international exports and international imports. The initial matrices are then generated using the bi-proportional apportionment method. This adjustment method is also known as iterative proportional fitting. Lahr and Mesnard (2004) provided an overview of this method and discussed its application in the field of economic research. There are two ways to build the initial matrix:

For the generic product *m,* the share of the origin region *O* 's export to the destination region *D* in the total import of the region *D* is equal to the ratio of the region *O* 's export to the total export from all regions except region *D*:

$$sc_m^{OD} = I_m^{DO} = I_m^D \cdot \frac{X_m^{O.reg}}{\sum_O X_m^{O.reg} - X_m^{D.reg}}, sc_m^{DD} = 0$$

For the generic product *m*, the share of the destination region *D* 's import from the origin region *O* in the total export of the region *O* is equal to the ratio of the region *D* 's import to the total import to all regions except region *O*:

$$sc_m^{OD} = X_m^{OD} = X_m^O \cdot \frac{I_m^{D.reg}}{\sum_D I_m^{D.reg} - I_m^{O.reg}}, sc_m^{OO} = 0$$

Then the deviations in the initial matrix are minimized by, alternatively, row scaling and column scaling iterations:

Row scaling: reduce/increase the value of each cell according to the ratio of the sum of all cells in the row to the corresponding value of "total export":

$${}^1sc_m^{OD} = {}^0sc_m^{OD} \cdot \frac{X_m^{O.reg}}{\sum_D {}^0sc_m^{OD}}$$

Column scaling: reduce/increase the value of each cell obtained in "row scaling" according to the ratio of the sum of all cells in the column to the corresponding value of "total import":

$${}^2sc_m^{OD} = {}^1sc_m^{OD} \cdot \frac{I_m^{D.reg}}{\sum_O {}^1sc_m^{OD}}$$

These OD flows are in terms of the sectoral production value. We assume that the technology of production is identical at both national and local level. Then, the national resource table of "products by activity" is taken as

reference to the composition of sectoral production. Once flows are converted into those in terms of product value, the COMEXT database is taken as price reference to convert the flows into those in terms of product weight. In this step, only principal material products are considered. The worldwide average FOB prices are used to convert the national flows, the country-specific FOB prices to convert international exports flows, the country-specific CIF prices to convert the international imports flows.

Finally, these flows of products can be converted into flows of freight types (dry bulk, liquid bulk, and other cargo), on the basis of the Sagmods model (Vierth, et al., 2017) and the correspondence between the transport statistics classification NST/R and the European classification for products CPA v2.1. Due to the different classification system, only the total value in the freight transport statistics by mode published by ISTAT are taken as constraints.

Results

The illustrative example is related to the freight mobility DSS under development for use of the government of the Lazio region in Italy. The zoning system is defined as: 378 municipalities in the Lazio region, 21 provinces in the Toscana, Umbria, Abruzzo, and Campania regions, 15 other Italian regions, 57 European and Mediterranean countries, and 11 supranational zones for the rest of the world.

The 414 local IO tables produced during the construction of MRIO model allow the analysis of local economy for each national study area. The MRIO model produces the production-consumption (P/C) flows between any pair of Italian study areas, or between one Italian and one foreign area. As output, there are 4 types of matrices:

- Matrices of trade flows in terms of either sectoral production value or product value: 63 national flows matrices with the dimension of 414*414, 29 exports matrices with the dimension of 414*68, 29 imports matrices with the dimension of 68*414.
- Matrices of trade flows in terms of product weight: 21 national flows matrices with the dimension of 414*414, 29 exports matrices with the dimension of 414*68, 29 imports matrices with dimension of 68*414.
- Matrices of freight flows in terms of weight: 3 national flows matrices, 3 exports matrices and 3 imports matrices.

Conclusions

Using the MRIO model to provide P/C flows is the prerequisite for the implementation of the DSS, but building the MRIO using disaggregated data is extremely resource consuming. The paper has provided a methodology to build the MRIO model using national IO tables and statistical data of population, employment, regional accounts, and international trade.

References

Cascetta, E., Di Gangi, M., Conigliaro, G., A multi-regional input-output model with elastic trade coefficients for the simulation of freight transport demand in Italy, Association for European Transport, 1996.

Eurostat, Easy Comext, accessible at: http://epp.eurostat.ec.europa.eu/newxtweb/mainxtnet.do.

Flegg, A. T., Webber, D., On the appropriate use of location quotients in generating regional input-output tables: Reply. In: Regional Studies, 31, 1997, pp. 795-805.

Flegg, A. T., Webber, C. D., Elliott, M. V., On the appropriate use of location quotients in generating regional input-output tables. In: Regional Studies, 29(6), 1995, pp.547-561.

Hewings, G. J., Jensen, R. C., Regional, Interregional and Multiregional Input-Output Analysis, edited by P. Nijkamp, Handbook of Regional and Urban Economics (Vol. I, pp. 295-355). Elsevier Science Publishers BV, 1986.

Isard, W., Drennan, Drennan, M. P., Miller, R. E., Saltzman, S., Thorbecke, E., Methods of Interregional and Regional Analysis, Ashgate, 1998.

ISTAT, Il Sistema di Tavole Input-Output - Anni 2015-2018, Roma, 2021, accessible at: https://www.istat.it/it/archivio/264985.

ISTAT, Trasporto Marittimo, accessible at: https://dati.istat.it/Index.aspx?DataSetCode=DCSC_TRAMAR#.

ISTAT, Trasporto merci su strada, accessible at: http://dati.istat.it/Index.aspx?DataSetCode=DCSC_TRAMERCIS1#.

Kim, U., Evaluation of Interregional Input-Output Model For Potential Use in the McCLELLAN-Kerr Arkansas River Multiple Purpose Project Impact Study, The Catholic University of America, Institute of Social and Behavioral Research. Washington, D.C.: National Technical Information Service, U.S. Department of Commerce, 1974.

Lahr, M. L., & Mesnard, L. D., Biproportional Techniques in Input-Output Analysis: Table Updating and Structural Analysis. In: Economic Systems Research, vol. 16, No. 2, 2004, pp. 115-134. doi:10.1080/0953531042000219259.

Kanemoto, K., Murray, J., What is MRIO: Benefits and Limitations. In: The Sustainability Practitioner's Guide to Multi-Regional Input-Output Analysis, edited by Lenzen, M., Murray, J., Common Ground Publishing LLC, Champaign, Illinois, USA, 2013.

Oosterhaven, J., Stelder, D., Regional and Interregional IO Analysis. Faculty of Economics and Business, University of Groningen, Groningen, 2007. Accessed in June 2014 at: http://www.regroningen.nl/irios/doc/Regional%20IO%20Analysis.pdf.

Round, J. I., An interregional input-output approach to the evaluation of nonsurvey methods, Journal of Regional Science (18), 179-94, 1978.

Vierth, I., Lindgren, S., Jong, G. d., Baak, J., Hovi, I. B., Berglund, M., Edwards, H., Recommendation for a new commodity classification for the national freight model Samgods, Centre for Transport Studies, Stockholm, 2017.

An advanced hybrid traffic flow model for mixed traffic flow

R. Di Pace[a], F. Storani[a], R. Jiang[b], S. de Luca[a]

a Department of Civil Engineering, University of Salerno, Fisciano (Salerno) 84084, Italy

b Laboratory of Transport Industry of Big Data Application Technologies for Comprehensive Transport, Ministry of Transport, Beijing Jiaotong, University, Beijing 100044, China

This paper proposes an enhanced traffic flow model that can support the presence of human-driven and connected vehicles in a mixed traffic flow condition. It is based on the hybrid model H – CA&CTM; Hybrid Cellular Automata Cell Transmission Model of Storani et al. (2022), which combines the meso-microscopic Cellular Automata model (CA; Nagel and Schreckenberg, 1992) and the macroscopic Cell Transmission Model (CTM; Daganzo, 1994). The whole model can represent: i) the Human-driven vehicles mode, ii) the Adaptive cruise control mode, and iii) the Cooperative adaptive cruise control mode. In more detail: the considered CTM was adapted from Yao et al. (2022), while the CA model was adapted from Jiang et al. (2021). The model was tested on a ring-shaped arc.

Autonomous driver identification using vehicle trajectory data

M. A. Makridis[a], A. L. Marin[b],1, G. Fontaras[c], MJ Ramírez-Quintana[c], A. Kouvelas[a]

[a] *Institute for Transport Planning and Systems, Department of Civil, Environmental and Geomatic, Engineering, ETH Zürich, 8032, Switzerland*

[b] *VRAIN, Universitat Politècnica de València, València 46002, Spain*

[c] *European Commission – Joint Research Centre, Ispra, 2749, Italy*

Prominent behavioural differences exist between human-driven vehicles (HDs) and automated-driven ones (ADs). The complexity of road traffic dynamics is primarily attributed to the heterogeneity of individual driver characteristics. Therefore, driver-type identification presents enormous potential in traffic monitoring, management and control, safety, driver understanding, and energy efficiency. We propose a methodological framework that uses a sophisticated behavioural feature design and deep learning to identify the driver type (i.e., HD or AD) from raw trajectory observations. The implemented empirical mode decomposition-based design drastically increases the efficiency of any employed deep learning architecture. The employed bidirectional long short-term memory (bLSTM) architecture outperforms other solutions in the limited literature. Finally, we demonstrate for the first time the ability of such an approach to generalize on unseen data through concept drift. The results demonstrate the robustness of the proposed approach.

Category 13. Freight transport

Maximum likelihood estimation of freight transport modal chain choice logit models from aggregate secondary data

P. Delle Site[a], L. Persia[b], Q. Zhang[a]

[a] *Niccolò Cusano University, Rome, Italy*

[b] *Sapienza University, Rome, Italy*

Introduction

We deal with non-urban freight transport. The simulation of the modal chain choice is an essential component of any decision support system (DSS). A survey of models and data used for estimation is found in de Jong (2014). Flows by modal chain in base year for the origin-destination (od) pairs of the adopted zoning are needed to assign demand to the multi-modal network. Assignment provides tonne-km, vehicle-km and vehicle-hour travelled, with the associated environmental, safety and economic impacts. At the same time, these flows are needed for forecasting aims, in cases where they are used in combination with an incremental logit model (see: Ortúzar and Willumsen, 2011, for multinomial logit; Bates et al., 1987, for nested logit) to provide flows in future scenarios. This is because the incremental form of logit models pivots from the base-year modal chain shares, while using only the terms in the utility functions that are subject to change.

Most often, od freight flows by modal chain are not available in base year. Clearly, they cannot be obtained using models available from other studies, because alternative-specific constants are not transferable. Therefore, there is a need to provide estimates using secondary data and models. In the paper, we refer to data as secondary when they result from spatial aggregations of od flows. Logit models, either multinomial or nested, are used.

In the next section, we report on the methodology that is proposed to estimate base-year od flows by modal chain from secondary data. In the subsequent section, we present results in a case study related to the freight transport DSS that is being developed for one regional government in Italy.

Methodology

Assume neither disaggregate nor aggregate data at the level of the od pairs of the adopted zoning are available. Data available relate to traffic in tonnes for distinct modal chains between selected geographic areas or in selected nodes. Examples of traffic in nodes include the number of tonnes per year arriving by ship to a port, or the number of tonnes per year leaving by train in container or swap bodies from a road-rail terminal. It is possible to treat traffic in a node as aggregation of od flows, if a preliminary all-or-nothing assignment of the od flows to the nearest node of the modal chain is performed. Assume the modal chain choice is modelled using either a multinomial or a nested logit.

The methodology in the sequel applies to any segmentation of demand. Transtools, the decision support system developed within the Framework Programmes of the European Commission (Jensen et al., 2019), uses three distinct chain choice models according to load type: solid bulk, liquid bulk and other. The other type includes container and general cargo.

The expected value of the od flow in tonnes on the modal chain alternative i is:

$$X_{odi} = X_{od} P_{odi},$$

where X_{od} is the total, known, od flow and P_{odi} the logit probability that a shipment on the od pair uses the modal chain alternative. For simplicity, the demand segment index is omitted. The utilities of the modal chain alternatives, which contribute to the logit probabilities P_{odi}, depend linearly on the travel time and monetary cost evaluated for the od pair and alternative.

The coefficients in the expressions of the utilities, namely the coefficients of travel time and monetary cost and the alternative specific constants, are estimated using maximum likelihood. The likelihood function is constructed as follows.

Let h denote the index of the traffic statistic available. Take the example of the traffic arriving by ship to a port. Every tonne has a probability $\hat{P}_h$ of being counted in the traffic statistic. In the example, probability $\hat{P}_h$ is the total probability of the events consisting in the arrival of a tonne from one of the od pairs that use the port. Therefore, we can write:

$$\hat{P}_h = \sum_{o,d,i} a_{odih} \frac{X_{od}}{\sum_{od} b_{odh} X_{od}} P_{odi},$$

where:

a_{odih} is 1 if the od pair and modal chain alternative is relevant to traffic statistic h, it is 0 otherwise,

b_{odh} is 1 if the od pair is relevant to traffic statistic h, it is 0 otherwise.

The log-likelihood function is:

$$\log L = \sum_h \left[A_h \log \hat{P}_h + B_h \log\left(1 - \hat{P}_h\right) \right],$$

$$B_h = \sum_{od} b_{odh} X_{od} - A_h,$$

where A_h is the traffic in tonnes of statistic h. The log-likelihood function takes into account that, for each traffic statistic h, there are A_h tonnes using a subset of modal chain alternatives, there are B_h tonnes using the remaining alternatives.

Maximum likelihood estimators are obtained by unconstrained maximization of the log-likelihood. Since there is no evidence of concavity, a global optimization approach is needed because of the possibility of local maxima. The typical heuristic that is used includes two steps. First, a candidate hyper-rectangle in the space of the coefficients is explored. Second, the best point found by the exploration step is used as starting point of the local search algorithm. For the exploration step, a recently proposed technique is the one based on the Lissajous curve (Ziadi et al., 2020). This provides a more uniform exploration of the candidate region compared with a purely random strategy. For the local search step, the classical, derivative-free, Nelder-Mead algorithm is used (Nocedal and Wright, 2000).

Maximum likelihood estimators are, for large samples, normally distributed with covariance matrix (Newey and McFadden 1994):

$$COV = \frac{\Im^{-1}}{N} = \frac{1}{N} \left(\nabla_{\boldsymbol{\beta}\boldsymbol{\beta}} \log L \right)^{-1},$$

where $\Im$ is the Fisher information matrix (the covariance matrix of scores), N is the total number of observations of the available traffic statistics, $\boldsymbol{\beta}$ is the vector of coefficients, $\nabla_{\boldsymbol{\beta}\boldsymbol{\beta}} \log L$ is the Hessian matrix of the log-likelihood function. All matrices are evaluated at the maximum likelihood point. Tests of hypotheses about true values of the coefficients are performed using the t-statistic associated with each coefficient. The application is, however, problematic. This is because the number N of observations associated with the available traffic statistics is not determined. This is different from aggregate estimation of passenger mode choice models where the observation unit is, clearly, the individual passenger.

Results

The illustrative example relates to the freight transport DSS which is being developed for use of one regional government in Italy. In Italy there are 20 regions. The region considered is Lazio, which includes the Rome metropolitan city. To the aim of simulating the internal, outbound, inbound and crossing flows of the region, zoning extends to the global dimension. Internally, each zone is a municipality. Externally, the size of the zones increases with distance from Lazio. The total number of zones is 482, of which 378 are internal zones.

The DSS includes a production/consumption (P/C) flow model, a multi-modal network model, a modal chain choice model, and a traffic assignment model. The P/C flow model is a Multi-Regional Input-Output (MRIO) model. MRIO provides P/C flows in tonnes/year. The multi-modal network model provides the od travel times (in time units per shipment) and the od monetary costs (in EUR/tonne).

There are three modal chain choice models, one for each load type, as in Transtools. The alternatives are shown in Figure 1. For the other goods load type, the model provides the shares of container and RoRo traffic. Systematic utilities of the alternatives includes travel time, monetary cost and an alternative specific constant. Coefficients of travel time and monetary cost are common across alternatives.

Inputs for estimation include the od flows provided by the MRIO model, the matrices of od travel times and monetary costs provided by the multi-modal network model, and a selection of available traffic statistics. Traffic statistics include flows using road between Lazio and other Italian regions, traffic at ports of Lazio, container

traffic at the main regional road-rail terminal. All inputs refer to 2018 base year. Lack of additional data on rail traffic in tonnes/year required a few ad-hoc assumptions.

According to results of the estimation of multinomial logit models, both coefficients of travel time and monetary cost have the correct sign. Thus, the estimated models can be used for forecasting aims, with no need to use the Transtools models. Application to a sample of od pairs has provided realistic shares.

Figure 130. Choice trees

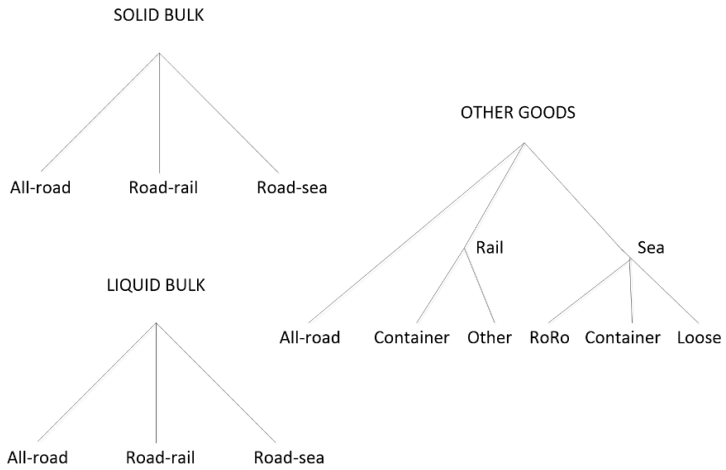

Conclusions

Providing estimates of the od flows by modal chain is key to application of the DSS to both base and future years. Od flows by modal chain need to be assigned to the multi-modal network to provide estimates of traffic indicators, such as vehicle-hour and vehicle-km, that enable impact assessment in the base year. For future years, base year flows by modal chain are needed to enable the use of logit models in incremental form. Data available most frequently for the base year do not provide modal flows at the spatial level of the adopted zoning. The paper has provided a methodology for their estimation based on secondary data. A comment is in order. The accuracy of the estimates is affected by the input data that are used. This calls, in turn, for accuracy of the outputs provided by trade flow and network models. Availability of rail traffic statistics with the proper units (tonnes/year) is a criticality.

References

Bates, J.J., Ashley, D.J., Hyman, G., The nested incremental logit model: theory and application to modal choice. *Proceedings of the 15th PTRC Summer Annual Meeting*, University of Bath, UK, September 1987.

de Jong, G., Mode choice models. In: *Modelling Freight Transport*, edited by L. Tavasszy and G. de Jong, Elsevier, Amsterdam, 2014, pp. 117-141.

Jensen, A.F., Thorhauge, M., de Jong, G., Rich, J., Dekker, T., Johnson, D., Ojeda Cabral, M., Bates, J., Nielsen, O.A., A disaggregate freight transport chain choice model for Europe, *Transportation Research Part E: Logistics and Transportation Review*, Vol. 121, 2019, pp.43-62.

Newey, W.K., McFadden, D., Large sample estimation and hypothesis testing. Chapter 36 in*: Handbook of Econometrics - Volume 4*, edited by R.F. Engle and D. McFadden, Elsevier, Amsterdam, 1994, pp. 2111-2244.

Nocedal, J., Wright, S., *Numerical Optimization*, Springer-Verlag, New York, 2000.

Ortúzar, J. d. D., Willumsen, L., *Modelling Transport*, Wiley, Hoboken NJ, 2011.

Ziadi, R., Bencherif-Madani A., Ellaia R., A deterministic method for continuous global optimization using a dense curve, *Mathematics and Computers in Simulation*, Vol. 178, 2020, pp. 62-91.

Privacy-preserving Coordination for Cross-carrier Truck Platooning

H. Blache [a], P. Laharotte [a], N. El Faouzi [a]

[a] *Univ. Gustave Eiffel, Univ. Lyon, ENTPE, LICIT-ECO7 UMR T9401,F-69675, Lyon (France)*

Introduction

The implementation of Automated and Connected Vehicle systems on the road while ensuring its safety is now a major challenge in the transportation field. Nevertheless, depending on the strategies adopted, their deployment can take a considerable amount of time [1], which challenges their rapid implementation. Thus, the reduction of the number of testing scenarios is one of the major issues today in the context of certification and validation for new intelligent transport systems. Multiple approaches were developed to design testing process for CAV. While the *distance-based* approach [2] remains naive and inefficient, a competitive approach raised in the literature is the scenarios-based approach[cite]. The *distance-based* approach consists in driving a vehicle on the road until the validation is reached, i.e., a sufficient variety of situations is met by the vehicle under test. In contrast, the scenarios-based approaches develop methodologies to directly guide the vehicle toward relevant scenarios. Nowadays, it should be noted that some exploratory work has been done to identify and/or reduce the scenarios [3-4]. However, to the best of our knowledge, there is no procedure in the current literature to analyse and drastically reduce a multitude of scenarios in order to evaluate them. The objective is therefore to identify, group and reduce the scenarios to be tested. The innovative approach proposes simultaneously to reduce the abstract layer of scenarios (**functional scenarios**) to be tested and analyse them a priori in order to propose experience plans exhaustively covering the scope of possibilities.

Methodology

The overall methodology is summarized in Fig.1 and broken down into 6 steps:

1. **Step 1 - Generation of functional scenarios by an ontology:** it concerns the process of defining an ontology and the exhaustive set of functional scenarios using this ontology.
2. **Step 2 - Criticality qualification of a subset of Functional Scenarios:** it focuses on the data processing that will assign a criticality distribution to the functional scenarios, then a critical index.
3. **Step 3 - Extraction of underlying and latent relationship between ontology attributes and criticality index of functional scenarios:** based on the Latent Dirichlet Allocation (LDA) [5] clustering process, some underlying topics and clusters are generated and enable to associate criticality index degree to ontology attributes generating functional scenarios.
4. **Step 4 - Generalisation of the underlying features to qualify any functional scenario:** based on a partial least square method, the reconstruction process takes advantage of the formulation of the underlying topics resulting from LDA to predict *a priori* the criticality of any new functional scenario.
5. **Step 5 - Clustering of scenarios between semantic and criticality terms:** based on hierarchical ascendant classification (HAC), the functional scenarios are classified based on the difference between the Euclidean distance of the words versus the a priori criticality difference of the scenarios. For each scenario i and scenario j, the distance equal to:

$$Dist(i,k) = \frac{Dist_{word}\ (i,k)}{Diff_{criticity}(i,k)}$$

   where $Dist_{word}(i,k)$ is the Euclidean distance of the scenario binary vector i and j, and $Diff_{criticity}(i,k)$ is the difference in criticality between scenario i and j.

6. **Step 6 - Reduction of the number of functional scenarios in each cluster:** Selection of representative scenarios for each group in terms of scenario criticality and word representation.

Figure 131. Methodology of reduction of scenarios in 6 steps

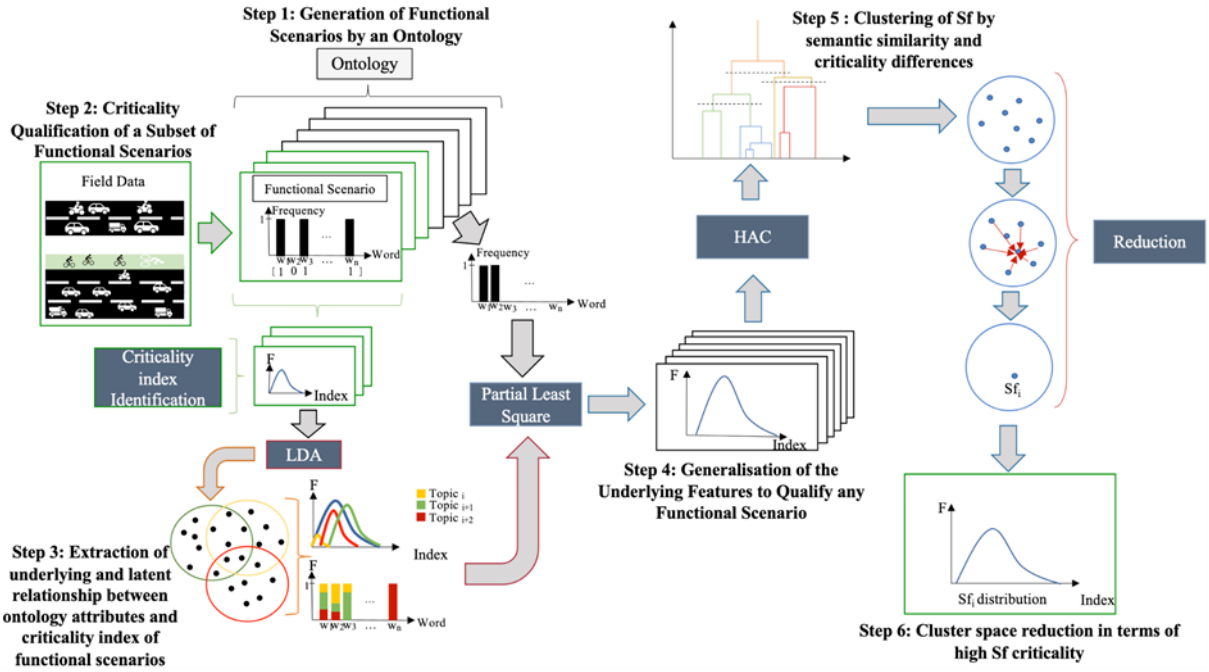

Results

Representation of a functional scenario

Fig.2 shows an example of a scenario generated with the ontology. This ontology generates a scenario in 5 layers (all independent). Layer 5 represents the weather, Layer 4 represents the dynamic and static objects, Layer 3 represents the temporal changes (e.g., road works), Layer 2 represents the road infrastructure and Layer 1 represents the road topology. In addition, the vehicle objective is added to the scenarios that sets up its starting point of arrival and its ending point.

Figure 132. 5-layer representation of functional scenario

Layer 5	- Illuminance: Day - Sky Condition: Sunny - Particule Matter: No Particule	- Temperature: Medium - Weather Disturbances: No Disturbances	
Layer 4	- Dynamique element crossing: No Dynamique element crossing	- Vehicule: Car, Commercial Vehicle - Volume of Traffic: Medium	- Statics: No Static Elements
Layer 3	- Temporary Problem: No Temporary Problem		
Layer 2	- Lights Signage: No Light Signage - Signs: NoSigns		
Layer 1	- RoundAbout: No RoundAbout - Junction: Simple Junction	- Road 1: 3 Lane Right Direction, Straight, Plane, Dry, Uniform, Traffic Lane	- Road 2: 3 Lane Right Direction, Straight, Plane, Dry, Uniform, Traffic Lane

Latent Dirichlet Allocation Results

The results of the LDA can be seen in Fig.3. According to the elbow method, we find an optimal number of topics equal to 5 (for 36 scenarios). Each topic can be interpreted as the distribution of a "typical" functional scenario with its own criticality index. For example, a very critical "Sf" and a less critical one. Another convincing result is the distribution of topics in each Sf, this is interpreted by the contribution of a more or less critical topic in each Sf.

Figure 133. Latent Dirichlet Allocation results:(a) topic distribution (b) topics distribution in each functional scenario

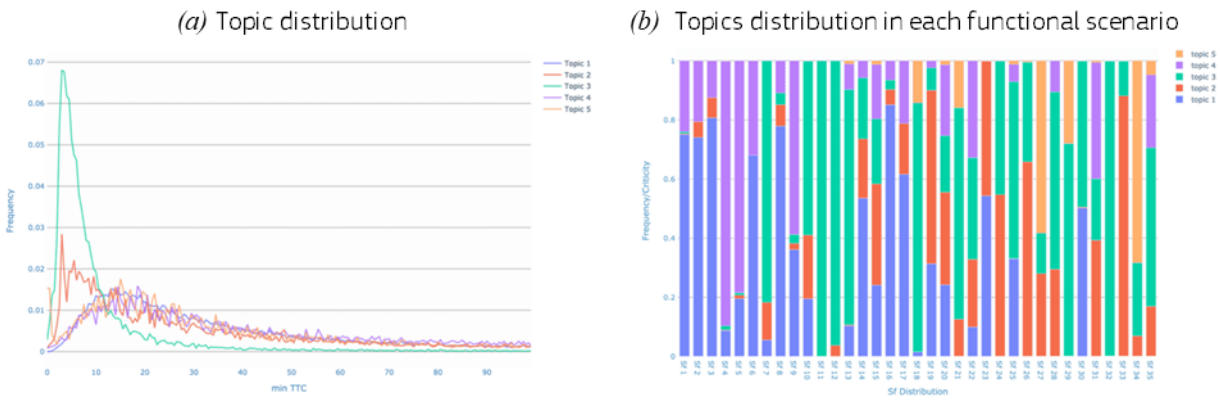

Partial Least Mean Square Results (Reconstruction)

Fig 4 illustrates the gap between a priori estimated criticality indices and observed values drawn from field test data. We compared our model with two other methods, a classical KNN method and a least squares method. In addition, Table I shows the different performance indices. First, using the R2, we notice that the two least squares methods perform better than the KNN method. However, the classical least squares method underestimates the high criticality index scenarios contrary to our model.

Figure 134. Comparison of the reconstructed criticality with the real indices of 3 methods (LDA + Partial Square in red, LDA + Least Square in blue, KNN in green)

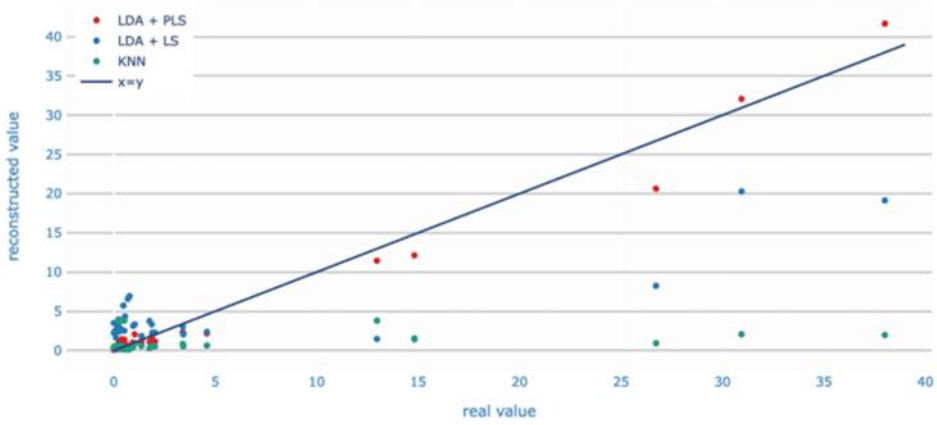

Table 25. Performance index of the reconstruction

Index	LDA+PLS	KNN	LDA+LS
RMSE	1,47	9,34	6,15
Max Error	6,09	36,02	18,86
R2	0,97	0,08	0,53

Clustering and reduction of functional scenario

Fig.5 shows the results of our strategy to select the most critical scenario. This method is compared with two other methods: random drawing of the same number of scenarios and drawing of the most critical scenarios corresponding to the same number of scenarios drawn in our method. We can see that even though the maximum tragedy allows us to cover a little more overall criticality, our method enables better coverage of all the words of our scenarios, i.e., the scope of possibilities.

Figure 135. Result of clustering and reduction

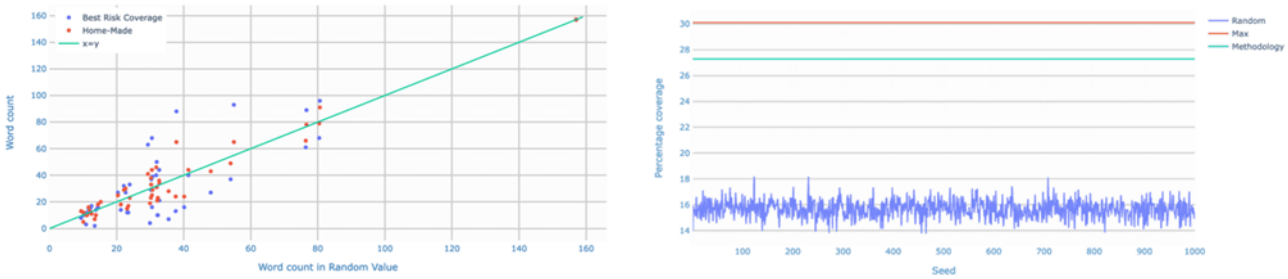

Conclusion

This new reduction methodology has potential in several ways. First, unlike many functional scenario generations, the emphasis is on the stochastic aspect of the words to be more in line with the philosophies of the simulation tools (e.g., the travel demand profile). The a priori generation of new functional scenarios difficult to observe in the field does not emerge in the literature despite its potential. The choice of reducing the most critical scenario of a group seems relevant in view of the diversity of the scenario but also of its potential hazard, compared to other approaches.

Nevertheless, this approach has some limitations, such as the number of data processed in the field and also the actual profile of the "artificially" generated scenarios and the over (or under) estimation of criticality for some scenarios. The next steps will be to process more data to strengthen findings and eventually identify replication abilities in simulations for the validation of CAV systems.

References

[1] N. Kalra and S. M. Paddock, “Driving to safety: How many miles of driving would it take to demonstrate autonomous vehicle reliability?” Transportation Research Part A: Policy and Practice, vol. 94, pp. 182–193, Dec. 2016. [Online]. Available: https://www.sciencedirect.com/science/article/pii/S0965856416302129.

[2] S. Riedmaier, T. Ponn, D. Ludwig, B. Schick, and F. Diermeyer, “Survey on Scenario-Based Safety Assessment of Automated Vehicles,” IEEE Access, vol. 8, pp. 87 456–87 477, 2020, conference Name: IEEE Access.

[3] L. Vater, A. Putz, L. Tellis, and L. Eckstein, “Test Case Selection Method for the Verification of Automated Driving Systems,” ATZelectronics worldwide , vol. 16, no. 11, pp. 40–45, Nov. 2021. [Online]. Available: https://doi.org/10.1007/s38314-021-0701-0.

[4] S. Riedmaier, D. Schneider, D. Watzenig, F. Diermeyer, and B. Schick, “Model Validation and Scenario Selection for Virtual-Base Homologation of Automated Vehicles,” Applied Sciences, vol. 11, no. 1, p. 35, Jan. 2021, number: 1 Publisher: Multidisciplinary Digital Publishing Institute. [Online]. Available: https://www.mdpi.com/2076-3417/11/1/35.

[5] D. M. Blei, A. Y. Ng, and M. I. Jordan, “Latent dirichlet allocation,” Journal of machine Learning research, vol. 3, no. Jan, pp. 993–1022, 2003.

Optimal modal shares for freight transport in Sweden

S. Ollila[ab], M. Börjesson[ab]

[a] *VTI*

[b] *Linköping University*

This paper estimates welfare optimal modal shares of freight transport in Sweden. Transport demand is derived from a multinominal logit model accounting for a simultaneous choice of transport mode and shipment size. We estimate modal shares given internalized external costs and study impact of internalization on transport costs, external costs and governmental revenues. Internalization shifts freight from rail to road and waterborne transport. However, the average changes in modal shares across origin-destination pairs are minor.

Category 14. Safety

Zoning cities for relief transport in disaster management

S.A Bagloee[a], M. Sarvi[a]

[a] *The University of Melbourne, Victoria 3010, Australia*

Introduction

In recent decades, the number and magnitude of disasters have grown significantly (Wang et al., 2018, Hsieh and Feng, 2020). In the aftermath of a disaster, the first and foremost action is to deploy search and rescue (SaR) teams and aids to disaster-hit areas which could be a mammoth logistical task (Holguín-Veras et al., 2014). Hence road network restoration in early hours is of highest importance which requires a proper damage assessment of the road infrastructure (Özdamar and Ertem, 2015). With today's technology, satellite images and remote sensing can assist authorities in their operational planning and decision making (Sakuraba et al., 2016). Hence, in early hours data is available, the question is how to allocate road restoration operations to various aid centers. To this end the literature lacks some vivid gaps: (i) methods that deal with large-scale disasters are not readily available, (ii) models' computational burdens might prevent them from being used in actual disasters, (iii) from practical and academic perspectives, real-time algorithms (fast algorithms) designed for optimal resource allocation and operation planning are in high demand (Özdamar and Ertem, 2015).

To address these shortcomings, we, in this study, develop a decision support system for zoning a city on a real-time basis after a disaster hits which is two folds: what is the capability of each aid center after initial assessment and which roads must be cleaned up first to provide access to the aid centers.

To this end, we formulate these two questions integrated as a single mixed integer problem (MIP) which is solved analytically (i.e. exact solutions not heuristic).

Literature review

An exhaustive review of the literature on humanitarian operations in disaster relief operations, as well as modeling approaches, can be found in (Kovács et al., 2017, Kovács and Spens, 2007, McCoy, 2008, Manopiniwes and Irohara, 2014).

Duque et al. (2016) investigate roads restoration after a disaster by minimizing the time to get to rural towns aiming. Yan et al. (2014) study emergency repair problems under large-scale supply-demand perturbations. Fiondella (2013) examines the vulnerability of a transportation network in the wake of emergency response. Yan et al. (2012) present a task support scheduling model for a given emergency repair task. Liberatore et al. (2014) address the problem of planning for recovery of damaged elements of a road network as a multi-criteria formulation. Aksu and Ozdamar (2014) maximize network accessibility for all locations in a target zone during the restoration operations. Sakuraba et al. (2016) address the road network accessibility and the worktroops scheduling problems. Kasaei and Salman (2016) investigate clearing blocked roads by minimizing the time to reconnect the road network.

To the best of our knowledge, partitioning cities based on the aid centers' operations right after a disaster has not been explicitly addressed in the literature (we call it real-time or online zoning).

Mathematical formulation

We formulate the OZP as a network flow problem that is to send one unit of commodity from a dummy origin to each destination such that total traversed time is minimized. All the notations used in the formulation of the OZP is introduced in Table 1. The OZP can be written as follows:

$$\text{OZP: } \underset{x_{ij},y_{ij},B}{Minimize} Z(x_{ij},y_{ij}) = \sum_{(i,j)\in A\cup A'} x_{ij}.t_{ij} + B, \quad (1)$$

$$\text{s.t.} \qquad \sum_{(i,j)\in A'} c_{ij}.y_{ij} \le B \qquad (2)$$

$$y_{ij} = \{0,1\} \qquad (i,j) \in A' \qquad (3)$$

$$\sum_j x_{kj} - \sum_j x_{ik} = \begin{cases} -1 & k \in D \\ |D| & k = o \\ 0 & o.w. \end{cases} \qquad (4)$$

$$x_{ij} \leq M.y_{ij}(i,j) \in A' \qquad (5)$$

$$B \leq \bar{B} \quad (6)$$

$$x_{ij} \geq 0, (i,j) \in A \cup A'. \quad (7)$$

The first term of Equation (1) is to minimize the total traverse time (from the origin to the destinations). The second term of the objective function is to find the most optimal budget value. Note that, since it is a minimization problem and the dummy links from the origin to destinations are labeled with a high traverse time, minimization of the total traverse time is equivalent to restoration of the network from the aid centers to the destinations. Constraints (2) and (3) ensures feasibility of the solutions with respect to the costs and the budget. Constraint (4) ensures flow conservation at each node of the network. Constraint (5) ensures that a damaged road (i,j)∈A∪A^'or the only access road of an aid center j is open (i.e., x_ij≥0), if and only if, the corresponding binary decision variable is set to be y_ij=1, otherwise (y_ij=0), the damaged (access) road is closed (x_ij≤M.0=0). Note that Mis a sufficiently large value. Constraint (6) imposes an upper bound to the optimal value of the budget (note that B¯is the maximum available budget). By releasing the budget's upper bound to infinity, the OZP can then provide the optimal value for the budget which has valuable practical implications.

Table 26 Notation used for the shelter location problem

Symbol	Description
A	Set of undamaged roads including the dummy directional links.
$A^{'}$	Set of damaged roads as well as the access roads representing the aid centers. For the latter, $(i,j) \in A^{'}$, the end node denotes the location of the respective aid center.
c_{ij}	The restoration cost of the road $(i,j) \in A^{'}$, if it is a damaged road the cost includes expense related to the debris clean up, repairment and construction. If it is an access road to an aid center the cost includes expenses related to the equipment and procurement etc.
B	A limited budget.
$\bar{B}$	An upper bound to budget, or the maximum available budget.
y_{ij}	Binary decision variables pertaining to $(i,j) \in A^{'}$. If it is assigned the value of $y_{ij} = 1$, the respective link is open and operational, otherwise ($y_{ij} = 0$) it is closed.
x_{ij}	A continuous variable denoting traffic flow on the directional roads $(i,j) \in A \cup A^{'}$.
t_{ij}	Traverse time (or delay) of the road$(i,j) \in A \cup A^{'}$
D	Set of destinations,
o	The dummy origin simply called the origin.
$\|D\|$	The cardinality of the set of destinations which is the total number of the SaR teams to dispatch from the origin
Z	Total traverse time (the objective function)

Numerical tests

The methodology algorithm is coded with Python linked to MS-Excel as a user interface and calls MATLAB and GAMS/CPLEX to solve the MINLP, we set a very fine convergence gap (i.e., 0.001%) to arrive at an exact and precise solution.

The case-study of Melbourne is tested to demonstrate computational efficiency of the proposed methodology when addressing real-life problems. We consider 40 candidate aid centers scattered all around the city. The

Melbourne's road network consists of 510 nodes and 2100 directional roads which account for all the main roads (excluding the local roads). The city has been divided into 199 main zones to be served by aid centers. Figure 1 shows the Melbourne's network and the locations of the candidate aid centers.

Figure 136. A zoning map, decomposition of the city based on the aid centers

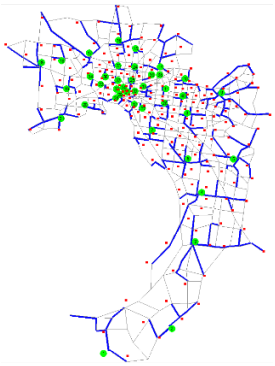

Optimal budget

We solve the OZP as stated in formulation (1) to (7) resulting in selection of 37 aid centers out of 40, restoration of 307 roads out of 1622 which accounts for total budget of 344 (i.e., 344 = 37*2 + 307*1) and total traverse time of 1472.98 (hence, value of the objective function is 1816.98 = 1472.98 + 344). Figure 1 exhibits locations of the selected aid centers as well as the roads to be restored in the context of the destinations. As can be seen, the city (roads and destinations) has been decomposed based on the coverage area of the aid centers, which are the mission areas assigned to the respective aid centers. Moreover, the total number of households or other land uses falling into the coverage area of an aid center can be considered as the capacity of the respective aid center. That is to inform decision-makers and authorities of how much supply, relief materials and rescue team must be provided to each aid center.

Minimum budget, minimum connectivity

In the above solution, the budget of 344 is optimal. Nevertheless, for practical purposes, it is also important to know the minimum budget, such that for every destination there exist at least an access route to an aid center? This results in a least-cost zoning map. An intuitive way is to conduct a sensitivity analysis on various values of the budget as shown in Table 2.

Table 27. Melbourne case study, sensitivity analysis on the value of the budget

Budget	Objective function	Number of aid centers	Number of links	traverse time
344	1816.98	37	270	1472.98
340	1819.25	36	268	1479.25
330	1825.63	35	260	1495.63
320	1839.68	32	256	1519.68
310	1872.16	31	248	1562.16
300	1943.74	25	250	1643.74
290	2111.92	20	250	1821.92
280	2409.18	15	250	2129.18
271	5886.50*	6	259	5627.50

Conclusion

In this study, we addressed online zoning of a city immediately after a disaster based on the operation of aid centers for real-life examples. In the meantime, restoration of transport connectivity from aid center to the disaster-hit areas is also sought. The online zoning problem (OZP), was formulated as a linear programming problem and solved using GAMS/CPLEX. The results show that the OZP can be solved exactly in few minutes even for large-sized cases such as the case of Melbourne. The proposed methodology can also be used to elicit

more insight into the managerial aspects of the post-disaster operation. In particular, it is important to know the optimal budget as well as a minimum budget to set up aid center and a zoning map based on which one can make sure no area is left behind in the relief operations.

References

AKSU, D. T. & OZDAMAR, L. 2014. A mathematical model for post-disaster road restoration: Enabling accessibility and evacuation. Transportation research part E: logistics and transportation review, 61, 56-67.

DUQUE, P. A. M., DOLINSKAYA, I. S. & SÖRENSEN, K. 2016. Network repair crew scheduling and routing for emergency relief distribution problem. European Journal of Operational Research, 248, 272-285.

FIONDELLA, L. An algorithm to prioritize road network restoration after a regional event. Technologies for Homeland Security (HST), 2013 IEEE International Conference on, 2013. IEEE, 19-25.

HOLGUÍN-VERAS, J., TANIGUCHI, E., JALLER, M., AROS-VERA, F., FERREIRA, F. & THOMPSON, R. G. 2014. The Tohoku disasters: Chief lessons concerning the post disaster humanitarian logistics response and policy implications. Transportation research part A: policy and practice, 69, 86-104.

HSIEH, C.-H. & FENG, C.-M. 2020. The highway resilience and vulnerability in Taiwan. Transport policy, 87, 1-9.

KASAEI, M. & SALMAN, F. S. 2016. Arc routing problems to restore connectivity of a road network. Transportation Research Part E: Logistics and Transportation Review, 95, 177-206.

KOVÁCS, G., SPENS, K. & MOSHTARI, M. 2017. The Palgrave Handbook of Humanitarian Logistics and Supply Chain Management, Springer.

KOVÁCS, G. & SPENS, K. M. 2007. Humanitarian logistics in disaster relief operations. International Journal of Physical Distribution & Logistics Management, 37, 99-114.

LIBERATORE, F., ORTUÑO, M. T., TIRADO, G., VITORIANO, B. & SCAPARRA, M. P. 2014. A hierarchical compromise model for the joint optimization of recovery operations and distribution of emergency goods in Humanitarian Logistics. Computers & Operations Research, 42, 3-13.

MANOPINIWES, W. & IROHARA, T. 2014. A review of relief supply chain optimization. Industrial Engineering and Management Systems, 13, 1-14.

MCCOY, J. 2008. Humanitarian response: improving logistics to save lives. American journal of disaster medicine, 3, 283-293.

ÖZDAMAR, L. & ERTEM, M. A. 2015. Models, solutions and enabling technologies in humanitarian logistics. European Journal of Operational Research, 244, 55-65.

SAKURABA, C. S., SANTOS, A. C., PRINS, C., BOUILLOT, L., DURAND, A. & ALLENBACH, B. 2016. Road network emergency accessibility planning after a major earthquake. EURO Journal on Computational Optimization, 4, 381-402.

WANG, C., SUN, J., RUSSELL JR, R. & DAZIANO, R. A. 2018. Analyzing willingness to improve the resilience of New York City's transportation system. Transport Policy, 69, 10-19.

YAN, S., CHU, J. C. & SHIH, Y.-L. 2014. Optimal scheduling for highway emergency repairs under large-scale supply–demand perturbations. IEEE Transactions on Intelligent Transportation Systems, 15, 2378-2393.

YAN, S., LIN, C. & CHEN, S. 2012. Optimal scheduling of logistical support for an emergency roadway repair work schedule. Engineering Optimization, 44, 1035-1055.

Identifying Safety Improvement Sites on Low-Volume Roads: Heuristic Safety Models

A. Al-Kaisy[a], S. Raza[b]

[a] *Professor, Western Transportation Institute, Bozeman, Montana, United States*

[b] *Graduate Research Assistant, Western Transportation Institute, Bozeman, Montana, United States*

Introduction

Rural low-volume roads (LVRs) are an integral part of the United States highway system. These roads are typically two-lane, two-way highway facilities with lower functional classification, and many of them are unpaved roads serving remote rural areas. Further, some of the LVRs are outside the jurisdiction of state highway departments as they are owned and operated by local government agencies such as counties, townships, and tribal governments.

While LVRs play a significant role in connecting rural communities and moving crops from farms to markets, they also pose unique challenges for highway departments, particularly in terms of traffic safety. According to a recent government report, only 19% of people in the US live in rural areas, however, 31% of the vehicle miles traveled and 43% of all fatal crashes occurred on rural highways (NHTSA, 2022). This highlights the importance of enhancing safety on rural roads, including those with low traffic volumes, and the need for incorporating LVRs into states' safety improvement programs to ensure progress toward vision zero objectives. Moreover, to implement roadway safety improvement projects, it is essential to identify candidate sites through network screening. Over the years, various network screening methods for crash hotspot locations have been developed and implemented. The traditional and widely used network screening methods such as the Empirical Bayes (EB) method and crash frequency/rate methods are resource intensive and require extensive historical crash and traffic data at individual sites. These methods are easily implemented on roadways with higher traffic volumes and more frequent crashes. However, on LVRs, crash occurrences, particularly fatal and serious injury crashes, are sporadic and infrequent due to low traffic volumes. Besides, it is expected that many of the property damage only (PDO) and other less serious crashes (minor and possible injury for instance) may go unreported on LVRs. This makes it challenging to identify hotspots and treat sites that are in greatest need of safety improvements using traditional network screening methods. Therefore, it is imperative to develop a new network screening method for identifying safety improvement sites specifically on LVRs where the use of the conventional network screening methods is deemed impractical.

Proposed Methodology: Heuristic Safety Models

Given the limitations of the conventional network screening methods on LVRs, a new method is needed with the following requirements in mind: 1) the method should not rely solely on crash history in identifying sites for safety improvements, and 2) the method should require a minimal amount of information that can easily be acquired by local agencies and can reasonably be applied by staff with a limited technical background.

The proposed method consists of heuristic safety models, for roadway segments and intersections, that were developed using the guidance and safety principles in the Highway Safety Manual (HSM). The HSM is the premier guidance document in the United States for conducting quantitative safety analyses in the highway project planning and development processes (AASHTO 2010). A key component of the HSM is the use of safety performance functions (SPFs), also known as crash prediction models. SPFs are mathematical models that estimate the expected number of crashes on a particular roadway type based on various factors such as traffic volume, speed, and roadway features. Another important aspect of the HSM is the use of crash modification factors (CMFs). A crash modification factor is a multiplicative factor that indicates the proportion of crashes that would be expected due to the presence of a roadway feature, or upon implementing a safety countermeasure (e.g., lane widening, shoulder rumble strips, etc.). Using the HSM, transportation professionals can make data-driven decisions about road safety and prioritize investments in safety programs.

The proposed heuristic safety models consist of assigning a score to each individual site that is part of the roadway network based on roadway characteristics, crash history, and traffic exposure over the analysis period. In these models, roadway characteristics are assigned scores based on the presence of certain roadway features (e.g., horizontal curve, grade, etc.). These scores were developed based on the rural two-lane highways crash modification factors (CMFs) provided in the Highway Safety Manual, the Federal Highway Administration CMFs clearinghouse (FHWA, 2020), or published in the existing literature. Roadway characteristics are expressed as simple classified variables that do not require exact values or access to detailed databases. The observed crashes involve the use of fatal and serious injury crashes as well as the remaining injury and property damage-

only (PDO) crashes in assigning scores to specific sites. Unlike fatal and serious injury crashes, it is expected that many of the PDO and less serious crashes (e.g., possible injury) may go unreported on low-volume roads. Further, it is reasonable to think that local agencies have knowledge of the recent fatal and serious injury crashes occurring within their jurisdictions, as such crashes represent unusual occurrences. Fatal and serious injury crashes are assigned scores in a way to ensure that their sites will receive further consideration regardless of existing physical roadway features. Traffic exposure is another component of the proposed safety models. The models assign a multiplier (multiplicative factor) in adjusting the relative risk score based on traffic level.

Upon systemically applying the safety models assigning scores to all sites that are part of the roadway network, a list of high-priority sites (ranked from highest to lowest scores) can be established and used for further investigation and potential safety treatments. Usually, two priority lists are established: one for roadway segments and one for intersections.

Roadway Segments: Proposed Model

For segments, the following roadway features were included in the methodology: total roadway width (lane width + shoulder width), horizontal curvature, grade, driveway density, roadside (side slope and fixed objects), roadway surface type (paved vs unpaved), and pavement condition. Roadway surface type and pavement condition were included in the methodology for their potential effects on safety despite the fact that these factors are not included in the HSM (Souleyrette et al., 2010). This is primarily because some of the low-volume roads owned and operated by local governments are unpaved and some are paved with pavement in poor condition, and they constitute an integral part of local road networks. The scoring scheme for roadway segments is shown in Table 1. For the purpose of this project, roadway segments refer to roadway sections with similar (or uniform) cross-sections and roadside features.

The use of a scoring scheme and classified variables eliminated the need to access detailed information and extensive databases. The scoring scheme can be structured in a simple questionnaire format where the user must determine the presence of certain roadway characteristics, observed crashes, and traffic conditions in a user-friendly manner. In the following, a few clarifications are provided for the development of the safety model.

1. In developing scores for roadway physical characteristics, crash modification factors (CMFs) were used as a guide in assigning the relative scores to different roadway characteristics or risk factors. Specific values of roadway characteristics for typical scenarios were used as a guide in deriving the relative scores for risk factors used in this table. The objective was to use scores that generally maintain the relative safety impacts of various risk factors in the proposed model.
2. As the Average Daily Traffic (ADT) is part of the HSM safety performance functions (not the CMFs), multiplicative factors (referred to as multipliers here) were used to account for the different ranges of traffic level. The multipliers for various traffic levels were estimated using the HSM safety performance functions for rural two-lane highways. It was decided to use a multiplier for traffic speed as well so that all traffic variables are treated similarly in the proposed model. The multiplier for traffic speed was derived using the crash modification factor from a study referenced in the CMF clearinghouse (Ksaibati et al. 2009).
3. The scores assigned to observed crashes were mainly selected to ensure that sites with one or more fatal or serious injury crashes receive further consideration/review for potential safety improvements regardless of the geometric features present.

Intersections: Proposed Model

For local road intersections, a separate model was developed using intersection characteristics, historical crash data, and traffic exposure as shown in Table 2. In this model, a baseline score is used to ensure that the relative risk compound score (RRCS) does not assume a negative value regardless of intersection characteristics and crash history. The presence of left-turn lanes and lighting are believed to improve safety at the intersection, thus the negative scores. Again, the scores for fatal and serious injury crashes were selected to ensure that intersections with one or more fatal or serious injury crashes receive further consideration/review for potential

Table 28. Safety model showing ranking scheme for roadway segments

LVR Segments Ranking Scheme	
Safety-Related Questions	**If yes, add:**
Risk Factors	
Total width (TD)	
TD ≤ 20 ft.?	7
20 ft. < TD ≤ 24 ft.?	4
Horizontal curve?	
Flatter curve (R ≥300 ft.)	30
Sharper curve (R<300 ft.)	60
Grade steeper than ± 4%?	3
Six or more driveways per mile?	5
Side slope steeper than 1V:3H?	4
Fixed objects within 15 ft of travel lane?	4
Unpaved Road?	14
Poor pavement condition? (ruting, potholes, etc.)	7
Crash History?	
Fatal or serious injury crashes (N_1)	N_1 X 80
Other crashes (N_2)	N_2 X 5
Relative Risk Compound Score (RRCS)	
Speed ≥ 50 mph?	RRCS X 1.25
Got ADT?	
ADT *≤ 300*	RRCS X 1.0
300 < ADT ≤ 600	RRCS X 3.0
600 < ADT ≤ 1000	RRCS X 5.0
ADT > 1000	RRCS X 7.0
Global Risk Score (GRS)	

safety improvements. The method considers crashes occurring in the intersection conflict area as well as intersection-related crashes occurring on intersection approaches. Intersection ADT (ADTint) is used as an indicator of traffic exposure at the intersection. It is defined as the sum of the ADT for the two crossing roadways (e.g., major and minor roads) or the sum of the ADTs for intersection approaches divided by two (when ADTs of opposing approaches are different).

Upon systemically applying the scoring method for all sites that are part of the roadway network, a list of high-priority sites ranked on their scores (from highest to lowest) can be established and used for further investigation and potential safety treatments.

Concluding Remarks

This study proposed novel heuristic safety models to predict the relative level of safety for a roadway segment or intersection using roadway, crash, and traffic data. The main application of the proposed safety models is to screen the rural highway network for sites that are in most need of safety investigations and potential improvements. The main merits of the proposed safety models are summarized below.

1. The models utilize simple classified variables for roadway characteristics and traffic variables that do not require exact values or access to detailed databases. This is very important for small agencies lacking access to detailed databases and technical staff such as counties, townships, and tribal governments. Further, the proposed models could be used with and without traffic exposure data.
2. While the main utility of the proposed safety models is for rural low-volume roads mostly owned and operated by local governments, the models are also applicable to high-volume roads often owned and operated by state agencies. The development of the heuristic safety models was primarily based on the Highway Safety Manual guidance on two-lane rural highways regardless of traffic exposure.

Table 29. Safety Model Showing Ranking Scheme for Intersections

LVR Intersections Ranking Scheme	
Safety-Related Questions	**If yes, add:**
Baseline Score	50
Roadway Factors	
Skew angle > 20 deg ?	10
Non-controlled intersection?	60
Lighting?	-5
Left-turn lanes on non-controlled approach?	-30
Crash History?	
Fatal or serious injury crashes (N_1)	N_1 X 80
Other crashes (N_2)	N_2 X 5
Relative Risk Compound Score (RRCS)	
Got ADT?	
$ADT_{int} \leq 600$	RRCS X 1.0
$600 < ADT_{int} \leq 1200$	RRCS X 2.0
$1200 < ADT_{int} \leq 2000$	RRCS X 4.0
$ADT_{int} > 2000$	RRCS X 6.0
Global Risk Score (GRS)	

3. The proposed methodology could also be used in making the decisions needed for the implementation of systemic safety improvements at the network level. Many states use systemic improvements at the network level to address roadway features associated with certain crash types that are separate from their ongoing network screening and hot-spot identification process. Systemic safety improvements consist of low-cost safety countermeasures, which makes it a good fit for low-volume roads (given the limited resources).

It is important to keep in mind that while the HSM is the main reference document for performing safety analyses in the U.S., it represents the general U.S. context which could be different from that in a specific state or region. Further, the proposed models are only meant for use in a comparative analysis such as for network screening applications or for comparing multiple improvement alternatives at a specific site. This is because the models cannot be used to predict crash numbers or crash rates at any specific site. The next phase of this research is currently ongoing and aims at validating the effectiveness of the proposed safety models using extensive field data from the state of Oregon in the United States.

Acknowledgment

The authors would like to acknowledge the financial support to this project by the Montana Department of Transportation (MDT).

References

American Association of State Highway and Transportation Officials (AASHTO). *Highway Safety Manual*, First edition. Washington, D.C., USA, 2010.

Federal Highway Administration (FHWA). *Crash Modification Factors Clearinghouse*. http://www.cmfclearinghouse.org, Accessed on February 2, 2023.

Ksaibati, K., Zhong, C., Evans, B. "*WRRSP: Wyoming Rural Road Safety Program*" Report No. FHWA-WY-09/06F, Wyoming Department of Transportation, Cheyenne, Wyoming, USA, 2009.

National Highway Traffic Safety Administration (NHTSA). Rural-Urban Comparison of Traffic Fatalities. Washington, D.C., USA, 2022.

Souleyrette, R., Caputcu, M., McDonald, T., Sperry, R., Hans, Z., and D. Cook. "*Safety Analysis of Low-Volume Rural Roads in Iowa*," Institute for Transportation, InTrans Project 07-309, Iowa State University, Ames, Iowa, USA, 2010.

Using a Cloud-based simulation environment for assessing future safety-critical scenarios with ADS

J. Casas[a], A. Cabrera[a], N. Parera[b], A. Tejada[c]

[a] *Aimsun SLU.*

[b] *IDIADA*

[c] *TNO*

Introduction

Technologies, such as Autonomous Driving Systems (ADS) are evolving rapidly and manufacturers must ensure that their future deployments will behave in the expected manner, and will be efficient at the system level when considering environmental aspects, such as pollutant emissions in case of IC engines or battery consumption with Electrical vehicles (EV), or traffic performance, such as reducing traffic congestion and delay time (see Poczter and Jankovic, 2014; Fagnant and Kockelman, 2015 and Elvik at al 2019 for an extensive taxonomy review of the potential impacts on Connected and Autonmous Transport systems (CATS)).

Traffic simultion software is a crucial tool for evaluating the safety and performance of Connected and Automated Vehicles (CAVs), allowing engineers and researchers to model and analyze complex traffic scenarios in a controlled and simulated environment. In doing so, they can identify potential safety risks and evaluate the performance of CAV systems before they are deployed in the real world.

There are several key advantages of using traffic simulation for the assessment of CAV safety:

- Flexibility: Traffic simulation allows researchers to simulate a wide range of traffic scenarios, including different road conditions, traffic patterns, and infrastructure elements. This allows them to identify potential safety risks and evaluate the performance of CAV systems in a variety of conditions.
- Repeatability: Traffic simulation provides a consistent and repeatable environment for testing, allowing researchers to conduct multiple simulations with the same conditions and evaluate the results. This helps to ensure the validity and reliability of the results.
- Cost-effectiveness: Compared to real-world testing, traffic simulation is be much less expensive, as they do not require the construction of test tracks or the use of physical vehicles. This makes it possible to perform a large number of simulations and evaluate a wide range of scenarios at a lower cost.
- Improved accuracy: Traffic simulation can be calibrated and validated using real-world data, allowing them to accurately represent real-world conditions. This can provide a more accurate picture of the performance of CAV systems in the real world.

Most prior research has performed traffic efficiency assessment on connected and/or automated vehicles (e.g., Makridis et al. 2018 and Tympakianaki et al 2022) and safety evaluation (Miqdady et al., 2023; Rahman; 2019) have been based on the abstraction of CAV behavior representing the full CAV system. Other approaches are based on plugging the CAV system as external component into a traffic simulator, for example (Liming et al 2021) bridges Aimsun Next, a traffic modeling and traffic network simulation tool, integrating it with Robot Operating System (ROS), an open-source meta-operating system, to develop a co-simulation platform bridging traffic simulations with ego-vehicle CAV simulations.

This paper describes a simulation environment for assessing future safety-critical situations in mixed scenarios with manual driven and automated vehicles.

The SAFE-UP simulation environment

The approach of having co-simulation between a traffic simulator and an ADS was considered by the research project SAFE-UP[22] (www.safe-up.eu) as the starting point for its simulation environment. The goal of SAFE-UP was to ascertain future safety-critical traffic interactions by means of behavioral simulations with the following goals:

[22] The SAFE-UP project has received funding from the European Union's Horizon 2020 research and innovation programme under Grant Agreement 861570.

— Extend existing microsimulation tools incorporating enhanced behavioural models for VRU's, automated vehicles, and manually driven vehicles.

— Develop metrics to describe non-safety-critical and safety-critical traffic interactions for future mobility systems.

— Identify safety-critical scenarios for future mobility systems that mix VRU's, automated and manually driven vehicles.

The requirements of a simulation environment for achieving the expected goals could be summarized as: a) a Plug-in to the traffic simulator new enhanced behavioural models for VRU's and manually driven vehicles, b) the Co-simulation of scenarios with multiples instances of AVs for representing realistic penetration rates of automated vehicles and c) the Potential for a massive number of simulations for assessing future safety-critical situation based on Monte Carlo experiments.

The simulation environment is based on Aimsun Next traffic simulator (Aimsun, 2022), where the integration of all behavioural models (manual driver, AV, Powered Two-wheeler, Pedestrian and Bike) is based on two types of technologies available in Aimsun Next, each with a different purpose: a) External Agent Interface (EAI) – allows the user to simulate in Aimsun Next microscopic simulation, externally controlled vehicles, for example, a human driver in a simulator, an autonomous vehicle controller, or an experimental control system being tested in a simulation environment, and b) Aimsun Microscopic Simulator Behavioural Models Software Development Kit (microSDK) allows the user to replace Aimsun Next microscopic models (car-following, lane-changing, etc.) with their own behavioural models, programmed in C++.

The system integration architecture consisted of Aimsun Next platform running in one computer with all behavioural models integrated using MicroSDK for the Human driver and PTW model as part of a dynamic library, while behavioural models, for AVs, cycling and pedestrians are integrated using the EAI and can run in different computers using TCP/IP communication.

The simulation integration framework requires all behavioural models have the same view of the infrastructure, having a common digital map. This common digital map selected is OpenDrive format (https://www.asam.net/standards/detail/opendrive/). OpenDRIVE is an open format specification to describe a road network's logic. It's objective is to standardize the logical road description to facilitate the data exchange between different driving simulators and traffic simulators.

The requirements of having potentially massive numbers of simulations and having multiple instances of AVs in the same simulation impose a strong requirement on computation power. This requirement leads to the need to migrate the simulation environment to Amazon Web services (AWS) using cloud technology.

The AWS cloud deployment architecture is composed of multiple containers, each container acts as an independent computer with its own operating system. These machines communicate with each other through a virtual TCP/IP network inside the cloud. The deployment architecture is as shown in Figure 1.

Figure 137. Architecture of the SAFE-UP AWS deployment

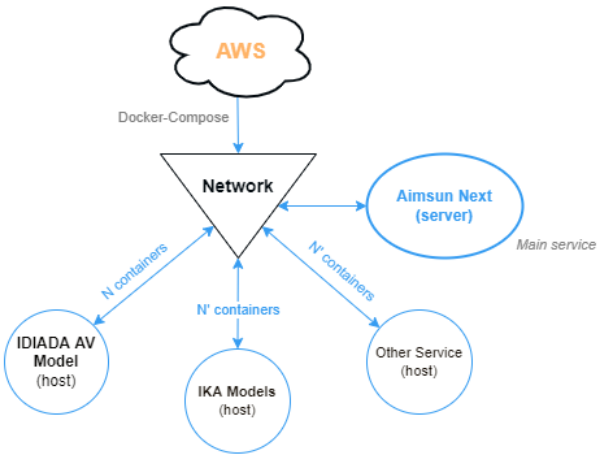

As can be seen in Figure 2 the AWS integration consists of one Aimsun Next container which runs the Aimsun road network with the Human driver model and the Powered Two-Wheeler model as dynamic libraries. This acts as the main service and is connected to the rest using TCP/IP communication through an External Agent

Interface (EAI). Then, one container for the bike model (managing all instances of bikes) and pedestrian model (managing all instances of pedestrians). Finally, one container with the AV model, in this case one instance of the container is required for each AV that will run in the simulated network, i.e. as many instances of the containers as AVs to be simulated. These different containers communicate using a network generated using Amazon Elastic Compute Cloud and a set of Docker instructions.

The main advantage of this architecture is the scalability in computational power. This translates into avoiding two limitations that can happen in private computing infrastructure, with no practical limit on the maximum number of AVs that can run in a simulation and no practical limit on the amount of simulation that can be run independently in parallel (each simulation represents a simulation of a single scenario).

To reproduce the experimental workflow necessary, a series of steps are required, as shown in the schematic in Figure 1. In general terms, it consists of running two scripts that have all the general information for the simulation to be set and run. These generate and place the files needed to run the given simulation on the AWS. Also, they indicate where to store the outputs. From that point, the process is controlled by the container settings and the AWS and no further action is required to run the simulation. When the simulation ends, the results need to be retrieved from the Amazon S3 bucket where they are stored.

Figure 138. AWS simulations workflow

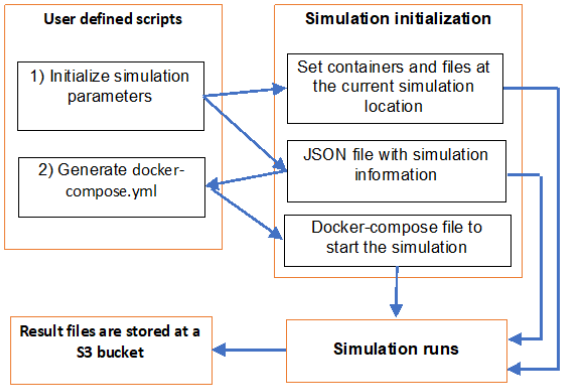

Figure 139. AWS S3 file and folder structure

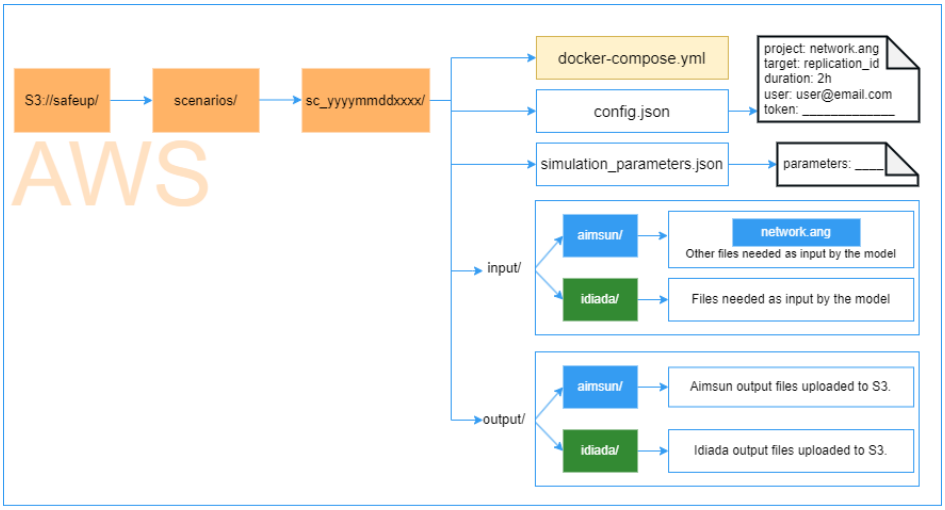

Two python scripts are required, one to define the simulation parameters and another to generate the folder structure and files required to execute all the experiments. This includes a configuration file of the scenario (common to all the containers), the simulation parameters JSON file that provides Aimsun Next with the required variables, and the YML file required to execute the experiment in AWS.

Finally, second python script copies the needed files into the Amazon S3 bucket, see Figure 62.

The first script defines the variables to set all the simulations, including how many of the containers will be needed for each of them. Then, the second script reads those requirements and builds a scenario for each of those contexts so that they can be executed. For each scenario, a folder (or bucket, in AWS terminology) contains everything needed for its execution (one single simulation). Inside, the YML file holds the instructions to instantiate the network and containers, the simulation parameters JSON file holds the variables that set the context for that specific scenario and the configuration JSON file holds technical information the containers will need to start the simulation.

Having this bucket ready, executing it is straightforward. Login to AWS with an account with permission to run Amazon Elastic Compute Cloud tasks and write the launch command. The YML file will do the rest and the results will be uploaded to the output folder of the scenario's AWS S3 bucket.

Conclusion

In conclusion, traffic simulators play a critical role in the assessment of CAV safety, providing a flexible, repeatable, cost-effective, and accurate tool for evaluating the performance of CAV systems. These simulators can help to identify potential safety risks and provide valuable insights into ways to improve the safety of CAVs. This paper describes the simulation environment for assessing future safety-critical scenarios overcoming computational requirements and scalability aspects related to the number of AVs co-simulated. The project SAFE-UP deployed this simulation environment allowing a design of a Monte Carlo experiments and their analysis. Currently the project is assessing 1000 simulations with 500 without AVs and 500 with Avs and shortly will have available the analysis comparing the base line against a future scenario with Avs.

Acknowledgements

This work was supported by the European Union's Horizon 2020 research and innovation programme under Grant Agreement 861570.

References

Aimsun (2022). Aimsun Next 22 User´s Manual. Aimsun Next Version 22.0.2, Barcelona, Spain.

Elvik, R. et al. (2019). A taxonomy of potential impacts of connected and automated vehicles at different levels of implementation. Deliverable D3.1 of the H2020 project LEVITATE.

Fagnant, D.J., Kockelman, K. (2015). Preparing a nation for autonomous vehicles: opportunities, barriers and policy recommendations, Transportation Research Part A: Policy and Practice 77, pp. 167–181.

Gao, L., Bai, W., Leary, R., Varadarajan, K., and Brennan, S., ROS Integration of External Vehicle Motion Simulations with an AIMSUN Traffic Simulator as a Tool to Assess CAV Impacts on Traffic, IFAC-PapersOnLine, Volume 54(20), 2021, pp 870-875,ISSN 2405-8963, https://doi.org/10.1016/j.ifacol.2021.11.281.

Miqdady T., de Oña R., Casas J. andde Oña J., "Studying Traffic Safety During the Transition Period Between Manual Driving and Autonomous Driving: A Simulation-Based Approach," in *IEEE Transactions on Intelligent Transportation Systems*, doi: 10.1109/TITS.2023.3241970.

NATIONAL HIGHWAY TRAFFIC SAFETY ADMINISTRATION (2008), National Motor Vehicle Crash Causation Survey, Report DOTHS 811 059, U.S. Department of Transportation, 2008.

Poczter, S.L., luka M. Jankovic, L.M. (2014). The Google car: driving toward a better future?, Journal of Business Case Studies (JBCS) 10 (1), pp. 7-14.

Tympakianaki, A., Nogues, L, Casas, J, Brackstone M., Oikonomou, M., Vlahogianni, E, Djukic, T. and Yannis, G.. (2022). Autonomous Vehicles in Urban Networks: A Simulation-Based Assessment. Transportation Research Record: Journal of the Transportation Research Board. 2676. 036119812210905. 10.1177/03611981221090507.

Rahman, M.S., Abdel-aty, M., lee, J., Rahman, M.H. (2019). Safety benefits of arterials' crash risk under connected and automated vehicles, Transportation Research Part C: Emerging Technologies 100, pp. 354-371.

Analyse the effect of fog on the perception

M. M. Chaar[a], G. Weidl[a], J. Raiyn[a]

[a] *Connected urban mobility, Faculty of Engineering, University of University of Applied Sciences, Aschaffenburg, Germany*

Introduction

Autonomous vehicles (AVs) aspire to operate without human drivers. An AV is equipped with a big number of sensors and devices to ensure safety. These sensors and devices collect a large amount of data every second, which is needed for navigation. The new generations of cars are becoming increasingly automated from currently SAE L3 to L4 and L5 (fully automated). A new challenge faced by the designers of connected autonomous vehicles is the management of big input data in real-time under weather conditions, such as fog, snow, cloud, and heavy rain (Zhai et al., 2020; Zhang, et al., 2020). Weather conditions cause discomfort to drivers and the traffic efficiency is affected negatively (Jägerbrand and Sjöbergh, 2019). Adverse weather conditions affect directly, the safety of the driver by reducing his safety margin due to a low visibility distance and/or low friction. Fog conditions also decrease the reliability of camera-base systems due to altered image quality (Chincholkar & Rajapandy, 2019).

Deep-learning methods have the potential to significantly improve the ability to manage big input data and make a short-term travel forecasting in real-time by extracting the attributes of collected big input data under fog conditions. Equipping vehicles with driving automation systems aims to increase the driving comfort and eliminate the human errors, which are responsible for the majority of accidents (Raiyn, 2022). The main goal of this study is reducing the AV accidents by improving the detection of the traffic anomalies under fog conditions. Our contribution will promote a better understanding of the relationship between traffic flow characteristics and crash risk under fog conditions. It will help driver assistance system to develop better crash prevention measures under fog conditions. The novelty of this study is generating a training set of images of extreme fog condition with various possibilities and attempts to calibrate the confidence level using the model uncertainty based on optimized Bayesian network (Weidl et al., 2018).

Related research

Adverse weather condition is one of the most important factors that influences the critical-safety events. Various studies have shown that human drivers have a reduced desire to travel under foggy and snowy conditions. On other hand, adverse weather conditions, such as heavy fog, rain, snow, and sandstorms are considered dangerous restrictions of the functionality of the installed devices on autonomous vehicles, that impact the performance of the detection algorithm and could cause massive detection errors (Bejelic et al., 2020). The uncertainty and invisibility present a challenge for autonomous vehicles. Most of published detection approaches have been aiming to distinguish between scenes with clear and foggy weather situations during the day and night (Jose et al., 2022). According to our knowledge, this paper is the first study that presents a dataset based on synthesised images with different fog densities (25%, 50%, 75%, 100%). The novelty of our algorithm is to perform data analysis and vehicles' detection based on unsupervised learning.

Methodology

Deep-learning (DL) methods are some of the most useful tools in the area of machine learning (Li et al., 2018). A DL system learns the features of a dataset and then combines them to achieve a specific goal. In this study, a DL method is proposed for the early detection of traffic under fog condition. It is composed of two main phases: training and testing. The system proposed here is composed of four phases: (1) preparation of the dataset, (2) a training phase, (3) a testing phase, and (4) a performance metrics phase. For the preparation of the dataset, we have used Carla simulation to generate images with different visibility of fog conditions. The advantages of the Carla simulation are allowing to generate a synthesis image, which can be of any type, such as fog conditions in day and night.

In the training phase, we made two steps. Firstly, we utilized ResNet18 to classify the fog density. In the second step we performed object detection, which implements YoloV5 algorithm with backbone based on EfficientNet (Li et al., 2022). Neck Network uses a combination of SPP (Spatial Pyramid Pooling), which divides images into sub-regions and pools features at multiple scales to enable efficient recognition of objects in images of varying sizes and positions, and PAN (Path Aggregation Network), which aggregates features from different levels of a convolutional neural network to improve accuracy. The Head network of YoloV5 is responsible for predicting the bounding box and its class to localize the objects trained for each class of fog separately.

Algorithm description

This study aimed to develop a real-time crash risk prediction model-based DL under fog conditions.

The training data includes fog-related images with different density rate. The training datasets have been generated with Carla simulation. They consisted of more than 30000 images to classify the fog density and 50000 images for object detection with three classes of vehicles (car, truck and other). From this data we used 80% for training and 20% for validation.

The CNN (ResNet18) has been applied to extract the image features and to detect the density of the fog in five scales, i.e. fog density 0% (clear weather), 25%, 50%, 75% and 100%. The so trained model for each class of fog density has been used to detect and classify the objects, as illustrated in **Figure 140**.

Figure 140. Algorithm description

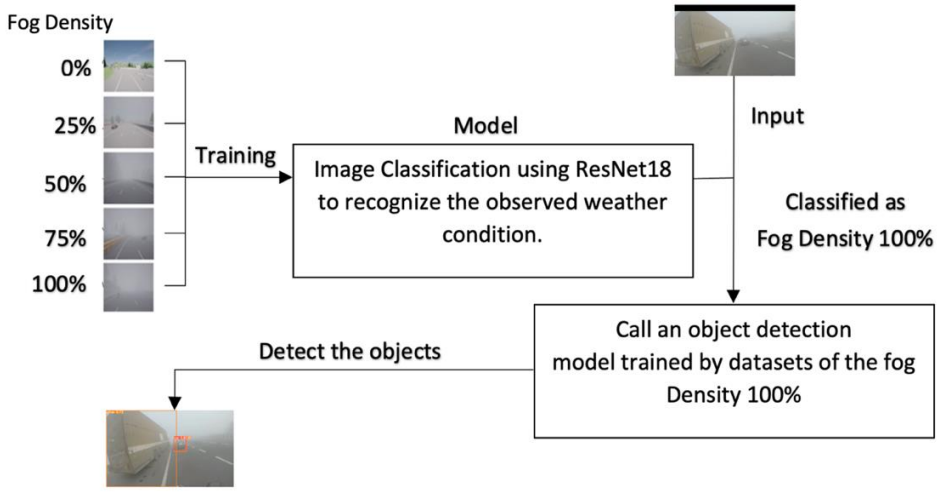

Source: Authors' elaborations.

Discussion and conclusion

The algorithm is designed to increase the accuracy of object detection under severe weather conditions as shown in **Table 30**. We use YoloV5 for object detection.

Table 30. Summary of results of the object detection, based on training using yolov5 algorithm for different foggy conditions

Fog Density	Precision	Recall	mAP50	mAP50-95
0%	0.724	0.737	0.793	0.651
25%	0.771	0.722	0.778	0.596
50%	0.754	0.785	0.825	0.665
75%	0.822	0.775	0.828	0.654
100%	0.759	0.747	0.814	0.651

Source: Authors' elaborations.

The algorithm's performance metrics decreases gradually when we validate object detection on images with a fog density different from what the model was trained for (see **Table 31**). The training accuracy is measured by mean average precision (mAP50) threshold intersection over union (IOU=50). Therefore, we can enhance perception under severe weather conditions (see **Figure 141**) by using the algorithm depicted in **Figure 140**. Next, the vehicles' counting algorithm and the dynamic trend of traffic flow will establish the tendency for a

possible congestion on an observed road segment and develop control strategy to improve the traffic flow efficiency and safety under severe foggy conditions.

Figure 141. Detection of vehicles, the density of the fog in this photo is 100% as generated by Carla simulations

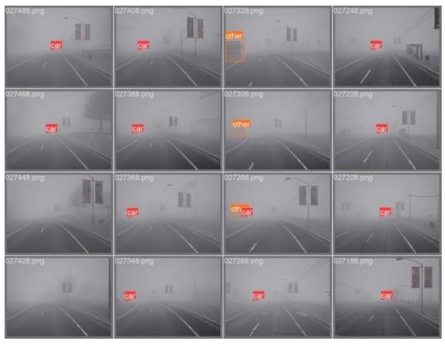

Source: *Authors' elaborations.*

Table 31. Evaluation results of the YoloV5, trained for different fog density (metric mAP50)

		Validation Data				
	Fog Density	0%	25%	50%	75%	100%
Training Data	0%	**0.793**	0.573	0.237	0.186	0.188
	25%	0.51	**0.778**	0.429	0.323	0.388
	50%	0.31	0.305	**0.825**	0.607	0.607
	75%	0.274	0.259	0.668	**0.828**	0.684
	100%	0.246	0.347	0.754	0.704	**0.814**

Source: *Authors' elaborations.*

References

Li, J., Cheng, H., Guo, H. and Qiu, S. *Survey on Artificial Intelligence for Vehicles, Automotive Innovation*, Springer, 2018. https://doi.org/10.1007/s42154-018-0009-9.

Zhai, B., Lu, J., Wang, Y. and Wu, B. *Real-time prediction of crash risk on freeways under fog conditions*, International Journal of Transportation Science and Technology, 9 (2020) 287–298.

Weidl, G., Madsen, A. L., Wang, S. R., Kasper, D., Karlsen, M. „*Early and Accurate Recognition of Highway Traffic Maneuvers Considering Real-World Application: A Novel Framework Using Bayesian Networks*", June 2018 IEEE Intelligent Transportation Systems Magazine 10(3):146 – 158, DOI: 10.1109/MITS.2018.2842049.

Raiyn, J. *Detection of Road Traffic Anomalies Based on Computational Data Science,* Discover Internet of things, 2,6, 2022. (https://doi.org/10.1007/s43926-022-00025-y).

Jägerbrand, A.K. and Sjöbergh, J. *Speed responses of trucks to light and weather conditions*, Cogent Engineering, 6:1, 2019. 1685365, DOI:10.1080/23311916.2019.1685365.

Zhang, Y., Carballo, A., Yang, H. and Takeda, K. *Perception and sensing for autonomous vehicles under adverse weather conditions*: A survey, ISPRS Journal of Photogrammetry and Remote Sensing, 196 (2023) 146177.

Chincholkar S, Rajapandy M. *Fog image classification and visibility detection using CNN*. Advances in Intelligent Systems and Computing. 2019;:249–57.

Li X, Cai Z, Zhao X. Oriented-yolov5: A *real-time oriented detector based on Yolov5*. 2022 7th International Conference on Computer and Communication Systems (ICCCS). 2022.

Bijelic M, Gruber T, Mannan F, Kraus F, Ritter W, Dietmayer K, et al. *Seeing through fog without seeing fog: Deep multimodal sensor fusion in unseen adverse weather*. 2020 IEEE/CVF Conference on Computer Vision and Pattern Recognition (CVPR). 2020.

M. B. Jensen, M. P. Philipsen, A. Møgelmose, T. B. Moeslund, and M. M. Trivedi. *Vision for looking at traffic lights: Issues, survey, and perspectives*. IEEE Transactions on Intelligent Transportation Systems, 17(7):1800–1815, 2016. 2.

Jose Valanarasu JM, Yasarla R, Patel VM. Transweather: *Transformer-based restoration of images degraded by adverse weather conditions*. 2022 IEEE/CVF C*onference on Computer Vision and Pattern Recognition (CVPR)*. 2022.

Data-Driven Safety Assessment of Adaptive Cruise Control

A. Sharma[a], D. Chen [a], Z. Zheng[b], Y. Xie[a]

[a] *Civil and Environmental Engineering, University of Massachusetts, Lowell, United States of America*

[b] *The University of Queensland, School of Civil Engineering, Faculty of Engineering, Architecture, and Information Technology, Brisbane, Australia*

Introduction

The Adaptive Cruise Control (ACC) system is a widely used driver-assistant system and plays a critical role in ensuring safety. However, the research indicates ACC system is unreliable under emergency braking and improvements are needed for better safety performance (Mattas et al., 2020). In this research, we use the Surrogate Safety Measure (SSM) and data analysis techniques to perform safety assessment of ACC controllers. The objectives include (1) understanding the impact of ACC Car-Following (CF) setting (such as Speed and Headway) on safety; (2) comparing performance of different ACC controllers; (3) analyzing kinematic parameters to unveil the fundamental risk factors during ACC functioning; and (4) suggesting improvements to design safer ACC controller. This extended abstract will briefly introduce safety metrics used, dataset, and preliminary results based on our earlier empirical experiments conducted in Massachusetts (T. Li et al., 2022).

Methodology

The stopping distance requirement is used to derive the collision-free safety metric, called Emergency Surrogate Safety Metric (ESSM). The main idea is to assess whether the follower is able to avoid collision if the leader conducts *emergency braking*. The philosophy of the ESSM is based on the physics of kinematics as proposed in our earlier work (Chen et al., 2023), which is also consistent with the distance-based fuzzy surrogate safety measures introduced in (Mattas et al., 2020). Moreover, Y. Li et al. (2017) has also embraced similar philosophy in safety evaluation of Adaptive Cruise Control.

Emergency Surrogate Safety Measure

Here we consider an initial situation that the leader traveling at speed v_l suddenly conducts emergency braking using its maximum deceleration capability, b_l, until it stops. The follower, traveling at v_f, will react to the emergency braking using its maximum deceleration capability b_f to avoid collision, but the reaction will occur *after* a response delay τ. During the response delay period, the follower continues its original kinematics, i.e., to continue its acceleration a, which is assumed constant in the response delay period. Based on such kinematics, we derive the minimum safe spacing (SS0), the initial spacing (bumper to bumper inter-vehicle distance) that guarantees that the follower will not collide with the leader for the entire response process until both vehicles stop. The SS0 derivation varies with the relative deceleration of follower compared to the leader as derived in Chen et al. (2023). For simplicity, we assume that the leader and follower have the same deceleration capability $b_l = b_f = b$. Our full paper will include the other cases where $b_f \neq b_l$. With $b_l = b_f = b$, the minimum spacing occurs when both vehicles have stopped, and the formulation of SS0 is given below in Equation (1).

$$S_l = -\frac{v_l^2}{2 * b_l} \; and \; S_f = \frac{\left(v_f + \left(a - b_f\right) * \tau\right)^2}{-2 * b_f} - \frac{1}{2} * \left(a - b_f\right) * \tau^2 \quad (1)$$

$$SS0 = S_f - S_l \quad (2)$$

$$SS0 = v_f * \tau + v_f * \tau * \frac{a}{b} + \frac{1}{2} * a * \tau^2 \left(1 + \frac{a}{b}\right) + \frac{v_f^2 - v_l^2}{2b} \quad (3)$$

Here, S_l and S_f denote the travel distance when they stop.

We define the Emergency Surrogate Safety Measure ($ESSM$) as the net distance per Equation (4), where S_0 is the actual spacing, l_c is the vehicle length and B_D is the additional safety buffer. Accordingly, the collision will occur if ESSM is smaller than zero, otherwise, it's collision-free. Besides, the value of $ESSM$ will indicate the collision severity. For preliminary analysis, we assume $l_c = 5\,m,\; B_D = 2\,m$.

$$ESSM = S_0 - l_c - B_D - SS0 \quad (4)$$

Risk Duration (RD)

Risk duration (RD) is the time-based SSM. It is defined as the continuous time duration with $ESSM < 0$, as shown in Figure 2 and defined in Equation (5). RD will capture the risk persistence.

$$T = t_f - t_i \; where \; ESSM(t) < 0 \; \forall \; t\epsilon \; (t_i, t_f) \quad (5)$$

Figure 142. Leader Follower profile after braking

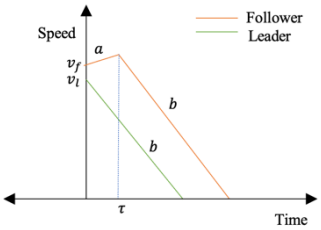

Figure 143. Risk Duration Representation

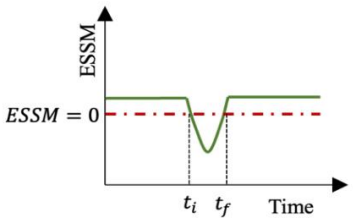

Dataset

The Massachusetts CF oscillation experiments consists of 3-vehicle platoon (Human driven vehicle (HDV) followed by ACC1 and then ACC2). A typical trajectory of the lead HDV is shown in Figure 3. The car-following characteristics captured during the experiments include headway, speed level; oscillation amplitude, and acceleration and deceleration (Mild, Strong), etc. For each model, the sample size is ninety-six oscillation cycles covering each ACC parameter setting twice. This study includes three different ACC controllers. (For details, please refer T. Li et al., 2022).

Figure 144. Desired Speed Profile of Lead V

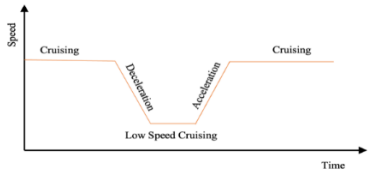

Figure 145. Speed Profile of HDV-ACC1 (Model X)

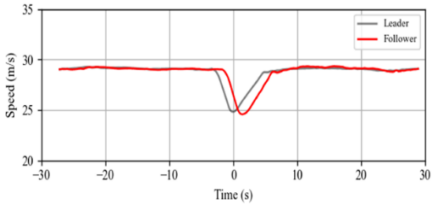

Figure 146. Actual Spacing, SS0 and ESSM Profile (An example from Model X)

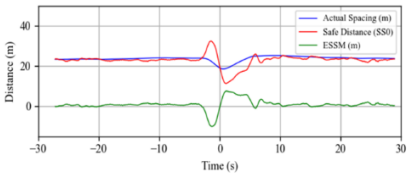

Results and Discussion

We applied the derivation of SS0 and ESSM to all leader-follower pairs in ACC data collected. Specifically, for a trajectory pair, each given point (actual trajectories of leader and follower) presents an initial condition, and we assess "what if the leader suddenly applies an emergency braking from this time on". If $ESSM < 0$, it

indicates that collision will occur if the leader applies emergency braking from this instance on. Therefore, corresponding to each point of the trajectory pair, we obtain an $ESSM$. One typical example of speed profile of HDV-ACC1 from one model, (referred to as Model X) is shown in and ESSM in (with $b = 0.5 * g\frac{m}{s^2}$, $\tau = 0.8s$) where g is acceleration due to gravity.

Safety Evaluation using TTC and ESSM

In this section, we present the result of ESSM for one ACC model (Model X). Note that since we have a three-vehicle platoon, our analysis includes ACC1 that follows the human leader and ACC2 that follows ACC1. In our evaluation, we use $b = 0.5 * g\frac{m}{s^2}$, $\tau = 0.8s$, where g is the gravity. The τ value is consistent with our empirical measurement of the response delay in T. Li et al. (2021).

The minimum ESSM of each oscillation cycle corresponds to the most critical instance of that driving cycle. ESSM analysis shows that, for ACC1 the mean of minimum ESSM for headway 1 is -3.03m, and 80 % of cases have collision risk (i.e., the minimum ESSM is smaller than 0). For headway 3 the mean of minimum ESSM is 3.59m, and the follower is under risk of collision. Note that headway 1 and 3 correspond to the minimum and medium headway settings. It's expected that the risk in headway 1 is much larger than headway 3. Yet, the percentage of case under risk is surprisingly high in headway 1. While the value will decrease if a much larger b is used, the risk is still significant. This suggests that headway 1 is too aggressive from the safety perspective.

Interestingly, the safety risk in ACC2 seems smaller than ACC1. Specifically, for ACC2 that follows ACC1, the mean minimum ESSM value for headway 1 is – 1.54m and 60% of cases are under the collision risk. Similarly, for headway 3, the mean of minimum ESSM is 7.27 m and no risk of collision. Note that for ACC1 and ACC2, the oscillation cycles have the same sample size and parameter setting. So, the outcomes are comparable. We suspect that this is because ACC2 has some anticipation effect that allows ACC2 to respond more promptly to the leader's deceleration. We will fully investigate this in the full paper.

Here we also compare our ESSM with the conventional safety surrogate measurement, time-to-collision (TTC). Specifically, we calculated the minimum TTC for each oscillation cycle to capture the most critical instance, similar to the minimum ESSM. Based on the literature, a threshold of 4s is commonly used for TTC (Ali et al. 2020; Li. et al. 2017). A TTC below this threshold is considered safety critical. Based on this standard, surprisingly, neither ACC1 nor ACC2 are under the risk of collision. The results here suggest that the conventional TTC evaluation is too conservative in assessing the safety risk.

Results from different ACC models

The safety risks of three different ACC models are presented in Figure 8 and Figure 11for ACC1 and ACC2, respectively. Note that all three ACC models have the same setting of driving experiments, and the data are comparable. Under the minimum headway, for ACC1, the safety risk is highest in Model X, followed by Model Y, and Model Z is much smaller; see the blue, green, and pink lines, respectively. Interestingly, for the difference between ACC1 and ACC2, it's significant in Model X (higher risk in ACC1; see the blue and yellow lines in Figure 8). But such difference is negligible for Model Y (see green and red line in Figure 8) and Model Z (see pink and purple line in Figure 8). In fact, the CDF of ACC2 of Model X becomes similar to the CDF of ACC1/2 of Model Y. These results suggest that platoon effect exists in some ACC models and a vehicle's position in a platoon matters when considering safety risk.

For the maximum headway, surprisingly, Model X still has a significant proportion of cases under collision risk for ACC1 (see blue and yellow line in Figure 11). For Model Y and Z, No collision risk in any of the cases. Note that the headway value itself is not directly comparable across different ACC models. The safety risk is a holistic indicator that captures the effect of the headway value and the ACC behaviors.

The result here suggests that Model X exhibits a higher risk at the maximum headway.

Figure 147. ESSM Distribution ACC1 Model X (m)

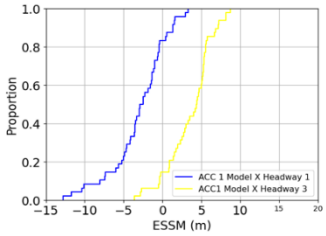

Figure 148. TTC Plot of ACC1 Model X (sec)

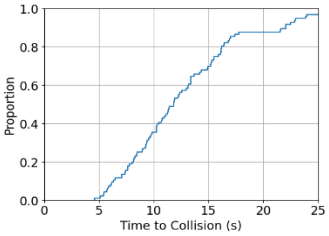

Figure 149. ESSM Distribution of all ACC controller in Minimum Headway (m)

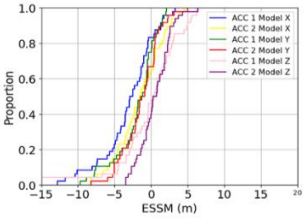

Figure 150. Minimum Headway of Model X (m)

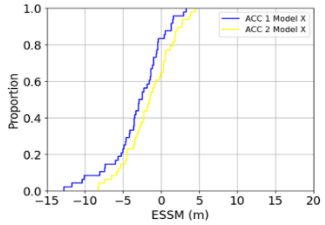

Figure 151. TTC Plot of ACC 2 Model X (sec)

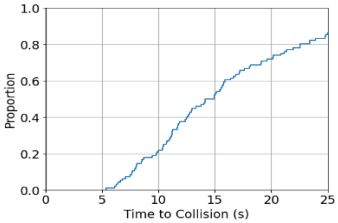

Figure 152. ESSM Distribution of all ACC controller in Maximum Headway (m)

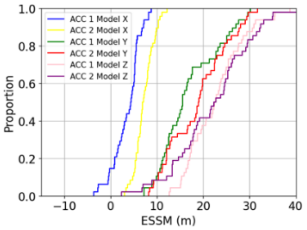

Conclusions

In this abstract, we present our data-driven safety assessment on the ACC models. We find that under the minimum headway, the ACC is under significant risk of collision, which is consistent in all three ACC models. Model X also exhibits a platoon effect, with smaller risk in ACC2.

The full paper will conduct in-depth analysis of car-following parameter analysis to understand the impact of ACC CF behavior on safety, particularly the contributions of the kinematic terms (e.g., response delay, deceleration capability). Based on that, we aim to derive insights onto controller design to improve the safety performance. We will also investigate the platoon effect. Lastly, we will compare the risk of ACC controllers and human driving using the NGSIM data.

References

Ali, Y., Sharma, A., Haque, M. M., Zheng, Z., & Saifuzzaman, M. (2020). The impact of the connected environment on driving behavior and safety: A driving simulator study. *Accident Analysis and Prevention*, *144*. https://doi.org/10.1016/j.aap.2020.105643.

Chen, D., Sharma, A., & Zheng, Z. (2023, January 10). *REVISIT GIPPS' CAR-FOLLOWING MODEL-WE HAVE BEEN WRONG :TRBAM_23_03835*.

Li, T., Chen, D., Zhou, H., Laval, J., & Xie, Y. (2021). Car-following behavior characteristics of adaptive cruise control vehicles based on empirical experiments. *Transportation Research Part B: Methodological*, *147*, 67–91. https://doi.org/10.1016/j.trb.2021.03.003.

Li, T., Chen, D., Zhou, H., Xie, Y., & Laval, J. (2022). Fundamental diagrams of commercial adaptive cruise control: Worldwide experimental evidence. *Transportation Research Part C: Emerging Technologies*, *134*. https://doi.org/10.1016/j.trc.2021.103458.

Li, Y., Li, Z., Wang, H., Wang, W., & Xing, L. (2017). Evaluating the safety impact of adaptive cruise control in traffic oscillations on freeways. *Accident Analysis and Prevention*, *104*, 137–145. https://doi.org/10.1016/j.aap.2017.04.025.

Li, Y., Wang, H., Wang, W., Xing, L., Liu, S., & Wei, X. (2017). Evaluation of the impacts of cooperative adaptive cruise control on reducing rear-end collision risks on freeways. *Accident Analysis and Prevention*, *98*, 87–95. https://doi.org/10.1016/j.aap.2016.09.015.

Mattas, K., Makridis, M., Botzoris, G., Kriston, A., Minarini, F., Papadopoulos, B., Re, F., Rognelund, G., & Ciuffo, B. (2020). Fuzzy Surrogate Safety Metrics for real-time assessment of rear-end collision risk. A study based on empirical observations. *Accident Analysis and Prevention*, *148*. https://doi.org/10.1016/j.aap.2020.105794.

Roadside LiDAR sensors for data privacy conform VRU detection

M. Ilic[a], M. Margreiter[a], S. Alvarez-Ossorio[a], M. Pechinger[b], K. Bogenberger[a]

[a] *Chair of Traffic Engineering and Control, Technical University Munich, Germany*

[b] *Department of Electrical Engineering, University of Applied Sciences Augsburg, Germany*

Introduction

LiDAR (Light Detection and Ranging) technology uses laser beams to measure distances and create high-resolution 3D models of the sensor's environment, including both static and dynamic objects. LiDAR sensors always incorporate two main components: A transmitter that emits light pulses with typical wavelengths between 250 to 1600 nm and a receiver that collects the reflected light pulses, converts the optical signal into an electrical quantity, and calculates the elapsed time between light pulse emission and collection of reflected photons. From this elapsed time, the distance between the LiDAR transmitter and the target reflecting the light pulse can be calculated (Roritz et al., 2022). LiDAR sensors can be categorized according to the beam steering of the emitted light pulse: Mechanical LiDAR sensors utilize a rotating assembly to create wide (typically 360°) fields of view (FOV), whereas solid-state LiDAR sensors avoid the use of rotating mechanical components leading to lower signal-to-noise ratios, narrower FOV and lower acquisition costs (Yahyaei et al., 2022; Khader et al., 2020).

Application-wise, LiDAR sensors can be grouped into stationary systems, mobile systems, and airborne systems. While mobile LiDAR systems are installed on road vehicles, trains, or boats and collect data within the flow of traffic, airborne LiDAR systems are mounted on aircrafts and capture features of the ground and built environment. Contrary to mobile and airborne systems, stationary LiDAR's are typically mechanical sensors installed at a fix position in the infrastructure (e.g., on a traffic pole) and they monitor a wide FOV around the sensor (Chang et al., 2014). Recently, pilot tests have been conducted to gather knowledge about optimal sensor installation heights and limitations of the system. A minimum installation height of 2.0 – 2.5 m is recommended in several publications to minimize occlusion effects limiting the detection accuracy. Furthermore, the use of several sensors at one location has proven to minimize occlusions due to the fusion of the data gathered by the individual sensors (Xu et al., 2018; Zhang et al, 2019).

In urban traffic, particularly at intersections, complex situations arise as multiple road users compete for limited space and collisions with motorized vehicles pose a high risk of severe injuries for VRU such as pedestrians and cyclists (Denk et al., 2022). Stationary LiDAR systems, capable of detecting motorized vehicles as well as VRU, could enable new urban traffic control and safety applications (Álvarez-Ossorio et al., 2023). In this paper we illustrate the use of roadside LiDAR systems for urban traffic control and safety applications by presenting the data collection process as well as the subsequent data processing of an exemplary hardware setup installed at a university campus in Germany. The outcome of the raw data processing is an object list containing information about all road users, which is suitable for utilization in numerous urban traffic control and safety applications.

Methodology

The exemplary hardware setup shown in Figure 1 was installed at the campus of the University of Applied Sciences Augsburg and consists of a sensor pole and an electric cabinet. The sensor pole holds the LiDAR sensor system used for this study as well as a roadside unit (RSU) for communication with connected vehicles and further stationary sensors. The used LiDAR system consists of two mechanical LiDAR devices: A mid-range 360° sensor (Ouster OS1-64) enables the detection of objects in a distance of up to 75 m to the sensor system, while a complementary blind spot sensor (RS-Bpearl) ensures the detection of objects closer to the sensor system.

The LiDAR sensor system (as well as the RSU and further sensors) is bi-directionally connected to the local network through a Power-over-Ethernet (PoE) switch, ensuring the transmission of the collected raw data to the computing units. The computing unit allocated to the LiDAR sensor system is responsible for the pre-processing and object detection from the transmitted LiDAR raw data, resulting in an object list containing information about all road users. Additionally, an external network gateway enables remote access to the described system.

Figure 153. Exemplary hardware setup, including network connections and computing units.

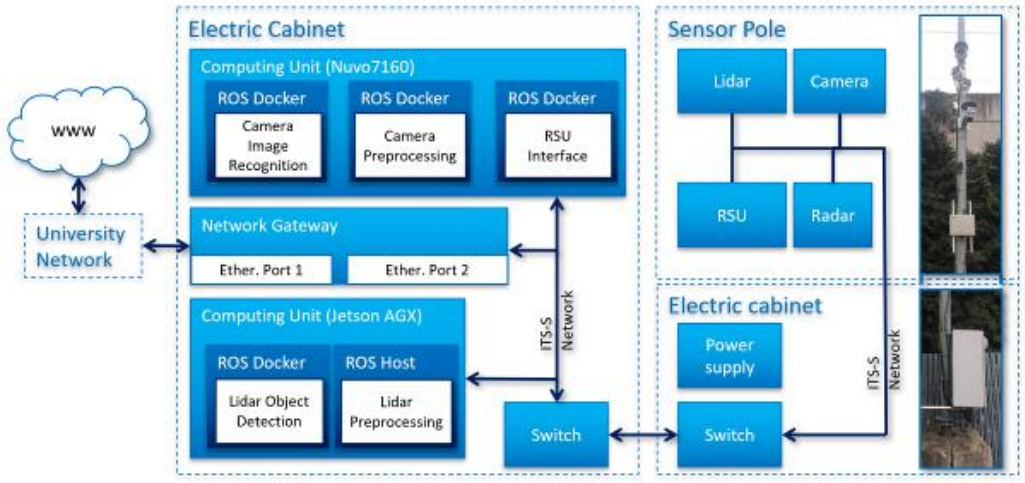

Source: Authors' elaborations.

Results

The raw data collected by the LiDAR sensors is a point cloud containing 3-dimensional coordinates and the intensity of reflection for each point sensed around the sensor. From this point cloud, a trained algorithm can detect different road users, classify them according to their type and track them over time. Figure 2 shows a visualization of the LiDAR point cloud (left) as well as the subsequent object detection and classification (right) indicated by the bounding boxes around the objects.

Figure 154. LiDAR point cloud (left) with object detection and classification (right)

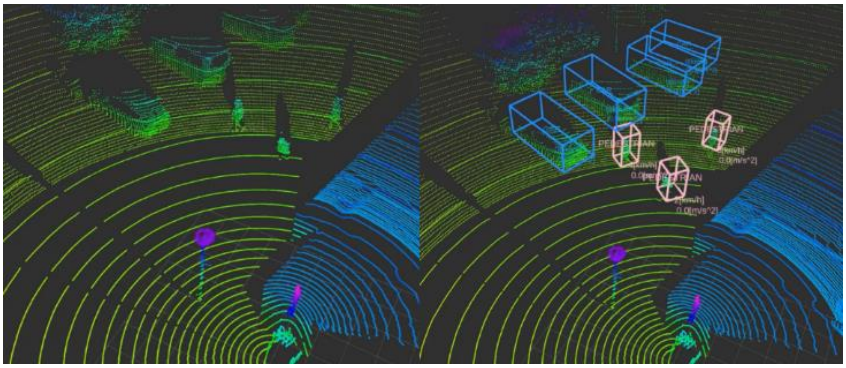

Source: Authors' elaborations.

The visualization of the collected LiDAR point cloud shows the difference in the two individual LiDAR sensors: While the mid-range LiDAR provides a comparably dense point cloud after a certain distance to the sensor location, the blind-spot LiDAR senses the area closer to the sensor with a lower density. In addition, occlusions appear where objects reflect the emitted light pulses and prevent them from reaching surfaces behind the objects. Both the low density of the acquired point cloud and the presence of occlusion can lead to limited object detection and classification capabilities, which can be counteracted by the use of more than one sensor system as described earlier. The tracking of detected objects over several continuous measurements allows for the generation of object lists containing information about all road users. A schematic pseudo-object list corresponding to **Figure 2** is shown in **Table 1**. Every line of the object list contains the information of one object at a given Unix *timestamp*. When an object is detected for the first time it receives a unique numerical *id*, which is used in all future observations in which the system re-identifies that object. Furthermore, the type and dimensions of the bounding box are given for each object, as well as the position, heading angle, speed, and acceleration for each *timestamp*.

Table 32. Pseudo-object list corresponding to Figure 2

Timestamp	ID	Classification	Position[1] x/y/z	Bounding Box Dimension x/y/z	Heading	Speed /Acceleration
1676019731	1	Car	5.0/7.5/0.0	2.7/5.5/1.7	140°	0 / 0
1676019731	5	Pedestrian	4.3/4.0/0.0	0.4/0.4/1.7	60°	1.2 / -0.08
1676019732	1	Car	5.0/7.5/0.0	2.7/5.5/1.7	140°	0 / 0
1676019732	5	Pedestrian	4.3/4.0/0.0	0.4/0.4/1.7	63°	1.1/ -0.02

([1]) In a local or global coordinate system

Source: Authors' elaborations.

Conclusions

LiDAR sensors have numerous strengths -and some weaknesses- in comparison to alternative sensor technologies currently used in roadside monitoring applications such as inductive loops and video sensors. One of the clear advantages of LiDAR is its excellent capabilities for measuring distance, in theory with accuracies under a couple of centimeters for ranges over 150 meters, as opposed to several-meter accuracies obtained with video sensors (Berk, 2019). In practice, however, the LiDAR sensor's effective detection and tracking range is significantly smaller depending on the type of sensor, characteristics of the target object, environmental conditions, etc. (Zhang et al.,2020). Another relevant benefit of LiDAR technology is that it is based on active detection, rather than passive detection, and it therefore performs independently of the lighting conditions. Furthermore, LiDAR sensors do not record sensitive personal data (e.g., facial attributes, vehicle's plate number, etc.) and therefore overcome data privacy issues common with video recordings.

Among its main disadvantages, LiDAR sensors provide only a rough identification of the object contours due their limited angular resolution, nor detect the texture of the objects. Furthermore, the quality of the object detection is affected under severe weather conditions (e.g., fog, snow, and heavy rain), although to a much lesser degree than for video sensors. Besides, in most cases the negative weather impacts can be mitigated in the short and mid-range with additional signal processing (Van Brummelen et al., 2018). The high price of LiDAR sensors is a major obstacle hindering their popularization in roadside applications, but it has decreased significantly in the last decade and will continue to do so as it becomes more extended in the automotive industry. Furthermore, we argue that the life-cycle-cost rather than the acquisition cost of the sensors should be taken into account since the former might turn them competitive to conventional sensors (e.g., inductive loops). This is because LiDAR sensors are not affected by construction works and several lanes and approaches can be monitored simultaneously with a single device (Sobie, 2016). The tracking of moving objects using only one LiDAR sensor still presents difficulties in contexts with frequent occlusions, particularly in areas with many pedestrians. However, this issue can be mitigated in the future by using sensors with higher resolution, implementing advanced tracking methods such as Kalman filters, and fusing the point cloud of several sensors located apart from each other (Margreiter et al., 2022).

As discussed in this work, LiDAR technology is an innovative and promising solution to perform roadside data collection of all traffic participants and it could provide valuable information to understand and model the complex interactions between different modes. This technology has gained maturity in the last decade and it is becoming more affordable. Besides, if future regulations ease the use of video sensors in public areas, it would be possible to fuse the data from video and LiDAR sensors. Thus, the former could capture the context, contribute to the classification and tracking of objects, and collect body pose information (valuable, for example, for short-term pedestrian movement prediction); while the latter could provide an accurate 3D map, speed measurements, etc.

Acknowledgements

The authors want to thank LiangDao GmbH for the cooperation in the field of sensor hardware and data processing algorithms.

References

Álvarez-Ossorio, S. and Margreiter, M., '*Predicting Pedestrian Crossing Intention at Signalized Intersections Using Roadside LiDAR Sensors',* Transportation Research Board, Washington, D.C., 2023, doi: 10.13140/RG.2.2.12255.12963.

Berk, M., *'Safety Assessment of Environment Perception in Automated Driving'*, PhD thesis. Technische Universität München, 2019.

Chang, J.C., Findley, D.J., Cunningham, C.M., Tsai, M.K., *'Considerations for Effective Lidar Deployment by Transportation Agencies'*, Transportation Research Records: Journal of the Transportation Research Board, No. 2440, Transportation Research Board of the National Academies, Washington, D.C., 2014, pp. 1-8, doi: 10.3141/2440-01.

Denk, F., Brunner, P., Huber, W., Margreiter, M., Bogenberger, K., Kates, R., *'Assessment of traffic safety interventions using virtual randomized controlled trials: potential of connected and automated driving including V2X for collision reduction at urban intersections'*, IEEE 25th International Conference on Intelligent Transportation Systems (ITSC), virtual, 2022, doi: 10.1109/ITSC55140.2022.9921764.

Khader, M. and Charlan, S., '*An Introduction to Automotive LIDAR*', Texas Instruments, Dallas, Texas, 2020.

Margreiter, M., Stüger, P., Ilic, M., Bogenberger, K. and Mohr, W., '*The Munich Test Bed for Connected and Automated Mobility*', mobil.TUM, Singapore, 2022.

Roriz, R., Cabral, J. and Gomes, T., '*Automotive LiDAR Technology: A Survey*', IEEE Transactions on Intelligent Transportation Systems, vol. 23, no. 7, pp. 6282-6297, 2022, doi: 10.1109/TITS.2021.3086804.

Sobie, C., '*Life Cycle Cost Analysis of Vehicle Detection Technologies and their Impact on Adaptive Traffic Control Systems*', Northern Arizona University, 2016.

Van Brummelen, J., O'Brien, M., Gruyer, D., Najjaran, H., *'Autonomous vehicle perception: The technology of today and tomorrow'*, Transportation Research Part C: Emerging Technologies, vol 89, 2018, pp. 384-406, doi: 10.1016/j.trc.2018.02.012.

Xu, H., Tian, Z., Wu, J., Liu, H., Zhao, J., 'High Resolution Micro Traffic Data from Roadside LiDAR Sensors for Connected Vehicles and New Traffic Applications', Center for Advanced Transportation Education and Research, University of Nevada, Nevada, 2018.

Yahyaei, M., Seifert, G., Hempen, T. and Huber, W., '*Review of Exteroceptive Sensors for Autonomous Driving*', IEEE 25th International Conference on Intelligent Transportation Systems (ITSC), virtual, 2022, doi: 10.1109/ITSC55140.2022.9922379.

Zhang, J., Xiao, W., Coifman, B., Mills, J.P. *'Vehicle Tracking and Speed Estimation from Roadside Lidar'*; IEEE Journal of Selected Topics in Applied Earth Observations and Remote Sensing 13, pp. 5597–5608, 2020, doi: 10.1109/JSTARS.2020.3024921.

Zhang, Z., Zheng, J., Xu, H., Wang, X., *'Vehicle Detection and Tracking in Complex Traffic Circumstances with Roadside LiDAR'*, Transportation Research Records: Journal of the Transportation Research Board, No. 2673, Transportation Research Board of the National Academies, Washington, D.C., 2019, doi: 10.1177/0361198119844457.

Understandability of accident risk information on road information boards

R. Katsumura [a], T. Yoshii [a], T. Tsubota [a], Y. Orino [b]

[a] *Ehime University, Japan*

[b] *Central Nippon Expressway Co., Ltd., Japan*

Introduction

Recently, a large amount of traffic data and accidents record has been able to be obtained. By using these data, likelihood of accident occurrence has been able to be estimated by accident risk estimation models. These models can evaluate the expected value of causing accident per unit veh-kms or during moving a specific road section. This paper defines these values as "accident risk". The information of the accident risk is expected to improve traffic safety by being used by drivers and by traffic administrators. One is because, when a driver is moving under the traffic situation with high accident risk, he could be more careful driving by getting the information about the accident risk. The other is because, by understanding the accident risk, traffic administrators are expected to implement effective traffic safety measures when the accident risk increases. The aim of this study is to understand which type of accident risk information and which type of information presentation method is more understandable by drivers and traffic administrators.

Types of accident risk information and types of methods at information presentation

(a) Types of accident risk information

2 types of accident risk information are considered in this study. One is the information of “accident risk”, which shows the expected value of causing accident during moving a specific road section. The other one is the information of “probability of being affected by an accident”, which shows the probability of accident occurrence by someone else.

Naturally, drivers have more interest on accident risk by themselves than accident risk by someone else. But the expected value is extremely small, e.g. once per 1 million travels. Therefore, the information about accident risk has little impact on drivers. On the other hand, information about probability of being affected by an accident is rather large, e.g. once per 20 travels. In this reason, the latter information may have more impact on drivers.

The accident risk is calculated by equation (1).

$$E_k^N = \sum_{i \in A_k} R_i \cdot d_i \qquad (1)$$

$$R_i = \frac{n_i \cdot 10^8}{d_i \cdot q_i \cdot (24 \times 365)} \qquad (2)$$

where,

E_k^N : Expected value of causing accident per single travel at route *k* [accidents/100million/km]

A_k : A set of road sections on route *k*

R_i : Accident risk on road section *i* [accidents/100million/km]

d_i : Distance of road section *i* [km]

n_i : Number of accidents on road section *i* [accidents/year]

q_i : Traffic flow rate at road section *i* [vehs/hour]

The probability of being affected by an accident is defined by equation (3). Then the expected value of numbers being affected by an accident per single travel at a route is calculated by equation (4).

$$D_i = T \cdot q_i \cdot R_i \cdot 10^{-8} \qquad (3)$$

$$E_k^M = \sum_{i \in A_k} D_i \cdot d_i \qquad (4)$$

where,

D_i : Probability of being affected by an accident at road section *i* [/km]

T : Average incident handling time [hour]

E_k^M : Expected value of numbers affected by an accident per single travel at route *k* [ ]

(b) Types of methods at information presentation

Regarding the method of presenting information, 2 types of criteria are considered. One is how to show the value of accident risk. 2 presentation methods, by numeric numbers or by colors on a graphic image, are tested. The other one is how to provide the information. 2 presentation methods, via variable message sign (VMS) or via graphic information board (GIB), are tested.

Table 1 shows the combination of the type of accident risk information and the type of information presentation. Also, Figure 1 shows the image of these types of information.

Table 33. Types of provided information

Type	Accident Risk	Presentation method	
A	causing accidents	numeric numbers	VMS (text)
B	being affected by accidents		
C	causing accidents		GIB (graphic image)
D	being affected by accidents		
E	causing accidents	colors	
F	being affected by accidents		

Source: Authors' elaborations.

Figure 155. Image of each Information type A to F

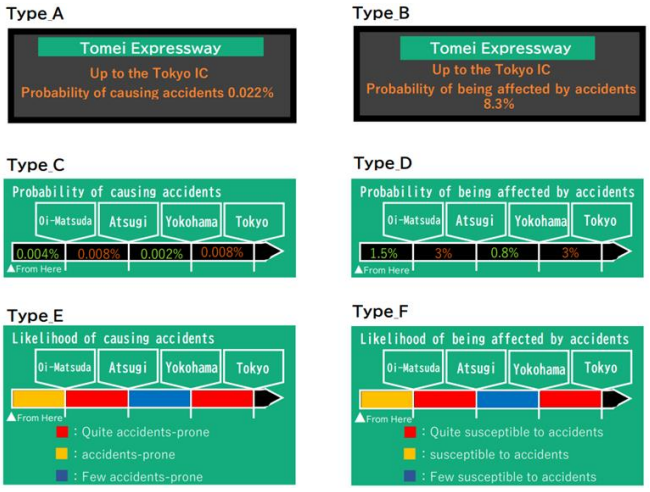

Source: Authors' elaborations.

Questionnaire survey

A questionnaire survey was conducted to understand which types of information is easier for drivers and traffic administrators to understand and to understand the usefulness of each information respondents consider. As shown in Table 2, the questionnaire sheets were distributed to drivers by hand at a rest area on the Matsuyama Expressway in Ehime Prefecture, and to traffic administrators at the NEXCO Central Japan Road Control Center, and both were collected by mail. They were distributed on July 31 (Sun.), 2022, on August 9 (Tue.), 2022 respectively. As for the number of copies, 300 sheets were distributed to drivers, of which 138 copies were collected, for a collection rate of 46%, and 40 copies were distributed to traffic controllers, of which 40 copies were collected, for a collection rate of 100%.

Table 34. Outline of questionnaire survey

Item	Content	
Respondent	Drivers	Traffic administrators
Distribution place	Matsuyama Expressway Ishizuchisan Service Aria（inbound lane）	Central Nippon Expressway Co.,Ltd. Traffic Control Center
Distribution date	July 31 (Sunday), 2022	August 9 (Tuesday), 2022
Number of distributed sheets	300	40
Number of collected sheets (Response rate)	138 (46%)	40 (100%)
Number of valid votes	138	40
Method	Distribution by hand, collection by mail	

Source: Authors' elaborations.

A result of the analysis

One of the results of the analysis is follows. The respondents were requested to answer to the question below.

"Please arrange the information from A to F in the order that easy to understand."

Then, the Ordered Logit Model was applied to the answers using the equation (5).

$$Y=a_1 \cdot x_1+a_2 \cdot x_2+a_3 \cdot x_3+a_{12} \cdot x_1 \cdot x_2+a_{12} \cdot x_1 \cdot x_3+\text{const}+\varepsilon \qquad (5)$$

where,

Y : answer in 6 ranks (most understandable:6,...,worst:1)

x_1 : accident information dummy(1: causing accident, 0: being affected by accidents)

x_2 : color information dummy(1: colors, 0: numeric numbers)

x_3 : information board dummy(1: GIB, 0: VMS)

$a_1, a_2, \ldots$: regression coefficients

Table 13 shows the estimation results. This result shows that the accident risk information using color information and using GIB information are easily understood by the respondents. Also, accident risk information in causing accidents is easily understood in case of using color information. From these results, it can be concluded that type E is most understandable one among the 6 types of information shown in Figure 1.

Table 35. Estimation results of ordered logistic regression analysis on ease of understanding

Explanatory variables	Coeff.	t-value
Intercept	2.04	8.75**
Color information dummy	1.53	8.74**
GIB information dummy	1.06	5.54**
causing accidents dummy * color information dummy	0.88	4.09**
Number of samples	1020	
		**p:<.01,*p:<.05

Source: Authors' elaborations.

Summary

Through the analysis, several knowledge have been obtained about the understandability of the accident risk information. In the future research, effect of the accident risk information provision is tested by providing it on actual information board.

References

Nishiuchi, H., Dito, T., Hyodo, S., Kurauchi, S., and Yoshii, T., *Provide An Accident Risk Information by Variable Message System and Analysis on Drivers Cognitive Tendency of Safe Driving*, The 62th Civil Engineering Planning Research Conference, 2020.

Virtual simulations to estimate the residual safety risk of automated driving systems as part of the multi-pillar approach

O.M.G.C. Op den Camp[a], E. de Gelder[a], S.H. Kalisvaart[a]

[a] *TNO Integrated Vehicle Safety, The Netherlands*

Introduction

If the number of traffic casualties in the EU [1] continues to decrease at the current rate, the target of Vision Zero (reducing road deaths to almost zero by 2050 [2]) will not be met. Moreover, the road traffic system is changing rapidly, due to: changes in the existing mobility system (e.g., increasing share of cycling, the increased share of older road users); the introduction of new mobility systems such as connected, cooperative, automated driving; shared mobility concepts; and new enabling technologies such as artificial intelligence and wireless V2X-communication [3]. Simultaneously, vehicles are increasingly automated—especially shuttles, buses, and passenger cars. The goal of automation is to make mobility services available and safe for all, including vulnerable road users (VRUs). At the same time, automation can provide more comfort to drivers and passengers and increase the efficiency of the mobility system.

Authorities are being asked to allow vehicles equipped with new advanced communication and automation technologies onto public roads. The improvement of road safety only partly results from vehicle innovation and development; innovative infrastructure solutions are also required. In addition, authorities (from local to EU levels) seek to increase road safety through policies and regulations. A Safe System [4] approach recognizes the shared responsibility of different stakeholders to increase road safety. Road authorities and consumer testing organizations (such as Euro NCAP) have expressed a clear need for establishing a safety assessment framework that:

- is capable of dealing with the great challenges and fast developments in technology, not only now but also in the future. The framework should also consider the safety impact of infrastructure solutions and regulatory changes.
- requires a feasible testing effort. The increasing role of virtual testing using simulations is foreseen, as the seemingly infinite number of possible situations needs to be handled efficiently.
- conforms with European Union and UN regulations as well as international standards such as ISO and SAE. The framework must not only link to such standards, but also feed them with more comprehensive and powerful insights for prospective assessments.
- is capable of handling the changing role of the human driver, evolving as a result of new transport modalities at various automation and communication levels.
- is fair, comparable, and clear. Although the assessment procedure can be complicated, its results should be unambiguous, easily understood, and explainable to authorities and the general public.

An important metric in such a framework is the residual safety risk when a vehicle is allowed onto the road [5]. The concept of risk is widely understood, and basing the safety assessment on that concept helps create a fair and acceptable assessment process. The United Nations Economic Commission for Europe (UNECE) WP.29 Working Party on Automated/Autonomous and Connected Vehicles (GRVA) has developed the New Assessment/Test Methods (NATM) Master Document, where a multi-pillar approach is envisaged, as shown in Figure 1. In this abstract, we propose how to determine estimates for the residual safety risk making use of *virtual simulations*, and how this is in agreement with and a further fulfilment of the UNECE multi-pillar approach.

Figure 156. The multi-pillar approach for safety assessment of CCAM[23] systems

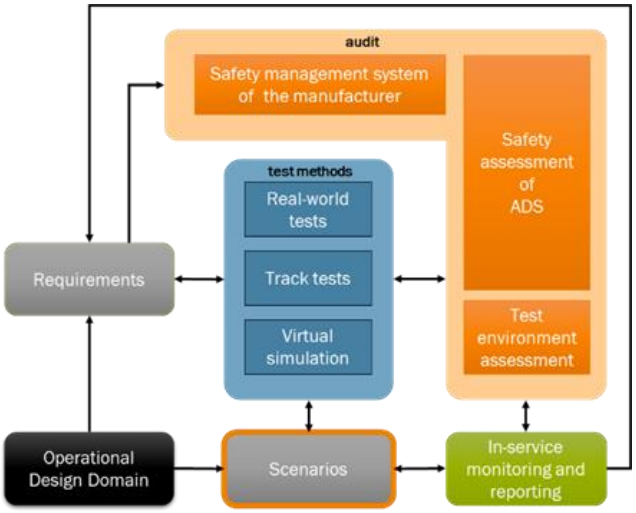

Source: Adapted from Donà et.al. 2022 [6].

Methodology

The safety assessment framework from Figure 156 makes use of predictive virtual simulation (hereafter simply 'simulation') in addition to physical tests. Simulation makes it possible to evaluate a large number of scenarios and its variations that are necessary for testing complex and integrated CCAM systems that can no longer be tested individually (like in Euro NCAP). Following the IEEE definition of a test, which is explained in [7], a test is an evaluation of test criteria (what we are going to evaluate using the test), under a set of specified conditions (the testcase, in what situations are we going to evaluate the test criteria), using metrics to express the outcome of the test quantitatively and a reference of what would be an acceptable outcome. In principle, this evaluation has to be done for all scenarios that the vehicle might encounter during its lifetime on the public road.

A clear, important and insightful outcome of a (virtual) test is the residual safety risk, i.e., the probability of harm as a consequence of the response of the CCAM to a scenario C_i. This is expressed as [5]:

$$Risk(C_i) = E(C_i) \times P_C(C_i) \times S(C_i),$$

in which $Risk(C_i)$ is the risk resulting from scenario C_i, $E(C_i)$ is the exposure of C_i (i.e. the probability that the vehicle encounters C_i on the road), $P_C(C_i)$ is the probability of ending up in a collision given a scenario C_i, and $S(C_i)$ is the severity of injuries resulting from the possible collision. The methodology of risk quantification making use of virtual simulations is clearly explained by De Gelder, et al. [5]. This paper also shows how to estimate an upper bound of the total residual safety risk once 'all' possible scenarios C_i for the CCAM system have been evaluated in simulation:

$$Risk\ (\sum_i C_i) \leq \sum_i Risk\ (C_i).$$

In other words, the total residual risk is smaller or equal to the sum of the risk values computed for the individual scenarios. To compute the risk upper bound for a certain CCAM system requires:

3. A structured overview of the scenarios that can occur on the public road, including the statistics regarding the exposure of these scenarios (what is the probability of ending up in a specific scenario, e.g., expressed per hour of driving). To provide this information, different scenario database initiatives have been established (e.g., as described in [8]). TNO established the StreetWise scenario database [9].

(23) Connected, Cooperative, Automated Mobility system.

4. A description of the Operational Design Domain (ODD, according to [10]) to select those scenarios from the scenario database that are relevant for the CCAM system under test.
5. A sampling strategy to specify, out of the infinite number of possible situations, a finite number of (virtual) tests that cover the ODD sufficiently well. Those situations in which the CCAM system unintentionally leaves its ODD need also to be considered in risk quantification.
6. A simulation toolchain and a simulation model for the CCAM system under test, to compute the probability of collision and the resulting severity (harm) in each test. An example of a scheme of a simulation framework is provided in [11]. Technical specification ISO 21934-2 drafted to provide guidelines on how to establish such a virtual simulation framework for safety assessment of automated vehicle functions [12].
7. An analysis of the confidence of the result based on the assumptions made in the procedure described above, given the limitations of the data and the number of tests [13].

Results

In [13], De Gelder and Op den Camp quantify the uncertainty in risk estimation in a use case of an Adaptive Cruise Control algorithm (described by Xiao et al. [14]) in response to three typical highway scenarios: a lead vehicle decelerating (LVD), a vehicle cutting in to continue driving in the ego vehicle lane (Cut-in) and the ego vehicle approaching a slower lead vehicle (ASV). The uncertainty of the results is calculated for three factors. As the data for identifying scenarios might be limited (e.g., limited number of hours of data collection for scenario mining), the identified scenarios and their variations in the dataset may not be fully representative for the variations in real traffic (insufficient degree of completeness for the ACC's ODD). Moreover, a limited amount of data also influences the reliability of estimation of the exposure values, i.e., the probability density functions of the scenario parameters. A third source of uncertainty results from the fact that only a limited number of simulations can be performed and the selected simulations should cover the ODD well.

Figure 157 shows the estimated risk of a collision per hour of driving for the three mentioned scenario categories. The horizontal axis shows the number of hours of data that is used as a basis for the risk calculations. The number of simulations (with importance sampling) is 10.000 for all risk calculations. The coloured areas mark the estimated uncertainty, which decreases with the increase of the amount of data that is used. The decrease of the uncertainty with an increasing number of simulations is not shown in this figure.

Figure 157. Estimated risk of a collision per hour of driving for three scenario categories

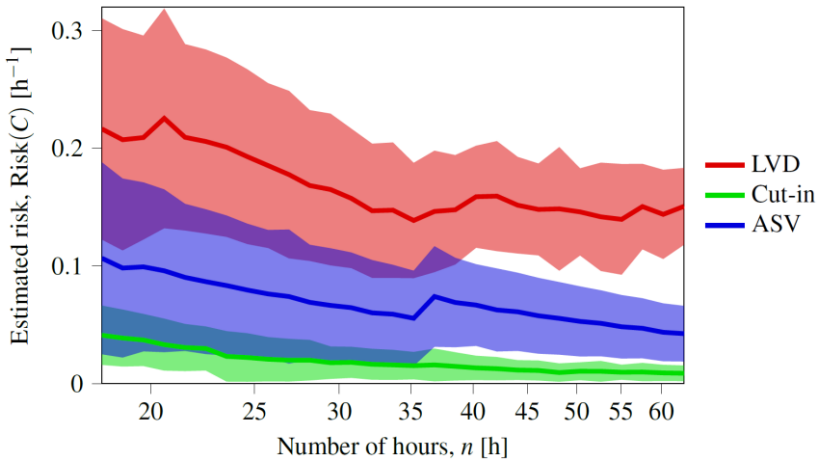

Source: De Gelder and Op den Camp 2023 [13].

Discussion

Virtual simulations form an increasingly important pillar in safety assessment of CCAM systems. As a result of the seemingly infinite number of scenarios that such systems might encounter on the public road and to which they need to respond appropriately, physical testing on a proving ground and field operational testing on the road to cover all these scenarios and their variations is far from feasible. Besides the validity of the models and methods used for simulation, also the interpretation of the large number of simulation results poses a challenge to all stakeholders involved in safety assessment. An intuitive and easily understood metric is the

residual safety risk, e.g., expressed as the probability of harm per hour of driving on the road using the CCAM system. For the safe introduction of a newly developed CCAM system, it must be assured (as a minimum requirement) that the safety risk is lower than the existing state of the art and that the current safety state is not compromised. Using simulation results in this way, requires an analysis of the confidence in the safety risk estimate. This paper provides an example of how to estimate a confidence interval. Further research is needed to estimate the influence of other factors in safety assessment using virtual simulation, such as model inaccuracies.

Acknowledgement

The work presented in this abstract is part of the V4SAFETY project. The V4SAFETY project is funded by the European Union under grant agreement 101075068. Content reflects only the authors' view and neither CINEA nor the European Commission is responsible for any use that may be made of the information it contains.

References

[1] European Road Safety Observatory, „Road safety targets Monitoring Report," [Online]. Available: https://ec.europa.eu/transport/ road_safety/system/files/2021-07/.

[2] European Commission, „European Sustainable and Smart Mobility Strategy Plan," 2021. [Online]. Available: https://transport.ec.europa.eu/transport-themes/mobility-strategy_en.

[3] J. Piao en M. McDonald, „Advanced driver assistance systems from autonomous to cooperative approach.," Transport Reviews, vol. 28, nr. 5, pp. 659-684, 2008.

[4] SWOV, „Sustainable Road Safety, SWOV Fact sheet," 2019. [Online]. Available: https://www.swov.nl/en/facts-figures/factsheet/sustainable-road-safety.

[5] E. de Gelder, H. Elrofai, A. K. Saberi, O. Op den Camp, J.-P. Paardekooper and B. de Schutter, "Risk Quantification for Automated Driving Systems in Real-World Driving Scenarios," IEEE Access, vol. 9, pp. 168953 - 168970, 2021.

[6] R. Donà, B. Ciuffo, A. Tsakalidis, L. Di Cesare, C. Sollima, M. Sangiogi en M. C. Galassi, „Recent Advancements in Automated Vehicle Certification: How the Experience from the Nuclear Sector Contributed to Making Them a Reality," Energies, vol. 15, 2022.

[7] E. Stellet, M. R. Zofka, J. Schumacher, T. Schamm, F. Niewels and J. M. Zöllner, "Testing of Advanced Driver Assistance Towards Automated Driving: A Survey and Taxonomy on Existing Approaches and Open Questions," in IEEE 18th International Conference on Intelligent Transportation Systems, 2015.

[8] SAKURA, SIP-adus and HEADSTART projects, "White Paper: Towards the Harmonization of Safety Assessment Methods," 2021. [Online]. Available: https://www.headstart-project.eu/wp-content/uploads/2021/12/211209_HEADSTARTSAKURA_WP_Final-draft.pdf.

[9] H. Elrofai, J.-P. Paardekooper, E. de Gelder, S. Kalisvaart and O. Op den Camp, "StreetWise position paper, scenario-based safety validation of connected and automated driving," 2018. [Online]. Available: https://publications.tno.nl/publication/34626550/AyT8Zc/TNO-2018-streetwise.pdf.

[10] SAE On-Road Automated Driving (ORAD) committee, "SAE J3016, Taxonomy and Definitions for Terms Related too On-Road Motor Vehicle Automated Driving Systems," SAE International, 2018.

[11] E. de Gelder, Performance assessment of automated vehicles using real-world driving scenarios, Delft, the Netherlands: PhD thesis, Delft University of Technology, ISBN: 978-94-6384-362-1, 2022.

[12] ISO 21934, „Road vehicles — Prospective safety performance assessment of pre-crash technology by virtual simulation, Part 2: Guidelines for application," International Organization for Standardization, expected 2023.

[13] E. de Gelder and O. Op den Camp, "How certain are we that our automated driving system is safe?," accepted for Traffic Injury Prevention, Special issue for the ESV 2023 conference, Yokohama, 2023.

[14] L. Xiao, M. Wang and B. Van Arem, "Realistic Car-Following Models for Microscopic Simulation of Adaptive and Cooperative Adaptive Cruise Control Vehicles," Transportation Research Record, SAGE Publications Sage CA, vol. 2623, no. 1, pp. 1 - 9, 2017.

Use of vehicle trajectory information in deep learning model for predicting traffic accident occurrence

T. Tsubota[a], T. Yoshii[a], Y. Isago[b], J. Xing[c]

a Ehime University

b Chuden Engineering Consultants

c Nippon Expressway Research Institute Company Limited

Introduction

This study investigates the use of probe vehicle trajectory data into the deep learning model for predicting the likelihood of traffic accident occurrence on an expressway. Traffic accidents are a big concern of society in many countries because the accidents cause severe losses on economy due to damages on road facilities and induced traffic congestions. In reducing the number of traffic accidents, prediction of the likelihood of traffic accident occurrence is essential for devising appropriate traffic management in timely manner. The likelihood of accident occurrence, or the "traffic accident risk" hereafter, dynamically changes depending on various factors, such as traffic conditions, road environments and road geometries (Hyodo and Yoshii (2015)). Recent development in measuring and storing traffic flow data has enabled the evaluation of the impact of such factors on accident risks as well as estimating traffic accident risks under various conditions considering the factors (Hyodo and Yoshii (2015).

In traffic accident analysis, the statistical method has long been a major analysis approach. Shankar, et al (Shankar, et al. (1997)) identified that number of traffic accidents have linear relationship with road geometries, such as number of curves and maximum slopes. Not only the static factors, but also the contribution of dynamic factors have been analyzed. Andry and Yagar (1993) demonstrated that accidents are more likely to occur under rain weather. There have been many attempts to include the traffic flow conditions as a risk factor of statistical regression analysis, and revealed that accident risk tends to be higher in congestion (Wang, et al. (2013)) and also when variation in speed and/or occupancy are higher (Golob, et al (2004)). However, it is challenging to carry out statistical regression analysis techniques when considering interactions among factors. Neural Network (hereafter, 'NN') is applied to the analysis instead of statistical analysis. NN models are computational ones defined as a set of processing units, represented by artificial neurons. They can handle nonlinear relationships and interactions among factors (Lin, et al. (2015)). One of the NN-based approach include the model proposed by Tsubota et al (2020), which predicts the likelihood of traffic accident occurrence in 2 hours ahead from the prediction start time. The traffic features are represented by three variables: speed, traffic volume and OCC; then the CNN was employed to learn the traffic features prior to accident occurrence. Although the results demonstrated that the proposed model classifies the accident occurrence with good accuracy, the method is only feasible on the expressway network densely equipped with traffic detectors.

The present study aims to employ detailed probe vehicle trajectory data to represent traffic states to be fed into a CNN-based accident prediction model.

Methodology

Problem settings

This study develops a convolutional neural network (CNN) model for predicting the accident occurrence on an expressway route with 15km stretch length in 30 minutes ahead from the prediction start time. The model is based on the VGG16 model (Simonyan and Zisserman (2015)), which is trained using the original dataset without transfer learning. The model input consists of a vehicle trajectory image data depicted by probe vehicle data. The input image data has time-space dimensions, and the trajectories on the time-space plane represent the traffic flow conditions along the study route for the past one hour.

A major difficulty of using the probe trajectory image data is that the number of probe vehicles changes over time. Figure 1 illustrates the trajectory image from the same road section at the same time on the same day. The trajectory on the left is drawn using all available probe vehicles, while the one on the right is drawn using half of the probe vehicles. Although the traffic states are identical, the images appear quite different. Hance it is virtually impossible to recognize that they are the same traffic conditions when these trajectory images are fed as input data into an accident prediction CNN model. Therefore, it is necessary to either fix the number of vehicles in all trajectory maps through sampling or to fix the sampling rate of probe cars to all traffic.

Figure 158. Sample of vehicle trajectory images of all available probe vehicles (left) and half of the data (right)

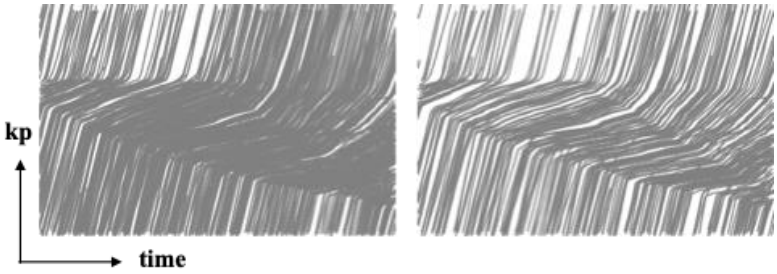

Source: Authors' elaborations.

In addition, probe data can provide information on vehicle speed based on time and position information. Therefore, we considered how to input the vehicle speed information into the trajectory images. First, when a trajectory image is created using only time and location information, a black-and-white trajectory lines are drawn. In the case of a black-and-white image, the color information is represented as 0 or 1, so the speed information is represented by the slope of the trajectory lines on a time-space plane. For color images, on the other hand, the color information is represented by a numerical value between 0 and 255, so the speed can be expressed as a numerical value by mapping the speed value to the color information value.

This study investigates the appropriate method to input the probe vehicle trajectory image to the CNN-based accident prediction model. In particular, four types of trajectory images are prepared and tested as illustrated in Figure 2.

Sampling method of probe trajectories

Two sampling methods are compared for creating trajectory images. The first method is fixed sampling (i.e., fixed number sampling), where the number of vehicles is set to approximately 100, and the number of trajectories is fixed. The trajectory image after sampling shows that the number of trajectories remains the same for all time period. However, in this case, the density remains constant, and only the slope of the trajectory represents the speed information of traffic flow, leading to a loss of traffic volume information. Another method is fixed sampling of the probe sampling rate (i.e., fixed rate sampling). In this method, the sampling rate of probe car is set to 10% of the all vehicles. The trajectory image after sampling can reflect the change in the number of trajectories. In this case, the change in the density of trajectory lines adds information on traffic volume in addition to the trajectory slope.

Figure 159. Four types of trajectory images tested in this study

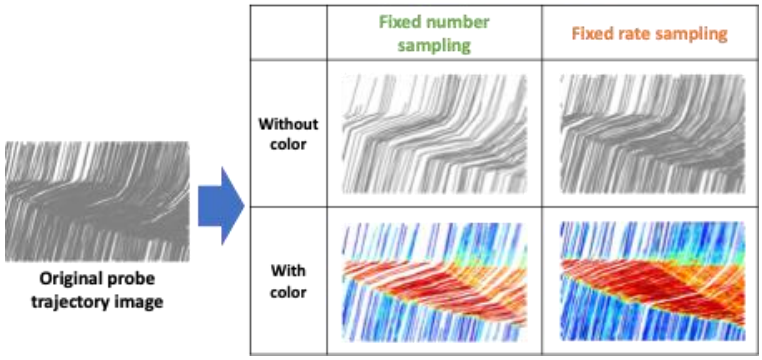

Source: Authors' elaborations.

Label data

Each input sample, which represents the traffic flow and weather feature in the past one hour, is associated with the accident occurrence in the next two hours on the study route. If traffic accidents occur in the next two hours, the corresponding input sample is labeled as "Accident (1)"; otherwise "No accident (0)". Regarding the accident types, only crash and sideswipe accidents are considered in the present study.

Data and study site

This study analyses a 15.4km stretch from Atsugi IC to Yokohama-Machida IC in the inbound direction of Tomei expressway, Japan. The probe vehicle data and traffic accident records are collected for two months from 1st January to 29th February 2020, during which 33 crash-type accident occurred.

Results

Accident risk prediction model was trained using the four types of trajectory data (Figure 2). Prediction performance of each model was evaluated using the F1 score. Results are summarized in Figure 3. The comparison between with and without color revealed that the color information on the trajectory image is effective in developing accident prediction model. Regarding the sampling method, fixed rate sampling resulted in better performance, suggesting that the trajectory images based on fixed rate sampling properly represent the traffic flow characteristics and more appropriate for the input data of the accident prediction model.

Conclusions

This study investigated the appropriate method of inputting trajectory image data obtained from probe vehicle data into an accident prediction model. Sampling methods for the probe vehicles were investigated, and a sampling method that fixes the penetration rate of probe vehicles was found to be suitable. Finally, the effect of colored trajectory image on learning accuracy was examined, and it was found that learning accuracy improved with coloration based on speed information.

It should be noted that this study utilized very limited number of samples from only two months period. In future research, probe data should be collected for longer period for comprehensive analysis, including fusion with detector data and weather data.

Figure 160. Comparison of the prediction performance

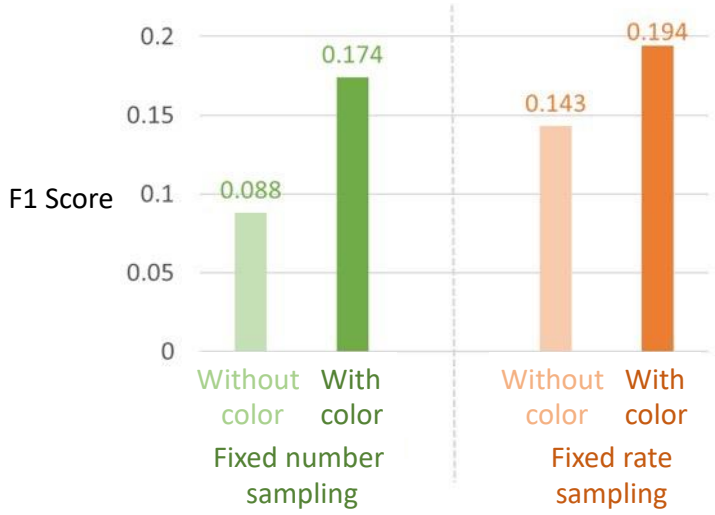

Source: Authors' elaborations.

References

Andrey, J., Yagar, S.: A temporal analysis of rain-related crash risk. Accident Analysis and Prevention, Vol.25 (4), pp.465–472, 1993.

Golob, F.T., Recker, W.W., Alvarez, V.M.: Freeway safety as a function of traffic flow, Accident Analysis and Prevention, Vol 36 (6), pp. 933-946, 2004.

Hyodo, S. and Yoshii, T., 'Analysis of the impact of the traffic states on traffic accident risk', Proceedings of 22st World Congress on Intelligent Transportation Systems (Scientific Paper), ITS-2863, Bordeaux, 2015.

Lin, L., Wang, Q., and Sadek, A. W. : A novel variable selection method based on frequent pattern tree for real-time traffic accident risk prediction, Transportation Research Part C Emerging Technology, vol. 55, pp. 444–459, 2015.

Shankar, V., Milton, J. and Mannering, F.: Modeling Accident Frequen-cies as Zero -Altered Probability Processes: An Empirical inquiry, Acci-dent Analysis and Prevention, Vol. 29, pp.829-837, 1997.

Simonyan. K. and Zisserman, A.: Very Deep Convolutional Networks for Large-Scale Image Recognition, arXiv:1409.1556, 2015.

Tsubota. T., Yoshii, T., and Xing, J.: PREDICTION OF TRAFFIC ACCIDENT LIKELIHOOD ON INTERCITY EXPRESSWAY BY CONVOLUTIONAL NEURAL NETWORK, Artificial Intelligence and Data Science, Vol. 1 (1), 2020.

Wang, C.; Quddus, M.; Ison, S. A spatio-temporal analysis of the impact of congestion on traffic safety on major roads in the uk, Transportmetrica A, Vol 9, pp.124–148, 2013.

Use of vehicle test data and changes in mileage patterns over time

R.E. Wilson[a], J. Thomas[a]

[a] *University of Bristol, United Kingdom*

Introduction and Background

Most vehicles in Great Britain (GB: England, Scotland, and Wales) that are over three years of age are required to undergo a statutory annual safety test, known as the MOT. Since 2010, a complete record of pseudonymised test results has been made available (Department for Transport, 2021) to researchers, via the United Kingdom (UK: GB plus Northern Ireland) government's open data initiative, backdated to 2005 when the system first became digitised. Fields for each test include its date, a coarse geography for the test location, a unique vehicle identifier, and most importantly, the vehicle's odometer reading – together with vehicle-related data such as make, model, and colour, but more crucially fuel type, engine capacity, and date of first use (from which the vehicle's age can be inferred). We realised some time ago (Wilson et al., 2013a) the potential for this data to provide estimates of total miles driven, at regional or national scale, put simply, by differencing consecutive odometer readings for the same vehicle, then summing over the vehicle population.

Of course, most developed countries compute and publish official statistics for total miles driven each year - in the United Kingdom, these are known as the National Road Traffic Estimates (NRTE) (Department for Transport, 2018). The usual approach is to derive such statistics from either automatic or manual vehicle counts on suitably sampled road segments and then to scale up. With this methodology, it is straightforward to provide statistics for different regions, different months / seasons, different road classes, and for strata of easily observed vehicle types, such as cars, light goods, heavy goods, and motorcycles. In future, Automatic Number Plate Recognition (ANPR) could facilitate lookups into vehicle licensing databases and potentially access more detailed vehicle information, however, is presently not used in the NRTE methodology.

In contrast, when using MOT data to estimate total mileages, useful vehicle properties, such as fuel type and vehicle age, naturally fall out. However, the use of MOT has some drawbacks: for example, using the open data release, mileage must be attributed to the test geography, which is presumably correlated to, but not the same as, where the miles were driven. In fact, in a large-scale project 2012-2017, we were also given confidential access and linkage to a vehicle licensing database which gave a fine-scale geography, known as the LSOA (Office for National Statistics, 2021), for the home address of each vehicle's registered keeper. The UK's national census provides quite detailed data at LSOA level, and we were thus able to characterise which socio-economic groups did the most driving and the most polluting (noting that the age and class of vehicles owned is also a key factor) (Chatterton et al, 2015), along with other policy-facing work (Cairns et al., 2017).

However, in this paper we wanted to return to the open data set and stimulate its use by international researchers. There are several reasons why this timely. Firstly, the open set is now extremely mature and well developed: containing the complete record of approximately 600M test results 2005-2021 inclusive, of approximately 67M distinct vehicles. Even the crudest analysis shows some clear trends in vehicle use over time, including perhaps the beginning of the "peak car" phenomenon. Most topically, the open data allows some first insights to vehicle use during the COVID-19 pandemic, which are not available by any other method.

Methodology

The open test data may be arranged so that associated to each vehicle $\mathcal{V}_i$ is a sequence of tests $\mathcal{T}_i^j$, $j = 1,2,\dots,N_i$, to each of which may be associated a triple $(t_i^j, x_i^j, \mathcal{L}_i^j)$. Here t_i^j and x_i^j denote the date and odometer reading (in miles) of the respective test, and $\mathcal{L}_i^j$ denotes the location of the test in terms of a *postcode area*, of which there are 120 in GB, with populations ranging from the tens of thousands to 1.9M (B – Birmingham). Note $t_i^1 \le t_i^2 \le \cdots \le t_i^{N_i}$. (NB a vehicle may have multiple tests on the same day if it does not pass.) Also, one expects $x_i^1 \le x_i^2 \le \cdots \le x_i^{N_i}$, although in practice in addition to 'clocking' (the illegal rolling back of an odometer), there are data entry errors, and the test triples should be filtered and/or cleaned using a set of principles which is beyond the scope of this paper to describe.

Here we process the triples with the *straddling rate* method introduced by (Wilson et al, 2013a). For a query date t^*, one seeks vehicles $\mathcal{V}_i$ with inter-test *intervals* for which $t_i^j \le t^* < t_i^{j+1}$, to which one attributes the mileage rate

$$\overline{r}_i = \frac{x_i^{j+1} - x_i^j}{t_i^{j+1} - t_i^j},$$

which assumes crudely that the vehicle accrues miles at a uniform rate between the two dates. We may then examine the distribution of $\overline{r}_i$ over vehicles, or compute statistics such as a population average which we denote by $\overline{r}$. Note in addition we may also filter populations by properties of vehicles, e.g., age, fuel type, etc., or by locations of tests. Of course, t^* may also be varied to study changes in mileages over time. However, some caution is required in inferring rapid changes in $\overline{r}(t^*)$, because in a setting where the inter-test interval is typically a year, $\overline{r}(t^*)$ convolves miles driven for up to one year before and after t^* itself — see (Wilson et al., 2013b) for a detailed discussion.

Finally, to each vehicle we also associate a triple $(t_i^0, 0, \mathcal{L}_i^1)$, where t_i^0 is the recorded date of first use in the associated vehicle's properties. Thus the *first use* interval $[t_i^0, t_i^1)$ may be queried to calculate contributions to mileage rates for vehicles in the first three years of life, leading up to their first tests. However, unfortunately, caution is required if t^* is within three years of the end of the data set, as the returned rates $\overline{r}_i$ will be incomplete, because some vehicles driving at t^* will not have a test within the provided data.

Results

Due to page limits, we restrict ourselves here to an analysis of total miles driven over time, and a closer inspection of how the mileage reduction that occurred during the pandemic was distributed.

Firstly, we estimate average daily mileage rates for the entire vehicle population with straddle dates set to the 1st July 2006-2021, to characterise each respective year, see Figure 1(a). Even before the pandemic, we observe a steady decline in per-vehicle average mileage that is particularly marked in vehicles under three years old – suggesting perhaps significant long-term change in travel behaviours. Note also that these newer vehicles drive significantly more on average than older vehicles and are given a separate curve here as the method to estimate their mileage is different, as we discussed above. They also do not display the sharp decline in mileage that older vehicles display in the pandemic, although this might be because the method to estimate their mileage loses robustness from 2018 onwards, as discussed above.

Figure 161. (a) Average per-vehicle mileage over time. (b) Registered vehicle populations in GB. (c) Comparison of official NRTE total mileage statistics and our test-based method

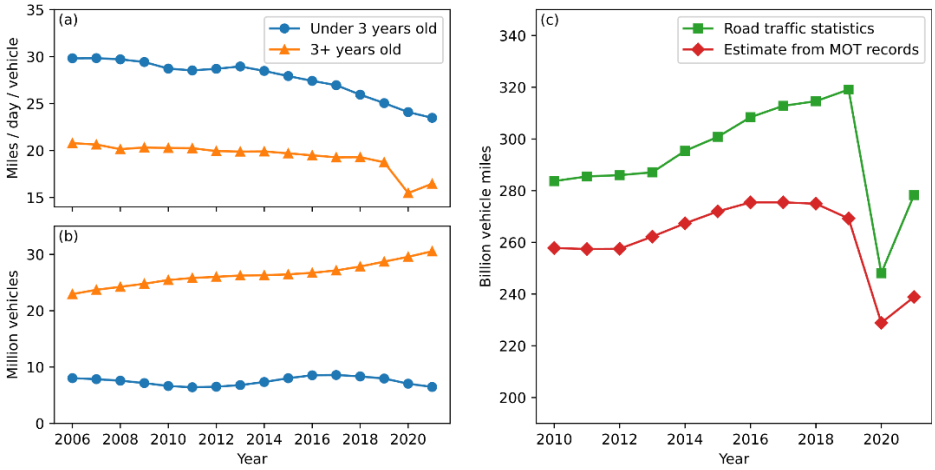

Source: Own analysis.

Next, we attempt to reproduce the NRTE statistics for total miles driven in GB. To do this we use other open data (Department for Transport and Driver and Vehicle Licensing Agency, 2022) that gives counts of vehicles registered each year in different age brackets, see Figure 1(b). This is more robust than counting the matching intervals from the test data, owing to the various cleaning procedures we have used that have filtered that set. Note that generally, the number of vehicles in circulation has increased, but via an increase in the older population (i.e., vehicles not retiring). The counts can then be multiplied by the respective per-vehicle average mileage rates to synthesise our own NRTE estimates, which can be compared with the official statistics based

on roadside counts, see Figure 1(c). Note our method consistently undershoots the official NRTE – this finding is robust to a wide range of variations in the above methodology and suggests that there may be sampling problems with the official NRTE itself. Note that both methods suggest an overall increase over time in total miles driven, due to the increasing vehicle population, and a sharp reduction due to the pandemic.

Table 36. Distributions of daily mileage in the pandemic versus base year 2013, represented by percentiles, based on inter-test intervals

	Statistics – miles per day									
	2013					**Pandemic**				
	Ave	**10%**	**25%**	**75%**	**90%**	**ave**	**10%**	**25%**	**75%**	**90%**
All	19.9	4.3	9.5	26.3	37.9	15.5	2.7	6.3	20.6	31.2
10+ years old	15.3	2.2	6.3	21.2	30.6	12.5	1.6	4.4	17.2	26.5
Postcode SW	14.1	2.5	5.8	18.2	26.5	11.8	1.7	4.1	15.3	24.0
Diesels	26.3	8.0	14.2	33.6	48.0	19.5	4.7	9.2	25.2	37.6

Source: Own analysis.

Finally, we considered how the reduction in mileage observed during the pandemic has been distributed over geography, age of vehicles, fuel type, and so on – a great many combinations of calculations are possible, so here we present just a small set of examples. Note it is important to understand the distribution of mileage rates across populations, which are known to resemble a shifted gamma distribution (Wilson et al., 2013a). This is because we want to know whether it is high or low mileage drivers who have contributed most to the observed reductions. Our method uses 2013 as a base year and compares percentiles of per-vehicle mileages with those for the pandemic (straddle date 1st January 2021). For robust comparison, we consider only inter-test intervals, i.e., for vehicles of three years of age and older. See Table 1.

The first finding is that per vehicle mileage reduced by about a quarter overall. However, the proportional reductions in higher mileage vehicles are less – about a sixth. The effect is even more marked for older vehicles (here 10+ years old), which drive less on average, but have experienced both a lower proportional loss on average (less than a fifth) and an even stiffer response in high mileage vehicles (reduction less than a seventh). A possible explanation is that essential workers are represented strongly in the higher mileage users, and due to modest pay, tend to own older vehicles.

Due to their large size, there are no purely rural postcode areas. However, SW (south west London) is an example of a purely urban area. Not surprisingly, mileage in SW is lower than average. However, SW's pandemic reductions are proportionately very small (a seventh on average, and almost negligible at the top end). Possible explanations include a higher proportion of essential trips, or differing social attitudes to compliance with pandemic guidance, amongst a highly privileged socio-economic group.

Our final computations concern diesel cars – which are driven more on average as (anecdotally) they tend to be preferred by salesmen, executives etc. who drive large numbers of motorway miles. However, the pandemic proportional reductions for diesels are larger in all percentile groups, markedly so in the high mileage vehicles. A possible explanation is that teleworking has especially reduced travel demand in this group.

Conclusion

We have shown how GB's open MOT test data can be used to compute alternative traffic statistics that do not rely on roadside counts, and to explore how mileage varies across different groups (age of vehicles, geography, fuel type etc.) in addition to how it is distributed within those groups. Note, our figures consistently undershoot official NRTE traffic estimates to a degree which raises questions about the correctness of the NRTE's sampling and scaling methods.

We have shown that in the pandemic, higher mileage vehicles reduced their mileage proportionately less than lower mileage vehicles, and this and strata-based analyses raise intriguing hypotheses for more detailed studies. Results for a richer range of strata will be presented at the ISPRA meeting.

Finally, we should note that mileages for some vehicles that were first used during the pandemic will only be calculable in 2024 when they first present for test at three years old. It therefore remains for future work, in 1-2 years' time, to complete the picture of pandemic driving patterns using the open MOT test data source.

References

Cairns, S., Anable, J., Chatterton, T., Wilson, E. and Morton, C., *MOToring Along: The lives of cars seen through licensing and test data*, RAC Foundation, London, 2017.

Chatterton, T., Barnes, J., Wilson, R.E., Anable, J. and Cairns, S., 'Use of a novel dataset to explore spatial and social variations in car type, size, usage and emissions', *Transportation Research Part D: Transport and Environment*, Vol. 39, 2015, pp. 151-164.

Department for Transport, *Traffic statistics methodology review: overview*, downloaded from https://www.gov.uk/guidance/road-traffic-statistics-information, 2018.

Department for Transport, *MOT testing data user guide*, V5.0, downloaded from https://www.data.gov.uk/dataset/e3939ef8-30c7-4ca8-9c7c-ad9475cc9b2f/anonymised-mot-tests-and-results, 2021.

Department for Transport and Driver and Vehicle Licensing Agency, *Vehicle licensing statistics: notes and definitions*, downloaded from https://www.gov.uk/government/collections/vehicles-statistics, 2022.

Office for National Statistics, *A Beginner's Guide to UK Geography*, V1.0, downloaded from https://geoportal.statistics.gov.uk/documents/a-beginners-guide-to-uk-geography-2021-v1-0-1, 2021, pp. 23-24.

Wilson, R.E., Cairns, S., Notley, S., Anable, J., Chatterton, T. and McLeod, F. (2013a), 'Techniques for the inference of mileage rates from MOT data', *Transportation Planning and Technology*, Vol. 36, No. 1, pp. 130-143.

Wilson, R.E., Anable, J., Cairns, S., Chatterton, T., Notley, S., and Lees-Miller, J.D. (2013b), 'On the estimation of temporal mileage rates', *Transportation Research Part E: Logistics and Transportation Review*, Vol. 60, pp. 126-139.

Assessing the Robustness of Multi-Agent Deep Reinforcement Learning for Collaborative Navigation under Adversarial V2V Attacks

L. Parada[a], H. Tiana, P. Angeloudis[a]

[a] *Centre for Transport Studies, Department of Civil and Environmental Engineering, Imperial College London, UK*

Introduction

Adversarial attacks can severely impact the performance and safety of autonomous systems, including Connected Autonomous Vehicles (CAVs). One common form of adversarial attack is to use messages that contain misleading information that can lead to a collision (Owoputi & Ray, 2022). For example, consider the scenario depicted in Figure 1, where an attacker agent can send a message to a victim agent indicating that an intersection is clear, even though it is not. As a result, the victim agent may not be able to stop in time, leading to a collision.

To carry out these types of attacks, attackers often use V2V (vehicle-to-vehicle) ad-hoc networks (Wang et al., 2020). These networks allow vehicles to communicate with each other directly without relying on a centralized infrastructure. This approach makes it easier for attackers to launch attacks, as they can send messages to target agents without being detected easily.

Existing approaches of adversarial attacks on autonomous systems mainly focus on input domains such as images (Szegedy et al., 2014), point clouds (Gleave et al., 2021), and text. There is a lack of research on adversarial robustness in multi-agent autonomous systems, which distribute computation across different entities and transmit encoded messages within a communication network. Moreover, adversarial attacks have been studied almost exclusively in the context of prediction and not in the context of control (e.g. using Deep Reinforcement Learning).

In this study, we assess the robustness of Multi-agent Deep Reinforcement Learning for collaborative navigation under malicious attacks. For this, we introduce attacks in the form of adversarial messages to the V2V network in a challenging driving scenario. We show that even small perturbations to key features of the observation space can result in higher collision probability. Moreover, we train a robust multi-agent controller that can effectively defend against malicious messages and reduce the collision probability.

Figure 162. Effect of an adversarial message on a safety-critical driving scenario

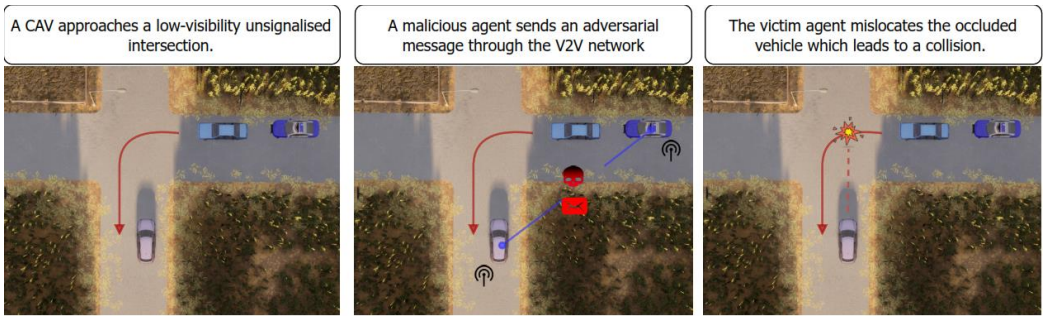

Related Work

Adversarial attacks on Deep Neural Networks are a type of attack where small and imperceivable perturbations can drastically change the behaviour of a neural network, resulting in false outputs. These attacks were first discovered in the context of image classification (Szegedy et al., 2014) and have since been extended to other applications, such as semantic segmentation (Xie et al., 2017) and reinforcement learning (Gleave et al., 2021; Huang et al., 2017).

There are two main types of adversarial DNN attacks - white box and black box - depending on whether the attacker has access to the target neural network's weights. In a white box attack (Goodfellow et al., 2014; Szegedy et al., 2014), the attacker has full access to the weights and can generate adversarial examples using gradient-based optimization. In contrast, a black box (Sun et al., 2020) attack is conducted without knowledge of the target network weights, and real-world knowledge can be leveraged to inject adversaries that resemble common objects.

A few recent works have addressed DNN attacks directly on the V2X communication network. In particular, (Gleave et al., 2021), explored attacks on multi-agent intermediate representations. They showed that adversarial messages could substantially degrade the overall performance when the ratio between malicious and benign agents is relatively high. Moreover, they explored both black and white box attacks over the communication network. They demonstrated that successful defence mechanisms could be employed against white-box attacks; however, when defending against black-box attacks, a more robust message aggregation component should be devised.

Methodology

The MARL problem can be represented as a Decentralised Partially Observable MDP (Dec-POMDP). This problem can be defined by the tuple $\langle N, S, A^i, T, R, O^i \rangle$, where N is a finite set of agents, S is the set of states, A^i is the set of actions for agent i, T is the transition function, R is the reward function, O^i is the set of observations.

To navigate the intersection, we implement the collaborative DRL navigation pipeline presented in figure 2. This figure also shows the message-passing module, which represents the V2V ad-hoc network. We assume that vehicles have high-level observations of the environment, such as pose, velocity, and acceleration. Moreover, CAVs can sense nearby vehicles and send encoded messages to other CAVs in the scene. The aggregated message is then decoded and used to take actions using a Deep Q-Network (DQN) controller.

We create a gym environment consisting of two CAVs and one human-driven vehicle navigating an unsignalized occluded intersection, using the CARLA autonomous driving simulator as the engine. As shown in the figure, the CAV approaching the intersection from the south has an occluded observation and cannot directly see the human-driven vehicle coming from the east. Using the V2V network, another CAV coming from the east can send the occluded vehicle's position and velocity in real-time.

Each CAV's set of actions corresponds to three high-level decisions: to speed up, slow down, or do nothing. On the other hand, the human-driven vehicle does not take action, and it uses the Intelligent Driver Model (IDM) (Treiber et al., 2000) to navigate the intersection. As for the reward function, it is comprised of two components: a penalty for collisions and a positive reward that is proportional to the vehicles' speed.

We implement adversarial attacks in the form of messages that contain misleading information that may directly lead to a collision. We assume that the attacker agent sends the message over a V2V ad-hoc network and that the victim agent cannot distinguish between a malicious or a benign message. To generate adversarial messages, we use a Gaussian noise injection procedure (Gu & Rigazio, 2015) over the true observations of the occluded vehicle. More complex methods, such as NES (Wierstra et al., 2008) have been proposed to generate adversarial examples, but in this study, we aim to show that even a simple noise injection method can substantially increase the probability of collision in challenging scenarios.

The Gaussian noise injected to the true observation of agent i is given by $\theta^i = O^i + \sigma\delta$, where $\delta \sim \mathcal{N}(0, I)$. We apply the noise injection directly to the observation of the occluded vehicle, i.e., to its position and velocity. We use the parameter σ to represent different levels of attack intensity.

To develop a robust multi-agent reinforcement learning (MARL) controller, we incorporate Gaussian noise into the learning process. During each step of training, we sample from a Gaussian distribution with a fixed value of σ, which allows us to determine the observation of the occluded vehicle. By utilising this method, we are able to train a more resilient MARL controller.

Figure 163. Message-sharing MARL framework. The vehicle in red corresponds to the malicious agent that sends an adversarial message to nearby CAVs

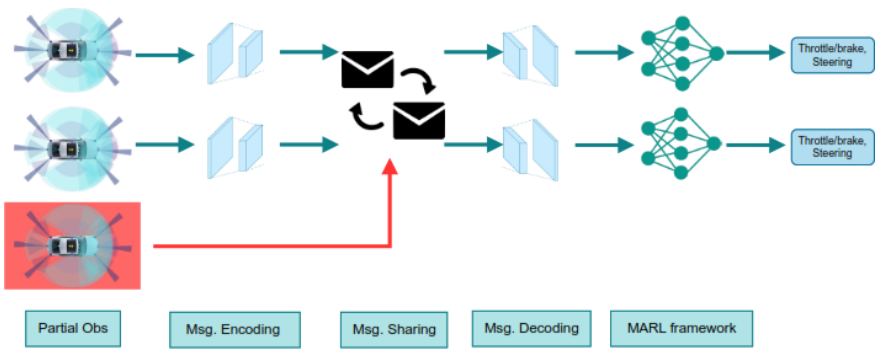

Results

All experiments were conducted using a 10-core, 3.70Ghz Intel Core i9-10900X CPU and an Nvidia GTX 3090 GPU. The models were trained for 600 episodes, and the resulting policies were evaluated over 10 test episodes. We compared the controllers based on the collision rate (ratio of testing episodes that ended with a collision) and the average speed.

The effect of adversarial messages on the base collaborative control model and the robust model were compared and the results are presented in Table 1. The experiment involved injecting noise as an adversarial message with an intensity of 80%. The results indicate that perturbations to the occluded vehicle's pose can lead to confusion of the base controller and result in higher collision rates. When the adversarial messages were introduced to the base model, the testing episodes' average speed remained high, but the controller failed to account for the observation changes and adapt to the adversarial noise.

In contrast, the robust model exhibited a more stable performance with lower collision rates while maintaining high average speeds. To further investigate the attack intensity, different values for the parameter σ were utilized, and the results are shown in Figure 3. As the attack intensity increased, higher collision rates were observed for both models. However, the robust model's rate of increase was considerably lower, with a maximum collision rate of approximately 15%.

Table 37. Evaluation of attacks over the base and the robust collaborative MARL model

Collaborative model	Type of Attack	Avg. Test Reward	Collision Rate (%)	Avg. Speed (km/hr)
Base	No Attack	130.72 ± 12.52	0.0 ± 0.0	75.06 ± 5.67
	Location	60.35 ± 25.25	35.12 ± 23.87	72.25 ± 14.12
	Location + Speed	62.66 ± 30.23	33 ± 18.25	70.01 ± 18.44
Robust	No Attack	100.45 ± 25.34	2.0 ± 1.5	67.44 ± 6.13
	Location	87.66 ± 22.23	12.45 ± 10.12	68.44 ± 12.13
	Location + Speed	70.01 ± 26.26	14.88 ± 9.33	63.44 ± 15.13

Figure 164. Average collision rate as a function of the intensity of the adversarial attack for the Base (orange) and Robust (blue) models

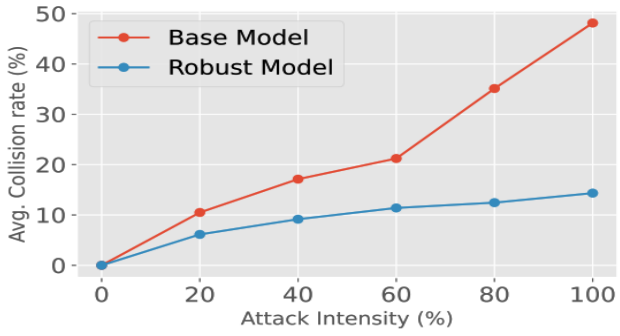

Conclusions

In this study, we evaluate the robustness of Multi-agent Deep Reinforcement Learning for navigation under adversarial messages. Specifically, we investigate how small Gaussian perturbations to the observation space can substantially increase collision probability in an occluded driving scenario. To mitigate this vulnerability, we developed a robust multi-agent controller capable of defending against malicious messages and preventing potential collisions. The results suggest that this approach allows to effectively reduce the collision probability. Although, it should be noted that the multi-agent controller trained with different levels of noise still leads to a

considerable number of collisions. Thus, other methods that can guarantee collision-free trajectories should be studied.

References

Gleave, A., Dennis, M., Wild, C., Kant, N., Levine, S., & Russell, S. (2021). Adversarial Policies: Attacking Deep Reinforcement Learning (arXiv:1905.10615). arXiv. http://arxiv.org/abs/1905.10615.

Goodfellow, I., Shlens, J., & Szegedy, C. (2014). Explaining and Harnessing Adversarial Examples. ArXiv 1412.6572.

Gu, S., & Rigazio, L. (2015). Towards Deep Neural Network Architectures Robust to Adversarial Examples (arXiv:1412.5068). arXiv. http://arxiv.org/abs/1412.5068.

Huang, S., Papernot, N., Goodfellow, I., Duan, Y., & Abbeel, P. (2017). Adversarial Attacks on Neural Network Policies (arXiv:1702.02284). arXiv. https://doi.org/10.48550/arXiv.1702.02284.

Owoputi, R., & Ray, S. (2022). Security of Multi-Agent Cyber-Physical Systems: A Survey. IEEE Access, 10, 121465–121479. https://doi.org/10.1109/ACCESS.2022.3223362.

Sun, J., Cao, Y., Chen, Q. A., & Mao, Z. M. (2020). Towards Robust LiDAR-based Perception in Autonomous Driving: General Black-box Adversarial Sensor Attack and Countermeasures (arXiv:2006.16974). arXiv. https://doi.org/10.48550/arXiv.2006.16974.

Szegedy, C., Zaremba, W., Sutskever, I., Bruna, J., Erhan, D., Goodfellow, I., & Fergus, R. (2014). Intriguing properties of neural networks (arXiv:1312.6199). arXiv. https://doi.org/10.48550/arXiv.1312.6199.

Treiber, M., Hennecke, A., & Helbing, D. (2000). Microscopic Simulation of Congested Traffic. In D. Helbing, H. J. Herrmann, M. Schreckenberg, & D. E. Wolf (Eds.), Traffic and Granular Flow '99 (pp. 365–376). Springer Berlin Heidelberg. https://doi.org/10.1007/978-3-642-59751-0_36.

Wang, T.-H., Manivasagam, S., Liang, M., Yang, B., Zeng, W., Tu, J., & Urtasun, R. (2020). V2VNet: Vehicle-to-Vehicle Communication for Joint Perception and Prediction. ArXiv:2008.07519 [Cs]. http://arxiv.org/abs/2008.07519.

Wierstra, D., Schaul, T., Peters, J., & Schmidhuber, J. (2008). Natural Evolution Strategies. 2008 IEEE Congress on Evolutionary Computation (IEEE World Congress on Computational Intelligence), 3381–3387. https://doi.org/10.1109/CEC.2008.4631255.

Xie, C., Wang, J., Zhang, Z., Zhou, Y., Xie, L., & Yuille, A. (2017). Adversarial Examples for Semantic Segmentation and Object Detection (arXiv:1703.08603). arXiv. https://doi.org/10.48550/arXiv.1703.08603.

Annex – ISTDM Commitees

- *Organising Commitee*
  - Biagio Ciuffo (Chair, European Commission Joint Research Centre)
  - Maria Cristina Galassi (Co-chair, European Commission Joint Research Centre)
  - Soyoung Ahn (University of Wisconsin, US)
  - Jaume Barceló (Universitat Politècnica de Catalunya, ES)
  - Ludovic Leclercq (University Gustave Eiffel, FR)
  - Carlos Lima Azevedo (Technical University of Denmark, DK)
  - Ronghui Liu (University of Leeds, UK)
  - Bat-Hen Nahmias-Biran (Ariel University, IL)
  - Carolina Osorio (HEC Montreal, CA / Google, US)
  - Vincenzo Punzo (University of Napoli Federico II, IT)
  - Meng Wang (Technical University of Dresden, DE)
- *Local organising committee*
  - Louison Duboz, (Program coordinator, European Commission Joint Research Centre)
  - Florentin Ungureanu (Administrative coordinator, European Commission Joint Research Centre)
  - Riccardo Donà (European Commission Joint Research Centre)
  - Ada Garus (European Commission Joint Research Centre)
  - Konstantinos Mattas (European Commission Joint Research Centre)
  - Andromachi Mourtzouchou (European Commission Joint Research Centre)
  - Ewelina Sujka (European Commission Joint Research Centre)
  - Sandor Vass (European Commission Joint Research Centre)
  - Jaime Sierra Munoz (European Commission Joint Research Centre)
  - Elitsa Trifonova (European Commission Joint Research Centre)
- *ISTDM steering committee*
  - Jaume Barceló (Universitat Politècnica de Catalunya)
  - Edward Chung (Hong Kong Polytechnic University)
  - Nour-Eddin El Faouzi (University of Lyon)
  - Masao Kuwahara (Tohoku University)
  - Hani Mahmassani (Northwestern University)
  - Majid Sarvi (The University of Melbourne)
  - Alexander Skabardonis (University of California, Berkeley)
  - Yafeng Yin (University of Michigan)

— *Scientific committee*

- Yasuo Asakura (Tokyo Institute of Technology, Japan)
- Kay Axhausen (ETH Zürich, Switzerland)
- Jaume Barceló (Technical University of Catalonia, Spain)
- Alexandre Bayen (University of California, Berkeley, United States)
- Michael Bell (University of Sydney, Australia)
- Chandra Bhat (University of Texas, Austin, United States)
- Stephen Boyles (University of Texas, Austin, United States)
- Joseph Chow (New York University, United States)
- Panayotis Christidis (European Commission Joint Research Centre, Spain)
- Edward Chung (Hong Kong Polytechnic University, Hong Kong)
- Riccardo Donà (European Commission Joint Research Centre, Italy)
- Nour-Eddin El Faouzi (ENTPE, France)
- Georgios Fontaras (European Commission Joint Research Centre, Italy)
- Ziyou Gao (Beijing Jiaotong University, China)
- Nikolas Geroliminis (EPFL, Switzerland)
- Haijun Huang (Beihang University, China)
- Wenlong Jin (University of California, Irvine, United States)
- Masao Kuwahara (Tohoku University, Japan)
- William Lam (Hong Kong Polytechnic University, Hong Kong)
- Jorge Laval (Georgia Institute of Technology, United States)
- Seungjae Lee (University of Seoul, South Korea)
- Henry Liu (University of Michigan, United States)
- Ronghui Liu (University of Leeds, United Kingdom)
- Hong Lo (Hong Kong University of Science and Technology, Hong Kong)
- Hani Mahmassani (Northwestern University, United States)
- Michail Makridis (ETH Zurich, Switzerland)
- Konstantinos Mattas (European Commission Joint Research Centre, Italy)
- Eric J. Miller (University of Toronto, Canada)
- Marcello Montanino (University of Napoli Federico II, Italy)
- Yu (Marco) Nie (Northwestern University, United States)
- Yanfeng Ouyang (University of Illinois at Urbana–Champaign, United States)
- Kaan Özbay (New York University, United States)
- Elena Paffumi (European Commission Joint Research Centre, Italy)
- Markos Papageorgiou (Technology University of Crete, Greece)
- Ferenc Pekar (European Commission Joint Research Centre, Italy)
- Srinivas Peeta (Georgia Institute of Technology, United States)
- Bin Ran (University of Wisconsin, United States)
- Stephen Ritchie (University of California, Irvine, United States)

- Majid Sarvi (University of Melbourne, Australia)
- James Sayer (University of Michigan Transportation Research Institute, United States)
- Amer Shalaby (University of Toronto, Canada)
- Yasuhiro Shiomi (Ritsumeikan University, Japan)
- Alexander Skabardonis (University of California, Berkeley, United States)
- Agachai Sumalee (Hong Kong Polytechnic University, Hong Kong)
- Lijun Sun (McGill University, Canada)
- S. Travis Waller (University of New South Wales, Australia)
- Yinhai Wang (University of Washington, United States)
- S.C. Wong (University of Hong Kong, Hong Kong)
- Hai Yang (Hong Kong University of Science and Technology, Hong Kong)
- Toshio Yoshii (Ehime University, Japan)
- Lei Zhang (University of Maryland, United States)

List of figures

List of tables

GETTING IN TOUCH WITH THE EU

In person

All over the European Union there are hundreds of Europe Direct centres. You can find the address of the centre nearest you online (european-union.europa.eu/contact-eu/meet-us_en).

On the phone or in writing

Europe Direct is a service that answers your questions about the European Union. You can contact this service:

— by freephone: 00 800 6 7 8 9 10 11 (certain operators may charge for these calls),

— at the following standard number: +32 22999696,

— via the following form: european-union.europa.eu/contact-eu/write-us_en.

FINDING INFORMATION ABOUT THE EU

Online

Information about the European Union in all the official languages of the EU is available on the Europa website (european-union.europa.eu).

EU publications

You can view or order EU publications at op.europa.eu/en/publications. Multiple copies of free publications can be obtained by contacting Europe Direct or your local documentation centre (european-union.europa.eu/contact-eu/meet-us_en).

EU law and related documents

For access to legal information from the EU, including all EU law since 1951 in all the official language versions, go to EUR-Lex (eur-lex.europa.eu).

Open data from the EU

The portal data.europa.eu provides access to open datasets from the EU institutions, bodies and agencies. These can be downloaded and reused for free, for both commercial and non-commercial purposes. The portal also provides access to a wealth of datasets from European countries.

Science for policy

The Joint Research Centre (JRC) provides independent, evidence-based knowledge and science, supporting EU policies to positively impact society

EU Science Hub
joint-research-centre.ec.europa.eu

@EU_ScienceHub
EU Science Hub - Joint Research Centre
EU Science, Research and Innovation
EU Science Hub
@eu_science

Publications Office
of the European Union